Energy Recovery at Thermodynamic Expansion and Thermal Boosting Through Convection in Flat Plate Solar Thermal Systems

Zakir Khan

The thesis is submitted in partial fulfilment of the requirements of Faculty of Science and Technology, Bournemouth University for the degree of Doctor of Philosophy

February 2018

NanoCorr, Energy & Modelling Research Group (NCEM)

Faculty of Science and Technology, Bournemouth University, UK

Copyright Statement

Reprint permission

Reprints from published papers can be made subject to permission from the respective publishers.

Abstract

Fossil fuels have served mankind to meet energy needs in both domestic and commercial applications for a considerable length of time. However, fossil fuels have environmental implications such as emission of harmful gases, depletion of ozone layer and climate change. Moreover, the ever rising prices and limited resources of fossil fuels have obstructed the uninterrupted supply of energy. Therefore, there is a dire need to develop renewable energy technologies that can sustain energy supply with increasing demands. Due to inexhaustible amount of clean solar energy, engineers and researchers are engaged in developing technologies to minimise dependency on fossil fuels. Solar collectors are utilised to use solar heat to increase the heat energy of thermo-fluids or heat transfer fluid (HTF), which can operate Organic Rankine Cycle (ORC) to generate electricity. However, the extensive gain from solar energy is restricted due to unreliability of solar energy during changing weathers and lack of availability at nights. Therefore, thermal energy storage (TES) system can provide a viable solution to respond to varying levels of solar energy.

Literature review indicated that phase change materials (PCM) based latent heat storage (LHS) systems are promising TES technique due to their high thermal storage density, operation at isothermal conditions and wide range availability of PCMs. However, large-scale practical utilisations of LHS systems are limited due to restrained charging and discharging rates caused by low thermal conductivity of PCM. Hence, this research is focused on numerical and experimental analyses conducted in developing an efficient and effective TES technology with novel heat transfer mechanism and novel thermal storage materials to sustain continuous generation of heat and power for low temperature practical applications.

In this research, numerical investigations were conducted to propose an optimum and novel design solution for shell and tube heat exchanger with multiple tube passes and longitudinal fins for improved thermal performance. Parametric investigations were conducted to examine the influence of number and orientations of tube passes in the shell container, geometrical dimensions of longitudinal fins, construction material for shell, tube passes and longitudinal fins, and operating temperature of HTF on phase transition rate and overall enthalpy of LHS system. Further, the proposed design was developed and commissioned with a connection to flat plate solar collector to examine

thermal performance at varied operating conditions. Paraffin (RT44HC) was employed as PCM in shell container and water was utilised to circulate in tube passes to transfer thermal energy gained at solar collector to paraffin in shell container. Thermal performance was evaluated by conducting series of charging and discharging cycles at varied operating conditions to examine the charging/discharging rate, accumulative thermal energy gain/release and mean charging/discharging power. Furthermore, numerical and experimental analyses were conducted to evaluate nano-additives enhanced paraffin samples, which were developed by incorporating aluminium oxides (Al_2O_3), aluminium nitride (AlN) and graphene nano-platelets (GNP) nano-additives in base paraffin. Based on numerical and experimental results and recommendations, numerical simulations were conducted on coupled thermal performance enhancement techniques with longitudinal fins and graphene nano-additives enhanced paraffin samples. It was noticed that phase transition rate for coupled thermal performance enhancement techniques was significantly enhanced by 75.46% as compared to no longitudinal fins orientation with pure paraffin. Likewise, the proposed LHS system can efficiently charge and discharge 14.36 MJ and 12 MJ of thermal energy in as less as 3 h and 1.5 h, which ensures the large-scale practical utilisation in both domestic and commercial applications.

List of Publications

Journal Publications

1. Khan, Z., Khan, Z. A., and Ghafoor, A., 2016. A review of performance enhancement of pcm based latent heat storage system within the context of materials, thermal stability and compatibility. Energy Conversion and Management, 115, 132-158. IF 5.589, Q1
2. Khan, Z., Khan, Z. A., and Tabeshf, K., 2016. Parametric investigations to enhance thermal performance of paraffin through a novel geometrical configuration of shell and tube latent thermal storage system. Energy Conversion and Management, 127, 355–365. IF 5.589, Q1
3. Khan, Z. and Khan, Z. A., 2017. Experimental investigations of charging/melting cycles of paraffin in a novel shell and tube with longitudinal fins based heat storage design solution for domestic and industrial applications. Applied Energy, 206, 1158-1168. IF 7.182, Q1
4. Khan, Z. and Khan, Z. A., 2017. An experimental investigation of discharge/solidification cycle of paraffin in novel shell and tube with longitudinal fins based latent heat storage system. Energy Conversion and Management, 154, 157-167. IF 5.589, Q1
5. Khan, Z. and Khan, Z. A., 2018. Experimental and numerical investigations of nano-additives enhanced paraffin in a shell and tube heat exchanger: a comparative study. Applied Thermal Engineering. IF 3.771, Q1
6. Khan, Z., Khan, Z. A., and Sewell, P., 2018. Thermodynamic performance of a novel shell-and-tube heat exchanger incorporating paraffin as thermal storage solution for domestic and commercial applications. Applied Energy. IF 7.900, Q1 (Under Review)

Conference Proceedings

7. Khan, Z., Khan, Z. A., and Helvaci H. U., 2016 (Invited). Investigation of phase change rate and thermal energy storage of paraffin based latent heat storage system. 5th International Symposium on Energy Challenges and Mechanics (ECM5), Inverness, Scotland, UK, July 10-14. (Accepted)

8. Khan, Z. and Khan, Z. A., 2017. Development in paraffin based thermal storage system through shell and tubes heat exchanger with vertical fins. ASME 2017 11th International Conference on Energy Sustainability, Charlotte, North Carolina, USA, June 26–30.
9. Khan, Z. and Khan, Z. A., 2018. Shell-and-tube based thermal energy system coupled with flat plate solar collector. Advanced Energy Materials (AEM 2018), University of Surrey, England, September 10-12. (Accepted)

Table of Contents

List of Figures

List of Tables

Nomenclature

A_s	Surface area (m^2)
C_p	Specific heat capacity (kJ/kg. K)
$D_{i,t}$	Inner diameter of tube (m)
$D_{i,s}$	Inner diameter of shell (m)
d	Diameter (m)
ΔT_{pc}	Interval for phase transition process (°C)
$\boldsymbol{F}$	Buoyant volume force (Pa/m)
f	Liquid fraction of PCM
$\boldsymbol{g}$	Gravitational acceleration (m/s^2)
H	Specific enthalpy (J)
h	Heat transfer coefficient (W/m^2. K)
$\bar{h}$	Average heat transfer coefficient (W/m^2. K)
k	Thermal conductivity (W/m. K)
k_B	Boltzmann constant (1.38×10^{-23} J/K)
L	Latent heat of fusion (kJ/kg)
l	Length of tube (m)
m	Mass flow rate (kg/s)
M_W	Molecular weight of paraffin
N_A	Avogadro number
Nu	Nusselt number
p	Pressure (Pa)
P_c	Mean charging power (kW)
P_d	Mean discharging power (kW)
Pr	Prandtl number
q	Heat transfer rate (W)
$\dot{q}$	Heat flux density (W/m^2)
Q_s	Accumulative thermal energy storage (kJ)
Re	Reynolds number
$S\boldsymbol{u}$	Momentum source term
t	Time (s)
t_c	Total charging time (s)
t_d	Total discharging time (s)
t_m	Total phase transition time (s)

Δt	Time interval for data collection (sec)
$T_{HTF,in}$	Inlet temperature of HTF (°C)
$T_{HTF,out}$	Outlet temperature of HTF (°C)
T_l	PCM temperature in liquid phase (°C)
T_s	PCM temperature in solid phase (°C)
T_o	Heating/cooling temperature (°C)
$T_{m,i}$	Mean inlet temperature of HTF (°C)
$T_{m,o}$	Mean outlet temperature of HTF (°C)
T_{pc}	Phase transition temperature (°C)
T_{ref}	Reference phase transition temperature (°C)
$\boldsymbol{u}$	Velocity vector (m/s)
u_m	Fluid velocity in tube (m/s)
$\dot{V}$	Volume flow rate of HTF (m^3/sec)
V_{pcm}	Volume of PCM (m^3)
W_{np}	Weight of nano-additives particle
x	Horizontal distance (m)

Greek symbols

α	Small constant value, 10^{-4}
β	Coefficient of thermal expansion (1/K)
ρ	Density (kg/m^3)
δ_{VF}	Volume concentration of nano-additives in base PCM
μ	Dynamic viscosity (kg/m· s)
κ	Morphology constant for mushy zone, ranging from 10^4 – 10^9

Subscripts

in	Inlet
out	Outlet
np	Nano-additives particle
pcm	Phase change material
$npcm$	Nano-additives enhanced PCM
r	Required

Abbreviations

Al_2O_3	Aluminium oxide

AlN	Aluminium nitride
GNP	Graphene nano-platelets
HFE	Hydrofluoroether
HTF	Heat transfer fluid
LHS	Latent heat storage
ORC	Organic Rankine cycle
PCM	Phase change material
TES	Thermal energy storage
SHS	Sensible heat storage

Acknowledgements

First and foremost, I would like to express my gratitude to my supervisor Professor Zulfiqar Khan for his unwavering support, perpetual motivation, collegiality and mentorship throughout this research project.

I would like to acknowledge Bournemouth University, UK and National University of Sciences and Technology (NUST), Pakistan for their financial and in-kind support to conduct this research.

I would also appreciate Future Energy Source Ltd, Poole, UK for providing in-kind support in conducting experimental work in their laboratories. I am thankful to Mr. Tony Camfield and Mr. Brian Camfield for their kind assistance in setting up the experimental setup at Future Energy Source Ltd, Poole, UK.

Finally, I would like to show my utmost respect and thankfulness to my beloved parents, my treasured brothers and respectable members of my entire family for their selfless and incessant support, prayers, motivation and encouragement.

Dedication

This thesis is dedicated to

my beloved parents Mr and Mrs Sadiq Khan

who have been a source of inspiration, encouragement and motivation

who showed me the purpose of life, to be compassionate and to spread positivity

who taught me to always remain loyal, determined and dedicated to work

the joy and pride on their face is my life biggest achievement

Thank you for shaping my future

God bless you

Author's Declaration

This report contains the original work of the author except otherwise indicated. This research is match funded by Bournemouth University, UK and National University of Science and Technology, Pakistan. Future Energy Source Ltd. have provided in-kind support and laboratory facilities. All contents of this report except materials from external referencing are subject to confidentiality under BU-NUST and BU-FES Ltd confidentiality and commercialisation contract.

Chapter 1 Introduction

1.1 Research background

Energy works as a backbone to global economic and social developments. To enable the rapid worldwide growth and advancements, an increase in energy demands for domestic and industrial applications is noticed. In order to meet the global energy demands, the total primary energy supply have indicated a rise of 150% from 1971 to 2015. Energy is categorised in three groups: fossil fuels, nuclear power and renewables, as shown in **Fig. 1. 1**. Fossil fuels are comprised of organic hydrocarbons such as natural gas, coal and oil. Fossil fuels are the main sources of global energy supply. In past four decades, the contribution of fossil fuels to global energy supply is relatively unchanged with a minimal reduction from 86% to 78.4% (REN21 2017). Oil and coal are the prime contributors with percentage total primary energy supply of 32% and 28%, respectively.

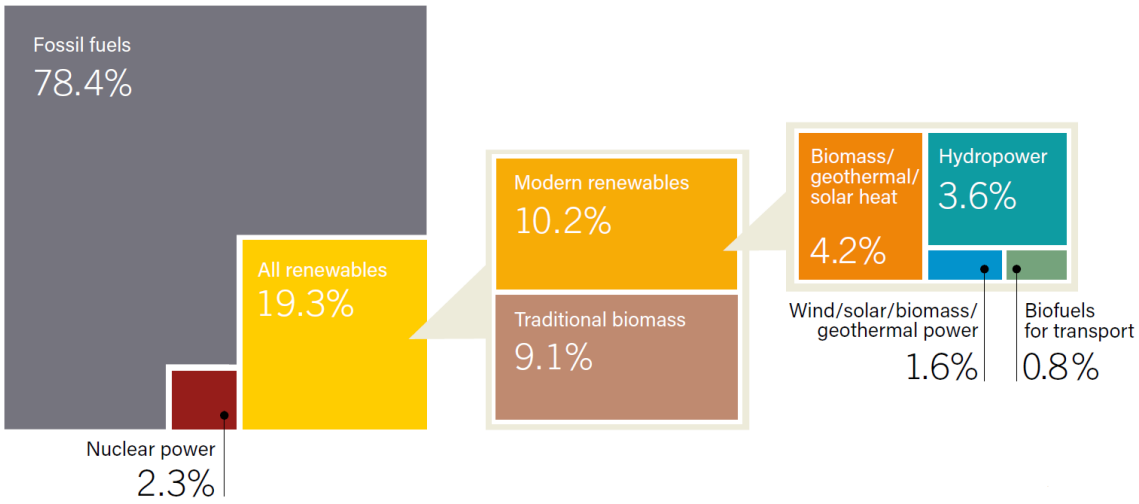

Fig. 1. 1 Energy contribution by fossil fuels, nuclear power and renewables to overall global energy consumptions in 2015 (REN21 2017)

However, the substantial usage of fossil fuels resources to meet global energy demands have significant implications in global warming and climate change (Suranovic, S. 2013; IEA 2015). The emission of greenhouse gases is considerably increased as compared to pre-industrial era level. The global emissions of CO_2 have expanded from 14 Gt to 33 Gt for 1970 to 2015, as shown in **Fig. 1. 2**. Due to large carbon content per unit energy release, coal is considered as the major source of CO_2 emission which is responsible for 45% of total global emissions. Since 1971 until 2015, the global emissions for oil were observed to be reduced from 50% to 35%, however the global

emissions of CO_2 for coal and natural gas were reported to be elevated from 38% and 15% to 45% and 20%, respectively.

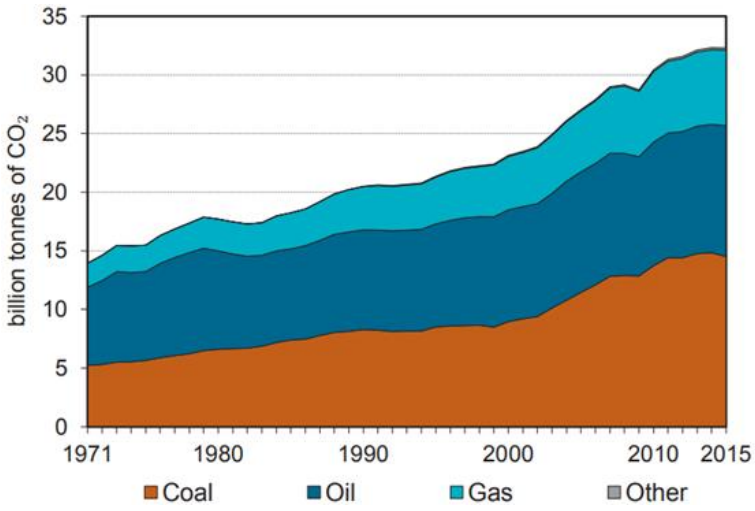

Fig. 1. 2 Contribution to global emissions of CO_2 by fossil fuel sources (IEA 2017).

Energy is crucial for residential, industrial sector, transport, services and generation of electricity and heat. However, transport sector and generation of electricity and heat are primarily responsible for producing two third of overall global emissions. In 2015, the transport sector was culpable the 24% of global emissions and generation of electricity and heat sector was liable for the largest 42% of emissions, as shown in **Fig. 1. 3**. Despite the fact that coal contains large carbon content, most countries still depend on it for generation of electricity and heat by combustion process. Since 1990 until 2015, a steady decline in share of oil for generation of electricity and heat is observed whereas; a slight increase for gas and a significant rise from 65% to 72% for coal is noticed. However, in last couple of years, a gradual transformation from coal to gas is noticed for generation of electricity and heat (IEA 2017).

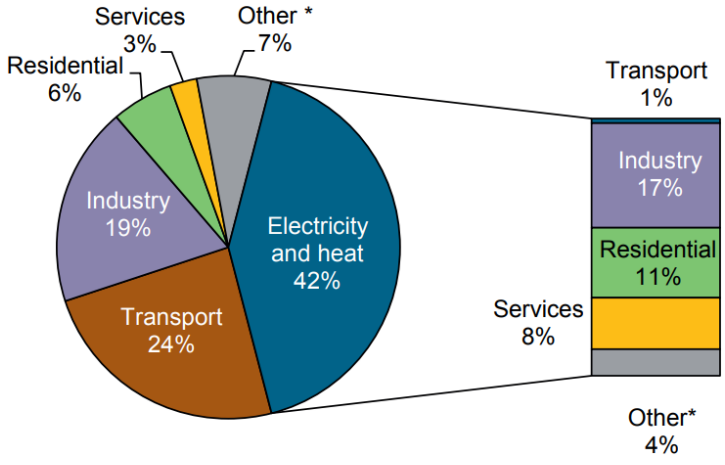

Fig. 1. 3 Various sectors contribution to global CO_2 emissions (IEA 2017)

Further to climate change and global warming concerns due to enormous emissions, fossil fuels have limited reserves in the world to sustain the global energy demand. According to (Petroleum, B. 2013), in view of the global fossil fuels consumptions rate, oil and gas reserves in the world will deplete within a century. In order to progress towards a clean, sustainable and low-carbon world, alternative sources of energy such as nuclear power and renewables are essential. However, the high-cost and hazardous nature of nuclear power limits its utilisation in large-scale power plants. Therefore, these alarming challenges have encouraged researchers, scientists and engineers to avert from high-cost and environmental hazardous technologies by developing technologies for renewable energy sources such as wind, solar, tidal, biomass, biofuels, geothermal and hydropower. As presented in **Fig. 1.1**, the contribution of biomass to global energy demand is higher as compared to any other renewable energy source. Regardless of being one the most promising and abundant sources of clean energy, the utilisation of solar energy sources for generation of heat and electricity is relatively smaller. Therefore, the need of developing technologies for clean, inexpensive and inexhaustible solar energy sources are essential for creating global advantages in terms of improved energy security and sustainability, reduced emissions of greenhouse gases and mitigation of climate change and global warming (Jacobson, M. Z. 2009).

However, the large-scale practical utilisation of solar energy for generation of heat and electricity is hindered by inconsistent and unpredictable nature of solar energy. Energy storage systems can provide a feasible solution to counter the discontinuous availability and variations of solar irradiance due to weather fluctuations. Energy storage systems are adaptable to wide-ranging heat and electricity generating technologies and therefore, it can play a fundamental role in energy security, reliability and improved performance along with reduced mismatch between overall energy demand and supply (Ibrahim, H. et al. 2008). It can also benefit in offsetting the temporary shortage or breakdown of conventional or primary energy sources by guaranteeing sustainable production of required energy demand, assist in peak-shaving and load management and therefore, it improves the overall system efficiency and fuel saving.

The various energy storage systems include mechanical, electrical, chemical and thermal storage systems, as shown in **Fig. 1. 4**. In mechanical storage systems, the pump hydropower is the oldest and most mature technology for bulk energy storage capacity and low lifetime cost. However, the limitations of pump hydropower systems are:

geographic specific technology, higher capital cost, longer construction time and large area occupancy. Similarly, compressed air and liquid air energy storage systems are dependent on mature components for a robust and inexpensive bulk storage capacity. However, these technologies are also geographic site specific and higher capital cost due to requirement of specific components to withstand higher temperature and pressure. Moreover, the flywheels are mostly employed for intermediate storage with rapid response, higher efficiency and higher power density. However, due to higher capital cost and energy supply over a shorter period of time limits the practical applications (Luo, X. et al. 2015).

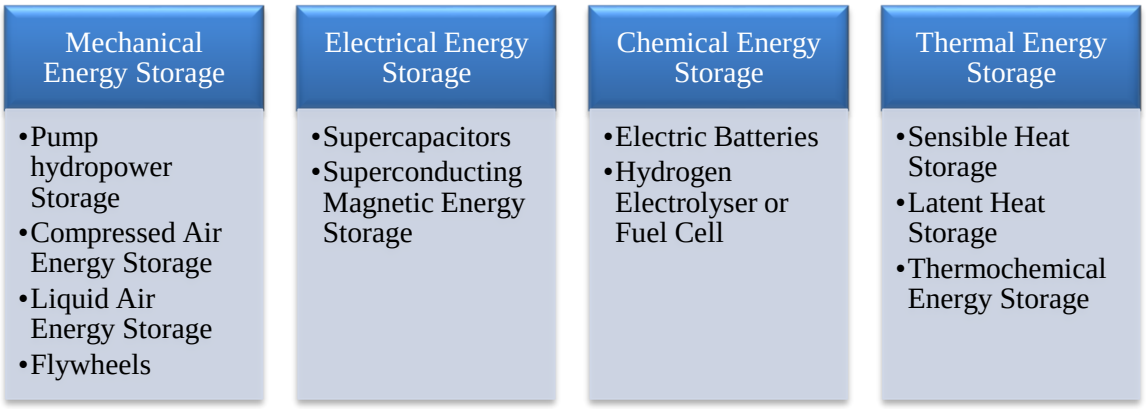

Fig. 1. 4 Various modes of energy storage systems

Electrical energy storage employs super-capacitors and superconducting magnetic energy storage technologies due to their higher efficiencies, quick response, longer life cycle and low maintenance. However, these technologies also supply energy for a shorter duration and requires higher capital cost. Likewise, the chemical energy storage involves electrochemical batteries (such as lithium-ion battery, lead-acid battery, sodium based batteries and redox-flow battery) and hydrogen electrolyser or fuel cells. The electrochemical batteries are mature technology with the ability to function at on-grid and off-grid scale capacity, higher efficiency and quick response. However, the low life cycle, higher capital cost, usage of some toxic material and challenging recycling hinders the practical utilisations (Chen, H. et al. 2009; Dunn, B. et al. 2011). The grid scale utilisation of various energy storage systems and their worldwide contribution is presented in **Fig. 1. 5**. Pumped hydropower storage system presented a comparatively significant contribution of 150 GW out of overall 156.4 GW and is followed by thermal storage systems with global contribution of 3.1 GW.

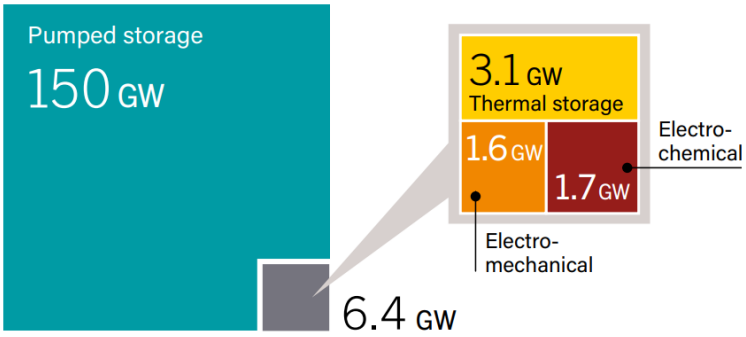

Fig. 1. 5 Total energy storage capacity connected to grid worldwide (REN21 2017)

Thermal energy storage (TES) include sensible heat storage (SHS), latent heat storage (LHS) and thermochemical energy storage. TES stores energy with changing the internal energy of thermal storage material. In SHS system, thermal energy is captured in thermal storage material with an increase in the temperature. Heat capacity and temperature gradient of thermal storage material are utilised to charge or discharge a SHS system. The quantity of TES depends on mass of thermal storage material, temperature gradient and specific heat capacity. Water, rock and concrete are a few examples of SHS materials. Likewise, the LHS system stores thermal energy during phase transition from solid to liquid or liquid to gas and releases it during phase change from liquid to solid or gas to liquid. In LHS system, phase change materials (PCM) are employed as thermal storage materials. The amount of TES are influenced by the mass, temperature gradient, specific heat capacity and latent heat of fusion of PCM. Paraffin, fatty acids, salt hydrates and eutectics are a few examples of LHS system. Similarly, thermochemical energy storage is categorised as reversible chemical reaction process and sorption process. In case of reversible chemical reaction process, the thermal energy is captured and released during breaking and reforming of molecular chemical bonding. Whereas, in case of sorption process, both thermo-chemical and thermo-physical aspects are involved and thermal energy is captured or released during breaking or binding sorbate and sorbent (N'tsoukpoe, K. E. et al. 2009). In this case, the quantity of TES depends on mass of thermal storage material, extent of conversion and heat of reaction (Sharma, A. et al. 2009b).

Due to relatively smaller cost of thermal storage materials, SHS systems are the most employed TES technique in practical applications. However, LHS systems are appraised as the most attractive thermal storage technique due to their wide range availability of thermal storage materials, relatively higher thermal storage density and

almost isothermal charging and discharging of thermal energy. Various comparative studies are conducted to examine the thermal storage performance of SHS and LHS systems. As illustrated in **Table 1**, the storage mass and volume is significantly reduced for LHS systems as compared to SHS system. Similarly, (Morrison, D. and Abdel-Khalik, S. 1978) and (Ghoneim, A. 1989) informed that the required mass to capture same quantity of thermal energy for rock based SHS system were more than seven times as compared to paraffin wax based LHS system and more than eight times as compared to $Na_2SO_4.10H_2O$ (salt hydrate) based LHS system. Therefore, in order to develop a compact TES system with high thermal storage density potential and ability to store thermal energy at various temperature ranges, PCM based LHS system is a preferable, feasible and realistic choice.

Table 1. 1 Comparison of various SHS and LHS systems (Hasnain, S. 1998)

	SHS system		LHS system	
Properties	Water	Rock	Paraffin	Salt Hydrate
Latent heat of fusion (kJ/kg)	-	-	269	280
Specific heat capacity (kJ/kg)	4.2	1.0	2.0	2.0
Density (kg/m^3)	1000	2240	800	2070
Mass required to store 10^6 kJ (kg)	16000	67000	3720	3570
Volume required to store 10^6 kJ (m^3)	16	30	4.7	1.7

1.2 Research motivation

NanoCorr Energy and Modelling (NCEM) research group at Bournemouth University, UK is actively committed to reinforce and achieve the set targets by climate change act, 2008 and Paris agreement, 2015 by developing novel technologies and materials for renewable energy sources. Previously, a large-scale flat plate collector was designed, fabricated and commissioned with effective building roof integration for efficient harvesting of solar energy at lower capital cost, minimum maintenance and adaptable scalability, under the PhD research project titled: “Research and development in novel alternative renewable energy technology” (Wen, Z. 2016). The experimental investigations indicated that the proposed design for flat plate collector with improved heat transfer mechanism between the circulation system and absorber, improved bonding conductivity and minimal convective losses had resulted in 43.50% and

46.07% operating efficiencies for unglazed and glazed configurations. Likewise, the mean useful output for unglazed and glazed configurations were noticed to be 1.00 and 1.29 GJ/m^2.year, respectively. Also, the economic evaluation of the proposed design showed a relatively shorter payback period of 2.4 - 6.5 years as compared to 8 - 12 years for commercial flat plate collectors. Similarly, another PhD research project was completed with a focus on simulating and experimenting novel and eco-friendly thermo-fluids in an organic Rankine cycle (ORC) for low temperature heat and power generation, under the title: "Experimental investigation and mathematical modelling of dynamic equilibrium of novel thermo-fluids for renewable technology applications" (Helvaci, H. U. 2017). Flat plate solar collector was employed as a heat source for generation of electricity through ORC. The low temperature heat and power generation was designed, simulated, commissioned and experimentally investigated with HFE 7000 due to their negligible ozone depletion and global warming potential. Furthermore, the thermo-physical performance of nano-additives enhanced refrigerants were numerically and experimentally examined. It was concluded that inclusion of nano-additives to refrigerants improved the heat transfer coefficient and reduced the entropy generation of the thermal system. Furthermore, the research group was involved in developing numerical design solutions and analytical formulations for developing novel thermo-fluids with improved thermal performance of ORC under a post-doctoral project titled: "Development and modelling of novel thermo-fluids".

This current project is focused on designing and simulating, commissioning and developing a novel LHS system coupled with flat plate solar collector and filled with novel and eco-friendly thermal storage material for effective and efficient charging of thermal energy during solar peak hours or from waste heat recovery sources and discharge it at equally higher rate upon demand to sustain continuous generation of heat and power to maximise its practical utilisations in both domestic and industrial low temperature applications (< 120 ^{o}C).

Due to unpredictable and intermittent nature of solar radiations, the desired LHS system should be capable of capturing maximum magnitude of thermal energy at peak hours with higher charging rate and release the thermal energy at equally higher discharging rate. However, the low thermal conductivity of PCM, which ranges from 0.2 – 0.7 W/m. K, obstructs the rapid charging and discharging of thermal energy from LHS systems and therefore, it reduces the large-scale practical utilisation (Zalba, B. et al. 2003; Farid,

M. M. et al. 2004; Cabeza, L. F. et al. 2011). Likewise, the thermal storage materials should demonstrate excellent compatibility with container material and heat exchanger for long-term thermo-physical stability and long life cycle of LHS systems (Porisini, F. C. 1988; Nagano, K. et al. 2004; Farrell, A. J. et al. 2006; Shukla, A. et al. 2008; Rathod, M. K. and Banerjee, J. 2013).

1.3 Research question

Due to intermittent and varying nature of solar energy sources, TES system is a crucial and practicable solution to limit the energy demand and supply mismatch by providing sustainable and uninterrupted supply of thermal energy for generation of heat or power. Therefore, the main research question addressed in this research project is:

Can a methodology for TES technology be designed, developed and commissioned with novel heat transferring mechanism and novel thermal storage materials to achieve rapid and efficient charging and discharging rate of higher thermal capacity for sustaining continuous generation of heat and power?

1.4 Aims and objectives

The aim of this research is to design and develop a novel TES technology that will be responsible for rapid capturing of excess amount of thermal energy from solar energy or other sources and release it at demand to sustain the continuous generation of heat or power. This research will be focused on numerical and experimental investigations of novel geometrical heat exchanger design solutions and nano-additives enhanced novel thermal storage materials for improved thermo-physical performance and long scale thermo-physical stability of TES systems.

In order to achieve the aforementioned aims, the following objectives are set for this research project:

1. To investigate and understand various possible modes of TES technologies within solar energy and energy recovery systems, and identification of various types of thermal storage materials, their thermo-physical stability and compatibility with several container materials and thermal performance enhancement techniques for maximum utilisation of thermal energy.
2. To conduct numerical simulations on a computational model that incorporates innovative geometrical configurations for LHS system, suitable thermal storage material and compatible container material for efficient heat distribution, higher

thermal storage capacity with improved charging/discharging rate and long-term thermo-physical stability.

3. To develop and simulate a numerical model that is capable to predict accurate enhancement in dynamic viscosity and thermal conductivity of nano-additives enhanced nano-PCM and to identify the influence of various nano-additives material, particle size, volume concentration and operating temperature on overall temperature distribution, phase transition rate and total enthalpy of LHS system.
4. To design, develop and commission an experimental setup for conducting charging and discharging cycles on novel LHS system coupled with flat plate solar collector and solar simulator at varied operating temperatures and volume flow rates. Based on experimental results, an optimum operating conditions are to be identified to achieve required thermal energy demands.
5. To identify the potential enhancement in thermo-physical performance and stability of nano-additives enhanced PCM by conducting several experimental charging and discharging tests at various operating conditions. Similarly, to examine the influence of nano-additives material, particle size and volume concentration on thermal behaviour of nano-PCM.
6. To conduct numerical investigations on combine heat transfer enhancement techniques of novel geometrical design solution of LHS system and novel nano-additives enhanced nano-PCM for calculating optimum thermal performance enhancement.

1.5 Novelty

This research project involves the following novelties:

1. To overcome the influence of low thermal conductivity of PCM on thermal performance of LHS systems, a novel geometrical orientation of shell and tube heat exchanger with longitudinal fins is designed and simulated. In order to attain optimum thermo-physical performance of LHS system, parametric investigations are conducted to examine the influence of various parameters on phase transition rate and thermal storage capacity of proposed LHS design solution. Parametric investigations include number and arrangements of tube passes in shell container, length and thickness of longitudinal fins, materials for shell container, tubes and fins, and operating temperatures of heat transfer fluid (HTF). Commercial grade paraffin (RT44HC) and water is employed as thermal storage material and HTF,

respectively. The proposed optimum design solution for LHS system offers significant enhancement in thermo-physical performance of LHS system with higher phase transition rate and higher thermal storage capacity. Moreover, this novel proposed design of LHS system has not been reported in previous literature and it is capable to easily integrate into solar thermal systems, industrial waste heat systems, peak-shaving and load management and others.

2. For nano-additives enhanced thermal storage materials, a novel numerical model is developed and simulated that considers the influence of nano-additives particle size and their volume concentration and varying temperature on effective dynamic viscosity and effective thermal conductivity. The previous models reported in literature fail to accurately estimate an increase in effective dynamic viscosity and effective thermal conductivity due to the reason that the previous models were developed for smaller volume concentration and large particle sizes. Furthermore, the numerical investigations discuss the impact of material, particle size and volumetric concentration of nano-additives on effective dynamic viscosity and thermal conductivity of nano-PCM and subsequently an influence on temperature distribution and natural convection, phase transition rates and overall system enthalpy.
3. The novel proposed design solution of LHS system is developed and commissioned with an integration to flat plate solar collector to conduct experimental charging and discharging tests. In previous literature, there is a lack of experimental investigations of multi-passes shell and tube heat exchanger with vertical longitudinal fins orientations. The vertical longitudinal fins are carefully designed and developed to improve effective heat transfer area and facilitate natural convection, which is the dominant mode of heat transfer during charging cycle. The influence of various operating temperatures and volume flow rates of HTF on temperature distribution, phase transition rate, total accumulative thermal energy and charging and discharging mean power of LHS system is comprehensively analysed and discussed. The experimental investigations will give significant understanding into practical utilisation of the novel proposed LHS design solution to match large-scale thermal energy demands.
4. Novel nano-additives enhanced thermal storage materials are developed by incorporating metal oxides, metal nitrides and carbon allotropes to commercial grade paraffin as base material. Aluminium oxide (Al_2O_3), aluminium nitride

(AlN) and graphene nano-platelets (GNP) are integrated to paraffin at varied volume fraction ranging from 1% to 5%. The prepared samples of nano-PCM are experimentally investigated in shell and tube heat exchanger by conducting a series of charging and discharging cycles at varied operating temperatures and volume flow rates. The literature also lacks the experimental examinations of nano-PCM in a proper shell and tube heat exchanger. Moreover, the influences of nano-additives material, respective particle size and volume fraction on overall temperature distribution, charging and discharging rate are analysed and discussed. Also, the optimum volume fraction of nano-additives is identified and established.

5. Numerical investigation of combine heat transfer technique by means of implementing shell and tube heat exchanger with longitudinal fins and nano-additives enhanced nano-PCM for ultimate thermal performance enhancement of LHS system.

1.6 Research methodology

The research methodologies adopted for this research project are in conjunction to achieve the set objectives, as listed below:

1. Detailed literature survey is conducted to give an understanding into the current developments in TES technologies in terms of potential low temperature (< 120 ^{o}C) PCMs and their thermo-physical stability for long-life cycle and various unique thermal performance enhancement techniques.
2. Numerical simulations are conducted on a computational design of novel geometrical configured LHS system in ANSYS Fluent software.
3. Numerical model is developed and simulated in ANSYS Fluent software for examining thermal performance enhancement of nano-additives based nano-PCM.
4. The novel design of LHS system is fabricated and commissioned with a connection to flat plate solar collector and solar simulator to conduct a series of experimental charging/discharging cycles at various operating temperatures and volume flow rates.
5. Experimental setup is developed to investigate the thermal performance enhancement of various nano-additives based nano-PCM samples in a shell and tube heat exchanger by conducting experimental charging/discharging cycles at varied operating conditions.

6. Numerical simulations in ANSYS Fluent software are conducted for combined heat transfer enhancement techniques of novel geometrical oriented LHS system with nano-PCM.

1.7 Thesis structure

This thesis is comprised of literature that has been published in journal articles and conference paper by the author (primary). In chapter 1, an introduction into the research background and research question is provided with summarised details of research aim, novelty and research methodologies to present an overview of the thesis.

In chapter 2, a detailed literature review is presented, focusing the evaluation of various groups of PCMs, their thermo-physical performance with respect to their long-term stability and compatibility with container materials, and various effective techniques to enhance the heat transfer mechanism and overall thermal performance of LHS system. Literature review is focused on current developments in PCMs based LHS systems. Moreover, the limitations and gaps in literature are identified. (*Paper I*).

In chapter 3, the analytical and numerical methodology implemented to simulate and analyse LHS systems are presented. At first, analytical models are simulated and analysed to acquire basic understanding of phase transition process, phase boundary movement and influence of operating temperature and volume flow rate of HTF on heat transfer coefficient, charging and discharging rate. In second stage, the numerical models are developed to conduct transient simulations on pure paraffin and nano-additives enhanced paraffin in a novel shell and tube heat exchanger based LHS system. A detailed description of physical models, initial and boundary conditions and computational procedure are provided. (*Paper II, III and VI*).

In chapter 4, the results acquired from analytical and numerical models simulations are discussed and analysed. Impact of varying operating conditions on phase front movement, heat transfer coefficient and total phase transition time of paraffin are discussed. Parametric investigations are conducted to optimise geometrical configurations and dimensions of novel shell and tube heat exchanger with multiple tube passes and longitudinal fins for improved thermal performance. Moreover, an optimum design solution for nano-additives enhanced paraffin as thermal storage material is proposed. (*Paper II, III and VI*).

In chapter 5, the experimental methodology implemented to conduct experimental tests on proposed design of shell and tube heat exchanger and nano-additives enhanced paraffin are presented. In first stage, the experimental setup is developed to examine the thermal performance of proposed design solution of shell and tube heat exchanger with pure paraffin based LHS system at various operating conditions generated with a connection to flat plate solar collector. The components comprising experimental setup are discussed in detail. In second stage, an experimental setup is devised to examine thermo-physical performance of nano-additives enhanced paraffin samples in shell and tube heat exchanger at varied operating conditions. The components involving experimental setup for evaluation of nano-additives enhanced paraffin samples are discussed along with sample preparation technique. (*Paper IV, V and VI*).

In chapter 6, the experimental results acquired from experimental investigations of novel shell and tube heat exchanger and nano-additives enhanced paraffin samples are discussed. Transient temperature response of pure paraffin/nano-additives enhanced paraffin samples to varied operating conditions are presented in terms of charging/discharging rate and mean charging/discharging power to analyse the viability and possible practical utilisation of the proposed LHS system. (*Paper IV, V and VI*).

In chapter 7, based on experimental results in chapter 6, a predictive model is developed and simulated to understand and examine practical utilisation of proposed LHS system to generate an uninterrupted mechanical work/ heat output. Also, the coupled thermal performance enhancement with longitudinal fins and nano-additives enhanced paraffin are simulated to examine optimum improvement in thermal performance of LHS system.

In chapter 8, the conclusions derived from numerical and experimental studies are provided with a reference to achievement of set objectives. Further, the recommendations for possible future developments are listed.

References and appendices are provided at the end of this thesis.

Chapter 2 Literature review

This chapter provides a detail literature survey to evaluate the merits and limitations of various groups of PCMs, their thermo-physical stability, their compatibility with container materials and techniques to enhance the overall thermal performance of TES system. This chapter will help in selecting appropriate thermal storage material and it will give an understanding to identify main key factors that influence long term enhanced thermal performance of TES system. This chapter summarises the literature review that has been published in the article "A review of performance enhancement of PCM based latent heat storage system within the context of materials, thermal stability and compatibility" by (Khan, Z. et al. 2016a) (refer to Appendix A – Paper I).

2.1 Latent heat storage systems

The thermodynamic definition of phase is: a state of matter that is physically and chemically homogenous. Kinetic energy of molecules differentiate between solid and liquids phases. In solid phase, the molecules are closely packed with almost zero mobility and energy transfers through vibration of molecules. Whereas, in liquid phase, the molecules are in higher disorder and thermal energy transfers through molecular motion and collisions. The phase transition of a material involves re-arrangements of molecules and formation/breaking of intermolecular forces which entails a large amount of thermal energy gain/release at specific range of phase change temperature. During phase transition, the thermal energy mainly influences the intermolecular forces, for instance, thermal energy is stored during melting and released during solidification (Dincer, I. and Rosen, M. 2002; Nield, D. A. and Bejan, A. 2006; Bergman, T. L. et al. 2011).

The phase transition of PCM can be categorised as solid–solid, solid–liquid, solid–gas and liquid–gas types. In solid–solid case, thermal energy is stored during transition from one crystalline form of material to another with relatively smaller latent heat capacity and volume change as compared to solid-liquid transitions. Therefore, it offers higher design flexibility and moderate container requirements. In solid-gas and liquid-gas cases, the latent heat of vaporisation is relatively higher as compared to solid-liquid but the higher volume change limits the large-scale practical utilisation in TES applications. Solid-liquid case is considered as an interesting and feasible option for TES applications

due to its large latent heat capacity and small volume change of about or less than 10% (Hasnain, S. 1998; Mehling, H. and Cabeza, L. F. 2007).

LHS systems utilise PCM as thermal storage materials. LHS systems provide an attractive and promising technological solution for TES as compared to SHS systems due to their high thermal storage density and the ability to capture thermal energy at almost isothermal temperature during phase transition. For instance, the amount of thermal energy required to melt 1 kg of ice is equal to 80 times the amount of energy required to raise the temperature of 1 kg of water by 1 ^{o}C. This shows that in case of latent heat storage, a small mass and volume is required to capture a large amount of thermal energy (Hasnain, S. 1998). LHS systems is essentially comprised of the following three components: a) an appropriate PCM with phase transition temperature in desirable range of temperature, b) a compatible container material for enclosing PCM and c) an effective heat exchanger. Thus, the development of an efficient and effective LHS system includes the detail understanding of phase change materials, their compatibility with container materials and an effective heat transfer mechanism.

2.1.1 Selection and classifications of PCM

The selection of an appropriate PCM for designing an effective and reliable LHS system should possess the following desirable thermo-physical, chemical, kinetic, economic and environmental properties:

a) Thermo-physical properties:

- Appropriate phase change temperature for accurate charging and discharging of thermal energy at right temperature for particular applications.
- Latent heat capacity and specific heat capacity should be higher for attaining small volumetric size of LHS system.
- Thermal conductivity should be higher for assuring rapid charging and discharging of latent portion of heat storage.
- Higher phase stability and no segregation for establishing heat storage capacity and higher density for minimising size of LHS system.
- Smaller volume change during phase transition and lower vapour pressure at operating temperature for reducing containment issues.

b) Chemical properties:

- Perfectly reversible melting and solidification of PCM during charging and discharging cycles.
- Long-term thermo-chemical stability to avoid degradation for ensuring longer reliable and useful life cycle.
- Compatibility with container and heat exchanger materials to avoid degradation and contaminations due to corrosion.
- Highly non-toxic, non-flammable and non-explosive to reduce safety concerns and wide practicability in domestic and commercial applications.

c) Kinetic properties:

- Higher nucleation rate to reduce the chances of subcooling which can hinder the discharge of latent portion of thermal energy during solidification process.
- Higher crystallisation rate.

d) Economic and environmental properties:

- Cost effective, abundant and available to be competitive with other TES technologies.
- Non-polluting and small embodied energy.
- Good recyclability and separation potential from other materials for economic and environmental benefits.

In last four decades, comprehensive research investigations are conducted to determine various materials as potential PCMs with broad ranging phase transition temperatures and latent heat capacities. These numerous quantity and diverse nature of PCMs are classified into three main groups of organic, inorganic and eutectic, as shown in **Fig. 2.1**. Each main group is branched into sub-groups with respective chemical composition, thermo-physical behaviour, strengths and limitations.

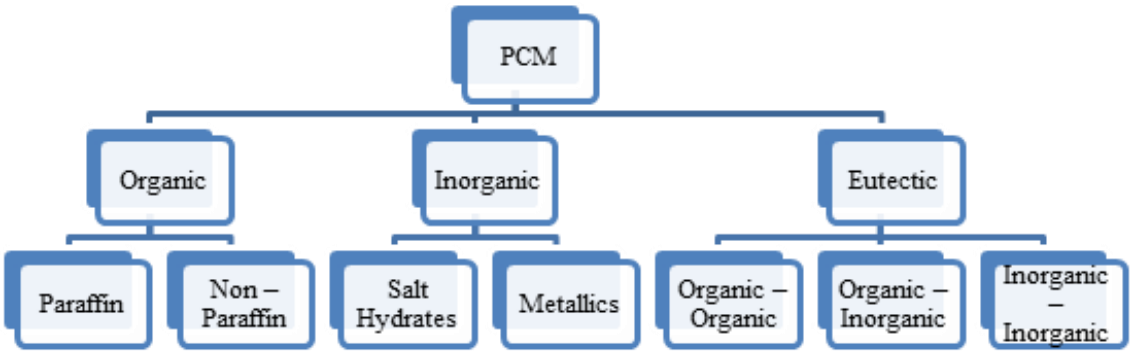

Fig. 2. 1 Classification of phase change materials

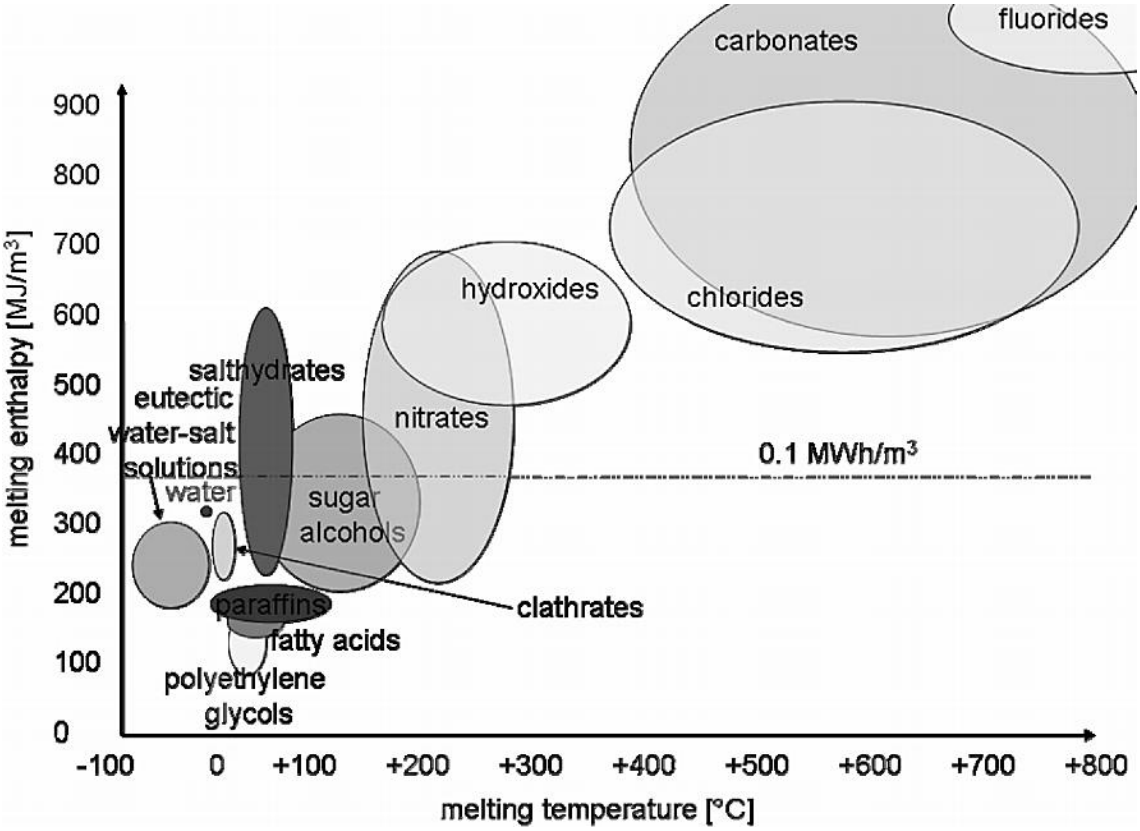

Fig. 2. 2 Classification of PCM with respect to melting temperature and volumetric enthalpy (MJ/m^3) (Mehling, H. and Cabeza, L. F. 2008)

2.1.1.1 Organic PCM

Organic materials based PCM are categorised into subgroups of paraffin and non-paraffins. Non-paraffins include wide-ranging fatty acids, sugar alcohols and glycols. Organic materials are ranging from melting temperature of 0 ^oC – 200 ^oC, as presented in **Fig. 2. 2**.

a) Paraffins

Paraffin is the most common and extensively studied group of organic PCMs. Paraffin is the technical name used for the mixture of hydrocarbon chains of alkanes with general formula of C_nH_{2n+2}. The chemical structure of linear alkanes are shown in **Fig. 2. 3**. The mixture of various linear alkanes result in paraffin with different desirable temperature. Paraffins are usually produced from petroleum distillation. Paraffins display almost identical properties and with an increase in chemical chain length, the developments in phase transition temperature and latent heat capacity are observed. The melting temperature and volumetric enthalpy of paraffins are ranged from -9.6 ^oC – 135 ^oC and 150 MJ/m^3 – 200 MJ/m^3, respectively (Khan, Z. et al. 2016a).

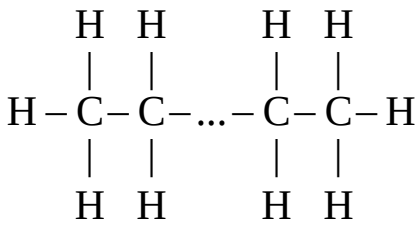

Fig. 2. 3 Chemical structure of paraffin

Paraffins are generally considered a potential and workable organic materials option for thermal storage due to their higher latent heat capacity, availability at wide-ranging phase transition temperatures, excellent thermal and chemical stability, good compatibility with metal containers and heat exchangers, congruent melting/solidification with no subcooling, lower vapour pressure, insoluble in water and non-reactant to chemical reagents and minimal environmental and safety constraints. In spite of numerous favourable attributes of paraffin, the low thermal conductivity (≅ 0.2 W/m. K), incompatibility with plastics (Lázaro, A. et al. 2006) and instability at higher temperature due to breakage of covalent bonding between molecules restricts the wide-ranging practical utilisation of paraffins (Abhat, A. 1983; Zalba, B. et al. 2003; Kenisarin, M. and Mahkamov, K. 2007; Sharma, A. et al. 2009a; Rathod, M. K. and Banerjee, J. 2013). **Table 2. 1** represents the list of common paraffins.

b) Non-paraffins

Non-paraffins organic materials are the largest subgroup of thermal storage materials, which include fatty acids, sugar alcohols and polyethylene glycol. The chemical structures of fatty acids, sugar alcohols and polyethylene glycol are presented in **Fig. 2. 4**. In case of fatty acids, the latent heat of fusion and availability at wide range of temperatures are similar to that of paraffins. Similarly, fatty acids present good thermal stability upon long thermal cycles and no subcooling. However, fatty acids have low practical utilisations due to their low thermal conductivity, poor compatibility with metal containers and heat exchangers due to corrosive and acidic nature, toxic and instable at higher operating temperatures due to high flammability and 2 – 2.5 times costly as compared to paraffins. Likewise, sugar alcohols have higher latent heat of fusion and higher density as compared to paraffins and are available at temperature ranging from 90 ^{o}C – 200 ^{o}C. However, sugar alcohols have slight subcooling which can limit the long-term practical utilisations. Moreover, literature lacks general

information about long-term thermo-physical stability and thermal performance of sugar alcohols and polyethylene glycols (Farid, M. M. et al. 2004; Mehling, H. and Cabeza, L. F. 2008; Sharma, A. et al. 2009a). **Table 2. 2** shows the list of some common non-paraffin organic thermal storage materials.

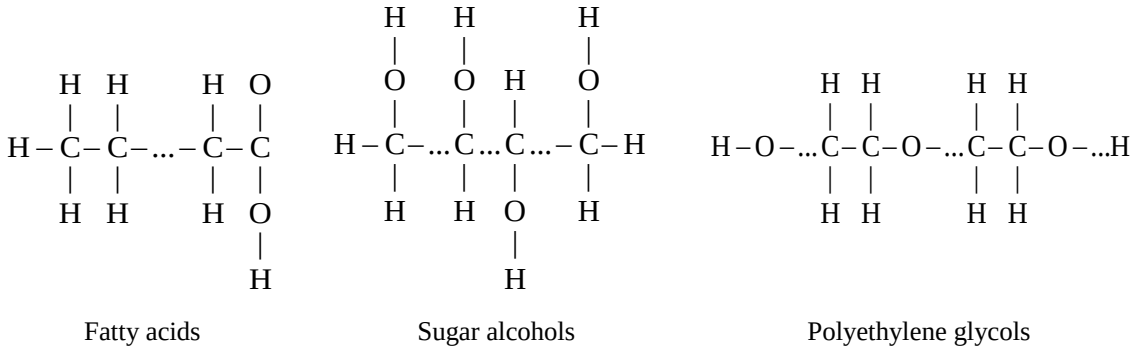

Fig. 2. 4 Chemical structure of fatty acids, sugar alcohols and polyethylene glycols

Table 2. 1 Examples of few common paraffins with thermo-physical properties (Mehling, H. and Cabeza, L. F. 2008; Sharma, A. et al. 2009a)

Paraffins	**Phase change temperature (°C)**	**Latent heat (kJ/kg)**	**Density (kg/m^3)**	**Thermal conductivity (W/m. K)**
n-Tetradecane $C_{14}H_{30}$	6	230	760 (liquid)	0.21 (solid)
n-Hexadecane $C_{16}H_{34}$	18	238	760 (liquid)	0.21 (solid)
n-Octadecane $C_{18}H_{38}$	28	245	814 (solid) 774 (liquid)	0.358 (solid) 0.148 (liquid)
n-Eicosane $C_{20}H_{42}$	38	283	779 (liquid)	-
n-Triacontane $C_{30}H_{62}$	66	-	775 (liquid)	-
n-Pentacontane $C_{50}H_{102}$	95	-	779 (liquid)	-
Polyethylene C_nH_{2n+2} (n up to 100000)	110 – 135	200	870 – 940 (solid)	-

Table 2. 2 Examples of few common non-paraffins with thermo-physical properties (Mehling, H. and Cabeza, L. F. 2008; Sharma, A. et al. 2009a)

Non-paraffins	Phase change temperature (°C)	Latent heat (kJ/kg)	Density (kg/m^3)	Thermal conductivity (W/m. K)
Fatty acids				
Caprylic acid $CH_3(CH_2)_6COOH$	16	149	981 (solid) 901 (liquid)	0.149 (liquid)
Capric acid $CH_3(CH_2)_8COOH$	32	153	1004 (solid) 886 (liquid)	0.149 (liquid)
Lauric acid $CH_3(CH_2)_{10}COOH$	42 to 44	178	1007 (solid) 870 (liquid)	0.147 (liquid)
Myristic acid $CH_3(CH_2)_{12}COOH$	58	186, 204	990 (solid) 861 (liquid)	0.17 (solid)
Palmitic acid $CH_3(CH_2)_{14}COOH$	61, 64	185, 203	989 (solid) 850 (liquid)	-
Sugar alcohols				
Xylitol $C_5H_7(OH)_5$	94	263	1500 (solid)	-
D-Sorbitol $C_6H_8(OH)_6$	97	185	1520 (solid)	-
Erythritol $C_4H_6(OH)_4$	120	340	1480 (solid) 1300 (liquid)	0.733 (solid) 0.326 (liquid)
D-Mannitol $C_6H_8(OH)_6$	167	316	1520 (solid)	-
Galactitol $C_6H_8(OH)_6$	188	351	1520 (solid)	-
Polyethylene glycol				
Diethylene glycol $C_4H_{10}O_3$	-10 to -7	-	1120 (liquid)	-
Triethylene glycol $C_6H_{14}O_4$	-7	-	1120 (liquid)	-
PEG400	8	100	1228 (solid) 1125 (liquid)	0.19 (liquid)
PEG600	17 to 22	127	1232 (solid) 1126 (liquid)	0.19 (liquid)
PEG6000	55 to 66	190	1212 (solid) 1085 (liquid)	-

2.1.1.2 Inorganic PCM

Inorganic materials as thermal storage materials are widely employed in practical applications due to their high latent heat of fusion per unit volume and availability at broad range of operating temperatures, as shown in **Fig. 2. 2**. Inorganic materials are divided into subgroups of salt hydrates, salts and metallics.

a) Salt hydrates

Salt hydrates are the composites of inorganic salts and water solution at discrete mixing ratio following the general formula of $AB.nH_2O$. The melting and solidification of salt hydrates are essentially the hydration and dehydration of salt, which resembles the thermodynamic phase transition between solid and liquid. Salt hydrates are the most studied and practically utilised group of PCMs due to their higher thermal storage density, relatively higher thermal conductivity, small volume change during phase transition, sharp melting point and availability at wide range of temperatures at relatively cheaper price (Sharma, A. et al. 2009a). Melting behaviour of salt hydrates are divided into three categories: congruent melting, incongruent melting and semi-congruent melting. In congruent melting, the anhydrous inorganic salt is completely soluble in water, whereas, in incongruent melting, it is not completely soluble. Similarly, in semi-congruent melting, the solid and liquid phases are in equilibrium during phase change process. The main drawback of salt hydrates are incongruent melting, phase segregation and subcooling during phase transition. In incongruent melting, the high density solid particles of salt settle at bottom of container and the solution is supersaturated. As a result, the reversible solidification process is not achievable with incongruent melting, phase segregation and subcooling issues and consequently, the low thermo-physical stability of salt hydrates is the main problem in practical utilisation (Arena, S. 2016). Moreover, salt hydrates are also corrosive to metal containers and toxic in nature. **Table 2. 3** shows some commonly employed salt hydrates as thermal storage materials.

b) Salts and metallics

For temperature higher than 150 ^{o}C, salts and metallics are the feasible options to be employed as thermal storage materials. The main advantages of salts are their higher phase transition temperature, higher latent heat of fusion, higher thermal conductivity and higher density (Rathod, M. K. and Banerjee, J. 2013). However, the higher capital

cost, corrosive nature towards metal containers and subcooling reduce their practical utilisation. Metallics include metals and metals eutectics which can be employed in higher temperature applications. Metallics possess higher latent heat per unit volume, higher thermal conductivity, low vapour pressure and insignificant volume change. However, the higher initial cost, low specific heat capacity and higher weight reduces the large-scale practical utilisations. The common metallics thermal storage materials are listed in **Table 2. 3**.

Table 2. 3 Examples of few common salt hydrates and metallics with thermo-physical properties (Mehling, H. and Cabeza, L. F. 2008; Sharma, A. et al. 2009a)

Salt hydrates	**Phase change temperature (^oC)**	**Latent heat (kJ/kg)**	**Density (kg/m^3)**	**Thermal conductivity (W/m. K)**
Salt hydrates				
$LiClO_3 \cdot 3H_2O$	8	155	1720 (solid) 1530 (liquid)	-
$CaCl_2 \cdot 6H_2O$	29	190	1710 (solid) 1562 (liquid)	1.088 (solid) 0.540 (liquid)
$Na_2SO_4 \cdot 10H_2O$	32	254	1485 (solid)	0.554 (solid)
$Na_2S_2O_3 \cdot 5H_2O$	48 to 55	209	1750 (solid) 1670 (liquid)	-
$Mg(NO_3)_2 \cdot 6H_2O$	90	163	1636 (solid) 1450 (liquid)	0.669 (solid) 0.490 (liquid)
$MgCl_2 \cdot 6H_2O$	117	169	1569 (solid) 1450 (liquid)	0.704 (solid) 0.570 (liquid)
Metallics				
Gallium	30	80.3	-	41
Cerrolow eutectic	58	90.9	-	-
Cerrobend eutectic	70	32.6	-	-
Bi–In eutectic	72	25	-	-
Bi–Pb–tin eutectic	96	-	-	-
$LiNO_3$	254	360	2140 (solid) 1780 (liquid)	1.37 (solid) 0.58 (liquid)
KNO_3	333	266	1900 (solid) 1890 (liquid)	0.5 (liquid)
MgCl	714	452	2140 (solid)	-
Na_2CO_3	854	276	2533 (solid)	-

In order to draw a comparison between various groups of thermal storage materials, a detailed literature review was conducted in our review article (Khan, Z. et al. 2016a), which considered both laboratory examined and commercially available PCMs. **Table 2** in Appendix A – Paper I discusses the comparison amongst various groups of PCMs with respect to the temperature range for materials availability, latent heat capacity, thermal conductivity, advantages and shortcomings with methods for improvement. It was manifested that the paraffins and salt hydrates could provide an advantageous and desirable thermal storage medium as compared to other subgroups. Therefore, paraffins and salt hydrates are exclusively considered for further investigations in this thesis. Likewise, **Table 3** and **Table 4** in Appendix A – Paper I provide the detailed list of various experimented and commercially available paraffins and salt hydrates thermal storage materials at varied range of phase transition temperatures, their latent heat capacity, thermal conductivity, density and long-term thermal cycle performance, respectively.

2.1.2 Thermo-physical stability and compatibility of PCMs with container materials

To develop a reliable and repeatable LHS system, the long-term thermo-physical stability of PCMs and their good compatibility with container materials of LHS systems are imperative. In last couple of decades, researchers have investigated the thermo-physical stability and compatibility with container materials due to rising interest in reliable and responsive LHS systems. Prior to producing large-scale commercial development of LHS systems, the PCMs should be investigated for long-term thermo-physical stability. Therefore, PCMs should be subjected to at least 3650 rapid thermal cycles in laboratory to ensure thermo-physical stability and reliability of LHS systems for 10 years.

2.1.2.1 Thermo-physical stability of PCMs

Thermo-physical stability of paraffins and salt hydrates are reviewed in detail (refer to Appendix A – Paper I). To conduct accelerated melting-solidification cycles, researchers have commonly utilised differential scanning calorimeter and electric hot plate setup or thermostatic bath or oven as thermal and cycling equipment.

In case of paraffins, due to identical chemical structure of chains of alkanes and no requirement for addition of thickener or nucleating agents, the paraffins do not

experience phase segregation and therefore, a good thermo-physical stability and reliability of paraffins are reported with insignificant variance in phase transition temperature and latent heat of fusion after accelerated thermal melting-solidification cycles. According to (Hadjieva, M. and Argirov, J. 1992), the phase transition temperature and latent heat of fusion for $C_{22.2}H_{44.1}$ and $C_{23.2}H_{40.4}$ were insignificantly varied from 47.1 ^{o}C – 46.6 ^{o}C and 57.1 ^{o}C – 57.8 ^{o}C, and 166 kJ/kg – 163 kJ/kg and 220 kJ/kg – 224 kJ/kg after 900 accelerated thermal cycles. Likewise, (Sari, A. et al. 2011) reported that n-heptadecane showed excellent thermo-physical stability with an insignificant variance of 18.4 ^{o}C – 18.9 ^{o}C in phase transition temperature and 84.7 kJ/kg – 94.5 kJ/kg in latent heat capacity after 5000 accelerated melt-freeze cycles. Similarly, (Sharma, S. et al. 1999; Sharma, A. et al. 2002; Shukla, A. et al. 2008; Alkan, C. et al. 2009) reported that thermo-physical properties of paraffins did not degrade by repeated thermal cycles.

In case of salt hydrates, the incongruent melting and phase separation causes the formation of additional hydrates with less water content and settle in bottom due to variation in densities, which drastically reduce the thermo-physical stability. In order to improve the thermo-physical stability of salt hydrates, the nucleating agents such as sodium chloride, strontium chloride hexahydrate, borax and disodium phosphate etc. and thickeners such as silica gel, attapulgite clay, polyacrylamide and polyvinyl alcohol etc. were proposed by researchers. Likewise, the addition of excess water were experimented which limited the formation of additional hydrates and increased solubility. In salt hydrates, calcium chloride hexahydrate ($CaCl_2$. $6H_2O$) along with nucleating agents, excess water and thickeners had presented good repeatability of phase transition temperature and latent heat capacity. (Kimura, H. and Kai, J. 1984; Feilchenfeld, H. and Sarig, S. 1985; Tyagi, V. and Buddhi, D. 2008) reported that $CaCl_2$. $6H_2O$ with nucleating agents and thickeners illustrated good repeatability and stability with no phase separation and insignificant degradation. However, (Marks, S. 1980; Porisini, F. C. 1988) reported that Glauber's salt (Na_2SO_4. $10H_2O$) with and without nucleating agents and thickeners had sustained drastic degradation in thermo-physical properties when subjected to accelerate thermal cycles. Likewise, (El-Sebaii, A. et al. 2009; El-Sebaii, A. et al. 2011) examined the thermal stability of magnesium chloride hexahydrate ($MgCl_2$. $6H_2O$) with sealed and unsealed container and addition of excess water. It was reported that in case of unsealed container, the phase transition

temperature and latent heat capacity deteriorated from 111.5 ^{o}C – 124.12 ^{o}C and 155.11 kJ/kg – 85 kJ/kg after 500 thermal melting-solidification cycles. Also, the unrestrained phase segregation and incompatibility with metal container in unsealed container orientation ruled out its practical utilisation in LHS systems. However, in case of sealed container, the thermo-physical degradation and phase segregation was minimal even after 1000 thermal melting-solidification cycles. It was reported that phase transition rate and latent heat capacity was insignificantly varied from 110.8 ^{o}C – 115.39 ^{o}C and 138 kJ/kg – 130.28 kJ/kg, respectively. Therefore, it is recommended to include an appropriate amount of nucleating agents, thickeners and excess water content to reduce the phase segregation and subcooling problems in salt hydrates for improved thermo-physical stability and reliability.

2.1.2.2 Compatibility of PCM and container materials

Long-term compatibility of PCM with container and heat exchanger materials are crucial for large scale practical utilisation of LHS systems. Prior to the design and development of LHS system for commercial or domestic applications, the thermal storage material with essential thermo-physical properties should be selected and its compatibility with container materials should be examined.

It is reported in literature that paraffins have good compatiblity with metal containers and heat exchangers. However, paraffins have illustrated poor compatibility with plastic containers which can reduce the long-term life cycle of LHS system. (Lázaro, A. et al. 2006) conducted a series of experiemtnal evaluation tests through visual inspection and gravimetric analysis on different paraffins against various plastic containers and it was informed that migration of paraffins in plastic containers and moisture sorption were observed. However, it was reported that high density polyethylene (HDPE) had illustrated relatively better compatibility with paraffins.

Due to corrosive nature of majority of salt hydrates, the compatibility with metal containers have caused serious complications. As presented in **Table 2. 4**, most of the salt hydrates are not compatible with copper and aluminium, which are the preferred construction materials for containers and heat exchangers of LHS systems due to their higher thermal conductivity and light weight as compared to stainless steel and carbon steel. (Cabeza, L. et al. 2001a, 2001b) investigated the corrosive nature of $CaCl_2$. $6H_2O$ at short term of 14 days and medium term of 75 days with brass, copper, aluminium,

stainless steel and carbon steel. It was reported that $CaCl_2$. $6H_2O$ was compatible with copper and brass but displayed corrosive behaviour against aluminium, stainless steel and carbon steel. Similarly, (Moreno, P. et al. 2014) examined the corrosive behaviour of eleven salt hydrates against copper, aluminium, stainless steel and carbon steel, as presented in **Table 2. 4**. It was observed that almost all salt hydrates had illustrated severe degradation to copper and aluminium samples, whereas stainless steel had presented good corrosive resistance, as shown in **Fig. 2. 5**.

Therefore, in order to develop a reliable, durable and long-lasting LHS system for practical utilisation in domestic and commercial applications, paraffins were appraised as a practicable and relatively advantageous thermal storage option over salt hydrates. The practical utilisation of salt hydrates were limited due to their complexities and deteriorations in thermo-physical performance caused by their corrosive nature and phase segregation problems. Therefore, paraffins were selected as thermal storage materials for designing and developing a robust and responsive LHS system due to their excellent thermo-physical stability and good compatibility with metal containers.

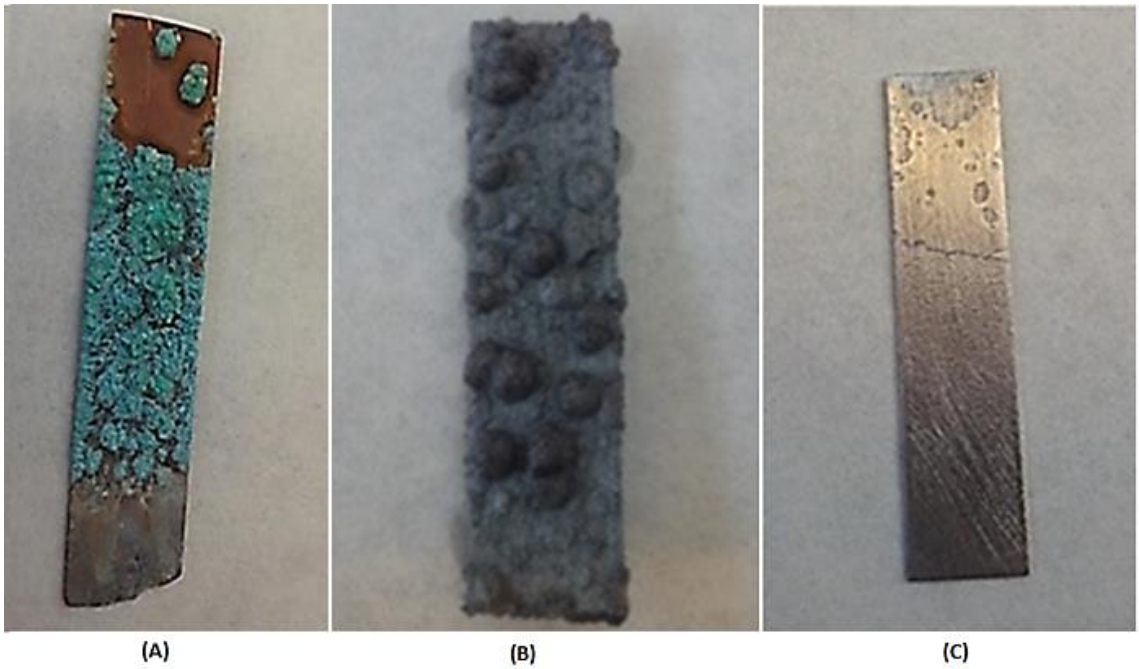

Fig. 2. 5 Corrosive behaviour of: (A) S10 against copper, (B) $ZnCl_2$. $3H_2O$ against aluminium and (C) $Zn(NO_3)_2$. $4H_2O$ against carbon steel (Moreno, P. et al. 2014). *Note: Investigation of corrosive behaviour of salt hydrates was out of scope of this thesis.

Table 2. 4 Salt hydrates compatibility with metal containers (Khan, Z. et al. 2016a)

PCM	**References**	**Container Materials**				
		Brass	Copper	Aluminium	Stainless steel	Carbon Steel
$Zn(NO_3)_2.6H_2O$	(Cabeza, L. et al. 2001a)	No	No	No	Yes	No
	(Cabeza, L. et al. 2001b)	No	No	No	Yes	No
$Na_2HPO_4.\ 12H_2O$	(Cabeza, L. et al. 2001a)	Yes	Yes	No	Yes	No
	(Cabeza, L. et al. 2001b)	Yes	Caution	No	Yes	Caution
$CaCl_2.6H_2O$	(Cabeza, L. et al. 2001a)	Yes	Yes	No	Caution	No
	(Cabeza, L. et al. 2001b)	Yes	Yes	Caution	Yes	Caution
$NaOAc.3H_2O$	(Cabeza, L. et al. 2002)	Caution	Caution	Yes	Yes	Yes
$Na_2S_2O_3.5H_2O$	(Cabeza, L. et al. 2002)	No	No	Yes	Yes	Yes
$Mg(NO_3)_2{\cdot}6H_2O$	(Farrell, A. J. et al. 2006)	No	No	Yes	Yes	No
Glauber's salt	(García-Romero, A. et al.			Al 1050 Yes		
($Na_2SO_4.10H_2O$)	2009)			Al 2024 No		
				Al 3003 Yes		
				Al 6063 Caution		
S10 (Na_2SO_4 + NH_4Cl + sepiolite)	(Moreno, P. et al. 2014)		No	Caution	Yes	No
C10 (Na_2SO_4 + H_2O + additives)	(Moreno, P. et al. 2014)		No	Yes	Yes	No
$ZnCl_2.3H_2O$	(Moreno, P. et al. 2014)		Yes	No	Yes	No
$NaOH.1.5H_2O$	(Moreno, P. et al. 2014)		No	No	Yes	Caution
$K_2HPO_4.\ 6H_2O$	(Moreno, P. et al. 2014)		Caution	No	Yes	No
S46 ($Na_2S2O_3.5H_2O$ +sepiolite+ fumed silica)	(Moreno, P. et al. 2014)		No	Caution	Yes	No
C48 ($CH_3OONa+H_2O$+ additives)	(Moreno, P. et al. 2014)		No	Yes	Yes	Yes
$MgSO_4.7H_2O$	(Moreno, P. et al. 2014)		No	Yes	Yes	No
$Zn(NO_3)_2.4H_2O$	(Moreno, P. et al. 2014)		No	No	Yes	No
$K_3PO_4.7H_2O$	(Moreno, P. et al. 2014)		No	No	Yes	Yes
$Na_2S_2O_3.5H_2O$	(Moreno, P. et al. 2014)		No	Caution	Yes	Caution

2.1.3 Effective heat exchanger mechanism for LHS system

The selection of heat transfer mechanism between thermal storage materials and HTF play a decisive role in designing and developing an efficient and responsive LHS system for practical applications. The productivity of LHS systems are significantly affected by low charging and discharging rates, which are caused by low thermal conductivity of PCMs (≈ 0.2 – 0.4 W/m· K). Therefore, it is imperative to adopt to various thermal performance enhancement techniques to overcome the shortcomings of LHS systems. As presented in **Fig. 2. 6**, the various thermal performance enhancement techniques implemented by various researchers to improve the charging/discharging rates and thermal storage capacity of LHS systems are geometrical configurations, inclusion of extended surfaces, addition of thermal conductive additives, multiple PCMs approach and encapsulations of PCM (Agyenim, F. et al. 2010; Dhaidan, N. S. and Khodadadi, J. 2015; Giro-Paloma, J. et al. 2016; Liu, L. et al. 2016). In this thesis, the numerical and experimental examinations for thermal performance enhancement of LHS system were focused on geometrical configurations, addition of extended surfaces and incorporation of thermal conductive additives techniques. Detailed discussion about other performance enhancement techniques can be found in Appendix A – Paper I.

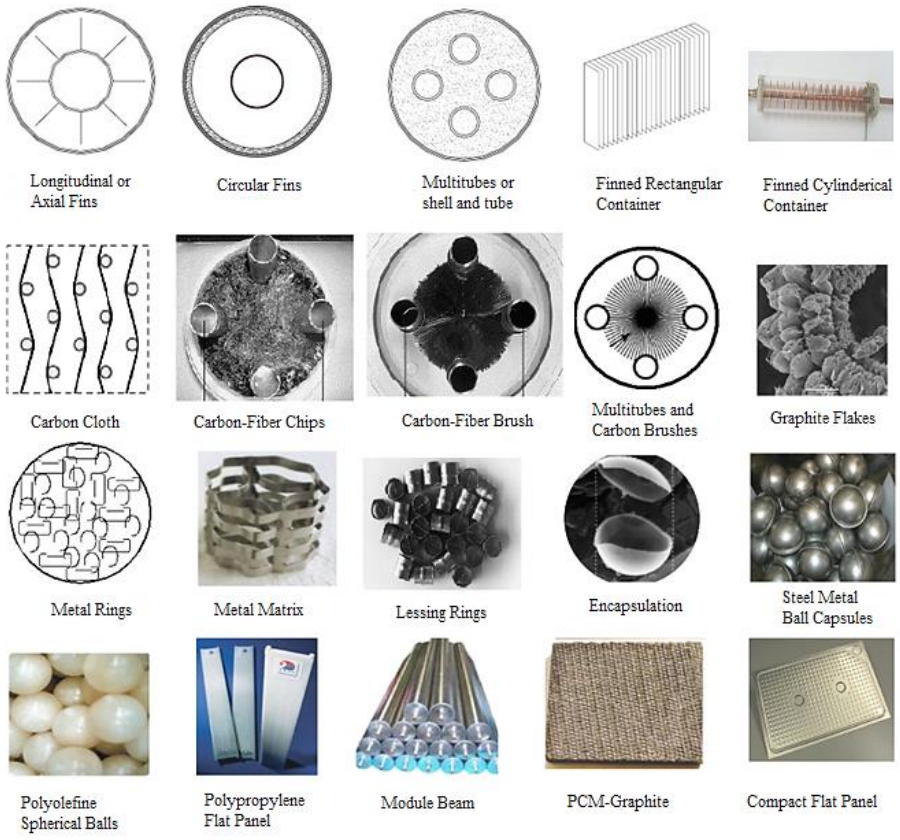

Fig. 2. 6 Thermal performance enhancement techniques adopted by researchers (Khan, Z. et al. 2016a)

2.1.3.1 Geometrical configuration of LHS system

The geometrical orientation of LHS system significantly influences the nature of heat transfer and subsequently, the accumulative thermal energy storage/release, charging/discharging rate and mean charge/discharge power. Thermal performance of LHS systems are directly influenced by the selection of container orientations. The typical container orientations investigated by researchers are: rectangular, spherical, cylindrical, concentric tubes and shell and tubes. Due to excellent integration to numerous engineering applications and minimal thermal energy losses, shell and tubes configurations based LHS systems are extensive inspected in literature.

The selection of container configuration is an important parameter for developing an effective and efficient LHS system. (Kamkari, B. et al. 2014) numerically examined the dynamic phase transition performance of PCM in a rectangular container with varied inclination angles of 0^o, 45^o and 90^o. The hot surface of container was set to an isothermal temperature and the other sides were set to adiabatic condition. It was informed that hot surface position was key to natural convection and consequently to overall heat transfer and phase transition rate. In case of vertical hot wall, conduction heat transfer dominated the thermal energy transfer at the start of charging cycle and as a result, the temperature contours were found to be in parallel to hot wall. However, as the liquid portion of PCM increased, the natural convection dominated the heat transfer by overcoming the viscous force with buoyant forces. Due to upward rise of high temperature molecules, the heat transfer at upper portion of container was increased, which produced a relatively higher melting rate. The temperature contours represented a reduction in temperature as descending along the solid-liquid interface, which resulted in lower heat transfer and melting rate at bottom portion. Likewise, a stratified liquid layer was observed due to accumulation of hot liquid PCM at upper portion of container. In case of hot surface at 45^o inclination, no stratified layer were observed and therefore, a relatively higher heat transfer and melting rate were achieved. Likewise, in case of horizontal hot surface orientation, the uniform temperature distribution resulted in twice as rapid melting rate as compared to vertical hot surface orientation. Likewise, (Lamberg, P. et al. 2004) conducted numerical investigations on phase transition performance of PCM in rectangular container with and without natural convection. It was informed that the melting time was reduced to almost half for LHS system with natural convection as compared to without natural convection case.

Similarly, the influence of natural convection on effective heat transfer, melt front movement and phase transition rate were investigated in cylindrical container by (Jones, B. J. et al. 2006; Shmueli, H. et al. 2010; Han, G.-S. et al. 2017). It was reported that as compared to rectangular orientation, the melting process was influenced by four various regimes, as follow: (i) conduction heat transfer, (ii) conduction and natural convection, (iii) natural convection and (iv) solid shrinkage, as shown in **Fig. 2. 7**. In solid shrinkage, the remaining solid portion of PCM was gradually melted by natural convection alone.

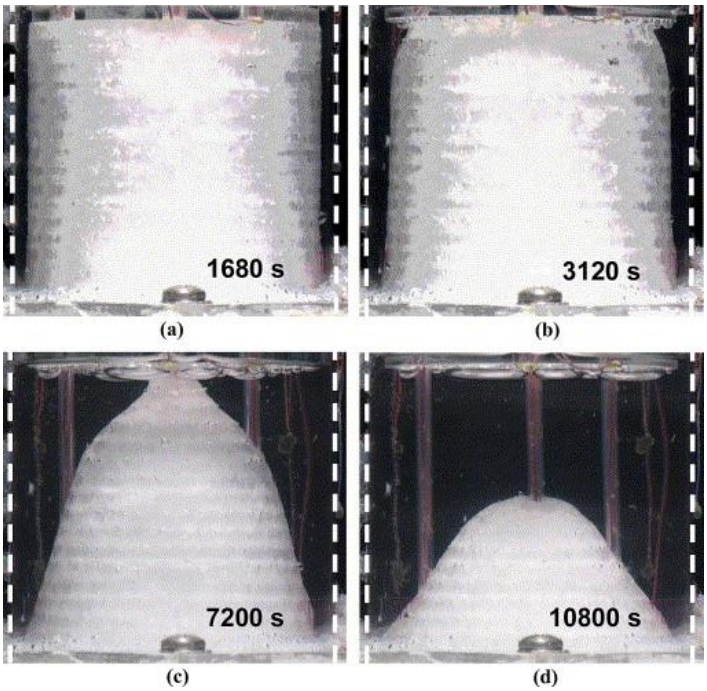

Fig. 2. 7 Melt front of paraffin wax in a vertical cylindrical container at various time intervals (Jones, B. J. et al. 2006).

(Esapour, M. et al. 2016) conducted numerical investigations on phase transition behaviour of PCM in a shell and multi-tubes configuration. The effect of increasing number of smaller multi-tubes as compared to single larger tube was analysed. It was informed that due to an increase in number of tubes, the molten regime was improved and therefore, the influence of natural convection was amplified. As a result, the melting rate was improved by 29% for four multi-tubes as compared to single tube orientation, as presented in **Fig. 2. 8**. Likewise, (Luo, K. et al. 2015) conducted numerical analyses to investigate the influence of number of tubes and their orientations in shell on phase transition rate. It was informed that with an increase in number of tubes to 4 and 9, the phase transition rate was improved by 2.5 and 5 times as compared to single tube

configuration. Moreover, the comparative analyses for relatively higher phase transition rate in rectangular, cylindrical and shell and tube orientations were conducted by (Zivkovic, B. and Fujii, I. 2001; Vyshak, N. and Jilani, G. 2007). It was reported that for same volume and effective heat transfer area, the shell and tube orientation had presented higher charging rate to accumulate equal amount of thermal energy.

In case of discharging cycle, the solidification process is initially dominated by natural convection which helps in discharging the sensible portion of thermal energy and therefore, the temperature of PCM drops to phase transition temperature. With the formation of solidified layer, conduction heat transfer dominates the extraction of thermal energy. The solidified layer of PCM behaves as an insulation medium due to their low thermal conductivity, which results in reduced phase transition rate. Therefore, the vertical or horizontal orientation of LHS system has an insignificant influence on phase transition rate during discharging cycle (Allen, M. J. et al. 2015; Seddegh, S. et al. 2016).

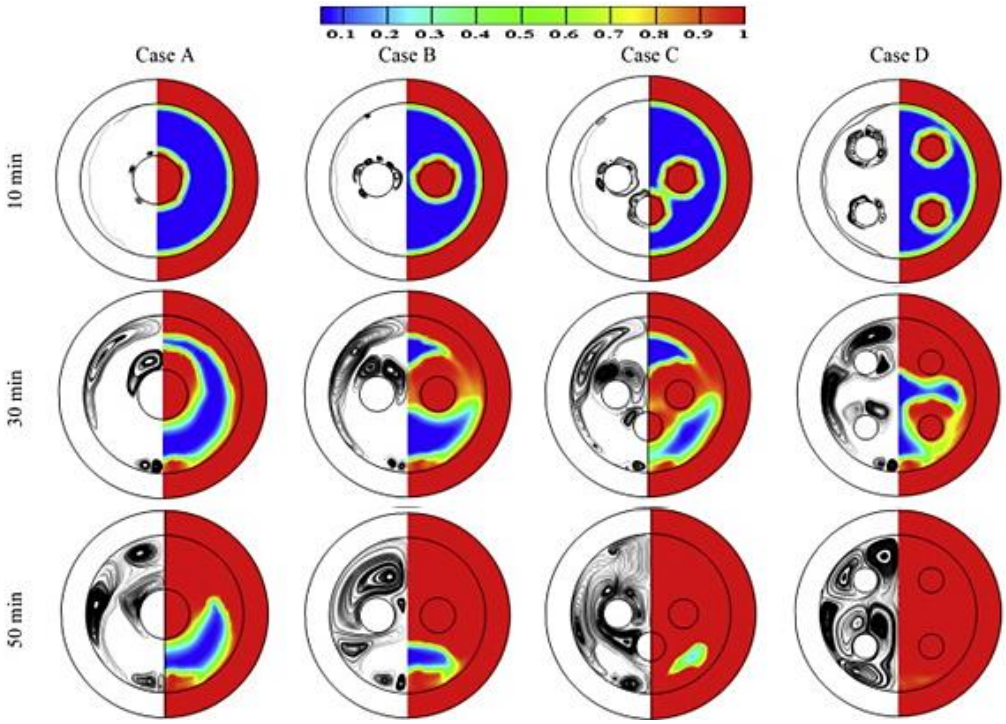

Fig. 2. 8 Transient liquid fractions for various shell and multi-tubes orientations (Esapour, M. et al. 2016).

2.1.3.2 Inclusion of extended surfaces

The inclusion of extended surfaces are practiced for countering the low thermal conductivity of PCM by improving the effective surface area for heat transfer. The geometrical configuration and orientation of extended surfaces play an essential role in

improving phase transition rate, accumulative thermal energy/discharge rate and mean charge/discharge power. Due to natural convection dominated melting process, the extended surfaces geometry, number and orientation in container are critical for optimum enhancement in thermal performance of LHS system.

The effect of extended surfaces number, height and thickness on overall thermal performance of LHS system were numerically simulated and analysed by (Shatikian, V. et al. 2005; Tao, Y. and He, Y. 2015; Ren, Q. and Chan, C. L. 2016; Wang, P. et al. 2016). It was observed that with an increase in number of fins, their length and thickness, the phase transition rate was amplified due to improved heat transfer rate and thermal distribution across the container. However, the excessive addition of fins would obstruct the liquid phase movement, which would disrupt the natural convection and consequently the enhancement in phase transition rate and temperature distribution would be affected. Therefore, the small number of lengthy fins were recommended over large number of smaller fins. Similarly, the thicker fins had presented uniform temperature along the height of fins whereas, the thinner fins had experienced temperature gradient. Uniform temperature provision is desirable for higher phase transition rate however, the thermal storage capacity would be compromised with an increase in fins thickness. Therefore, an optimum number of fins, their length and thickness should be identified for particular container orientation to gain most appropriate enhancement in thermal performance.

Influence of longitudinal fins on phase transition rate in concentric tube configuration was simulated by (Li, Z. and Wu, Z.-G. 2015). It was noticed that the melting and solidification rate were improved by a fraction of 14% as compared to without fins orientation. Likewise, (Darzi, A. A. R. et al. 2016) reported an enhancement of 39%, 73%, 78% and 82% in melting rate and 28%, 62%, 75% and 85% in solidification rate with an inclusion of 4, 10, 15 and 20 longitudinal fins as compared to without fins case. It was observed that due to conduction dominant solidification process, the impact of inclusion of extended surfaces were more pronounced as compared to melting process. Similarly, (Yuan, Y. et al. 2016) numerically investigated the influence of longitudinal fins angles on phase transition rate in concentric tube based LHS system. It was informed that longitudinal fins angle significantly influenced the melting process. Two longitudinal fins were installed at four angles of 0^o, 30^o, 45^o and 90^o, and it was informed that the melting rate for longitudinal fins with 0^o angle was relatively higher.

Therefore, the number and orientation of extended surfaces in container are critical for an appropriate thermal performance enhancement.

Beside longitudinal fins, the various designs of extended surfaces for thermal performance enhancement include rectangular, radial, pinned, helical and triplex fins. Various comparative studies were conducted by (Agyenim, F. et al. 2009; Caron-Soupart, A. et al. 2016; Lohrasbi, S. et al. 2017) to determine the most suitable design solution for extended surfaces which is capable of producing relatively higher phase transition rate, mean charge/discharge power, accumulative thermal energy storage/discharge with easier and rapid manufacturing and integration into container. It was reported that longitudinal fins based LHS systems had established relatively higher thermal performance and provided an easier integration to shell and tube or other container orientations.

2.1.3.3 Addition of thermal conductive additives

The low thermal conductivity of PCM can be overcome by addition of thermal conductive additives to achieve improved thermal storage and discharge performance. The various types of thermal conductive additives include metal matrices and structures, metal nano-particles, metal-oxides nano-particles, metal-nitrides nano-particles, carbon fibres and graphite.

(Velraj, R. et al. 1999) conducted a comparative analysis on thermal performance enhancement with inclusion of longitudinal fins and lessing rings techniques in a cylindrical LHS system. It was observed that the total solidification time for longitudinal fins and lessing rings were $1/4^{th}$ and $1/9^{th}$ of the solidification time for plain cylindrical LHS system, respectively. However, it was also noticed that the inclusion of longitudinal fins and lessing rings had compromised the overall thermal storage capacity by 7% and 20%, respectively. Therefore, an optimum concentration of lessing rings should be identified to achieve a required phase transition rate and thermal storage capacity. Similarly, (Mesalhy, O. et al. 2005; Du, Y. and Ding, Y. 2016) suggested that metal matrix and metal foam with higher thermal conductivity and optimum porosity should be employed to achieve required improvement in phase transition rate.

Due to higher thermal conductivity (24 – 270 W/m. K) and excellent absorbability of graphite, an extensive research is reported in literature that investigates the thermal performance enhancement of LHS systems with inclusion of graphite. (Haillot, D. et al.

2008) informed that the effective thermal conductivity for graphite composites were ranged from 5 – 50 W/m. K as compared to pure PCM range of 0.2 – 1 W/m. K. Despite the significant enhancement in thermal conductivity, it was informed that the thermal storage capacity was significantly reduced with inclusion of graphite (Sarı, A. and Karaipekli, A. 2007; Duan, Z.-j. et al. 2014). The porosity of graphite is essential parameter for effectiveness of enhanced overall thermal performance. The smaller mean pore size of graphite can complicate the impregnation of PCM and can obstruct the molecular moment which could decrease the latent portion of thermal energy capacity. Conversely, an increase in mean pore size can cause leakage issues due to reduced capillary forces. Moreover, the chemical and mechanical procedures for preparation of graphite composites are time and energy consuming. Therefore, a relatively simpler technique of dispersion of nano-particles is preferred.

(Mettawee, E.-B. S. and Assassa, G. M. 2007) conducted experimental tests to investigate the enhancement in thermal performance of paraffin wax with incorporation of various mass fractions of aluminium nano-particles. It was reported that the charging and discharging rate was significantly improved with an increase mass fraction of aluminium nano-particles. Likewise, (Zeng, J. et al. 2006) reported a significant enhancement with inclusion of silver nano-particles to 1-tetradecanol. However, it was informed that the increase in mass fraction of metal nano-particles had adverse effect on latent heat capacity of LHS system. Overall thermal storage capacity was reduced from 234.2 kJ/kg for pure 1-tetradecanol to 119.4 kJ/kg for composite with 0.5 mass fraction.

To achieve desirable thermal conductivity and thermal storage capacity, the inclusion of metal oxides or nitrides provide a feasible and relatively cost effective enhancement technique. (Harikrishnan, S. et al. 2014) conducted experimental examinations on the influence of TiO_2, ZnO and CuO nano-particles addition to lauric acid and stearic acid mixture base material. It was reported that with addition of 1 wt% of nano-additives, the thermal conductivity was improved by 34.85%, 46.97% and 62.12%, respectively. Likewise, (Venkitaraj, K. et al. 2017) studied the impact of varying mass fraction of aluminium oxide on thermal performance enhancement of LHS system. It was informed that with an increase in mass fraction from 0.1% – 1%, the overall thermal conductivity of composites were increased from 18.11% – 51.79% as compared to pure PCM. Similarly, (Wang, W. et al. 2009) noticed an enhancement in thermal conductivity from 0.3847 W/m. K – 0.7661 W/m. K with an increase in concentration of aluminium

nitride nano-particles from 5% – 30%, respectively. It was also reported that an increase in nano-particles concentration had minimal impact on phase transition temperature. Furthermore, (Awad, A. et al. 2018) reported an improvement in effective thermal conductivity of potassium nitrate salt (KNO_3) with inclusion of Fe_2O_3 and CuO nano-additives. In case of 0.5 wt%, the thermal conductivity was increased from 0.359 W/m. K to 0.524 and 0.536 W/m. K, respectively.

It was concluded from literature review that the thermal conductivity of base materials could be significantly enhanced by incorporating thermal conductive additives. However, the latent heat capacity would be compromised with inclusion of excessive quantity of additives. Also, the excessive inclusion of additives could significantly augment the dynamic viscosity which could adversely affect the impact of natural convection on melting process. Therefore, an optimum quantity of nano-particle additives should be identified for an appropriate thermal performance enhancement of LHS system.

2.2 Limitations and gaps in literature

Detailed literature review of LHS systems identified the following limitations and gaps in terms of geometrical orientation of container along with extended surfaces and nano-additives enhanced thermal storage materials:

1. The literature review identified that shell and tube heat exchanger based LHS systems have relatively better thermal storage performance and provision of easier integration into practical applications. However, there is a lack of literature on vertical shell and tube configurations with multiple tube passes for higher thermal storage capacity. Similarly, the inclusion of longitudinal fins for thermal performance enhancement had presented a relatively higher thermal performance, however the vertical configuration of longitudinal fins in shell and tube heat exchanger with multiple tube passes have not been reported in previous literature. Therefore, there is a need for numerical and experimental examinations of novel vertical shell and tube heat exchanger with optimum multiple tube passes and optimum geometrical dimensions, construction material and orientation of longitudinal fins in the shell container to produce high thermo-physical stability and enhanced thermal performance of LHS system.

2. It can be concluded from literature review that the inclusion of metal oxides, metal nitrides and carbon allotropes nano-additives in base material can significantly enhance thermal conductivity and charging/discharging rate on the expense of thermal storage capacity. However, there is lack of literature on experimental examinations of aluminium oxide (Al_2O_3), aluminium nitride (AlN) and graphene nano-platelets (GNP) based paraffin composites with varied mass fractions in an actual shell and tube heat exchanger based LHS system. Likewise, the literature review identified that the previously implemented numerical models for estimation of effective thermal conductivity and dynamic viscosity of nano-additives enhanced composites are inaccurate because those models were developed for smaller concentration and large particles. Therefore, there is a need to conduct experimental and numerical examinations to draw a comparison metal oxide, metal nitride and carbon allotrope based paraffin composites in an actual shell and tube orientation based LHS system. Also, there is a need to implement a numerical model that is capable of accurate prediction of effective thermal conductivity and dynamic viscosity of paraffin composites by considering the influence of nano-additives material, their particle size, volume concentration and operating temperature.
3. Finally, there is a lack of research on coupling two thermal performance enhancement techniques, such as inclusion of longitudinal fins and incorporation of nano-additives, which would establish a LHS system with significantly higher charging/discharging rate, accumulative thermal energy storage/discharge and mean charge/discharge power and consequently enable large-scale practical utilisation.

2.3 Selections and conclusions

Based on literature review of various types of thermal storage materials, their compatibility with heat exchanger and container materials and thermal performance enhancement techniques, the following selections and conclusions are made considering the limitations in literature:

1. The comparison among various types of PCMs with respect to temperature range for materials availability, latent heat capacity, thermal conductivity, advantages and shortcomings with methods for improvement, it was established that paraffins and salt hydrates are relatively advantageous and desirable thermal storage

mediums. However, the requirement of nucleating agents, thickeners and excess water content to reduce the phase segregation and subcooling problems along with corrosive nature can increase the complexity and deterioration of thermo-physical performance of salt hydrates based LHS systems. Therefore, paraffins were selected as thermal storage materials due to their excellent thermo-physical stability and good compatibility with metal containers for developing a durable and reliable LHS system. Commercial grade paraffins ranging from 0 ^{o}C – 90 ^{o}C are available from (Anon. 2017). In this thesis, the numerical and experimental investigations were conducted on paraffin (RT44HC) with phase transition temperature of 44 ^{o}C. Based on practical application, paraffin with different phase transition temperature could be selected and employed in the proposed LHS system.

2. Due to excellent compatibility of paraffins with metal containers, the usual construction materials for heat exchanger such as copper, aluminium, nickel, tin, cast iron and steel was selected to be numerically investigated for their impact on thermo-physical performance of LHS system. Copper and aluminium were preferred due to their higher thermal conductivity which would be essential for higher thermal performance of LHS systems.
3. In case of effective heat exchanging mechanism, vertical shell and tube heat exchanger based LHS system were selected due to their comparatively higher thermal performance, easier integration into numerous practical applications and minimal thermal losses. Likewise, longitudinal fins were selected as extended surfaces due to their simpler geometry and insignificant obstructions towards natural convection or liquid moment, excellent temperature distribution in container and minimal reduction in thermal storage capacity. Moreover, metal oxides (Al_2O_3), metal nitrides (AlN) and carbon allotropes (GNP) were selected as nano-additives to be incorporated in base paraffin for thermal performance enhancement due to their relatively higher thermal conductivity performance and lower reduction in thermal storage capacity of LHS systems. Therefore, this thesis would be focused on numerical and experimental investigations of novel LHS system comprising of vertical shell and tube heat exchanger with longitudinal fins and nano-additives enhanced paraffin as thermal storage medium.

Chapter 3 Numerical methodology

This chapter provides a detailed discussion on the analytical and numerical methodology adopted for designing a novel LHS system with enhanced thermal performance. Based on knowledge acquired in chapter 2, SOLIDWORKS software was exercised to model various orientations of shell and tube heat exchanger with longitudinal fins based LHS system. ANSYS Fluent software was implemented for discretisation of governing equations to numerically simulate the melting and solidification processes on the proposed models for LHS system. Parametric investigations were conducted by simulating a transient numerical model to investigate the influence of various positioning and orientations of tubes and longitudinal fins in shell container, geometrical dimensions of longitudinal fins, materials for shell and tube heat exchanger and longitudinal fins and operating conditions on phase transition rate and overall thermal storage capacity of LHS system. Moreover, thermal performance enhancement due to incorporation of various nano-additives such as metal oxides, metal nitrides and carbon allotropes with varied volume concentrations, particle size and operating conditions were numerically simulated in ANSYS Fluent software. Based on numerical investigations, an optimum design solution with novel nano-PCM for LHS system were proposed. Therefore, this chapter will help in understanding the influence of various parameters on thermal performance of LHS system and will also explain the basic numerical simulation techniques that could be implemented for designing LHS system with optimum thermal storage performance. This chapter summarises the literature that has been published in the articles: "Parametric investigations to enhance thermal performance of paraffin through a novel geometrical configuration of shell and tube latent thermal storage system" by (Khan, Z. et al. 2016b) (refer to Appendix A – Paper II), "Development in paraffin based thermal storage system through shell and tubes heat exchanger with vertical fins" by (Khan, Z. and Khan, Z. A. 2017a) (refer to Appendix A – Paper III) and "Experimental and numerical investigations of nano-additives enhanced paraffin in a shell and tube heat exchanger: a comparative study" by (Khan, Z. and Khan, Z. A. 2018) (refer to Appendix A – Paper VI).

3.1 Mathematical models for LHS systems

3.1.1 Analytical models

3.1.1.1 Stefan problem approach for 1-dimensional semi-infinite layer

Prior to developing a numerical model for transient phase change or moving boundaries problems, an analytical approach known as *Stefan problem* was implemented on a simple 1-dimensional semi-infinite rectangular slab to acquire basic understanding of phase transition process and phase boundary movement. (Stefan, J. 1889) developed an analytical model for ice formation problem to predict the solid phase boundary movement with respect to time. The proposed analytical model was comprised of following assumptions:

1. This analytical model could only be implemented to a simple geometry as presented in **Fig. 3. 1**. The semi-infinite layer of rectangular slab could be melted/solidified by assigning constant heating/cooling temperature T_o to the left surface of the geometry extending towards right till infinity.
2. Variations in volume, density and thermal conductivity due to phase transition between solid and liquid was neglected.
3. Overall thermal storage capacity were comprised of sensible and latent portion of heat capacity. In Stephan problem, the sensible portion of heat capacity was neglected and thus, the latent portion of heat capacity was considered at phase transition temperature.
4. Natural convection was neglected and conduction was assumed as an only and dominant mode of heat transfer, which would result in linear temperature profiles during phase transition.
5. Paraffin material was assumed to be in initial solid/liquid phase during melting/solidification process and at a uniform phase transition temperature T_{pc}. Likewise, a constant heating/cooling temperature T_o was assigned to left surface of the geometry.

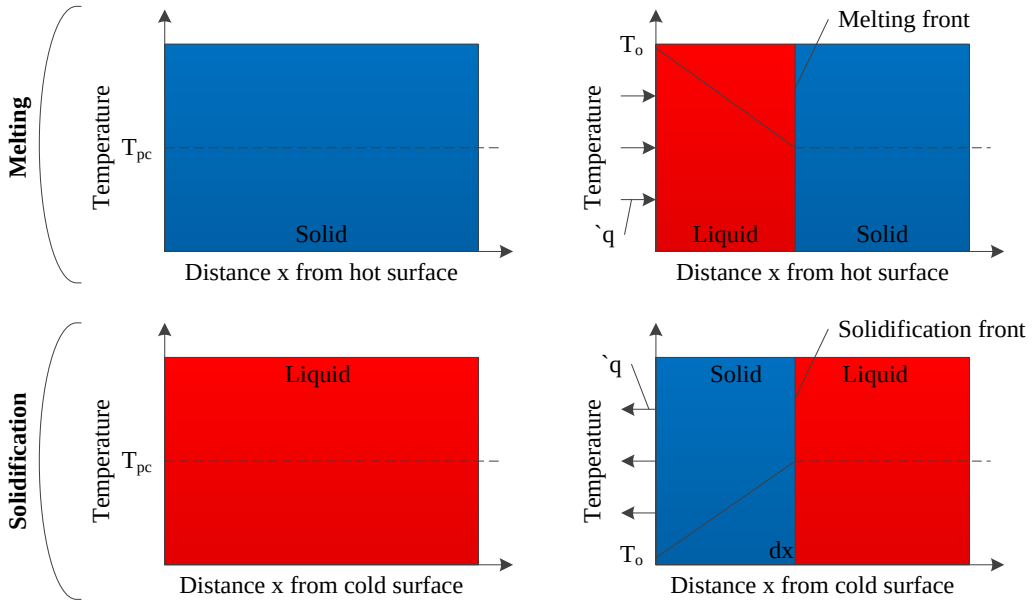

Fig. 3. 1 Melting and solidification process of a 1- dimensional semi-infinite layer of paraffin. Left side plots represent initial conditions and right side represent melting/solidification front movement conditions after time interval (t).

By neglecting sensible portion of thermal energy, the amount of heat transferred from the hot surface was completely stored as latent heat by melting the solid phase, as represented by melting front. Therefore, the heat flux density $\dot{q}$ at the hot surface was then given by (Hahn, D. W. and Ã–zisik, M. N. 2012):

$$\dot{q} = \rho L \frac{dx}{dt} \tag{3. 1}$$

where ρ, L, x and t represented density (kg/m^3), latent heat of fusion (kJ/kg) of paraffin, horizontal distance from hot/cold surface (m) and time (s), respectively. Likewise, due to neglecting natural convection and assuming that heat transfer was conduction dominant, the heat flux density from the surface to melting front, which was at distance x from hot surface, was estimated by Fourier law (Bergman, T. L. et al. 2011), as follow:

$$\dot{q} = k \frac{T_o - T_{pc}}{x} \tag{3. 2}$$

where k represented thermal conductivity (W/m. K) of paraffin. Equating Eq. (3. 1) and Eq. (3. 2), the following form could be derived:

$$k\frac{T_o - T_{pc}}{x} = \rho L\frac{dx}{dt} \tag{3. 3}$$

Re-arranging Eq. (3. 3) and integrating it for time interval $t = 0$ to $t = t$, as follow:

$$\int_{0}^{t} \frac{k\left(T_o - T_{pc}\right)}{\rho L}.dt = \int_{x(0)}^{x(t)} x.dx \tag{3. 4}$$

$$\frac{k\left(T_o - T_{pc}\right)}{\rho L}.t = \frac{1}{2}x_{(t)}^2 \tag{3. 5}$$

In order to equate the time required for melting front to move a distance $x_{(t)}$ away from hot surface, Eq. (3. 5) was rearranged as follow:

$$t = \frac{\rho L x_{(t)}^2}{2k\left(T_o - T_{pc}\right)} \tag{3. 6}$$

Likewise, to locate the distance $x_{(t)}$ covered by melting front away from hot surface after time interval *t*, Eq. (3. 5) could be rearranged as follow:

$$x_{(t)} = \sqrt{\frac{2k\left(T_o - T_{pc}\right)}{\rho L}.t} \tag{3. 7}$$

Moreover, Eq. (3. 2) and Eq. (3. 7) were simplified to calculate heat flux density as a function of time *t*, as follow:

$$q_{(t)} = \sqrt{\frac{k\rho L\left(T_o - T_{pc}\right)}{2.t}} \tag{3. 8}$$

As illustrated in Eq. (3. 7) and Eq. (3. 8), parameters such as thermal conductivity *k*, density ρ, latent heat capacity *L*, phase transition temperature T_{pc}, inlet temperature of hot surface T_o and time *t* significantly influence the melting front movement or melting rate and heat flux density. These equations were produced for melting process, in solidification process the temperature gradient could be changed from $(T_o - T_{pc})$ to $(T_{pc} - T_o)$.

3.1.1.2 Energy balance method

Energy balance method was implemented to design an analytical model to calculate the inlet/outlet temperature of HTF, heat transfer coefficient, charging and discharging rates of selected thermal capacity of paraffin in a shell and tube heat exchanger based LHS system. Impact of operating temperature and mass flow rates on charging and discharging rate could be calculated using this analytical model. In order to simplify the complex geometrical configuration of shell and tube heat exchanger with multi-tube passes, each tube pass was assumed as a concentric tube and the length of concentric tubes was equivalent to the running length of multi-tube passes, as shown in **Fig. 3. 2**.

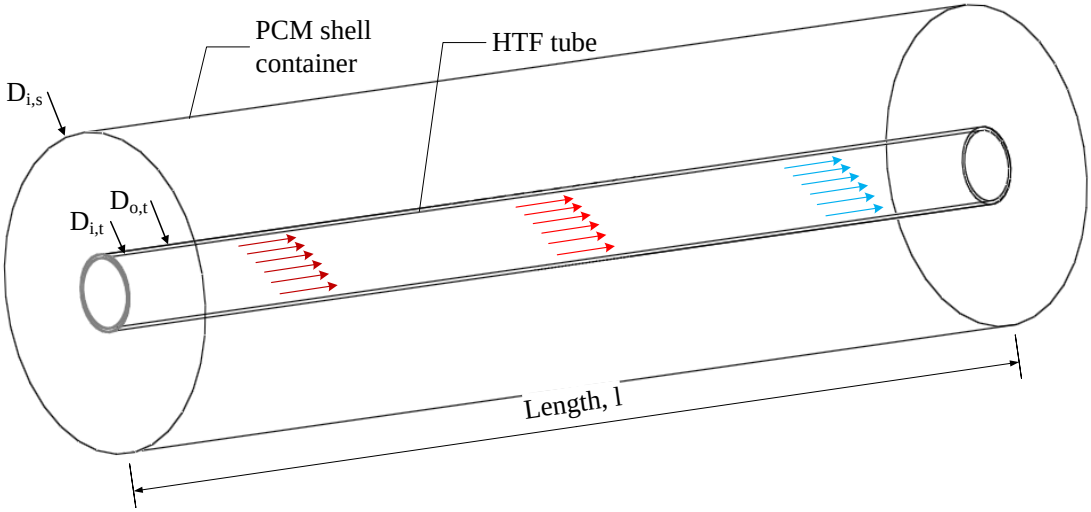

Fig. 3. 2 Geometrical representation of single tube in shell configuration

The analytical model was based on the following essential assumptions:

1. Steady state conditions and fully developed flow for HTF were assumed.
2. Phase transition temperature for paraffin was assumed as constant and subcooling was neglected. Moreover, the variations in volume, density and thermal conductivity due to phase transition between solid and liquid were neglected.
3. Due to relatively higher thermal conductivity of HTF tube wall, the conduction resistance in tube was neglected and the convection resistance in liquid paraffin was ignored as well.
4. Sensible heat storage was ignored due to its minimal heat storage capacity as compared to latent portion of heat storage. Likewise, constant inlet temperature of HTF and perfect adiabatic conditions were applied to outer surface of shell.

Energy balance approach was employed considering the adiabatic outer surface of shell and negligible thermal resistance and therefore, the total thermal energy released by high temperature HTF was completely arrested by paraffin in shell container. Therefore, the total heat transfer rate q was calculated as follow (Bergman, T. L. et al. 2011):

$$q = mC_p\left(T_{m,o} - T_{m,i}\right) = mC_p dT_m \tag{3. 9}$$

$$q = hA_s\left(T_{pc} - T_m\right) = h(\pi D_{i,t} dx)(\Delta T) \tag{3. 10}$$

where $m, C_p, h, A_s, D_{i,t}, T_m$ and T_{pc} represented mass flow rate of HTF (kg/s), specific heat capacity of HTF (kJ/kg. K), heat transfer coefficient (W/m^2. K), surface area of tube (m^2), inner diameter of tube (m), mean temperature of HTF in tube (^{o}C) and phase transition temperature of paraffin (^{o}C), respectively. Similarly, $dT_m = \left(T_{m,o} - T_{m,i}\right)$ and $\Delta T = T_{pc} - T_m$. Hence, the following equation was produced by rearranging Eq. (3. 9) and Eq. (3. 10):

$$\frac{dT_m}{dx} = -\frac{d(\Delta T)}{dx} = \frac{\pi D_{i,t} h}{mC_p}\Delta T \tag{3. 11}$$

Subsequently, Eq. (3. 11) was rearranged to integrate for entire length l of shell and tube, as follow:

$$\int_{\Delta T_i}^{\Delta T_o} \frac{d(\Delta T)}{\Delta T} = -\frac{\pi D_{i,t}}{mC_p}\int_0^l h.dx \tag{3. 12}$$

$$\int_{\Delta T_i}^{\Delta T_o} \frac{d(\Delta T)}{\Delta T} = -\frac{\pi D_{i,t} l}{mC_p}\left(\frac{1}{l}\int_0^l h.dx\right) \tag{3. 13}$$

$$\mathrm{In}\frac{\Delta T_o}{\Delta T_i} = -\frac{\pi D_{i,t} l}{mC_p}\bar{h} \tag{3. 14}$$

In Eq. (3. 14), $\bar{h}$ represented average heat transfer coefficient, $\Delta T_o = T_{pc} - T_{m,o}$ and $\Delta T_i = T_{pc} - T_{m,i}$. Therefore, Eq. (3. 14) can be rearranged as follow:

$$\frac{T_{pc} - T_{m,o}}{T_{pc} - T_{m,i}} = \exp\left(-\frac{\pi D_{i,t} l}{mC_p}\bar{h}\right) \tag{3. 15}$$

The outlet temperature $T_{m,o}$ was calculated from Eq. (3. 15) for known values of geometrical parameters, thermo-physical properties and inlet temperature of HTF. Likewise, the average heat transfer coefficient $\bar{h}$ was evaluated by simply employing dimensionless numbers such as Reynolds number, Prandtl number and Nusselt number. Reynolds number Re was operated to evaluate the nature of HTF flow, whether laminar or turbulent, and was calculated using the following equation:

$$\mathrm{Re} = \frac{\text{inertial forces}}{\text{viscous forces}} = \frac{\rho u_m D_{i,t}}{\mu} = \frac{4m}{\pi D_{i,t}\mu} \tag{3. 16}$$

where u_m and μ represented fluid velocity in tube (m/s) and dynamic viscosity of HTF (kg/m· s). Similarly, Prandtl number Pr, the ratio of viscous diffusion rate to thermal diffusion rate, was calculated as follow:

$$\mathrm{Pr} = \frac{\mu/\rho}{k/C_p\rho} = \frac{C_p\mu}{k} \tag{3. 17}$$

Similarly, the non-dimensional Nusselt number Nu is the ratio of convection heat transfer to conductive heat transfer. Nusselt number for turbulent and fully developed flow was calculated by implementing Dittus-Boelter equation (Bergman, T. L. et al. 2011), as follow:

$$Nu = \frac{hD_{i,t}}{k} = 0.023\,\mathrm{Re}^{4/5}\,\mathrm{Pr}^{n} \tag{3. 18}$$

Eq. (3. 18) was implemented to estimate the average heat transfer coefficient $\bar{h}$ and consequently, outlet temperature $T_{m,o}$ was calculated from Eq. (3. 15). Likewise, the total thermal energy storage by paraffin was estimated by assigning calculated values in Eq. (3. 9). Moreover, the overall charging or discharging time t_m for paraffin in shell and tube heat exchanger configuration was estimated by following relation:

$$t_m = \frac{mL}{q} = \frac{\rho l}{q}\left(\frac{\pi(D_{i,s}^2 - D_{o,t}^2)}{4}\right)L \tag{3. 19}$$

where $D_{i,s}$ and $D_{o,t}$ represented the inner diameter of shell (m) and outer diameter of HTF tube (m), respectively.

3.1.2 Numerical models

3.1.2.1 Mathematical formulation for pure paraffin

Numerical model was developed based on governing equations to simulate transient charging and discharging cycles of LHS system. In order to bring simplicity to transient numerical model and shorten the computation time, the following assuming were made:

1. Due to higher thermal conductivity of metal tubes as compared to paraffin, the thickness and conduction resistance in HTF tubes were neglected. Likewise, outer boundary of the shell was assumed to be under perfect adiabatic conditions.
2. Volumetric expansion of paraffin during phase transition was neglected and the nature of natural convection was assumed as laminar.
3. Uniform initial temperature was assigned to entire computational domain of paraffin and constant boundary temperature was assigned to HTF tubes to transfer thermal energy between HTF in tubes and paraffin in shell.

The governing equations computed for investigating the phase transition rate and overall thermal capacity of LHS system during charging and discharging cycles included continuity, momentum and energy conservation equations, as described:

Continuity conservation equation:

$$\frac{\partial \rho}{\partial t} + \nabla.(\rho \mathbf{u}) = 0 \tag{3. 20}$$

Momentum conservation equation:

$$\rho \frac{\partial \mathbf{u}}{\partial t} + \rho(\mathbf{u}.\nabla)\mathbf{u} = -\nabla p + \mu \Delta \mathbf{u} + \mathbf{F} + S\mathbf{u} \tag{3. 21}$$

Energy conservation equation:

$$\rho \frac{\partial (C_p T)}{\partial t} + \rho \nabla.(C_p T \mathbf{u}) = k \Delta T + q \tag{3. 22}$$

where ρ and $\mathbf{u}$ in Eq. (3. 20) represented density (kg/m^3) and velocity vector (m/s), and p, μ, $\mathbf{F}$ and $S\boldsymbol{u}$ in Eq. (3. 21) represented pressure (Pa), dynamic viscosity (kg/m.s), buoyant volume force (Pa/m) and momentum source term and $C_{p,}\, T, k$ and q in Eq. (3.

22) represented specific heat at constant pressure (kJ/kg.K), temperature (^oC), thermal conductivity (W/m.K) and heat source term (W/m^3), respectively.

Buoyant volume force term **F** in Eq. (3. 21) was responsible for buoyancy driven upward rise of high temperature paraffin molecules and resulting in dominant natural convection heat transfer. Therefore, the natural convection influence on phase transition rate was controlled by Boussinesq approximation term (Gray, D. D. and Giorgini, A. 1976) for buoyant volume force, as follow:

$$F = \rho \mathbf{g} \beta (T - T_{ref}) \tag{3. 23}$$

where **g**, β and T_{ref} showed gravitational acceleration (m/s^2), coefficient of thermal expansion (1/K) and reference phase transition temperature (^oC), respectively. Likewise, enthalpy-porosity technique (Voller, V. R. and Prakash, C. 1987) was implemented for identification of liquid fraction during phase transition process. The computational domain of paraffin was considered as porous medium and the porosity in each mesh element was compared as equivalent to liquid fraction. For instance, at fully solidified state, the porosity was equal to zero and consequently, the liquid fraction in computational domain was zero as well. The momentum source term $\boldsymbol{Su}$ in Eq. (3. 21) was regulating the porosity in computational domain of paraffin and was calculated by implementing Kozeny-Carman equation (Nield, D. A. and Bejan, A. 2006), as follow:

$$S\mathbf{u} = \frac{\kappa(1-f)^2}{(\alpha + f^3)}\mathbf{u} \tag{3. 24}$$

where κ, α and f represented the morphology constant for mushy zone which range from 10^4 – 10^9, small constant value such as 10^{-4} to circumvent division by zero and liquid fraction of paraffin during phase transition, respectively. The phase transition phenomena occurred during temperature interval of $T_s \le T \le T_l$ and therefore, the liquid fraction term f was estimated using the following relations:

$$f = \begin{cases} 0 & T < T_s \\ \dfrac{T - T_s}{T_l - T_s} & T_s \le T \le T_l \\ 1 & T > T_l \end{cases} \tag{3. 25}$$

where T_s and T_l represented temperature of paraffin during solid phase and liquid phase, respectively. Temperature interval for phase transition process, represented by ΔT_{pc}, was noticed as influencing parameter in identifying the phase transition rate. For higher ΔT_{pc} value, the phase transition rate was underestimated and therefore, a longer phase transition time was noticed, likewise for lower ΔT_{pc} value, the phase transition rate was slightly overestimated and thus, a shorter phase transition time was recorded. Moreover, the effective specific enthalpy was calculated from the combined specific enthalpies of paraffin in solid and liquid phase. Likewise, the effective specific heat capacity was derived from differentiation of effective specific enthalpy with respect to temperature, as follow:

$$\rho H = \rho C_p T = f_s \rho_s H_s + f_l \rho_l H_l \tag{3. 26}$$

$$C_p = \frac{\partial}{\partial T}\left[\frac{f_s \rho_s H_s + f_l \rho_l H_l}{\rho}\right] \tag{3. 27}$$

$$C_p = \frac{1}{\rho}\left(f_s \rho_s C_{p,s} + f_l \rho_l C_{p,l}\right) + (H_l - H_s)\frac{\partial}{\partial T}\left[\frac{\left(f_l \rho_l - f_s \rho_s\right)}{2\rho}\right] \tag{3. 28}$$

Likewise, the difference between specific enthalpy of paraffin at liquid and solid phase in Eq. (3. 28) was equivalent to latent heat capacity of paraffin: $L = (H_l - H_s)$.

3.1.2.2 Mathematical formulation for nano-PCM

By incorporating nano-additives into base paraffin, the thermal performance of LHS system could be enhanced. To investigate the influence of nano-additives material, particle size and volumetric concentration on thermo-physical performance of nano-PCM based LHS system, a numerical model was developed based on governing equations and theoretical relations for mixture of two components. The governing equations employed for nano-PCM were the same continuity, momentum and energy conservation equations as discussed in above section for pure paraffin (refer to Appendix A – Paper VI). However, the thermo-physical properties of pure paraffin was altered by inclusion of nano-additives and were estimated from mixture of two component relations, as follow:

$$\rho_{npcm} = \delta_{VF}\rho_{np} + \left(1 - \delta_{VF}\right)\rho_{pcm} \tag{3. 29}$$

$$C_{p,npcm} = \frac{\delta_{VF}\rho_{np}C_{p,np} + (1-\delta_{VF})\rho_{pcm}C_{p,pcm}}{\rho_{npcm}} \quad (3.30)$$

$$L_{npcm} = \frac{(1-\delta_{VF})\rho_{pcm}L_{pcm}}{\rho_{npcm}} \quad (3.31)$$

where the indices np, pcm and $npcm$ represented nano-additive particle, paraffin as base PCM and nano-additives enhanced PCM or nano-PCM, respectively. Likewise, δ_{VF} showed the volume concentration or volume fraction of nano-additives in base PCM.

Moreover, the effective thermal conductivity and dynamic viscosity of nano-PCM were computed by implementing semi-empirical models proposed by (Corcione, M. 2011). Corcione proposed semi-empirical models were accounting for nano-additives particle size, volume concentration and operating temperature of composite nano-PCM. The previous standard models and theories proposed by (Maxwell, J. C. 1881) and (Bruggeman, V. D. 1935; Hamilton, R. and Crosser, O. 1962; Xuan, Y. et al. 2003) for valuation of effective thermal conductivity of nano-additives enhanced nano-PCM and models proposed by (Einstein, A. 1906) and (De Bruijn, H. 1942; Brinkman, H. 1952; Krieger, I. M. and Dougherty, T. J. 1959; Batchelor, G. 1977) for estimation of dynamic viscosity of nano-PCM, failed to accurately predict enhancement in thermal conductivity and dynamic viscosity with inclusion of nano-additives due to the reason that these proposed standard models were developed for larger particle size and smaller volumetric concentration of nano-additives and were not considering the influence of operating temperature. The effective thermal conductivity were estimated by implementing (Corcione, M. 2011) semi-empirical model, as follow:

$$k_{npcm} = k_{pcm}\left(1 + 4.4\,\mathrm{Re}^{0.4}\,\mathrm{Pr}^{0.66}\left(\frac{T_{npcm}}{T_{pc}}\right)^{10}\left(\frac{k_{np}}{k_{pcm}}\right)^{0.03}\delta_{VF}{}^{0.66}\right) \quad (3.32)$$

where Re and Pr represented the non-dimensional Reynolds number of nano-additives enhanced nano-PCM and non-dimensional Prandtl number of pure paraffin, respectively. The respective Reynolds number and Prandtl number were estimated using the following equations:

$$\mathrm{Re} = \frac{2\rho_{pcm} k_B T_{npcm}}{\pi \mu_{pcm}^2 d_{np}} \tag{3. 33}$$

$$\mathrm{Pr} = \frac{\mu_{pcm} C_{p,pcm}}{k_{pcm}} \tag{3. 34}$$

where k_B and d_{np} represented the Boltzmann constant (1.38 x 10^{-23} J/K) and diameter of nano-additive particle (m), respectively. Similarly, (Corcione, M. 2011) semi-empirical model was implemented for computing dynamic viscosity of nano-PCM, as follow:

$$\mu_{npcm} = \frac{\mu_{pcm}}{1 - 34.87 (d_{np}/d_{pcm})^{-0.3} \delta_{VF}^{1.03}} \tag{3. 35}$$

where μ_{pcm} and d_{pcm} represented the dynamic viscosity of pure paraffin as a function of temperature and equivalent diameter of pure paraffin, respectively. The dynamic viscosity of paraffin as a function of temperature was calculated using following relation (Kandasamy, R. et al. 2008):

$$\mu_{pcm} = 0.001 \exp\left(-4.25 + \frac{1790}{T_{pcm}}\right) \tag{3. 36}$$

Also, the equivalent diameter of pure paraffin was calculated as follow:

$$d_{pcm} = 0.1 \left(\frac{6 M_W}{\pi N_A \rho_{pcm,o}}\right)^{1/3} \tag{3. 37}$$

where N_A, M_W and $\rho_{pcm,o}$ represented the Avogadro number, molecular weight of paraffin and density of paraffin at $T_{pcm} = 20$ ℃, respectively.

3.2 Numerical simulations for LHS systems

The physical models, boundary conditions and computational procedure selected for numerical simulations of charging and discharging cycles of LHS system will be discussed in this section.

3.2.1 Physical models

As discussed earlier in section 2.3, thermal performance enhancement techniques selected in this thesis included geometrical configuration of shell and tube heat exchanger with extended surfaces based enhancement and nano-additives enhanced

paraffin. Therefore, two physical models were developed for investigating novel design solution for optimum thermal performance of LHS systems. First model was centred on investigations of novel design solution of LHS systems based on geometrical orientations of shell and tube heat exchanger with multiple passes and longitudinal fins and second model was based on examinations of optimum thermal enhancement with inclusion of nano-additives to base paraffin.

3.2.1.1 Physical model I – Geometrical configuration and extended surfaces

Geometrical configuration of heat exchanger to transfer thermal energy between paraffin and HTF has pronounced impact on overall thermal performance of LHS system. Therefore, in order to design a novel geometrical configured shell and tube heat exchanger with longitudinal fins enhancement for efficient and responsive thermal performance and easier integration to flat plate solar thermal system, several geometrical orientations were simulated, as presented in **Fig. 3. 3**. Initially, trial and error method was exercised to simulate various geometrical orientations of shell and tube heat exchanger with various number of tube passes, their orientation in shell container, longitudinal fins dimensions and their construction material to generate an optimum geometrical design solution with capability of rapid charging in less than 10 hours and with least reduction to overall thermal storage capacity of LHS system. As a result, a physical model based on novel geometrical orientation of shell and tube heat exchanger with longitudinal fins were developed, as presented in **Fig. 3. 4**. Parametric investigations were conducted for further enhancements in geometrical design configuration.

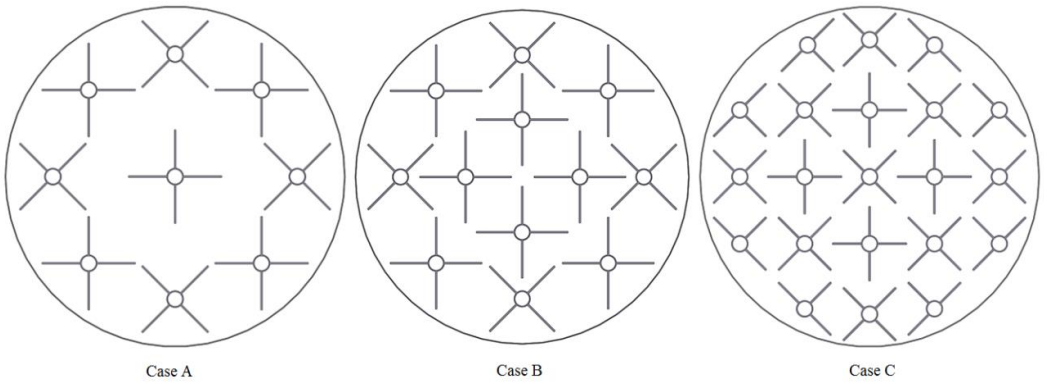

Fig. 3. 3 Various geometrical design configurations of shell and tube heat exchanger with longitudinal fins (Khan, Z. et al. 2016b)

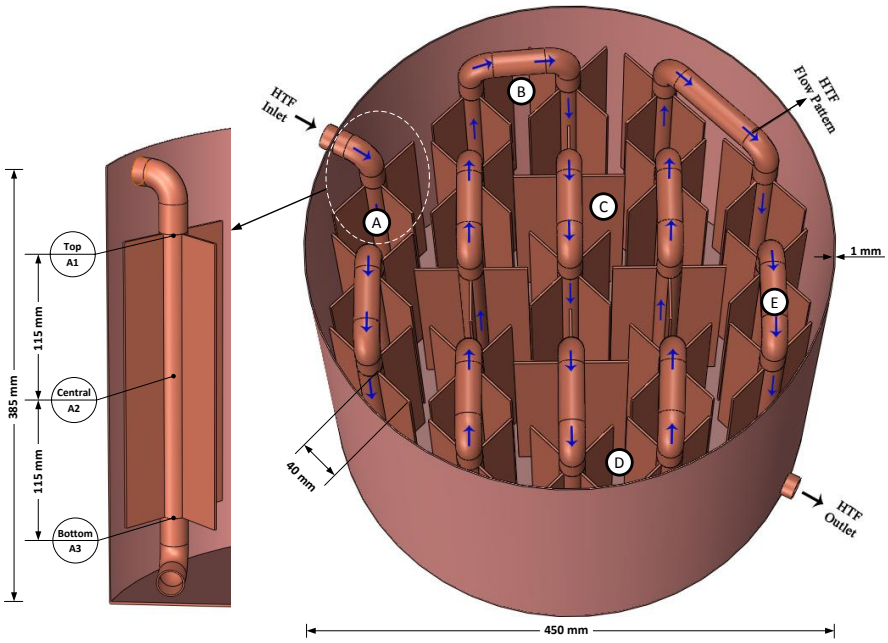

Fig. 3. 4 Physical model I - Proposed novel design of shell and tube heat exchanger with longitudinal fins based LHS system (Khan, Z. and Khan, Z. A. 2017a)

Paraffin (RT44HC) was selected as thermal storage material that would be filled in shell container and water was chosen as HTF that would flow in tubes of heat exchanger to provide/extract thermal energy during charging/discharging cycles, respectively. Thermo-physical properties of commercial grade paraffin (RT44HC) are listed in **Table. 3. 1**.

Table 3. 1 Thermal and physical properties of commercial grade paraffin (RT44HC) and nano-additives (Anon. 2017; Khan, Z. and Khan, Z. A. 2018)

Properties	**Base material**	**Nano-additives**		
	Paraffin	Al_2O_3	AlN	GnP
Density (kg/m^3)	800 (solid) 700 (liquid)	3500	3300	400
Thermal conductivity (W/m.K)	0.2 (solid) 0.2 (liquid)	36	180	3000
Specific heat capacity (kJ/kg. K)	2.0	0.765	0.74	0.643
Latent heat of fusion (kJ/kg)	255	-	-	-
Phase change temperature (^{o}C)	42-44	-	-	-

3.2.1.2 Physical model II – Inclusion of nano-additives to base paraffin

To reduce computational and experimental cost, a relatively smaller shell and tube heat exchanger was selected to investigate the thermal performance enhancement by inclusion of nano-additives to base paraffin, as presented in **Fig. 3. 5**. The shell and

tubes of heat exchanger were made of acrylic plastic and stainless steel, respectively. The outer diameter, thickness and length of shell container were 60 mm, 5 mm and 185 mm, respectively. Likewise, the outer diameter and thickness of seven stainless steel tubes were 6 mm and 1 mm, respectively. Nano-PCM samples were filled in shell container, whereas water was directed to flow in the tubes to transfer heat, as illustrated in **Fig. 3. 5**. Moreover, the thermo-physical properties of selected nano-additives are listed in **Table 3. 1**.

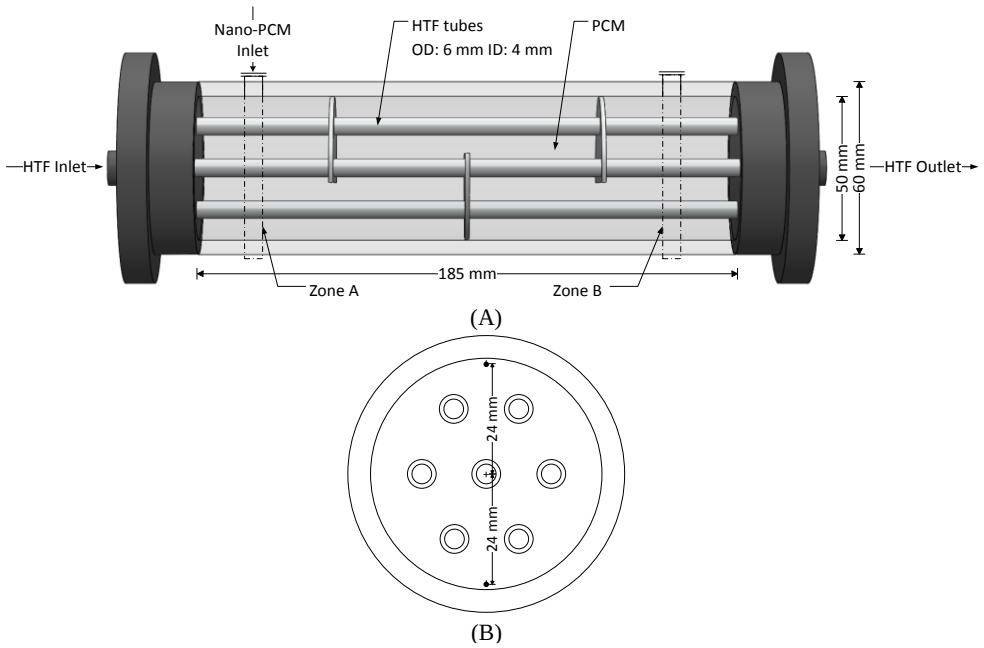

Fig. 3. 5 Physical model II - Shell and tube heat exchanger for nano-additives enhanced nano-PCM (Khan, Z. and Khan, Z. A. 2018)

3.2.2 Initial and boundary conditions

During charging cycles for both physical models, the entire mass of paraffin was assumed to be in complete solid state at initial temperature of 15 ^{o}C. As shown in **Table 3. 1**, the phase transition temperature of paraffin is 44 ^{o}C, therefore the initial temperature of 15 ^{o}C ensured the solid phase of paraffin. Moreover, the tubes were assigned various constant boundary temperatures, which had temperature gradient between PCM and HTF ranged from 10 ^{o}C – 25 ^{o}C. Similarly, the exterior boundary of shell was assumed to be under adiabatic condition.

During discharging cycles for both physical models, the entire computational domain of paraffin were assumed to be in completely liquid state at initial temperature higher than phase transition temperature. The selected initial temperature was 52 ^{o}C, which ensured complete liquid phase of paraffin. Similarly, the various constant boundary

temperatures for tubes were selected in the range of 5 ^{o}C – 20 ^{o}C, which could replicate the municipal cold water temperature.

3.2.3 Computational procedure and discretisation of governing equations

ANSYS Fluent software was operated to discretise the governing equations for computational models of LHS system. The design modeller of ANYSYS Fluent software could be used for drawing the geometry of physical models, however the proposed physical models in this thesis were drawn and developed in SolidWorks and were imported in Fluent workbench. Fluent meshing tool was utilised for generating fine meshing of complex geometry of physical models.

To reduce computational cost, parallel processing was implemented to utilise all 8 processors of the workstation. The transient computational models for melting and solidification processes were simulated using pressure-based solver. The solution pattern followed by pressure-based solver is illustrated in **Fig. 3. 6**. The governing equations in melting and solidification processes were coupled to each other and nonlinear in nature therefore, the solver computed various iterative solutions for all governing equations for entire computational domain until solution convergence was achieved. Similarly, pressure-implicit with splitting of operators (PISO) scheme was implemented for pressure-velocity coupling in momentum equation. PRESTO! and second order upwind schemes were implemented for spatial discretisation of pressure, momentum and energy governing equations. Moreover, the absolute convergence criterion was adopted with residual value of 10^{-6} for continuity, velocities and energy equations.

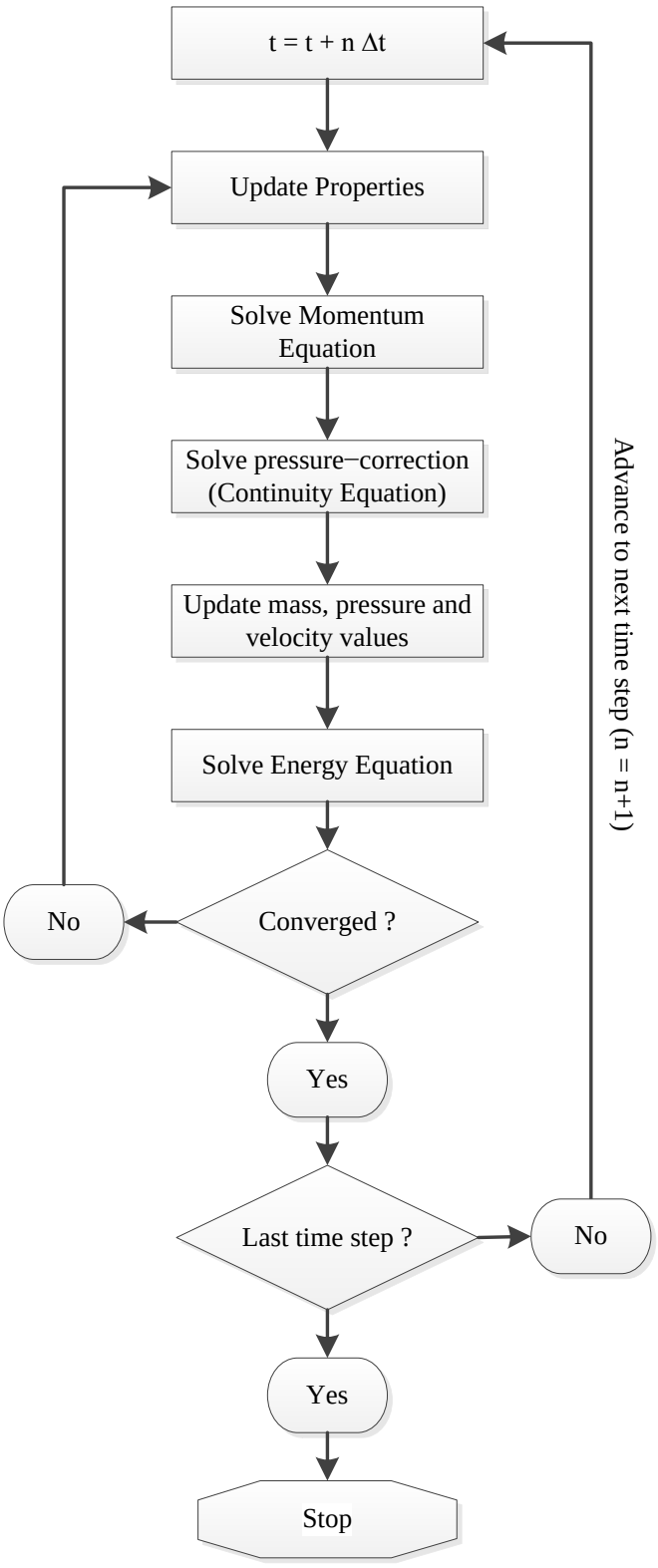

Fig. 3. 6 Flow diagram of solution procedure for transient computational model (Fluent, A. 2009)

To ensure accuracy of numerical simulation results, the mesh and time step independency was examined by conducting a series of simulations for both physical

models at varied mesh sizes and time steps, as given in **Table 3. 2**. It was noticed that for physical model I, the mesh size and time step independency was achieved at 57861 and 1 min, respectively. Likewise, the mesh size of 27420 and time step of 0.1 s ensured mesh and time step independency. The computational models for pure paraffin and nano-additives enhanced nano-PCM was validated with experimental results, as depicted in **Fig. 3. 7**. It was observed that numerical and experimental results are in good agreement with mean absolute percentage error of 3.44% for pure paraffin and 2.53% for nano-PCM, respectively.

Table 3. 2 Mesh size and time step independency for physical model I. Phase transition interval ΔT_{pc} for this case was set to 1 °C (Khan, Z. et al. 2016b)

Case	Mesh Numbers	HTF temperature (°C)	Time step (min)	Melt time (min)	Percent Error
I	28674	60	1	396	10.6
II	57861	60	1	443	-
III	61932	60	1	441	0.45
IV	57861	60	0.25	437	1.35
V	57861	60	0.5	452	2.03

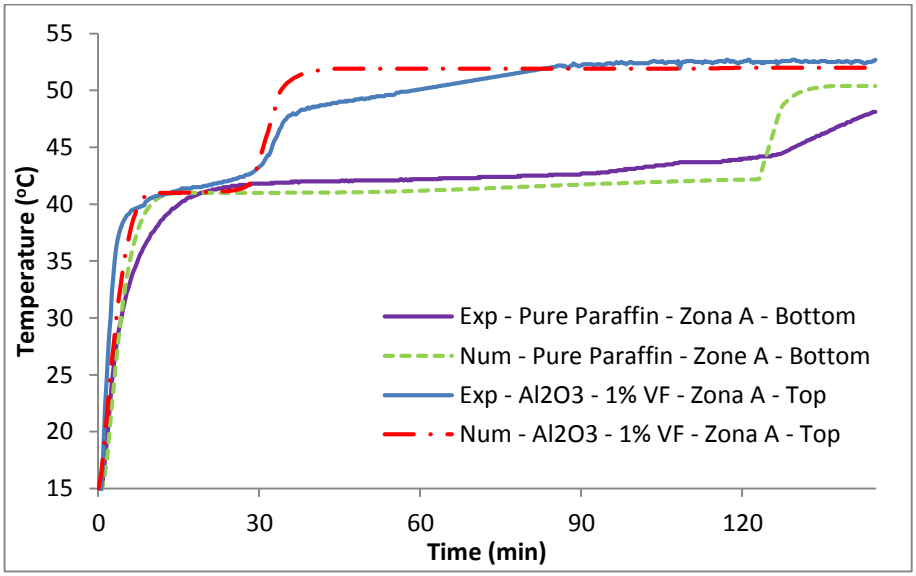

Fig. 3. 7 Validation of numerical and experimental results attained for physical model II during melting process at inlet temperature of 52 °C (Khan, Z. and Khan, Z. A. 2018).

Chapter 4 Numerical simulations results and discussions

This chapter provides detail discussion on the results acquired from simulation of analytical and numerical models proposed in previous chapter for enhanced thermal performance of LHS systems. Initially, the 1-dimenstional analytical models for simpler geometries were simulated in MATLAB workspace to examine the influence of various operating conditions and thermo-physical characteristics of paraffin on phase transition rate and heat flux density of LHS systems. Subsequently, the numerical models for physical model I and II were simulated in ANSYS Fluent workbench to investigate the influence of various design parameters and operating conditions on overall thermal performance of proposed LHS system. This chapter will discuss the optimum design solution for shell and tube heat exchanger with longitudinal fins configuration and nano-additives enhanced paraffin as thermal storage material for improved thermo-physical performance of LHS system. The literature in this chapter has been published in the articles: "Parametric investigations to enhance thermal performance of paraffin through a novel geometrical configuration of shell and tube latent thermal storage system" by (Khan, Z. et al. 2016b) (refer to Appendix A – Paper II), "Development in paraffin based thermal storage system through shell and tubes heat exchanger with vertical fins" by (Khan, Z. and Khan, Z. A. 2017a) (refer to Appendix A – Paper III) and "Experimental and numerical investigations of nano-additives enhanced paraffin in a shell and tube heat exchanger: a comparative study" by (Khan, Z. and Khan, Z. A. 2018) (refer to Appendix A – Paper VI).

4.1 Analytical models results

4.1.1 Stefan problem approach for 1-dimensional semi-infinite layer

The melting and solidification processes for 1-dimensional semi-infinite layer was simulated to examine the impact of various hot/cold surface temperatures and time intervals on melting/solidification front movement and charging/discharging heat flux density, respectively. **Fig. 4. 1** and **Fig. 4. 2** represent the impact of various hot surface temperatures on melting front movement and heat flux density during melting process. It was observed that with an increase in hot surface temperature, the temperature gradient increased which resulted in an increased melting front moment and therefore, a larger portion of paraffin underwent phase transition from solid to liquid. As illustrated in **Fig. 4. 1**, with an increase in hot surface temperature from 52 ^{o}C to 67 ^{o}C, the

distance x covered by melting front away from hot surface was augmented from 16.80 mm to 26.56 mm by charging the system at constant surface temperatures for 4 hours. Likewise, with an increase in temperature gradient by increasing hot surface temperatures from 52 ºC to 67 ºC, the heat flux density after charging the system for 2 hours was augmented from 168.3 W/m^2 – 266.15 W/m^2, respectively.

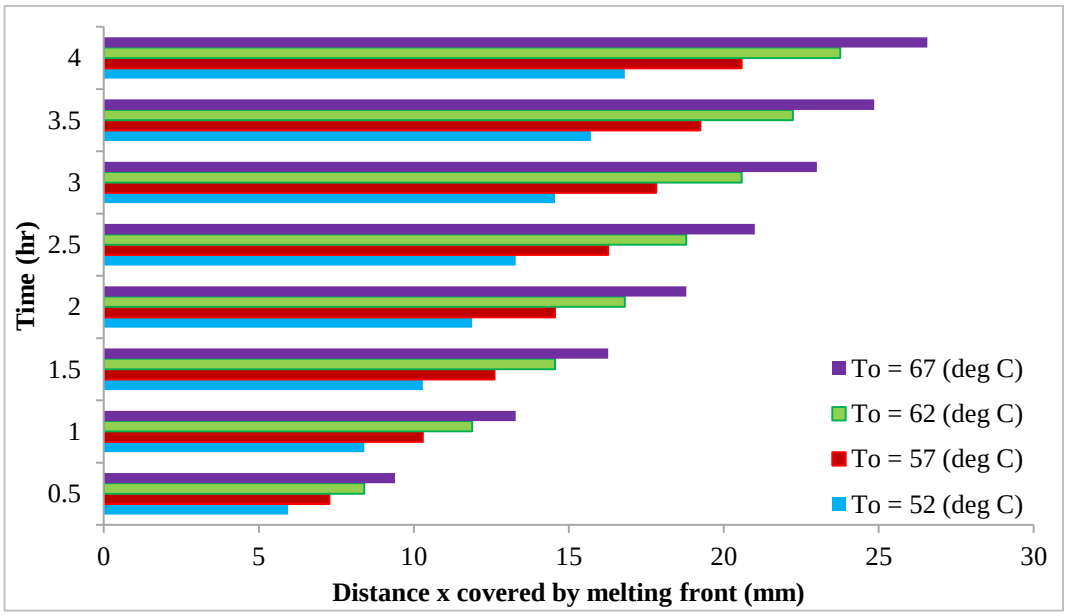

Fig. 4. 1 Phase front movement away from hot surfaces during melting process at various time intervals and hot surface temperatures

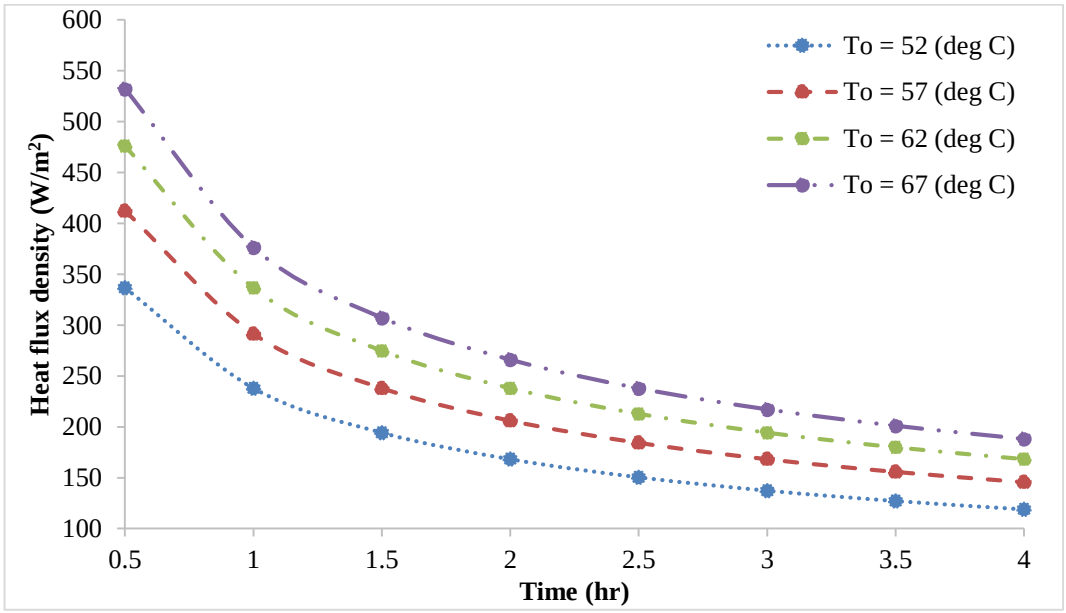

Fig. 4. 2 Heat flux density with respect to varying hot surface temperatures and time intervals during melting process

Similarly, in solidification process, the distance covered by phase front away from cold surface and heat flux density at various time intervals and operating temperatures are illustrated in **Fig. 4. 3** and **Fig. 4. 4**, respectively. It was observed that as the temperature of cold surface was decreased from 20 ^{o}C to 5 ^{o}C, a higher temperature gradient was generated and therefore, the amount of paraffin experiencing phase transition from liquid to solid phase was increased, as well as the heat flux density. It can be noticed from **Fig. 4. 3** that with an increase in temperature gradient by reducing the cold surface temperature from 20 ^{o}C to 5 ^{o}C, the distance covered by solidified front away from cold surface was increased from 26.03 mm to 33.18 mm, after discharging the system for 4 hours at constant surface temperatures. Likewise, the heat flux density was improved from 260.76 W/m^2 – 332.42 W/m^2, after discharging the system for 2 hours.

Therefore, it was concluded that the thermo-physical properties of paraffin (such as thermal conductivity, latent heat capacity, density and phase transition temperature) and operating temperature of hot surface or HTF demonstrated significant impact on phase transition rate or phase front movement and heat flux density of LHS system.

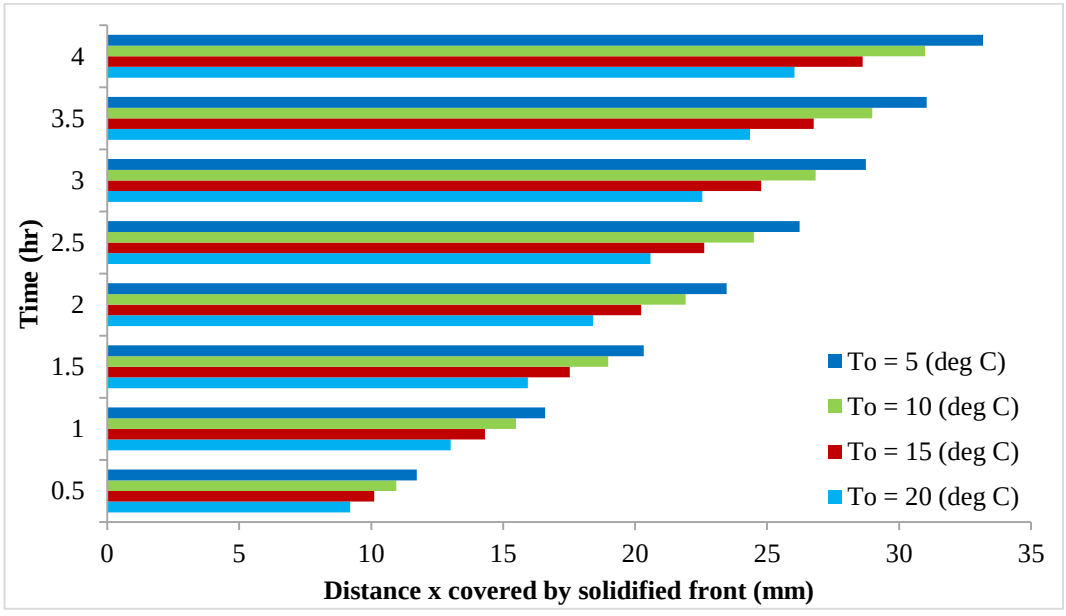

Fig. 4. 3 Phase front movement away from cold surfaces during solidification process at various time intervals and surface temperatures

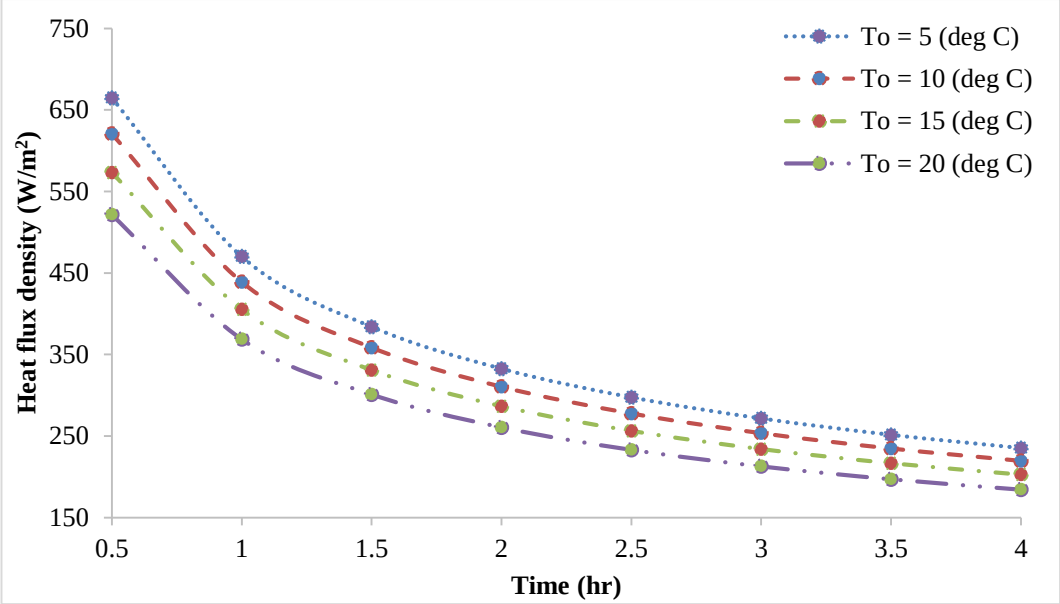

Fig. 4. 4 Heat flux density during solidification process at various time intervals and surface temperatures

4.1.2 Energy balance method for shell and tube heat exchanger

In energy balance approach, the energy released by high temperature water during melting process was assumed to be completely captured by paraffin in shell. The impact of varying operating temperatures and mass flow rates of water on heat transfer coefficient, overall heat transfer rate and phase transition rate were investigated by implementing energy balance technique to simple shell and tube heat exchanger based LHS system, as presented in **Fig. 3. 2**.

The influence of varying operating inlet temperatures of water on overall thermal performance of paraffin in shell and tube heat exchanger is illustrated in **Table 4. 1**. It was noticed that at constant mass flow rate, the thermo-physical characteristics of water was influenced by increasing operating temperature and subsequently, the nature of fluid flow (laminar or turbulent), thermal diffusion rate and mode of heat transfer (conductive or convective) were influenced. Dynamic viscosity of water was decreased due to increasing operating temperature of water from 52 ^{o}C – 67 ^{o}C and therefore, the viscous forces were reduced as compared to inertial forces. Thus, the turbulent nature of water flow was progressed. Similarly, due to an increase in specific heat capacity and reduction in dynamic viscosity of water with an increasing operating temperature, the viscous diffusion rate overcame thermal diffusion rate. Moreover, the heat transfer coefficient was enhanced by 14.17% with an increase in operating temperature. Furthermore, due to improved heat transfer coefficient, the rate of heat transfer between

water and paraffin was considerably augmented from 954.402 W to 2446.559 W and consequently, the total time required to melt paraffin in shell was reduced by 66.08%.

Table 4. 1 Influence of varying inlet temperature of HTF on melting process of paraffin in shell and tube heat exchanger based LHS system

Inner diameter of HTF tube (m)	0.02			
Outer diameter of HTF tube (m)	0.022			
Running length (m)	6.72			
Latent heat of paraffin (RT44HC) (J/Kg)	255000			
Density of paraffin (kg/m^3)	800			
Phase transition temperature of paraffin (^{o}C)	44			
Mass flow rate of water (kg/s)	0.02458			
Inlet temperature of water (^{o}C)	52	57	62	67
Dynamic viscosity of water (kg/s.m)	0.0005293	0.000488	0.0004517	0.0004197
Thermal conductivity of water (W/m.K)	0.645	0.651	0.656	0.660
Specific heat capacity of water (J/kg.K)	4182.22	4184.02	4186.12	4188.67
Reynolds number	2956.379	3206.581	3464.271	3728.405
Prandtl number	3.432	3.136	2.882	2.664
Nusselt number	19.907	20.677	21.446	22.212
Heat transfer coefficient (W/(m^2.K))	641.993	673.042	703.426	732.996
Outlet temperature of water (^{o}C)	42.716	42.946	43.115	43.237
Heat transfer rate (W)	954.402	1445.325	1943.127	2446.559
Total melting time of paraffin (hr)	3.099	1.889	1.353	1.051

Likewise, the impact of varying mass flow rate of water on thermal performance of paraffin in a shell and tube heat exchanger based LHS system is presented in **Table 4. 2**. It was observed that at constant operating temperature, thermo-physical properties of water remained unchanged with varying mass flow rate and therefore, the Prandtl number remained constant. However, the inertial forces were significantly enhanced with increasing mass flow rate and therefore, the turbulent nature of flow was improved, which resulted in a higher convective heat transfer rate. As a result, the heat transfer coefficient was significantly enhanced by a fraction of 74.66% with an increase in mass flow rate from 0.02458 kg/s to 0.04936 kg/s. Due to higher heat transfer coefficient, the heat transfer between water and paraffin was improved from 954.402 W to 1855.955 W. Due to higher rate of heat transfer, the total time required to melt entire mass of paraffin in shell was decreased by 48.56%.

Table 4. 2 Influence of varying mass flow rate of HTF on melting process of paraffin in shell and tube heat exchanger based LHS system

Latent heat of paraffin (RT44HC) (J/Kg)	255000			
Density of paraffin (kg/m^3)	800			
Phase transition temperature of paraffin (^{o}C)	44			
Inlet temperature of water (^{o}C)	52			
Dynamic viscosity of water (kg/s.m)	0.0005293			
Thermal conductivity of water (W/m.K)	0.645			
Specific heat capacity of water (J/kg.K)	4182.22			
Prandtl number	3.432			
Mass flow rate of water (kg/s)	0.02458	0.03290	0.04113	0.04936
Reynolds number	2956.379	3957.555	4946.943	5936.452
Nusselt number	19.907	25.138	30.051	34.771
Heat transfer coefficient (W/(m^2.K))	641.993	810.707	969.152	1121.357
Outlet temperature of water (^{o}C)	42.716	42.831	42.927	43.009
Heat transfer rate (W)	954.402	1261.734	1560.771	1855.955
Total melting time of paraffin (hr)	3.099	2.344	1.895	1.594

Likewise, during solidification process, the influence of varying inlet temperature and mass flow rate of water on thermal performance of paraffin in shell and tube heat exchanger based LHS system is illustrated in **Table 4. 3** and **Table 4. 4**, respectively. It was observed that with a decrease in inlet temperature of HTF, the temperature gradient between water and paraffin was augmented and therefore, the heat transfer coefficient was improved and consequently, a relatively higher heat transfer rate was achieved to extract thermal energy from paraffin by flowing water at constant flow rate. As illustrated in **Table 4. 3**, the total solidification time was decreased by a fraction of 37.6% as the inlet temperature was reduced from 20 ^{o}C – 5 ^{o}C. Moreover, at constant inlet temperature of 10 ^{o}C, an increase in mass flow rate demonstrated an increase in heat transfer coefficient and as a result, the heat transfer rate was improved from 2654.2 W to 4993.9 W, as presented in **Table 4. 4**. Due to higher heat transfer rate, the total solidification time for paraffin in shell was reduced by a fraction of 46.79% as the mass flow rate was increased from 0.0249 kg/s to 0.0499 kg/s. Therefore, it was deduced from energy balance technique that the operating temperature and mass flow rate of water are critical parameters for designing an optimum thermal performance of LHS system.

Table 4. 3 Influence of varying inlet temperature of HTF on solidification process of paraffin in shell and tube heat exchanger based LHS system

Latent heat of paraffin (RT44HC) (J/Kg)	255000			
Density of paraffin (kg/m^3)	700			
Phase transition temperature of paraffin (^{o}C)	42			
Mass flow rate of water (kg/s)	0.0249			
Inlet temperature of water (^{o}C)	5	10	15	20
Dynamic viscosity of water (kg/s.m)	0.001507	0.001298	0.001134	0.001004
Thermal conductivity of water (W/m.K)	0.579	0.587	0.595	0.603
Specific heat capacity of water (J/kg.K)	4202.81	4192.33	4185.85	4182.11
Reynolds number	1055.654	1225.818	1403.411	1585.001
Prandtl number	10.939	9.269	7.975	6.961
Nusselt number	12.366	13.264	14.125	14.947
Heat transfer coefficient (W/(m^2.K))	358.027	389.237	420.249	450.685
Outlet temperature of water (^{o}C)	33.227	35.334	37.049	38.438
Heat transfer rate (W)	2964.776	2654.205	2306.513	1927.049
Total solidification time of paraffin (hr)	0.698	0.780	0.898	1.074

Table 4. 4 Influence of varying mass flow rate of HTF on solidification process of paraffin in shell and tube heat exchanger based LHS system

Latent heat of paraffin (RT44HC) (J/Kg)	255000			
Density of paraffin (kg/m^3)	700			
Phase transition temperature of paraffin (^{o}C)	42			
Inlet temperature of water (^{o}C)	10			
Dynamic viscosity of water (kg/s.m)	0.001298			
Thermal conductivity of water (W/m.K)	0.587			
Specific heat capacity of water (J/kg.K)	4192.33			
Prandtl number	9.269			
Mass flow rate of water (kg/s)	0.0249	0.0333	0.0416	0.0499
Reynolds number	1225.818	1634.456	2043.046	2451.684
Nusselt number	13.264	16.693	19.955	23.089
Heat transfer coefficient (W/(m^2.K))	389.237	489.973	585.728	677.712
Outlet temperature of water (^{o}C)	35.334	34.722	34.236	33.833
Heat transfer rate (W)	2654.205	3453.636	4232.140	4993.994
Total solidification time of paraffin (hr)	0.780	0.599	0.489	0.415

4.2 Numerical models results

The numerical models discussed in section 3.1.2 were simulated for both physical models I and II to propose an optimum design solution for an effective and responsive LHS system. In first stage, the transient numerical simulations were conducted for identification of optimum geometrical configurations of shell and tube heat exchanger with multiple tube passes and longitudinal fins as extended surfaces for improved thermal performance. Therefore, physical model I was investigated with pure paraffin as thermal storage material at various operating conditions and with various affecting geometrical parameters to produce an optimised design solution. In second stage, the novel thermal storage material was proposed by conducting series of numerical simulations on nano-additives enhanced paraffin in physical model II. In third stage, the proposed design of novel shell and tube heat exchanger with extended longitudinal fins and proposed nano-additives enhanced novel thermal storage materials was simulated.

4.2.1 First stage: Design solution of shell and tube heat exchanger for LHS system

In this stage, the trial and error method was implemented for identification of geometrical orientation of shell and tube heat exchanger with multiple tube passes and longitudinal fins with relatively better thermal performance. Likewise, the parametric investigations were conducted based on geometrical dimensions of longitudinal fins, construction material for shell, tubes and fins, and operating conditions to determine an optimum design solution for LHS system.

4.2.1.1 Geometrical orientation of shell and tube heat exchanger

In order to reduce computational time, two dimensional transient numerical simulations were conducted on various geometrical orientations to investigate the respective phase transition rate of paraffin. Due to vertical orientations of shell and tube heat exchanger (refer to **Fig. 3. 4**), the top view cross section was selected as geometrical computational domain for numerical simulation. As might be expected that due to selection of top view cross section, the effect of natural convection on phase transition rate was neglected.

The phase transition rates of paraffin in various geometrical configurations, which were previously illustrated in **Fig. 3. 3**, were simulated at constant inlet temperature of 62 ^{o}C to investigate the influence of various number of tube passes with longitudinal fins and their positioning in shell container. The melting fraction of paraffin for each case of geometrical orientation are illustrated in **Fig. 4. 5**. It was noticed that due to an increase

in the number of tube passes from 9 to 21 for case A to C, the volume of paraffin in shell container was compromised, however, the effective surface area for heat transfer was significantly improved which had generated a higher phase transition rate.

Due to low thermal conductivity of paraffin, the geometrical orientation of tube passes with longitudinal fins in shell container should be in uniform proximity to paraffin. It was noticed that the geometrical positioning of tube passes in shell container was widely apart in case A, which affected the uniformity of heat transfer across the shell container. As a result, the melted fraction of paraffin was 65.75%, 95.45% and 99% after charging at constant inlet temperature for 5 h, 10 h and 15 h, respectively. Moreover, the effective surface area for heat transfer was improved by increasing the number of tube passes from 9 to 12 for case B and consequently, the melted fraction of paraffin was 71.85%, 96.07% and 99.5% after charging at constant inlet temperature for 4 h, 8 h and 12 h, respectively. Furthermore, the effective surface area for heat transfer was increased by increasing number of tube passes to 21 for case C and therefore, the melted fraction was 84%, 94.2% and 98.25% after charging for 3 h, 4 h and 5 h, respectively. As illustrated in **Fig. 4. 5**, the phase transition rate of paraffin in case C was significantly higher than case A and case B due to improved effective surface area for heat transfer. Likewise, the increased number of tube passes with longitudinal fins generated a dominant conduction heat transfer across the shell container (Khan, Z. et al. 2016b).

Likewise, the impact of longitudinal fins on phase transition rate of paraffin was investigated by simulating geometrical orientation in case C with and without longitudinal fins. It was deduced that phase transition rate of paraffin was significantly improved by a fraction of 69.75% for longitudinal fins orientation as compared to no fins orientation.

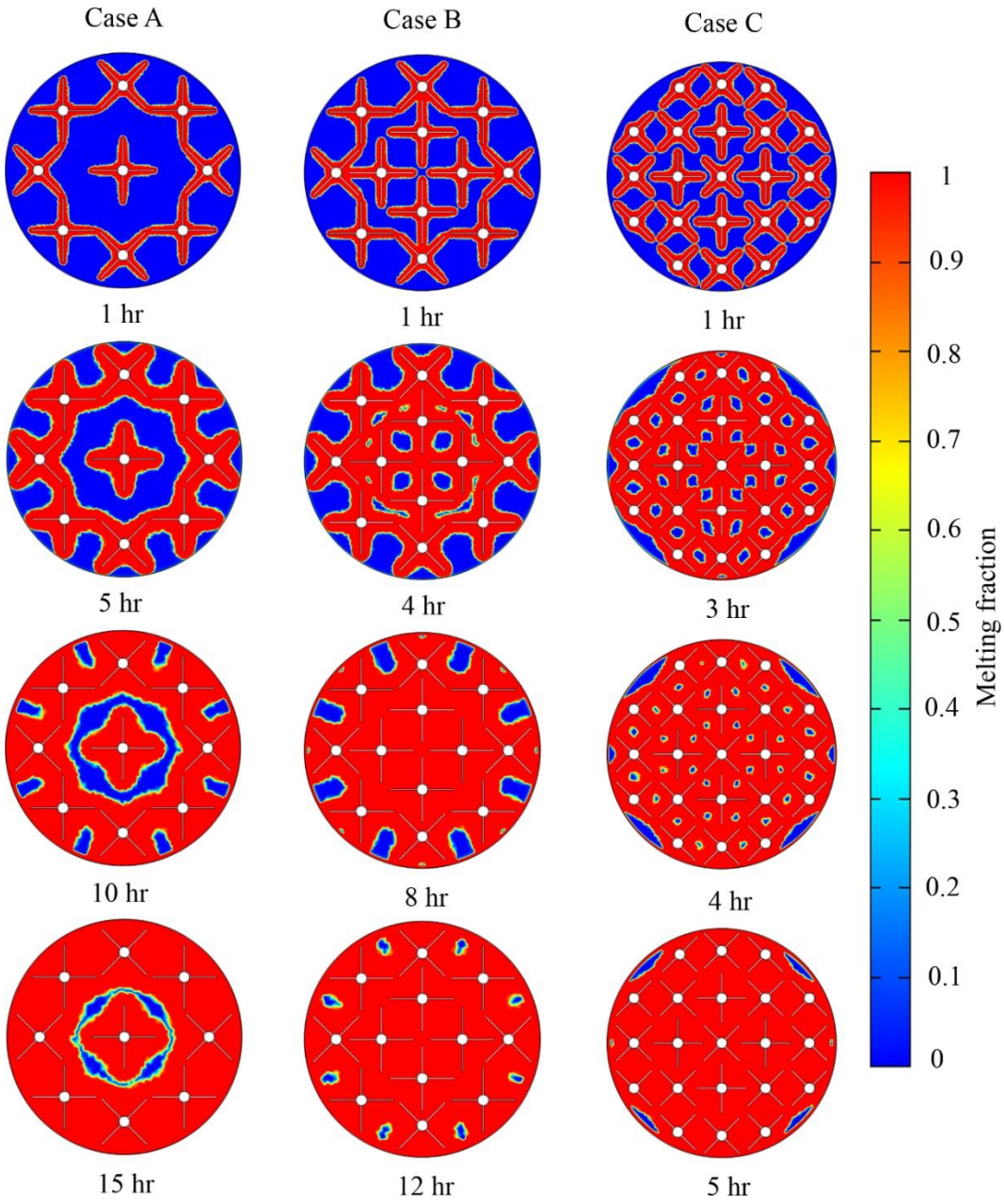

Fig. 4. 5 Melting fraction of paraffin at various time intervals while charging at constant inlet temperature of 62 °C. Phase transition interval $\Delta \boldsymbol{T_{pc}}$ for this case was set to 1 °C (Khan, Z. et al. 2016b)

4.2.1.2 Geometrical dimensions of longitudinal fins

Following to the selection of case C as geometrical orientation for shell and tube heat exchanger, the geometrical dimensions of longitudinal fins are crucial to the optimum thermal performance enhancement of LHS system. Therefore, parametric investigations were conducted to investigate the impact of longitudinal fins length and thickness on phase transition rate and thermal storage capacity of LHS system. Moreover, heat transfer from tubes to paraffin was kept constant at 62 °C and the phase transition interval ΔT_{pc} was set to 0.1 °C.

The impact of varying longitudinal fins length on phase transition rate is illustrated in **Fig. 4. 6**. It was noticed that with an increase in fins length from 12.70 mm to 38.10 mm, the effective surface area for heat transfer was improved and therefore, a dominant conduction heat transfer was generated. Similarly, in case of longitudinal fins length of 38.10 mm, a relatively better temperature distribution in shell container was generated. As a result, the melting fraction of paraffin for all cases were recorded to be 64.34%, 82.80%, 92.06% and 96.86% after charging at constant inlet temperature for 2 h, respectively. Therefore, it was concluded that the phase transition rate was significantly enhanced by increasing longitudinal fins length. Likewise, an increase in fins length from 12.70 mm to 38.10 mm had an insignificant impact on reduction in thermal storage capacity, such as it reduced from 10.971 MJ to 10.762 MJ, respectively.

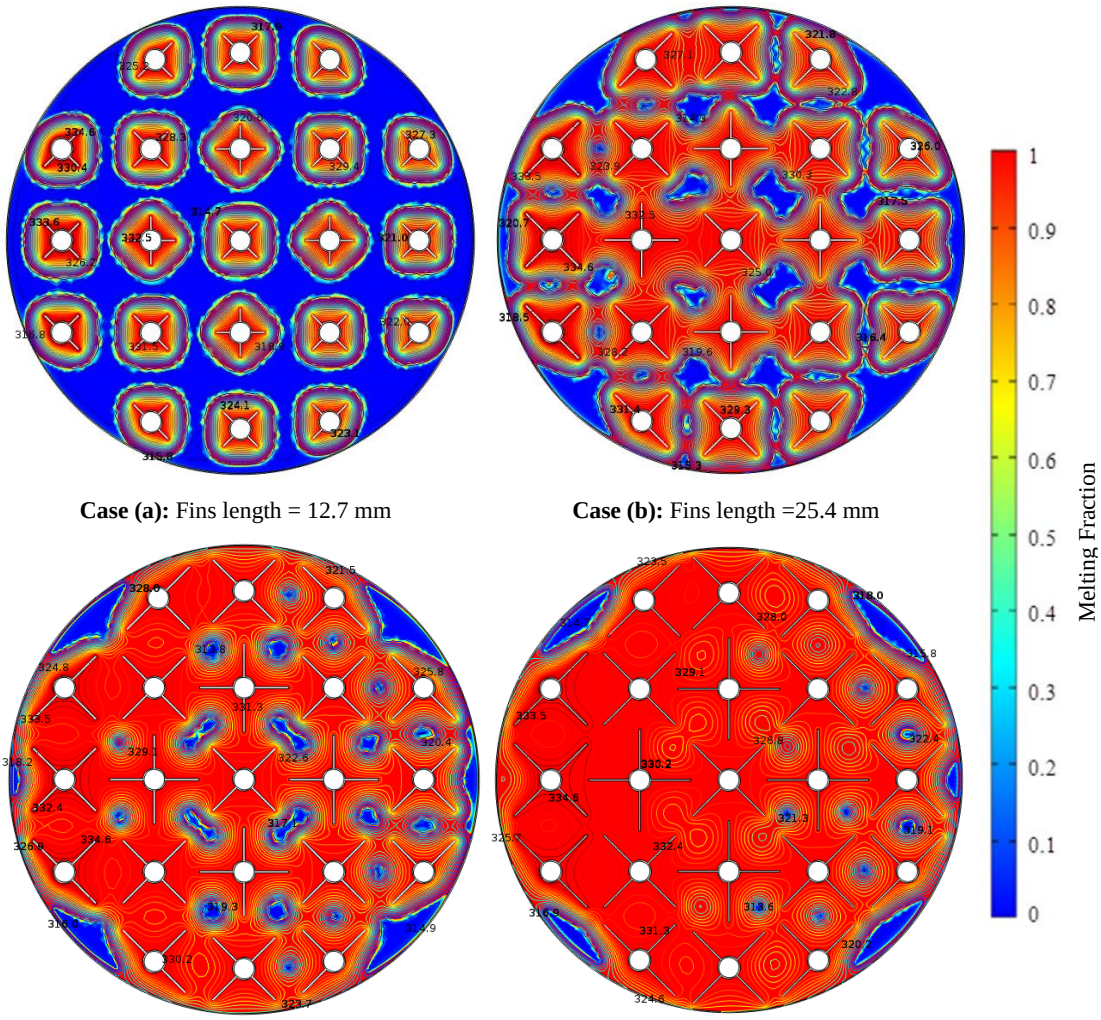

Case (a): Fins length = 12.7 mm

Case (b): Fins length =25.4 mm

Case (c): Fins length = 31.75 mm

Case (d): Fins length =38.10 mm

Fig. 4. 6 Impact of longitudinal fins length on melting rate of paraffin in LHS system while charging at constant inlet temperature of 62 °C. Phase transition interval ΔT_{pc} for this case was set to 0.1 °C (Khan, Z. and Khan, Z. A. 2017a).

Similarly, the influence of longitudinal fins thickness on phase transition rate and thermal storage capacity of LHS system was examined by conducting parametric investigations on fins thickness ranging from 1 mm to 4 mm, as shown in **Fig. 4. 7**. Longitudinal fins length was set constant at 38.10 mm. It was noticed that with an increase in fins thickness, the temperature distribution in shell container was improved which resulted in relatively higher phase transition rate. The total time required to melt entire mass of paraffin in shell container was reduced by a fraction of 22.68% by increasing fins thickness from 1 mm to 4 mm. However, an increase in fins thickness compromised the volume for paraffin in shell container and therefore, the thermal storage capacity was reduced from 10.919 MJ to 10.292 MJ, respectively. Therefore, an optimum geometrical length and thickness of 38.10 mm and 1.5 mm were determined.

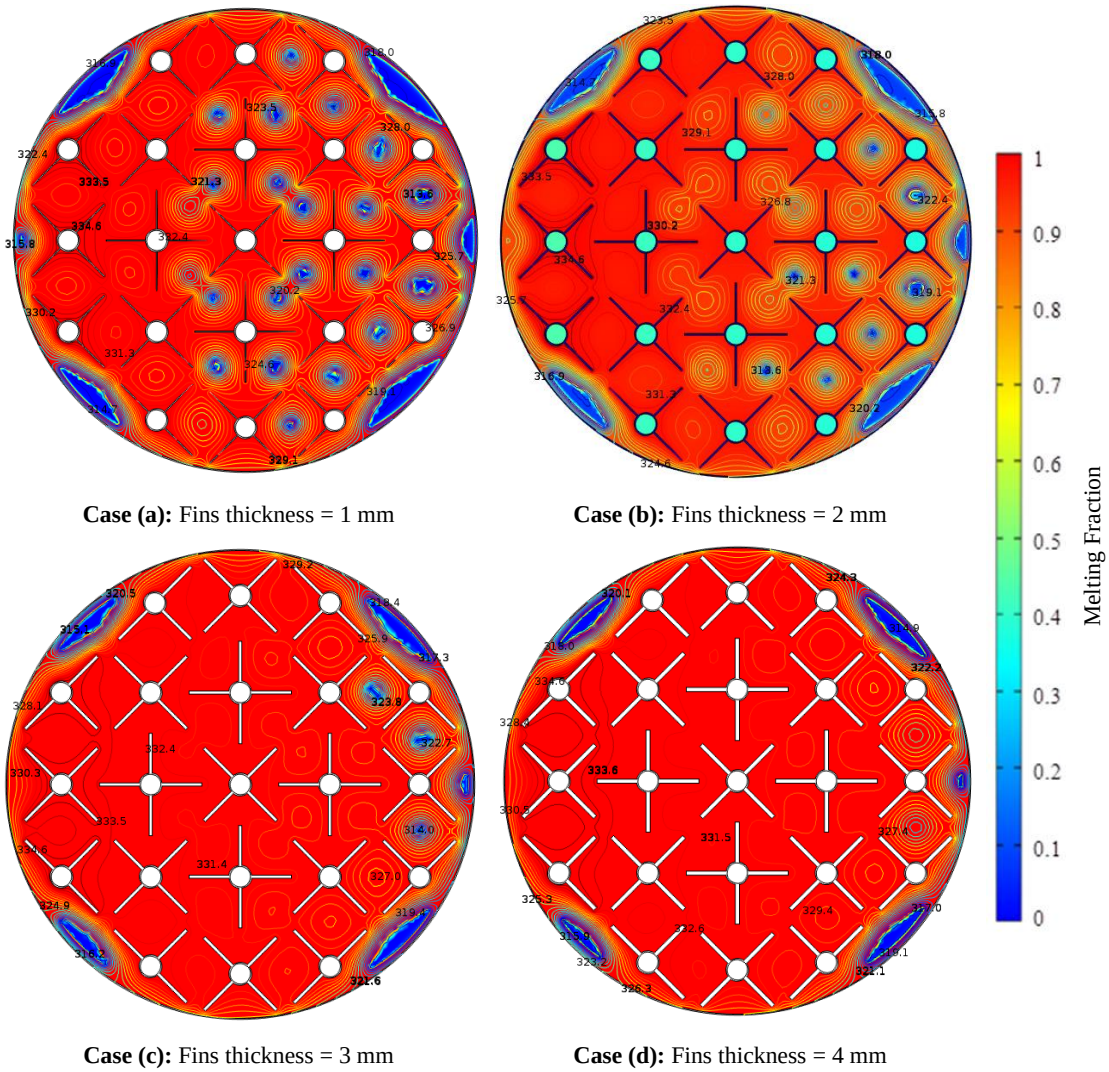

Case (a): Fins thickness = 1 mm

Case (b): Fins thickness = 2 mm

Case (c): Fins thickness = 3 mm

Case (d): Fins thickness = 4 mm

Fig. 4. 7 Impact of longitudinal fins thickness on melting fraction of paraffin in LHS system while charging at constant inlet temperature of 62 ^{o}C. Phase transition interval ΔT_{pc} for this case was set to 0.1 ^{o}C (Khan, Z. and Khan, Z. A. 2017a).

4.2.1.3 Material for shell, tubes and fins

Low thermal conductivity of paraffin can be countered by employing shell and tube heat exchanger with extended surfaces. However, the construction material of shell, tubes and longitudinal fins of proposed geometrical orientation are crucial to optimum enhancement in thermal performance of LHS system. Hence, numerical simulations were conducted on number of commonly employed construction material such as steel, cast iron, tin, nickel, aluminium and copper to investigate their influence on phase transition rate of paraffin, as shown in **Table 4. 5**. It was noticed that materials with higher thermal conductivity had significant enhancement in heat transfer rate and therefore, the time required to completely melt paraffin in shell container was significantly reduced. As presented, the phase transition time for aluminium and copper was significantly reduced by a fraction of 21.61% and 23.68% as compared to steel. Thus, copper and aluminium were considered as suitable construction materials for shell, tubes and longitudinal fins. In this thesis, copper was employed as construction material for shell, tubes and fins.

Table 4. 5 Impact of various construction materials on phase transition rate of paraffin in LHS system. Phase transition interval ΔT_{pc} for this case was set to 1 ^{o}C (Khan, Z. et al. 2016b)

Materials	Thermal Conductivity (W/m. K)	Percent Liquid Fraction					Complete Melting Time (h)
		2 h	4 h	6 h	8 h	10 h	
Steel AISI 4340	44.5	63.92	85.23	95.53	99.25	100	9.67
Cast Iron	50	65.06	86.23	96.19	99.46	100	9.34
Tin	67	67.30	87.69	97.30	99.71	100	8.92
Nickel	90	68.57	88.32	97.78	99.85	100	8.75
Aluminium 6063	201	72.77	92.19	99.08	100		7.67
Aluminium	238	73.05	92.68	99.15	100		7.58
Copper	400	73.63	93.69	99.34	100		7.38

4.2.1.4 Impact of operating conditions

Following to selection of geometrical configuration and construction material for shell and tube heat exchanger with multiple passes and longitudinal fins, the phase transition rate and thermal storage capacity at various operating temperatures ranging from 52 ^{o}C to 62 ^{o}C were simulated. It was noticed that with an increase in inlet temperature, the temperature gradient between paraffin in shell and water as HTF in tubes was improved which resulted in higher heat transfer rate. Hence, due to improved heat transfer, the

phase transition rate was significantly enhanced. As presented in **Fig. 4. 8**, the melting fraction of paraffin in shell container was recorded to be 86.71%, 97.84% and 99.9% for inlet temperature of 52 ^{o}C, 57 ^{o}C and 62 ^{o}C, respectively. Furthermore, the sensible portion of thermal energy was significantly boosted with an increase in inlet temperature and as a result, the overall thermal storage capacity of LHS system was augmented from 10.16 MJ to 11.06 MJ as the inlet temperature was raised from 52 ^{o}C to 62 ^{o}C, respectively.

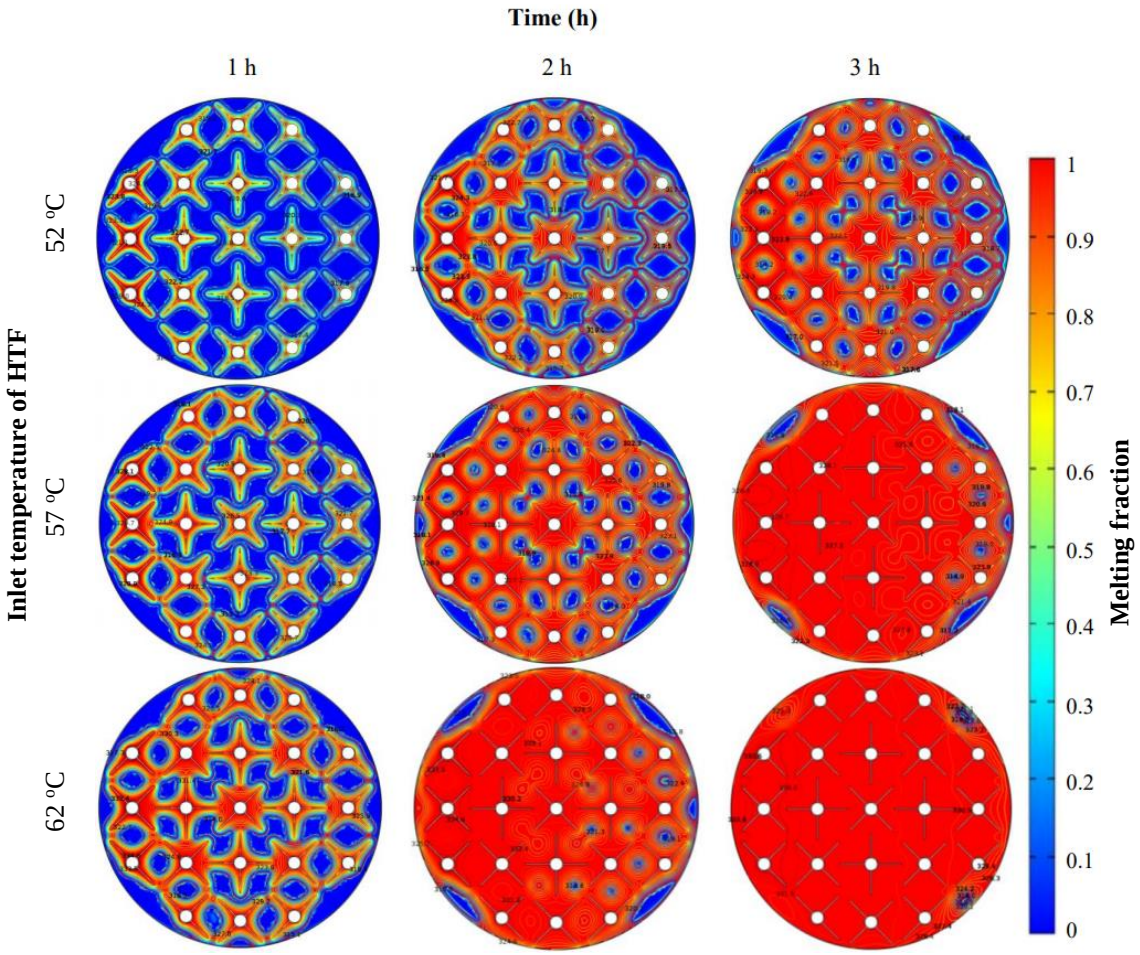

Fig. 4. 8 Phase transition rate of paraffin at various time intervals and inlet temperatures. Phase transition interval ΔT_{pc} for this case was set to 0.1 ^{o}C (Khan, Z. and Khan, Z. A. 2017a).

4.2.1.5 Influence of natural convection

As mentioned earlier, the numerical simulation conducted on the selected top view cross section of vertical shell and tube heat exchanger did not account for the influence of natural convection on melting process of paraffin in vertical direction. Thus, in order to examine the influence of natural convection on temperature distribution and phase transition rate of paraffin in vertical direction, a three dimensional transient numerical

simulation was conducted at constant inlet temperature of 62 ^{o}C. Due to computational complexity of transient numerical simulation in a three dimensional computational domain, a small section of shell was selected as computational domain to reduced computational cost and time, as illustrated in **Fig. 4. 9**. Paraffin in selected section was subjected to constant wall temperature at pipe surfaces and longitudinal fins surfaces, as presented with red colour in **Fig. 4. 9**.

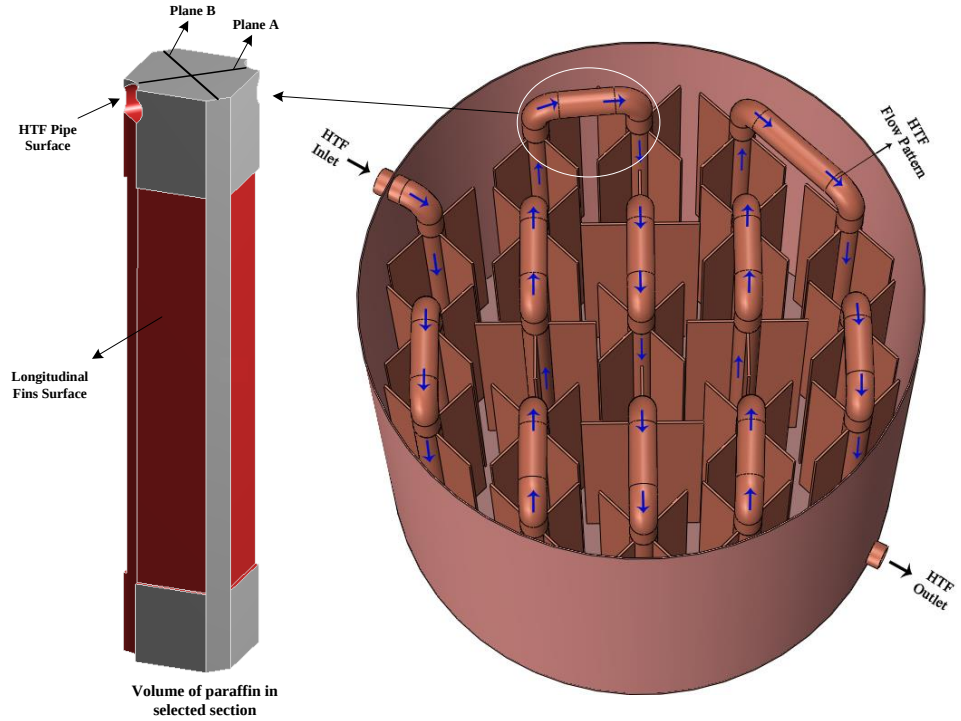

Fig. 4. 9 Selected section in shell container as computational domain for 3-dimensional transient simulation to examine impact of natural convection on vertical temperature distribution and melting rate. Red colour surfaces demonstrate constant wall temperature of 62 ^{o}C.

It was deduced that natural convection had significant influence on phase transition rate and temperature distribution in vertical direction due to upward rise of high temperature paraffin molecules, as presented in **Fig. 4. 10** and **Fig. 4. 11**. It was noticed that conduction was the dominant mode of heat transfer at initial stages of melting process. However, as the paraffin melted at locations nearer to tube surface and longitudinal fins, the buoyant forces in liquid portion of paraffin started to overcome the viscous forces and thus an upward rise of high temperature molecules were recorded. During this stage, the natural convection was noticed as the dominant mode of heat transfer. The accumulation of high temperature liquid paraffin molecules at the top portion of shell container resulted in a relatively higher phase transition rate of paraffin. Subsequently, as the entire mass of paraffin was melted at top portion of shell container, the liquid

paraffin molecules transferred thermal energy to solid paraffin at central portion of shell container. However, due to upward rise of high temperature molecules, the heat transfer rate at central and bottom portion were relatively lower and consequently, the phase transition rate was comparatively slow. Hence, it was observed that natural convection was crucial for thermal performance of LHS system and therefore, the dynamic viscosity of paraffin at various temperatures had significant influence on phase transition rate and temperature distribution. Moreover, it was verified that the proposed design of vertical shell and tube heat exchanger with longitudinal fins had not interrupted the buoyance driven natural convection during melting process.

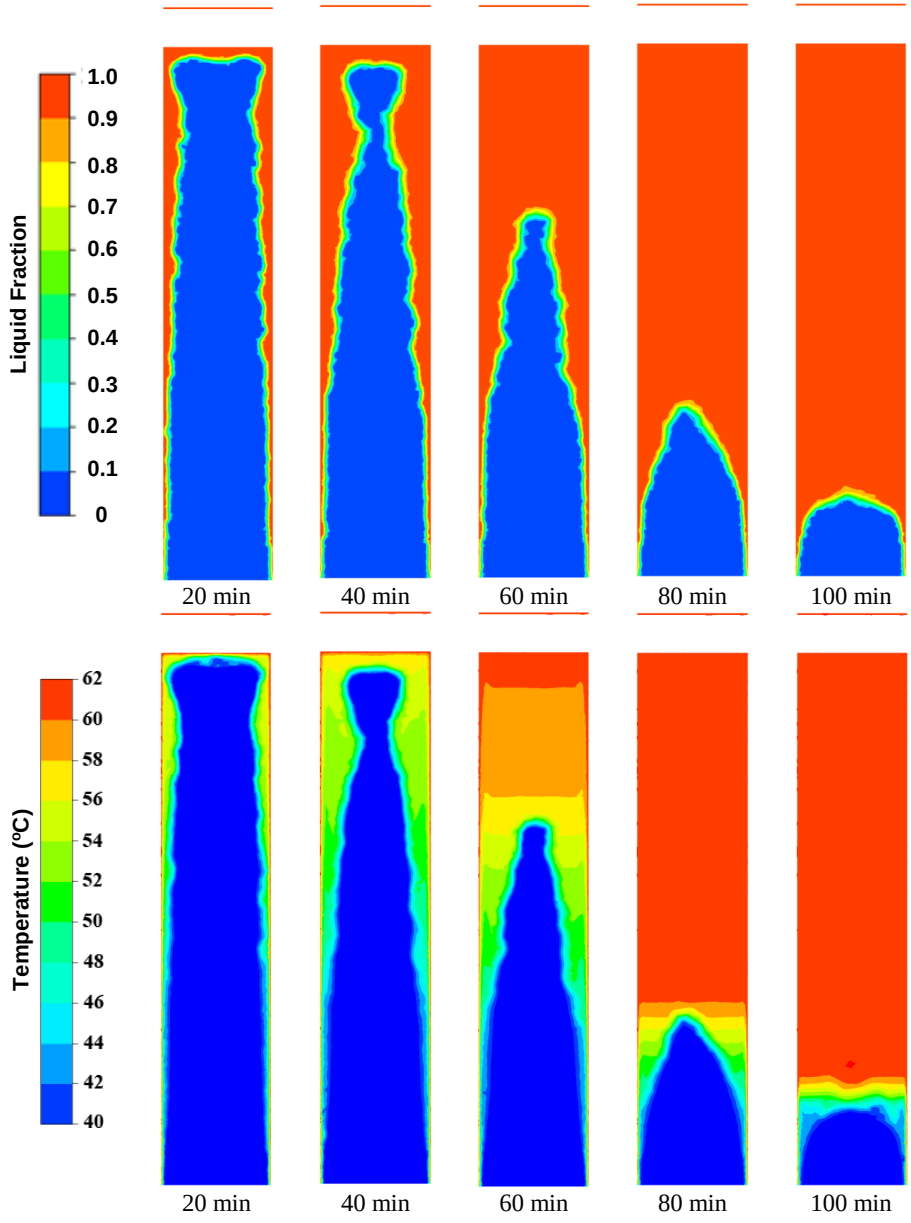

Fig. 4. 10 Melting fractions and temperature contours of paraffin at plane A during various time intervals of melting process at constant inlet temperature of 62 °C. Phase transition interval ΔT_{pc} was set to 0.1 °C.

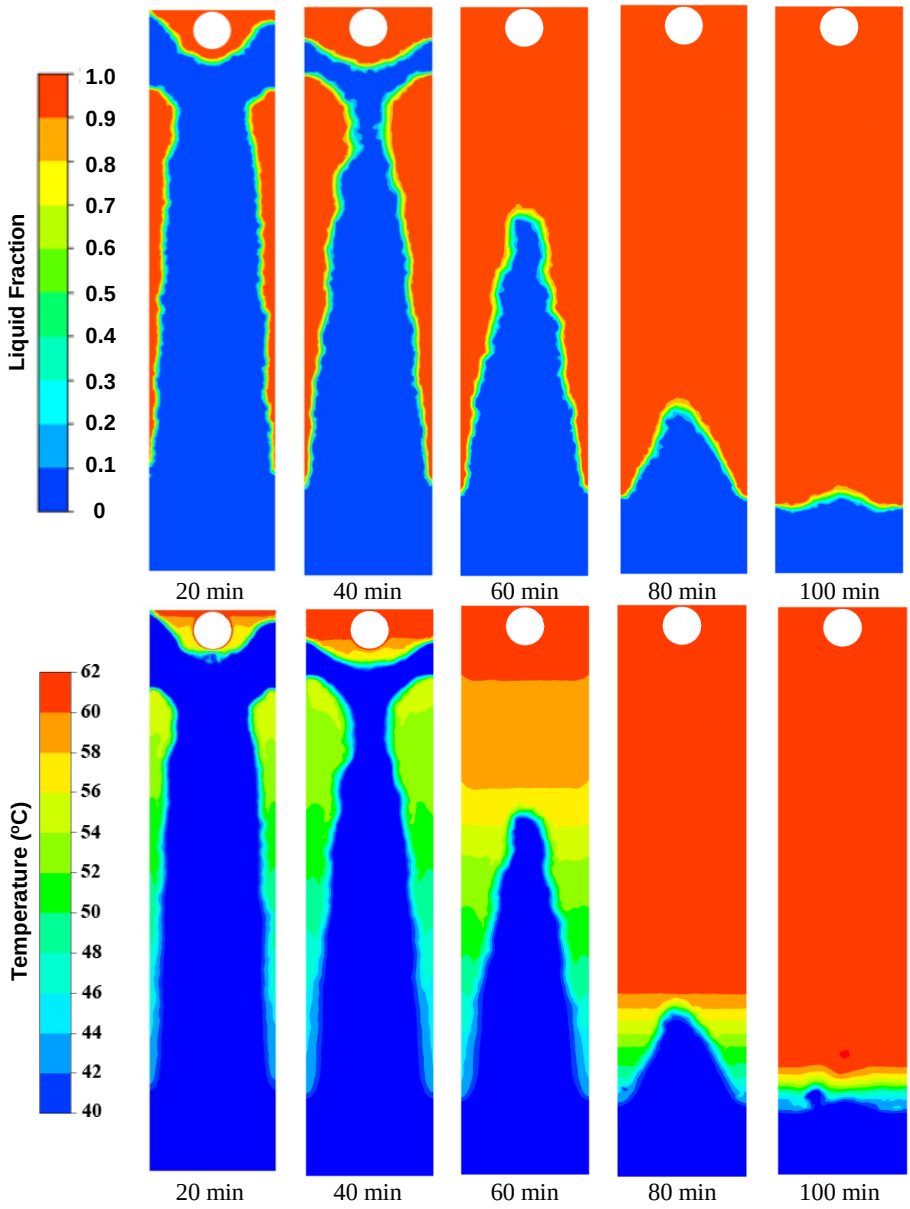

Fig. 4. 11 Melting fractions and temperature contours of paraffin at plane B during various time intervals of melting process at constant inlet temperature of 62 °C. Phase transition interval ΔT_{pc} was set to 0.1 °C.

As discussed earlier, the phase transition temperature interval ΔT_{pc} significantly influence the phase transition rate. Parametric investigations of ΔT_{pc} were conducted to identify an appropriate value for accurate numerical simulation results, as presented in **Fig. 4. 12**. It was observed that as the value for ΔT_{pc} was increased, the phase transition rate was underestimated and vice versa. For instance, the time required to completely charge the paraffin at bottom position of selected section was 2.57 h, 3.78 h and 4.08 h for ΔT_{pc} value of 0.025, 0.1 and 1, respectively. Therefore, for accurate prediction of melting/solidification front, phase transition rate and temperature distribution, the

numerical simulations results should be compared to experimental results for each simulation scenario to identify accurate value for ΔT_{pc}.

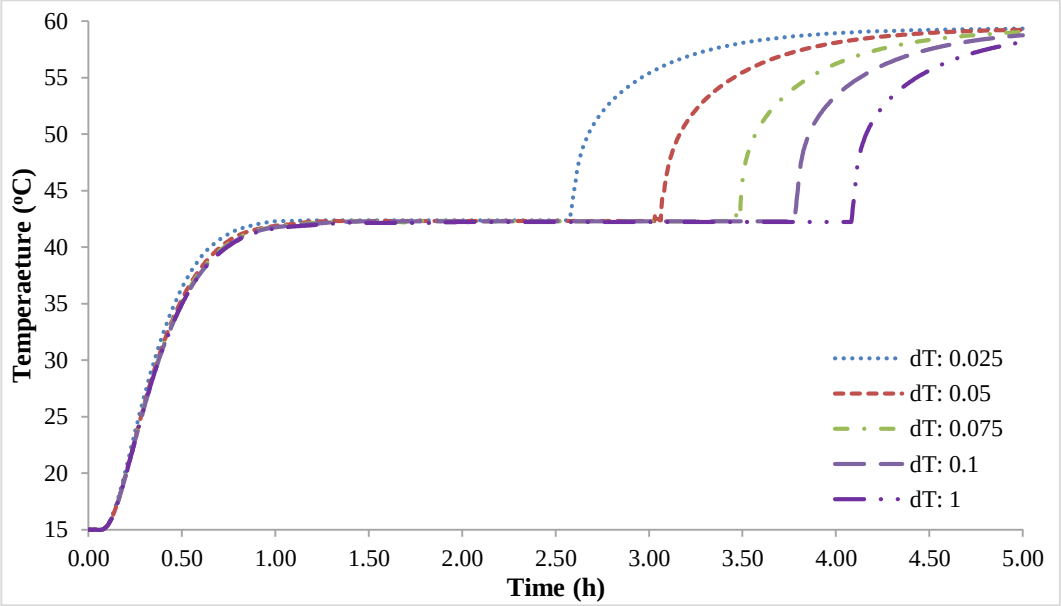

Fig. 4. 12 Impact of phase transition temperature interval ΔT_{pc} on transient temperature profiles of paraffin at bottom position of selected section. The inlet temperature was kept constant at 62 ºC.

4.2.2 Second stage: Novel nano-additive enhanced thermal storage materials

It was observed in previous section that the thermal performance of paraffin in shell and tube heat exchanger with multiple passes and longitudinal fins was significantly enhanced due to improved surface area for heat transfer, vertical orientation of longitudinal fins to support buoyancy driven natural convection and optimal positioning of tube passes and longitudinal fins to create better thermal distribution in shell container. However, the overall thermal performance could be further enhanced by incorporating high thermal conductive nano-additives to base paraffin. In this stage, the governing equations and mathematical formulations for nano-PCM were discretised and solved by considering nano-additives enhanced paraffin in physical model II of shell and tube heat exchanger as computational domain. Transient numerical simulations considered the influence of natural convection, material of nano-additives, their concentration and particle size on phase transition rate, temperature distribution and overall enthalpy of LHS system.

4.2.2.1 Influence of nano-additives on thermo-physical properties

The impact of various concentrations of aluminium oxide (Al_2O_3), aluminium nitride (AlN) and graphene nano-platelets (GNP) nano-additives on thermo-physical properties were computed by implementing mathematical formulations for nano-PCM, as presented in **Table 4. 6**. The selected range of volume concentration of nano-additives were 1%, 2%, 3%, 4% and 5%.

Thermo-physical properties of nano-additives have significant influence on overall thermo-physical performance of nano-PCM samples. It was noticed that as the volume concentration of nano-additives were increased, the effective density of nano-PCM sample for Al_2O_3 and AlN nano-additives were increased due to relatively higher density of nano-additives as compared to base paraffin. However, due to smaller density of GNP nano-additives, the effective density of nano-PCM samples were reduced. In case of Al_2O_3 and AlN nano-additives samples with 5% volume concentration, the effective density of nano-PCM samples were increased by 20% and 18.57% as compared to base paraffin, respectively. Likewise, in case GNP, the effective density of nano-PCM samples with 5% volume concentration were reduced by 2.14% as compared to base paraffin. Due to constant volume of shell container, the overall weight of LHS system was increased with an increase in density of nano-PCM samples.

Moreover, the effective specific heat capacity and latent heat were significantly influenced by thermo-physical properties of nano-additives. It was noticed that with an increase in volume concentration of nano-additives, the specific heat capacity and latent heat of nano-PCM samples were reduced, as illustrated in **Table 4. 6**. The impact of Al_2O_3 and AlN nano-additives were more pronounced as compared to GNP. In case of Al_2O_3 and AlN nano-PCM samples with 5% volume concentration, both specific heat capacity and latent heat were reduced by a fraction of 20.82% and 19.87% as compared to base paraffin, respectively. However, an insignificant reduction of 2.91% were noticed for GNP based nano-PCM. Therefore, GNP based nano-PCM samples were recommended for light weight and higher thermal capacity applications.

Similarly, the effect of nano-additives material, volume concentration and particle size on effective dynamic viscosity and thermal conductivity of nano-PCM were examined, as presented in **Fig. 4. 13**. Dynamic viscosity and thermal conductivity are equally crucial to natural convection, phase transition rate, temperature distribution and overall

thermal performance of thermal storage material in LHS system. It was noticed that with inclusion of nano-additives, the effective dynamic viscosity and thermal conductivity were significantly improved as compared to base paraffin. However, due to relatively smaller particle size of GNP nano-additives, the enhancement in dynamic viscosity of GNP based nano-PCM samples were more significant as compared to Al_2O_3 and AlN based samples. Similarly, due to relatively higher thermal conductivity of GNP nano-additives, the enhancement in effective thermal conductivity was noticed to be higher as compared to Al_2O_3 and AlN based samples. However, an increase in dynamic viscosity have adverse effects on natural convection, which could weaken the significance of improved thermal conductivity on phase transition rate.

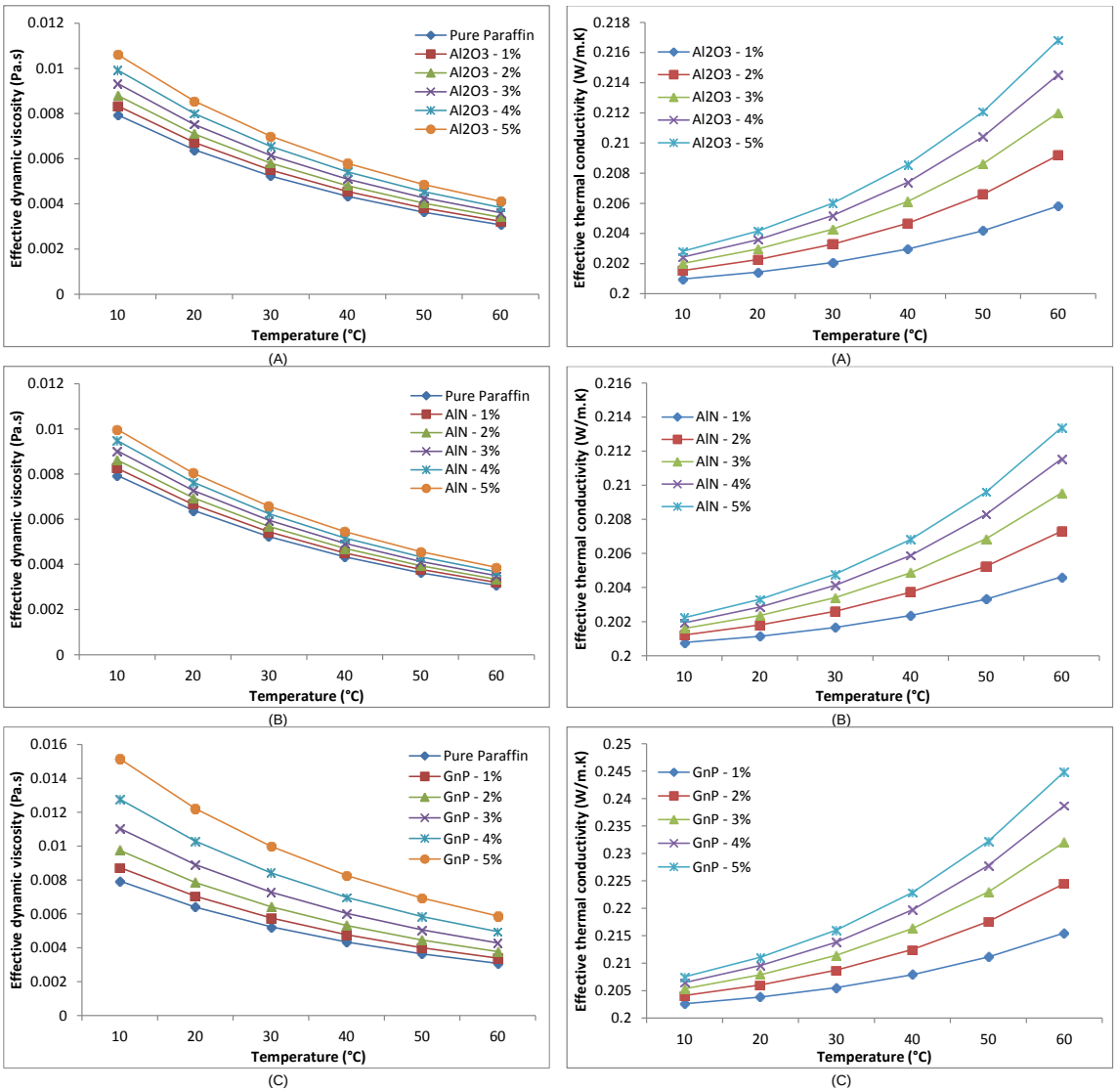

Fig. 4. 13 Influence of nano-additives and varied volume fractions on dynamic viscosity and thermal conductivity of nano-PCM samples (A) Al_2O_3, (B) AlN and (C) GNP (Khan, Z. and Khan, Z. A. 2018).

Table 4. 6 Impact of various concentrations of nano-additives on thermo-physical properties of nano-PCM

Volume of shell container (m^3)			0.0003		
Base material			**Paraffin (RT44HC)**		
Density of paraffin (kg/m^3) (Solid)			800		
Density of paraffin (kg/m^3) (Liquid)			700		
Specific heat capacity of paraffin (J/kg. K)			2000		
Latent heat (kJ/kg)			255		
Nano-additive material			**Al_2O_3**		
Density of nano-additive (kg/m^3)			3500		
Specific heat capacity of nano-additives (J/kg. K)			765		
Percent volume concentration	**1 %**	**2 %**	**3 %**	**4 %**	**5 %**
Density of nano-PCM (Solid)	827	854	881	908	935
Density of nano-PCM (Liquid)	728	756	784	812	840
Specific heat capacity (J/kg.K) (Solid)	1915.37	1836.08	1761.66	1691.66	1625.71
Specific heat capacity (J/kg.K) (Liquid)	1903.86	1814.84	1732.17	1655.21	1583.38
Latent heat (kJ/kg) (Solid)	244.207	234.098	224.608	215.682	207.272
Latent heat (kJ/kg) (Liquid)	242.740	231.388	220.848	211.034	201.875
Nano-additive material			**AlN**		
Density of nano-additive (kg/m^3)			3300		
Specific heat capacity of nano-additives (J/kg. K)			740		
Percent volume concentration	**1 %**	**2 %**	**3 %**	**4 %**	**5 %**
Density of nano-PCM (Solid)	825	850	875	900	925
Density of nano-PCM (Liquid)	726	752	778	804	830
Specific heat capacity (J/kg.K) (Solid)	1920.01	1844.72	1773.74	1706.70	1643.28
Specific heat capacity (J/kg.K) (Liquid)	1909.10	1824.49	1745.53	1671.68	1602.45
Latent heat (kJ/kg) (Solid)	244.800	235.200	226.149	217.600	209.514
Latent heat (kJ/kg) (Liquid)	243.409	232.620	222.551	213.134	204.307
Nano-additive material			**GNP**		
Density of nano-additive (kg/m^3)			400		
Specific heat capacity of nano-additives (J/kg. K)			643		
Percent volume concentration	**1 %**	**2 %**	**3 %**	**4 %**	**5 %**
Density of nano-PCM (Solid)	796	792	788	784	780
Density of nano-PCM (Liquid)	697	694	691	688	685
Specific heat capacity (J/kg.K) (Solid)	1989.96	1979.81	1969.57	1959.22	1948.76
Specific heat capacity (J/kg.K) (Liquid)	1988.53	1976.96	1965.30	1953.53	1941.65
Latent heat (kJ/kg) (Solid)	253.719	252.424	251.117	249.796	248.462
Latent heat (kJ/kg) (Liquid)	253.537	252.061	250.572	249.070	247.555

4.2.2.2 Thermal performance of nano-PCM samples

Prior to conducting transient thermal performance of nano-PCM samples in shell and tube heat exchanger as presented in physical model II, the base paraffin was initially simulated at various inlet temperatures of 47 ^{o}C, 52 ^{o}C and 57 ^{o}C to produce a reference line for comparison, as presented in **Fig. 4. 14**.

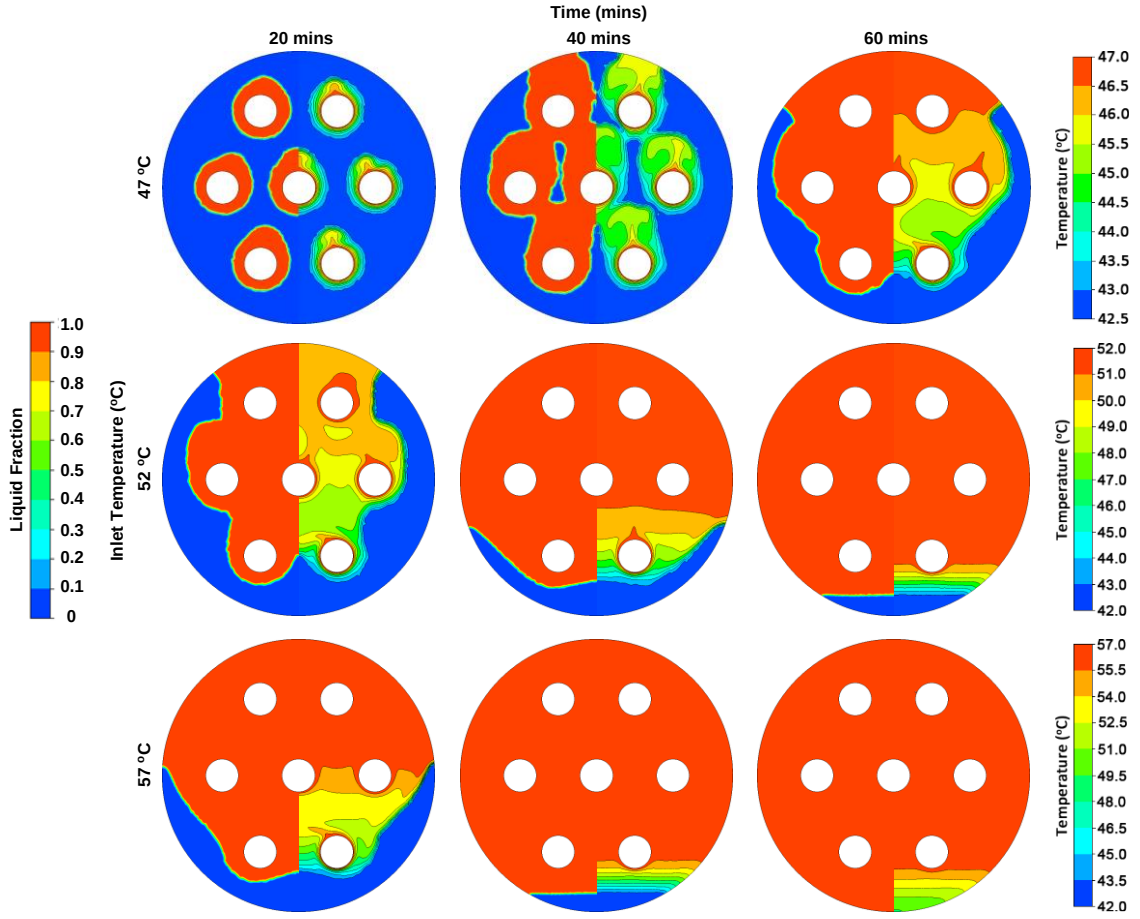

Fig. 4. 14 Melting fraction (left side) and temperature contours (right side) of base paraffin at various inlet temperatures in physical model II of shell and tube heat exchanger (Khan, Z. and Khan, Z. A. 2018).

During melting process, the heat transferred between HTF and paraffin in shell container was initially dominated by conduction heat transfer. Paraffin started melting around the surface area of HTF tubes. With an increase in melted fraction of paraffin around the HTF tubes, an upward rise of high temperature paraffin molecules were noticed and therefore, natural convection started dominating the heat transfer between HTF and paraffin in shell container. Due to upward rise of high temperature paraffin molecules, the phase transition rate of paraffin at top portion of shell container was relatively higher as compared to bottom portion, as illustrated by liquid fraction and

temperature contours in **Fig. 4. 14**. Moreover, it was observed that an increase in inlet temperature of HTF had significantly improved the phase transition rate and sensible portion of thermal energy storage. For instance, the phase transition rate was improved by a fraction of 56.96% and 72.60% as the inlet temperature of HTF was increased from 47 ^{o}C to 52 ^{o}C and 57 ^{o}C, respectively. Similarly, due to an increase in sensible portion of thermal energy, the overall enthalpy of system was improved from 299 kJ/kg to 309 kJ/kg and 310 kJ/kg, respectively.

After simulating pure paraffin in physical model II, the transient simulations of nano-PCM samples were conducted. **Fig. 4. 15** illustrate the influence of various volume concentrations of nano-additives on temperature contours and overall thermal storage enthalpy of LHS system. It was noticed that while charging at constant inlet temperature of 52 ^{o}C, the temperature contours for Al_2O_3, AlN and GNP based nano-PCM samples had presented a small variation. This was in contradiction to higher thermal conductivity of GNP based nano-PCM samples. However, the reason behind was the relatively higher dynamic viscosity of GNP based nano-PCM samples which weakened the influence of natural convection on phase transition rate and temperature distribution. As a result, the temperature distributions for all samples were presenting small variance. Whereas, due to relatively higher specific heat capacity, higher latent heat and lower density of GNP based nano-PCM samples, the total enthalpy of the samples were relatively higher as compared to Al_2O_3 and AlN based samples.

For controlled volume, the overall thermal storage capacity of LHS system would be reduced with an inclusion of nano-additives, due to occupancy of volume by nano-additives. Therefore, as compared to pure paraffin, the nano-additives enhanced samples would present a reduction in overall enthalpy of the system. The enthalpy of pure paraffin at 52 ^{o}C was recorded to be 309 kJ/kg. As presented in **Fig. 4. 16**, with an inclusion of 1% volume concentration of Al_2O_3, AlN and GNP nano-additives, the overall enthalpy of the system was reduced by 4.75%, 4.46% and 0.55% as compared to pure paraffin, respectively. Similarly, in case of 5% volume concentration, the reduction was noticed to be 20.58%, 19.64% and 2.88%, respectively.

To conclude, GNP based nano-additives were recommended for thermal performance enhancement due to their lower effective density, higher specific heat capacity, higher latent heat and higher overall enthalpy of LHS system. Also, it was observed that Al_2O_3

and AlN based nano-PCM samples had presented relatively higher phase transition rate as compared to pure paraffin, however due to significant increase in weight and reduction in thermal storage capacity, the widespread practical utilisation could be affected.

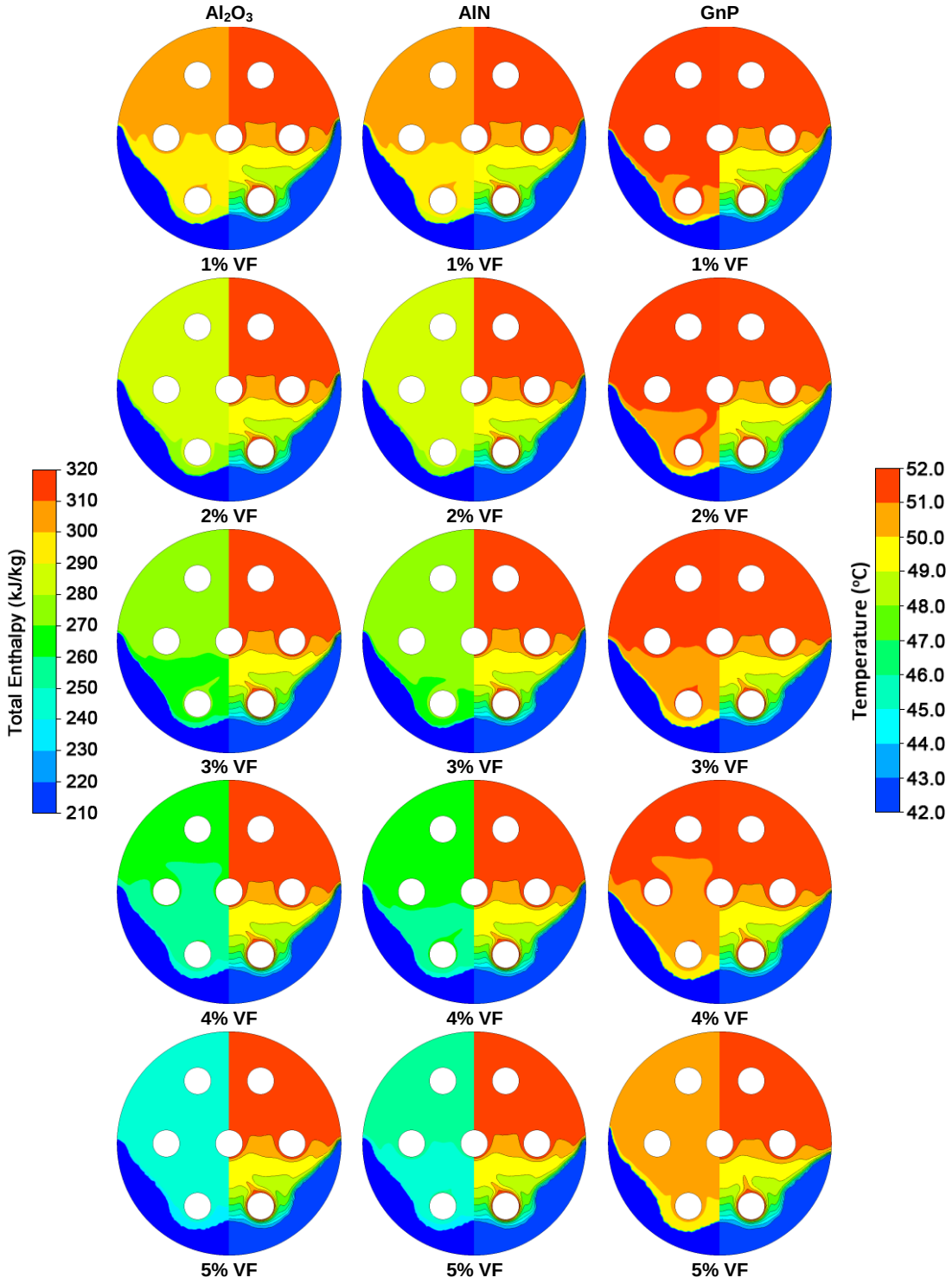

Fig. 4. 15 Total enthalpy (left side) and temperature contours (right side) of nano-PCM samples attained after charging for 0.5 h at constant inlet temperature of 52 °C (Khan, Z. and Khan, Z. A. 2018).

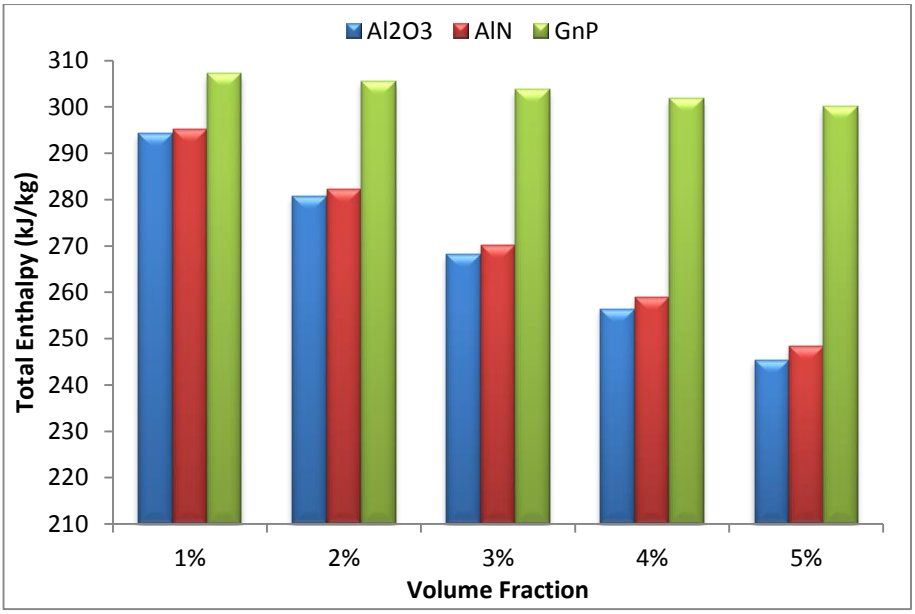

Fig. 4. 16 Impact of varying volume fraction of nano-additives materials on overall enthalpy of LHS system

4.2.3 Third stage: Coupled thermal performance enhancement with longitudinal fins and nano-PCM

In third stage, the proposed novel design solution for shell and tube heat exchanger (first stage) with nano-additives enhanced thermal storage material (second stage) was simulated to examine coupled thermal performance enhancement of LHS system. This section is discussed in detail in **Chapter 7**.

Chapter 5 Experimental methodology

This chapter discuss the details regarding experimental methodology adopted to examine the thermal performance enhancement of novel design solution for shell and tube heat exchanger and nano-additives enhanced paraffin based LHS system. Experimental methodology was divided into two stages. In first stage, based on numerical simulations conducted in chapter 4, the proposed novel design solution of shell and tube heat exchanger with multiple tubes passes and longitudinal fins was developed, commissioned and experimented at various operating conditions generated with a connection to flat plate solar collector. A series of charging and discharging cycles of paraffin in the novel design of shell and tube heat exchanger were experimented at varied operating conditions. In second stage, various samples of nano-additives enhanced paraffin were developed and experimented for enhanced thermal performance at varied operating conditions. This chapter summarises the literature that has been published in the articles: "Experimental investigations of charging/melting cycles of paraffin in a novel shell and tube with longitudinal fins based heat storage design solution for domestic and industrial applications" by (Khan, Z. and Khan, Z. A. 2017c) (refer to Appendix A – Paper IV), "An experimental investigation of discharge/solidification cycle of paraffin in novel shell and tube with longitudinal fins based latent heat storage system." by (Khan, Z. and Khan, Z. A. 2017b) (refer to Appendix A – Paper V) and "Experimental and numerical investigations of nano-additives enhanced paraffin in a shell and tube heat exchanger: a comparative study." by (Khan, Z. and Khan, Z. A. 2018) (refer to Appendix A – Paper VI).

5.1 First stage: Novel design solution of shell and tube heat exchanger

5.1.1 Testing room and experimental procedure

The proposed shell and tube heat exchanger based LHS system was developed and connected to flat plate solar collector to examine at various operating conditions in a testing room, as illustrated in **Fig. 5. 1**. The testing room was consisting of two sections. The two sections for flat plate solar collector and solar simulator to generate required temperature conditions and another section for thermal storage system were separated by an inner partition wall. The outer walls of testing room were built of strong and thick insulating boards to create controllable operating conditions and testing environments

for comparative analysis. Testing room was also equipped with ventilating fan to generate a free or forces convection environment over solar collector.

The schematic of experimental layout for charging and discharging cycles on paraffin in shell and tube heat exchanger is presented in **Fig. 5. 2**. The experimental setup was comprised of flat plate solar collector, solar simulators, latent heat storage tank, circulation centrifugal pump, connections to municipal/building water tank, flow meters, thermocouples and data acquisition unit with computer. LHS tank included shell and tube heat exchanger with paraffin as thermal storage material in shell container and water as HTF in tubes.

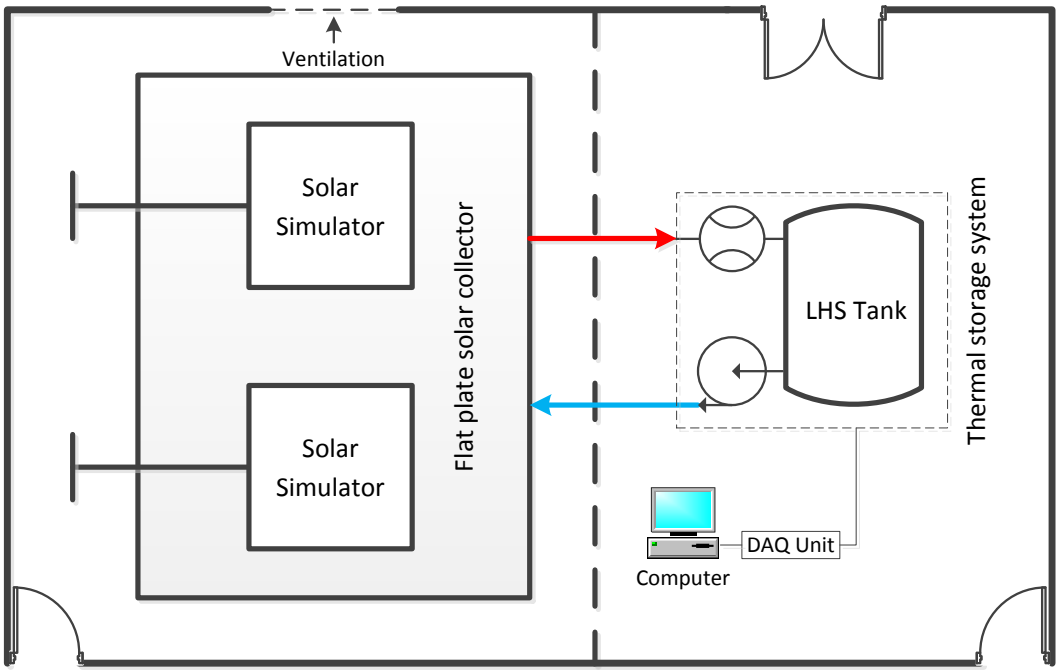

Fig. 5. 1 Schematic illustration of experimental setup in testing room

During charging cycles, the entire loop of tubes was initially filled up with water by connecting it to building water supply through control valve 1 and the water was drained out through control valve 4. Through this procedure, the air trapped in the tubes along the whole system loop was released by switching on air release valve (not mentioned in **Fig. 5. 2**) and also, a constant initial temperature of about 10 ^{o}C was generated, which provided a good baseline temperature for all experimental cycles. The drainage was stopped by turning off control valve 4 and subsequently, the water from building water tank was turned off by control valve 1. In order to start the charging cycle, control valve 2 and 3 were operated and adjusted to generate a required constant flow rate in range of 1.5 l/min to 3.0 l/min. Solar simulators were utilised to generate

radiations heat output which was converted into thermal energy and transferred into water in flat plate solar collector. High temperature water was then directed to pass through the tubes passes in LHS tank, where thermal energy was transferred to paraffin. The low temperature water at outlet of LHS tank was pumped back to flat plate solar collector. The close loop was operated until all thermocouples in LHS tank logged temperature readings higher than phase transition temperature of paraffin.

During discharging cycles, control valve 2 and 3 were switched off and control valve 1 and 4 were operated to direct low temperature water from building water tank through tube passes in LHS tank to extract thermal energy from paraffin. Flat plate solar collector and centrifugal pump remained idle during discharging cycle. Control valves 1 and 4 were adjusted to generate a required flow rate in range of 1.5 l/min to 3.0 l/min for discharging cycles. The low temperature water from building water tank were circulated in tube passes to extract thermal energy from paraffin and therefore, the high temperature water at outlet of LHS tank could be utilised for desirable practical applications. This open loop discharging cycle was operated until all thermocouples in LHS tank logged temperature reading lesser than phase transition temperature of paraffin and the temperature gradient between inlet and outlet temperature of water is less than 5 ^{o}C.

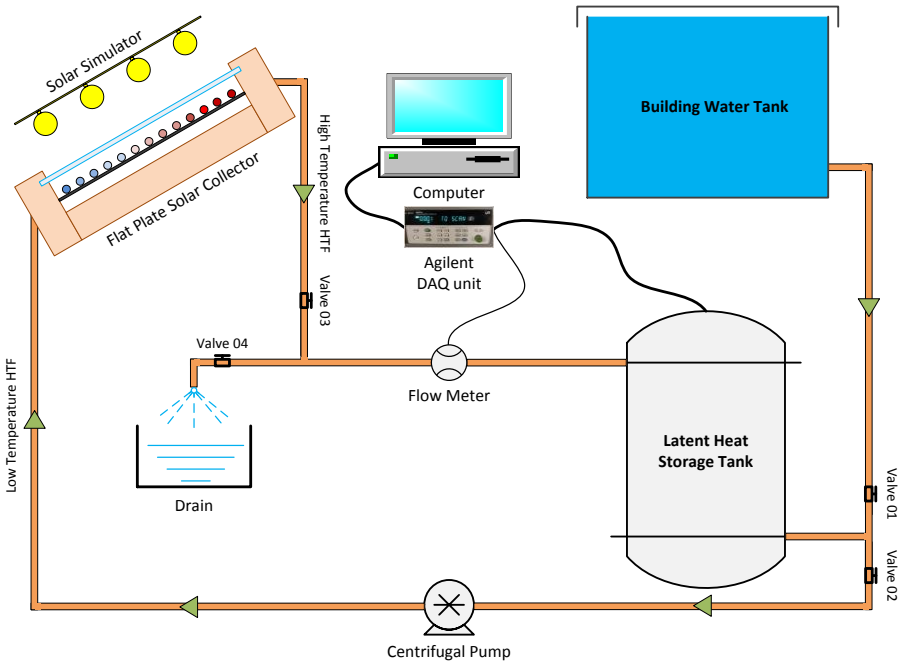

Fig. 5. 2 Experimental layout for conducting charging and discharging cycles of proposed LHS unit (Khan, Z. and Khan, Z. A. 2017c)

5.1.2 Thermal storage system components

The components comprising thermal storage system are detailed in this section.

5.1.2.1 Flat plate solar collector and solar simulator

The solar collector and simulator setup utilised in this research was previously designed, developed and commissioned with and without glazing configuration by (Wen, Z. 2016) and employed in ORC for generation of heat and electricity by (Helvaci, H. U. 2017). Solar collector was consisting of glazing cover, stainless steel absorber, serpentine copper tubing for water circulation system and insulation. Glazing cover was prepared from 2 mm thick transparent glass sheet for dampening convection and radiation heat losses from solar collector. Transmittance and emissivity of glazing cover were 0.9 and 0.92, respectively. Similarly, stainless steel S280 sheet of 1 mm thickness was employed as absorber and to attain higher absorptivity, the absorber sheet was painted to dark black surface. Absorptivity, emissivity and thermal conductivity of absorber sheet were 0.9, 0.9 and 50 W/m.K, respectively. Likewise, serpentine copper tubing was utilised for water circulation in solar collector to extract thermal energy from absorber sheet. Outer diameter, thickness and running length of copper tubing were 10 mm, 1 mm and 57.5 m, respectively. Moreover, Celotex sheets were used for insulating the back and sides of solar collector to reduce thermal losses. The thickness and thermal conductivity of insulating sheets were 100 mm and 0.022 W/m.K, respectively.

Solar simulator was employed to provide steady thermal energy to solar collector through radiations. It was consisting of two lightening machines with each of them equipped with six quartz-halogen lamps and each lamp was able to radiate 1 kW heat output. In order to identify an optimum distance of solar simulator from solar collector to cast constant radiations at each point on solar collector, a pyranometer was operated and a distance of 2 m was identified. Moreover, solar simulators had an inbuilt control system for adjusting required radiance heat output and operation time of experiment. Due to close loop operation of charging cycles, the outlet temperature of HTF from solar collector would consistently increase therefore, the solar simulators were manually operated to emit required heat output for sustaining constant outlet temperature of HTF from solar collector. The solar collector and solar simulator setup in testing room for generation of controllable operating conditions and testing environments is illustrated in **Fig. 5. 3**.

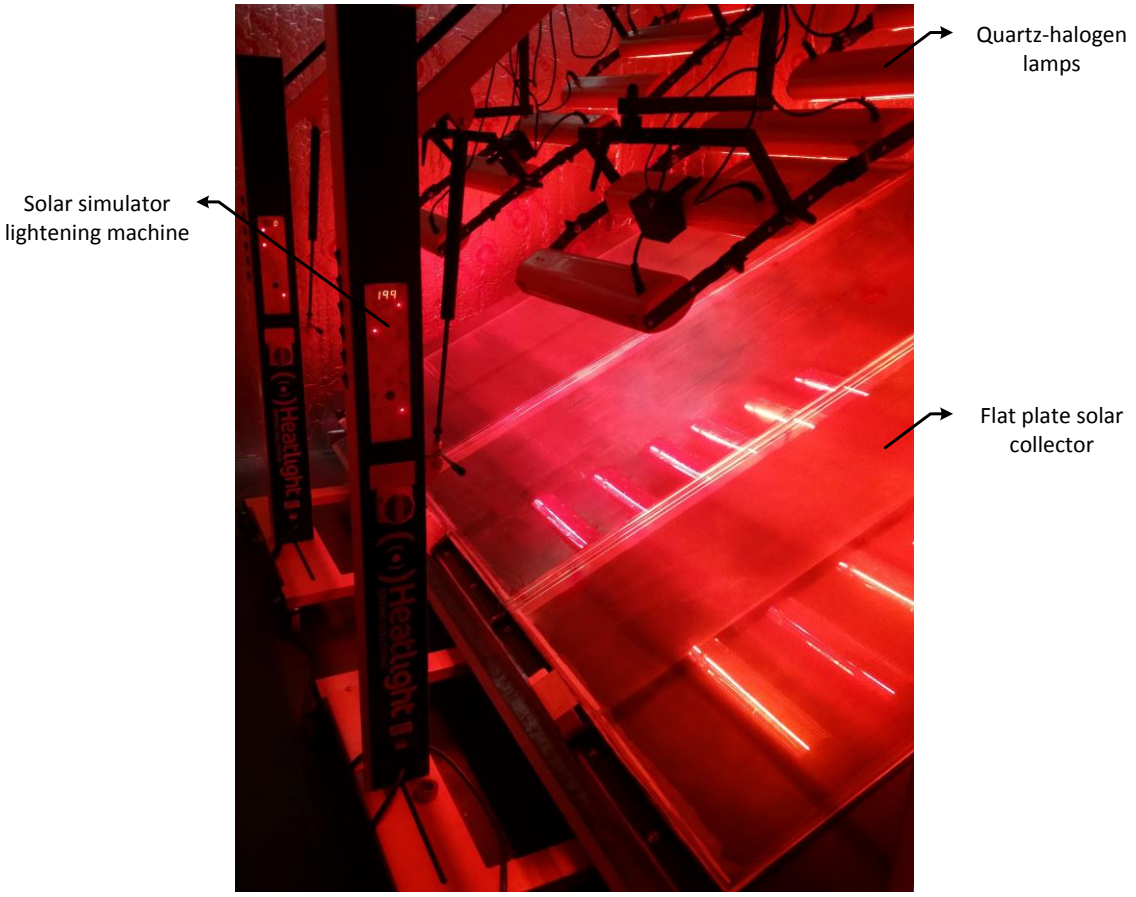

Fig. 5. 3 Pictorial representation of solar collector and solar simulator setup in testing room

5.1.2.2 Shell and tube heat exchanger

During charging cycles, the high temperature HTF from solar collector was directed to pass through tube passes in shell and tube heat exchanger to transfer thermal energy to paraffin in shell container. The proposed design of shell and tube heat exchanger with multiple passes and longitudinal fins (see **Fig. 3. 4**) was developed by implementing following steps:

Step 1: To begin with, the copper pipe with outer diameter and thickness of 22 mm and 1 mm was cut into 21 pieces, using pipe reamer, with each piece having a length of 1 feet. After that, a wooden mould was made to accurately hold the copper pipe and copper longitudinal fins for soldering, as illustrated in **Fig. 5. 4**. The length, thickness and height of longitudinal fins were 40 mm, 1.5 mm and 230 mm, respectively.

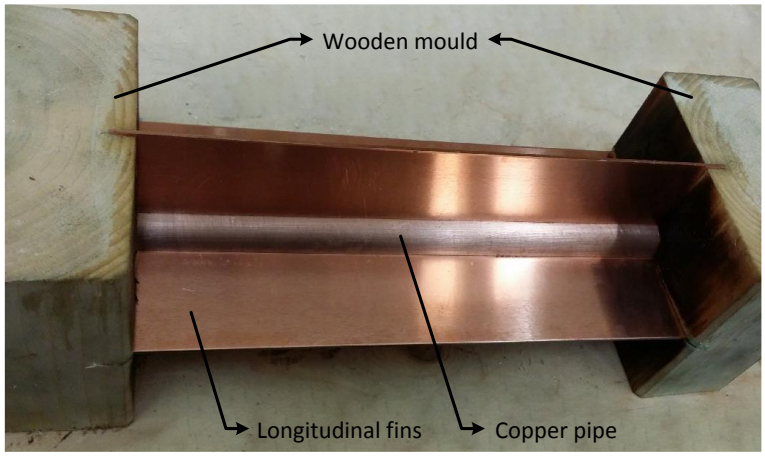

Fig. 5. 4 Step 1: Wooden mould to hold copper pipe and longitudinal fins at right accurate position

Step 2: In next step, the copper pipe and longitudinal fins were soldered using flux material to avoid oxidation, lead free wire (BS EN 29453) as filler and MAPP gas torch to bond both metals. Likewise, the fittings to link tube passes in shell container were carefully soldered to avoid any future leakages. Pictorial depiction of tube passes and fittings are given in **Fig. 5. 5**.

Soldered copper tube and longitudinal fins

Fittings to link tube passes

Fig. 5. 5 Step 2: Soldered copper tube with longitudinal fins and fittings to link tube passes

Step 3: The top view of proposed design of shell and tube heat exchanger was printed on a wooden frame and was precisely cut to accurately position tube passes before soldering the fittings to relevant tube passes. In such manner, the entire geometry of tube passes were linked through fittings, as presented in **Fig. 5. 6**.

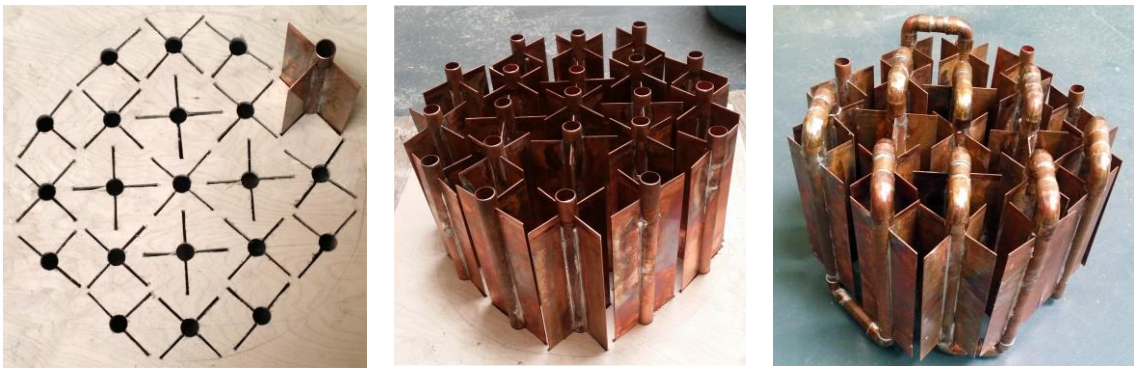

Fig. 5. 6 Step 3: Placement of tube passes in wooden frame and soldering fittings to create proposed tube passes pattern in shell container

Step 4: Finally, the tube passes and longitudinal fins geometry was placed in the shell container and connections to inlet and outlet were made, as presented in **Fig. 5. 7**. Shell container was made of copper with the outer diameter, thickness and height of 450 mm, 1 mm and 385 mm, respectively. The outer surface of shell container was properly insulated with chlorofluorocarbon-free envirofoam of 50 mm thickness to lessen thermal losses and reduce the influence of surrounding conditions.

Prior to pouring liquid paraffin in shell container, leak tests were conducted to examine any leakage as otherwise the thermo-physical properties of the system could be affected. Joints and elbows were given special attention due to their high prone to leakage. Air compressor was connected to inlet of LHS tank and both control valves 1 and 2 (see **Fig 5. 2**) were turned off to generate high pressure of 4 bar within tube passes. Foamy leak detector was applied to joints and elbows but no leakage was detected. Similarly, in order to cross examine, pressurised water was pumped into tube passes and was left for 48 hours to spot any leakage at the bottom of LHS tank. No leakage was detected in water leak test either. After leak tests, liquid paraffin (RT44HC) was poured in shell container. Due to density variation of liquid and solid phases of paraffin, the volume of paraffin slightly shrunk as it solidified. Shell container lid was placed and sealed to avoid heat losses and influence of ambient conditions on thermal performance of LHS system. Furthermore, the detailed specifications of shell and tube heat exchanger are illustrated in **Table 5. 1**.

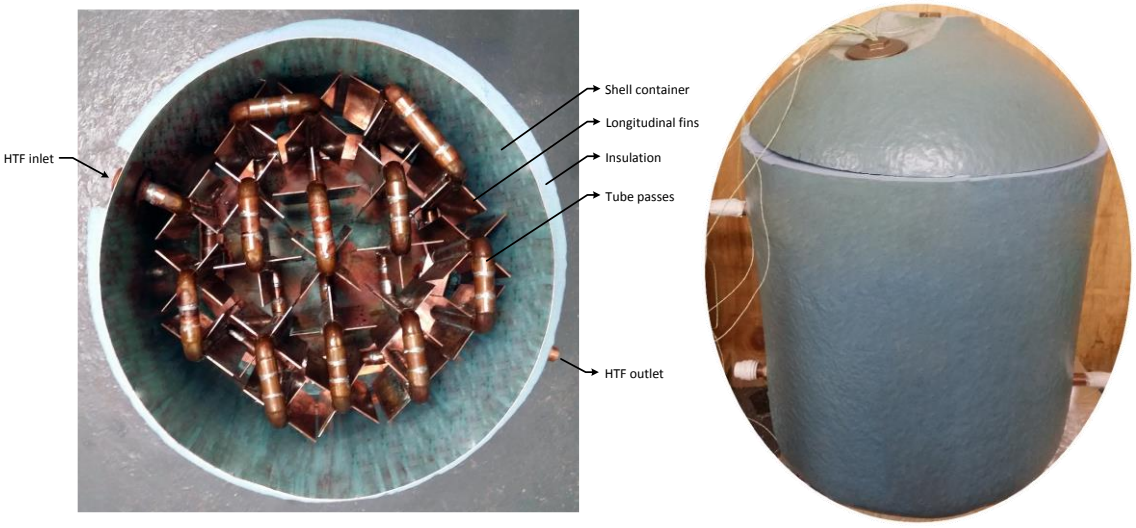

Fig. 5. 7 Step 4: Pictorial representation of developed proposed design of shell and tube heat exchanger.

Table 5. 1 Detailed specification of proposed design of shell and tube heat exchanger based LHS system (Khan, Z. and Khan, Z. A. 2017c)

Total volume of shell	V_S	60.7E+06	mm^3
Running length of tube		8.2	m
Volume occupied by tube	V_T	3.12E+06	mm^3
Surface area of longitudinal fins		1.43E+05	mm^2
Volume occupied by fins	V_F	1.05E+06	mm^3
Volume of LHS unit	$V_{LHS} = V_S - V_T - V_F$	56.5E+06	mm^3
Mass of paraffin		40	kg
Packing factor of PCM	$\frac{V_{PCM}}{V_{LHS}}$	0.824	solid
		0.942	liquid

5.1.2.3 Centrifugal pump

During charging cycles, the high temperature water as HTF at outlet of solar collector was directed to pass through the tube passes in shell and tube heat exchanger to transfer thermal energy to paraffin in shell container. Therefore, the temperature of water dropped as thermal energy was transferred to paraffin. In order to complete the charging cycles, a close loop operation was adopted to pump water back to solar collector to gain thermal energy and transfer it to paraffin in shell and tube heat exchanger. Centrifugal pump was employed to circulate water in the close loop operation of charging cycle, as presented in **Fig. 5. 8**.

Fig. 5. 8 Pictorial representation of centrifugal pump employed in charging cycle to circulate water between solar collector and LHS unit.

5.1.2.4 Measuring components and data acquisition system

In order to examine thermal performance of paraffin in LHS unit at varied flow rates, the experimental investigations were conducted by adjusting respective control valve (see **Fig. 5. 2**) during charging/discharging cycles to generate a required constant flow rate. Turbine flow meter (Titan FT2 Hall Effect) was installed to measure the constant flow rates, which had a flow range of 0.60 l/min to 10 l/min and accuracy of 1.0%, as illustrated in **Fig. 5. 9**.

Fig. 5. 9 Picture of Titan FT2 Hall Effect turbine flow meter

To examine thermal performance of paraffin in shell container during charging and discharging cycles, fifteen thermocouples were installed at five selected zones within shell container and at three vertical positions at each zone. Five selected zones were sections in shell container closer to inlet (A), centre (C), container boundaries (B and D) and outlet (E), as shown in **Fig. 3. 4**. Also, the three selected vertical positions were top,

central and bottom, which were at 115 mm distance to each other. Thermocouples were also installed at copper tube at inlet and outlet of LHS unit to record transient temperature response of HTF. Thermocouples used were K-type with an accuracy of ± 0.18%. Similarly, in order to measure irradiance on flat plate solar collector during charging cycles, pyranometer (Kipp & Zonen CMP3) was utilised, as presented in **Fig. 5. 10**. The spectral range of pyranometer was between 300 nm to 2800 nm and the ability to measure solar irradiance was up to 2000 W/m^2.

Fig. 5. 10 Photograph of Kipp & Zonen CMP3 pyranometer (Source: Kipp & Zonen)

Turbine flow meter and thermocouples data were recorded and logged in computer with a help of data acquisition unit (Agilent 34972A), as shown in **Fig. 5. 11**. Agilent software was operated in computer to record the flow rate and temperature data at time step of 10 s. Agilent data acquisition unit was also capable of measuring and converting various DC/AC volts, DC/AC currents and frequencies.

Fig. 5. 11 Agilent 34972A data acquisition unit.

5.2 Second stage: Nano-additives enhanced paraffin

In second stage of experimental methodology, the nano-additives enhanced paraffin samples were prepared and investigated at varied operating conditions in shell and tube heat exchanger.

5.2.1 Experimental procedure

In order to examine thermal performance of various nano-additives enhanced paraffin samples in an actual shell and tube heat exchanger, an experimental step was formulated as illustrated in **Fig. 5. 12**. Experimental setup included a water tank with electric heater, shell and tube heat exchanger, nano-additives enhanced paraffin samples as thermal storage materials, centrifugal pump for circulation of water, manual flow control valves, connections to building/municipal water supply and a versatile data acquisition system (VDAS) with computer. To reduce experimental time and cost, the flat plate solar collect and proposed shell and tube heat exchanger with longitudinal fins were replaced with water tank with electric heater and horizontal shell and tube heat exchanger with shell container volume of 300 ml. A digital temperature controller was operated to control electric heater in water tank for ensuring constant inlet temperature of water.

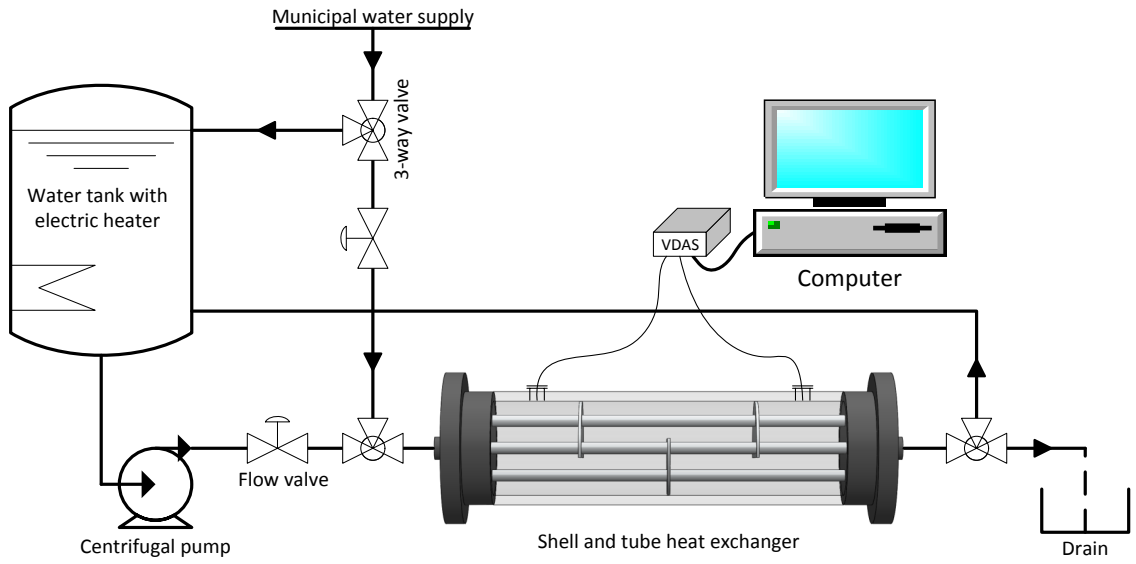

Fig. 5. 12 Schematic layout of experimental setup for second stage investigations of nano-PCM samples (Khan, Z. and Khan, Z. A. 2018)

Prior to conducting charging cycles, the municipal water was circulated in tubes to generate a constant initial temperature of nano-additives enhanced paraffin sample in

shell container and to produce a baseline for comparison. In meantime, the digital temperature controller for electric heater was set to required inlet temperature of water. As the required temperature in water tank was established, the centrifugal pump was turned on to circulate high temperature water from water tank to through the tubes of heat exchanger. Thermal energy was transferred from high temperature water in tubes to nano-additives enhanced paraffin samples in shell container. Water at outlet of heat exchanger was guided back to water tank to complete a close loop operation of charging cycles and to reduce electric heater cost. Similarly, the charging cycles were examined at three varied inlet temperatures of 47, 52 and 57 ^{o}C. Moreover, the manual operated control valves were regulated to create a required volume flow rate for charging cycles in the range of 1.5 l/min – 3 l/min. The charging cycles were completed with all thermocouples in shell container registering temperature value higher than phase transition temperature of paraffin.

Prior to discharging cycles, the initial temperature of paraffin samples were raised to maintain a constant temperature of 50 ^{o}C to produce a baseline for all discharging cycles. As illustrated in **Fig. 5. 12**, the 3-way valves were adjusted to exclude water tank with electric heater and centrifugal pump, and to direct the low temperature water flow from municipal through the tubes in heat exchanger to drain or could be used for desirable practical application. Low temperature water extracted thermal energy from paraffin samples in shell container and therefore, solidification of paraffin samples were started. This open loop operations of discharging cycles were completed once all thermocouples in shell container registered temperature values lesser than phase transition value.

5.2.2 Thermal storage system components

The components comprising thermal storage system in second stage are discussed in this section.

5.2.2.1 Nano-PCM samples preparation

To prepare a novel nano-additives enhanced paraffin for optimal thermal performance of LHS system, three groups of nano-additive materials were selected, which were aluminium oxide (Al_2O_3), aluminium nitride (AlN) and graphene nano-platelets (GNP). The suppliers and specifications of selected base material and nan-additives are given in **Table 5. 2**. Various samples of nano-additives were developed for experimental

investigations, as presented in **Table 5. 3**. To incorporate accurate concentration of nano-additives based paraffin samples, the required mass of nano-additives was computed from the following equation:

$$W_{np} = \left(\frac{\delta_{VF}}{100 - \delta_{VF}} \right) \left(\rho_{np} V_{pcm} \right) \times 10^3 \tag{5. 1}$$

Similarly, the volume of base material paraffin required for specific volume concentration sample was calculated using the following equation:

$$V_{pcm,r} = \left(V_{pcm} - \left(\frac{W_{np}}{\rho_{np} \times 10^3} \right) \right) \times 10^6 \tag{5. 2}$$

Table 5. 2 Materials suppliers and specifications (Khan, Z. and Khan, Z. A. 2018)

Materials	Dealers	Particle size	Purity
Paraffin (RT44HC)	Rubitherm Technologies GmbH		99.9%
Al_2O_3	EPRUI Nanoparticles and Microspheres Co. Ltd	30 - 60 nm	99.9%
AlN	Sigma-Aldrich Co. Ltd	<100 nm	99%
GnP	Ionic Liquids Technologies GmbH	6 - 8 nm	99.5%

Table 5. 3 Nano-PCM samples prepared for experimental tests (Khan, Z. and Khan, Z. A. 2018)

Sample	Nano-additives	Volume fraction	W_{np}: Mass of nano-additives added (g)	$V_{pcm,r}$: Volume of paraffin filled in beaker (ml)
A	Al_2O_3	1%	10.606	296.96
B	Al_2O_3	3%	32.474	290.72
C	Al_2O_3	5%	55.263	284.21
D	AlN	1%	10	296.96
E	GNP	1%	1.212	296.96

Upon equating the required volume of base material paraffin and mass of nano-additives for respective volume concentration sample, the ultrasonic emulsification technique was adopted to prepare nano-PCM sample, as illustrated in **Fig. 5. 13**.

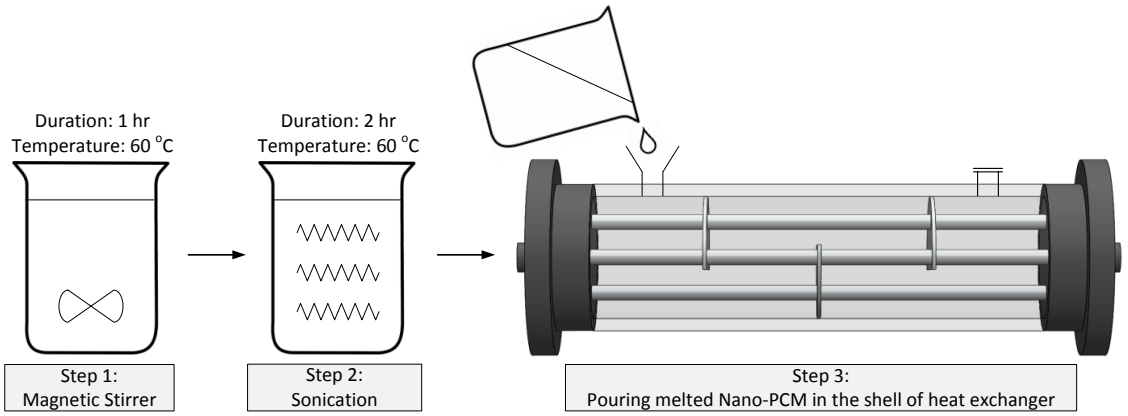

Fig. 5. 13 Schematic layout of steps followed during nano-PCM samples preparation and loading in shell and tube heat exchanger (Khan, Z. and Khan, Z. A. 2018)

In step 1, the volume of liquid paraffin was filled in beaker and the mass of nano-additives were added. A good suspension of nano-additive particles in base material paraffin was developed by subjecting the mixture to strong agitation using magnetic stirrer for 1 hour. Hotplate with stirrer (Stuart, model: US152) was used as magnetic stirrer, which had the stirrer speed ranging from 100-2000 rpm and the maximum hot plate temperature ranging up to 325 ºC. For each sample, the hot plate temperature was set to 75 ºC to ensure liquid phase of paraffin throughout the beaker.

In step 2, the complete dispersion of nano-additives particles in base paraffin was achieved by subjecting the mixture to magnetic stirrer and intensive ultra-sonication for 2 h. Ultrasonic process system (model: P100) was employed to disperse nano-additives particles in base paraffin, which had the operating frequency ranged from 20 kHz to 40 kHz. The pictorial representation of magnetic stirrer and sonication process of Al_2O_3 based nano-PCM is illustrated in **Fig. 5. 14**.

In step 3, the prepared sample of nano-additive based paraffin was poured in the shell container of heat exchanger to conduct series of charging and discharging cycles for thermal performance evaluation, as presented in **Fig. 5. 15**.

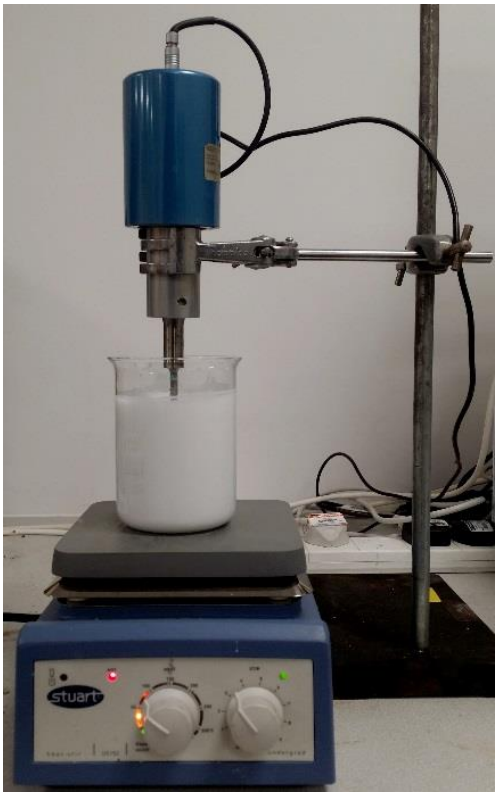

Fig. 5. 14 Pictorial illustration of magnetic stirrer and sonication processes of Al_2O_3 – 1% VF sample.

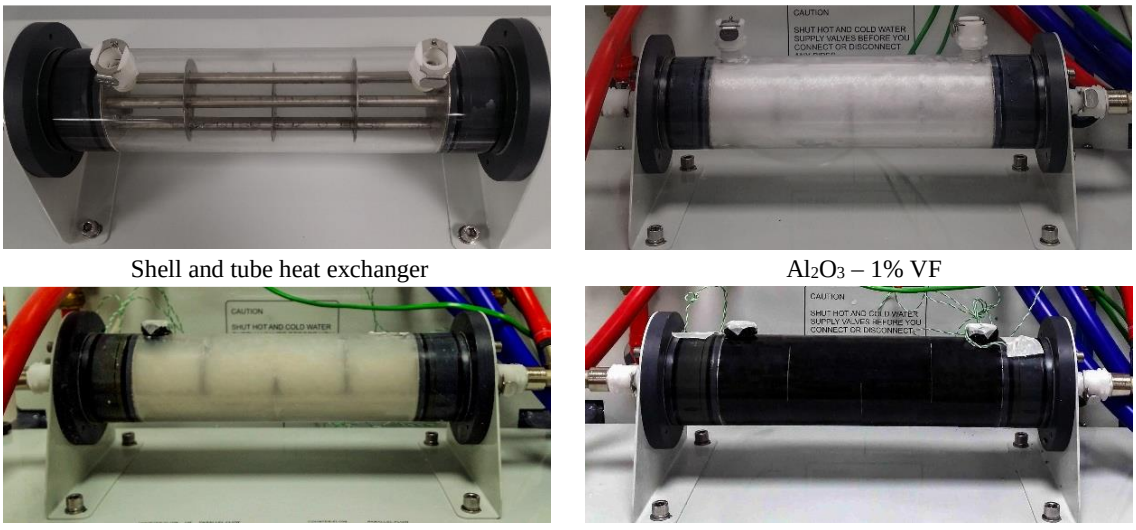

Shell and tube heat exchanger | Al_2O_3 – 1% VF

AlN – 1% VF | GNP – 1% VF

Fig. 5. 15 Pictorial illustration of shell and tube heat exchanger filled with various nano-additives samples

5.2.2.2 Shell and tube heat exchanger

In order to investigate thermal performance of nano-additives enhanced paraffin samples in an actual heat exchanger, the shell and tube heat exchanger with bundle of seven tubes were selected, as presented in **Fig. 5. 15**. The shell container was made of acrylic plastic thickness, length and outer diameter of 5 mm, 185 mm and 60 mm,

respectively. Likewise, the tubes were made of stainless steel with thickness and outer diameter of 1 mm and 6 mm, respectively. In ordered to minimise thermal losses to surrounding, the outer boundary of shell container was insulated with 50 mm thick glass wool. Liquid nano-PCM sample was poured in shell container whereas, water was utilised to circulate in tubes as HTF.

5.2.2.3 Measuring components and data acquisition system

During charging cycles, the hot water was circulated in close loop from water tank through the tubes in heat exchanger and returned back to water tank via centrifugal pump (Stuart Turner, model: PH 35 ES). The flow rate of inlet water during charging or discharging cycles was controlled by regulating flow control valves.

Similarly, the transient temperature response of nano-additives enhanced paraffin samples were recorded by installing four K-type thermocouples in shell container at two zones (A and B) and two vertical positions (top and bottom), as shown in **Fig. 3. 5 (B)**. Two selected zones in shell container were sections closer to inlet and outlet of heat exchanger and the vertical positioning of thermocouples were ± 24 mm from central position. Also, two thermocouples were attached to the inlet and outlet of heat exchanger to record transient temperature response of water.

To record transient temperature response and flow rate value, the data captured by sensors were transferred to computer via versatile data acquisition system (VDAS) (model: VDAS MKII). VDAS software was operated in computer to record temperature and flow rate readings at time step of 5 s. VDAS software was also capable of estimating thermal energy storage/retrieval from paraffin samples in shell container by water.

Chapter 6 Experimental results and discussions

This chapter provides detailed discussion on experimental results acquired from thermal performance enhancement of paraffin in novel design solution of shell and tube heat exchanger with multiple passes and longitudinal fins and nano-additives enhanced paraffin samples in shell and tube heat exchanger, as elaborated in previous chapter. In first stage, various charging and discharging cycles were experimented at varied operating conditions to understand and analyse the applicability of proposed LHS system in practical applications. Similarly, in second stage, the nano-additives enhanced paraffin samples were subjected to number of charging and discharging cycles at varied operating conditions to identify an optimal thermal performance. The influence of natural convection, operating temperatures and volume flow rates of water on phase transition rate, accumulative thermal energy storage/release, mean charge/discharge power and thermal distribution in paraffin in shell container were analysed and discussed. This chapter will give detailed understanding of how to adjust operating conditions to supply the required thermal energy demand. The content of this chapter has been published in the following articles: "Experimental investigations of charging/melting cycles of paraffin in a novel shell and tube with longitudinal fins based heat storage design solution for domestic and industrial applications" by (Khan, Z. and Khan, Z. A. 2017c) (refer to Appendix A – Paper IV), "An experimental investigation of discharge/solidification cycle of paraffin in novel shell and tube with longitudinal fins based latent heat storage system." by (Khan, Z. and Khan, Z. A. 2017b) (refer to Appendix A – Paper V) and "Experimental and numerical investigations of nano-additives enhanced paraffin in a shell and tube heat exchanger: a comparative study." by (Khan, Z. and Khan, Z. A. 2018) (refer to Appendix A – Paper VI).

6.1 First stage: Novel design solution of shell and tube heat exchanger

6.1.1 Charging cycles

During charging cycles, the solar simulator was operated to increase thermal energy of water in solar collector, which was then directed to flow through tube passes in shell and tube heat exchanger to transfer it to paraffin in shell container. Paraffin absorbed thermal energy from water and phase transition from solid to liquid occurred. Charging cycle was completed once entire mass of paraffin in shell container was melted and all

fifteen thermocouples in shell container registered temperature readings higher than phase transition temperature of paraffin. Thermal performance of paraffin in proposed shell and tube heat exchanger was investigated at varied range of inlet temperatures and volume flow rates, as illustrated in **Table 6. 1**. It was noticed from Reynolds number that turbulent flow was preferred due to better heat transfer performance over laminar flow. Flow rates of water ranged from 1.5 l/min to 3.0 l/min and were selected with an accordance to thermal performance of flat plate solar collector. Volume flow rates could not be increased more otherwise flat-plate solar collector would not perform effectively and the desired inlet temperature of water could not be achieved. Likewise, the range of inlet temperatures of water were selected while considering temperature gradient of 10, 15, 20 and 25 ^{o}C between inlet temperature of water and phase transition temperature of paraffin.

Table 6. 1 Range of experimental charging cycles conducted (Khan, Z. and Khan, Z. A. 2017c)

Set of experiments	Inlet temperature of HTF	Flow rate of HTF	Reynolds number
1-4	52, 57, 62, 67 ^{o}C	1.5 l/min	2950, 3200, 3450, 3700
5-8	52, 57, 62, 67 ^{o}C	2.0 l/min	4000, 4300, 4600, 4900
9-12	52, 57, 62, 67 ^{o}C	2.5 l/min	4950, 5350, 5750, 6150
13-16	52, 57, 62, 67 ^{o}C	3.0 l/min	5900, 6400, 6900, 7400

Prior to analysing and discussing experimental results, three repeatability tests were conducted at constant inlet temperature of 62 ^{o}C and volume flow rate of 1.5 l/min to examine the consistency of experimental results. Temperature profiles of paraffin at three vertical positions at zone C are illustrated in **Fig. 6. 1**. It was observed that phase transition time for paraffin at all three positions were almost identical, with a standard deviations of 0.008, 0.029 and 0.033 at top, central and bottom positions, respectively. Therefore, it was observed that the experimental results from repeatability tests were highly reliable and repeatable and similarly, the thermal performance of paraffin in shell and tube heat exchanger was indicating good thermal stability. Moreover, a slight variation in sensible portion of thermal energy storage was developed due to small variation in inlet temperature of water from solar collector.

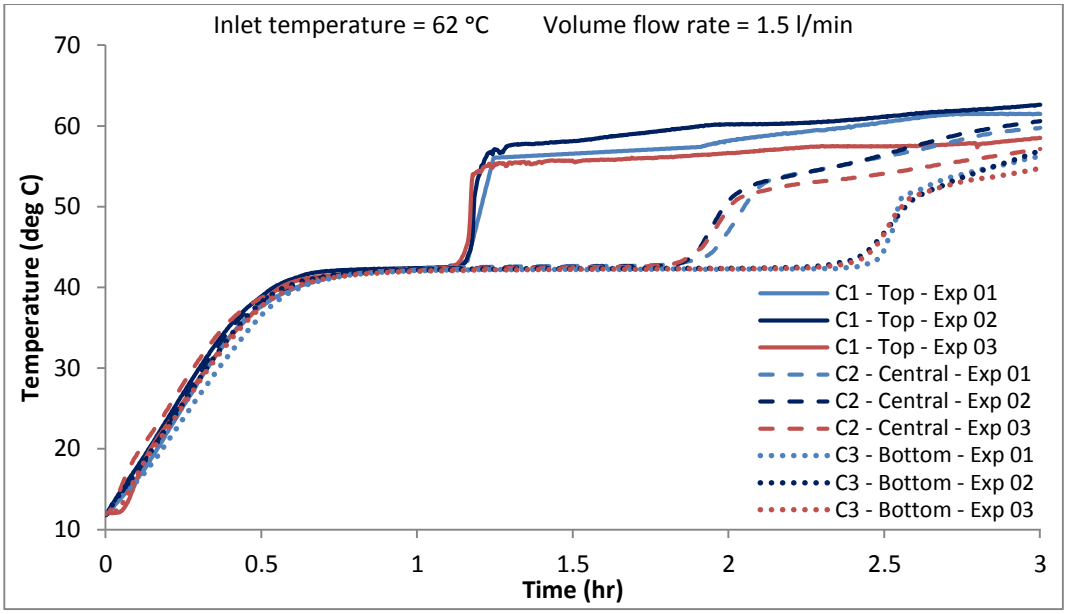

Fig. 6. 1 Transient temperature profiles of paraffin at three vertical positions at zone C while conducting repeatability tests at constant inlet temperature and volume flow rate (Khan, Z. and Khan, Z. A. 2017c).

6.1.1.1 Temperature distribution in shell container

A detailed examination of thermal distribution in paraffin in shell container was studied prior to conducting charging cycles at varying operating conditions. This examination was conducted to help understand the effective mode of heat transfer and phase transition rate at various zones and positions. Therefore, a charging cycle was conducted at inlet temperature of 62 ^{o}C and volume flow rate of 1.5 l/min and the transient temperature response from all fifteen thermocouples in shell container were recorded.

The pictorial representation of melting process of paraffin in shell container at various time intervals is shown in **Fig. 6.2**. It was observed that due to higher temperature gradient between inlet temperature of water and paraffin at inlet section (zone A) of shell container, the phase transition rate was significantly higher as compared to other zones. Thermal energy was transferred from water to paraffin as it was flowing through tube passes. Due to thermal energy transfer at inlet sections, the temperature of water at forthcoming sections of shell container were proportionately reducing. Therefore, due to relatively smaller temperature gradient at later sections in shell container, the phase transition rate was comparatively lower. It was noticed that after 1 hour of charging at constant inlet temperature, the paraffin at inlet sections (zone A and B) were indicating phase transition from solid to liquid or mushy state, whereas the later sections (zone C, D and E) were still in either solid or mushy state. Likewise, it was noticed that after 2

hours of charging, the paraffin at top positions in entire shell container were in liquid state. Moreover, it was noticed that paraffin adjacent to tube passes and longitudinal fins were rapidly melted due to proximity to heat transfer surface. With an increase in amount of liquid paraffin nearer to tube passes and longitudinal fins, the buoyant forces overcame viscous forces and consequently, an upward rise of paraffin molecules were observed. Temperature and density gradient between top and central/bottom positions strengthened buoyant forces to overcome viscous forces. Due to upward rise of liquid paraffin, natural convection became a dominant mode of heat transfer and influenced the rapid phase transition rate of paraffin at top position as compared to central and bottom position. The effect of natural convection on phase transition rate of paraffin at top positions across shell container was evident, as presented in **Fig. 6. 2**. Similarly, due to upward rise of high temperature paraffin molecules, the temperature of paraffin at top position was generally higher as compared to central and bottom positions. Additionally, due to smaller temperature gradient at bottom positions, the heat transfer rate was relatively weaker. For instance, the paraffin alongside shell boundaries were in either solid or mushy state even after charging for 3 hours. It was also noticed that vertical orientation of shell and tube heat exchanger with longitudinal fins significantly improved the effective heat transfer surface area and assisted natural convection without restricting liquid paraffin vertical movement.

Transient temperature response of paraffin registered during charging cycles by all fifteen thermocouples is presented in **Fig. 6. 3 (I)**. Due to conduction dominated heat transfer at start and a relatively smaller specific heat capacity as compared to latent heat capacity of paraffin, a linear rise in paraffin temperature from initial value of 10 ^{o}C to 40 ^{o}C was noticed. Therefore, the portion of sensible heat storage in solid phase was rapidly achieved. After sensible heat storage, the temperature profile indicated slower and gradual rise in paraffin temperature from 40 ^{o}C to 44 ^{o}C, which was influenced by a relatively higher latent heat capacity of paraffin. During latent heat storage, the phase transition from solid to mushy to liquid phase was observed. After completion of latent portion of heat storage, the paraffin temperature was instantly increased which indicated sensible heat storage in liquid phase. Moreover, it was observed from **Fig. 6. 3 (I)** that temperature of paraffin at top position in entire shell container was higher as compared to central and bottom positions. It was noticed that due to natural convection, the phase transition rate of paraffin at top position at zone C was significantly augmented by a

fraction of 65.21% and 113.04% as compared to central position and bottom position, respectively.

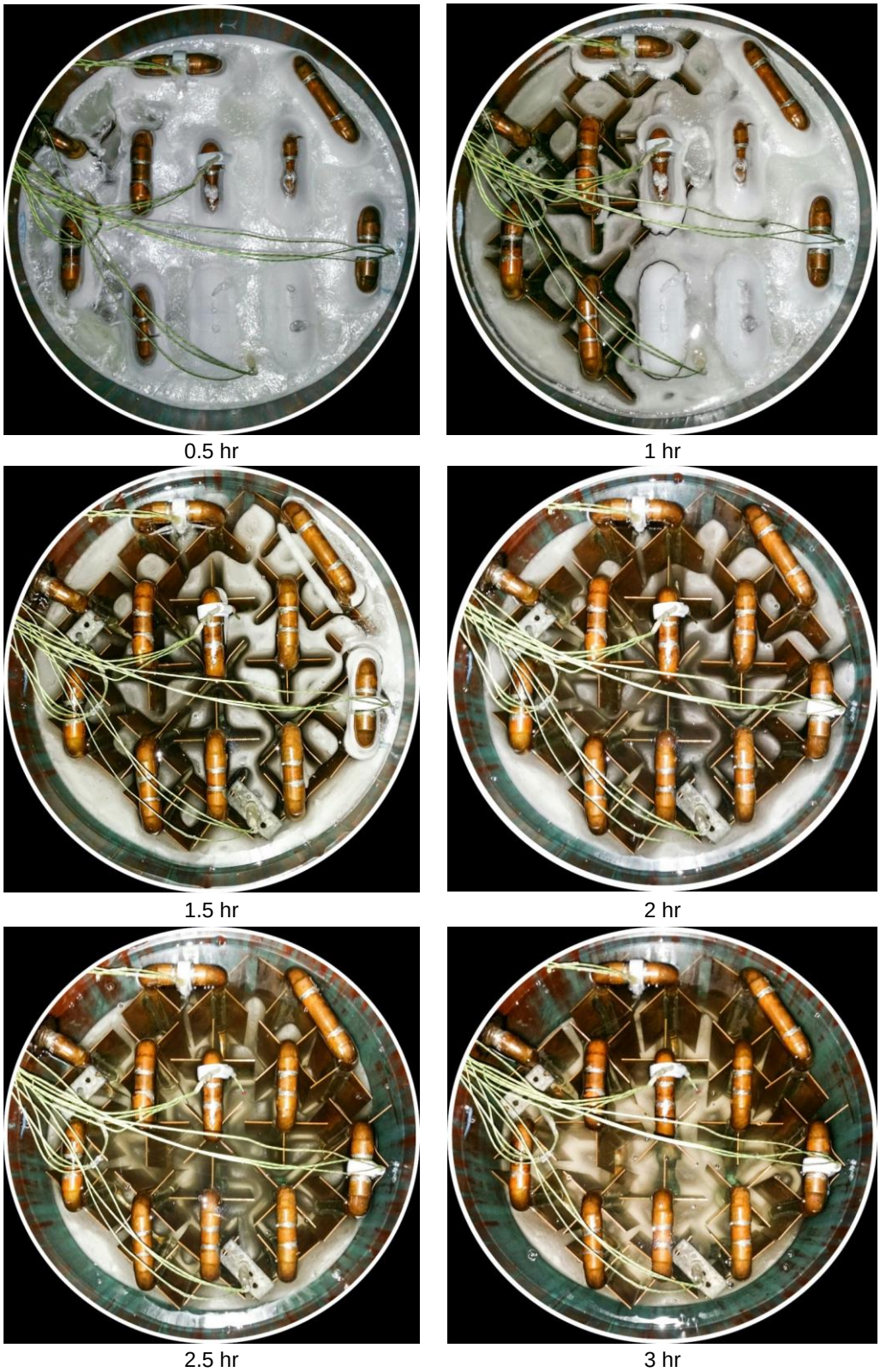

Fig. 6. 2 Pictorial depiction of melting process of paraffin in shell container while charging at inlet temperature of 62 ^{o}C and volume flow rate of 1.5 l/min (Khan, Z. and Khan, Z. A. 2017c).

6.1.1.2 Influence of inlet temperature on charging rate

The impact of weather fluctuations and solar off-peak hours on thermal performance of paraffin based LHS system was investigated by conducted experimental tests at four varied inlet temperatures of water. The selected range of inlet temperature of water was 52, 57, 62 and 67 ^{o}C, as presented in **Table 6. 1**. In this set of experiments, the volume flow rate of water was set constant to 1.5 l/min.

It was noticed from experimental results that due to an increase in inlet temperature of water, the temperature gradient between paraffin and water was improved and consequently, the heat transfer rate was augmented. Due to higher heat transfer rate between paraffin and water, the melting time for paraffin was significantly reduced. Transient temperature response of paraffin to various inlet temperatures of water was recorded by thermocouples installed in shell container, as presented in **Fig. 6. 3 (II)**. It was observed that due to relatively smaller temperature gradient, the phase transition rate of paraffin for inlet temperature of 52 ^{o}C was significantly low as compared to other inlet temperatures of water. It was noticed that due to an increase in temperature gradient by increasing inlet temperature from 52 ^{o}C to 57, 62 and 67 ^{o}C, the phase transition time of paraffin at top position at zone D was significantly increased by a fraction of 38.54%, 47.24% and 53.7%, respectively. Similar enhancement in phase transition rate was noticed for paraffin at central and bottom positions. Therefore, the overall average enhancement in phase transition rate of paraffin, due to an increase in inlet temperature from 52 ^{o}C to 57, 62 and 67 ^{o}C, was evaluated to be 22.83%, 39.04% and 50.08%, respectively.

Moreover, it was observed that the sensible heat storage in liquid paraffin was augmented with an increase in inlet temperature and consequently, the overall thermal storage capacity of LHS system was improved. Similarly, the thermal distribution in paraffin in shell container was relatively improved by increasing temperature gradient in all sections in shell container.

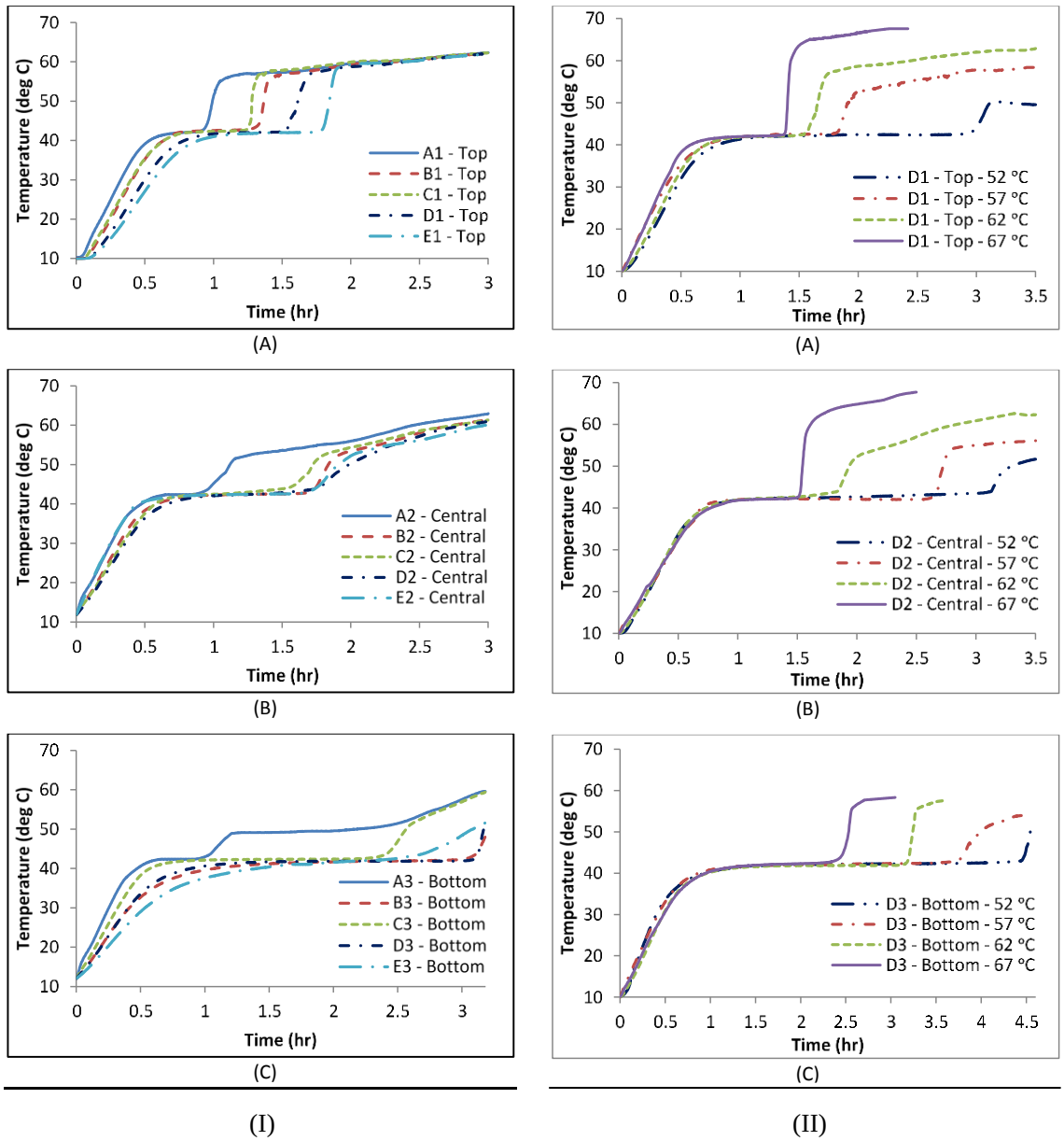

Fig. 6. 3 (I): Thermal distribution in shell container while charging at inlet temperature of 62 °C and volume flow rate of 1.5 l/min, (A) thermocouples installed at vertical top positions at all five zones, (B) central positions and (C) bottom positions. (II): Transient temperature profiles acquired from thermocouples at all three vertical positions at zone D while charging at constant flow rate of 1.5 l/min but four varied inlet temperatures such as 52, 57, 62 and 67 °C (Khan, Z. and Khan, Z. A. 2017c).

6.1.1.3 Influence of volume flow rate on charging rate

To examine the influence of operating volume flow rate of water on thermal performance of paraffin in proposed design of shell and tube heat exchanger, sixteen experimental tests were conducted at varying volume flow rate of 1.5, 2.0, 2.5 and 3.0 l/min, as presented in **Table 6. 1**. Transient temperature response of paraffin in shell container to varying volume flow rates of water are illustrated in **Fig. 6. 4**.

It was noticed that the sensible heat storage (an increase in paraffin temperature from 15 ^{o}C to 40 ^{o}C) was almost identical for the range of varying volume flow rates, however the influence on latent heat storage (an increase in paraffin temperature from 40 ^{o}C to 44 ^{o}C) was noticeable. The reason behind was that the initial phases of charging cycles were influenced by conduction heat transfer and due to low thermal conductivity of paraffin, the overall thermal resistance offered was hindering the rate of conduction heat transfer. Thus, an increase in volume flow rate had an insignificant impact on phase transition rate in earlier stages of charging cycles. However, due to formation of liquid paraffin, natural convection started dominating the heat transfer between water and paraffin. Likewise, due to an increase in volume flow rate, the turbulent nature of flow in tubes was augmented which resulted in an improved heat transfer coefficient. Thus, the phase transition rate of paraffin was improved with an increase in heat transfer rate. After completion of latent heat storage, the sensible heat storage in liquid phase of paraffin was again insignificantly influenced by varying volume flow rate.

As presented in **Fig. 6. 4 (A)**, the phase transition rate was enhanced by a fraction of 6.56%, 18.53% and 19.91% as the volume flow rate was increased from 1.5 l/min to 2.0, 2.5 and 3.0 l/min, respectively. Likewise, as illustrated in **Fig. 6. 4 (D)**, an enhancement of 19.24%, 21.65% and 30.98% was noticed with an increase in volume flow rate. Moreover, it was observed that with an increase in constant inlet temperature of water such as 62 ^{o}C and 67 ^{o}C, the influence of increasing volume flow rates on phase transition rates were becoming insignificant. The reason behind was that with an increase in constant inlet temperature of water, the temperature gradient between paraffin and water was increased which diminished the further enhancement due to varying volume flow rates. For instance, at constant inlet temperature of 67 ^{o}C, the phase transition rate of paraffin was enhanced by a fraction of 1.67%, 2.04% and 7.72% with an increase in volume flow rates from 1.5 l/min to 2.0, 2.5 and 3.0 l/min, respectively. To conclude, it was construed from experimental investigations that the phase transition rate of paraffin was significantly influenced by varying volume flow rates, however the influence was weakened with an increase in constant inlet temperature of water.

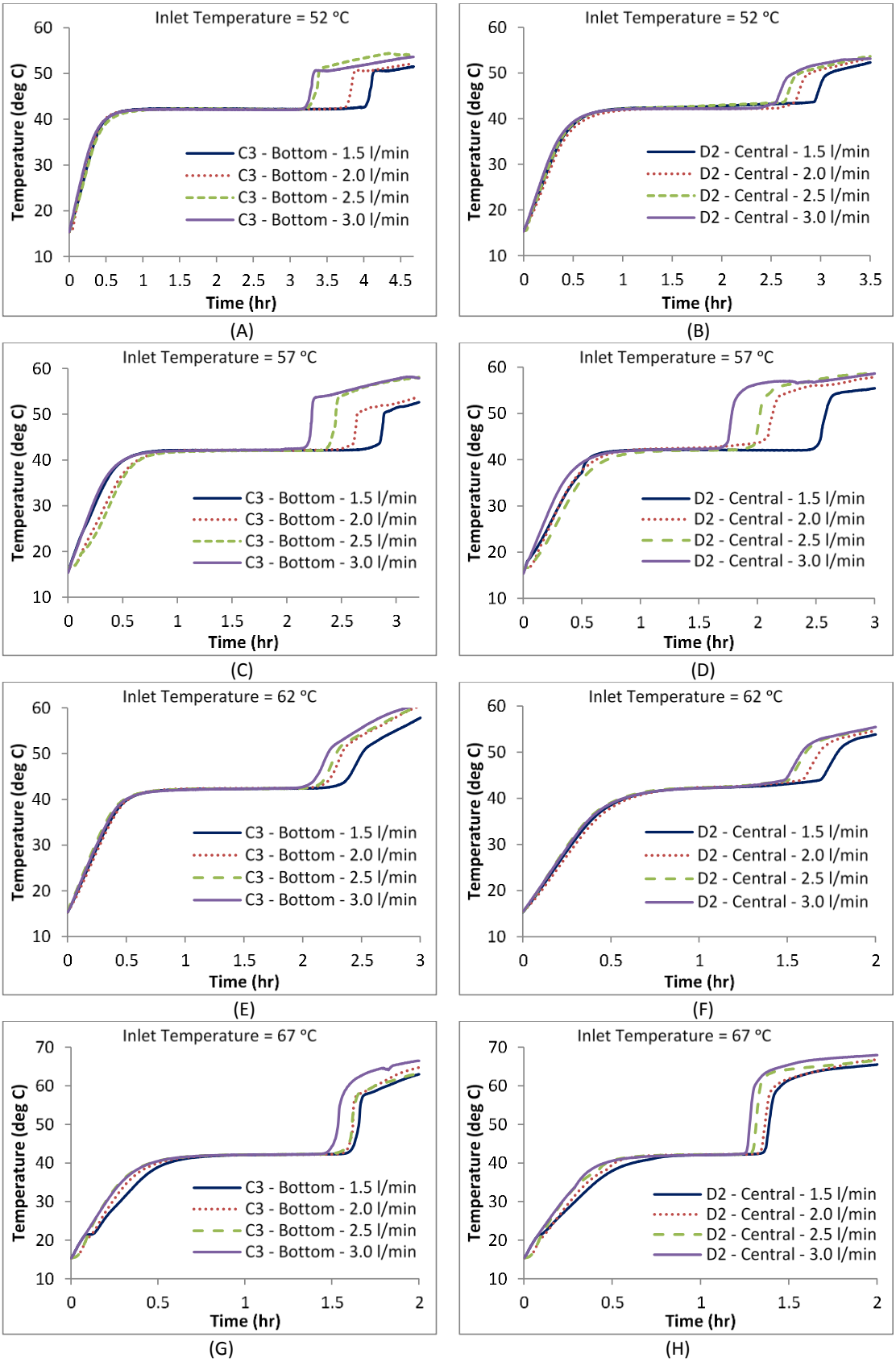

Fig. 6. 4 Transient temperature response of paraffin at bottom position at zone C and central position at zone D to varied volume flow rates and various constant inlet temperatures of water (Khan, Z. and Khan, Z. A. 2017c).

6.1.1.4 Mean charging power

Thermal performance of paraffin based shell and tube heat exchanger was evaluated by calculating mean charging power at various operating conditions. The mean charging power was estimated from change in enthalpy of water at inlet and outlet of LHS unit. Thermocouples installed at inlet and outlet of LHS unit registered the temperature readings for charging cycles. Accumulative thermal energy storage Q_s by paraffin was estimated by computing a subsection integral method which incorporated variations in density, specific heat capacity and temperature of water at inlet and outlet of LHS unit, as follow:

$$Q_s = \sum \dot{V} \left(\frac{\rho_{in} + \rho_{out}}{2} \right) \left(\frac{C_{p,in} + C_{p,out}}{2} \right) \left(T_{HTF,in} - T_{HTF,out} \right) \Delta t \quad (6.1)$$

where $Q_s, \dot{V}, \rho, C_p, T_{HTF}$ and Δt represented total thermal energy storage (kJ), volume flow rate of water (m^3/sec), density of water (kg/m^3), specific heat capacity of water (kJ/kg.K), temperature of water (^oC) and time interval (sec) at which temperature data was registered by thermocouples. Moreover, the mean charging power P_c was calculated using the following equation:

$$P_c = \frac{Q_s}{t_c} \quad (6.2)$$

where P_c and t_c represented the mean charging power (kW) and total time lapsed for completing charging cycle.

Impact of varying operating conditions on mean charging power were analysed by fixing constant initial temperature and mass of paraffin in LHS unit. As illustrated in **Fig. 6. 5**, the mean power was significantly influenced by an increasing inlet temperature. The reason behind was an increase in temperature gradient which resulted in a higher heat transfer rate and therefore, the mean charging power was significantly enhanced. It was observed that for a constant volume flow rate of 1.5 l/min, the mean charging power was enhanced by a fraction of 14.82%, 59.28% and 69.71% with an increase in inlet temperature from 52 ^oC to 57, 62 and 67 ^oC, respectively. In the same manner, an increase in volume flow rate demonstrated a noticeable enhancement in mean charging power. However, mean charging power enhancement due to increasing volume flow rate was relatively moderate as compared to increasing inlet temperature.

For instance, at constant inlet temperatures of 52, 57, 62 and 67 ^{o}C, the mean charging power was improved by a fraction of 16.28%, 24.39%, 10.94% and 7.19% with an increase in volume flow rate from 1.5 l/min to 2.0 l/min, respectively.

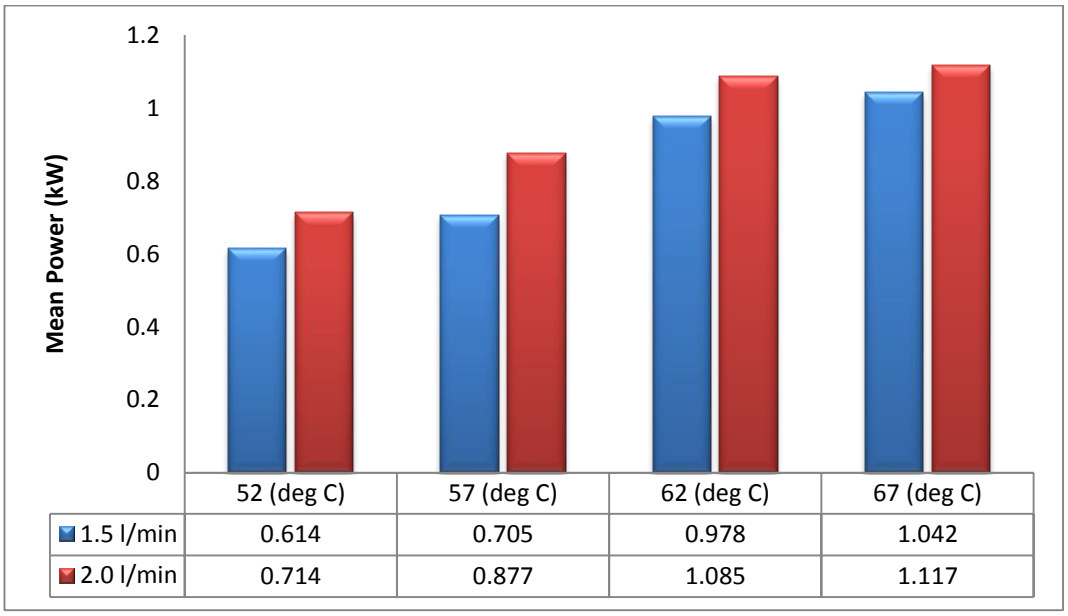

	52 (deg C)	57 (deg C)	62 (deg C)	67 (deg C)
1.5 l/min	0.614	0.705	0.978	1.042
2.0 l/min	0.714	0.877	1.085	1.117

Fig. 6. 5 Mean charging power of LHS unit at varied inlet temperatures and volume flow rates (Khan, Z. and Khan, Z. A. 2017c)

6.1.2 Discharging cycles

During discharging cycles, the flat plate solar collector and centrifugal pump remained inactive and the low temperature water from municipal/building water tank was directed to circulate through the tube passes in heat exchanger and extract thermal energy from paraffin in shell container. High temperature paraffin in shell container released thermal energy to low temperature water flowing in tubes passes and consequently, a phase transition of paraffin from liquid to solid was commenced. Also, the low temperature water gained thermal energy from paraffin and thus, a high temperature water at outlet of LHS unit was collected. As illustrated in **Fig. 5. 2**, the control valves 2 and 3 were turned off and control valves 1 and 4 were turned on to generate an open loop operation of discharging cycles. Control valves 1 and 4 were regulated to produce a required volume flow rate in the range of 1.5 l/min to 3.0 l/min. Similarly, the thermal performance of paraffin during discharging cycles were investigated by conducting experimental tests at three varied inlet temperatures of 5 ^{o}C, 10 ^{o}C and 15 ^{o}C.

In order to provide a good baseline for comparison of discharging cycles at varied operating conditions, the discharging cycles were initiated once all thermocouples

installed at top positions in shell container were registering paraffin temperature value equal to 62 ^{o}C. Moreover, the discharging cycles were completed when all thermocouples registered temperature values lesser than phase transition temperature of paraffin and the temperature gradient between inlet and outlet of water was smaller than 5 ^{o}C.

6.1.2.1 Temperature distribution in shell container

Prior to conducting discharging cycles of paraffin in proposed shell and tube heat exchanger with longitudinal fins at varied operating conditions, a discharging cycle was conducted at inlet temperature of 10 ^{o}C to examine and analyse the temperature distribution in shell container and help understand the dominant mode of heat transfer, development of solidification front and phase transition rate of paraffin at various zones in shell container.

The pictorial illustrations of solidification front movement of paraffin in shell container at various time intervals during discharging cycles at inlet temperature of 10 ^{o}C, as presented in **Fig. 6. 6**. It was noticed that due to higher temperature gradient between low temperature water in tube and high temperature paraffin in shell container, the formation of solidified layer around tube passes and longitudinal fins were more prominent. It showed that the higher heat transfer rate at initial stages discharged the sensible and latent portion of thermal energy from paraffin closer to tube passes and longitudinal fins to water in tubes, as shown at time interval of 0.25 h. In shell container, the transparent portion represented liquid paraffin and white layers around tube passes and longitudinal fins represented solidified paraffin. Likewise, it was noticed that due to relatively higher temperature gradient at inlet section (zone E), the phase transition rate from liquid to solid phase was more prominent and therefore, the thickness of solidified layers across longitudinal fins were comparatively thicker than other section in shell container. At time interval of 0.75 h, it was noticed that paraffin at top position in entire shell container was in mushy phase whereas, the paraffin in between longitudinal fins remained in liquid phase due to low thermal conductivity of solidified layer of paraffin across longitudinal fins and tube passes. Unlike charging cycles, natural convection had minimal influence on solidification front movement in discharging cycles. Conduction heat transfer dominated discharging cycles. It was noticed that after conducting discharging cycle for 1 h, the mass of paraffin at top position at central section (zone C) in shell container was completely solidified whereas,

the rest of the sections in shell container illustrated mushy phase. The reason behind higher phase transition rate of paraffin at central section (zone C) in shell container was due to the presence of closely packed longitudinal fins, which augmented the conduction heat transfer rate and phase transition rate. Finally, at time interval of 1.25 h, the paraffin at top positon at all sections in shell container had completely discharged latent portion of thermal energy to water in tubes and had transformed from liquid to solid phase.

The transient temperature response of paraffin to discharging cycle was registered by thermocouples installed in shell container. An average of temperature profiles registered by thermocouples installed at top, central and bottom position for each zone is illustrated in **Fig. 6. 7**. It was observed that due to higher temperature gradient at inlet section (zone E), the phase transition rate was higher for paraffin at zone E and compared other zones. It was noticed that the sensible portion of thermal energy at all zones in shell container were discharge at equal rate whereas, the latent portion of thermal energy was discharged at higher rate at sections closer to inlet section (zone E) and followed by central section (zone C) and outlet section (zone B and zone A). Temperature gradient between water in tubes and paraffin in shell container was reduced as the water flows in tube passes. The reason behind was the extraction of thermal energy from paraffin and consequent rise in the temperature of water as the flow progresses in tube passes. Therefore, the heat transfer rate was effected and the phase transition rate of paraffin was relatively reduced at outlet section (zone A) in shell container. As latent portion of thermal energy was completely discharged, the paraffin temperature was instantly declined due to smaller sensible portion of thermal energy.

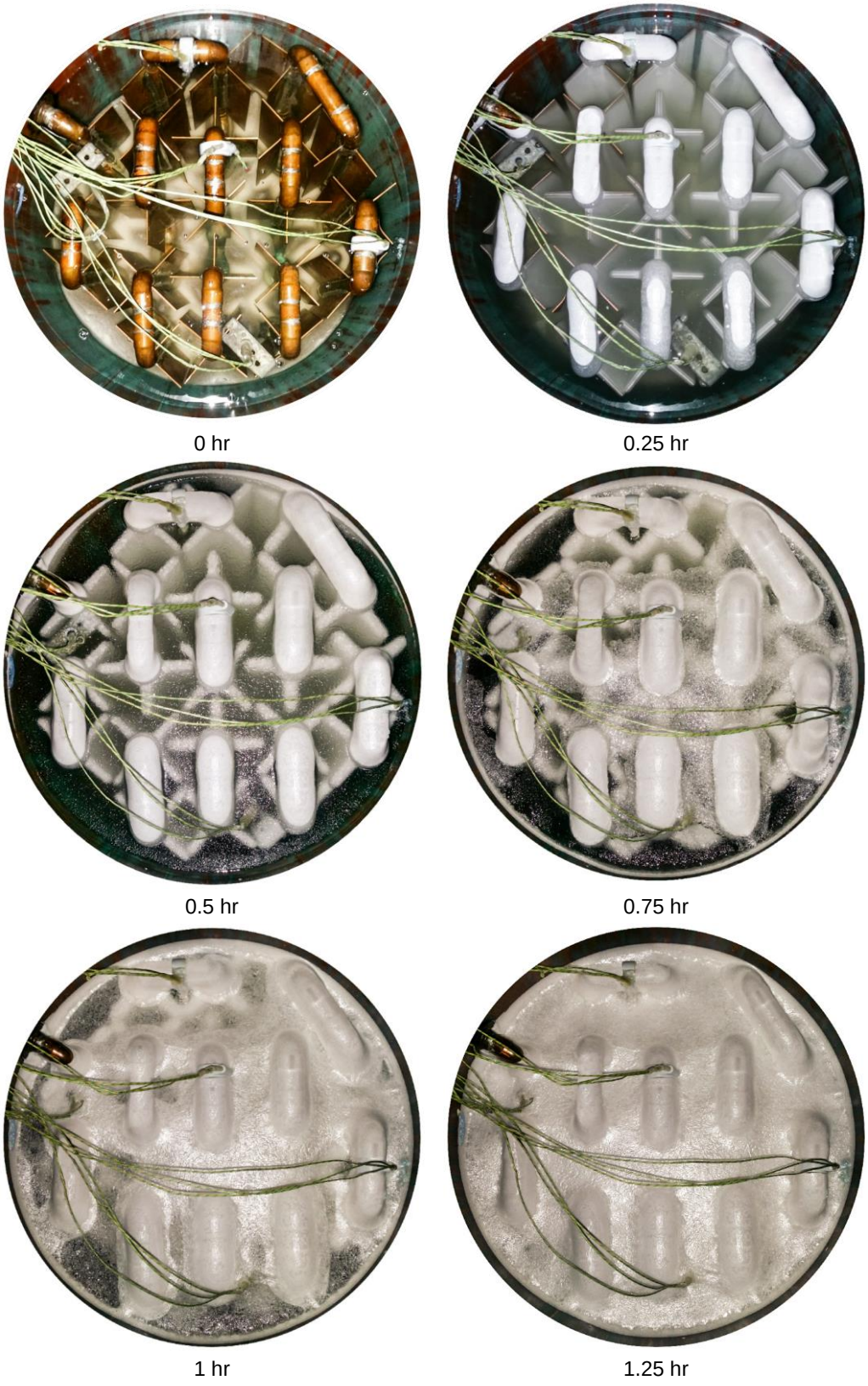

Fig. 6. 6 Pictorial illustration of solidification front of paraffin in shell container at various time intervals during discharging at inlet temperature of 10 ^{o}C and volume flow rate of 1.5 l/min (Khan, Z. and Khan, Z. A. 2017b).

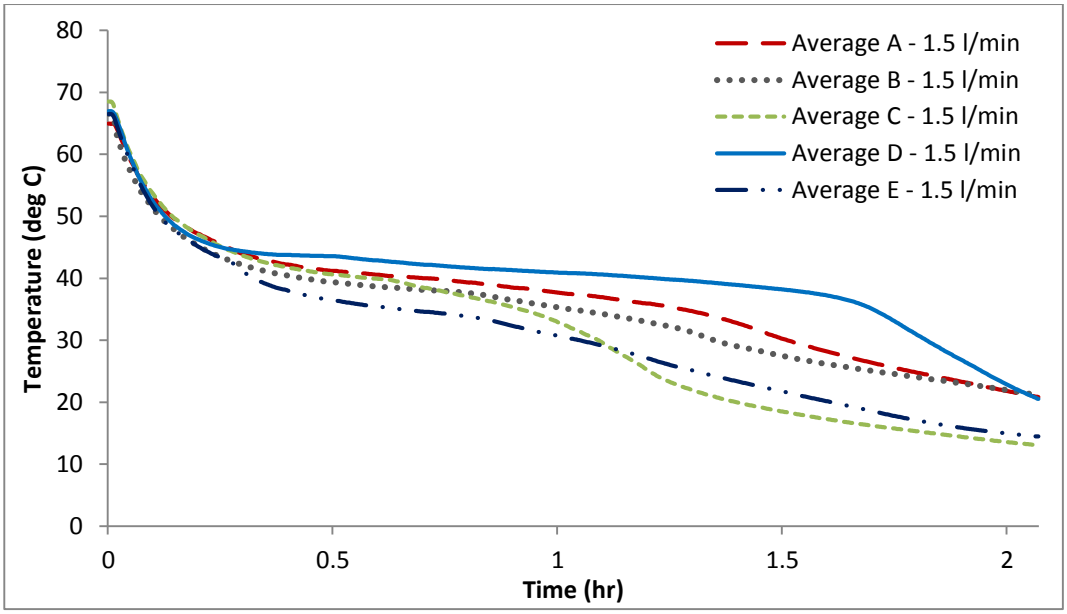

Fig. 6. 7 Average temperature profiles of three vertically installed thermocouples at each of five zones while discharging at inlet temperature of 10 °C and volume flow rate of 1.5 l/min (Khan, Z. and Khan, Z. A. 2017b).

6.1.2.2 Influence of inlet temperature on discharging rate

To investigate thermal response of paraffin in proposed design of shell and tube heat exchanger to discharging cycles at varied operating conditions, three inlet temperatures of water were examined: 5 °C, 10 °C and 15 °C. However, the volume flow rate of inlet water was kept constant to 1.5 l/min. Transient thermal response of paraffin to discharging cycles at varied operating conditions were recorded by thermocouples installed at three vertical positions and five zones across shell container and plotted against time interval in **Fig. 6. 8**. During discharging cycles, water was circulated in tube passes and thermal energy was extracted from paraffin in shell container and therefore, the outlet water temperature was increased. Transient variations in outlet water temperature for discharging cycles at varied operating temperatures are illustrated in **Fig. 6. 8 (H)**.

Similar to charging cycles, the phase transition rate of paraffin during discharging cycles were significantly influenced by varied inlet temperatures of water. It was noticed that sensible portion of thermal energy discharge by paraffin in shell container to varied inlet temperature of water in tube was identical. However, the latent portion of thermal energy discharge was significantly influenced by varied inlet temperature of water. It was observed that the total solidification time for paraffin in shell container at

top position at outlet section (zone A) was significantly decreased as the temperature gradient was increased by decreasing inlet temperature of water from 15 ^{o}C to 10 ^{o}C and 5 ^{o}C. Total solidification time of paraffin at top position at zone A was 1.38 h for inlet temperature of 15 ^{o}C, as shown in **Fig. 6. 8 (A)**. Total solidification time was reduced by a fraction of 9.01% and 17.43% as the inlet temperature was reduced from 15 ^{o}C to 10 ^{o}C and 5 ^{o}C, respectively. Furthermore, the sensible thermal energy discharge after solidification showed a rapid decline in paraffin temperature.

Paraffin at central position along vertical axis had experienced higher phase transition rate as compared to top and bottom position. This reason behind was the congestion and proximity of longitudinal fins to paraffin at central position. It was noticed that the total solidification time for paraffin at central position at zone B was reduced from 1.06 h to 0.88 h and 0.76 h as the inlet temperature was reduced from 15 ^{o}C to 10 ^{o}C and 5 ^{o}C, respectively (see **Fig. 6. 8 (B)**). Likewise, the total solidification time of paraffin at central position at zone D was reduced by a fraction of 23.58% and 48.11%, respectively (see **Fig. 6. 8 (E)**). Furthermore, the sensible thermal energy discharge after solidification was identical due to conduction dominant heat transfer.

During discharging cycles at varied inlet temperatures of water, the thermal energy was extracted from paraffin in shell container and the temperature of water in tubes was increased. Outlet temperature of water was significantly influenced by varied inlet temperatures of water. It was noticed that as the inlet temperature of water was decreased from 15 ^{o}C to 5 ^{o}C, the temperature gradient between water and paraffin was enhanced and therefore, thermal energy was extracted from paraffin at higher rate. Therefore, a higher water temperature at outlet was achieved for a shorted period of time, as presented in **Fig. 6. 8 (H)**. Whereas, with an increase in inlet water temperature, the temperature gradient was reduced and consequently, thermal energy was extracted at relatively lower rate. Thus, high temperature water was attained at outlet for a longer period of time. Furthermore, it was observed that with further increase in inlet temperature, the outlet temperature could be further enhanced and for even higher period of time, which can guarantee to be a workable solution for large scale practical applications.

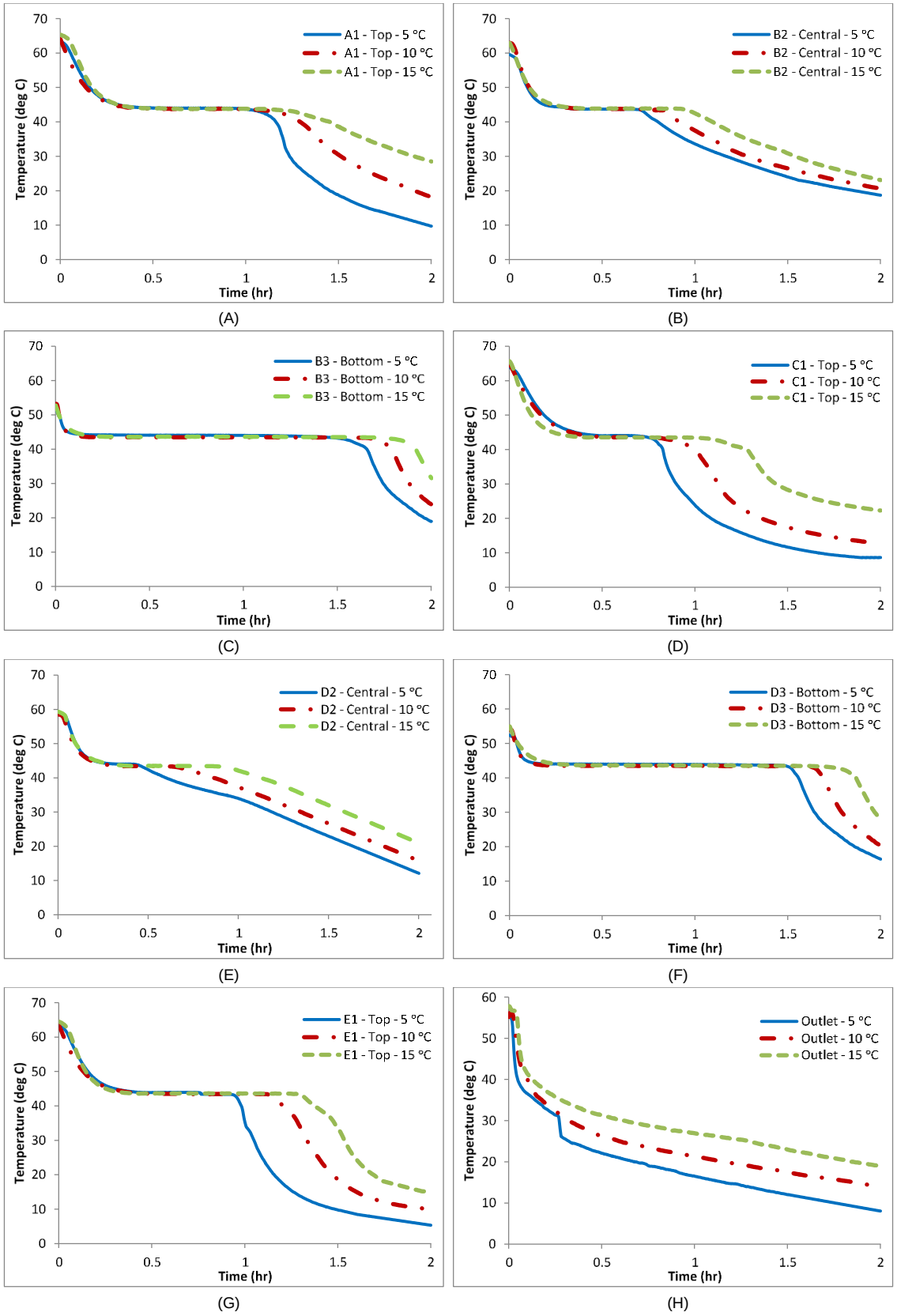

Fig. 6. 8 Transient temperature response of paraffin in shell container to discharging at varied inlet temperatures of water such as 5 ºC, 10 ºC and 15 ºC and at constant volume flow rate of 1.5 l/min (Khan, Z. and Khan, Z. A. 2017b).

6.1.2.3 Influence of volume flow rate on discharging rate

The impact of varying operating volume flow rates conditions of water on phase transition rate of paraffin in shell container were investigated by conducting a series of discharging cycles at varied volume flow rates of 1.5, 2, 2.5 and 3 l/min and constant inlet temperature of 10 ^{o}C. Transient temperature response of paraffin in shell container was recorded by thermocouples installed in shell container, as illustrated in **Fig. 6. 9**.

Similar to inlet temperature of water, the variation in volume flow rates of water had illustrated an insignificant impact on sensible thermal energy discharge of paraffin in shell container. Whereas, the total time required to discharge latent portion of thermal energy from paraffin in shell container was significantly reduced by an increase in volume flow rate. Likewise, the sensible portion of thermal energy discharge from solid paraffin in shell container had presented a minimal impact due to varying volume flow rates of water.

As presented in **Fig. 6. 9**, the total solidification time for paraffin at top position at outlet section (zone A) was significantly reduced by a fraction of 9.03%, 14.98% and 28.19% as volume flow rate of water was increased from 1.5 l/min to 2, 2.5 and 3 l/min, respectively. Likewise, the total solidification time for paraffin at top position at central section (zone C) was reduced by a fraction of 11.04%, 21.22% and 27.32%, respectively. Similarly, the paraffin at top position at inlet section (zone E) had presented total solidification time reduction of 6.76%, 13.05% and 19.81% with an increase in volume flow rate of water from 1.5 l/min to 2, 2.5 and 3 l/min, respectively.

Similarly, it was observed that for a constant inlet temperature of water, the heat transfer rate between water in tubes and paraffin in shell container was enhanced with an increase in volume flow rates. The reason behind was that with an increase in volume flow rate, the turbulent nature of water in tubes was augmented and therefore, a higher heat transfer coefficient was produced. Therefore, with an increase in volume flow rate, a relatively higher capacity of thermal energy was extracted from paraffin in shell container and consequently, the phase transition rate was enhanced. However, the higher volume flow rates of inlet water would produce a lower output temperature. Thus, in order to maintain a higher outlet temperature to meet a required demands for a practical application, a smaller volume flow rate should be considered. Furthermore, the operating temperature and volume flow rate conditions of inlet water should be

regulated in order to produce a required outlet temperature and mean power for practical applications.

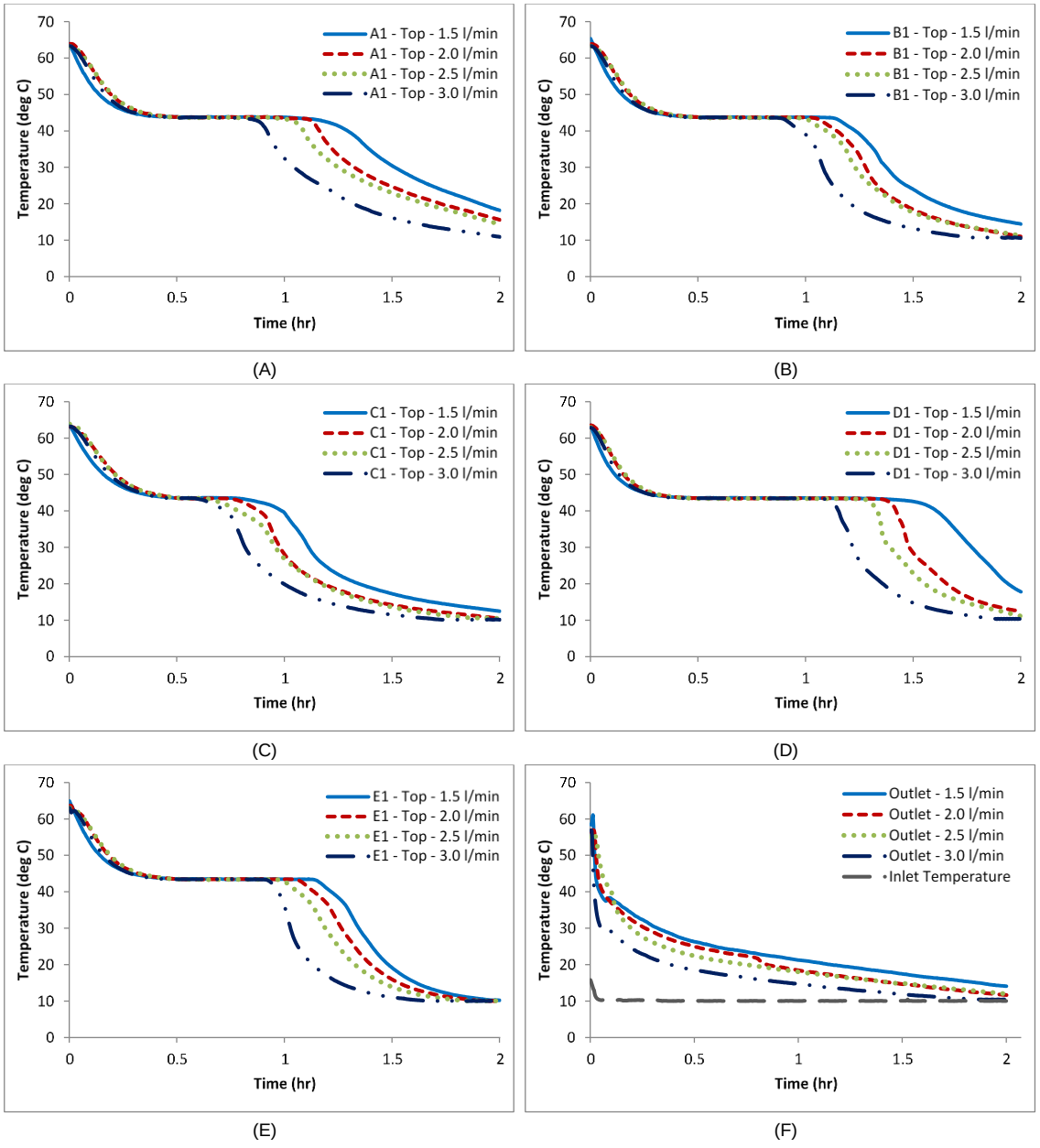

Fig. 6. 9 Transient temperature response of paraffin in shell container to discharging at varied volume flow rates of water such as 1.5, 2.0, 2.5 and 3.0 l/min and at constant inlet temperature of 10 ^{o}C (Khan, Z. and Khan, Z. A. 2017b).

6.1.2.4 Mean discharging power

To examine thermal performance of paraffin in proposed design of shell and tube heat exchanger with longitudinal fins, the accumulative thermal energy discharge and mean discharge power were calculated at varied operating conditions. Accumulative thermal energy discharge Q_d and mean discharge power P_d were computed from a subsection

integral method which considered average density, specific heat capacity, temperature gradient and time interval to record transient temperature data for discharging cycle, as follow:

$$Q_d = \sum \dot{V} \left(\frac{\rho_{in} + \rho_{out}}{2} \right) \left(\frac{C_{p,in} + C_{p,out}}{2} \right) \left(T_{HTF,out} - T_{HTF,in} \right) \Delta t \quad (6.3)$$

$$P_d = \frac{Q_d}{t_d} \quad (6.4)$$

The impact of varied volume flow rates of water on accumulative thermal energy discharge from paraffin was examined, as presented in **Fig. 6. 10**. Inlet temperature of water was set constant to 10 ^{o}C. It was noticed that with an increase in volume flow rate of water, the overall thermal resistance to convective heat transfer in water was reduced and therefore, a relatively higher amount of thermal energy was discharged by water from paraffin. It was observed that while discharging paraffin for 1.5 h at volume flow rates of 1.5, 2, 2.5 and 3 l/min, the accumulative thermal energy discharged by water was 10604 kJ, 11150 kJ, 11521 kJ and 12055 kJ, respectively. Likewise, the discharging time of paraffin was reduced by a fraction of 24% as the volume flow rates was increased from 1.5 l/min to 3 l/min.

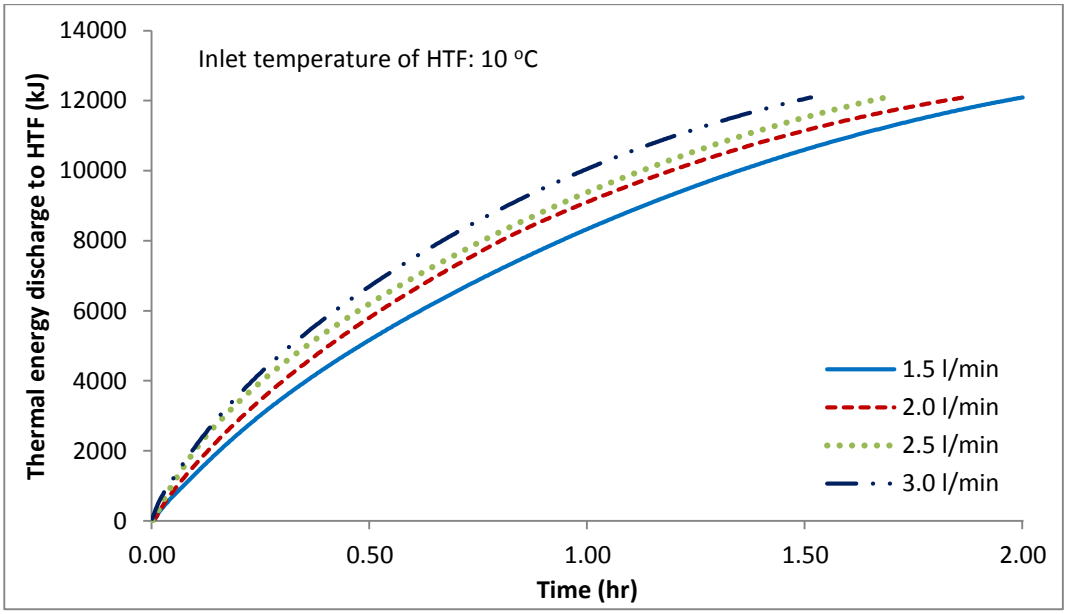

Fig. 6. 10 Accumulative thermal energy discharge by paraffin to water at varied volume flow rates of 1.5, 2.0, 2.5 and 3.0 l/min and at constant inlet temperature of 10 ^{o}C (Khan, Z. and Khan, Z. A. 2017b).

Furthermore, the impact of varying operating conditions on mean discharge power of paraffin was examined, as illustrated in **Fig. 6. 11**. It was noticed that for a constant inlet temperature of 15 ^{o}C, the mean discharge power was linearly increased with an increase in volume flow rate from 1.5 l/min to 2.0, 2.5 and 3.0 l/min. As presented, the mean discharge power was enhanced by a fraction of 18.24%, 33.58% and 49.75%, respectively. Similarly, for constant inlet temperature of 10 ^{o}C, the enhancement in mean discharge power acquired with an increase in volume flow rate was 6.85%, 13.47% and 26.49%. Likewise, in case of inlet temperature of 5 ^{o}C, the mean discharge power was increased by a fraction of 7.31%, 17.98% and 33.70%, respectively. Furthermore, in case of varying inlet temperatures and constant volume flow rates, the mean discharge power of paraffin had demonstrated significant enhancement. For instance, in case of varying inlet temperatures and constant volume flow rate of 3 l/min, the mean discharge power was increased from 1.959 kW to 2.125 and 2.38 kW as the inlet temperature was decreased from 15 ^{o}C to 10 ^{o}C and 5 ^{o}C, respectively. Therefore, it was evident from experimental investigations that by adjusting inlet temperature and flow rate of water, the required power and temperature demands for practical applications could be achieved.

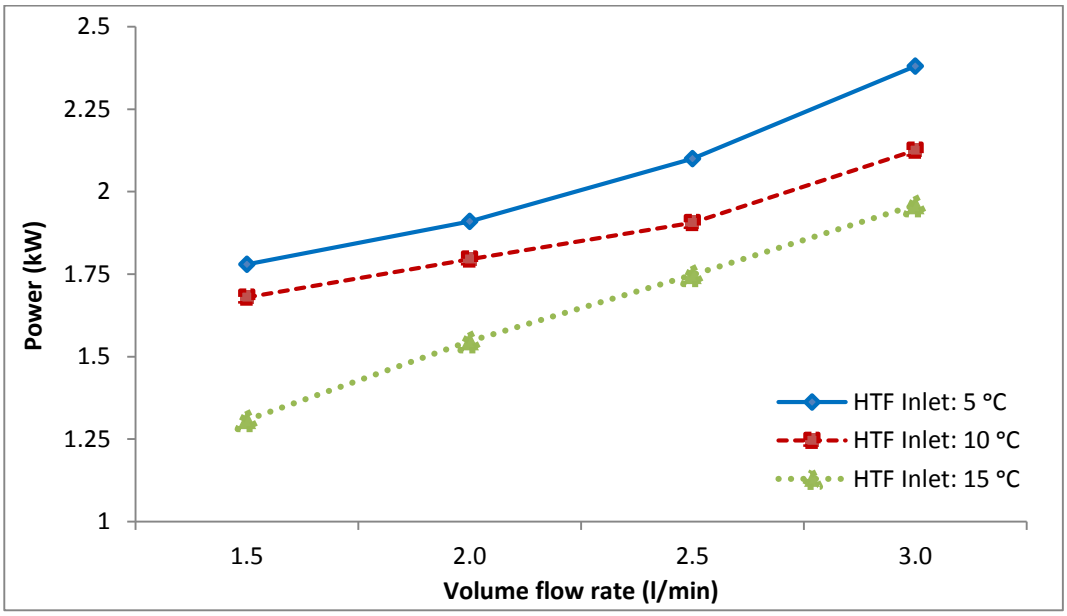

Fig. 6. 11 Mean discharging power of LHS unit at three varied inlet temperatures and four volume flow rates (Khan, Z. and Khan, Z. A. 2017b).

6.2 Second stage: Nano-additives enhanced paraffin

To understand relative thermal performance enhancement with an inclusion of nano-additives in base paraffin, the thermal performance of base paraffin during charging/discharging cycles at varied operating conditions were investigated in shell and tube heat exchanger (see **Fig. 5. 12**) to provide a good reference for evaluation of nano-additives enhanced paraffin samples. Following to investigation of base paraffin in shell and tube heat exchanger, the nano-additives enhanced paraffin samples, as presented in **Table 5. 3**, were investigated by conducting charging/discharging cycles at various operating conditions to identify nano-additive material with volume concentration for optimum thermal performance enhancement.

6.2.1 Charging cycles

Nano-PCM samples were prepared by ultrasonic emulsification technique and loaded in shell container of heat exchanger, as illustrated in **Fig. 5. 13**. High temperature water was pumped through the heat exchanger tubes to transfer thermal energy to nano-PCM sample in shell container. Charging cycle was completed when all four thermocouples in shell container registered temperature higher than phase transition temperature. In order to investigate thermal response of nano-PCM samples to varied operating conditions, three inlet temperatures were experimented such as 47 ^{o}C, 52 ^{o}C and 57 ^{o}C. Similarly, the impact of four volume flow rates ranging from 1.5 l/min – 3.0 l/min were experimented. However, due to small volume of shell and tube heat exchanger, such as 300 ml, the impact of varying volume flow rates of water on thermal performance of nano-PCM samples were insignificant.

6.2.1.1 Influence of nano-additives volume concentrations

Due to inclusion of high thermal conductive nano-additives, the effective thermal conductivity of paraffin was enhanced and therefore, the heat transfer rate and charging/discharging rate was significantly enhanced. However, with inclusion of nano-additives, the effective dynamic viscosity of paraffin was also augmented, which had adverse impacts on buoyancy driven natural convection. Therefore, an optimum volume concentration of nano-additives should be identified to achieve desired thermal performance enhancement of LHS system.

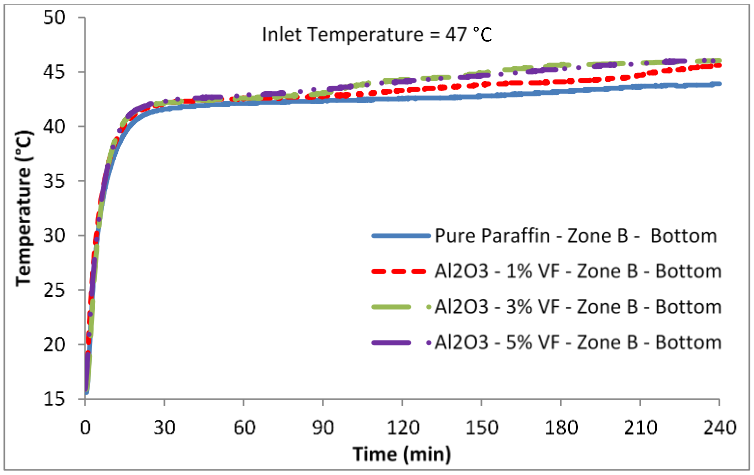

(A)

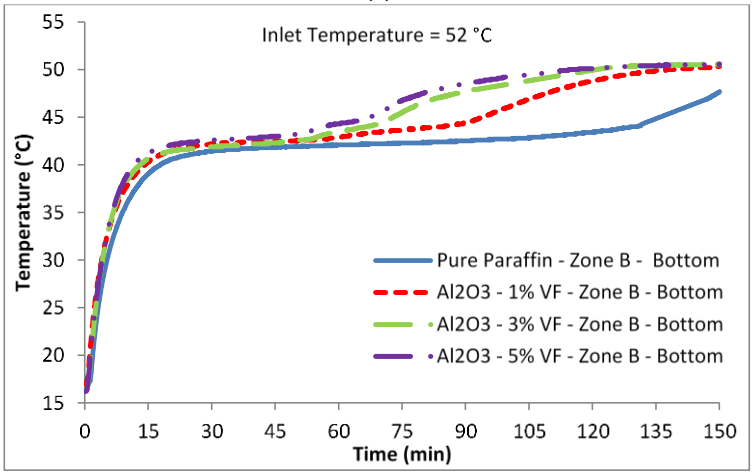

(B)

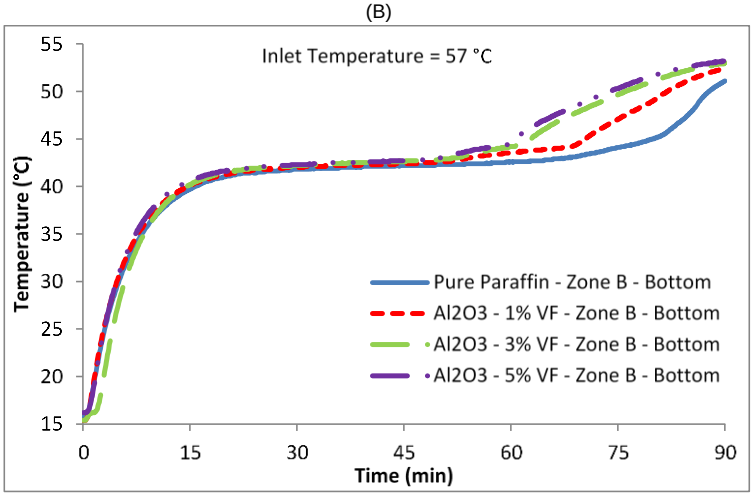

(C)

Fig. 6. 12 Transient temperature profiles acquired from thermocouple installed at bottom position at outlet section (zone B) of shell container during charging cycles of pure paraffin and Al_2O_3 nano-additives enhanced paraffin samples with varied volume fractions of 1%, 3% and 5% at three varied inlet temperatures of 47 ºC, 52 ºC and 57 ºC (Khan, Z. and Khan, Z. A. 2018).

In order to determine the influence of nano-additives inclusion to base paraffin and optimum volume concentration of nano-additives, Al_2O_3 based nano-PCM samples

were prepared with volume fraction of 1%, 3% and 5%. Thermal performance enhancement of nano-PCM samples were experimented with reference to base paraffin at varied inlet temperatures of 47 ^{o}C, 52 ^{o}C and 57 ^{o}C, as presented in **Fig. 6. 12**.

It was evident that while charging at constant inlet temperature of 47 ^{o}C, the charging rate was significantly enhanced by a fraction of 33.75%, 55.41% and 56.25% for Al_2O_3 based nano-PCM samples as compared to base paraffin, respectively. Similarly, in case of charging at constant inlet temperature of 52 ^{o}C, the charging rate was improved by a fraction of 35.92%, 48.80% and 56.37%, respectively. Moreover, while charging at constant inlet temperature of 57 ^{o}C, the charging rate was increased by a fraction of 11.36%, 21.71% and 24.74%, respectively.

It was deduced from experimental investigations that the inclusion of nano-additives to paraffin had significantly enhanced the heat transfer rate and charging rate. However, it was noticed that thermal performance was just slightly enhanced with an increase in volume concentration from 3% to 5%. This was due to the fact that with an increase in volume concentration, the dynamic viscosity was significantly augmented, which was the reason for adverse effects on natural convection and overall charging rate. Furthermore, the density and overall weight of LHS system was also increased with an increase in volume concentration. Thus, it was construed that for optimal thermo-physical performance, the volume concentration of nano-additives should not exceed 3%.

6.2.1.2 Influence of various nano-additive materials

In order to examine the impact of various nano-additives materials on thermal performance enhancement of LHS system, nano-PCM samples were prepared with 1% volume concentration of Al_2O_3, AlN and GNP, as shown in **Table 5. 3**. Nano-PCM samples were investigated at three varied inlet temperatures of 47 ^{o}C, 52 ^{o}C and 57 ^{o}C. Transient temperature response of base paraffin and nano-PCM samples to varied inlet temperatures were registered by thermocouples installed at top and bottom position at inlet section (zone A) of shell container, as presented in **Fig. 6. 13**.

It was noticed that for inlet temperature of 47 ^{o}C, the charging rates at top position at inlet section (zone A) for Al_2O_3, AlN and GNP based nano-PCM samples were significantly improved by a fraction of 9.04%, 18.74% and 37.85% as compared to base paraffin, respectively. Similarly, the charging rates at bottom position were enhanced by

a fraction of 33.75%, 35.90% and 62.56%, respectively. For inlet temperature of 52 °C, the phase transition rates at top position were enhanced by a fraction of 6.42%, 27.27% and 57.22% and at bottom position, it was augmented by 32.70%, 36.40% and 38.07%, respectively. Moreover, for inlet temperature of 57 °C, the charging rates at top position were improved by 19.04%, 28.57% and 49.78% and at bottom position, it was improved by 28.01%, 36.47% and 44.57%, respectively.

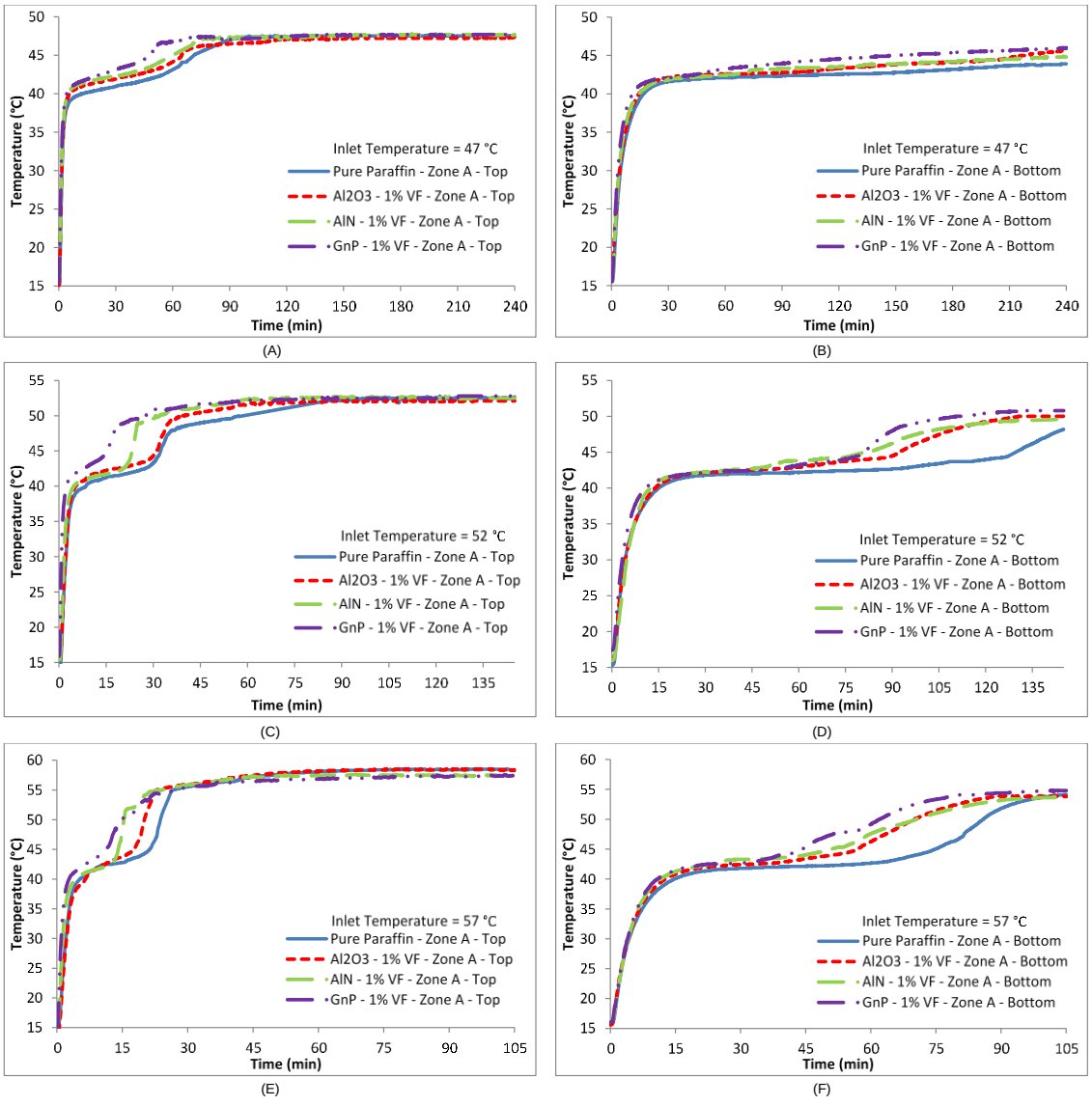

Fig. 6. 13 Transient temperature profiles acquired from thermocouples installed at top and bottom position at inlet section (zone A) of shell container during charging cycles of pure paraffin and Al_2O_3, AlN and GNP nano-additives enhanced paraffin samples with volume fraction of 1% at three varied inlet temperatures of 47 °C, 52 °C and 57 °C (Khan, Z. and Khan, Z. A. 2018).

It was deduced from experimental examinations that the effective thermal conductivity was increased due to inclusion of nano-additives and consequently, the charging rate

was significantly increase. It was also deduced that for constant volume concentration, GNP based nano-PCM samples demonstrated relatively better thermal performance. Also, due to relatively smaller density of GNP nano-additive particles, the overall weight of LHS system was not increased. Therefore, an optimum thermo-physical performance of LHS system could be achieved with addition of GNP nano-additives to base paraffin.

6.2.2 Discharging cycles

Following to charging cycles, thermal performance of nano-PCM samples in shell container were examined by conducting discharging cycles. Municipal water was channelled through the heat exchanger tubes to extract thermal energy from base paraffin or nano-PCM samples in shell container. Open loop discharging cycle was completed when all thermocouples in shell container registered temperature reading lesser than phase transition temperature of paraffin.

6.2.2.1 Influence of nano-additives volume concentrations

Similar to charging cycles, the impact of volume concentrations of nano-additives on thermal performance of LHS system was examined by conducting discharging cycles on base paraffin and Al_2O_3 based nano-PCM samples with volume fraction of 1%, 3% and 5%. Transient temperature response to discharging cycles were recorded by thermocouple installed at bottom position at inlet section (zone A) in shell container, as presented in **Fig. 6. 14**. It was noticed that the effective thermal conductivity was enhanced with inclusion of Al_2O_3 nano-additives and consequently, the discharging rate was significantly augmented. In case of discharging at constant inlet temperature of 15 ^oC, the discharging rate was enhanced by a fraction of 28.45%, 39.05% and 39.52% for Al_2O_3 based nano-PCM samples as compared to base paraffin, respectively. Similar to charging cycles, an insignificant enhancement in discharging rate was noticed with an increase in volume concentration from 3% to 5%. Hence, it was concluded that for optimal thermal performance, the volume concentration of nano-additives should not exceed 3%.

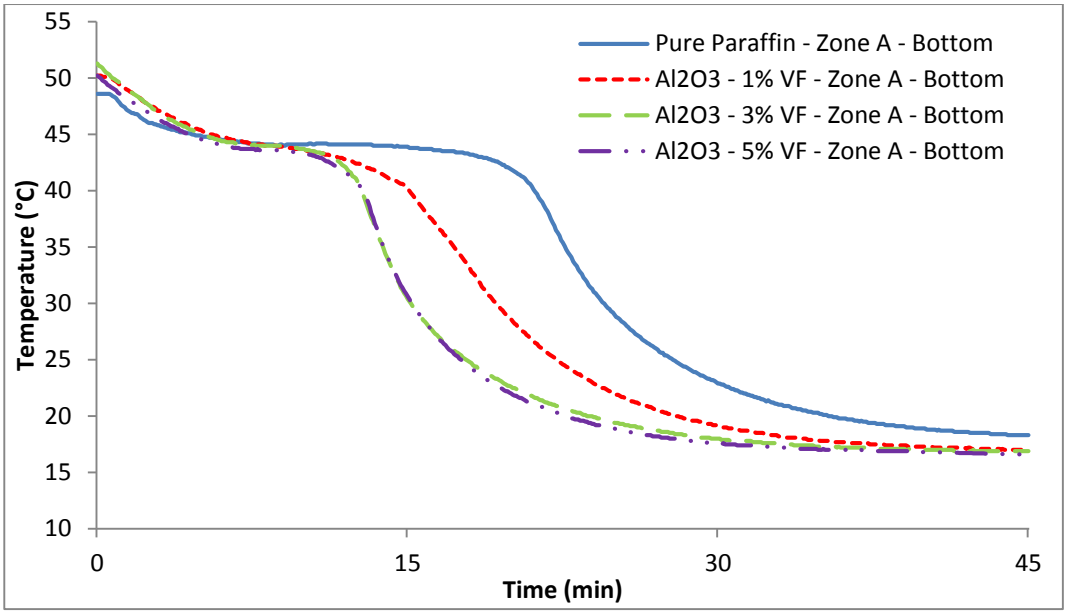

Fig. 6. 14 Transient temperature profiles acquired from thermocouple installed at bottom position at inlet section (zone A) of shell container during discharging cycles of pure paraffin and Al_2O_3 nano-additives enhanced paraffin samples (Khan, Z. and Khan, Z. A. 2018).

6.2.2.2 Influence of various nano-additive materials

To examine the impact of various nano-additives materials on thermo-physical performance of LHS system, the discharging cycles were conducted for base paraffin and nano-PCM samples with 1% volume concentration of Al_2O_3, AlN and GNP nano-additives. Inlet temperature for discharging cycles were set constant to 15 ^oC. Likewise, the transient temperature response of base paraffin and nano-PCM samples were recorded from thermocouple installed at bottom position at outlet section (zone B), as illustrated in **Fig. 6. 15**.

It was observed that for constant inlet temperature, the discharging rate for nano-PCM samples with 1% volume concentration of Al_2O_3, AlN and GNP nano-additives were enhanced by a fraction of 14.63%, 34.95% and 41.46% as compared to base paraffin, respectively. It was evident from transient temperature profiles that GNP and AlN based nano-PCM samples had presented significantly higher discharging rate due to their higher effective thermal conductivity. However, GNP based nano-PCM sample was recommended and preferred due to relatively lighter weight and higher charging performance.

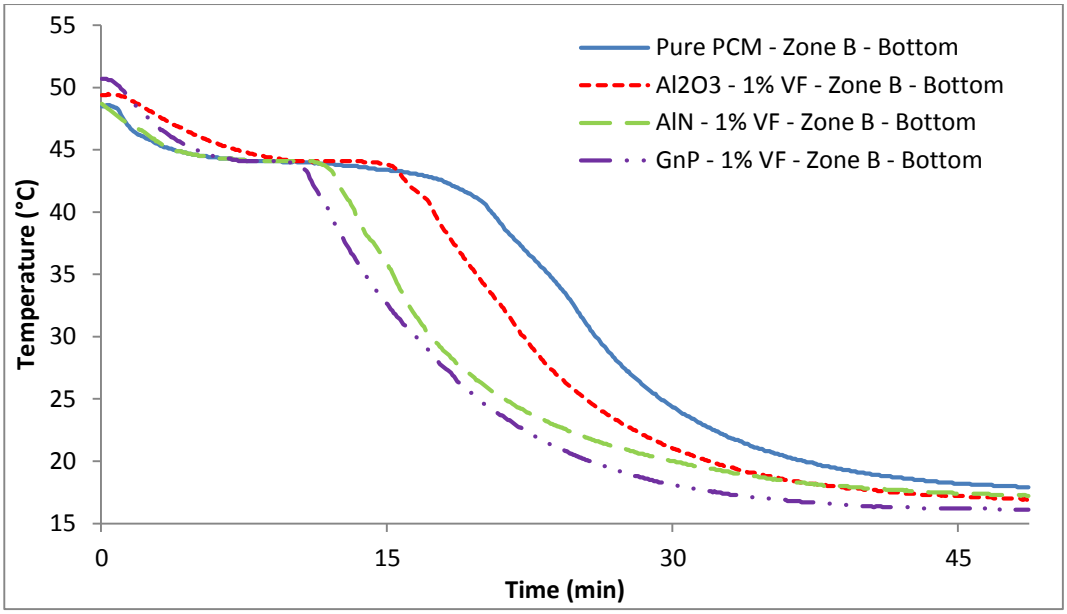

Fig. 6. 15 Transient temperature profiles acquired from thermocouples installed at bottom position at outlet section (zone B) of shell container during discharging cycles of pure paraffin and Al_2O_3, AlN and GNP nano-additives enhanced paraffin samples (Khan, Z. and Khan, Z. A. 2018).

Chapter 7 Predictive modelling and analytics

This chapter discusses the predictive modelling and analytics based on experimental results to forecast thermal performance of proposed designed of LHS system at varied operating conditions. Non-linear regression technique was implemented to develop equations for outlet temperature of water for proposed designed LHS system. Moreover, a general equation was generated for outlet temperature of water as a factor of inlet temperature of water and time interval. Furthermore, the proposed design of shell and tube with multiple passes and longitudinal fins coupled with graphene nano-additives enhanced paraffin as thermal storage material was simulated in ANSYS Fluent workbench to investigate coupled thermal performance enhancement.

9.1 Governing equation for proposed LHS system

It was informed by (Helvaci, H. and Khan, Z. A. 2016) that a mechanical work of 146.74 W was generated at rotary expander in ORC. Inlet and outlet temperatures of organic refrigerant (HFE 7000) at rotary expander were 45.41 ^{o}C and 36.36 ^{o}C, respectively. In order to analyse whether or not the proposed designed solution of LHS system is capable of sustaining continuous generation of mechanical work at rotary expander, the provision of desired higher inlet temperature of organic refrigerant at rotary expander is essential. It can be noticed from **Fig. 6. 8 (H)** that with an increase in inlet temperature during discharging cycles, a higher outlet temperature was produced for an even longer period of time. However, the experimental discharging cycles of LHS system were conducted at inlet temperatures of 5, 10 and 15 ^{o}C. Therefore, the non-linear regression technique was adopted to generate correlations between inlet temperature, outlet temperature and time interval for respective proposed designed LHS system to predict outlet temperature profiles at varied higher inlet temperature of 20, 25, 30 and 35 ^{o}C.

It can be observed from the experimental results in **Fig. 6. 8 (H)** that the outlet temperature profiles followed logarithmic declination trend. Hence, the logarithmic trend line equation was generated and the coefficient of determination R^2 was calculated to examine the accuracy of predicted equations. It was noticed that as compared to polynomial and power declination trend equations, the logarithmic declination trend equation produced a relatively better coefficient of determination R^2. Furthermore, generalized reduction gradient (GRG) nonlinear algorithm was implemented to optimise

the logarithmic declination trend equations for outlet temperature at various inlet temperatures, as given below:

$$T_{HTF,in} = 5℃; \quad T_{HTF,out} = -9.224In(t) + 14.9842 \tag{7. 1}$$

$$T_{HTF,in} = 10℃; \quad T_{HTF,out} = -8.445In(t) + 19.9842 \tag{7. 2}$$

$$T_{HTF,in} = 15℃; \quad T_{HTF,out} = -7.694In(t) + 24.9842 \tag{7. 3}$$

It can be noticed from Eq. (7. 1) to Eq. (7. 3) that outlet temperature at varied inlet temperatures were influenced by logarithmic time intervals and two coefficients which behaved linearly with an increase in inlet temperature from 5 ^{o}C – 15 ^{o}C. Therefore, a general governing equation was developed for outlet temperature as a factor of inlet temperature and time intervals, as given below:

$$T_{HTF,out} = \left(\lambda T_{HTF,in} - \Phi\right)In(t) + T_{HTF,in} + \Phi \tag{7. 4}$$

where $\lambda = 0.153$ and $\Phi = 9.9842$ are coefficients for respective volume flow rate of 1.5 l/min and proposed design of LHS system. In order to examine the accuracy of governing equation, the predicted outlet temperature profiles for inlet temperature of 10 ^{o}C and 15 ^{o}C were compared with experimental outlet temperature profiles, as presented in **Fig. 7. 1**. It can be observed that the predicted outlet temperature profiles are in good agreement with experimental temperature profiles. The mean absolute percentage error between predicted and experimental results were calculated to be 4.01%.

In similar manner, the developed governing equation was computed to predict the output temperature response to various inlet temperatures of HTF such as 20, 25, 30 and 35 ^{o}C, as presented in **Fig. 7. 2**. It was noticed that with an increase in inlet temperature, the gradient between paraffin and HTF was reduced and hence the thermal energy was discharged for longer period of time. In other words, in case of higher inlet temperature, a relatively smaller thermal energy was required to raise the output temperature and therefore, a higher outlet temperature was acquired for longer period of time. For instance, at inlet temperature of 35 ^{o}C, a higher outlet temperature in the range of 40 ^{o}C was can be generated for 4 hours.

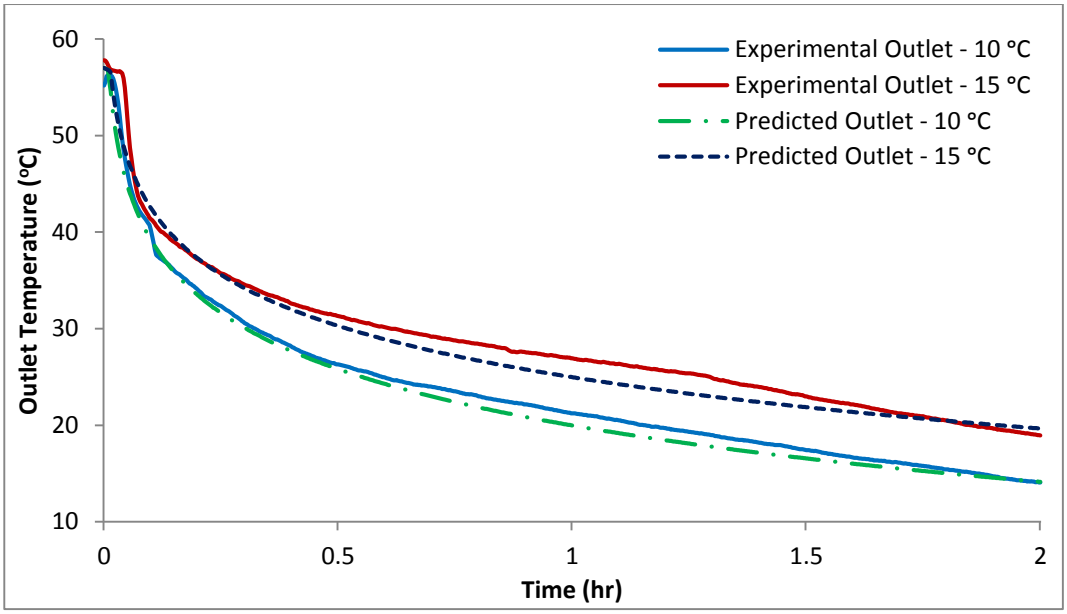

Fig. 7. 1 Validation of predicted and experimental results of outlet temperature profiles at varied inlet temperatures of 10 °C and 15 °C.

Hence, it can be deduced that for close loop operation at higher inlet temperature of organic refrigerant, the proposed LHS system is proficient of generating higher temperature output to sustain uninterrupted generation of mechanical work at rotary expander. Further, to generate mechanical work for even longer period of time, the proposed LHS systems can be arranged in series sequence and for generating higher mechanical work output, the proposed LHS systems can be assembled in parallel sequence.

It was informed by (Khan, Z. et al. 2016a) that paraffins with higher phase transition temperature possess almost identical density, thermal conductivity and viscosity. Therefore for higher outlet temperature demands, the current employed paraffin (RT44HC) in shell container can be substituted with higher phase transition temperature paraffin such as RT70HC, RT80HC, RT90HC, etc (Anon. 2017). Therefore, the proposed design of shell and tube with multiple tube passes and longitudinal fins can be employed for numerous domestic and industrial applications to meet wide ranging temperature demands.

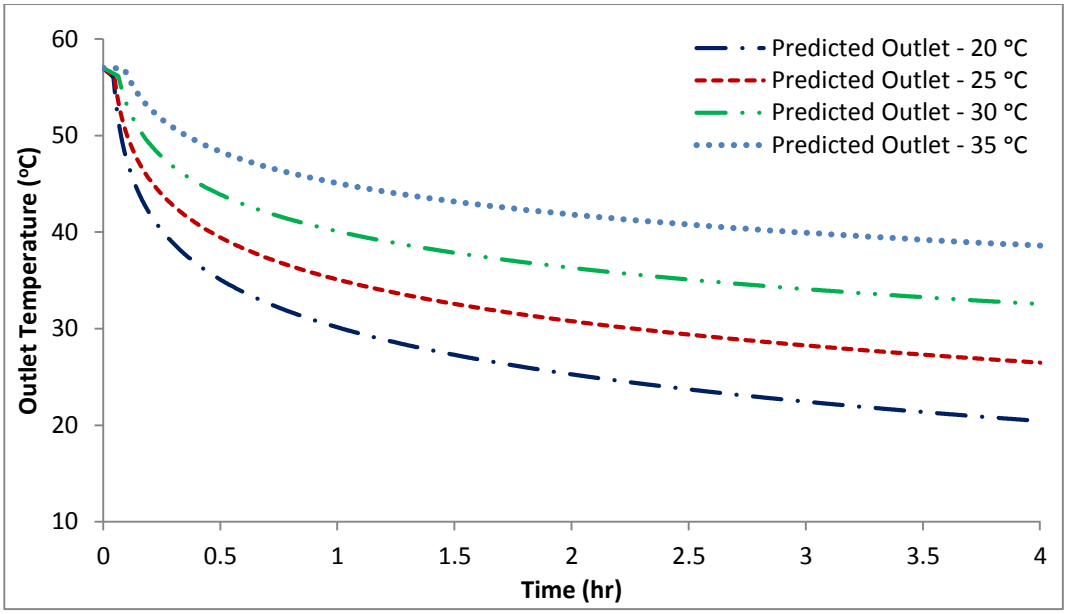

Fig. 7. 2 Predicted outlet temperature profiles at varied time intervals and at various inlet temperatures of 20, 25, 30 and 35 °C.

9.2 Coupled thermal performance enhancement with longitudinal fins and nano-PCM

Numerical and experimental investigations have demonstrated significant thermal performance enhancement of paraffin at varied operating conditions in proposed shell and tube heat exchanger with multiple tube passes and longitudinal fins. Inclusion of longitudinal fins countered the low thermal conductivity of paraffin in shell container and therefore, a higher charging and discharging rate is achieved. Likewise, it was determined from numerical and experimental analysis that inclusion of GNP nano-additives can significantly enhance the effective thermal conductivity of paraffin, which can result in higher charging and discharging rate. In this section, the proposed design of novel shell and tube heat exchanger with extended longitudinal fins (see **Fig. 3. 4**) and proposed graphene nano-platelets enhanced novel thermal storage materials was simulated to examine coupled thermal performance enhancement.

Fig. 7. 3 illustrates the impact of coupled thermal performance enhancement techniques on melting fractions and enthalpy contours of pure paraffin and GNP enhanced paraffin samples in shell container while charging at constant inlet temperature of 62 °C. Three volume concentrations of GNP nano-additives were selected: 1%, 2% and 3%. It was noticed that as compared to pure paraffin, the nano-additives enhanced paraffin samples presented relatively higher charging rate due to improved effective thermal

conductivity. It was also detected that the charging rate was increased with an increase in volume concentration of nano-additives. For instance, while charging at constant inlet temperature of 62 ^{o}C for 3 hour, the complete liquid fraction for pure paraffin and GNP enhanced paraffin samples were 92.12%, 93.6%, 94.5% and 95.5%, respectively.

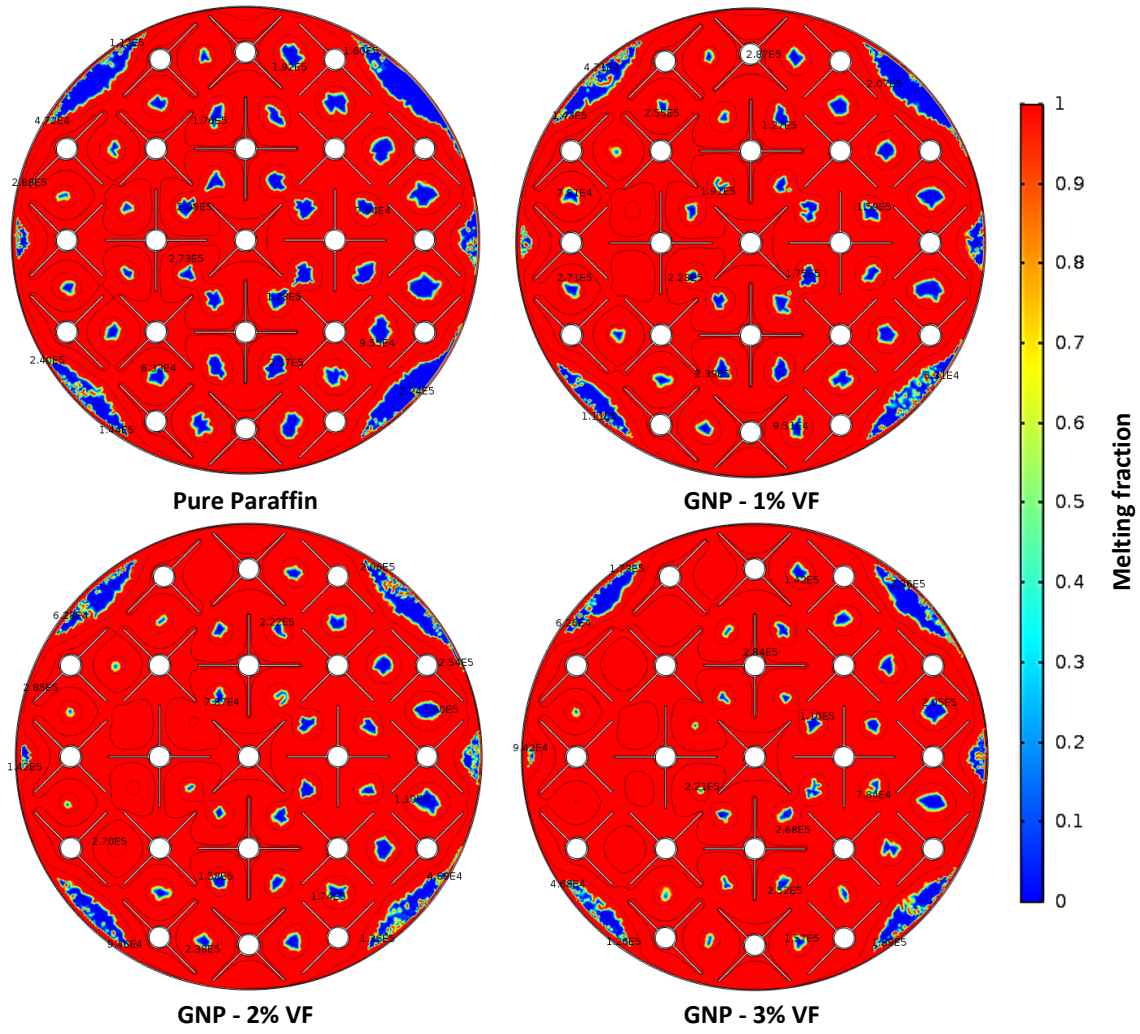

Fig. 7. 3 Melting fractions and enthalpy contours of pure paraffin and nano-additives enhanced paraffin samples during charging at constant inlet temperature of 62 ^{o}C for 3 hour. Phase transition interval ΔT_{pc} for this case was set to 0.1 ^{o}C.

Likewise, the transient temperature profiles of paraffin and nano-additives enhanced paraffin samples acquired at inlet section (zone A) and boundary section (zone B) were plotted in **Fig. 7. 4** and **Fig. 7. 5**, respectively. It was noticed that the phase transition rate at zone A was significantly enhanced with inclusion of GNP nano-additives and the enhancement was further augmented with an increase in volume concentration. For instance, the phase transition rate for nano-additive enhanced paraffin sample with 3% volume concentration was 24.17% higher as compared to pure paraffin. Likewise, it was

noticed that at zone A, the transient temperature profiles represented a relatively higher phase transition rate for nano-additives enhanced paraffin as compared to pure paraffin. However, the improvement in phase transition rate due to an increase in volume concentration from 1% – 3 % was insignificant at zone B. Total melting time required for pure paraffin and nano-additives enhanced paraffin samples at zone B were recorded to be 4.11 h, 3.59 h, 3.56 h and 3.52 h, respectively. Therefore, as compared to pure paraffin, a significant enhancement in charging rate was achieved with inclusion of GNP nano-additives. Moreover, it was noticed that phase transition rate for coupled thermal performance enhancement techniques was significantly enhanced by 75.46% as compared to no longitudinal fins orientation with pure paraffin.

However, it was observed that with an inclusion of longitudinal fins and nano-additives, the volume occupied by paraffin was compromised and consequently the overall thermal storage capacity was slightly reduced, as presented in **Fig. 7. 6**. As compared to no fins orientation with pure paraffin, the overall thermal storage capacity was reduced from 10.48 MJ to 10.03 MJ with inclusion of GNP nano-additives with 3% volume concentration. Hence, the significant enhancement in phase transition rate and minimal reduction in overall thermal storage capacity support and recommend the coupled enhancement technique with inclusion of longitudinal fins and nano-additives.

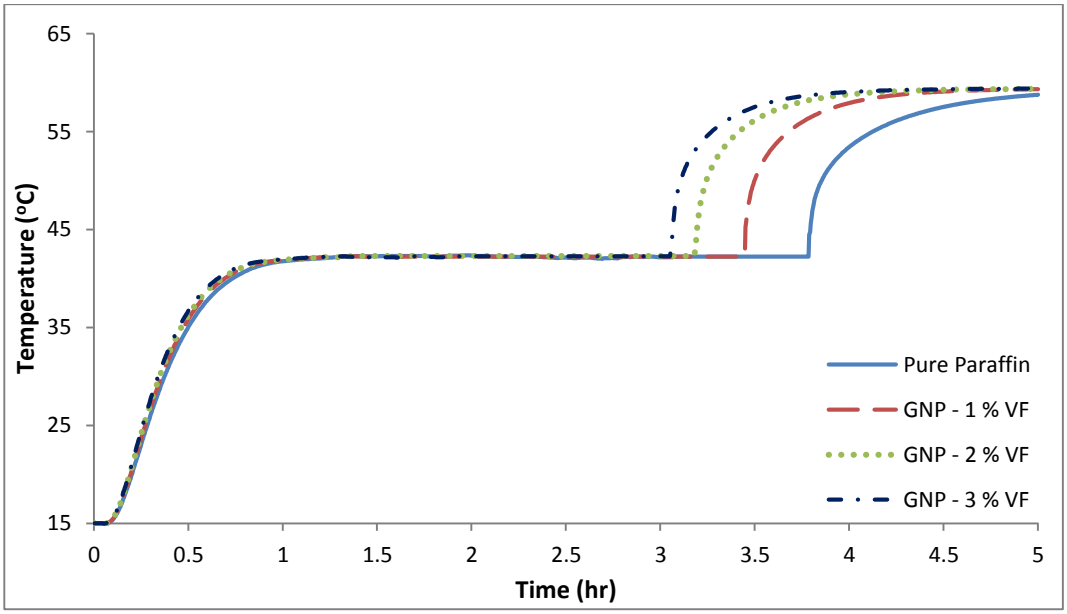

Fig. 7. 4 Transient temperature profiles acquired at inlet section (zone A) for pure paraffin and nano-additives enhanced paraffin samples during charging at constant inlet temperature of 62 °C. Phase transition interval ΔT_{pc} for this case was set to 0.1 °C.

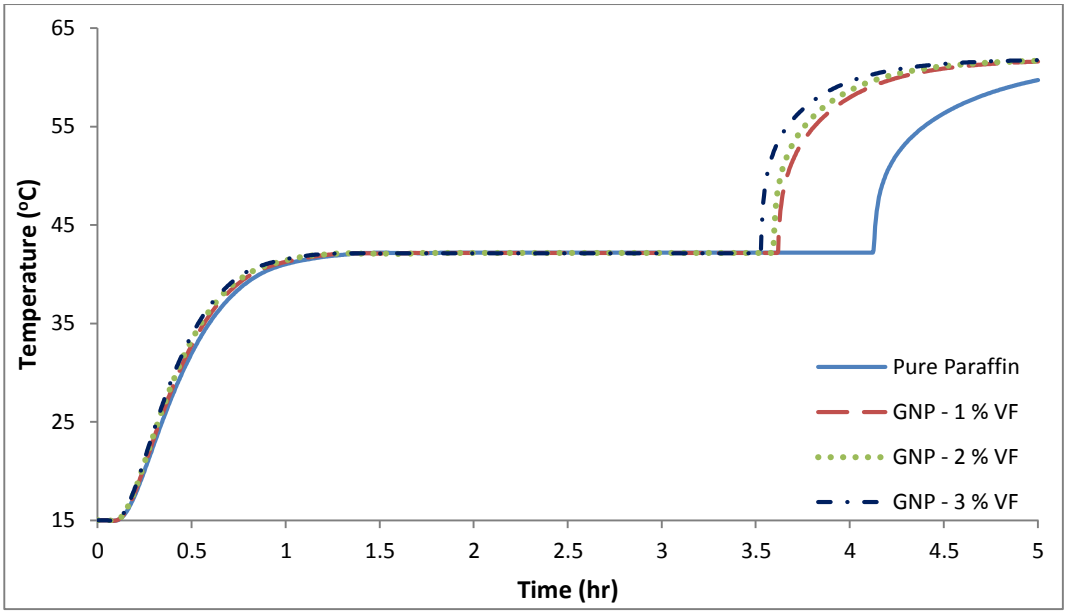

Fig. 7. 5 Transient temperature profiles acquired at shell container boundary section (zone B) for pure paraffin and nano-additives enhanced paraffin samples during charging at constant inlet temperature of 62 °C. Phase transition interval ΔT_{pc} for this case was set to 0.1 °C.

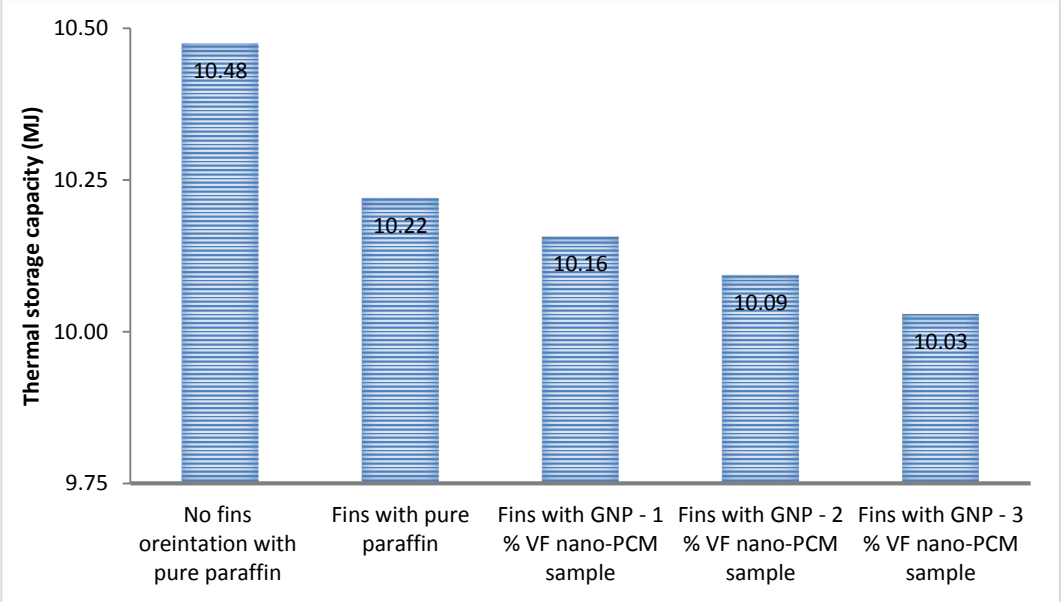

Fig. 7. 6 Overall thermal storage capacity (MJ) of pure paraffin and nano-PCM samples with varied volume concentrations

Chapter 8 Conclusions and future work

This chapter provides the conclusions derived from numerical and experimental analyses conducted in developing an efficient and effective thermal energy storage technology with novel heat transfer mechanism and novel thermal storage materials to sustain continuous generation of heat and power for low temperature practical applications. These conclusions are discussed with an instance of fulfilling the set objectives of this thesis.

8.1 Achieving the set objectives of this thesis

- **Investigation and identification of various possible thermal storage system for solar energy or heat recovery sources**

These conclusions are based on the literature survey conducted in Chapter 2. In literature survey, various subgroups of organic and inorganic thermal storage materials were studied and analysed as potential candidates for LHS systems on the basis of their chemical composition, thermo-physical performance, long term thermo-physical stability and compatibility with container materials. Paraffin and salt hydrates were established as favourable thermal storage materials due to their higher latent heat capacity, availability at wide range of temperatures for low temperature applications and relatively cheaper price. However, due to corrosive nature, phase segregation and subcooling problems of salt hydrates, the complexity to design and develop a long-life cycle LHS system was increased. Therefore, paraffin was selected as thermal storage material due to their excellent compatibility with metal container, no phase segregation or subcooling, good thermo-physical stability and repeatability, and good environmental properties. Likewise, copper was selected as preferable and feasible construction material for heat exchanger to overcome the influence of low thermal conductivity of paraffin on charging/discharging rate of LHS system. Moreover, the literature survey advocated the utilisation of vertical shell and tube heat exchanger due to its easier integration to number of practical applications, higher thermal performance and minimal thermal losses. Longitudinal fins were identified advantageous over radial fins due to their better temperature distribution in vertical shell container, simpler geometrical integration to tubes, minimal thermal storage reduction and excellent facilitation to natural convection. Furthermore, metal oxides, metal nitrides and carbon allotropes were recognised as potential nano-additives to incorporate in base paraffin to

enhance effective thermal conductivity. Finally, the coupled thermal performance enhancement with longitudinal fins and nano-additives was proposed for developing an efficient and effective thermal energy storage system for large-scale practical applications.

- **To conduct numerical simulations for designing a novel geometrical orientated heat exchanger for LHS system**

These conclusions are based on the numerical analyses conducted in Chapter 3 and 4. Based on recommendations conferred in Chapter 2, the computational model comprising novel geometrical orientation of shell and tube heat exchanger with multiple tube passes and longitudinal fins was simulated to investigate the influence of various design parameters and operating conditions on overall thermal performance of proposed LHS system. Commercial grade paraffin (RT44HC) was employed as thermal storage material in shell container and water was utilised as HTF in tube passes. Parametric investigations were conducted focusing on the influence of number of tube passes and their orientation in shell container, geometrical dimensions of longitudinal fins, construction material for shell, tubes and fins, and operating conditions to determine an optimum design solution for LHS system. Transient numerical simulations presented that with an increase in tube passes from 9 – 21, the effective surface area for heat transfer was significantly enhanced and consequently, a dominant conduction heat transfer was generated across shell container. It was noticed from transient simulations of charging cycles at constant inlet temperature of 62 ^{o}C that the melted fraction of paraffin was significantly increased from 65.72% – 98.25% as the tube passes was increased from 9 – 21, respectively. Moreover, it was noticed that as compared to no fins orientation, the charging rate of paraffin in shell container was increased by 69.75% as compared to proposed longitudinal fins orientation. Furthermore, the geometrical dimensions of longitudinal fins were found to be crucial to optimal thermal performance. Parametric investigations indicated that longitudinal fins length have more profound impact on phase transition rates as compared to fins thickness. The effective surface area for heat transfer was increased as the longitudinal fins length was increased from 12.70 mm to 38.10 mm and consequently, the melted fraction of paraffin was significantly increased from 64.34% to 96.86% while charging at constant inlet temperature of 62 ^{o}C for 2 hours. Similarly, it was noticed that with an increase in longitudinal fins thickness from 1 mm to 4 mm, the overall thermal storage capacity

was reduced from 10.919 MJ to 10.292 MJ. Subsequently, the optimum length and thickness of longitudinal fins were determined as 38.10 mm and 1.5 mm, respectively. Also, the numerical simulations indicated that due to higher thermal conductivity of copper as construction material, the melting rate was enhanced by 23.68% as compared to steel. Therefore, copper was selected as construction material for shell, tubes and longitudinal fins. Moreover, it was noticed that with an increase in inlet temperature of HTF, the temperature gradient between paraffin in shell container and water in tube passes was enhanced and consequently, the phase transition rate and sensible portion of thermal energy storage was increased. For instance, with an increase in inlet temperature from 52 ^{o}C – 62 ^{o}C, the overall enthalpy was increased from 10.16 MJ – 11.06 MJ, respectively.

Moreover, the impact of natural convection on phase transition rate and vertical temperature distribution in shell container was simulated. It was noticed that the proposed design of shell and tube heat exchanger with multiple passes and longitudinal fins did not interrupt the impact of buoyance driven natural convection on phase transition rate of paraffin in shell container.

- **To develop mathematical model and conduct transient numerical simulations on nano-additives enhanced thermal storage material**

These conclusions are based on the numerical analyses conducted in Chapter 3 and 4. In order to develop nano-additives enhanced thermal storage material, a numerical model was developed and simulated to examine the influence of various nano-additive material, particle size, volume concentration and operating temperature on overall thermal performance enhancement of LHS system. Transient numerical simulations were conducted to examine the influence of effective thermal conductivity and effective dynamic viscosity on phase transition rate. Due to higher thermal conductivity and lower particle size of GNP nano-additives, the effective thermal conductivity and dynamic viscosity was significantly enhanced with an increase in volume concentration from 1% – 5%. It was noticed that as compared to pure paraffin, the effective thermal conductivity for GNP based nano-additives with 5% volume concentration was increased by a fraction of 22.5% and consequently, the phase transition rate was significantly enhanced. However, due to an increase in dynamic viscosity with inclusion of nano-additives, the effective dynamic viscosity was improved which provided

resistance to natural convection. Therefore, the optimum enhancement in phase transition rate was influenced. Besides the enhancement in phase transition rate, the effective density and overall weight of LHS system was significantly increased with inclusion of Al_2O_3 and AlN nano-additives, due to their relatively higher density as compared to GNP nano-additives. Similarly, the overall enthalpy was reduced with inclusion of nano-additives. For instance, as compared to pure paraffin case, the overall enthalpy was reduced by a fraction of 20.58%, 19.64% and 2.88% for Al_2O_3, AlN and GNP based nano-PCM samples with 5% volume concentration. Hence, the numerical analyses indicated that GNP nano-additives are preferable to be incorporated in base paraffin due to their relatively lower effective weight, higher phase transition rate and higher overall enthalpy of LHS system.

- **To design, develop and commission an experimental setup to analyse thermal performance of novel LHS system coupled with flat plate solar collector**

These conclusions are based on the experimental analyses conducted in Chapter 5 and 6. Based on numerical analyses, the proposed design of shell and tube heat exchanger with multiple passes and longitudinal fins was fabricated and commissioned with flat plate solar collector. Paraffin (RT44HC) was employed in shell container and water was utilised to circulate in tube passes to transfer thermal energy gained at solar collector to paraffin in shell container. Several charging and discharging cycles were experimented at varied operating temperatures and volume flow rates of inlet water to examine the effects on temperature distribution in paraffin in shell container, effective modes of heat transfer, charging/discharging rate, accumulative thermal energy storage/discharge and mean charging/discharging power. It was deduced that the natural convection significant influenced phase transition rate during charging cycles whereas, the influence was not minimal during solidification rate. Likewise, the longitudinal fins had successfully augmented the charging and discharging rate of paraffin in shell container. It was noticed that due to natural convection influence on charging cycles, the phase transition rate at top position of shell container was 65.21% and 113.04% higher than central and bottom position, respectively. Likewise, with an increase in inlet temperature from 52 ^oC to 67 ^oC, the mean charging rate and mean charging power was enhanced by 50.08% and 69.71%, respectively. Moreover, with an increase in volume flow rate from 1.5 l/min to 3.0 l/min, the charging rate and mean charging power was improved by 30.98% and 24.39%, respectively. Furthermore, the discharging cycles at

varied operating conditions demonstrated conduction as dominant mode of heat transfer. It was noticed that with a reduction in inlet temperature from 15 ^{o}C to 5 ^{o}C, the discharging rate and mean discharging power was augmented by 48.11% and 36.08%, respectively. Likewise, the heat transfer rate between paraffin in shell container and water in tube passes was increased with an increase in volume flow rate from 1.5 l/min to 3.0 l/min. Hence, the discharging rate and mean discharging power was enhanced by a fraction of 24% and 26.49%, respectively. Therefore, it was proved from experimental investigations that the required charging/discharging rate, accumulative thermal energy storage/discharge and mean charging/discharging power demands for practical applications can be achieved by regulating inlet temperature and volume flow rate of water.

- **To conduct experimental analyses of nano-additives enhanced thermal storage material**

These conclusions are based on the experimental analyses conducted in Chapter 5 and 6. Nano-additives enhanced paraffin samples were prepared using ultrasonic emulsification technique and experimentally investigated in a shell and tube heat exchanger at varied inlet temperatures and volume flow rates. Nano-PCM samples were loaded in shell container whereas, water was channelled in tubes to conduct a series of charging and discharging cycles. An optimum volume concentration for nano-additives was identified by investigating three samples of Al_2O_3 nano-additives enhanced paraffin with volume concentration of 1%, 3% and 5%. It was noticed that while charging at inlet temperature of 47 ^{o}C, the charging rate for nano-PCM samples were increased by a fraction of 3.75%, 55.41% and 56.25% as compared to pure paraffin, respectively. Similarly, while discharging at inlet temperature of 15 ^{o}C, the discharging rate was increased by 28.45%, 39.05% and 39.52% as compared to pure paraffin. Hence, it was evident from experimental results that with an increase in volume concentration from 3% to 5%, the phase transition rate was only slightly improved. Therefore, it was deduced that the volume concentration of nano-additives should not exceed 3% for an optimum thermo-physical performance of LHS system. Similarly, for constant volume concentration of nano-additives, GNP based nano-PCM sample demonstrated relatively higher phase transition rate as compared to Al_2O_3 and AlN based nano-PCM samples. For instance, while charging at inlet temperature of 57 ^{o}C, the charging rate for Al_2O_3, AlN and GNP nano-additives based nano-PCM samples were improved by 28.01%,

36.47% and 44.57% as compared to pure paraffin, respectively. Similarly, the discharging rates were augmented by 14.63%, 34.95% and 41.46% as compared to pure paraffin, respectively. Thus, for optimal thermo-physical performance enhancement of LHS system, GNP nano-additives enhanced paraffin with volume concentration not exceeding 3% was recommended.

- **To conduct numerical simulations on coupled thermal performance enhancement techniques**

These conclusions are based on the numerical analyses conducted in Chapter 7. Transient numerical simulations were conducted on proposed design of shell and tube heat exchanger with multiple tube passes and longitudinal fins with GNP nano-additives enhanced paraffin as thermal storage material. It was deduced that with coupled thermal performance enhancement the phase transition rate was enhanced by 75.46% as compared to no longitudinal fins orientation with pure paraffin. Therefore, in order to increase practical utilisation of LHS system in both domestic and commercial applications, the proposed coupled thermal performance enhancement techniques should be implemented to achieve the required thermal energy demand.

The main research question is successfully addressed by devising a numerical and experimental methodology to design, develop and commission a novel geometrical orientated heat exchanger with nano-additives enhanced thermal storage materials based thermal storage system for low temperature domestic and commercial applications; featuring higher charging/discharging rate, higher thermal storage capacity and higher mean charging/discharging power for sustaining continuous generation of desired mechanical power or heat.

8.2 Future work

In future work, the proposed design of heat exchanger with nano-additives enhanced paraffin is needed to be experimentally examined with an integration into ORC to observe the real time generation of mechanical power during off-peak solar hours. In ORC, water will be replaced with HFE 7000 to product the mechanical power at rotary expander. LHS system will be employed to either supplement solar collector or replace it during off-peak solar hours to maintain continuous and low cost mechanical power. Also, the thermal performance of LHS system during charging and discharging cycles with HFE 7000 as working HTF require experimental investigations. In next stage,

nano-additives enhanced thermo-fluids should be employed to gain an optimum advantage from solar energy gain at collector, storage in proposed LHS system and generation of mechanical power at rotary expander. Also, the proposed LHS system should be experimentally tested with an integration to heat recovery systems and building heating systems to perform energy management, peak-shaving and to analyse the reduction profile in building natural gas and electricity cost.

Furthermore, experimental analyses are required to validate the thermal performance of proposed LHS system in series and parallel configurations for generating higher thermal storage capacity to produce higher mechanical power for longer period of time. Moreover, in order to meet higher outlet temperature demands in practical applications, the higher phase transition temperature paraffin such as RT70HC, RT80HC, RT90HC, etc. are required to be employed in shell container to conduct experimental analyses at varied operating conditions. To achieve long-term thermo-physical stability and compatibility with construction materials, paraffins were selected. However, to achieve further reduction in initial capital cost of LHS system, salt hydrates with good thermo-physical stability and compatibility with copper heat exchanger and containers (i.e. $CaCl_2$. $6H_2O$) need to be employed and experimentally analysed. For corrosive salt hydrates, the encapsulation technique for thermal performance enhancement should be adopted to improve long-term practical utilisation in varied applications.

For mass production and commercialisation, the construction and manufacturing techniques are recommended to be reconsidered and standardised to reduction production cost and time, and increase precision. The components of LHS system are also recommended to be standardised to achieve widespread and long-life utilisation in both domestic and industrial application. Moreover, a control system should be devised and developed to operate the proposed LHS system by considering weather forecast, building energy demands, electricity and natural gas peak-shaving profiles in a control algorithm to arrange an optimised management strategies for timely charging and discharging of LHS system.

Also, the understanding and possibility of utilising LHS system for cold storage and/or seasonal storage with an integration to geothermal heat pump is an interesting research area for future work. CFD analyses are recommended for conducting initial feasibility examination.

References

Abhat, A., 1983. Low temperature latent heat thermal energy storage: heat storage materials. *Solar energy*, 30 (4), 313-332.

Agyenim, F., Eames, P. and Smyth, M., 2009. A comparison of heat transfer enhancement in a medium temperature thermal energy storage heat exchanger using fins. *Solar Energy*, 83 (9), 1509-1520.

Agyenim, F., Hewitt, N., Eames, P. and Smyth, M., 2010. A review of materials, heat transfer and phase change problem formulation for latent heat thermal energy storage systems (LHTESS). *Renewable and Sustainable Energy Reviews*, 14 (2), 615-628.

Alkan, C., Kaya, K. and Sarı, A., 2009. Preparation, thermal properties and thermal reliability of form-stable paraffin/polypropylene composite for thermal energy storage. *Journal of Polymers and the Environment*, 17 (4), 254-258.

Allen, M. J., Sharifi, N., Faghri, A. and Bergman, T. L., 2015. Effect of inclination angle during melting and solidification of a phase change material using a combined heat pipe-metal foam or foil configuration. *International Journal of Heat and Mass Transfer*, 80, 767-780.

Anon. , 2017. *Rubitherm® Technologies GmbH*, *http://www.rubitherm.eu/en/* [online]. Available from: http://www.rubitherm.eu/en/ [Accessed

Arena, S., 2016. *Modelling, design and analysis of innovative thermal energy storage systems using PCM for industrial processes, heat and power generation.* Universita'degli Studi di Cagliari.

Awad, A., Navarro, H., Ding, Y. and Wen, D., 2018. Thermal-physical properties of nanoparticle-seeded nitrate molten salts. *Renewable Energy*, 120, 275-288.

Batchelor, G., 1977. The effect of Brownian motion on the bulk stress in a suspension of spherical particles. *Journal of fluid mechanics*, 83 (1), 97-117.

Bergman, T. L., Incropera, F. P., DeWitt, D. P. and Lavine, A. S., 2011. *Fundamentals of heat and mass transfer*. John Wiley & Sons.

Brinkman, H., 1952. The viscosity of concentrated suspensions and solutions. *The Journal of Chemical Physics*, 20 (4), 571-571.

Bruggeman, V. D., 1935. Berechnung verschiedener physikalischer Konstanten von heterogenen Substanzen. I. Dielektrizitätskonstanten und Leitfähigkeiten der Mischkörper aus isotropen Substanzen. *Annalen der physik*, 416 (7), 636-664.

Cabeza, L., Illa, J., Roca, J., Badia, F., Mehling, H., Hiebler, S. and Ziegler, F., 2001a. Immersion corrosion tests on metal-salt hydrate pairs used for latent heat storage in the 32 to 36° C temperature range. *Materials and Corrosion*, 52 (2), 140-146.

Cabeza, L., Illa, J., Roca, J., Badia, F., Mehling, H., Hiebler, S. and Ziegler, F., 2001b. Middle term immersion corrosion tests on metal-salt hydrate pairs used for latent heat storage in the 32 to 36° C temperature range. *Materials and Corrosion*, 52 (10), 748-754.

Cabeza, L., Roca, J., Nogués, M., Mehling, H. and Hiebler, S., 2002. Immersion corrosion tests on metal-salt hydrate pairs used for latent heat storage in the 48 to 58° C temperature range. *Materials and Corrosion*, 53 (12), 902-907.

Cabeza, L. F., Castell, A., Barreneche, C., De Gracia, A. and Fernández, A., 2011. Materials used as PCM in thermal energy storage in buildings: a review. *Renewable and Sustainable Energy Reviews*, 15 (3), 1675-1695.

Caron-Soupart, A., Fourmigué, J.-F., Marty, P. and Couturier, R., 2016. Performance analysis of thermal energy storage systems using phase change material. *Applied Thermal Engineering*, 98, 1286-1296.

Chen, H., Cong, T. N., Yang, W., Tan, C., Li, Y. and Ding, Y., 2009. Progress in electrical energy storage system: A critical review. *Progress in Natural Science*, 19 (3), 291-312.

Corcione, M., 2011. Empirical correlating equations for predicting the effective thermal conductivity and dynamic viscosity of nanofluids. *Energy Conversion and Management*, 52 (1), 789-793.

Darzi, A. A. R., Jourabian, M. and Farhadi, M., 2016. Melting and solidification of PCM enhanced by radial conductive fins and nanoparticles in cylindrical annulus. *Energy Conversion and Management*, 118, 253-263.

De Bruijn, H., 1942. The viscosity of suspensions of spherical particles.(The fundamental η-c and φ relations). *Recueil des travaux chimiques des Pays-Bas*, 61 (12), 863-874.

Dhaidan, N. S. and Khodadadi, J., 2015. Melting and convection of phase change materials in different shape containers: A review. *Renewable and Sustainable Energy Reviews*, 43, 449-477.

Dincer, I. and Rosen, M., 2002. *Thermal energy storage: systems and applications*. John Wiley & Sons.

Du, Y. and Ding, Y., 2016. Towards improving charge/discharge rate of latent heat thermal energy storage (LHTES) by embedding metal foams in phase change materials (PCMs). *Chemical Engineering and Processing: Process Intensification*, 108, 181-188.

Duan, Z.-j., Zhang, H.-z., Sun, L.-x., Cao, Z., Xu, F., Zou, Y.-j., Chu, H.-l., Qiu, S.-j., Xiang, C.-l. and Zhou, H.-y., 2014. CaCl2· 6H2O/Expanded graphite composite as form-stable phase change materials for thermal energy storage. *Journal of Thermal Analysis and Calorimetry*, 115 (1), 111-117.

Dunn, B., Kamath, H. and Tarascon, J.-M., 2011. Electrical energy storage for the grid: a battery of choices. *Science*, 334 (6058), 928-935.

Einstein, A., 1906. Eine neue bestimmung der moleküldimensionen. *Annalen der Physik*, 324 (2), 289-306.

El-Sebaii, A., Al-Amir, S., Al-Marzouki, F., Faidah, A. S., Al-Ghamdi, A. and Al-Heniti, S., 2009. Fast thermal cycling of acetanilide and magnesium chloride hexahydrate for indoor solar cooking. *Energy conversion and Management*, 50 (12), 3104-3111.

El-Sebaii, A., Al-Heniti, S., Al-Agel, F., Al-Ghamdi, A. and Al-Marzouki, F., 2011. One thousand thermal cycles of magnesium chloride hexahydrate as a promising PCM for indoor solar cooking. *Energy Conversion and Management*, 52 (4), 1771-1777.

Esapour, M., Hosseini, M., Ranjbar, A., Pahamli, Y. and Bahrampoury, R., 2016. Phase change in multi-tube heat exchangers. *Renewable Energy*, 85, 1017-1025.

Farid, M. M., Khudhair, A. M., Razack, S. A. K. and Al-Hallaj, S., 2004. A review on phase change energy storage: materials and applications. *Energy conversion and management*, 45 (9), 1597-1615.

Farrell, A. J., Norton, B. and Kennedy, D. M., 2006. Corrosive effects of salt hydrate phase change materials used with aluminium and copper. *Journal of materials processing technology*, 175 (1), 198-205.

Feilchenfeld, H. and Sarig, S., 1985. Calcium chloride hexahydrate: A phase-changing material for energy storage. *Industrial & engineering chemistry product research and development*, 24 (1), 130-133.

Fluent, A., 2009. 12.0 User's Guide, 2009. *Fluent Inc., New Hampshire.[Links]*.

García-Romero, A., Delgado, A., Urresti, A., Martín, K. and Sala, J., 2009. Corrosion behaviour of several aluminium alloys in contact with a thermal storage phase change material based on Glauber's salt. *Corrosion Science*, 51 (6), 1263-1272.

Ghoneim, A., 1989. Comparison of theoretical models of phase-change and sensible heat storage for air and water-based solar heating systems. *Solar Energy*, 42 (3), 209-220.

Giro-Paloma, J., Martínez, M., Cabeza, L. F. and Fernández, A. I., 2016. Types, methods, techniques, and applications for microencapsulated phase change materials (MPCM): A review. *Renewable and Sustainable Energy Reviews*, 53, 1059-1075.

Gray, D. D. and Giorgini, A., 1976. The validity of the Boussinesq approximation for liquids and gases. *International Journal of Heat and Mass Transfer*, 19 (5), 545-551.

Hadjieva, M. and Argirov, J., 1992. Thermophysical properties of some paraffins applicable to thermal energy storage. *Solar Energy Materials and Solar Cells*, 27 (2), 181-187.

Hahn, D. W. and Ã–zisik, M. N., 2012. *Heat conduction*. John Wiley & Sons.

Haillot, D., Py, X., Goetz, V. and Benabdelkarim, M., 2008. Storage composites for the optimisation of solar water heating systems. *Chemical engineering research and design*, 86 (6), 612-617.

Hamilton, R. and Crosser, O., 1962. Thermal conductivity of heterogeneous two-component systems. *Industrial & Engineering chemistry fundamentals*, 1 (3), 187-191.

Han, G.-S., Ding, H.-S., Huang, Y., Tong, L.-G. and Ding, Y.-L., 2017. A comparative study on the performances of different shell-and-tube type latent heat thermal energy storage units including the effects of natural convection. *International Communications in Heat and Mass Transfer*, 88, 228-235.

Harikrishnan, S., Deenadhayalan, M. and Kalaiselvam, S., 2014. Experimental investigation of solidification and melting characteristics of composite PCMs for building heating application. *Energy Conversion and Management*, 86, 864-872.

Hasnain, S., 1998. Review on sustainable thermal energy storage technologies, Part I: heat storage materials and techniques. *Energy conversion and management*, 39 (11), 1127-1138.

Helvaci, H. and Khan, Z. A., 2016. Experimental study of thermodynamic assessment of a small scale solar thermal system. *Energy Conversion and Management*, 117, 567-576.

Helvaci, H. U., 2017. *Experimental investigation and mathematical modelling of dynamic equilibrium of novel thermo-fluids for renewable technology applications.* Bournemouth University.

Ibrahim, H., Ilinca, A. and Perron, J., 2008. Energy storage systems—characteristics and comparisons. *Renewable and sustainable energy reviews*, 12 (5), 1221-1250.

IEA, 2015. Energy and Climate Change *International Energy Agency (IEA), 21st UN Conference of the Parties (COP21)*. Paris.

IEA, 2017. CO2 emissions from fuel combustion-highlights. *IEA, Paris* *http://www.iea.org/publications/freepublications/publication/CO2EmissionsfromFuelCombustionHighlights2017.pdf*.

Jacobson, M. Z., 2009. Review of solutions to global warming, air pollution, and energy security. *Energy & Environmental Science*, 2 (2), 148-173.

Jones, B. J., Sun, D., Krishnan, S. and Garimella, S. V., 2006. Experimental and numerical study of melting in a cylinder. *International Journal of Heat and Mass Transfer*, 49 (15), 2724-2738.

Kamkari, B., Shokouhmand, H. and Bruno, F., 2014. Experimental investigation of the effect of inclination angle on convection-driven melting of phase change material in a rectangular enclosure. *International Journal of Heat and Mass Transfer*, 72, 186-200.

Kandasamy, R., Wang, X.-Q. and Mujumdar, A. S., 2008. Transient cooling of electronics using phase change material (PCM)-based heat sinks. *Applied Thermal Engineering*, 28 (8), 1047-1057.

Kenisarin, M. and Mahkamov, K., 2007. Solar energy storage using phase change materials. *Renewable and Sustainable Energy Reviews*, 11 (9), 1913-1965.

Khan, Z., Khan, Z. and Ghafoor, A., 2016a. A review of performance enhancement of PCM based latent heat storage system within the context of materials, thermal stability and compatibility. *Energy Conversion and Management*, 115, 132-158.

Khan, Z., Khan, Z. and Tabeshf, K., 2016b. Parametric investigations to enhance thermal performance of paraffin through a novel geometrical configuration of

shell and tube latent thermal storage system. *Energy Conversion and Management*, 127, 355-365.

Khan, Z. and Khan, Z. A., 2017a. Development in paraffin based thermal storage system through shell and tubes heat exchanger with vertical fins, *Proceedings of the ASME 2017 11th International Conference on Energy Sustainability, ES 2017*: ASME.

Khan, Z. and Khan, Z. A., 2017b. An experimental investigation of discharge/solidification cycle of paraffin in novel shell and tube with longitudinal fins based latent heat storage system. *Energy Conversion and Management*, 154, 157-167.

Khan, Z. and Khan, Z. A., 2017c. Experimental investigations of charging/melting cycles of paraffin in a novel shell and tube with longitudinal fins based heat storage design solution for domestic and industrial applications. *Applied Energy*.

Khan, Z. and Khan, Z. A., 2018. Experimental and numerical investigations of nano-additives enhanced paraffin in a shell and tube heat exchanger: a comparative study. *Applied Thermal Engineering*.

Kimura, H. and Kai, J., 1984. Phase change stability of CaCl 2· 6H 2 O. *Solar Energy*, 33 (6), 557-563.

Krieger, I. M. and Dougherty, T. J., 1959. A mechanism for non-Newtonian flow in suspensions of rigid spheres. *Transactions of the Society of Rheology*, 3 (1), 137-152.

Lamberg, P., Lehtiniemi, R. and Henell, A.-M., 2004. Numerical and experimental investigation of melting and freezing processes in phase change material storage. *International Journal of Thermal Sciences*, 43 (3), 277-287.

Lázaro, A., Zalba, B., Bobi, M., Castellón, C. and Cabeza, L. F., 2006. Experimental study on phase change materials and plastics compatibility. *AIChE journal*, 52 (2), 804-808.

Li, Z. and Wu, Z.-G., 2015. Analysis of HTFs, PCMs and fins effects on the thermal performance of shell–tube thermal energy storage units. *Solar Energy*, 122, 382-395.

Liu, L., Su, D., Tang, Y. and Fang, G., 2016. Thermal conductivity enhancement of phase change materials for thermal energy storage: A review. *Renewable and Sustainable Energy Reviews*, 62, 305-317.

Lohrasbi, S., Gorji-Bandpy, M. and Ganji, D. D., 2017. Thermal penetration depth enhancement in latent heat thermal energy storage system in the presence of heat pipe based on both charging and discharging processes. *Energy Conversion and Management*, 148, 646-667.

Luo, K., Yao, F.-J., Yi, H.-L. and Tan, H.-P., 2015. Lattice Boltzmann simulation of convection melting in complex heat storage systems filled with phase change materials. *Applied Thermal Engineering*, 86, 238-250.

Luo, X., Wang, J., Dooner, M. and Clarke, J., 2015. Overview of current development in electrical energy storage technologies and the application potential in power system operation. *Applied Energy*, 137, 511-536.

Marks, S., 1980. An investigation of the thermal energy storage capacity of Glauber's salt with respect to thermal cycling. *Solar Energy*, 25 (3), 255-258.

Maxwell, J. C., 1881. *A treatise on electricity and magnetism*. Vol. 1. Clarendon press.

Mehling, H. and Cabeza, L. F., 2007. Phase change materials and their basic properties. *Thermal energy storage for sustainable energy consumption.* Springer, 257-277.

Mehling, H. and Cabeza, L. F., 2008. *Heat and cold storage with PCM*. Springer.

Mesalhy, O., Lafdi, K., Elgafy, A. and Bowman, K., 2005. Numerical study for enhancing the thermal conductivity of phase change material (PCM) storage using high thermal conductivity porous matrix. *Energy Conversion and Management*, 46 (6), 847-867.

Mettawee, E.-B. S. and Assassa, G. M., 2007. Thermal conductivity enhancement in a latent heat storage system. *Solar Energy*, 81 (7), 839-845.

Moreno, P., Miró, L., Solé, A., Barreneche, C., Solé, C., Martorell, I. and Cabeza, L. F., 2014. Corrosion of metal and metal alloy containers in contact with phase change materials (PCM) for potential heating and cooling applications. *Applied Energy*, 125, 238-245.

Morrison, D. and Abdel-Khalik, S., 1978. Effects of phase-change energy storage on the performance of air-based and liquid-based solar heating systems. *Solar Energy*, 20 (1), 57-67.

N'tsoukpoe, K. E., Liu, H., Le Pierrès, N. and Luo, L., 2009. A review on long-term sorption solar energy storage. *Renewable and Sustainable Energy Reviews*, 13 (9), 2385-2396.

Nagano, K., Ogawa, K., Mochida, T., Hayashi, K. and Ogoshi, H., 2004. Performance of heat charge/discharge of magnesium nitrate hexahydrate and magnesium

chloride hexahydrate mixture to a single vertical tube for a latent heat storage system. *Applied thermal engineering*, 24 (2), 209-220.

Nield, D. A. and Bejan, A., 2006. *Convection in porous media*. Springer Science & Business Media.

Petroleum, B., 2013. Statistical review of world energy-full report.

Porisini, F. C., 1988. Salt hydrates used for latent heat storage: corrosion of metals and reliability of thermal performance. *Solar Energy*, 41 (2), 193-197.

Rathod, M. K. and Banerjee, J., 2013. Thermal stability of phase change materials used in latent heat energy storage systems: a review. *Renewable and Sustainable Energy Reviews*, 18, 246-258.

REN21, 2017. *Renewables 2017 Global Status Report*. Paris: REN21 Secretariat.

Ren, Q. and Chan, C. L., 2016. GPU accelerated numerical study of PCM melting process in an enclosure with internal fins using lattice Boltzmann method. *International Journal of Heat and Mass Transfer*, 100, 522-535.

Sari, A., Eroglu, R., Bicer, A. and Karaipekli, A., 2011. Synthesis and thermal energy storage properties of erythritol tetrastearate and erythritol tetrapalmitate. *Chemical Engineering & Technology*, 34 (1), 87-92.

Sarı, A. and Karaipekli, A., 2007. Thermal conductivity and latent heat thermal energy storage characteristics of paraffin/expanded graphite composite as phase change material. *Applied Thermal Engineering*, 27 (8), 1271-1277.

Seddegh, S., Wang, X. and Henderson, A. D., 2016. A comparative study of thermal behaviour of a horizontal and vertical shell-and-tube energy storage using phase change materials. *Applied Thermal Engineering*, 93, 348-358.

Sharma, A., Sharma, S. and Buddhi, D., 2002. Accelerated thermal cycle test of acetamide, stearic acid and paraffin wax for solar thermal latent heat storage applications. *Energy Conversion and Management*, 43 (14), 1923-1930.

Sharma, A., Tyagi, V., Chen, C. and Buddhi, D., 2009a. Review on thermal energy storage with phase change materials and applications. *Renewable and Sustainable energy reviews*, 13 (2), 318-345.

Sharma, A., Tyagi, V. V., Chen, C. and Buddhi, D., 2009b. Review on thermal energy storage with phase change materials and applications. *Renewable and Sustainable energy reviews*, 13 (2), 318-345.

Sharma, S., Buddhi, D. and Sawhney, R., 1999. Accelerated thermal cycle test of latent heat-storage materials. *Solar Energy*, 66 (6), 483-490.

Shatikian, V., Ziskind, G. and Letan, R., 2005. Numerical investigation of a PCM-based heat sink with internal fins. *International Journal of Heat and Mass Transfer*, 48 (17), 3689-3706.

Shmueli, H., Ziskind, G. and Letan, R., 2010. Melting in a vertical cylindrical tube: numerical investigation and comparison with experiments. *International Journal of Heat and Mass Transfer*, 53 (19), 4082-4091.

Shukla, A., Buddhi, D. and Sawhney, R., 2008. Thermal cycling test of few selected inorganic and organic phase change materials. *Renewable Energy*, 33 (12), 2606-2614.

Stefan, J., 1889. Uber einige probleme der theorie der warmeletung. *Sitzer. Wien. Akad. Math. Naturw.*, 98, 473-484.

Suranovic, S., 2013. Fossil fuel addiction and the implications for climate change policy. *Global Environmental Change*, 23 (3), 598-608.

Tao, Y. and He, Y., 2015. Effects of natural convection on latent heat storage performance of salt in a horizontal concentric tube. *Applied Energy*, 143, 38-46.

Tyagi, V. and Buddhi, D., 2008. Thermal cycle testing of calcium chloride hexahydrate as a possible PCM for latent heat storage. *Solar Energy Materials and Solar Cells*, 92 (8), 891-899.

Velraj, R., Seeniraj, R., Hafner, B., Faber, C. and Schwarzer, K., 1999. Heat transfer enhancement in a latent heat storage system. *Solar energy*, 65 (3), 171-180.

Venkitaraj, K., Suresh, S., Praveen, B., Venugopal, A. and Nair, S. C., 2017. Pentaerythritol with alumina nano additives for thermal energy storage applications. *Journal of Energy Storage*, 13, 359-377.

Voller, V. R. and Prakash, C., 1987. A fixed grid numerical modelling methodology for convection-diffusion mushy region phase-change problems. *International Journal of Heat and Mass Transfer*, 30 (8), 1709-1719.

Vyshak, N. and Jilani, G., 2007. Numerical analysis of latent heat thermal energy storage system. *Energy conversion and management*, 48 (7), 2161-2168.

Wang, P., Yao, H., Lan, Z., Peng, Z., Huang, Y. and Ding, Y., 2016. Numerical investigation of PCM melting process in sleeve tube with internal fins. *Energy Conversion and Management*, 110, 428-435.

Wang, W., Yang, X., Fang, Y., Ding, J. and Yan, J., 2009. Enhanced thermal conductivity and thermal performance of form-stable composite phase change materials by using β-Aluminum nitride. *Applied Energy*, 86 (7), 1196-1200.

Wen, Z., 2016. *Research and development in novel alternative renewable energy technology*. Bournemouth University.

Xuan, Y., Li, Q. and Hu, W., 2003. Aggregation structure and thermal conductivity of nanofluids. *AIChE Journal*, 49 (4), 1038-1043.

Yuan, Y., Cao, X., Xiang, B. and Du, Y., 2016. Effect of installation angle of fins on melting characteristics of annular unit for latent heat thermal energy storage. *Solar Energy*, 136, 365-378.

Zalba, B., Marín, J. M., Cabeza, L. F. and Mehling, H., 2003. Review on thermal energy storage with phase change: materials, heat transfer analysis and applications. *Applied thermal engineering*, 23 (3), 251-283.

Zeng, J., Sun, L., Xu, F., Tan, Z., Zhang, Z., Zhang, J. and Zhang, T., 2006. Study of a PCM based energy storage system containing Ag nanoparticles. *Journal of Thermal Analysis and Calorimetry*, 87 (2), 371-375.

Zivkovic, B. and Fujii, I., 2001. An analysis of isothermal phase change of phase change material within rectangular and cylindrical containers. *Solar Energy*, 70 (1), 51-61.

Appendices

Appendix A: Publications

Paper I

A review of performance enhancement of PCM based latent heat storage system within the context of materials, thermal stability and compatibility.

Zakir Khan [a]*, Zulfiqar Khan [a], Abdul Ghafoor [b]

[a] Bournemouth University, Sustainable Design Research Cluster, Fern Barrow, Talbot Campus, Poole, Dorset BH12 5BB, UK.

E-mail: zkhan@bournemouth.ac.uk

[b] SMME, National University of Sciences and Technology (NUST), NUST Campus H-12, Islamabad, Pakistan.

E-mail: principal@smme.nust.edu.pk

Corresponding Author:

[a]* Bournemouth University, Sustainable Design Research Cluster, Fern Barrow, Talbot Campus, Poole, Dorset BH12 5BB, UK.

E-mail: zkhan2@bournemouth.ac.uk

Tel.: +44 74592490691

Abstract

Phase change materials (PCM) with their high thermal storage density at almost isothermal conditions and their availability at wide range of phase transitions promote an effective mode of storing thermal energy. Literature survey evidently shows that paraffins and salt hydrates provide better thermal performance at competitive cost. This review paper is focused on the classification of various paraffins and salt hydrates. To acquire long term productivity of LHS system, the thermo-physical stability of both paraffins and salt hydrates; and their compatibility with various plastic and metallic container materials play a vital role. Likewise, the lower thermal conductivity of PCMs affects the thermal performance of LHS system. This article reviews the various thermo-physical performance enhancement techniques such as influence of container shape and its orientation, employment of fins and high conductivity additives, multi-PCM approach and PCM encapsulation. The performance enhancement techniques are focused to improve the phase transition rate, thermal conductivity, latent heat storage capacity and thermo-physical stability. This review provides an understanding on how to maximize thermal utilization of PCM. This understanding is underpinned by an analysis of PCM-Container compatibility and geometrical configuration of the container.

Keywords

Thermal energy storage, Latent heat, Phase change materials, Thermal stability, Heat transfer

Table of Contents

1. Introduction

The continuous and expeditious rise in worldwide economic development is followed up by a strong demand of continuous supply of energy. Energy generated from fossil fuel have fulfilled and served human needs for a long era. However, the fossil fuel resources are limited and due to their fluctuating pricings, the availability of uninterrupted supply of energy is highly uncertain. Moreover, the higher use of conventional fossil fuel is responsible for immense damage to environment, due to emission of harmful gases and impurities in air that leads to recent global warming. These serious challenges have motivated engineers and scientists all over the world to develop technologies to utilize sources of renewable energy so as to avert from technologies that cause environmental hazards, high cost for energy generation and avoid establishing new costly power plants.

Thermal energy storage (TES) system is considered a very critical technology, which possess a great adaption to renewable energies. The storage of excess energy that would otherwise be wasted could work as to bridge the gap between energy requirements and generation. Solar thermal energy can be stored during solar peak hours and it can be utilized during off peak hours/night times, using TES system. Likewise, both in cold and hot climates, electricity consumption varies significantly during day and night timings, due to space heating and air conditioning. Therefore, an effective power consumption management can be achieved by using TES system to store the thermal heat or coolness in off peak loads hours and use it during peak loads hours.

The unpredictable and varying nature of renewable energy affects the supply and demand gap of energy, which can be sorted by adopting robust and responsive energy storage technique. However, the speedy energy storage and its reclamation has been a major challenge. TES can be classified into sensible heat storage (SHS), latent heat storage (LHS) and thermo-chemical categories of heat storage systems. SHS is the most commonly exercised method, e.g. water and rock bed are used to store heat in solar heating systems and in air based heating systems, respectively. However, LHS system is considered the most promising technique for storing thermal energy due to their wide range of availability of PCMs, higher thermal storage density and almost isothermal operation of thermal storage/retrieval. Morrison [1] and Ghoneim [2] reported that to store equal amount of thermal energy from a unit collector area, the storage mass for rock (SHS) will be seven times to that of paraffin 116 wax (LHS), five times to that of medicinal paraffin (LHS) and eight times to that of $Na_2SO_4.10H_2O$ (LHS).

Telkes and Raymond were the pioneers to investigate PCMs in 1940s. However, PCMs were ignored until the energy crisis in late 1970s and early 1980s, which motivated scientists to explore the usage of PCMs in solar heating systems and other applications. Since then, a good amount of research has been carried out to assess the thermal performance of PCMs in LHS system. Research has explored the design fundamentals, transient behaviour, system optimization and various field applications of PCMs in LHS system. Although, LHS system is more promising than SHS but it lacks practical applications due to low thermal conductivity, poor thermo-physical stability, corrosive nature of PCMs towards its container material, phase segregations and subcooling, irregular melting, volume variation during phase transition and higher cost.

The flexibility of PCM to store and retrieve thermal energy at desired time enables it to be employed in broad range of practical applications. A number of comprehensive review articles have been published with a focus on the encapsulation of PCMs; their different types and techniques, encapsulate materials and their utilization in concentrated solar power plants, heat recovery systems, solar thermal heating systems and various

passive residential thermal control applications [3-5]. In recent years, a considerable amount of research has been conducted in identification of various novel PCM composites which possess enhanced form-stability, thermal conductivity and thermal storage density [6-8]. Similarly, metal matrix and metal nanoparticle based phase change composites have presented better thermal conductivity than the typical PCMs and thus it indicates a new paradigm for TES systems [9].

This review paper is focused on classification and selection of PCMs for LHS system. A comprehensive review of organic paraffins and inorganic salt hydrates is presented as these groups of PCMs possess high phase change enthalpy, sharp melting point, cost effectiveness and abundant availability. Also, both paraffins and salt hydrates are the most studied and commercially used groups of PCMs. For long term utilization of LHS system, it is essential that the PCMs should possess long term thermo-physical stability and hold a good compatibility with container material. This review article presents the thermo-physical stability of paraffins and salt hydrates; and their compatibility with various plastic and metallic containers. Due to low thermal conductivity of organic and inorganic PCMs, the productivity of LHS system during thermal energy storage and retrieval is highly affected. This article reviews the performance enhancement techniques such as the effect of container configurations, inclusion of extended surfaces and fins, additives for enhancing thermal conductivity, employing multi-PCMs and encapsulation of PCMs. This review will help in selecting reliable PCM and compatible container material, with efficient geometric configurations to achieve maximum thermal utilization of PCM based LHS system.

2. Classification of latent heat storage materials

LHS system uses PCM as thermal energy storage medium. Thermal energy transfer occurs when PCM is melted from solid to liquid or solidified from liquid to solid. During the phase transition of PCM, thermal energy is stored or retrieved. PCM phase transition occurs at nearly constant temperature and unlike sensible storage medium such as water, rocks or masonry; PCM captures 5-14 times more heat per unit volume. Plenty of research is carried out in identifying several groups of suitable PCMs . The selection of PCM for thermal storage system shall possess desirable thermo-physical, chemical, kinetic and economic properties, as summarized in Table 1.

Table 1

Key design properties of PCM for storage purposes.

Thermal	Physical	Chemical	Kinetic	Economic
Appropriate phase transition temperature	Low vapour pressure (<1 bar)	Compatible with container material	High crystallization rate	Cost effective
High latent heat of fusion and specific heat	High density and small volume change	Long term chemical cycling stability	High nucleating rate to avoid supercooling	Abundant
High thermal conductivity	High phase stability	Highly non-flammable, non-toxic and non-explosive		Available

For the past four decades, an extensive research is carried out in identification of various nature of PCMs in a wide range of phase transition temperature and latent heat of fusion including organic materials (e.g.

paraffins, fatty acids), inorganic materials (e.g. salt hydrates, metallic) and eutectics (e.g. mixture of organic-organic, inorganic-inorganic and organic-inorganic materials). Each group of PCMs have their own properties, strengths and limitations. Table 2 shows the detail comparison of various groups of PCMs. It is evident from table 2 that paraffins and salt hydrates can provide a better thermal energy storage medium than others.

Paraffins are made up of mixture of alkanes of type C_nH_{2n+2}. They possess almost similar properties and an increase in chain length ensure higher melting point and latent heat of fusion [10, 11]. Paraffins are widely used as thermal energy storage medium due to their good latent heat values (60 - 269 kJ/kg and ≅ 150 MJ/m^3), varied range of phase transition temperature, low vapour pressure, chemical stability and inert to metal containers, no tendency to supercooling and commercially available in reasonable cost. Paraffins are nontoxic [11, 12]. Table 3 presents the list of thermo-physical properties of paraffins studied by many researchers and commercially manufactured. Besides various favourable properties, paraffins also have some undesirable characteristics which limit applications such as: low thermal conductivity (≅ 0.2 W/mK) and incompatibility with plastic containers [11, 13-15].

Salt hydrates are compounds of inorganic salt and water of general formula $AB.nH_2O$. Solid-liquid transitions of salt hydrates are actually the dehydration and hydration of salt. Salt hydrates are extensively studied and most important group of PCMs, due to their high latent heat of fusion per unit volume (86 - 328 kJ/kg and ≅ 350 MJ/m^3), higher thermal conductivity than paraffins (≅ 0.7 W/mK) and cheaper cost than paraffins [16]. However, during melting of salt hydrates some anhydrous salt or lower hydrates and water formation takes place and due to difference in densities the anhydrous salt (or lower hydrates) settles at the bottom of the container reducing the active volume of heat storage. Salt hydrates also experience supercooling because of their poor nucleating properties. Moreover, some salt hydrates are corrosive towards container materials [15, 17]. Table 4 presents the thermo-physical properties of salt hydrates found in literature and some of the manufacturing companies.

Table 2

Comparison of various PCM groups.

Classification	**Ref.**	**Organic Materials**		**Inorganic Materials**		**Eutectics** [b]
		Paraffins	Fatty Acids	Salt Hydrates	Metallic [a]	
Formula	[11, 14]	C_nH_{2n+2} (n=12-50)	$CH_3(CH_2)_{2n}.COOH$	$AB.nH_2O$	-	-
Melting Point	[11, 13]	-12-135 ^oC	-7-187 ^oC	-33-120 ^oC	29.8 - 125 ^oC	-30.6 - 93 ^oC
Latent Heat	[11, 13, 14]	60 - 269 kJ/kg	125 - 250 kJ/kg	86 - 328 kJ/kg	25 - 90.9 kJ/kg	100 - 267 kJ/kg
Thermal Conductivity	[13, 15]	0.2 W/m K	0.2 W/m K	0.7 W/m K	40.6 W/m K	0.680 W/m K
Density (kg/m^3)	[11-14]	760 (liquid), 900 (Solid)	878 (liquid), 1004 (solid)	1937 (liquid), 2180 (solid)	5910 (solid)	1530 (liquid), 1640 (solid)
Key Features		1. Increase in chain length results in increased melting point and latent heat. 2. Most commercially used PCMs.	1. Unlike paraffin, each material possesses its own properties. 2. Variation in latent heat and melts over a wide range.	1. Alloys of water and inorganic salts. 2. Greater phase change enthalpy. 3. Most studied group of PCMs	1. Due to larger weight, it is not seriously considered.	1. No phase segregation during phase transition. 2. Mixture of two or many organic or inorganic or both components.
Advantages		1. Chemically stable, safe, reliable and non-corrosive. 2. No tendency to supercooling or segregation. 3. Good latent heat of fusion. 4. Compatible with all metal containers. 5. Less expensive and available.	1. High latent heat of fusion. 2. Sharp phase transformation. 3. Fatty acids show reproducible melting and freezing. 4. No supercooling.	1. High latent heat of fusion per unit volume. 2. High thermal conductivity. 3. Small volume change than others. 4. Higher density. 5. Sharp melting point. 6. Available and cheap.	1. High thermal conductivity. 2. Low vapour pressure. 3. High heat of fusion per unit volume.	1. Good thermal conductivity. 2. High latent heat of fusion per unit volume.

Disadvantages	1. Low thermal conductivity and density. 2. Incompatible with plastic container. 3. High volume change, volatile and inflammable. 4. No well-defined sharp melting point.	1. Low thermal conductivity. 2. Low flash point. 3. Instable at high temperature and highly inflammable. 4. Toxic and mild corrosive. 5. 2-3 times expensive than paraffins.	1. Corrosion on metal containers. 2. Phase segregation. 3. Supercooling. 4. Lack of thermal stability. 5. Slightly toxic	1. Low specific heat capacity. 2. Low heat of fusion per unit weight. 3. Costly	1. Low latent heat of fusion per unit weight. 2. Very costly.
Method for improvement	1. Installation of Fins in storage unit. 2. Adding highly thermal conductive additives. 3. Adding fire-retardants	1. Fire retardant additives. 2. Thermal conductivity enhancement additives.	1. Nucleating and thickening agent additives. 2. Mechanical Stirring. 3. Use of excess water. 4. PCM encapsulation.		

[a] In metallic category, only potential low melting point PCMs are considered.

[b] In eutectic category, paraffin eutectics, fatty acid eutectics, salt hydrates eutectics, metallic eutectics, salt hydrates– metallic, paraffin– salt hydrates and paraffin– metallic eutectics are considered.

Table 3

Thermo-physical properties of Paraffins

Type of PCM	Ref.	Melting Point (°C)	Latent Heat of Fusion (kJ/kg)	Specific heat Capacity C_p (kJ/kg K)		Thermal Conductivity (W/m. K)		Density (kg/m^3)		Thermal Cycles
				Solid	Liquid	Solid	Liquid	Solid	Liquid	
Dodecane	[15]	−9.6	216				2.21			
RT-9 HC	[18]	-9	260	2		0.2	0.2	880	770	
RT 0	[18]	-1	225	2		0.2	0.2	880	770	
RT 3 HC	[18]	3	200	2		0.2	0.2	880	770	
n-Tetradecane	[12]	6	230							
	[15]	5.8-5.9	258-227			0.21				
RT 8 HC	[18]	8	200	2		0.2	0.2	880	770	
RT 10	[18]	10	190	2		0.2	0.2	880	770	
Paraffin C15	[11]	10	205							
n-Pentadecane	[15]	10	193.9						770	
Paraffin C_{16}	[11]	16.7	237.1							
RT 18 HC	[18]	18	250	2		0.2	0.2	880	770	
n-Heptadecane (C_{17} H_{36})	[19]	18.4	84.7							3000
	[12]	19	240			0.21			760	
Paraffin C_{17}	[11]	21.7	213							
Paraffin C_{16}–C_{18}	[12, 20, 21]	20-22	152							
Paraffin C_{13}–C_{24}	[12, 20]	22-24	189				0.21	900	760	
RT 25 HC	[18]	22-26	230	2		0.2	0.2	880	770	
n-Octadecane	[22, 23]	27.7	243.5	2.14	2.66	0.19	0.148	865	785	
RT 28 HC	[18]	27-29	245	2		0.2	0.2	880	770	
Paraffin C_{18}	[11, 12, 20]	28	244			0.15	0.148	814	774	
n-Octadecane	[15]	28	245			0.358	0.148	814	779	
RT 28 HC	[18]	28	245	2		0.2	0.2	880	770	
Paraffin C_{19}	[11]	32	222							
Paraffin wax	[21, 24]	32	251	1.92	3.26	0.514	0.224	830		
RT 35 HC	[18]	35	240	2		0.2	0.2	880	770	
Paraffin C_{20}	[11]	36.7	246							
Heneicosane	[15]	40	155.5-213					778		
Heptadecanone	[11]	41	201							
Paraffin C_{16}–C_{28}	[12]	42-44	189			0.21		910	765	
RT 44 HC	[18]	44	255	2		0.2	0.2	880	770	

Docosane	[15]	44	196.5-252							
Paraffin (70 wt%) + Polypropylene (30 wt%)	[25]	44.77	136.16							3000
P116-Wax	[2, 21, 22]	46.7	209	2.89	2.89	0.14	0.277	786		
Paraffin ($C_{22.2}$ $H_{44.1}$) (TG)	[26]	47.1	166							900
3-Heptadecanone	[11]	48	218							
Paraffin C_{20} – C_{33}	[12, 20]	48-50	189			0.21		912	769	
9-Heptadecanone	[11]	51	213							
Paraffin wax 53 (CG)	[26, 27]	53	184			2.05				1500
Paraffin wax 54 (CG)	[28]	53.32	184.48							1500
RT 55	[19]	55	172	2		0.2	0.2	880	770	
Paraffin C_{26}	[11]	56.3	256							
Paraffin ($C_{23.2}$ $H_{48.4}$) (TG)	[26]	57.1	220							900
Paraffin wax 60-62	[28]	57.78	129.7							600
Paraffin wax 58-60	[28]	58.27	129.8							600
Paraffin C_{22} – C_{45}	[12, 20]	58-60	189			0.21		920	795	
RT 64 HC	[18]	64	230	2		0.2	0.2	880	780	
Paraffin wax	[17]	64	173.6			0.346	0.167	916	790	
Paraffin C_{21} – C_{50}	[20]	66-68	189			0.21		930	830	
RT 70 HC	[18]	69-71	260	2		0.2	0.2	880	770	
Paraffin C_{33}	[11]	73.9	268							
Paraffin C_{311}	[11]	75.9	269							
Paraffin natural wax 811	[15]	82-86	85			0.72				
Paraffin natural wax 106	[15]	101-108	80			0.65				
Polyethylene	[12]	110-135	200					9110	870	

Table 4

Thermo-physical properties of Salt Hydrates

Type of PCM	Ref.	Melting Point (°C)	Latent Heat of Fusion (kJ/kg)	Thermal Conductivity (W/m. K)		Density (kg/m^3)		Thermal Cycles
				Solid	Liquid	Solid	Liquid	
SN 33	[12]	-33	245					
TH 21	[12]	-21	222					
SN 18	[12]	-18	268					
SP -13	[18]	-13	300	0.6				
STLN 10	[12]	-11	271					
SN 06	[12]	-6	284					
SLT 3	[12]	-3	328					
$LiClO_3 \cdot 3H_2O$	[12, 29]	8	253			1720	1530	
$CCl_3F.17H_2O$	[30]	8.5	210					100
$K_2HPO_4 \cdot 6H_2O$	[11]	14	109					
$NaOH_3$ $5H_2O$	[31]	15						5650
Na_2SO_4 1/2NaCl $10H_2O$	[31]	20						5650
$FeBr_3 \cdot 6H_2O$	[11]	21	105					
SP 21 E	[18]	21-23	160	0.6		1500	1400	
$Mn(NO_3) \cdot 6H_2O$	[20, 32]	25.9					1738	
SP 26 E	[18]	25-27	200	0.6		1500	1400	
$CaCl_2 \cdot 12H_2O$	[11]	29.8	174					
TH 29	[15, 32]	29	188	1.09				
Calcium chloride hexahydrate	[29, 33]	29.8	190.8	1.088	0.54	1802	1562	1000
($CaCl_2$ $6H_2O$)	[34]	23.26	125.4					1000
	[31]	27						5650
	[35]	28	86					1000
$LiNO_3 \cdot 3H_2O$	[20, 29, 32]	30	296					
$LiNO_3 \cdot 2H_2O$	[11]	30	296					
SP 31	[18]	31-33	220	0.6		1300	1100	
$Na_2SO_4 \cdot 3H_2O$	[20]	32	251					
Glauber's salt (Na_2SO_4	[36]	32.4	238					320
$10H_2O$)	[20, 31]	32	254	0.554		1485	1458	5650
$Na_2CO_3 \cdot 10H_2O$	[12]	32-36	246.5					
$CaBr_2 \cdot 6H_2O$	[12, 37]	34	115.5				1956	
$LiBr_2 \cdot 2H_2O$	[11]	34	124					
$Na_2HPO_4 \cdot 12H_2O$	[20, 29]	35-44	280	0.514		1522		
$Zn(NO_3)_2 \cdot 6H_2O$	[11, 12, 37]	36	147		0.469	1937	1828	
$FeCl_3 \cdot 6H_2O$	[12]	37	223					

$Mn(NO_3)\cdot 6H_2O$	[11]	37.1	115				1738	
$CoSO_4\cdot 7H_2O$	[11]	40.7	170					
$KF\cdot 2H_2O$	[11]	42	162					
$MgI_2\cdot 8H_2O$	[11]	42	133					
$CaI_2\cdot 6H_2O$	[11]	42	162					
$K_2HPO_4\cdot 7H_2O$	[11]	45	145					
$Ca(NO_3)_2\cdot 4H_2O$	[11, 20]	47	153					
$Zn(NO_3)_2\cdot 4H_2O$	[11, 12]	45-47	110					
STL 47	[12, 20]	47	221	1.34				
$Mg(NO_3)\cdot 2H_2O$	[11]	47	142					
$Fe(NO_3)_2\cdot 9H_2O$	[11]	47	155					
$Na_2SiO_3\cdot 4H_2O$	[11]	48	168					
$K_2HPO_4\cdot 3H_2O$	[11]	48	99					
$Na_2S_2O_3\cdot 5H_2O$	[12, 15, 20]	48-49	201-210			1750	1670	
$MgSO_4\cdot 7H_2O$	[12, 20]	48.5	202					
$Ca(NO_3)_2\cdot 3H_2O$	[11]	51	104					
$FeCl_3\cdot 2H_2O$	[11]	56	90					
$Ni(NO_3)_2\cdot 6H_2O$	[11]	57	169					
SP 58	[18]	56-59	250	0.6		1400	1300	
$MnCl_2\cdot 4H_2O$	[11]	58	151					
$MgCl_2\cdot 4H_2O$	[11]	58	178					
$Na(CH_3COO)\cdot 3H_2O$	[12, 15, 20]	58	264-267		0.63	1450	1280	
Sodium acetate trihydrate	[38]	58	230					500
($NaCH_3COO.3H_2O$)	[39]	58	252					100
$Fe(NO_3)_2\cdot 6H_2O$	[11, 20]	60	126					
NaOH	[12, 20]	64.3	227.6			1690		
$Na_3PO_4\cdot 12H_2O$	[11, 12]	65-69	190					
ClimSel C70	[12, 20]	70-71	194	0.7	0.5	1400	1400	
$Na_2P_2O_7\cdot 10H_2O$	[12, 20]	70	184					
$LiCH_3COO\cdot 2H_2O$	[11]	70	150					
E 72	[15]	72	140	0.58				
SP 70	[18]	69-73	150	0.6		1500	1300	
$Al(NO_3)_2\cdot 9H_2O$	[11]	72	155					
$Ba(OH)_2\cdot 8H_2O$	[20, 29, 37]	78	265-280	1.225	0.653	2070	1937	
E 83	[15]	83	152	0.62				
$Mg(NO_3)_2\cdot 6H_2O$	[15, 20, 37]	89	162.8	0.611	0.49	1636	1550	
TH 89	[12, 15]	89	149					
SP 90	[18]	88-90	150	0.6		1650		
$KAl(SO_4)_2\cdot 12H_2O$	[11]	91	184					
$(NH_4)Al(SO_4)\cdot 6H_2O$	[12]	95	269					

Magnesium chloride	[12, 40]	111.5	155.11	0.704	0.694	1569	1450	500
hexahydrate ($MgCl_2$ $6H_2O$)	[41]	110.8	138					1000
E 117	[15]	117	169	0.7				

3. Long term stability of PCMs

Long term useful life of LHS system is limited by poor thermo-physical stability of PCM and corrosion between PCM and its container material. In last two decades, many researchers have indicated the importance of long term stability of PCM-container system [12, 14, 17]. Murat and Khamid [15] suggested that prior to commercial development; the PCMs should be subjected to at least 1000 thermal cycles to examine the long term stability. In this section, a detail review is carried out on thermal stability and corrosion behaviour of various PCM-container materials.

3.1 Thermo-physical stability of PCM

In this section, the thermal stability of paraffins and salt hydrates has been reviewed.

3.1.1 Paraffins

Sari et al. [19] investigated thermal stability of microencapsulated n-heptadecane for 5000 melt-freeze cycles. Perkin Elmer Diamond DSC (Differential scanning calorimeter) and electric hot plate setup were used as thermal and cycling equipment. They observed good stability of thermo-physical properties of microencapsulated n-heptadecane as the melting point and latent heat of fusion before and after the 5000 thermal cycles varied from 18.4-18.9 ^oC and 84.7-94.5 kJ/kg, respectively.

Alkan et al. [25] conducted 3000 thermal cycles of paraffin and polypropylene composite. Setaram DSC 131 and electric hot plate setup were used as thermal and cycling equipment. The results from DSC depicted a small variation in melting point and latent heat of fusion of paraffin within the composite from 44.77-45.52 ^oC and 136.16-116.12 kJ/kg, respectively. It was deduced from stability tests that the composite can be used for solar heating applications.

Hadjieva et al. [26] studied variation in thermo-physical properties of three technical grade hydrocarbons $C_{22.2}H_{44.1}$, $C_{23.2}H_{40.4}$ and $C_{24.7}H_{51.3}$. DSC with Mettler TA 3000 system and thermostatic bath setup were used to conduct 900 thermal cycles. $C_{22.2}H_{44.1}$ showed a stable behaviour to thermal cycles with a minor change in melting point and latent heat, from 47.1-46.6 ^oC and 166-163 kJ/kg, respectively. Likewise, $C_{23.2}H_{40.4}$ displayed no degradation in the thermo-physical properties after 900 thermal cycles. The change in phase transition temperature and latent heat were negligible, such as from 57.1-57.8 ^oC and 220-224 kJ/kg, respectively. Whereas, $C_{24.7}H_{51.3}$ degraded abruptly showing low latent heat capacity and noticeable change in phase transition range. Because of cheap price and highest enthalpy, $C_{23.2}H_{40.4}$ was proposed an efficient material for LHS system.

Shukla et al. [28] evaluated three paraffin waxes of different temperature specified as sample A (m.p 58-60 ^oC), sample B (m.p 60-62 ^oC) and sample C (m.p 54 ^oC). Rheometric scientific ltd. DSC and oven were used to conduct 600 thermal cycles for sample A and B, whereas, sample C was examined for 1500 thermal cycles. DSC results indicated significant degradation in transition temperature and enthalpy of sample A and B.

However, sample C was most stable even after 1500 thermal cycles and was proposed as a good PCM for LHS system.

Sharma et al. [42] examined commercial grade paraffin wax 53. Rheometric scientific ltd. DSC and electric hot plate setup were used to conduct 300 accelerated melt-freeze cycles. Paraffin wax was found to be stable PCM with a small change in latent heat of fusion, from 184-165 kJ/kg. Later on, the same PCM was investigated for 1500 thermal cycles [27]. The results from DSC showed a slight change in melting point (53-50 ^{o}C), whereas, a noticeable change was observed in latent heat (184-136 kJ/kg).

Table 3 provides detail list of paraffins along with their transition temperature, latent heat of fusion, thermal conductivity, density and thermal cycles. The experimental results show that thermo-physical properties of paraffins do not degrade after repeated thermal cycles.

3.1.2 Salt Hydrates

Calcium chloride hexahydrate ($CaCl_2.6H_2O$) is the most studied PCM in salt hydrates group. $CaCl_2.6H_2O$ experiences continuous phase separation and causes either formation of $CaCl_2.4H_2O$ or other hydrates, with repeated thermal cycles, which settle down in the container.

Kimura and Kai [33] examined thermo-physical stability of $CaCl_2.6H_2O$ using Perkin elmer DSC and two tubes heat exchanger for carrying 1000 thermal cycles. They used excess water to control the formation of other hydrates and to increase solubility. NaCl was mixed for its good nucleating potentials. The mixture was tested for 1000 thermal cycles. They noticed a good repeatability of thermo-physical properties and no phase separation.

Fellechenfeld et al. [35] used strontium chloride hexahydrate as nucleating agent and silica gel as thickener in $CaCl_2.6H_2O$. They used Mettler DSC and water bath setup for performing 1000 thermal cycles. They noticed no phase separation and no degradation of thermo-physical properties. Also, Tyagi et al. [34] examined the thermal stability of $CaCl_2.6H_2O$, using TA Instruments DSC Q-100 to perform 1000 accelerated thermal cycles of cooling and heating and observed a small variation in latent heat of fusion but stability in transition temperature.

Marks [36] evaluated the thermal stability of pure Glauber's salt ($Na_2SO_4.10H_2O$) and thickened one. Attapulgite clay was employed as thickener and Borax ($Na_2B_4O_7.10H_2O$) was mixed as nucleating agent. Calorimeter and thermal cycling chamber were used to conduct 320 thermal cycles on both pure and thickened Glauber's salt. It was deduced from thermal cycles that thermo-physical properties of pure Glauber's salt degrade quicker than thickened mixture. However, it was reported that due to declination in thermal capacity, both pure and thickened Glauber's salt were rejected for long term LHS system.

Porisini [31] evaluated thermal stability of commercial grade salt hydrates specified as sample A ($NaOH.3.5H_2O$), sample B ($Na_2SO_4.½NaCl.10H_2O$), sample C ($CaCl_2.6H_2O$) and sample D ($Na_2SO_4.10H_2O$). He used thermostatic chamber to conduct 5650 thermal cycles on each sample. Sample A and sample B failed after 10 and 300 thermal cycles, respectively. Sample D also experienced declination in thermal properties after 100 thermal cycles. However, sample C showed good thermo-physical stability even after 5650 thermal cycles.

196 Kimura and Kai [30] investigated thermal stability of Trichlorofluoromethane heptadecahydrate
197 ($CCl_3F.17H_2O$). Polyacrylamide was added as thickener and Tetrabutyl ammonium fluoride hydrate was added
198 as nucleating agent. Perkin elmer DSC and glass beaker with water jacket were used to carry 100 thermal cycles
199 of the mixture. The PCM showed good thermal stability and it was concluded that it can be used for coolness
200 storage.

201 Wada et al. [38] conducted thermal stability test of three samples of sodium acetate trihydrate specified
202 as guaranteed grade, technical grade and technical grade with added thickener. Polyvinyl alcohol and sodium
203 pyrophosphate decahydrate were added as thickener and nucleating agent. Calorimeter and thermal bath were
204 used to carry 500 thermal cycles on each sample. It was reported that enthalpy capacity of guaranteed grade
205 sample degrade comparatively quicker than technical grade sample. It was also observed that technical grade
206 with thickener sample experienced little declination in thermo-physical properties during thermal test. Kimura
207 and Kai [39] also tested 220g of same sodium acetate trihydrate which was examined by Wada et al [38].
208 Disodium phosphate was used as nucleating agent and excess water to increase solubility. They prepared four
209 samples of different ratio of water. They observed phase separation for all four samples and no noticeable
210 improvement in stability of hydrate because of excess water. They concluded that due to severe phase
211 separation, this hydrate cannot be considered as a material for LHS system. The conclusion made by Wada et
212 al. [38] and Kimura and Kai [39] comes in contradiction. The reason for phase separation might be because of
213 the small amount of sample (30g) taken by Wada et al. [38] in comparison to Kimura and Kai [39].

214 Sebaii et al. [40] conducted thermal stability and container material compatibility tests of commercial
215 grade magnesium chloride hexahydrate ($MgCl_2.6H_2O$). Shimadzu DSC- 60 and Heraeus D-6450 electric oven
216 were used to carry out 500 thermal cycles and SEM for compatibility test. It was noticed that $MgCl_2.6H_2O$
217 experienced phase segregation in unsealed container even with excess water and was not compatible with
218 container material (aluminium or stainless steel). The changes in transition temperature (111.5–124.12 ^oC) and
219 latent heat of fusion (155.11-85 kJ/kg) were significant and thus it could not qualify to be used as thermal
220 storage material. Later on, the same researcher investigated thermal stability for 1000 thermal cycles of
221 $MgCl_2.6H_2O$ with sealed container and excess water [41]. It was observed that sealing of container and excess
222 of water improved thermo-physical stability with slight change in transition temperature (110.8-115.39 ^oC) and
223 latent heat of fusion (138-130.28 kJ/kg).

224 Table 4 provides detail list of salt hydrates along with their transition temperature, latent heat of fusion,
225 density and thermal cycles. The experimental results show that salt hydrates need nucleating agents and
226 thickeners to sustain long term thermal stability.

227 **3.2 Container-PCM compatibility**

228 For long term stability of LHS system, the compatibility between selected PCM and its container
229 material is considered very important.

230 Lazaro et al. [43] evaluated the compatibility of four commercial organic PCMs (C16-C18, RT20,
231 RT25 and RT26) and one inorganic PCM (TH24) against plastic materials (PP, LDPE, HDPE and PET). During
232 ten months of experimental investigations, through visual inspection and gravimetric analysis, moisture sorption

and migration of organic PCM in plastic containers were detected. The results depicted that due to highest mass variation in LDPE encapsulation, it was discarded against all PCMs. PET encapsulates material produced good mass stability against C16-C18, RT 20, RT 25 and RT 26. However, PP, PET and LDPE indicated increase in material mass due to moisture sorption during TH 24 molten salt test and therefore only HDPE encapsulate material were recommended.

Cabeza et al. [44] tested the corrosive nature of zinc nitrate hexahydrate ($Zn(NO_3)_2.6H_2O$), sodium hydrogen phosphate dodecahydrate ($Na_2HPO_4.12H_2O$) and calcium chloride hexahydrate ($CaCl_2.\ 6H_2O$) upon short term 14 days contact with metals. They observed that apart from stainless steel (Mat. No.1.4301), $Zn(NO_3)_2.6H_2O$ appeared to be extremely corrosive to brass (Ms58 Flach), steel (Mat. No. 1.0345), aluminium (EN AW-2007) and copper (E-Cu 57). $Na_2HPO_4.12H_2O$ proved to be compatible with brass, copper and stainless steel, whereas, it was found very corrosive against aluminium. $CaCl_2.\ 6H_2O$ was found compatible with brass and copper, while it was very corrosive against aluminium, stainless steel and steel.

Cabeza et al. [45] investigated the corrosive nature of same three salt hydrates, as in [44], upon medium term 75 days contact with metals. They reported that while using $Zn(NO_3)_2.6H_2O$ as thermal energy storage medium only stainless steel should be considered for container material. $Na_2HPO_4.12H_2O$ showed good compatibility with brass and stainless steel. Aluminium indicated aggressive corrosion, whereas, copper and steel corrode at slow rate. $CaCl_2.6H_2O$ was observed to have good compatibility with copper, brass and stainless steel but can corrode steel and aluminium at slow rate.

Cabeza et al. [46] conducted compatibility test of two salt hydrates sodium acetate trihydrate ($NaOAc.\ 3H_2O$) and sodium thiosulfate pentahydrate ($Na_2S_2O_3.\ 5H_2O$) with the same five metals as in [44]. It was reported that both salt hydrates showed good compatibility with aluminium, steel and stainless steel, however, both salt hydrates were aggressively corrosive towards brass and copper.

Farrell et al. [47] examined the galvanic coupling of aluminium-copper in contact with sodium sulphate decahydrate and sodium chloride eutectic and sodium acetate with additives. It was observed that aluminium alloy 2024 was corroded by both PCMs. The corrosion was more aggressive when aluminium was in contact with sodium acetate in the presence of copper.

Nagano et al. [48] inspected material compatibility of magnesium nitrate hexahydrate ($Mg(NO_3)_2.6H_2O$) with magnesium chloride hexahydrate ($MgCl_2.6H_2O$) as an additive, and six metals. Each metal sample was placed for 90 days in a glass tube of 60 ml at a constant temperature of 95^{o}C. It was reported that copper, steel and brass experienced strong corrosion with a 90 days mass loss of 0.11g, 0.0843g and 0.0284g, respectively. Stainless steel SUS 304 and SUS 316 underwent a very small mass loss of 0.00107g and 0.00017g, respectively. However, it can be seen from Fig. 1 that almost all the surface of SUS 304 and a small portion of SUS 316 were covered with dotted red-brown rust. Aluminium was the only metal that was not affected by the salt hydrates mixture.

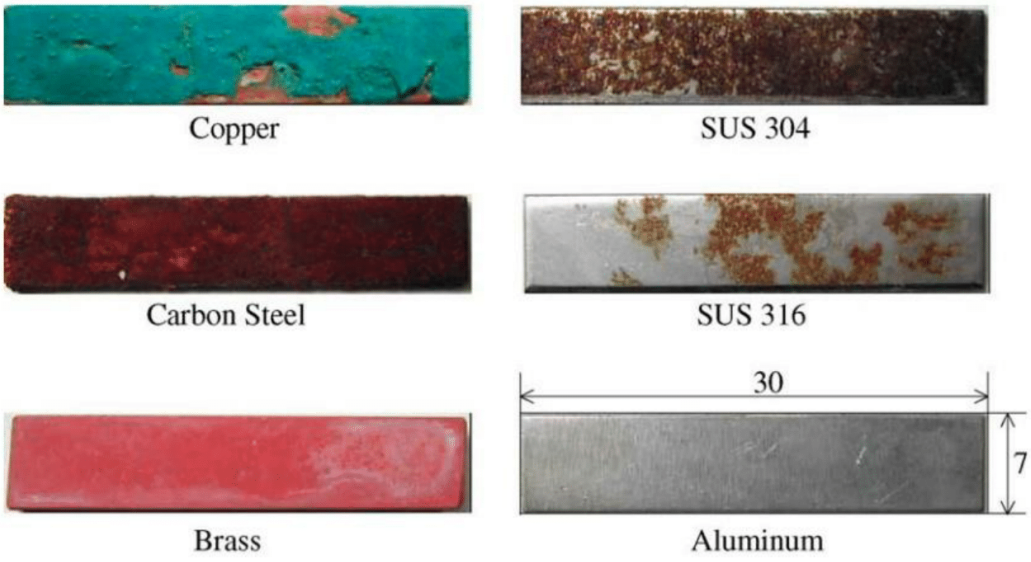

Fig.1. Mg $(NO_3)_2 \cdot 6H_2O$ compatibility test with metals [48].

Garcia et al. [49] studied the corrosion behaviour of commercial grade Glauber's salt ($NA_2SO_4. 10H_2O$) with aluminium alloys (Al 1050, 2024, 3003 and 6063). Aluminium alloy specimens were partly and fully immersed in the Glauber's salt for 90 days at 45°C. Al 2024 experienced strong pitting corrosion and degradation of PCM due to formation of Na-Al alkaline carbonates due to the reaction with CO_2 from the air. Al 1050 and 3003 displayed an excellent compatibility with Glauber's salt. Al 6063 also showed good resistance to corrosion when the sample was fully immersed, whereas a loss of brightness and stained surface was notice when it was partially immersed.

Pere et al. [50] presented the corrosion behaviour of two metals and two metal alloys in contact with eleven different salt hydrates used in cooling and heating applications. Each material specimen was examined after week 1, 4 and 12 to examine corrosion rate, salt precipitation and bubbles formation. They reported that commercial PCM S10 can only be used with stainless steel. Similarly, PCM C10 showed good compatibility with both aluminium and stainless steel. $NaOH.1.5H_2O$, $ZnCl_2.3H_2O$ and $K_2HPO_4.6H_2O$ were well suited with stainless steel, whereas $NaOH.1.5H_2O$ could also be used with carbon steel while $ZnCl_2.3H_2O$ and $K_2HPO_4.6H_2O$ could be used with copper. Stainless steel indicated good resistance to corrosion when brought in contact with heating application PCMs. Commercial PCM C48 also showed good compatibility with carbon steel and aluminium. $MgSO_4.7H_2O$ could be used with aluminium and $K_3PO_4.7H_2O$ was suitable to be used with carbon steel.

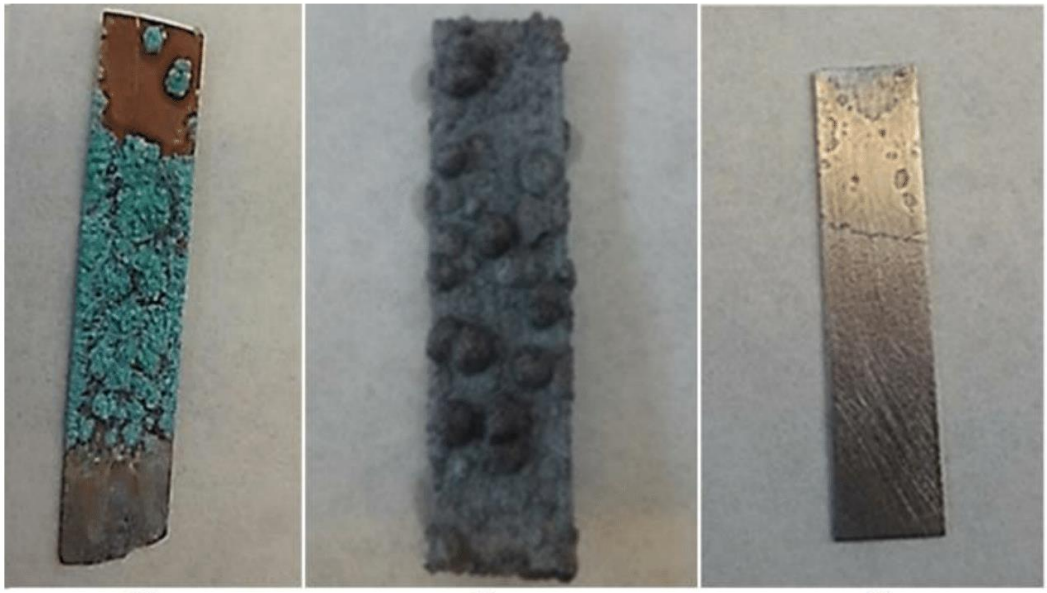

Fig.2. Corrosion tests results: (A) S10 - Copper corrosion test for 12 weeks (B) $ZnCl_2.3H_2O$ - Aluminium corrosion test for 12 weeks, and (C) $Zn(NO_3)_2.4H_2O$-Carbon steel corrosion test for 4 weeks.

Table 5 represents the experimental work carried out in identification of container-PCM compatibility. It is observed from literature that paraffins have poor compatibility with plastic containers; however, high density polyethylene (HDPE) has exhibited good compatibility with paraffins. Similarly, majority of inorganic salt hydrates have corrosive nature with metal containers; however, stainless steel has exhibited good compatibility.

293

Table 5

A list of compatible PCM with container material.

PCM	Ref.	Container Materials				
		Brass	**Copper**	**Aluminium**	**Stainless steel**	**Carbon Steel**
$Zn(NO_3)_2.6H_2O$	[44]	No	No	No	Yes	No
	[45]	No	No	No	Yes	No
$Na_2HPO_4.12H_2O$	[44]	Yes	Yes	No	Yes	No
	[45]	Yes	Caution	No	Yes	Caution
$CaCl_2.6H_2O$	[44]	Yes	Yes	No	Caution	No
	[45]	Yes	Yes	Caution	Yes	Caution
$NaOAc.3H_2O$	[46]	Caution	Caution	Yes	Yes	Yes
$Na_2S_2O_3.5H_2O$	[46]	No	No	Yes	Yes	Yes
$Mg(NO_3)_2 \cdot 6H_2O$	[47]	No	No	Yes	Yes	No
Glauber's salt	[49]			Al 1050 Yes		
($Na_2SO_4.10H_2O$)				Al 2024 No		
				Al 3003 Yes		
				Al 6063 Caution		
S10 (Na_2SO_4 + NH_4Cl + sepiolite)	[50]		No	Caution	Yes	No
C10 (Na_2SO_4 + H_2O + additives)	[50]		No	Yes	Yes	No
$ZnCl_2.3H_2O$	[50]		Yes	No	Yes	No
$NaOH.1.5H_2O$	[50]		No	No	Yes	Caution
$K_2HPO_4.6H_2O$	[50]		Caution	No	Yes	No
S46 ($Na_2S2O_3.5H_2O$ +sepiolite+	[50]		No	Caution	Yes	No
fumed silica)						
C48 (CH_3OONa+H_2O+ additives)	[50]		No	Yes	Yes	Yes
$MgSO_4.7H_2O$	[50]		No	Yes	Yes	No
$Zn(NO_3)_2.4H_2O$	[50]		No	No	Yes	No
$K_3PO_4.7H_2O$	[50]		No	No	Yes	Yes
$Na_2S_2O_3.5H_2O$	[50]		No	Caution	Yes	Caution

294

295 4. LHS system performance analysis and enhancement

296 LHS system with its high thermal storage density at nearly isothermal process provides a better choice
297 of heat storage. However, due to low thermal conductivity and poor thermo-physical stability of PCMs, the LHS
298 system productivity during charging and discharging processes are highly affected. As a result, large scale
299 practical utilization of LHS system remains inefficient. Therefore, it is necessary to enhance the shortcomings of
300 the LHS system by adopting various performance enhancement techniques. In recent years, few review papers
301 are published on thermal performance enhancement of LHS system [51-53]. These review papers have

highlighted the improvement in thermal conductivity of PCMs by using nanostructures, techniques to enhance the thermal performance of PCMs in concentrated solar power plants and the effect of inlet and outlet temperature, and mass flow rate of heat transfer fluid (HTF) on thermal performance of PCM. However, this section reviews the most recent developments in geometrical orientations of containers to enhance heat flow in order to boost the phase transition rate, thermal conductivity enhancement of PCMs by extended surfaces and additives, improvement in thermal storage capacity by multi PCM, and encapsulation of PCMs to ensure better thermal conductivity and thermo-physical stability. This section is focused on techniques that influence the phase transition rate, thermal conductivity, latent heat storage capacity and thermo-physical stability of PCMs.

4.1 PCM container configuration

After the selection of PCM, the geometry of PCM container plays an important role in thermal performance of LHS system. The PCM container geometric configuration has a direct impact on the heat transfer nature and ultimately affects the phase transition rate. PCM containers are of typically rectangular, concentric annular tube, spherical and shell and tube configurations. The most studied geometric configuration is shell and tube, for the fact that it has minimal heat loss characteristic and substantial utilization in engineering applications.

During melting process, heat is transferred from hot surface to PCM through conduction and as the heat transfer continues, the amount of melted PCM increases near hot surface and thus natural convection takes over. Lamberg at al. [54] simulated the melting time of PCM in rectangular container of 96mm height, 20mm thickness and 41mm depth; with and without natural convection. It was justified by comparison with experimental results that LHS system with natural convection took almost half melting time to that without convection consideration. Kamkari et al. [55] studied the dynamic thermal performance of lauric acid as PCM in rectangular container at different inclination angles of 0^o, 45^o and 90^o. The container hot wall was isothermally heated whereas the other walls were thermally insulated. Various experiments were conducted for hot wall temperatures of 55 ^{o}C, 60 ^{o}C and 70 ^{o}C. It was reported that hot wall positioning in rectangular container played a vital role in formation of natural convection currents and therefore affecting the heat transfer rate and melting rate. Initially, the heat transfer in vertical hot wall container was dominated by conduction as temperature contours were almost parallel to hot wall. The viscous forces were overcome by buoyant forces as the temperature of liquid PCM increased, and eventually the hot liquid PCM climbed along the vertical hot wall. The heat transfer was dominated by natural convection and therefore it increased the melting rate in upper portion of solid-liquid interface by increasing local heat transfer due to hot liquid PCM. The temperature of liquid PCM decreased as it descended along the solid-liquid interface and therefore the heat transfer at lower portion of container was found lesser than upper portion. Also, the accumulated hot liquid PCM at upper portion of container absorbed a considerable amount of heat from hot wall and resulted in stratified liquid layer. In case of 45^o inclination of hot wall, contrary to vertical hot wall observations, the stratified temperature layers did not appear at the upper portion of container which means that heat transferred from liquid to solid PCM and thus it increased the melting rate. In case of horizontal hot wall, the uniform temperature distribution along the solid-liquid interface resulted in uniform melting rate. The heat transfer enhancement ratio for horizontal hot wall container was found twice to that of vertical hot wall container, as shown in Fig. 3.

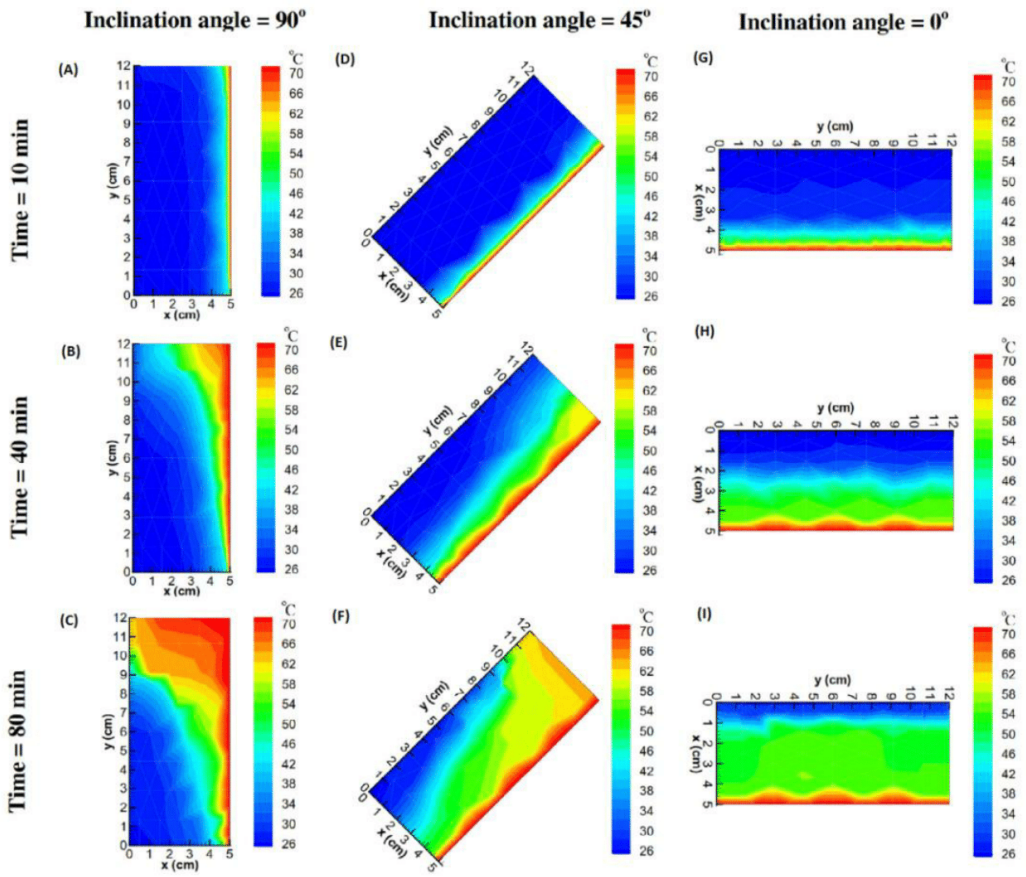

Fig.3. Temperature contours of rectangular container with different inclination angles when hot wall is at 70 °C [55].

Constrained and unconstrained melting of n-Octadecane in a sphere container is experimentally examined by Tan [56]. In constrained melting case, solid PCM is attached to thermocouple to prevent it from sinking to the bottom of sphere due to gravity. It was reported that in unconstrained melting case, the start of PCM melt was dominated by heat conduction across the sphere wall. As the PCM melted then due to difference in densities the solid PCM sank to the bottom. Therefore, the lower portion of solid PCM was melted by heat conduction from inner wall and the upper portion was melted by natural convection caused due to buoyancy effect. In constrained melting case, conduction heat was responsible for initial inward concentric melting and later the melting was dominated by natural convection, making an oval shape at the top half of solid PCM. The upper half of the solid PCM was melting at higher rate than the bottom half. Natural convection cells were formed at bottom half and it caused waviness profile at bottom of solid PCM.

The melting behaviour of n-eicosane in cylindrical container was studied by Jones et al. [57]. The experimental examination was focused on solid-liquid interface, temperature measurements and volumetric liquid fraction. Digital image processing technique was used to locate the melt front in cylindrical container. It was reported that melting process was dominated by four different regimes, such as (a) pure conduction, (b)

conduction and natural convection, (c) natural convection and (d) solid shrinkage. As shown in Fig. 5(a), the melt front was found thin and parallel to vertical hot boundaries of cylindrical container, it depicted that initially melting was dominated by conduction. It was noticed that as the melting increased, the melt front thickness along vertical direction varied, with maximum molten layer thickness was observed at top of container. It indicated the buoyant forces driven natural convection began to strengthen and moving the hot molten layer to top of container. However, the melt front was still almost uniform to vertical hot walls and it was suggested that this regime could be a mixed conduction and natural convection, as shown in Fig. 5(b). Later, the melting was found more influenced by natural convection and the molten layer thickness varied along the vertical hot walls, as shown in Fig. 5(c). Lastly, the top portion of PCM was completely melted by convection and this regime was called shrinking solid, as shown in Fig. 5(d). Similarly, Shmueli et al. [58] numerically investigated the melting behaviour of PCM in vertical cylindrical container, isothermally heated from sides, insulted at bottom and top portion of container was bare to air. The melting behaviour was found similar to that of Jones et al. [57].

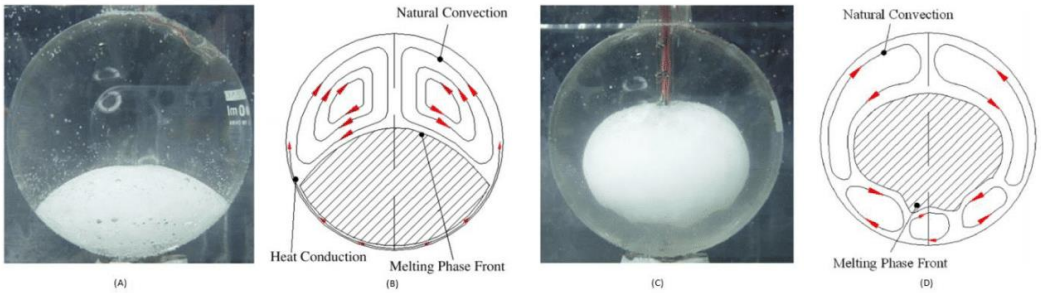

Fig.4. (a) Unconstrained melting inside sphere, (b) Representation of heat conduction and natural convection in unconstrained melting, (c) Constrained melting inside sphere and (d) Representation of natural convection in constrained melting [56].

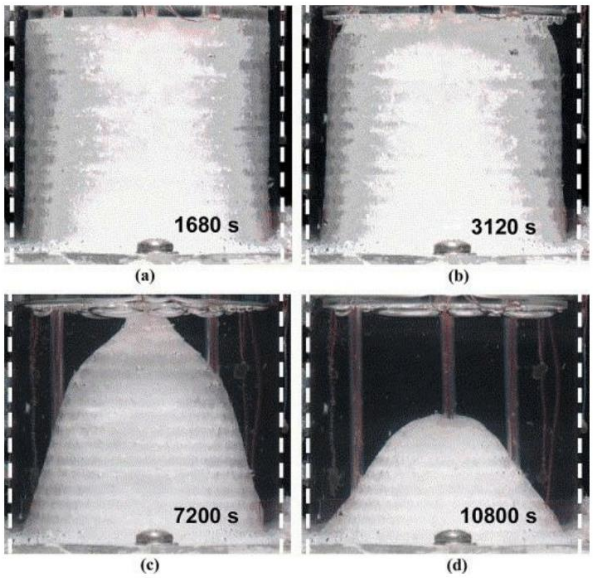

Fig.5. Melting nature of wax in cylindrical container with wall temperature of 45 ^{o}C at various time intervals such as; (a) 1680 seconds, (b) 3120 seconds, (c) 7200 seconds and (d) 10800 seconds [57].

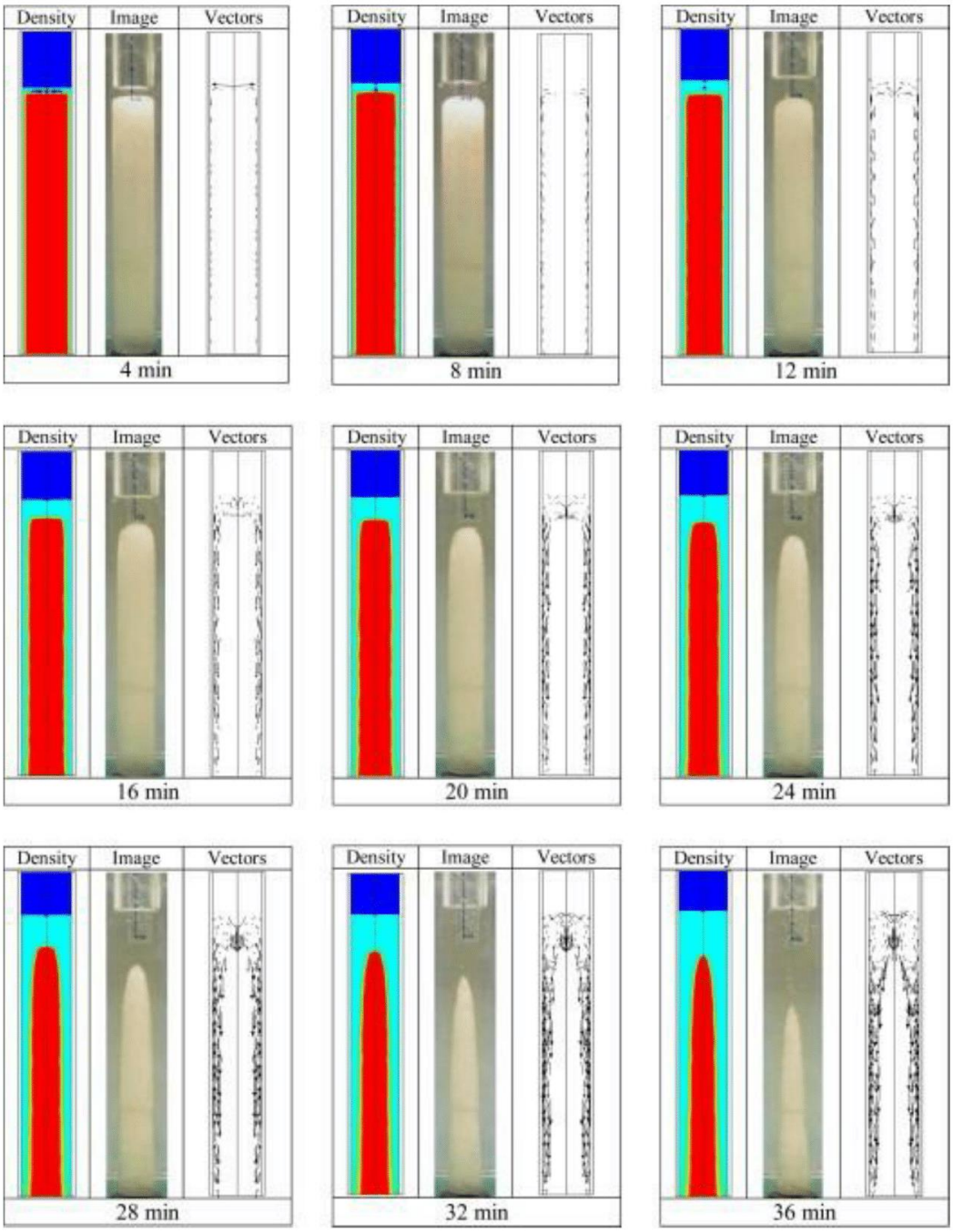

Fig.6. Comparison of simulate density and vector maps with experimental images [58].

Theoretical optimization of two different models of cylindrical containers is carried out by Esen et al. [21]. In the cylindrical model, the PCM was stored in pipe and HTF was flowing parallel in cylindrical portion. Whereas in pipe model, the PCM was stored in cylindrical side and HTF was flowing in pipe. A series of numerical tests were carried out to investigate the effect of different PCMs, radii of cylinder and pipe, mass flow

rate and inlet temperature of HTF on melting time. It was concluded from the results that pipe model required less time than cylindrical model to melt the PCM, due to the fact that thicker mass of PCM takes longer time to melt and less amount of heat loss from the HTF to surrounding.

Esapour et al. [59] investigated the melting behaviour of RT35 in various arrangements of shell and multi-tubes. As exhibited in Fig. 7, RT35 was stored in middle tube/shell, whereas HTF was made to flow in inner tubes and outer one .The effect of number of inner-tubes on charging process was analysed. It was reported that an increase in inner-tubes from 1 to 4 enlarged the molten region and therefore the regime was dominated by convection heat transfer, which led to enhanced melting rate. According to Fig. 8, in case A, both the heating surfaces (inner tube and outer tube) were installed wide apart which resulted in weak natural convection effects and thus the melting rate was slow. Whereas in case B, C and D, heat transfer surface was increased by distributing thinner tubes across the shell. The buoyant force increased as the vortices merged to form a large vortex and therefore the melting rate was accelerated. The utilization of 4 inner-tubes in shell reduced the melting time by 29% to that of single inner-tube.

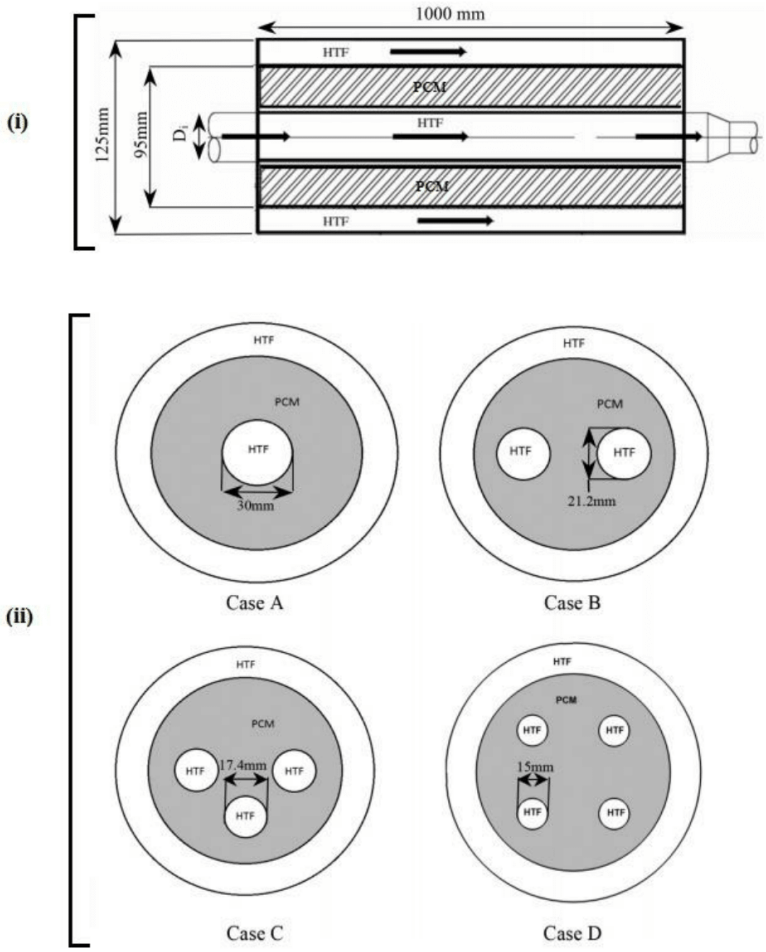

Fig.7. (i) Schematic of physical model of multi-tube configuration, (ii) Configuration of multi-tube cases [59].

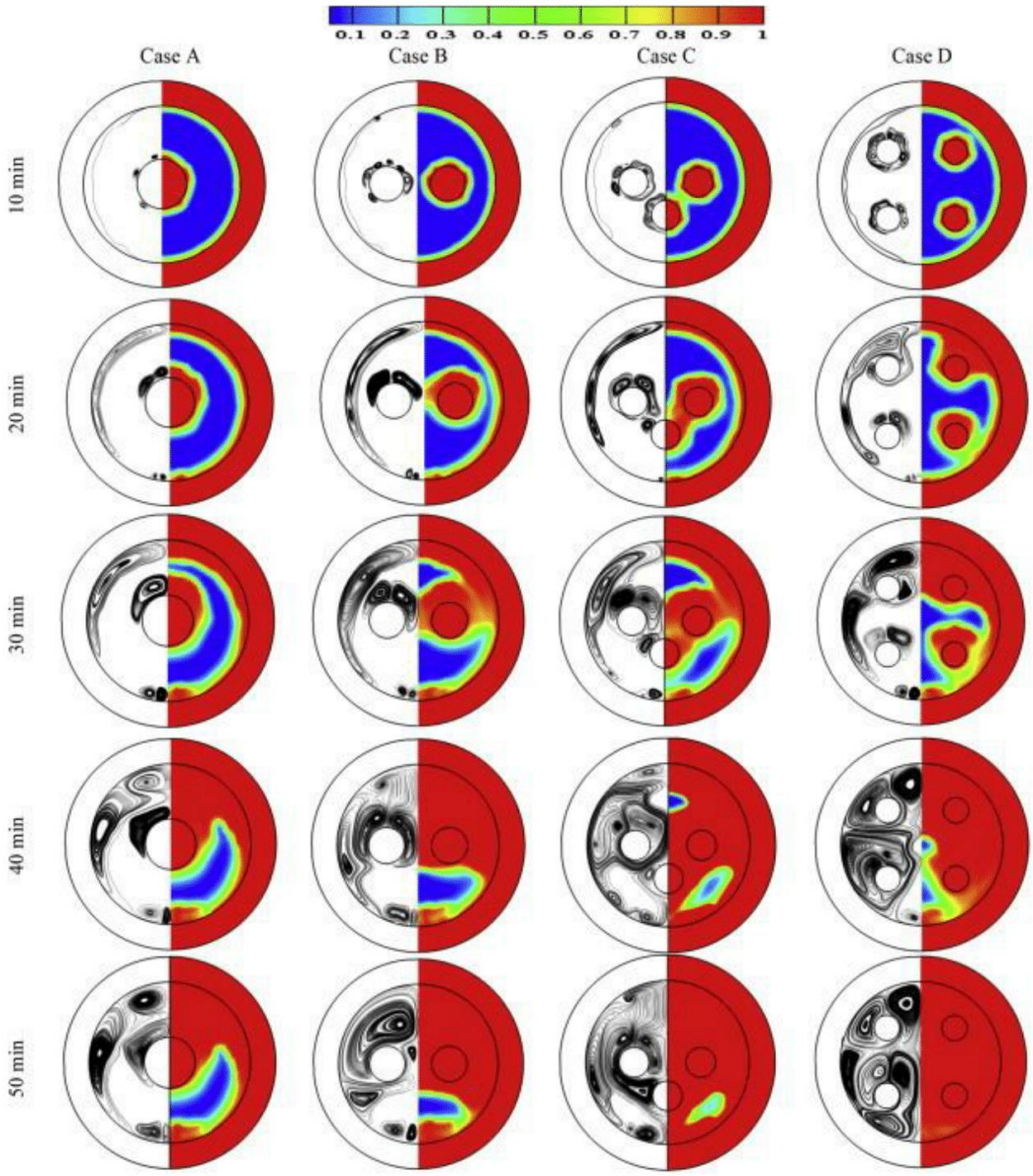

397

398 **Fig.8.** Liquid fraction contours for various multi-tube arrangements [59].

399 Vyshak and Jilani [60] conducted a comparative study on total melting time of PCM stored in
400 rectangular, cylindrical and cylindrical shell containers of same volume and heat transfer surface area. The
401 investigation was carried out for various values of PCM mass and inlet temperature of HTF. It was deduced that
402 cylindrical shell configuration took least time to store the same amount of thermal energy as compared to other
403 two configurations. It was also reported that with increase in mass of PCM, the cylindrical shell performance
404 was more pronounced, comparatively. The results showed that melting time for rectangular container was nearly
405 half to that of cylindrical container. Zivkovic and Fujii [61] also reported the similar results for rectangular and
406 cylindrical configuration.

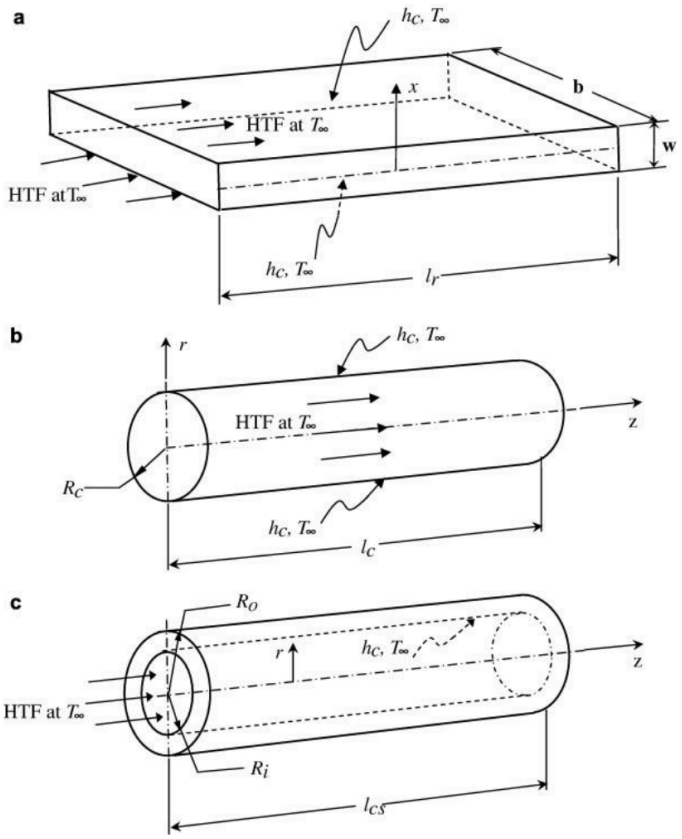

407

408 **Fig.9.** Comparison of various container models: (a) Rectangular container model, (b) cylindrical container
409 model and (c) cylindrical shell container model [60].

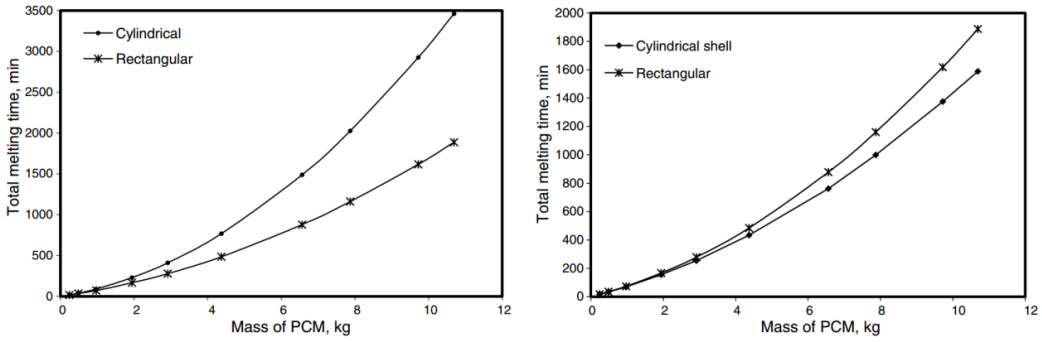

410

411 **Fig.10.** Comparison of total melting time vs mass of PCM for cylindrical and rectangular containers and
412 cylindrical shell and rectangular containers [60]

413 In case of solidification process, the heat transfer is dominated and influenced by conduction. Therefore,
414 the container orientation has insignificant influence on solidification rate. Seddegh et al.[62] numerically
415 evaluated the thermal behaviour of Paraffin wax in horizontal and vertical orientations of shell and tube
416 container. During melting process, it was noticed that the heat transfer in horizontal system was more effective

in melting the upper half of PCM than the lower half, whereas the vertical system presented an almost constant melting rate. Moreover, the comparative analysis showed that horizontal system provided better thermal performance in melting process than vertical system. During solidification process, the natural convection dominated the heat transfer at first, which rapidly reduced the temperature of PCM to its freezing point. The heat transfer was dominated by conduction as the PCM started to solidify around the HTF tube. Due to low thermal conductivity of PCM, the solidified PCM started behaving like insulating medium and thus it reduced the phase transition rate. Due to buoyancy, the liquid PCM was moving to the upper portion of container, whereas the solidification rate was faster in lower portion. Furthermore, the comparative analysis showed that the horizontal and vertical orientations had insignificant influence on solidification rate as the average temperature and solidification rate were almost same for both cases, as shown in Fig. 11. Similarly, Allen et al.[63] experimentally analysed the influence of cylindrical container inclination on solidification rate of n-Octadecane. It was observed that due to conduction dominated heat transfer, the orientation of cylindrical container had a minimal impact on the solidification rate of PCM.

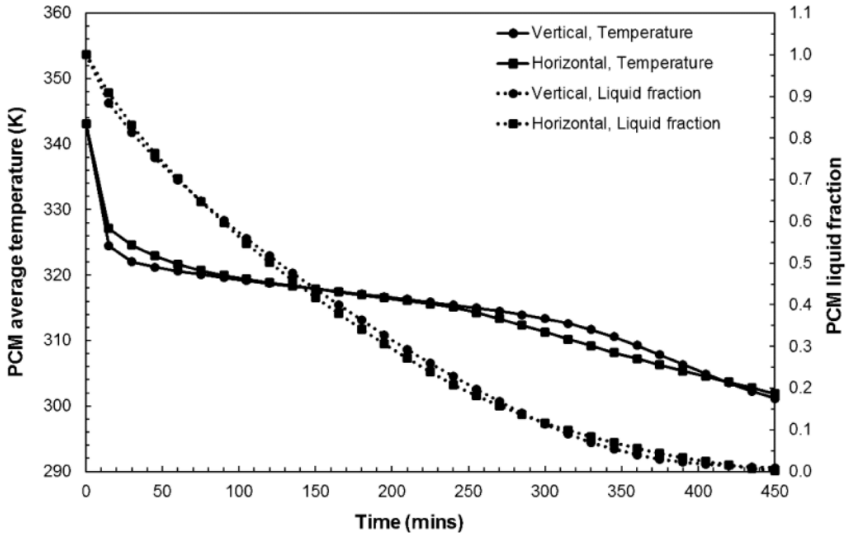

Fig.11. Comparison of PCM average temperature and liquid fraction in horizontal and vertical orientations of shell and tube container during solidification process [62]

In this section, the phase transitions of PCMs in various containers have been reviewed. It is noticed from review that conduction heat transfer and natural convection are responsible for melting behaviour of PCMs in containers with different shapes. In early stages of phase transition from solid to liquid, conduction plays a vital role in transferring excess amount of heat and is responsible for higher melting rate. Later, buoyant forces overcome viscous forces and buoyant forces driven flow depends on heat supply, operating conditions, thermo-physical properties of PCMs and container geometry. Container orientation and geometric parameters have great impact on the melting behaviour of PCMs, such as aspect ratio of rectangular and cylindrical containers, spherical capsules radius and annular cavity eccentricity. Therefore, the selection of PCM container shall be

441 carried with great attention, knowing the effect of geometry configuration on phase transition behaviour of
442 PCM.

443 **4.2 Heat exchanger surface area enhancement**

444 Extended surfaces and fins are employed in the heat exchanger to increase the heat transfer surface area.
445 Fins configuration and orientation play an important role in improving the performance of LHS system. Fins are
446 normally installed in lower heat transfer coefficient side because the fins efficiency rises with declination in heat
447 transfer coefficient. Therefore, fins are mostly on the PCM side.

448 Akhilesh et al. [64] numerically investigated the effect of adding more fins in rectangular container,
449 heated from top wall. It was observed that heat transfer area and thermal energy storage were increased by
450 increasing number of fins per unit length. However, thermal storage performance could not be enhanced any
451 further upon increasing the number of fins beyond a critical value. Gharebaghi and Sezai [65] studied the effect
452 of fins in rectangular container of PCM. It was noticed that inclusion of fins increased the heat transfer rate.
453 They also reported that horizontal fins with vertical heated walls provided double heat transfer rate to that of
454 vertical fins with horizontal heated walls. Thermal storage performance was enhanced by increasing the number
455 of fins and reducing the gap in-between fins. However, increase in number of fin beyond the critical value could
456 not provide considerable enhancement.

457 Lacroix and Benmadda [66] simulated the melting rate of PCM in rectangular container with horizontal
458 fins and vertical heated walls. The simulation was focused on investigating the effect of number of fins and their
459 length. It was concluded that large number of shorter fins (19 fins, each of 0.01m length) are less efficient in
460 improving the melting rate than few number of longer fins (4 fins, each of 0.03 m length). Even with small
461 temperature gradient, longer fins could improve the performance and it was found more efficient than increasing
462 the heated wall temperature.

463 Shatikian et al. [67] numerically studied the effect of fin thickness on melting rate. It was reported that
464 thicker fins experienced uniform temperature along the length of the fin, whereas thinner fins showed
465 temperature gradient. Temperature uniformity was desirable for better heat transfer but too thick fins would
466 reduce the storage capacity of container. Therefore, the thickness and number of fins should be optimized for
467 better performance of LHS system.

468 Stritih [68] experimentally investigated the fin effectiveness of rectangular container. Fin effectiveness is
469 defined as the ratio between heat flux with fins and heat flux without fins. It was noticed that heat flux with fins
470 was high and because of that fin effectiveness was high and resulted in 40% reduction in phase transition time.

471 Tao and He [69] numerically examined the effect of number of fins, fin thickness and fin height on
472 melting rate of PCM in horizontal concentric tube. It was noticed that an increase in fins number, thickness and
473 height amplified the thermal conductivity in lower portion of PCM causing enhanced heat transfer rate and
474 melting rate. However, excessively large number of fin, thickness and height would decrease the storage
475 capacity of PCM. Therefore, the recommended values for number of fins, dimensionless thickness and
476 dimensionless height were 7, 0.1 and 0.8, respectively.

Vertical fins effect with constant temperature horizontal wall on solidification time of high temperature PCM was simulated by Guo and Zhang [70]. It was observed that without fins the solidified front only moved in vertical direction, whereas with fins, simultaneous vertical and horizontal movement of solidified front was noticed. Solidification time observed linear declination with number of fins. Thermal energy discharge time was $1/30^{th}$ with fins to that without fins. Prior to critical value for fin thickness, it was observed that increasing fin thickness could decrease solidification time.

Lacroix [71] numerically studied the behaviour of LHS unit with shell and annular finned tube configuration, with PCM stored in shell side and HTF flowing in tube. Natural convection was considered by including effective thermal conductivity of PCM in conduction equation, as a function of Rayleigh number. It was concluded that annular fins enhanced the heat conduction for all values of mass flow rates and inlet temperatures. Maximum improvement in heat conduction was observed with moderate flow rate and small inlet temperature; whereas even with more number of fins, the increase in heat conduction was less significant with larger flow rate and inlet temperature. Similarly, Zhang and Faghri [72] studied the same shell and annular finned tube system and reported that fins proved to be very effective in tackling the depletion in performance caused by subcooling of PCM.

Rahimi et al. [73] experimentally examined the effect of flow rate, inlet HTF temperature and fin pitch on melting and solidification rate of R35 paraffin in fin and tube heat exchanger. An increase in flow rate from 0.2 L/min to 1.6 L/min enhanced turbulent nature of HTF and it resulted in improved melting rate, whereas the solidification rate was not affected significantly. Similarly, an increase in inlet temperature of HTF from 50 °C to 60 °C enhanced melting time, whereas, the enhancement was not impressive when inlet temperature was increased from 60 °C to 70 °C. It was noticed that solidification rate was more enhanced as compared to melting rate with employing fins. For 5mm fin pitch, the melting and solidification time decreased from 290 to 190 minutes and from 445 to 245 minutes, respectively. Increasing the fin pitch from 5mm to 15mm could not produce a significant difference in transition rates.

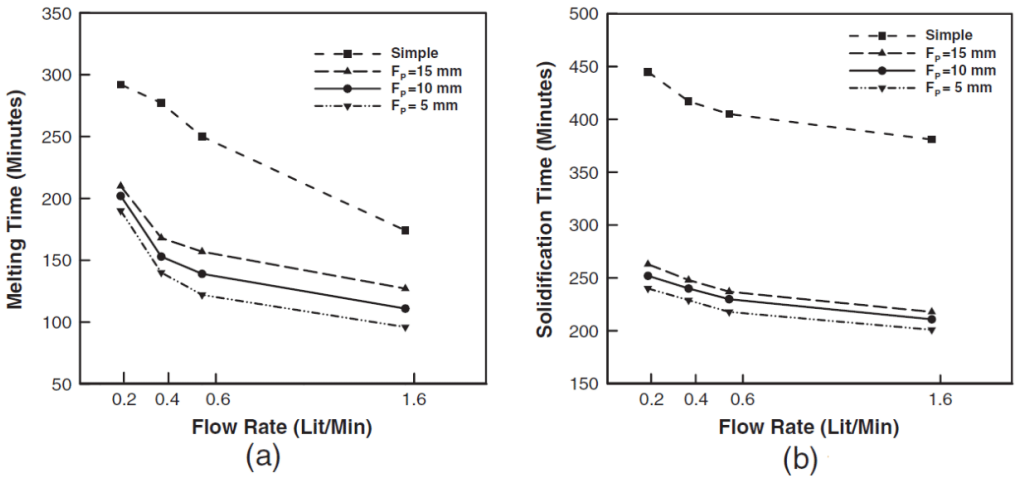

Fig.12. Effect of mass flow rate on phase transition rates for various fin pitch values: (a) melting rate and (b) solidification rate [73].

Choi and Kim [74] experimentally investigated the radial fins effect on solidification time of PCM in cylindrical container. Due to radial fins, enhancement in both radial and axial heat conduction were observed, which result in better heat recovery. It was also reported that at lower mass flow rate of HTF, solidification front was only found on fins portion nearby tube wall. Whereas for higher flow rate of HTF, solidified front was found on large fin portion and better utilization of fins could be made.

Velraj et al. [75] experimentally verified the increase in solidification rate of PCM in vertical concentric double tube, with PCM stored in inner tube with longitudinal fins. It was reported that the portion of liquid PCM which was at furthest from heat transfer surface could be covered by using longitudinal fins, which results in minimal resistance and higher thermal contact. It was noticed that increasing the number of fins in large tube was more effective and solidification time was $1/n^{th}$ times with fins to that without fins.

Rathod et al. [76] analysed the performance enhancement of LHS system by installing three longitudinal fins in shell and tube arrangement. It was noticed that an increase in inlet temperature of HTF is more effective than mass flow rate of HTF. Due to installation of fins, the melting time percentage decrease was 12.5% and 24.52% for the inlet temperature 80 ^{o}C and 85 ^{o}C, respectively. Similarly, the percentage decrease in solidification time was reported to be 43.6%.

An experimental study was carried by F. Agyenim et al. [77], to compare the thermal performance of erythritol in various geometric configurations of horizontal concentric tube, such as concentric tube without fins, with radial fins and with longitudinal fins. PCM charging cycle was carried out for 8 hours. It was reported that only longitudinal fin configuration has completely melted the PCM. During the discharging cycle, longitudinal fin configuration showed insignificant subcooling. Therefore, the longitudinal fin configuration was recommended for enhanced performance in concentric tube LHS system.

Medrano et al. [78] experimentally investigated the melting and solidification rate of organic PCM RT 35 in five commercially available heat exchangers. It was noticed that double pipe heat exchanger and plate type heat exchanger are not appropriate to be used as PCM containers. However, the double pipe with graphite matrix, double pipe with fins and compact heat exchanger can be utilized as heat storage containers. It was reported that compact heat exchanger produced highest average thermal power i.e. 1kW for both melting and solidification case. The normalized thermal power was found maximum in double pipe with graphite matrix, in range of 700–800 W/m^2–K.

As discussed, the inclusion of fins in LHS system enhances the storage performance and reduces the phase transition time. The number and size of fins play an important role in LHS system performance and promotion of natural convection. External fins have more impact on LHS system performance during solidification process than melting process. It is because melting process is dominant by convection, whereas solidification is governed by conduction. In addition, the number of fins in a LHS system can affect the thermal storage capacity of container due to small volume for PCM. Therefore, the fins number and size should be optimized for the system thermal performance enhancement and thermal energy storage capacity.

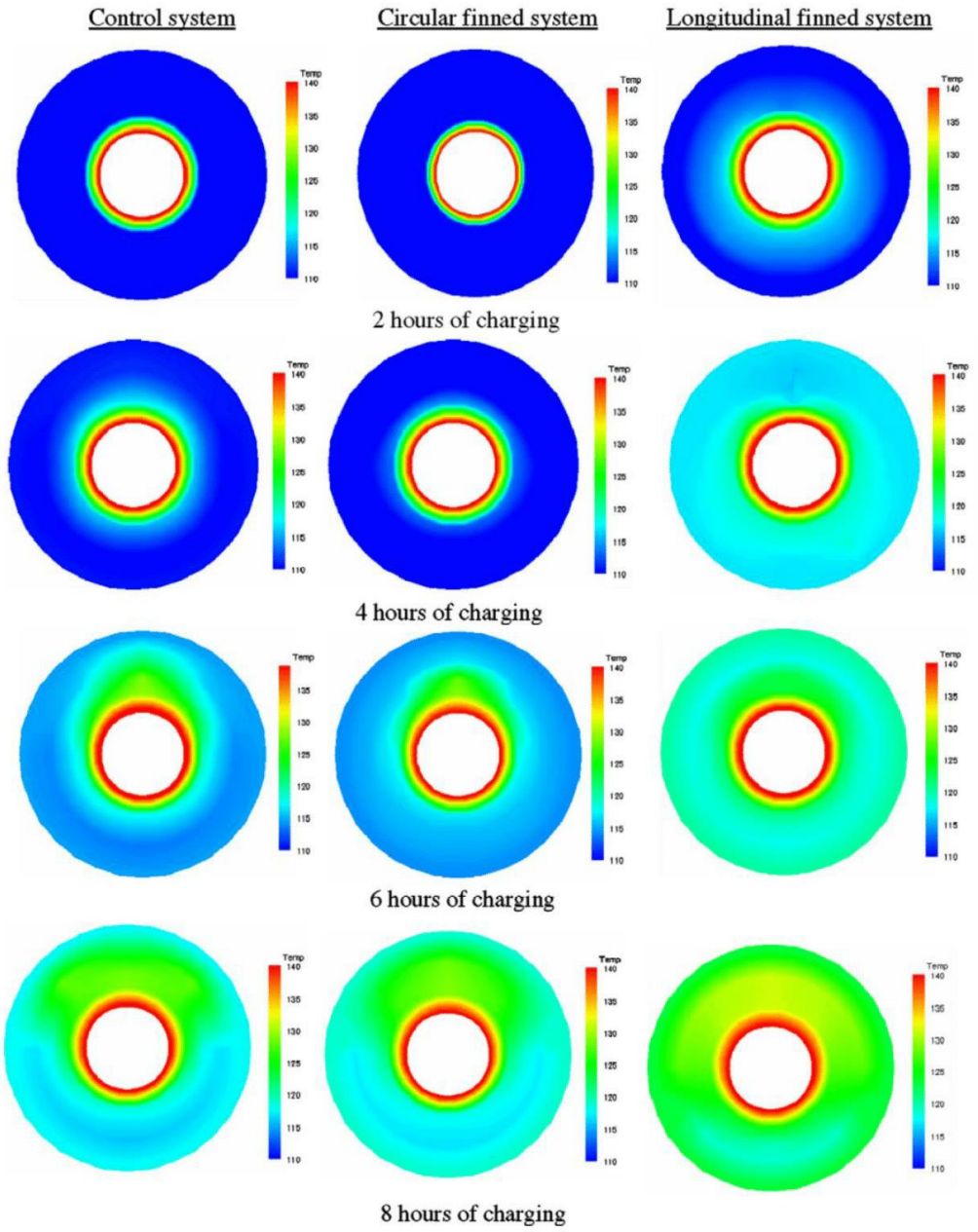

539

540 **Fig.13.** Comparison of thermal performance of erythritol in various geometric configurations: (i) Control system
541 (no fins), (ii) Circular finned system and (iii) Longitudinal finned system [77].

542 **4.3 PCM additives to increase the thermal conductivity**

543 Despite the fact that PCMs possess higher thermal storage density, the slower rate of melting and
544 solidification limits the potential practical applications of LHS system. This is due to lower thermal conductivity
545 of both organic and inorganic PCMs which ranges from 0.1 to 0.7 W/mK, as shown in Table 3 and Table 4. In

recent years, a subchapter of a book by Mehling and Cabeza [20], and portions of few review papers [52, 53, 79, 80] are published on this topic. However, this section thoroughly reviews the latest research developments in thermal conductivity enhancement of both paraffins and salt hydrates by using metal matrices and structures, expanded graphite, metal nanoparticles and carbon fibers. This section is focused on effect of addition of additives on thermal conductivity, latent heat storage capacity and transition rate of PCMs.

Melting and solidification rate can be enhanced by adding naturally available materials such as graphite, carbon fibers, copper, aluminium, metal matrices etc. Copper matrices enhanced the thermal conductivity of paraffin by approximately 80% as compared to aluminium matrices. Moreover, diamond coated copper matrices can further increase the thermal conductivity [81].

Mesalhy et al. [82] performed a numerical parametric study to identify the effects of employing solid matrices with different porosities of 0.85, 0.90 and 0.95; and thermal conductivity ratios on thermal performance of paraffin based LHS system. Thermal conductivity ratio, ks/kf ranged from 50-200. The term ks and kf represented the thermal conductivity of solid porous matrix and PCM, respectively. It was reported that thermal performance of LHS system was dependent on both porosity and thermal conductivity of employed matrix. Compared to pure paraffin, the addition of porous matrix increased the rate of melting and heat transfer rate. A decrease in matrix porosity resulted in increased thermal conductivity and melting rate of paraffin but it also dampened the convection motion. It was suggested that a matrix with high thermal conductivity and high porosity can enhance the storage performance in best way.

Due to high thermal conductivity and absorbability of graphite, it is used by many researchers as an additive in LHS system to improve thermal performance. Thermal conductivity of graphite ranges from 24 to 270 W/mK. Haillot et al. [83] characterized and elaborated composites of expanded graphite and several PCMs and reported an increase of thermal conductivity from 0.2 – 1 W/mK for pure PCM to 5 – 50 W/mK for composite. However, the inclusion of expanded graphite to RT-65 paraffin decreased the latent heat capacity from 170 – 140 kJ/kg. It showed that thermal capacity and thermal conductivity of LHS system depended on the amount of expanded graphite in composite.

Similarly, the effect on melting time, thermal conductivity and thermal capacity on composite of n-docosane (paraffin) and different mass fractions of expanded graphite is investigated by Sari and Karaipekli [84]. Liquid paraffin absorbed in pores of expanded graphite of 2%, 4%, 7% and 10% mass fraction, making a form-stable composite with no leakage due to capillary force and surface tension of expanded graphite. The density of 10% expanded graphite composite was less than pure paraffin. The increase in mass fraction of expanded graphite showed an increase in thermal conductivity but a decrease in thermal capacity. An optimum mass fraction of 10% expanded graphite resulted in four time increased thermal conductivity, causing about 32% reduction in melting time, and a small drop in thermal capacity from 194.6 - 178.3 kJ/kg.

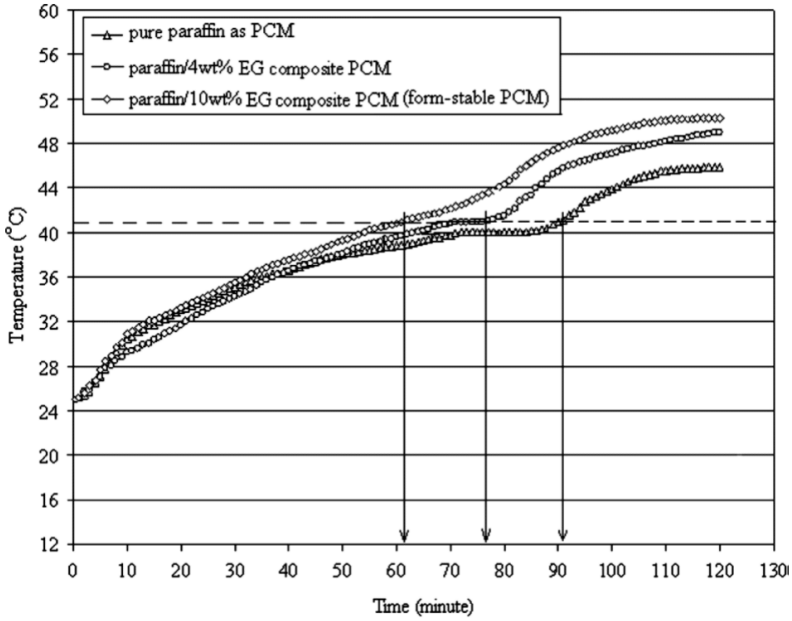

Fig.14. Melting time of pure paraffin and composite paraffin/EG [84].

An experimental investigation on thermal conductivity enhancement of $CaCl_2.6H_2O$ and expanded graphite composite was conducted by Z. Duan et al.[85] . OP-10 was added as a surfactant to improve the bonding energy and sealing performance of the composite. Various samples were prepared with expanded graphite mass fraction of 50%, 40%, 30%, 20% and 10%. DSC results showed that composite sample with 40% mass fraction of expanded graphite produced comparatively higher latent heat of fusion (145 kJ/kg), whereas sample of 50% mass fraction of expanded graphite provided lower latent heat of fusion (49.10 kJ/kg). TG analysis of composite samples evidently showed that the inclusion of OP-10 surfactant enhanced the thermal stability. Moreover, thermal constant analyser tests presented that that 50% mass fraction of expanded graphite improved the thermal conductivity of $CaCl_2.6H_2O$ (8.796 W/mK) by 14 times to that of pure $CaCl_2.6H_2O$ (0.596 W/mK).

Thermal performance enhancement of $Na_2SO_4.10H_2O$ and $Na_2HPO_4.12H_2O$ with expanded graphite was examined by Y. Wu and T. Wang [86]. Impregnation and physical blending techniques were used to prepare the composite sample of 3.5g of each salt hydrates with 1g of expanded graphite. The composite sample was coated with 0.2g of paraffin wax to restrain salt hydrates from phase segregation. It was reported that the composite sample demonstrated good thermal stability after 100 thermal cycles and presented good latent heat of fusion (172.3 kJ/kg). Moreover, the inclusion of expanded graphite increased the thermal conductivity of hydrated salts to 3.643 W/mK.

H.K. Shin et al.[87] investigated the thermal performance enhancement of sodium acetate trihydrate by inserting various weight percentages of expanded graphite. Carboxymethyl cellulose (CMC) was added as a thickening agent. It was reported that the PCM composite containing 2.5 wt% of expanded graphite and 5 wt% of thickening agent exhibited a high thermal conductivity of 1.85 W/mK and excellent thermal stability. On the

602 contrary, the same PCM composite sample with 5 wt% of graphite powder (particle size ≤ 50 μm) and 5 wt% of
603 CMC was prepared and investigated by M. Dannemand et al.[88]. The maximum thermal conductivity of
604 composite was reported to be 1.1 W/mK.

605 The results from various research shows that graphite is an excellent additive to enhance thermal
606 performance of LHS system. However, its porosity plays a vital role in effectiveness of improved thermal
607 performance. If the composite of small mean pore size graphite is selected then it may cause difficulty in
608 impregnation of PCM in porous media of graphite and hinders the molecular moment, which can decrease the
609 latent heat capacity. On the contrary, if the mean pore size is increased then it can cause leakage problem as
610 reduction in capillary forces. Moreover, the composite of graphite and PCM can be prepared by using chemical
611 or mechanical processes, which are time and energy consuming. Therefore, to avoid these shortcomings, another
612 simple technique to enhance thermal conductivity is dispersion of high thermal conductivity particles.

613 An experimental study was conducted on thermal conductivity enhancement of paraffin wax by
614 incorporating aluminium particles of 80 μm, with a mass fraction of 0.1, 0.3, 0.4 and 0.5, by Mettawee and
615 Assassa [89]. Mass fraction was the ratio of mass of aluminium powder to mass of compound of paraffin wax
616 and aluminium powder. During charging time, the heat transfer from solar collector to paraffin wax/aluminium
617 composite was increased as the mass fraction increase from 0.1 to 0.5. However, the increase in mass fraction
618 beyond 0.5 resulted in insignificant increase in heat transfer rate. For aluminium mass fraction of 0.5, the
619 thermal conductivity of composite increased and produced 60% reduction in charging time as compared to pure
620 paraffin wax. Similarly for discharging process, the composite of 0.5 mass fractions showed more homogenous
621 solidification. The highest mean daily efficiency of the LHS system increased from 54.8% for pure paraffin wax
622 to 94% for composite.

623 Performance enhancement of 1-tetradecanol (TD) and silver nanoparticle composite was investigated by
624 Zeng at al. [90], using TG-DSC, IR, TEM, XRD and thermal conductivity evaluation method. The investigated
625 composite samples were based on various mass fractions of 0.98, 0.94, 0.80, 0.50, 0.20 and 0.06. Mass fraction
626 was the ratio of mass of pure TD to the combined mass of TD and silver nanoparticles. It was reported that
627 thermal conductivity of composite increased with increase in the amount of silver nanoparticle. Thermal
628 conductivity enhancement was examined by the increase in temperature at particular time. It was noticed that
629 after 150 seconds of melting process, the pure TD was at 26 ^{o}C, whereas the composite of mass fraction of 0.06
630 was at 30 ^{o}C. Also, no interaction between TD and silver nanoparticle was noticed and the stability of composite
631 was found to be almost the same as to that of pure TD. However, thermal storage capacity of composite
632 decreased with increase in silver nanoparticle (234.2 kJ/kg for pure TD, 216.5 kJ/kg for composite of mass
633 fraction of 0.98 and 119.4 kJ/kg for composite of mass fraction of 0.50, respectively) and the phase transition
634 temperature was also reduced as compared to pure TD.

635 To improve the thermal conductivity of paraffin, various techniques such as vertical cylinder with
636 internal longitudinal fins, lessing rings and bubble agitation are studied by Velraj et al. [91]. In case of lessing
637 rings, hollow steel rings of 1 cm diameter were added in cylindrical paraffin container. Reduction in
638 solidification time was reported for both fins and lesser rings based LHS system. It was found that solidification
639 time for fins and lesser rings were 1/4th and 1/9th that of plain tube LHS system, respectively. However, the

inclusion of fins and lesser rings occupied 7% and 20% of total storage volume of container respectively and thus reducing the storage capacity of LHS system, as shown in Fig. 15. Therefore for large container size of LHS system, lesser rings will perform better than fins.

Due to higher density of metal particles and metal structures, there is a possibility that the additives can settle at the bottom of container and increasing the weight of container. As discussed in section 3.2, there are compatibility concerns between metals and PCMs. Therefore, researchers have been searching for low density but high thermal conductivity additives, which are compatible with all PCMs. Carbon fibers is much lighter as compared to metal particles and its thermal conductivity is almost equal to copper and aluminium. Also, it has a good corrosive resistant nature and possesses good compatibility with almost all PCMs, thus it can qualify for better alternative to improve thermal performance of LHS system. Elgafy and Lafdi [92] analytically and experimentally investigated the performance enhancement of Paraffin wax based LHS system by adding carbon nanofibers of 100nm outer diameter and 20µm average length. Samples of different mass ratio (1%, 2%, 3% and 4%) of carbon nanofibers were made using shear mixing and melting process. The composite showed an almost linear increase in thermal conductivity and output power with increase in mass ratio of carbon nanofibers, which resulted in increased solidification rate and insignificant reduction in storage capacity. The solidification time was reduced by 23% by using 1% mass ratio of carbon nanofibers. It was reported that further improvement in thermal performance can be achieved by uniform distribution of fibers.

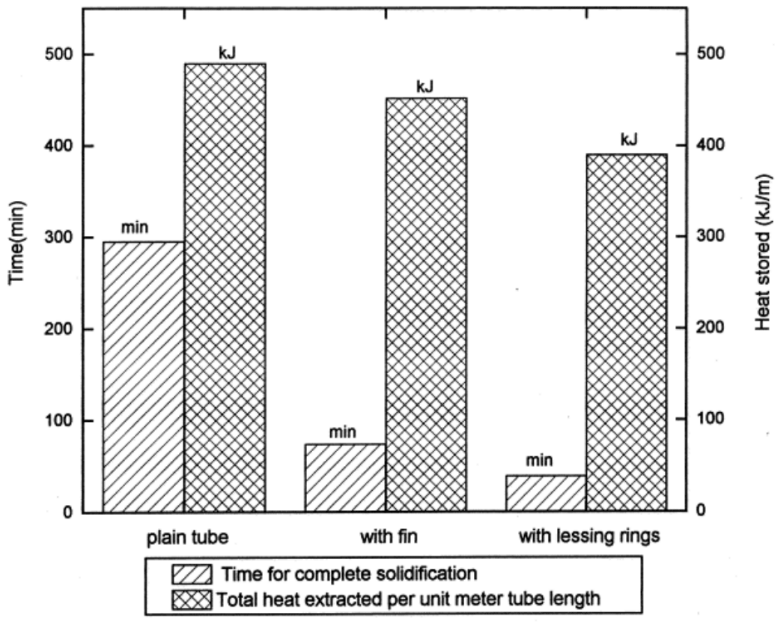

Fig.15. Solidification time and total heat storage capacity for various configurations [91].

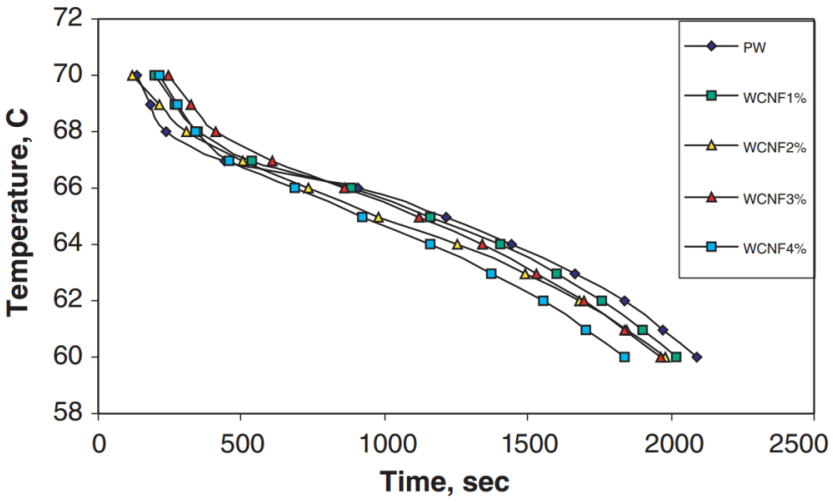

Fig.16. Solidification temperature with respect to time for various mass ratios of Carbon nanofibers [92].

Fukai et al. [93] inspected the effect of randomly and uniformly oriented carbon fibers on the thermal performance enhancement of paraffin wax based LHS system. Carbon fibers of 10µm diameter, 220 W/mK thermal conductivity and 2170 kg/m^3 density were packed with paraffin wax in a steel cylindrical capsule. It was found that effective thermal conductivity of uniformly oriented brush type was three times to that of randomly oriented type. Moreover, in case of small mass fraction of carbon fibers, the randomly oriented carbon fibers dampened the natural convection and thus resulted in lower melting rate than pure paraffin. Whereas, the higher melting rate in brush type orientation was not affected by loss in convection. Similarly, Fukai et al. [94] experimentally and numerically investigated the effect of inclusion of carbon fiber brushes in paraffin wax based LHS system. It was reported that an enhancement of 20% and 30% in charging and discharging respectively was achieved as compared to normal paraffin wax.

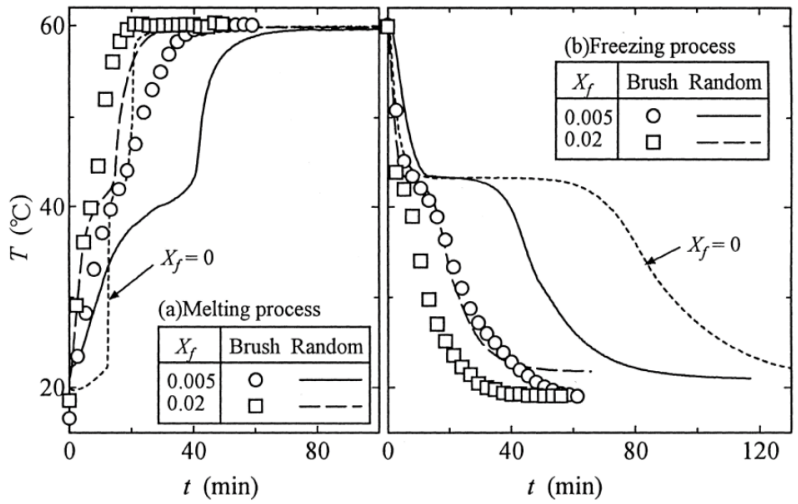

Fig.17. Transient temperature response to random type and brush type orientation of carbon fibers [93].

As reviewed in this section, the thermal conductivity of LHS system can be increased significantly by incorporating high conductivity additives and it can enhance the melting and solidification rate. However, the addition of additives can reduce the storage volume of PCM and it can lead to loss in storage capacity. Thus, an optimum mass of additives should be selected for enhancing thermal performance.

4.4 Multiple PCMs method

Instead of single PCM, using multiple PCMs technique has reported an increase in LHS system performance and storage capacity. During the charging and discharging process of the LHS system, the rate of heat transfer depends largely on the temperature difference between PCM melting temperature and HTF temperature. In single PCM case, the temperature of HTF decreases along the length of flow which results in temperature difference reduction. As a consequence, the rate of heat transfer decreases and therefore the LHS capacity reduces and most part of stored thermal energy is sensible energy. Whereas in multiple PCMs case, the storage medium consist of different PCMs in descending order of their melting temperatures, even if the temperature of HTF decreases the unit maintain almost a constant temperature difference. Multiple PCMs method yields constant heat flux to the PCM in melting process and to the HTF in solidification process.

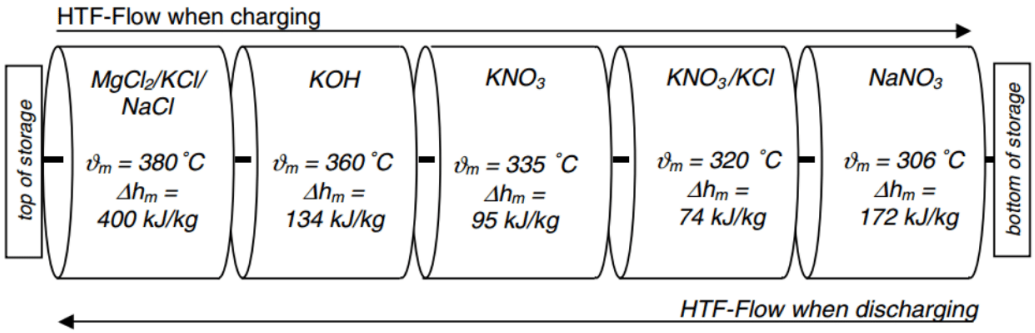

Fig.18. A schematic of multiple PCMs based LHS unit [95].

Wang et al [96] numerically investigated the performance enhancement of LHS system by employing multiple PCMs (PE, PG and NPG). It was suggested that an increase in number of PCMs would reduce the phase transition time. Numerical results indicated that phase transition for all PCMs were almost homogenous and with constant rate.

Mosaffa et al [97] numerically investigated the improved performance of free cooling system using multiple PCM based LHS system. The PCMs selected for investigation were $CaCl_2.6H_2O$, Paraffin C18 and RT25. Energy based optimization were used to find out the effect of length and thickness of PCM slab, and fluid passage gap on storage performance. It was reported that $CaCl_2.6H_2O$ and RT25 composite was very effective in maintaining the outlet air temperature below 27 ^oC for 8 hours and providing maximum heat absorbing capacity.

Gong and Mujumda [98] developed a one dimensional finite element heat conduction phase change model for melting and freezing processes of composite PCMs slabs. The model was used to investigate the performance of various arrangements of PCMs with descending order of their melting temperatures, thermo-physical properties and various boundary conditions for both melting and heating processes as shown in Table 6.

E_T and E_M represent the actual energy stored or retrieved in a cycle and maximum energy stored or retrieved, respectively. The ratio between E_T and E_M represents the LHS system performance. Upon reaching to steady reproducible state, the multiple PCM slab resulted in enhanced melting and solidification rate as compared to single PCM slab. The charge and discharge rate was enhanced from 21.9% to 31.7% by decreasing the thermal conductivity ratio from 1.0 to 0.1, and the percentage enhancement was decreased by periodic reduction in thermal diffusivity ratio. Increase in latent heat of multiple PCMs resulted in improved charge and discharge rate. It can also be observed from the table 6 that the melting and solidification rate can be enhanced by minimizing the temperature differences between boundary temperatures using multiple PCMs.

Table 6

Performance enhancement using multiple PCM [98]

	Property	**t_m=t_s (s)**	**Slab type**	**E_T (J/m^2)**	**E_T/E_M**	**Enhancement (%)**
Case	Thermal conductivity kl/ks					
1	1	650	Single	404,508	0.632	
			3-PCM	493,178	0.771	21.9
2	0.4	1150	Single	439265	0.774	
			3-PCM	534425	0.941	21.7
3	0.2	1950	Single	415613	0.764	
			3-PCM	517257	0.969	26.9
4	0.1	3375	Single	393120	0.723	
			3-PCM	517790	0.955	31.7
Case	Thermal diffusivity al/as					
1	1	650	Single	404508	0.632	
			3-PCM	493178	0.771	21.9
2	0.4	800	Single	552627	0.674	
			3-PCM	627102	0.765	13.5
3	0.2	1000	Single	704900	0.629	
			3-PCM	758942	0.678	7.67
Case	Latent heat (J/kg)					
1	2000	375	Single	263161	0.598	
			3-PCM	304540	0.692	15.7
2	4000	650	Single	404508	0.632	
			3-PCM	493178	0.771	21.9
3	8000	1200	Single	754818	0.726	
			3-PCM	945164	0.909	25.2
4	16000	2150	Single	1329710	0.723	
			3-PCM	1756840	0.955	32.1
Case	Temperature swing (^{o}C)					
1	T_{wm}= 80, T_m= 70, T_{wf}= 60	1750	Single	363228	0.757	-
2	T_{wm}= 80, T_{m1}= 75, T_{m2}= 70,	1750	3-PCM	457240	0.953	25.9

	T_{m3}= 65, T_{wf}= 60					
3	T_{wm}= 120, T_m=90, T_{mf}= 60	650	Single	404508	0.632	-
4	T_{wm}= 120, T_{m1}= 105, T_{m2}= 90, T_{m3}= 75, T_{wf}= 60	650	3-PCM	493178	0.771	21.9
5	T_{wm}= 160, T_m= 110, T_{wf}= 60	400	Single	465331	0.582	-
6	T_{wm}= 160, T_{m1}= 135, T_{m2}= 110, T_{m3}= 85, T_{wf}= 60	400	3-PCM	545623	0.682	17.3
7	T_{wm}=200, T_m= 130, T_{wf}= 60	350	Single	579027	0.603	-
8	T_{wm}= 200, T_{m1}= 165, T_{m2}= 130, T_{m3}= 95, T_{wf}=60	350	3-PCM	670265	0.698	15.8

Farid and Kansawa [99, 100] numerically and experimentally studied the performance enhancement of LHS system by employing three commercial waxes of different temperatures (44 ^oC, 53 ^oC and 64 ^oC) and reported an increase of 10-15% in heat transfer rate to that of single PCM unit. It was also reported that the phase transition of all PCMs started simultaneously.

Aldoss and Rahman [101] investigated the improvement in performance of multiple paraffins based LHS system by increasing the number of stages. Spherical capsule containing paraffin 40, paraffin 50 and paraffin 60 were used in various stages along the length of bed. It was observed that an increase in number of stages of multiple paraffins based LHS system resulted in enhanced rate of charge and discharge, increased heat transfer rate and improved storage capacity. However, increasing the number of stages more than three could not enhance the system significantly.

Wang et al [102] experimentally investigated the decrease in melting time of LHS unit consisting of three coaxial cylindrical containing stearic acid, sliced paraffin and lauric acid, respectively. LHS unit was dipped in water and experiments were conducted for different temperatures, for both multiple PCMs unit and single PCM (sliced paraffin) unit. The experimental results demonstrated that charging rate of multiple PCMs unit was enhanced and resulted in 37-42% reduction in melting time compared to single PCM.

4.5 PCM encapsulation

PCM encapsulation is a process of shelling the PCM with suitable coating material to keep it isolated from surrounding. The encapsulation process was invented by Barrett K Green in 1940s. Encapsulation ensures the sustainability of true composition of PCM that can be altered by connection with surrounding, reduces the possibility of surrounding reaction with PCM, improves thermal and mechanical stability, improves heat transfer rate and compatibility with hazardous PCMs that cannot be exposed to surrounding such as building temperature control, food storage and blood transport applications. Encapsulation of organic PCMs is given preference over salt hydrates for its non-corrosive nature and insignificant solubility in water. However, the inflammable nature of organic materials can be controlled by using inorganic coating materials. As shown in Fig. 19, chemical and physical are two broad manufacturing methods of PCM encapsulation. Physical encapsulation methods deal with large amount and rough surface encapsulation as compared to chemical techniques. Chemical encapsulation techniques result in better heat storage capacity than that of physical methods. In-situ

polymerization manufacturing technique with its smaller capsule size and excellent shell structure is preferred over others techniques. PCM encapsulation can be also be classified by different sizes such as macro, micro and nano encapsulation and various container shapes as spherical, cylindrical, tubular or rectangular. In last decade, several review articles and subchapters of books are published on this topic. Review articles on nanoencapsulation [103, 104] and microencapsulation [3, 105-107] are focused on various encapsulation types, techniques and applications. Similarly, the subchapters of books by Cabeza [20, 108] are focused on macro and micro encapsulation. This section reviews the updated research on thermal performance enhancement and thermo-physical stability of micro and macro encapsulated PCMs. This section is focused on effects of encapsulation on thermo-physical stability, latent heat storage capacity, thermal conductivity and phase transition rate.

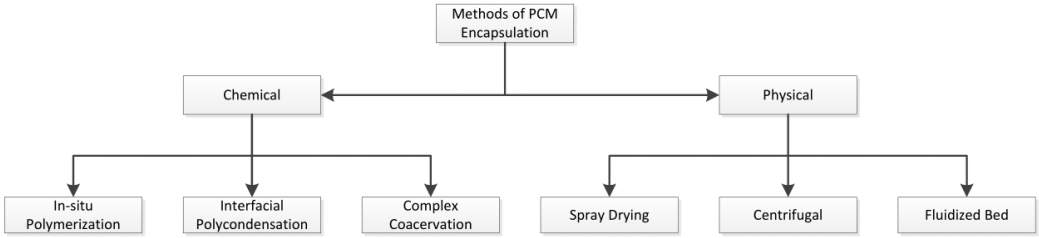

Fig.19. Various methods of PCM encapsulation.

4.5.1 Microencapsulation

Mechanical strength of encapsulated PCM can be identified by the core to coating ratio. An increase in core to coating ratio proceeds in deteriorating coating strength and increases possibility of PCM leakage from encapsulation, while a decrease in core to coating ratio can reduce the amount of PCM in encapsulation. Ohtsubo et al. [109] examined the mechanical stability of microcapsules by using mass median diameter factor (D) and wall thickness factor (T). It was noticed that for larger ratio of D and T, a smaller pressure is enough to break 50% of coating material of encapsulation. Zhang and Wang [110] synthesized microencapsulated PCM with n-octadecane as core material and polyurea as coating material. Core to coating ratio of 70/30 and 75/25 were examined, with mean particle size of 6.9 µm and 7.1µm, respectively. Lower core to coating ratio (70/30) produced better thermal stability, while the higher core to coating ratio (75/25) caused slippage of PCM at 200 ^{o}C.

Namwong et al. [111] investigated the latent heat capacity of microencapsulated PCM with octadecane as core material and divinylbenzene and methyl methacrylate (DVB-MMA) polymer as coating material. The average diameter of microcapsule was 3.2 µm. Three polymer samples were tested. The samples contained different percent weights of DVB and MMA such as 100:0, 50:50 and 30:70 wt%, respectively. The latent heat of all samples of microencapsulated PCM was reported to be 189 kJ/kg, 218 kJ/kg and 223 kJ/kg, respectively. It was observed that the latent heat of microencapsulated PCM increased as the percent weight of hydrophilic MMA increased to 70 wt%. Yu et al. [112] examined the thermal conductivity enhancement of microencapsulated n-octadecane. $CaCO_3$ was used as shell material. The spherical microencapsulated PCM was having a diameter of 5 µm. Three samples of various percent weights of core and shell material were tested such as 30:70, 40:60 and 50:50 wt%, respectively. Thermal conductivity of pure n- octadecane was 0.153 W/mK. It

771 was reported that thermal conductivity of all samples of microencapsulated PCM improved to 1.674 W/mK,
772 1.325 W/mK and 1.264 W/mK, respectively. Also, the microencapsulated PCM samples were subjected to 200
773 thermal cycles and it showed a good thermal stability and structural reliability. Yang et al. [113] examined the
774 performance enhancement of thermo-physical properties of microencapsulated n-octadecane. Silicon nitride and
775 polymethyl methacrylate polymer was used as shell material. Four samples of microencapsulated PCM were
776 tested. The percent weight of core materials ranged from 82.3 - 66.4 wt%. It was noticed that latent heat of
777 fusion reduced from 151.30 - 122.07 kJ/kg as the percent weight of core material decreased from 82.3 - 66.4
778 wt%. However, the mechanical strength of sample with 66.4 wt% of core material appeared to be four time
779 higher (16.24 mN) than ordinary PCM.

780 Sarier et al.[114] evaluated the thermal performance enhancement of two microencapsulated PCMs with
781 n-hexadecane and n-octadecane as core materials. Urea-formaldehyde was used as coating material. Silver
782 nanoparticles were added to core materials to improve the thermal performance of microencapsulated PCMs.
783 The average particle size of silver nanoparticles ranged from 163-496 nm. Six samples of microencapsulated
784 PCMs were tested. Four samples were containing 176.6 mmol of n-hexadecane and 0, 26, 52 and 104 mmol of
785 silver nanoparticles as core material, respectively. Likewise, two samples were containing 157.2 mmol of n-
786 octadecane and 0 and 26 mmol of silver nanoparticles as core material, respectively. For all samples, the core to
787 coating ratio by mass was kept constant at 1:1. It was reported that the latent heat capacity of microencapsulated
788 n-hexadecane increased from 115-137 kJ/kg as the amount of silver nanoparticles increased from 0-52 mmol.
789 Likewise, the thermal conductivity improved from 0.0557- 0.1231 W/mK as the amount of silver nanoparticles
790 increased from 0-104 mmol. In case of microencapsulated n-octadecane, the latent heat capacity improved from
791 117-168 kJ/kg and thermal conductivity increased from 0.0695- 0.0978 W/mK with addition of 26 mmol of
792 silver nanoparticles. The samples were also subjected to 100 thermal cycles and the results indicated a good
793 thermal stability and durability. Jiang et al.[115] used emulsion polymerization to synthesise paraffin wax
794 microencapsulates with methyl methacrylate-co-methyl acrylate (MMA-MA) as coating material and nano-
795 Al_2O_3 as additives to enhance thermal performance. Six samples were evaluated with varied mass ratio of nano-
796 Al_2O_3 (0, 5, 16, 27, 33 and 38 wt%). It was reported that thermal conductivity of microencapsulated PCM
797 samples improved from 0.2442-0.3816 W/mK as the mass ratio of nano-Al_2O_3 increased from 0-38 wt%.
798 However, the latent heat capacity of microencapsulated PCM decreased from 110.40-75.40 kJ/kg as the mass
799 ratio of nano-Al_2O_3 increased from 0-38 wt%, due to drop in content of paraffin wax. It was also noticed that the
800 microencapsulated PCM samples with nano-Al_2O_3 additives displayed better thermal stability.

801 Alkan et al. [116] studied the experimental preparation, characterization and calculating the thermal
802 behaviour of microencapsulated docosan-PMMA. The microencapsulated docosane was subjected to 5000
803 thermal cycles and the results depicted a good thermal stability and no chemical degradation. Ma et al. [117]
804 prepared spherical shape encapsulated paraffin-PMMA by UV irradiations to emulsion polymerization. The size
805 of encapsulated paraffin-PMMA was 0.5 – 2 µm. Thermal stability tests were conducted for 1000 thermal
806 cycles. The results showed a good thermal stability with melting point varied in a range of 33.40 – 35.71 ^oC and
807 latent heat varied from 99.8 – 95.6 kJ/kg.

4.5.2 Macroencapsulation

Howlader et al. [118] investigated the chemical and physical stability and thermal performance of larger capsules of size (2.833 mm diameter) with paraffin as core material. It was reported that after 1000 thermal cycles, the encapsulated paraffin showed a good thermal and structural stability, and stable thermal storage capacity. Alam et al. [119] experimentally investigated the thermo-physical stability of spherical encapsulated $NaNO_3$. The diameter of hemispherical pellets of $NaNO_3$ ranged from 12.5-25.5 mm. Firstly, the PCM was encapsulated by a layer of polymer (PTFE), having a thickness of 0.5-0.7 mm. Subsequently, it was coated with a thin layer of nickel (10-80 µm). Due to polymer layer in between molten PCM and nickel, the possibility of corrosion was reduced. The capsule was subjected to 2200 thermal cycles and the results showed excellent thermo-physical stability.

Cabeza et al. [120] studied the thermal storage behaviour of solar pilot plant with several modules of encapsulated PCM-graphite. A granular compound of sodium acetate trihydrate (90 vol.%) and graphite (10 vol.%) was encapsulated in aluminium container of size 8.8 cm x 31.5 cm. As shown in the Fig. 20, the inclusion of 2, 4 and 6 PCM modules carried a weight of 2.1 kg, 4.2 kg and 6.3 kg, and it occupied 2.05 vol.%, 4.1 vol.% and 6.16 vol.% of storage tank, respectively. An increase in thermal density of 40%, 57.2% and 66.7% was noticed for 1 K temperature difference in case of 2, 4 and 6 PCM modules, respectively. Thermal density increase was 6%, 12% and 16.4% for 8 K temperature difference, respectively. The inclusion of encapsulated PCM-graphite maintained the temperature of water top layer in storage tank above 54 °C for 10-12 hours. Similarly, Mehling et al. [121] investigated the inclusion of encapsulated paraffin-graphite in brass cylinders of size 10 cm x 30 cm. Thermal storage capacity was increased by 20% to 45% and the hot water storage duration was increased by 50% to 200%.

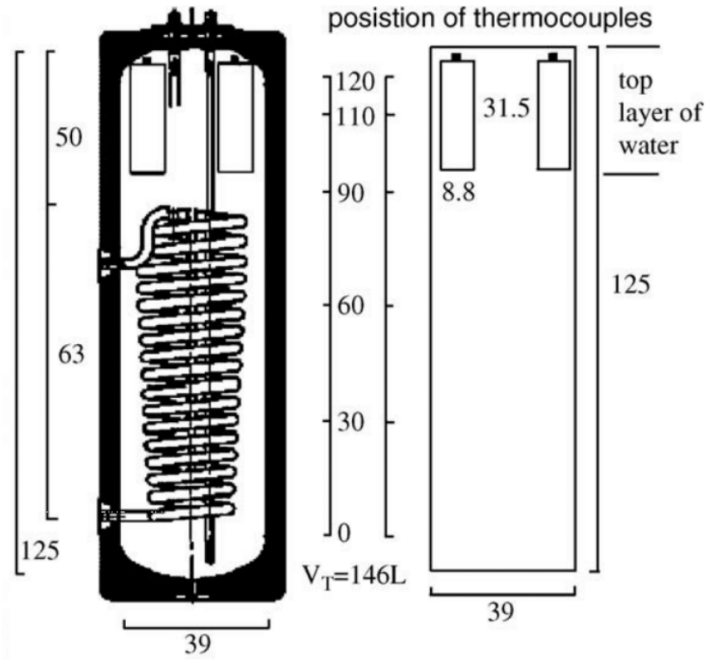

Fig.20. Schematic of 2 PCM modules embedded on the top portion of hot water storage tank [120].

Veerappan et al. [122] performed analytical study on influence of encapsulation size on melting and solidification rate. It was noticed that as the diameter of capsule increased from 4 cm to 12 cm, the melt time of encapsulated $CaCl_2.6H_2O$ also increased from 26 minutes to 192 minutes, respectively. Similarly, it was reported that increase in capsule diameter will reduce the solidification rate and therefore the encapsulated PCM will take more time to solidify as compared to small diameter. Calvet et al. [123] conducted numerical and experimental examination of improvement in phase transition rate of PCM composite in a spherical encapsulation. The diameter of capsule was 98mm. Graphite flakes and expanded graphite was incorporated as thermal conductivity enhancement additives. It was reported that the addition of 13%wt. of graphite flakes reduced both the melting and solidification time by 30% each. Whereas, the addition of 13%wt. of expanded graphite reduced the melting and solidification time by 60% and 40%, respectively. Zhang et al. [124] conducted numerical and experimental investigation to find the increase in solidification rate of $NaNO_3$ (60 wt%) and KNO_3 (40 wt%) composite in cylinder encapsulation. The capsule material was AISI 321. The outer diameter and height of capsule was 75mm and 77mm, respectively. Metallic foam was inserted as thermal conductivity enhancement additive. The cylindrical capsules were heated in electric furnace to melt the composite PCM and then subjected to air and water to measure the solidification time. In case of air cooling, the solidification time was reduced from 3600s for PCM composite with no enhancement to 2800s for PCM composite with metallic foam. However in case of water cooling, the solidification time of PCM composite with metallic foam reduced further to 700s.

Wai et al. [125] studied the effect of capsules shape, diameter and coating thickness on thermal performance of encapsulated PCM. It was reported that spherical capsule produced an excellent heat release performance as compared to cylindrical, plate and tube type capsules. It was observed that with increase in PCM diameter from 2mm to 5mm, the heat release rate decreased. As the coating thickness increase from 0.2 mm to 0.4 mm, the mechanical stability increased but it reduced the amount of PCM in capsule and therefore it affected the thermal storage capacity. Ismail and Henriquez [126] developed a model to study the effect of spherical capsule size, coating thickness and material, initial PCM temperature on solidification rate. It was observed that coating material of high thermal conductivity and smaller capsule size with low external temperature reduced the solidification time. Increase in internal radius of spherical capsule lead to increased solidification time. As constant mass of PCM resulted in constant internal radius of 0.05m, the critical external radius for copper, PVC and glass were found to be 17.46 m, 0.003 m and 0.054 m, respectively. Increase in coating thickness could enhance solidification rate, therefore external radius of copper and glass could be increased up to their critical values, whereas, PVC critical radius was found to be lower than internal radius, thus an increase in PVC external radius would reduce the solidification rate. Ismail and Moraes [127] also observed that solidification rate could be increased by using coating material of high thermal conductivity, smaller capsule diameter and lower external temperature. Fig. 21 summarises the various techniques used for thermal performance enhancement of PCM based LHS system.

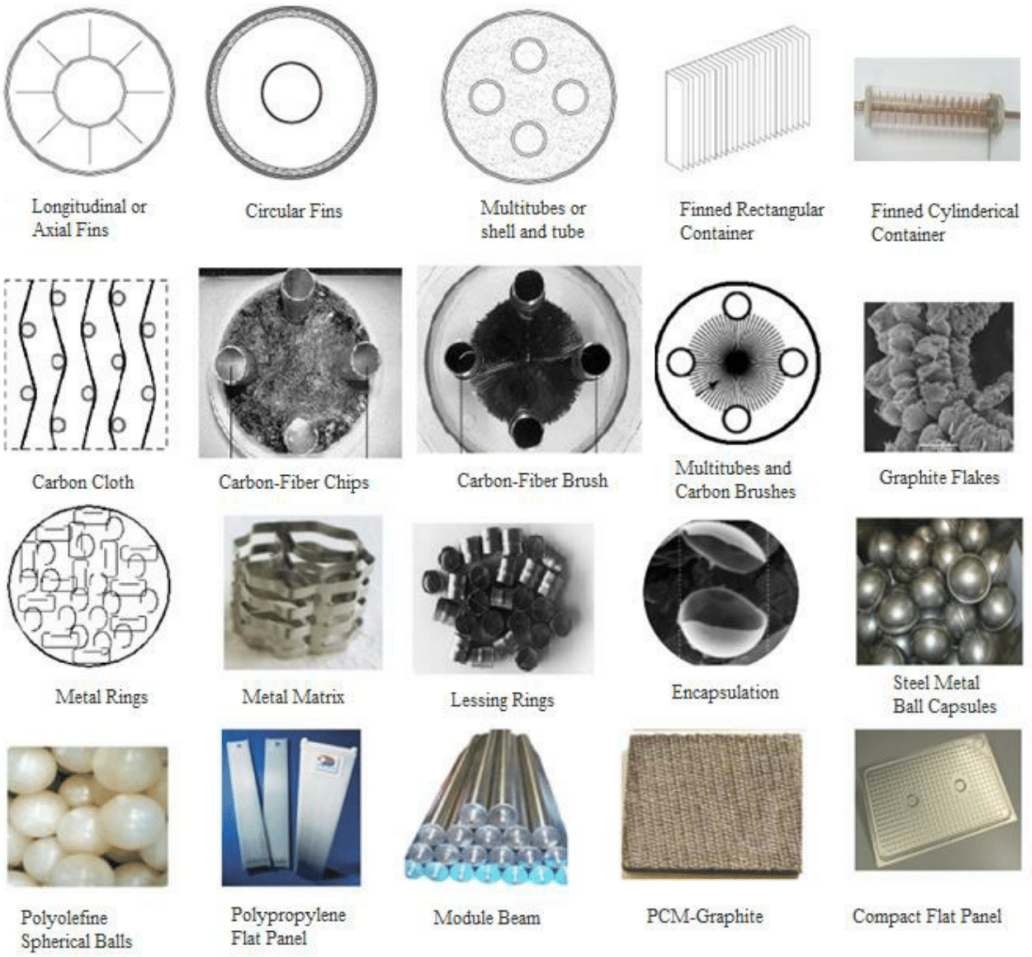

Fig.21. Various techniques used for enhancing thermal performance of LHS system. In this figure, the various techniques adopted by researchers are sequenced on the basis of subchapters of this review paper such as initially various configurations of fins are presented and it is followed by PCM additives to enhance thermal conductivity and lastly the PCM encapsulation techniques.

5. Conclusion

This review paper presents a detail literature survey focused on PCMs categorization, long term stability of PCMs and compatibility with container materials, thermal performance analysis and thermal performance enhancement techniques. Literature survey encouraged to draw the below given conclusions:

- For long term thermal performance of LHS system, the PCM needs to ensure thermal stability, chemical stability and corrosion resistance with container material upon subjecting to extended amount of repeated thermal cycles. After repeated cycles, the thermo-physical properties of PCM shall not change significantly. It can be deducted from the review that paraffins yield better thermal and chemical stability than salt hydrates after repeated thermal cycles. Salt hydrates faces phase segregation and supercooling,

880 which can be controlled by adding suitable thickener and nucleating agents. $CaCl_2.6H_2O$ is found as the
881 most studied salt hydrate. Before using industrial grade PCMs, it is advised to run the repeated thermal
882 cycle test to check the stability of thermo-physical properties.
883 • It is noticed that conduction heat transfer and natural convection are responsible for melting behaviour of
884 PCMs in containers with different shapes. In early stages, conduction heat transfer is dominant and as the
885 PCM melts down, natural convection dominates the melting of PCM. Container orientation and
886 geometric parameters have great influence on the melting behaviour of PCMs, such as aspect ratio of
887 rectangular and cylindrical containers, spherical capsules radius and annular cavity eccentricity. Thus, it
888 is important to make sure that the geometric configuration is suitable for certain PCM.
889 • An enhanced storage performance and phase transition rate can be achieved by using fins in LHS system.
890 The size and number of fins are vital in improving thermal performance of LHS system. It is noticed that
891 inclusion of fins has more impact on improving solidification rate than melting rate. The size and number
892 of fins should be optimized as inclusion of fins reduces storage volume for PCM in container and thus
893 the thermal storage capacity is also affected.
894 • The melting and solidification rate of PCM can be enhanced significantly by incorporating high thermal
895 conductivity additives as it will increase the thermal conductivity of LHS system. However, the inclusion
896 of high density additives can reduce storage volume for PCM in container and it can lead to loss in
897 storage capacity. Therefore, an optimized amount of additives can only be added to enhance thermal
898 performance.
899 • Utilization of multi-PCM can produce an increased thermal storage performance of LHS system. It is
900 useful in storing thermal energy at constant temperature difference. Multiple PCMs method yields
901 constant heat flux to the PCM in melting process and to the HTF in solidification process. Most of the
902 studies have been carried out on combination of arbitrary PCMs, thus there is a need of experimental
903 investigation of various combinations of actual PCMs.
904 • Thermal and mechanical stability is dependent on core-to-coating ratio of encapsulated PCM. Increased
905 ratio will produce weak shell and lower ratio will result in less amount of PCM in encapsulation.
906 Optimization of core-to-coating ratio is required. Similarly, encapsulate material shall possess high
907 thermal conductivity. Metallic encapsulates like copper, aluminium and steel can be good options but it is
908 challenging to manufacture. Salt hydrates for their high thermal conductivity, diffusion values and
909 mechanical strength can be a good choice as encapsulate materials for organic PCMs. Encapsulation
910 having higher thermal conductivity, lower temperature at external surface and smaller diameter of
911 capsule can increase solidification rate of LHS system.

912 **Acknowledgment**

913 The corresponding author's PhD is match funded by Bournemouth University, UK and National
914 University of Science and Technology (NUST), Pakistan. The author would like to extend sincere gratitude to
915 both parties.

916

References

[1] D. Morrison, S. Abdel-Khalik. Effects of phase-change energy storage on the performance of air-based and liquid-based solar heating systems. Solar Energy. 20 (1978) 57-67.

[2] A. Ghoneim. Comparison of theoretical models of phase-change and sensible heat storage for air and water-based solar heating systems. Solar Energy. 42 (1989) 209-20.

[3] J. Giro-Paloma, M. Martínez, L.F. Cabeza, A.I. Fernández. Types, methods, techniques, and applications for microencapsulated phase change materials (MPCM): A review. Renewable and Sustainable Energy Reviews. 53 (2016) 1059-75.

[4] R. Jacob, F. Bruno. Review on shell materials used in the encapsulation of phase change materials for high temperature thermal energy storage. Renewable and Sustainable Energy Reviews. 48 (2015) 79-87.

[5] M. Kenisarin, K. Mahkamov. Passive thermal control in residential buildings using phase change materials. Renewable and Sustainable Energy Reviews. 55 (2016) 371-98.

[6] B. Tang, L. Wang, Y. Xu, J. Xiu, S. Zhang. Hexadecanol/phase change polyurethane composite as form-stable phase change material for thermal energy storage. Solar Energy Materials and Solar Cells. 144 (2016) 1-6.

[7] B. Tang, Y. Wang, M. Qiu, S. Zhang. A full-band sunlight-driven carbon nanotube/PEG/SiO 2 composites for solar energy storage. Solar Energy Materials and Solar Cells. 123 (2014) 7-12.

[8] Y. Wang, B. Tang, S. Zhang. Single-Walled Carbon Nanotube/Phase Change Material Composites: Sunlight-Driven, Reversible, Form-Stable Phase Transitions for Solar Thermal Energy Storage. Advanced Functional Materials. 23 (2013) 4354-60.

[9] M. Liu, Y. Ma, H. Wu, R.Y. Wang. Metal Matrix–Metal Nanoparticle Composites with Tunable Melting Temperature and High Thermal Conductivity for Phase-Change Thermal Storage. ACS nano. 9 (2015) 1341-51.

[10] A. Abhat. Low temperature latent heat thermal energy storage: heat storage materials. Solar energy. 30 (1983) 313-32.

[11] A. Sharma, V. Tyagi, C. Chen, D. Buddhi. Review on thermal energy storage with phase change materials and applications. Renewable and Sustainable energy reviews. 13 (2009) 318-45.

[12] B. Zalba, J.M. Marín, L.F. Cabeza, H. Mehling. Review on thermal energy storage with phase change: materials, heat transfer analysis and applications. Applied thermal engineering. 23 (2003) 251-83.

[13] L.F. Cabeza, A. Castell, C. Barreneche, A. De Gracia, A. Fernández. Materials used as PCM in thermal energy storage in buildings: a review. Renewable and Sustainable Energy Reviews. 15 (2011) 1675-95.

[14] M.K. Rathod, J. Banerjee. Thermal stability of phase change materials used in latent heat energy storage systems: a review. Renewable and Sustainable Energy Reviews. 18 (2013) 246-58.

[15] M. Kenisarin, K. Mahkamov. Solar energy storage using phase change materials. Renewable and Sustainable Energy Reviews. 11 (2007) 1913-65.

[16] A.M. Khudhair, M.M. Farid. A review on energy conservation in building applications with thermal storage by latent heat using phase change materials. Energy conversion and management. 45 (2004) 263-75.

[17] M.M. Farid, A.M. Khudhair, S.A.K. Razack, S. Al-Hallaj. A review on phase change energy storage: materials and applications. Energy conversion and management. 45 (2004) 1597-615.

[18] Rubitherm® Technologies GmbH, http://www.rubitherm.eu/en/. 2015.

[19] A. Sari, R. Eroglu, A. Bicer, A. Karaipekli. Synthesis and thermal energy storage properties of erythritol tetrastearate and erythritol tetrapalmitate. Chemical Engineering & Technology. 34 (2011) 87-92.
[20] H. Mehling, L.F. Cabeza. Heat and cold storage with PCM. Springer2008.
[21] M. Esen, A. Durmuş, A. Durmuş. Geometric design of solar-aided latent heat store depending on various parameters and phase change materials. Solar Energy. 62 (1998) 19-28.
[22] H.A. Adine, H. El Qarnia. Numerical analysis of the thermal behaviour of a shell-and-tube heat storage unit using phase change materials. Applied mathematical modelling. 33 (2009) 2132-44.
[23] M. Lacroix. Numerical simulation of a shell-and-tube latent heat thermal energy storage unit. Solar energy. 50 (1993) 357-67.
[24] M. Huang, P. Eames, B. Norton. Thermal regulation of building-integrated photovoltaics using phase change materials. International Journal of Heat and Mass Transfer. 47 (2004) 2715-33.
[25] C. Alkan, K. Kaya, A. Sarı. Preparation, thermal properties and thermal reliability of form-stable paraffin/polypropylene composite for thermal energy storage. Journal of Polymers and the Environment. 17 (2009) 254-8.
[26] M. Hadjieva, J. Argirov. Thermophysical properties of some paraffins applicable to thermal energy storage. Solar Energy Materials and Solar Cells. 27 (1992) 181-7.
[27] A. Sharma, S. Sharma, D. Buddhi. Accelerated thermal cycle test of acetamide, stearic acid and paraffin wax for solar thermal latent heat storage applications. Energy Conversion and Management. 43 (2002) 1923-30.
[28] A. Shukla, D. Buddhi, R. Sawhney. Thermal cycling test of few selected inorganic and organic phase change materials. Renewable Energy. 33 (2008) 2606-14.
[29] H. Mehling, L.F. Cabeza. Phase change materials and their basic properties. Thermal energy storage for sustainable energy consumption. Springer2007. pp. 257-77.
[30] H. Kimura, J. Kai. Feasibility of trichlorofluoromethane (CCl 3 F, R11) heptadecahydrate as a heat storage material. Energy conversion and management. 25 (1985) 179-86.
[31] F.C. Porisini. Salt hydrates used for latent heat storage: corrosion of metals and reliability of thermal performance. Solar Energy. 41 (1988) 193-7.
[32] V.V. Tyagi, D. Buddhi. PCM thermal storage in buildings: a state of art. Renewable and Sustainable Energy Reviews. 11 (2007) 1146-66.
[33] H. Kimura, J. Kai. Phase change stability of CaCl 2· 6H 2 O. Solar Energy. 33 (1984) 557-63.
[34] V. Tyagi, D. Buddhi. Thermal cycle testing of calcium chloride hexahydrate as a possible PCM for latent heat storage. Solar Energy Materials and Solar Cells. 92 (2008) 891-9.
[35] H. Feilchenfeld, S. Sarig. Calcium chloride hexahydrate: A phase-changing material for energy storage. Industrial & engineering chemistry product research and development. 24 (1985) 130-3.
[36] S. Marks. An investigation of the thermal energy storage capacity of Glauber's salt with respect to thermal cycling. Solar Energy. 25 (1980) 255-8.
[37] I. Dincer, M. Rosen. Thermal energy storage: systems and applications. John Wiley & Sons2002.
[38] T. Wada, R. Yamamoto, Y. Matsuo. Heat storage capacity of sodium acetate trihydrate during thermal cycling. Solar Energy. 33 (1984) 373-5.
[39] H. Kimura, J. Kai. Phase change stability of sodium acetate trihydrate and its mixtures. Solar energy. 35 (1985) 527-34.

[40] A. El-Sebaii, S. Al-Amir, F. Al-Marzouki, A.S. Faidah, A. Al-Ghamdi, S. Al-Heniti. Fast thermal cycling of acetanilide and magnesium chloride hexahydrate for indoor solar cooking. Energy conversion and Management. 50 (2009) 3104-11.

[41] A. El-Sebaii, S. Al-Heniti, F. Al-Agel, A. Al-Ghamdi, F. Al-Marzouki. One thousand thermal cycles of magnesium chloride hexahydrate as a promising PCM for indoor solar cooking. Energy Conversion and Management. 52 (2011) 1771-7.

[42] S. Sharma, D. Buddhi, R. Sawhney. Accelerated thermal cycle test of latent heat-storage materials. Solar Energy. 66 (1999) 483-90.

[43] A. Lázaro, B. Zalba, M. Bobi, C. Castellón, L.F. Cabeza. Experimental study on phase change materials and plastics compatibility. AIChE journal. 52 (2006) 804-8.

[44] L. Cabeza, J. Illa, J. Roca, F. Badia, H. Mehling, S. Hiebler, et al. Immersion corrosion tests on metal-salt hydrate pairs used for latent heat storage in the 32 to 36° C temperature range. Materials and Corrosion. 52 (2001) 140-6.

[45] L. Cabeza, J. Illa, J. Roca, F. Badia, H. Mehling, S. Hiebler, et al. Middle term immersion corrosion tests on metal-salt hydrate pairs used for latent heat storage in the 32 to 36° C temperature range. Materials and Corrosion. 52 (2001) 748-54.

[46] L. Cabeza, J. Roca, M. Nogués, H. Mehling, S. Hiebler. Immersion corrosion tests on metal-salt hydrate pairs used for latent heat storage in the 48 to 58° C temperature range. Materials and Corrosion. 53 (2002) 902-7.

[47] A.J. Farrell, B. Norton, D.M. Kennedy. Corrosive effects of salt hydrate phase change materials used with aluminium and copper. Journal of materials processing technology. 175 (2006) 198-205.

[48] K. Nagano, K. Ogawa, T. Mochida, K. Hayashi, H. Ogoshi. Performance of heat charge/discharge of magnesium nitrate hexahydrate and magnesium chloride hexahydrate mixture to a single vertical tube for a latent heat storage system. Applied thermal engineering. 24 (2004) 209-20.

[49] A. García-Romero, A. Delgado, A. Urresti, K. Martín, J. Sala. Corrosion behaviour of several aluminium alloys in contact with a thermal storage phase change material based on Glauber's salt. Corrosion Science. 51 (2009) 1263-72.

[50] P. Moreno, L. Miró, A. Solé, C. Barreneche, C. Solé, I. Martorell, et al. Corrosion of metal and metal alloy containers in contact with phase change materials (PCM) for potential heating and cooling applications. Applied Energy. 125 (2014) 238-45.

[51] F. Agyenim, N. Hewitt, P. Eames, M. Smyth. A review of materials, heat transfer and phase change problem formulation for latent heat thermal energy storage systems (LHTESS). Renewable and Sustainable Energy Reviews. 14 (2010) 615-28.

[52] M. Liu, W. Saman, F. Bruno. Review on storage materials and thermal performance enhancement techniques for high temperature phase change thermal storage systems. Renewable and Sustainable Energy Reviews. 16 (2012) 2118-32.

[53] J. Khodadadi, L. Fan, H. Babaei. Thermal conductivity enhancement of nanostructure-based colloidal suspensions utilized as phase change materials for thermal energy storage: a review. Renewable and Sustainable Energy Reviews. 24 (2013) 418-44.

1035 [54] P. Lamberg, R. Lehtiniemi, A.-M. Henell. Numerical and experimental investigation of melting and
1036 freezing processes in phase change material storage. International Journal of Thermal Sciences. 43 (2004) 277-
1037 87.
1038 [55] B. Kamkari, H. Shokouhmand, F. Bruno. Experimental investigation of the effect of inclination angle on
1039 convection-driven melting of phase change material in a rectangular enclosure. International Journal of Heat and
1040 Mass Transfer. 72 (2014) 186-200.
1041 [56] F. Tan. Constrained and unconstrained melting inside a sphere. International Communications in Heat and
1042 Mass Transfer. 35 (2008) 466-75.
1043 [57] B.J. Jones, D. Sun, S. Krishnan, S.V. Garimella. Experimental and numerical study of melting in a cylinder.
1044 International Journal of Heat and Mass Transfer. 49 (2006) 2724-38.
1045 [58] H. Shmueli, G. Ziskind, R. Letan. Melting in a vertical cylindrical tube: numerical investigation and
1046 comparison with experiments. International Journal of Heat and Mass Transfer. 53 (2010) 4082-91.
1047 [59] M. Esapour, M. Hosseini, A. Ranjbar, Y. Pahamli, R. Bahrampoury. Phase change in multi-tube heat
1048 exchangers. Renewable Energy. 85 (2016) 1017-25.
1049 [60] N. Vyshak, G. Jilani. Numerical analysis of latent heat thermal energy storage system. Energy Conversion
1050 and Management. 48 (2007) 2161-8.
1051 [61] B. Zivkovic, I. Fujii. An analysis of isothermal phase change of phase change material within rectangular
1052 and cylindrical containers. Solar Energy. 70 (2001) 51-61.
1053 [62] S. Seddegh, X. Wang, A.D. Henderson. A comparative study of thermal behaviour of a horizontal and
1054 vertical shell-and-tube energy storage using phase change materials. Applied Thermal Engineering. 93 (2016)
1055 348-58.
1056 [63] M.J. Allen, N. Sharifi, A. Faghri, T.L. Bergman. Effect of inclination angle during melting and
1057 solidification of a phase change material using a combined heat pipe-metal foam or foil configuration.
1058 International Journal of Heat and Mass Transfer. 80 (2015) 767-80.
1059 [64] R. Akhilesh, A. Narasimhan, C. Balaji. Method to improve geometry for heat transfer enhancement in PCM
1060 composite heat sinks. International Journal of Heat and Mass Transfer. 48 (2005) 2759-70.
1061 [65] M. Gharebaghi, I. Sezai. Enhancement of heat transfer in latent heat storage modules with internal fins.
1062 Numerical Heat Transfer, Part A: Applications. 53 (2007) 749-65.
1063 [66] M. Lacroix, M. Benmadda. Numerical simulation of natural convection-dominated melting and
1064 solidification from a finned vertical wall. Numerical Heat Transfer, Part A Applications. 31 (1997) 71-86.
1065 [67] V. Shatikian, G. Ziskind, R. Letan. Numerical investigation of a PCM-based heat sink with internal fins.
1066 International Journal of Heat and Mass Transfer. 48 (2005) 3689-706.
1067 [68] U. Stritih. An experimental study of enhanced heat transfer in rectangular PCM thermal storage.
1068 International Journal of Heat and Mass Transfer. 47 (2004) 2841-7.
1069 [69] Y. Tao, Y. He. Effects of natural convection on latent heat storage performance of salt in a horizontal
1070 concentric tube. Applied Energy. 143 (2015) 38-46.
1071 [70] C. Guo, W. Zhang. Numerical simulation and parametric study on new type of high temperature latent heat
1072 thermal energy storage system. Energy Conversion and Management. 49 (2008) 919-27.
1073 [71] M. Lacroix. Study of the heat transfer behavior of a latent heat thermal energy storage unit with a finned
1074 tube. International Journal of Heat and Mass Transfer. 36 (1993) 2083-92.

[72] Y. Zhang, A. Faghri. Heat transfer enhancement in latent heat thermal energy storage system by using an external radial finned tube. Journal of Enhanced Heat Transfer. 3 (1996).
[73] M. Rahimi, A. Ranjbar, D. Ganji, K. Sedighi, M. Hosseini, R. Bahrampoury. Analysis of geometrical and operational parameters of PCM in a fin and tube heat exchanger. International Communications in Heat and Mass Transfer. 53 (2014) 109-15.
[74] J.C. Choi, S.D. Kim. Heat-transfer characteristics of a latent heat storage system using MgCl 2· 6H 2 O. Energy. 17 (1992) 1153-64.
[75] R. Velraj, R. Seeniraj, B. Hafner, C. Faber, K. Schwarzer. Experimental analysis and numerical modelling of inward solidification on a finned vertical tube for a latent heat storage unit. Solar Energy. 60 (1997) 281-90.
[76] M.K. Rathod, J. Banerjee. Thermal performance enhancement of shell and tube Latent Heat Storage Unit using longitudinal fins. Applied Thermal Engineering. 75 (2015) 1084-92.
[77] F. Agyenim, P. Eames, M. Smyth. A comparison of heat transfer enhancement in a medium temperature thermal energy storage heat exchanger using fins. Solar Energy. 83 (2009) 1509-20.
[78] M. Medrano, M. Yilmaz, M. Nogués, I. Martorell, J. Roca, L.F. Cabeza. Experimental evaluation of commercial heat exchangers for use as PCM thermal storage systems. Applied Energy. 86 (2009) 2047-55.
[79] D. Chung. A review of exfoliated graphite. Journal of Materials Science. 51 (2016) 554-68.
[80] L. Fan, J. Khodadadi. Thermal conductivity enhancement of phase change materials for thermal energy storage: a review. Renewable and Sustainable Energy Reviews. 15 (2011) 24-46.
[81] T. Fiedler, A. Öchsner, I.V. Belova, G.E. Murch. Thermal conductivity enhancement of compact heat sinks using cellular metals. Defect and Diffusion Forum. Trans Tech Publ2008. pp. 222-6.
[82] O. Mesalhy, K. Lafdi, A. Elgafy, K. Bowman. Numerical study for enhancing the thermal conductivity of phase change material (PCM) storage using high thermal conductivity porous matrix. Energy Conversion and Management. 46 (2005) 847-67.
[83] D. Haillot, X. Py, V. Goetz, M. Benabdelkarim. Storage composites for the optimisation of solar water heating systems. Chemical engineering research and design. 86 (2008) 612-7.
[84] A. Sarı, A. Karaipekli. Thermal conductivity and latent heat thermal energy storage characteristics of paraffin/expanded graphite composite as phase change material. Applied Thermal Engineering. 27 (2007) 1271-7.
[85] Z.-j. Duan, H.-z. Zhang, L.-x. Sun, Z. Cao, F. Xu, Y.-j. Zou, et al. CaCl2· 6H2O/Expanded graphite composite as form-stable phase change materials for thermal energy storage. Journal of Thermal Analysis and Calorimetry. 115 (2014) 111-7.
[86] Y. Wu, T. Wang. Hydrated salts/expanded graphite composite with high thermal conductivity as a shape-stabilized phase change material for thermal energy storage. Energy Conversion and Management. 101 (2015) 164-71.
[87] H.K. Shin, M. Park, H.-Y. Kim, S.-J. Park. Thermal property and latent heat energy storage behavior of sodium acetate trihydrate composites containing expanded graphite and carboxymethyl cellulose for phase change materials. Applied Thermal Engineering. 75 (2015) 978-83.
[88] M. Dannemand, J.B. Johansen, S. Furbo. Solidification behavior and thermal conductivity of bulk sodium acetate trihydrate composites with thickening agents and graphite. Solar Energy Materials and Solar Cells. 145 (2016) 287-95.

1115 [89] E.-B.S. Mettawee, G.M. Assassa. Thermal conductivity enhancement in a latent heat storage system. Solar
1116 Energy. 81 (2007) 839-45.
1117 [90] J. Zeng, L. Sun, F. Xu, Z. Tan, Z. Zhang, J. Zhang, et al. Study of a PCM based energy storage system
1118 containing Ag nanoparticles. Journal of Thermal Analysis and Calorimetry. 87 (2006) 371-5.
1119 [91] R. Velraj, R. Seeniraj, B. Hafner, C. Faber, K. Schwarzer. Heat transfer enhancement in a latent heat
1120 storage system. Solar energy. 65 (1999) 171-80.
1121 [92] A. Elgafy, K. Lafdi. Effect of carbon nanofiber additives on thermal behavior of phase change materials.
1122 Carbon. 43 (2005) 3067-74.
1123 [93] J. Fukai, M. Kanou, Y. Kodama, O. Miyatake. Thermal conductivity enhancement of energy storage media
1124 using carbon fibers. Energy Conversion and Management. 41 (2000) 1543-56.
1125 [94] J. Fukai, Y. Hamada, Y. Morozumi, O. Miyatake. Improvement of thermal characteristics of latent heat
1126 thermal energy storage units using carbon-fiber brushes: experiments and modeling. International Journal of
1127 Heat and Mass Transfer. 46 (2003) 4513-25.
1128 [95] F. Dinter, M.A. Geyer, R. Tamme. Thermal energy storage for commercial applications: a feasibility study
1129 on economic storage systems. Springer1991.
1130 [96] J. Wang, G. Chen, H. Jiang. Theoretical study on a novel phase change process. International journal of
1131 energy research. 23 (1999) 287-94.
1132 [97] A. Mosaffa, C.I. Ferreira, F. Talati, M. Rosen. Thermal performance of a multiple PCM thermal storage
1133 unit for free cooling. Energy Conversion and Management. 67 (2013) 1-7.
1134 [98] Z.-X. Gong, A.S. Mujumdar. Enhancement of energy charge-discharge rates in composite slabs of different
1135 phase change materials. International Journal of Heat and Mass Transfer. 39 (1996) 725-33.
1136 [99] M.M. Farid, A. Kanzawa. Thermal performance of a heat storage module using PCM's with different
1137 melting temperatures: mathematical modeling. Journal of solar energy engineering. 111 (1989) 152-7.
1138 [100] M.M. Farid, Y. Kim, A. Kansawa. Thermal performance of a heat storage module using PCM's with
1139 different melting temperature: experimental. Journal of Solar Energy Engineering. 112 (1990) 125-31.
1140 [101] T.K. Aldoss, M.M. Rahman. Comparison between the single-PCM and multi-PCM thermal energy storage
1141 design. Energy Conversion and Management. 83 (2014) 79-87.
1142 [102] J. Wang, Y. Ouyang, G. Chen. Experimental study on charging processes of a cylindrical heat storage
1143 capsule employing multiple-phase-change materials. International journal of energy research. 25 (2001) 439-47.
1144 [103] C. Liu, Z. Rao, J. Zhao, Y. Huo, Y. Li. Review on nanoencapsulated phase change materials: Preparation,
1145 characterization and heat transfer enhancement. Nano Energy. (2015).
1146 [104] T. Khadiran, M.Z. Hussein, Z. Zainal, R. Rusli. Encapsulation techniques for organic phase change
1147 materials as thermal energy storage medium: A review. Solar Energy Materials and Solar Cells. 143 (2015) 78-
1148 98.
1149 [105] M. Delgado, A. Lázaro, J. Mazo, B. Zalba. Review on phase change material emulsions and
1150 microencapsulated phase change material slurries: materials, heat transfer studies and applications. Renewable
1151 and Sustainable Energy Reviews. 16 (2012) 253-73.
1152 [106] A. Jamekhorshid, S. Sadrameli, M. Farid. A review of microencapsulation methods of phase change
1153 materials (PCMs) as a thermal energy storage (TES) medium. Renewable and Sustainable Energy Reviews. 31
1154 (2014) 531-42.

[107] C.-Y. Zhao, G.H. Zhang. Review on microencapsulated phase change materials (MEPCMs): fabrication, characterization and applications. Renewable and Sustainable Energy Reviews. 15 (2011) 3813-32.
[108] L.F. Cabeza. Advances in Thermal Energy Storage Systems: Methods and Applications. Elsevier Science & Technology2014.
[109] T. Ohtsubo, S. Tsuda, K. Tsuji. A study of the physical strength of fenitrothion microcapsules. Polymer. 32 (1991) 2395-9.
[110] H. Zhang, X. Wang. Synthesis and properties of microencapsulated n-octadecane with polyurea shells containing different soft segments for heat energy storage and thermal regulation. Solar Energy Materials and Solar Cells. 93 (2009) 1366-76.
[111] S. Namwong, M.Z. Islam, S. Noppalit, P. Tangboriboonrat, P. Chaiyasat, A. Chaiyasat. Encapsulation of octadecane in poly (divinylbenzene-co-methyl methacrylate) using phase inversion emulsification for droplet generation. Journal of Macromolecular Science, Part A. 53 (2016) 11-7.
[112] S. Yu, X. Wang, D. Wu. Microencapsulation of n-octadecane phase change material with calcium carbonate shell for enhancement of thermal conductivity and serving durability: synthesis, microstructure, and performance evaluation. Applied Energy. 114 (2014) 632-43.
[113] Y. Yang, X. Ye, J. Luo, G. Song, Y. Liu, G. Tang. Polymethyl methacrylate based phase change microencapsulation for solar energy storage with silicon nitride. Solar Energy. 115 (2015) 289-96.
[114] N. SARIER, E. ONDER, G. UKUSER. Silver Incorporated Microencapsulation of n-Hexadecane and n-Octadecane Appropriate for Dynamic Thermal Management in Textiles. Thermochimica Acta. (2015).
[115] X. Jiang, R. Luo, F. Peng, Y. Fang, T. Akiyama, S. Wang. Synthesis, characterization and thermal properties of paraffin microcapsules modified with nano-Al 2 O 3. Applied Energy. 137 (2015) 731-7.
[116] C. Alkan, A. Sarı, A. Karaipekli, O. Uzun. Preparation, characterization, and thermal properties of microencapsulated phase change material for thermal energy storage. Solar Energy Materials and Solar Cells. 93 (2009) 143-7.
[117] S. Ma, G. Song, W. Li, P. Fan, G. Tang. UV irradiation-initiated MMA polymerization to prepare microcapsules containing phase change paraffin. Solar Energy Materials and Solar Cells. 94 (2010) 1643-7.
[118] M. Hawlader, M. Uddin, H. Zhu. Encapsulated phase change materials for thermal energy storage: experiments and simulation. International Journal of Energy Research. 26 (2002) 159-71.
[119] T.E. Alam, J.S. Dhau, D.Y. Goswami, E. Stefanakos. Macroencapsulation and characterization of phase change materials for latent heat thermal energy storage systems. Applied Energy. 154 (2015) 92-101.
[120] L.F. Cabeza, M. Ibanez, C. Sole, J. Roca, M. Nogués. Experimentation with a water tank including a PCM module. Solar Energy Materials and Solar Cells. 90 (2006) 1273-82.
[121] H. Mehling, L.F. Cabeza, S. Hippeli, S. Hiebler. PCM-module to improve hot water heat stores with stratification. Renewable energy. 28 (2003) 699-711.
[122] M. Veerappan, S. Kalaiselvam, S. Iniyan, R. Goic. Phase change characteristic study of spherical PCMs in solar energy storage. Solar Energy. 83 (2009) 1245-52.
[123] N. Calvet, X. Py, R. Olivès, J.-P. Bédécarrats, J.-P. Dumas, F. Jay. Enhanced performances of macro-encapsulated phase change materials (PCMs) by intensification of the internal effective thermal conductivity. Energy. 55 (2013) 956-64.

1194 [124] H. Zhang, J. Baeyens, J. Degrève, G. Cáceres, R. Segal, F. Pitié. Latent heat storage with tubular-
1195 encapsulated phase change materials (PCMs). Energy. 76 (2014) 66-72.
1196 [125] J. Wei, Y. Kawaguchi, S. Hirano, H. Takeuchi. Study on a PCM heat storage system for rapid heat supply.
1197 Applied thermal engineering. 25 (2005) 2903-20.
1198 [126] K. Ismail, J. Henrıquez. Solidification of PCM inside a spherical capsule. Energy conversion and
1199 management. 41 (2000) 173-87.
1200 [127] K. Ismail, R. Moraes. A numerical and experimental investigation of different containers and PCM
1201 options for cold storage modular units for domestic applications. International Journal of Heat and Mass
1202 Transfer. 52 (2009) 4195-202.

Paper II

Energy Conversion and Management 127 (2016) 355–365

Contents lists available at ScienceDirect

Energy Conversion and Management

journal homepage: www.elsevier.com/locate/enconman

Parametric investigations to enhance thermal performance of paraffin through a novel geometrical configuration of shell and tube latent thermal storage system

Zakir Khan *, Zulfiqar Khan, Kamran Tabeshf

Bournemouth University, Faculty of Science and Technology, NanoCorr, Energy and Modelling (NCEM), Fern Barrow, Talbot Campus, Poole, Dorset BH12 5BB, UK

ARTICLE INFO

Article history:
Received 1 July 2016
Received in revised form 23 August 2016
Accepted 8 September 2016

Keywords:
Latent heat storage
Phase change material
Thermal conductivity
Heat transfer
Shell and tube

ABSTRACT

This paper presents a two-dimensional finite element computational model which investigates thermal behaviour of a novel geometrical configuration of shell and tube based latent heat storage (LHS) system. Commercial grade paraffin is used as a phase change material (PCM) with water is employed as a heat transfer fluid (HTF). In this numerical analysis, the parametric investigations are conducted to identify the enhancement in melting rate and thermal storage capacity. The parametric investigations are comprised of number and orientation of tube passes in the shell, longitudinal fins length and thickness, materials for shell, tube and fins, and inlet temperature of HTF. Numerical analysis revealed that the melting rate is significantly enhanced by increasing the number of tube passes from 9 to 21. In 21 passes configuration, conduction heat transfer is the dominant and effective mode of heat transfer. The length of fins has profound impact on melting rate as compared to fins thickness. Also, the reduction in thermal storage capacity due to an increase in fins length is minimal to that of increase in fins thickness. The influence of several materials for shell, tube and fins are examined. Due to higher thermal conductivity, the melting rate for copper and aluminium is significantly higher than steel AISI 4340, cast iron, tin and nickel. Similarly, the thermal storage capacity and melting rate of LHS system is increased by a fraction of 18.06% and 68.8% as the inlet temperature of HTF is increased from 323.15 K to 343.15 K, respectively. This study presents an insight into how to augment the thermal behaviour of paraffin based LHS system and ultimately, these findings inform novel design solutions for wide-ranging practical utilisation in both domestic and commercial heat storage applications.

1. Introduction

For a long era, the world energy requirements are served and assisted by fossil fuels. However, due to the number of downsides of using fossil fuels such as limited and depleting resources, inconsistent prices and emission of harmful gases have encouraged scientists and engineers to progress in technologies to take advantages of renewable energy. In order to respond to the unpredictable and fluctuating nature of renewable energy sources, latent heat storage (LHS) system provides a viable option. LHS utilises PCM to store surplus thermal energy within solar systems or heat recovery systems and retrieves it when needed, in order to minimise the gap between energy demand and supply [1,2].

However, due to low thermal conductivity of PCM, rapid energy storage and discharge has been a major obstacle. Therefore, LHS system requires a sensitive and responsive thermal energy storing and discharging technique. A significant body literature is available that deals with the enhancement of LHS system such as geometric orientations of LHS system [3,4], utilising extended surfaces [5,6], encapsulation of PCM [7–11], employing form stable PCM [12–17] and inclusion of high thermal conductivity additives to PCM [18–20].

To develop efficient and productive LHS systems, thermal behaviour of several configurations and orientations have been examined. PCMs are normally employed in rectangular, spherical, cylindrical and shell and tubes containers. Kamkari and Shokouhmand [21] conducted an experimental study to identify the effect of number of fins on heat transfer and melting rate of PCM in rectangular container. It was deducted that melting time for one fin and 3 fins were reduced by 18% and 37% as compared to without fins enclosure. However, an increase in number of fins resulted in

* Corresponding author.
E-mail addresses: zkhan2@bournemouth.ac.uk (Z. Khan), zkhan@bournemouth.ac.uk (Z. Khan), KTabeshf@bournemouth.ac.uk (K. Tabeshf).

http://dx.doi.org/10.1016/j.enconman.2016.09.030
0196-8904/

Nomenclature

C_p	specific heat at constant pressure (kJ/kg K)
F	volume force (Pa/m)
f	fraction of PCM in solid and liquid phase
f_s	fraction of PCM in solid phase
f_l	fraction of PCM in liquid phase
g	gravitational acceleration (m/s^2)
H	specific enthalpy (MJ)
k	thermal conductivity (W/m K)
L	latent heat of fusion (kJ/kg)
T	temperature of PCM (K)
T_s	temperature of solid region of PCM (K)
T_l	temperature of liquid region of PCM (K)
T_{pc}	phase change temperature (K)
p	pressure (Pa)
q	heat source term (W/m^3)
S	momentum source term
u	velocity (m/s)
α	small constant value
β	coefficient of thermal expansion (1/K)
κ	morphology constant of mushy zone
ρ	density (kg/m^3)
μ	dynamic viscosity (kg/m s)

Subscripts

s	solid phase of PCM
l	liquid phase of PCM

Acronyms

HTF	heat transfer fluid
LHS	latent heat storage
PCM	phase change material

reduced natural convection and thus the overall heat transfer rate was compromised. Kalbasi and Salimpour [22] numerically studied the impact of length and number of longitudinal fins on thermal performance of PCM in rectangular enclosure. It was reported that higher number of longitudinal fins with shorter length showed augmented natural convection as compared to few fins with longer length. It was recommended that an optimum value for fins length and number should be identified to optimise the system. On the contrary, Ren and Chan [23] reported that an increase in longitudinal fins length enhanced the melting rate of PCM and therefore small number of lengthy fins exhibited effective thermal performance as compared to large number of shorter fins.

Li and Wu [24] numerically investigated the influence of six longitudinal fins on melting rate of $NaNO_3$ in horizontal concentric tube. It was observed that extended fins can reduce the melting and solidification time by at least 14% compared to concentric tubes without fins. Darzi et al. [25] simulated the effect of number fins on melting and solidification rate of N-eicosane in horizontal concentric tube. It was noticed that melting time for 4, 10, 15 and 20 fins were reduced by 39%, 73%, 78% and 82% as compared to no fins case, respectively. Likewise, the solidification time was decreased by 28%, 62%, 75% and 85% as compared to no fins case, respectively. However, as an increase in fins number restrained natural convection, thus increase in fins presented more prominent influence on solidification than melting rate. Yuan et al. [26] simulated the impact of fins angle on melting rate of lauric acid in horizontal concentric tube. It was reported that fins angle plays a significant role in influencing melting rate. The different angles for installation of two fins were 0°, 30°, 45° and 90°. The melting rate for fins angle 0° was comparatively higher. Moreover, in case of fins angle 0°, an increase in inlet temperature of HTF from 60 °C to 80 °C reduced melting time by 59.24%.

Caron-Soupart et al. [27] conducted an experimental examination to identify the effect of vertical concentric tube orientations on melting rate, heat exchange power and storage density. Selected concentric tube orientations were consisted of a single HTF tube without fins, with longitudinal fins and with circular fins. It was noticed that the melting rate for tube with longitudinal fins and circular fins was significantly higher than that of the tube without fins. Likewise, the heat exchange power was increased by a factor of 10 for the fins orientations than without fins. However, due to provision of higher PCM volume, the tube without fins orientation exhibited higher thermal storage density. Likewise, Agyenim et al. [28] conducted an experimental investigation to identify the thermal response of erythritol as a PCM in three orientations of horizontal concentric tube. The three orientations were concentric tube with no fins, with circular fins and with longitudinal fins. It was noticed that after 8 h of charging, only longitudinal fins orientation was able to melt the entire PCM. Also, cumulative thermal energy storage for longitudinal fins was comparatively higher. During solidification process, longitudinal fins showed better thermal performance with reduced subcooling.

Rathod and Banerjee [29] experimentally evaluated the effect of three longitudinal fins on melting and solidification rate of stearic acid in shell and tube container. It was noticed that melting and solidification time was reduced by 24.52% and 43.6% as compared to without fins case, respectively. Luo et al. [30] numerically studied the impact of number of HTF tubes and their orientations in shell and tube container on thermal performance. It was observed that the required melting time for single HTF tube was 2.5 and 5 times than four and nine HTF tubes, respectively. Similarly, the thermal performance of centrosymmetric orientation is better than staggered and inline orientation. Esapour et al. [31] also examined the influence of number of HTF tubes in shell and tube container. It was noticed that by increasing the number of HTF tubes from 1 to 4, the melting time can be reduced by 29%. Therefore, it is evident that the number of HTF tubes has a good influence on thermal behaviour of LHS system.

Vyshak and Jilani [32] conducted a numerical study to compare the impact of rectangular, cylindrical, and shell and tube container orientations on melting rate of PCM. It was observed that for the same volume and heat transfer surface area, the melting rate for shell and tube configuration was comparatively higher.

Tao et al. [33] numerically investigated the influence of HTF tube geometry on melting time. The tested configurations involved smooth, dimpled, cone-finned and helical-finned tubes. It was reported that the melting time for dimple, cone-finned and helical-finned tube was reduced by 19.9%, 26.9% and 30.7% comparing to smooth tube, respectively. Likewise, Li et al. [34] reported that heat transfer rate can be significantly enhanced by employing internally ribbed tubes instead of smooth tubes. Furthermore, the influence of the numbers, geometrical configurations and orientations of fins on thermal behaviour of LHS system is discussed in [35–40].

The mass flow rate of HTF has a minimal influence on thermal behaviour as compared to inlet temperature of HTF and geometrical configuration of LHS system. Seddegh et al. [41] numerically examined the influence of vertical and horizontal orientation of

shell and tube container on thermal behaviour of LHS system. Moreover, it was noticed that mass flow rate of HTF has insignificant influence on melting rate. Kibria et al. [42] conducted numerical and experimental examination of paraffin wax in shell and tube container. It was deduced that mass flow rate of HTF has negligible effect on thermal performance. Also, Wang et al. [43] numerically investigated the enhancement in thermal performance of shell and tube container due to inlet temperature and mass flow rate of HTF. It was observed that the inlet temperature has more profound impact on melting rate and thermal storage capacity than mass flow rate of HTF. Thus, this article will not consider the parametric investigation of mass flow rate of HTF.

In this article, the parametric investigation of a novel geometrical configuration of a shell and tube model is conducted. This specific orientation of shell and tube with longitudinal fins has not been reported in literature. A two-dimensional computational model is applied to a novel shell and tube configuration. This article is focused on identifying the influence of number of tube passes and their orientation in the shell on the melting rate and thermal storage capacity. Moreover, the parametric investigations of fins length, fins thickness and materials for shell, tubes and fins are conducted to investigate the impact on thermal behaviour of LHS system. The influence of inlet temperature of HTF on melting rate and thermal storage capacity is also examined. This article will help in highlighting the parameters that can enhance the thermal performance of LHS system and therefore, the large scale practical utilisation in various domestic and industrial applications, time-saving and economic benefits can be achieved.

2. Numerical model

2.1. Physical model

Physical configuration of LHS system is presented in Fig. 1. Parametric investigations of novel shell and tube model has been conducted to address the enhancement of phase transition rate and thermal storage capacity. The geometrical parameters of shell and tube model are selected with an objective to develop an efficient and responsive LHS system that will be coupled with flat plate solar thermal system, which is previously designed and developed by Helvaci and Khan [44]. The outer diameter, length and thickness of the shell are 450 mm, 320 mm and 1 mm, respectively. The tube is connected with fins, each of 2 mm thickness. The fins are equidistant to each other. Commercial grade paraffin is selected as PCM for its high heat storage capacity, good chemical stability, no super-cooling, non-corrosiveness and low cost [6,45]. Water is made to flow in tube. The thermo-physical properties of paraffin are given in Table 1. Various configurations of shell and tube are examined, as depicted in Fig. 2. In all cases, the number of tube passes, fins number and fins geometry are selected to design a LHS system that is capable of melting entire mass of PCM within 10 h and with minimal reduction in thermal storage capacity. Likewise, the highest possible temperature attained by flat plate solar thermal system is in the range of 333.15 K [44]. To incorporate weather fluctuations, the selected range of inlet temperature of HTF is from 323.15 K to 343.15 K.

2.2. Governing equations

The governing equations to calculate the thermal performance and phase transition rate of PCM based LHS system are mass, momentum and energy conservation equations; which are described as follow:

Mass conservation:

$$\frac{\partial \rho}{\partial t} + \nabla \cdot (\rho \mathbf{u}) = 0 \tag{1}$$

Momentum conservation:

$$\frac{\partial (\rho \mathbf{u})}{\partial t} + \nabla \cdot (\rho \mathbf{u}\mathbf{u}) = -\nabla p + \nabla \cdot (\mu \nabla \mathbf{u}) + \mathbf{F} + S\mathbf{u} \tag{2}$$

Energy conservation:

$$\frac{\partial (\rho C_p T)}{\partial t} + \nabla \cdot (\rho C_p T \mathbf{u}) = \nabla \cdot (k \nabla T) + q \tag{3}$$

Table 1
Thermo-physical characteristics of paraffin [45].

Melting temperature, T_{pc}	41–44 °C or 314.15–317.15 K
Latent heat of fusion, L	255 (kJ/kg)
Specific heat, C_p	2.0 (kJ/kg K)
Thermal conductivity, k	0.2 (W/m K) (solid); 0.2 (W/m K) (liquid)
Density, ρ	800 (kg/m^3) (solid); 700 (kg/m^3) (liquid)
Dynamic viscosity, μ	0.008 (kg/m s)
Coefficient of thermal expansion, β	0.00259 (1/K)

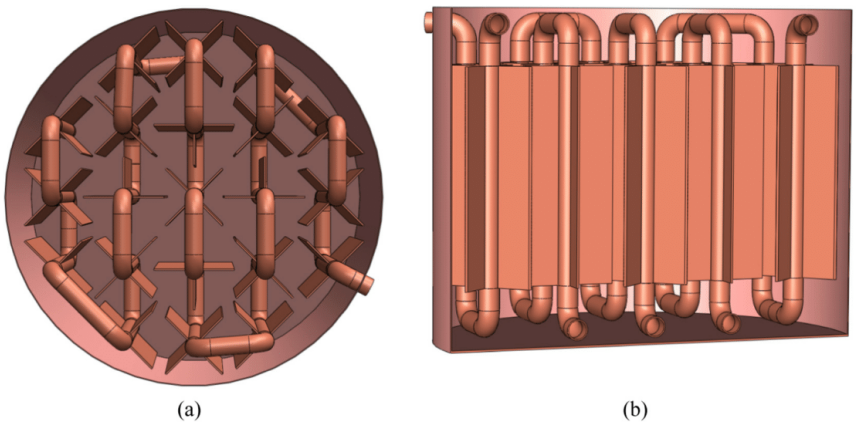

Fig. 1. Physical model of LHS system. (a) Top view and (b) cross section view.

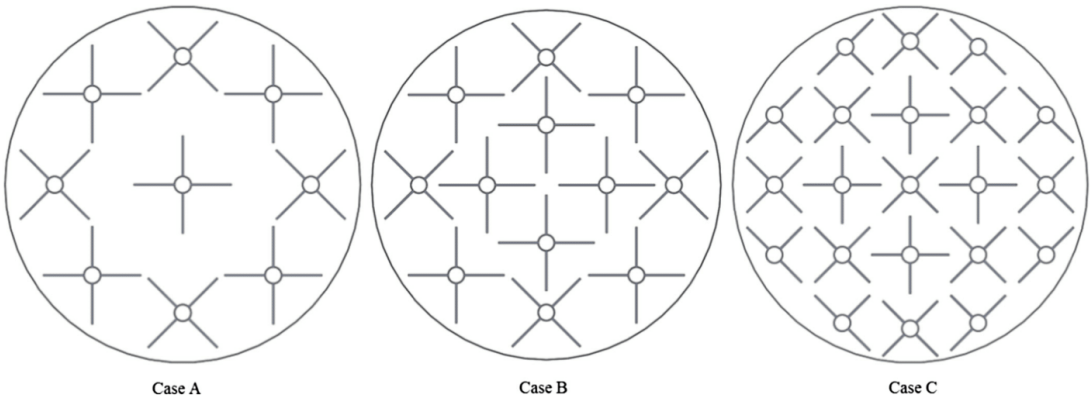

Fig. 2. Various configurations and orientations of shell and tube based LHS system.

where ρ, $\mathbf{u}$, p, μ, $\mathbf{F}$, S, C_p, k, T and q represents density (kg/m^3), velocity (m/s), pressure (Pa), dynamic viscosity (kg/m s), volume force (Pa/m), momentum source term, specific heat at constant pressure (kJ/kg K), thermal conductivity (W/m K), temperature (K) and heat source term (W/m^3), respectively. F in Eq. (2) can be estimated by using Boussinesq approximation [46,47] as follow:

$$\mathbf{F} = \rho \mathbf{g} \beta (T - T_{pc}) \tag{4}$$

where $\mathbf{g}$, β and T_{pc} shows gravitational acceleration (m/s^2), coefficient of thermal expansion (1/K) and phase change temperature (K), respectively. During phase transition, the enthalpy-porosity technique considers mushy zone as porous medium. The porosity and liquid fraction in each mesh element are assumed to be equivalent. In fully solidified mesh elements, the porosity is equal to zero. In order to reduce the velocity in solid region to zero, Kozeny-Carman equation is implemented to estimate the momentum source term S in Eq. (2), as follow [48,49]:

$$S = \frac{\kappa (1-f)^2}{(f^3 + \alpha)} \tag{5}$$

where κ represents morphology constant of mushy zone and α is a small value to avoid division by zero. In this study the values of κ and α are set to 10^7 and 10^{-4}, respectively. Further, the phase transition occurs in temperature interval of $T_s \leqslant T \leqslant T_l$. A smoothing function f is introduced which indicates the fraction of material in solid and liquid phase, as described below:

$$f = \begin{cases} 0 & T < T_s \\ \frac{T - T_s}{T_l - T_s} & T_s \leqslant T \leqslant T_l \\ 1 & T > T_l \end{cases} \tag{6}$$

where the indices s and l represent the solid and liquid phase of PCM, respectively. During phase transition interval, the specific enthalpy H can be defined as the combination of enthalpy in solid and liquid phase, as follow:

$$\rho H = f_s \rho_s H_s + f_l \rho_l H_l \tag{7}$$

To calculate effective specific heat capacity, Eq. (7) is differentiated with respect to temperature and simplified as follow:

$$C_p = \frac{\partial}{\partial T}\left[\frac{f_s \rho_s H_s + f_l \rho_l H_l}{\rho}\right] \tag{8}$$

$$C_p = \frac{1}{\rho}(f_s \rho_s C_{p,s} + f_l \rho_l C_{p,l}) + (H_l - H_s)\frac{\partial}{\partial T}\left[\frac{(f_l \rho_l - f_s \rho_s)}{2\rho}\right] \tag{9}$$

Eq. (9) indicates that effective specific heat capacity is the sum of sensible and latent heat components. The difference in enthalpies $H_l - H_s$ can be replaced with latent heat term L. Likewise, the thermal conductivity and density of PCM can be expressed as follow:

$$k = f_s k_s + f_l k_l \tag{10}$$

$$\rho = f_s \rho_s + f_l \rho_l \tag{11}$$

2.3. Initial and boundary conditions

As mentioned in Table 1, the phase transition temperature of PCM is 314.15 K. In the course of melting, the initial temperature of thermal storage unit is kept at room temperature at 298.15 K, which is less than melting temperature. It indicates that initially entire PCM is in solid phase. A constant boundary temperature is provided from HTF tube to PCM in shell, which ranges from 323.15 K to 343.15 K. The melting process starts at $t = 0$ s by supplying constant temperature from HTF tube walls. The exterior boundary of shell is assumed to be perfectly insulated.

2.4. Computational procedure and model validation

The governing equations are discretised by using finite element approach. In order to simplify the model, it is assumed that all tube passes transfer thermal energy to PCM at constant temperature T_h. The governing equations for HTF and PCM are simultaneously solved in entire computational domain due to coupled thermal energy transfer between HTF and PCM. Second order backward differentiation technique is employed for time stepping to check the relative tolerance. The relative tolerance is set to 0.001. The mesh independency and time stepping are validated by conducting a series of comparative investigations to find the influence of different mesh numbers and time steps on melt time. Case C from Fig. 2 is selected for this examination. Table 2 represent the impact of mesh numbers and time steps on the melt time. It is observed that when the time step is set to 1 min, the melt time for entire LHS system in case-II and case-III are 443 and 441, respectively. However, the difference in melt time for case-I and case-II is significant. Further, the melting fraction at a point, which is at 20 mm vertical distance from the outer boundary of central HTF tube, is illustrated in Fig. 3. It can be noticed from Fig. 3(b) that the melting fraction

Table 2
Validation of mesh independency and time stepping.

Case	Mesh numbers	HTF temperature (K)	Time step (min)	Melt time (min)	Percent error
I	28674	333.15	1	396	10.6
II	57861	333.15	1	443	–
III	61932	333.15	1	441	0.45
IV	57861	333.15	0.25	437	1.35
V	57861	333.15	0.5	452	2.03

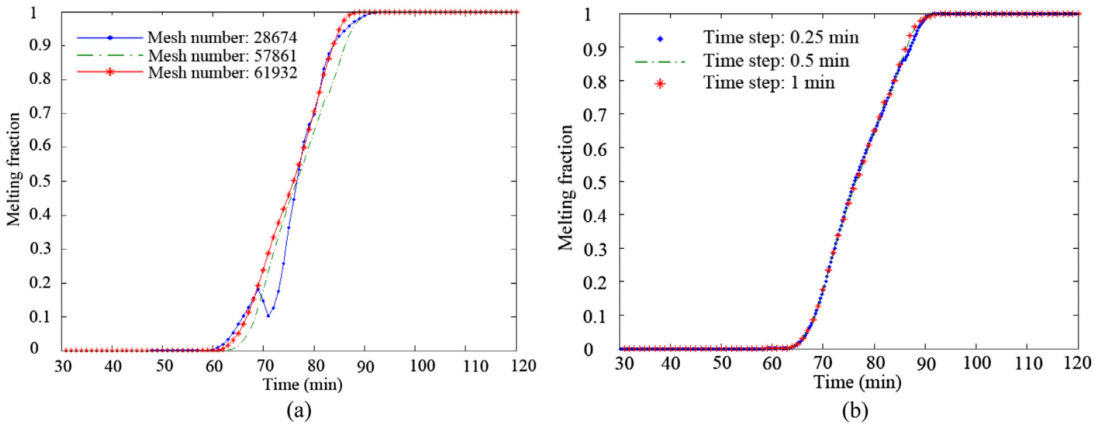

Fig. 3. (a) and (b) illustrates the mesh and time steps independency, respectively.

plots for all three time steps are almost identical. Therefore, the selected mesh numbers and time steps for this study are 57861 and 1 min, respectively.

The current computational model was validated by comparing the simulation results with experimental results which are reported by Liu and Groulx [50]. In their study, dodecanoic acid was employed as PCM in horizontal cylindrical container of 152.4 mm outer diameter. Copper pipe of 12.7 mm outer diameter was fitted through the centre of cylinder. Four fins were connected to copper pipe, each at 90°. Water was utilised as HTF through copper pipe. For validation purpose, the computational model was simulated using geometrical configuration, PCM, initial and boundary conditions and mass flow rate of HTF as reported in [50]. Fig. 4 depicts that both numerical results and experimental results are in good agreement.

3. Results and discussion

3.1. Numbers and orientations of tube passes

Fig. 5 demonstrates the melting fraction of PCM in various geometrical orientations of LHS system. The inlet temperature of HTF is set to 333.15 K for investigating the effect of numbers of tube passes on melting rate. The number of tube passes in case A, B and C are 9, 12 and 21, respectively. With an increase in tube pass, the volume of PCM in shell is compromised by tube and fins. On the contrary, it will increase the effective surface area for heat transfer and thus the low thermal conductivity of PCM can be improved. As a result, the melting rate of PCM can be significantly enhanced by increasing the tube passes.

In case A, the geometric orientation depicts that the tube passes are widely apart. It can be noticed that the tube pass at the centre and the tube passes near the boundary of shell are afar. Therefore, due to low thermal conductivity of PCM, the heat transfer is not very intense in this region. Initially, the melting process is dominated by conduction. It can be noticed from Fig. 5 that only 65.75% of PCM is melted after 5 h of heat transfer. With an increase in liquid percentage of PCM, the heat transfer is now dominated by convection. Further, the melting rate is reduced due to lack of conduction heat transfer. It can be observed that the liquid percentage of PCM is 95.45% and 99% after 10 h and 15 h of heat transfer, respectively. Likewise, even after 20 h, the PCM is not completely melted.

In case B, the surface area for heat transfer is increased by adding three more tube passes. Similar to case-A, the melting process is initially dominated by conduction. It is observed that after 4 h of heat transfer only 71.85% of PCM is in liquid phase. Convection dominates the heat transfer now and thus the melting rate reduces, as the liquid percentage of PCM is 96.07% and 99.5% after 8 h and 12 h, respectively. In case B, the entire PCM is melted in 15 h of continuous heat transfer.

In case C, the surface area for heat transfer is enhanced by increasing the number of tube passes to 21. In this case, the heat transfer is highly dominated by conduction as it can be seen that a huge percentage of PCM is melted within 3 h. It is noticed that the liquid percentage of PCM is 84%, 94.2% and 98.25% after 3 h, 4 h and 5 h of heat transfer, respectively. The entire PCM is melted in 7.5 h.

As depicted in Fig. 5, the melting rate for case C is significantly higher than case A and case B. It is noticed that due to higher effective surface area for heat transfer, the melt time for case C is about half as compared to case B. Also, due to the increase in tube passes, the heat transfer is dominated by conduction and therefore, the melting rate is improved significantly.

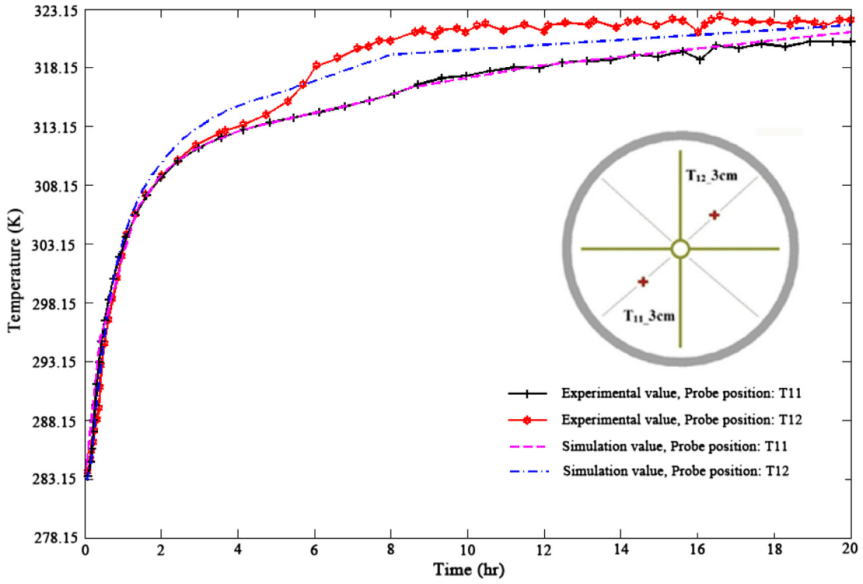

Fig. 4. Comparison of temperature profiles to validate numerical model with experimental results from [50]. For all cases, the inlet temperature and flow rate of HTF were set to 323.15 K and 1 L/min, respectively.

3.2. Longitudinal fins geometry

Fins geometry plays a significant role in enhancing the thermal performance of LHS system. Fig. 6 represents the effect of various fins lengths on melting fraction and temperature distribution in LHS system. Heat is transferred to LHS system for 4 h at inlet temperature of 333.15 K. The influence of various fins lengths ranging from 12.7 mm to 38.10 mm is investigated. Due to an increase in surface area, the thermal conduction enhances and consequently overall heat transfer improves. It is evident from Fig. 6 that the temperature distribution in entire system for case (d) is significantly better than other cases. After 4 h of heat transfer, the liquid fractions for case (a), (b), (c) and (d) are noted to be 59.2%, 72.98%, 83.86% and 94.66%, respectively.

It can be observed from Fig. 7 that as compared to case (a), the total melting time for case (e), (g) and (i) is reduced by 35.45%, 47.01% and 57.32%, respectively. However, it is noticed that the thermal storage capacity is reduced by increasing the fins length. It is noted that the thermal storage capacity for case (i) is 1.94% lesser than case (a). Due to higher melting rate, case (i) is selected for further investigations in this article.

Fig. 8 illustrates the impact of fins thickness on melting fraction and temperature distribution in LHS system. The HTF temperature is set to 333.15 K and the system is charged for 4 h. The effects of different fins thickness ranging from 1 mm to 5 mm are examined. It can be noticed from Fig. 8 that the melting fraction for all cases are almost similar after 4 h of heat transfer. The liquid fraction for case (a), (b), (c) and (d) are recorded to be 94.58%, 94.66%, 94.74% and 94.75%, respectively. Likewise, the fins thickness has minimal influence on the temperature distribution.

Fig. 9 represents the total melting time and variation in thermal storage capacity for all cases. It can be noticed that the total melting time for case (e), case (g) and case (i) is reduced by 10.25%, 13.25% and 16.45% as compared to case (a), respectively. However, an increase in fins thickness can limit the volume for PCM and therefore the thermal storage capacity of LHS system can be compromised. As shown in Fig. 9, the thermal storage capacity for case (i) is reduced by 5.7% as compared to case (a), respectively.

3.3. Shell, tube and fins materials

The low thermal conductivity of PCM can be boosted by employing higher thermal conductive shell, tube and fins. High thermal conductive materials play a vital role in improving the thermal performance of LHS system. In order to analyse the influence of material on thermal performance, the following materials are examined: steel AISI 4340, cast iron, tin, nickel, aluminium 6063, aluminium and copper. The inlet temperature of HTF is kept constant at 333.15 K for all materials. Table 3 represents the percent liquid fraction and complete melting time of PCM against various materials. It is observed that as the thermal conductivity of material increases, the heat transfer rate between HTF and PCM increases and therefore the melting rate of PCM strengthens. Due to higher thermal conductivity of copper, the required melting time for PCM is reduced by 23.68% as compared to steel AISI 4340. Likewise, aluminium and aluminium 6063 presents a good thermal performance, as the melting time is reduced by 18.84% and 17.88% comparing to cast iron, respectively. It is evident from Table 3 that copper and aluminium are the suitable materials to be employed as shell, tube and fins material.

3.4. Inlet temperature of HTF

In order to examine the influence of inlet temperature of HTF on melting rate and increase in enthalpy of LHS system, various inlet temperatures are investigated ranging from 323.15 K to 343.15 K. An increase in inlet temperature of HTF produces higher temperature difference between PCM and HTF and consequently the heat transfer rate is accelerated. Due to an increase in heat transfer, the melting rate of PCM is enhanced, as shown in Fig. 10. It is evident that LHS system in case (d) is at notable higher temperature compared to case (a) and thus majority of the PCM is either in

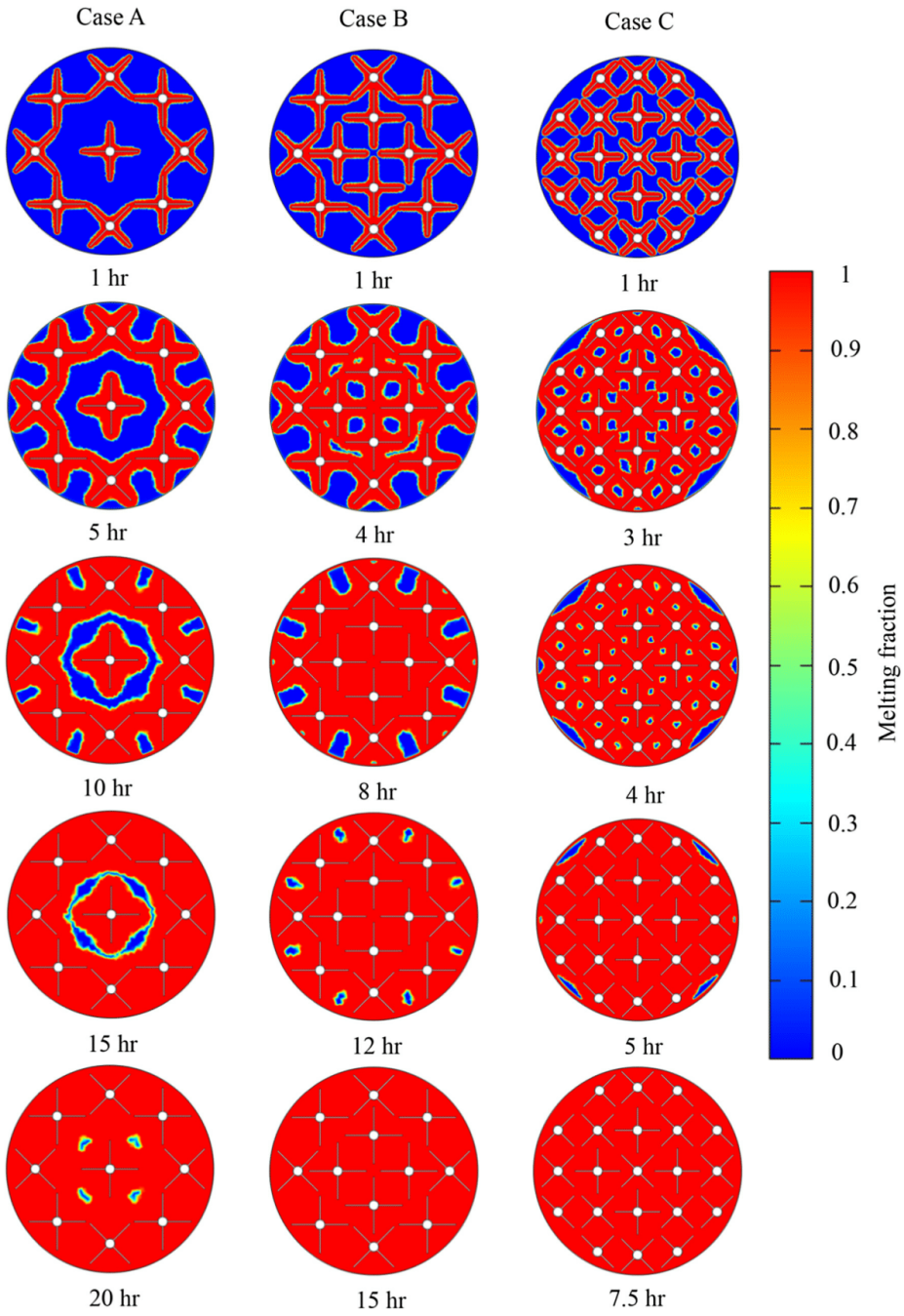

Fig. 5. Liquid fraction for all the three cases at inlet temperature of 333.15 K.

liquid state or mushy zone. After 4 h of heat transfer, the liquid fraction for case (a), (b) (c) and (d) are noted to be 66.71%, 92.93%, 93.65% and 99.55%, respectively. Fig. 11 illustrates that the total melting time is reduced by 42.8%, 52.4% and 68.8% as the inlet temperature of HTF is increased from 323.15 K to 328.15 K, 333.15 K and 343.15 K, respectively. Also, due to the

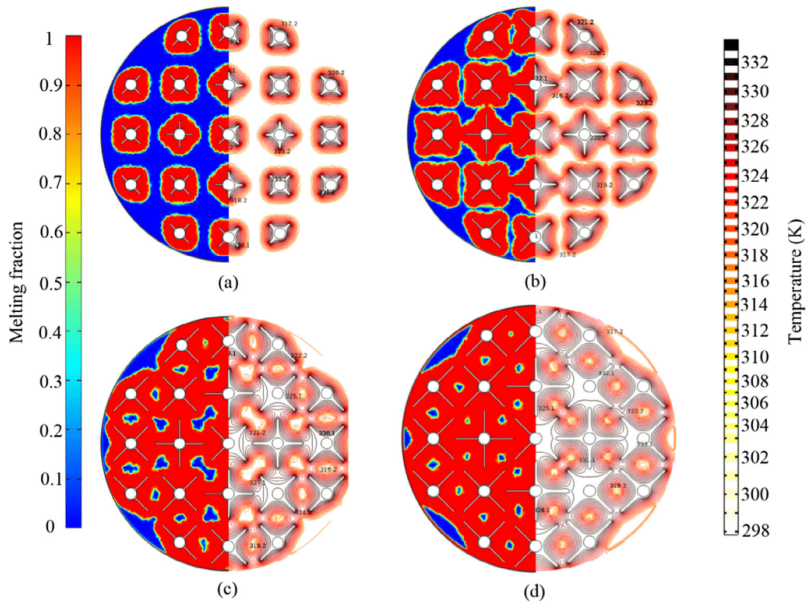

Fig. 6. Influence of fins length on melting fraction and temperature contours after charging for 4 h. Fins thickness is set to 2 mm for all cases. (a) Fins length = 12.7 mm, (b) fins length = 25.4 mm, (c) fins length = 31.75 mm and (d) fins length = 38.10 mm.

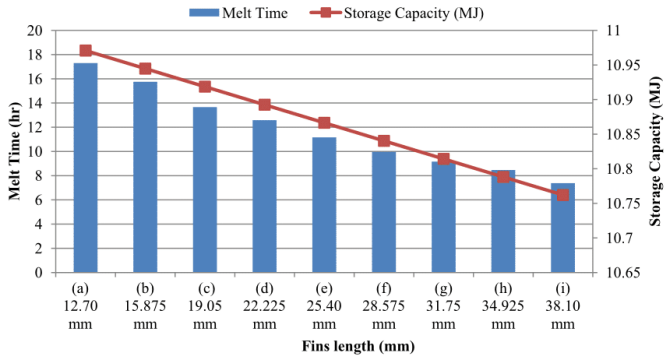

Fig. 7. Effects of fins length on total melt time and thermal storage capacity.

increase in inlet temperature, the sensible enthalpy of the system is also augmented, which results in enhancing the overall thermal storage capacity. Fig. 11 shows that the enthalpy of LHS system for case (c), case (e) and case (i) is increased by 4.52%, 9.03% and 18.06% as compared to case (a), respectively.

4. Conclusions

In this article, a computational model is employed to examine the thermal performance of novel shell and tube configuration based LHS system. Parametric investigation is conducted to inspect the improvement in thermal performance due to the number of tube passes, length and thickness of longitudinal fins, materials for shell, tube and fins, and inlet temperature of HTF. The augmented thermal behaviour of LHS system can attain both time and economic benefits, along with extensive and sustainable employment in both domestic and industrial applications. From the numerical results the following conclusions are reached:

- It is observed that as the number of tube passes is increased from 9 to 21, the thermal performance of the LHS system is significantly enhanced. This is due to the fact that the thermal conductivity and effective surface area for heat transfer increases by increasing the number of tubes. The heat transfer is dominated by conduction heat transfer and therefore the required melting time for 21 number of tube passes is reduced by 48.5% to that of 12 tube passes.
- The geometry of the fins plays a vital role in improving the thermal performance of LHS system. It is noticed that as the length

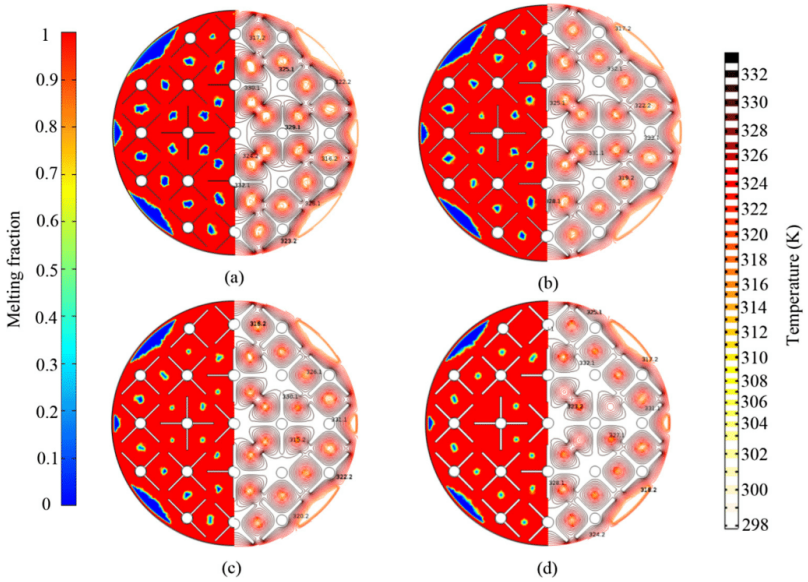

Fig. 8. Influence of fins thickness on melting fraction and temperature contours after charging for 4 h. (a) fins thickness = 1 mm, (b) fins thickness = 2 mm, (c) fins thickness = 3 mm and (d) fins thickness = 4 mm.

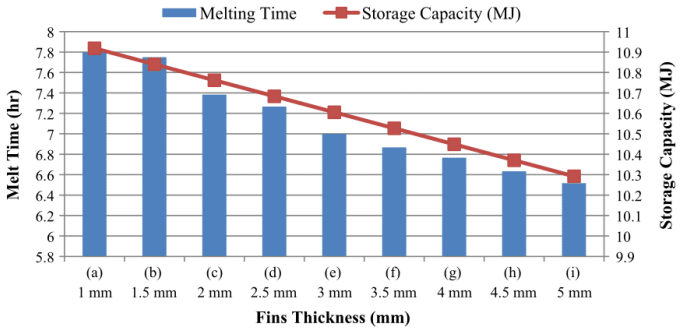

Fig. 9. Effects of fins thickness on total melt time and thermal storage capacity.

Table 3
Effect of shell, tube and fins material on melting rate of LHS system.

Materials	Thermal conductivity (W/(m K)) [51]	Percent liquid fraction					Complete melting time (h)
		2 h	4 h	6 h	8 h	10 h	
Steel AISI 4340	44.5	63.92	85.23	95.53	99.25	100	9.67
Cast iron	50	65.06	86.23	96.19	99.46	100	9.34
Tin	67	67.30	87.69	97.30	99.71	100	8.92
Nickel	90	68.57	88.32	97.78	99.85	100	8.75
Aluminium 6063	201	72.77	92.19	99.08	100		7.67
Aluminium	238	73.05	92.68	99.15	100		7.58
Copper	400	73.63	93.69	99.34	100		7.38

of the fins is increased from 12.7 mm to 38.10 mm, the thermal conductivity of the system improved and consequently the heat transfer between HTF and PCM. The melting time is reduced by 57.32% as the length of the fins is increased from 12.7 mm to 38.10 mm.

- Fins thickness influences the melting time of the PCM. However, it is observed that increase in fins length has more prominent effects on thermal performance than fins thickness. Also, the thermal storage capacity of system is decreased by 5.7% as the fins thickness is increased from 1 mm to 5 mm.

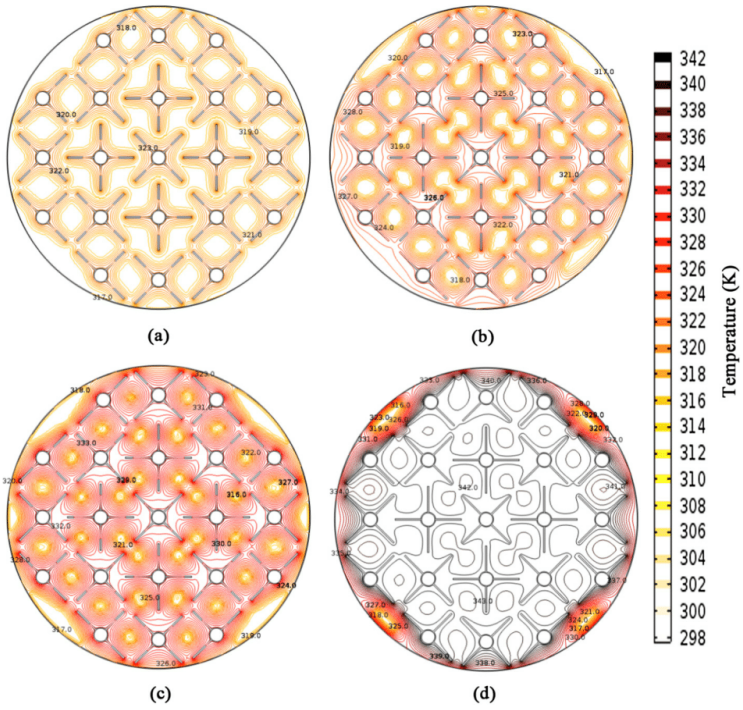

Fig. 10. Temperature contours of LHS system after 4 h of heat transfer. Various inlet temperatures of HTF are (a) 323.15 K, (b) 328.15 K, (c) 333.15 K and (d) 343.15 K.

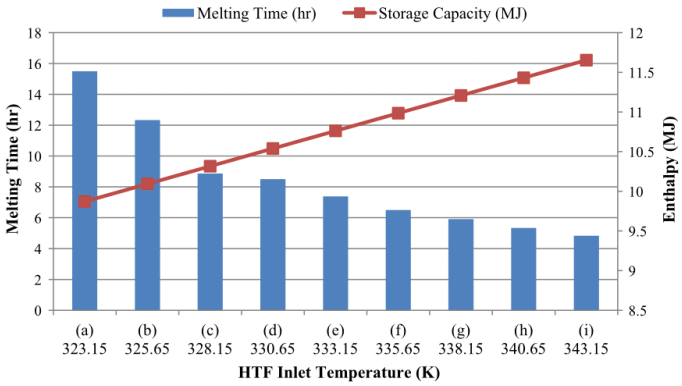

Fig. 11. Impact of inlet temperature of HTF on melting time and thermal storage capacity.

- Shell, tubes and fins material has significant effect on the thermal performance. It is recommended to use high thermal conductive material, which is compatible with PCM. It was observed that copper, aluminium and aluminium 6063 has considerably better thermal performance with paraffin as compared to steel AISI 4340.
- The enthalpy and melting rate is augmented by increasing the inlet temperature of HTF from 323.15 K to 343.15 K. Due to increase in inlet temperature, the sensible enthalpy increases and therefore the overall system thermal storage capacity is increased by 18.06%. Likewise, the melting time is reduced by 68.8%.

Acknowledgment

This project is match funded by Bournemouth University, UK and National University of Sciences and Technology (NUST), Pakistan within their international research collaboration initiative. The authors would like to acknowledge both financial and in-kind support provided by both universities.

References

[1] Farid MM, Khudhair AM, Razack SAK, Al-Hallaj S. A review on phase change energy storage: materials and applications. Energy Convers Manage 2004;45:1597–615.
[2] Sharma A, Tyagi V, Chen C, Buddhi D. Review on thermal energy storage with phase change materials and applications. Renew Sustain Energy Rev 2009;13:318–45.
[3] Dhaidan NS, Khodadadi J. Melting and convection of phase change materials in different shape containers: a review. Renew Sustain Energy Rev 2015;43:449–77.
[4] Archibold AR, Gonzalez-Aguilar J, Rahman MM, Goswami DY, Romero M, Stefanakos EK. The melting process of storage materials with relatively high phase change temperatures in partially filled spherical shells. Appl Energy 2014;116:243–52.
[5] Jegadheeswaran S, Pohekar SD. Performance enhancement in latent heat thermal storage system: a review. Renew Sustain Energy Rev 2009;13:2225–44.
[6] Khan Z, Khan Z, Ghafoor A. A review of performance enhancement of PCM based latent heat storage system within the context of materials, thermal stability and compatibility. Energy Convers Manage 2016;115:132–58.
[7] Salunkhe PB, Shembekar PS. A review on effect of phase change material encapsulation on the thermal performance of a system. Renew Sustain Energy Rev 2012;16:5603–16.
[8] Liu C, Rao Z, Zhao J, Huo Y, Li Y. Review on nanoencapsulated phase change materials: preparation, characterization and heat transfer enhancement. Nano Energy 2015;13:814–26.
[9] Giro-Paloma J, Martínez M, Cabeza LF, Fernández AI. Types, methods, techniques, and applications for Microencapsulated Phase Change Materials (MPCM): a review. Renew Sustain Energy Rev 2016;53:1059–75.
[10] Fan L-W, Zhu Z-Q, Xiao S-L, Liu M-J, Lu H, Zeng Y, et al. An experimental and numerical investigation of constrained melting heat transfer of a phase change material in a circumferentially finned spherical capsule for thermal energy storage. Appl Therm Eng 2016;100:1063–75.
[11] Zhang H, Baeyens J, Degrève J, Cáceres G, Segal R, Pitié F. Latent heat storage with tubular-encapsulated phase change materials (PCMs). Energy 2014;76:66–72.
[12] Tian B, Yang W, Luo L, Wang J, Zhang K, Fan J, et al. Synergistic enhancement of thermal conductivity for expanded graphite and carbon fiber in paraffin/EVA form-stable phase change materials. Sol Energy 2016;127:48–55.
[13] Liu Z, Zhang Y, Hu K, Xiao Y, Wang J, Zhou C, et al. Preparation and properties of polyethylene glycol based semi-interpenetrating polymer network as novel form-stable phase change materials for thermal energy storage. Energy Build 2016;127:327–36.
[14] Li R, Zhu J, Zhou W, Cheng X, Li Y. Thermal properties of sodium nitrate-expanded vermiculite form-stable composite phase change materials. Mater Des 2016;104:190–6.
[15] Feng L, Wang C, Song P, Wang H, Zhang X. The form-stable phase change materials based on polyethylene glycol and functionalized carbon nanotubes for heat storage. Appl Therm Eng 2015;90:952–6.
[16] Silakhori M, Fauzi H, Mahmoudian MR, Metselaar HSC, Mahlia TMI, Khanlou HM. Preparation and thermal properties of form-stable phase change materials composed of palmitic acid/polypyrrole/graphene nanoplatelets. Energy Build 2015;99:189–95.
[17] Zeng J-L, Gan J, Zhu F-R, Yu S-B, Xiao Z-L, Yan W-P, et al. Tetradecanol/expanded graphite composite form-stable phase change material for thermal energy storage. Sol Energy Mater Sol Cells 2014;127:122–8.
[18] Khodadadi J, Fan L, Babaei H. Thermal conductivity enhancement of nanostructure-based colloidal suspensions utilized as phase change materials for thermal energy storage: a review. Renew Sustain Energy Rev 2013;24:418–44.
[19] Fan L, Khodadadi J. Thermal conductivity enhancement of phase change materials for thermal energy storage: a review. Renew Sustain Energy Rev 2011;15:24–46.
[20] Liu L, Su D, Tang Y, Fang G. Thermal conductivity enhancement of phase change materials for thermal energy storage: a review. Renew Sustain Energy Rev 2016;62:305–17.
[21] Kamkari B, Shokouhmand H. Experimental investigation of phase change material melting in rectangular enclosures with horizontal partial fins. Int J Heat Mass Transf 2014;78:839–51.
[22] Kalbasi R, Salimpour MR. Constructal design of horizontal fins to improve the performance of phase change material rectangular enclosures. Appl Therm Eng 2015;91:234–44.
[23] Ren Q, Chan CL. GPU accelerated numerical study of PCM melting process in an enclosure with internal fins using lattice Boltzmann method. Int J Heat Mass Transf 2016;100:522–35.
[24] Li Z, Wu Z-G. Analysis of HTFs, PCMs and fins effects on the thermal performance of shell–tube thermal energy storage units. Sol Energy 2015;122:382–95.
[25] Darzi AAR, Jourabian M, Farhadi M. Melting and solidification of PCM enhanced by radial conductive fins and nanoparticles in cylindrical annulus. Energy Convers Manage 2016;118:253–63.
[26] Yuan Y, Cao X, Xiang B, Du Y. Effect of installation angle of fins on melting characteristics of annular unit for latent heat thermal energy storage. Sol Energy 2016;136:365–78.
[27] Caron-Soupart A, Fourmigué J-F, Marty P, Couturier R. Performance analysis of thermal energy storage systems using phase change material. Appl Therm Eng 2016;98:1286–96.
[28] Agyenim F, Eames P, Smyth M. A comparison of heat transfer enhancement in a medium temperature thermal energy storage heat exchanger using fins. Sol Energy 2009;83:1509–20.
[29] Rathod MK, Banerjee J. Thermal performance enhancement of shell and tube Latent Heat Storage Unit using longitudinal fins. Appl Therm Eng 2015;75:1084–92.
[30] Luo K, Yao F-J, Yi H-L, Tan H-P. Lattice Boltzmann simulation of convection melting in complex heat storage systems filled with phase change materials. Appl Therm Eng 2015;86:238–50.
[31] Esapour M, Hosseini M, Ranjbar A, Pahamli Y, Bahrampoury R. Phase change in multi-tube heat exchangers. Renewable Energy 2016;85:1017–25.
[32] Vyshak N, Jilani G. Numerical analysis of latent heat thermal energy storage system. Energy Convers Manage 2007;48:2161–8.
[33] Tao Y, He Y, Qu Z. Numerical study on performance of molten salt phase change thermal energy storage system with enhanced tubes. Sol Energy 2012;86:1155–63.
[34] Li Z, Tang G, Wu Y, Zhai Y, Xu J, Wang H, et al. Improved gas heaters for supercritical CO_2 Rankine cycles: considerations on forced and mixed convection heat transfer enhancement. Appl Energy 2016;178:126–41.
[35] Tao Y, He Y. Effects of natural convection on latent heat storage performance of salt in a horizontal concentric tube. Appl Energy 2015;143:38–46.
[36] Wang W-W, Wang L-B, He Y-L. Parameter effect of a phase change thermal energy storage unit with one shell and one finned tube on its energy efficiency ratio and heat storage rate. Appl Therm Eng 2016;93:50–60.
[37] Tiari S, Qiu S, Mahdavi M. Discharging process of a finned heat pipe–assisted thermal energy storage system with high temperature phase change material. Energy Convers Manage 2016;118:426–37.
[38] Al-Abidi AA, Mat S, Sopian K, Sulaiman MY, Mohammad AT. Experimental study of melting and solidification of PCM in a triplex tube heat exchanger with fins. Energy Build 2014;68:33–41.
[39] Mat S, Al-Abidi AA, Sopian K, Sulaiman MY, Mohammad AT. Enhance heat transfer for PCM melting in triplex tube with internal–external fins. Energy Convers Manage 2013;74:223–36.
[40] Hosseini M, Ranjbar A, Rahimi M, Bahrampoury R. Experimental and numerical evaluation of longitudinally finned latent heat thermal storage systems. Energy Build 2015;99:263–72.
[41] Seddegh S, Wang X, Henderson AD. A comparative study of thermal behaviour of a horizontal and vertical shell-and-tube energy storage using phase change materials. Appl Therm Eng 2016;93:348–58.
[42] Kibria M, Anisur M, Mahfuz M, Saidur R, Metselaar I. Numerical and experimental investigation of heat transfer in a shell and tube thermal energy storage system. Int Commun Heat Mass Transf 2014;53:71–8.
[43] Wang W-W, Zhang K, Wang L-B, He Y-L. Numerical study of the heat charging and discharging characteristics of a shell-and-tube phase change heat storage unit. Appl Therm Eng 2013;58:542–53.
[44] Helvaci H, Khan ZA. Mathematical modelling and simulation of multiphase flow in a flat plate solar energy collector. Energy Convers Manage 2015;106:139–50.
[45] Rubitherm® Technologies GmbH. <http://www.rubitherm.eu/en/>; 2016.
[46] Mohamad A, Kuzmin A. A critical evaluation of force term in lattice Boltzmann method, natural convection problem. Int J Heat Mass Transf 2010;53:990–6.
[47] Gray DD, Giorgini A. The validity of the Boussinesq approximation for liquids and gases. Int J Heat Mass Transf 1976;19:545–51.
[48] Nield DA, Bejan A. Convection in porous media. Springer Science & Business Media; 2006.
[49] Tiari S, Qiu S, Mahdavi M. Numerical study of finned heat pipe-assisted thermal energy storage system with high temperature phase change material. Energy Convers Manage 2015;89:833–42.
[50] Liu C, Groulx D. Experimental study of the phase change heat transfer inside a horizontal cylindrical latent heat energy storage system. Int J Therm Sci 2014;82:100–10.
[51] MatWeb. <http://www.matweb.com/index.aspx>; 2016.

Paper III

Proceedings of the ASME 2017 11th International Conference on Energy Sustainability
ES2017
June 26-30, 2017, Charlotte, North Carolina, USA

ES2017-3276

DEVELOPMENT IN PARAFFIN BASED THERMAL STORAGE SYSTEM THROUGH SHELL AND TUBES HEAT EXCHANGER WITH VERTICAL FINS

Zakir Khan
Nano Corr., Energy and Modelling Research Group, Faculty of Science and Technology, Bournemouth University.
Bournemouth, Dorset, UK

Zulfiqar Ahmad Khan
Nano Corr., Energy and Modelling Research Group, Faculty of Science and Technology, Bournemouth University.
Bournemouth, Dorset, UK

ABSTRACT

Researchers are committed to develop robust and responsive technologies for renewable energy sources to avert from reliance on fossil fuels, which is the main cause of global warming and climate change. Solar energy based renewable energy technologies are valued as an important substitute to bridge gap between energy demand and generation. However, due to varying and inconsistent nature of solar energy during weather fluctuations, seasonal conditions and night times, the complete utilisation of technology is not guaranteed. Therefore, thermal energy storage (TES) system is considered as an imperative technology to be deployed within solar energy systems or heat recovery systems to maximise systems efficiency and to compensate for varying thermal irradiance. TES system can capture and store the excess amount of thermal energy during solar peak hours or recover from systems that would otherwise discard this excess amount of thermal energy. This stored energy is then made available to be utilised during solar off peak hours or night times.

Phase change material (PCM) based TES system is appraised as a viable option due to its excellent adoption to solar and heat recovery systems, higher thermal storage density and wide range of materials availability. However, due to its low thermal conductivity (≅ 0.2 W/mK), the rapid charging and discharging of TES system is a challenge. Therefore, there is a need for efficient and responsive heat exchange mechanism to boost the heat transfer within PCM.

In this study, transient analysis of two-dimensional computational model of vertical shell and tube based TES system is conducted. Commercial grade paraffin (RT44HC) is employed in shell as thermal storage material due to its higher thermal storage density, thermo-physical stability and compatibility with container material. Water is made to flow in tubes as heat transfer fluid. In this numerical study, the parametric investigations are performed to determine the enhancement in charging rate, discharging rate and thermal storage capacity of TES system. The parametric investigations involve geometrical orientations of tubes in shell with and without fins, inlet temperature and volume flow rate of HTF.

It is evident from numerical results that due to increase in effective surface area for heat transfer by vertical fins, the charging and discharging rate of paraffin based TES system can be significantly increased. Due to inclusion of vertical fins, conduction heat transfer is dominant mode of heat transfer in both charging and discharging processes. Furthermore, vertical fins do not restrict natural convection or buoyancy driven flow as compared to horizontal fins. Similarly, the inlet temperature has a noticeable impact on both charging and discharging process. In melting process, the sensible enthalpy is boosted due to rise in inlet temperature and thus the whole system thermal storage capacity is enhanced. Likewise, the effect of volume flow rate of HTF on charging and discharging rate is moderate as compared to inlet temperature of HTF. The numerical results are validated by experimental results.

To conclude, these findings present an understanding into how to increase charging and discharging rate of TES system so as to provide feasible design solutions for widespread domestic and commercial utilisation of TES technology.

INTRODUCTION

Dependency on fossil fuels for power generation has instigated immense threat to clean air and ozone layer which are main sources behind recent global warming and climate change [1, 2]. Likewise, world power consumption is continuously increasing with economic development. Therefore, there is a need of developments in renewable energy sector to minimise reliance on fossil fuels for power generation.

Solar energy is termed as decisive renewable energy source for its enormous quantity of free and clean incident solar

radiations. Thus, the interest in utilising solar energy source to meet global energy demand has been boosted in recent years [3]. Nano Corr., Energy and Modelling Research Group at Bournemouth University, UK is keenly engaged in developing robust and responsive technologies to attain maximum benefit from solar energy sources [4-6].

However, due to highly unforeseeable and dubious nature of solar energy caused by weather fluctuations and day/night times, the far-reaching benefits are highly affected. In order to respond to unpredictable nature of solar energy, thermal energy storages (TES) system is gauged as a suitable option due to its great acceptance to solar energy. TES system can capture the excess thermal energy at solar peak periods and bring it into service during solar off-peak periods or night-time.

TES system is categorised into three groups, which are sensible heat storage (SHS), latent heat storage (LHS) and thermo-chemical system. In order to store same quantity of thermal energy, the required mass for rocks (SHS) will be seven times to organic paraffin (LHS) and eight times to salt hydrate (LHS) [7, 8]. Therefore, LHS is regarded as better option due to its higher thermal storage capacity, higher heat of fusion per unit volume, lower vapour pressure, phase change materials (PCM) availability in wide range of temperatures and almost isothermal thermal energy storage and retrieval [9, 10].

Despite these favorable properties, PCMs have low thermal conductivity (≅ 0.2 W/mK), which hinders rapid charging and discharging of LHS system and thus the practical utilisation is highly affected. Hence, LHS system requires a responsive heat transfer mechanism within PCM to boost thermal charging rate and discharging rate. In past 2 decades, substantial research has been conducted to identify techniques for enhancing thermal performance of LHS system. Among all techniques, geometrical configuration with extended surfaces[11, 12], addition of high thermal conductivity additives [13, 14] and encapsulation techniques [15, 16] have been studied the most.

In this paper, two dimensional transient computational model of shell and tube with longitudinal fins based LHS system is simulated to find effective parameters that promise rapid melting and solidification of PCM in LHS system. This paper is focused on studying impact of longitudinal fins, geometrical configurations of fins and operating conditions on thermal performance of LHS system. Moreover, experimental examinations are conducted to validate the simulated computational model. This paper will give an insight and understanding into how to improve charging and discharging rate of LHS system so as to enlarge its practical utilisation in domestic and industrial applications.

PHYSICAL MODEL

The schematic of LHS system connected to flat-plate solar collector is represented in Fig. 1. The model is comprised of LHS tank, flat-plate solar collector, pump and connection to mains water supply. The serpentine type flat-plate solar collector is previously designed and developed in Nano Corr., Energy and Modelling Research Group at Bournemouth University, UK by Helvaci and Khan [4, 5]. Shell and tube heat exchange mechanism is designed for LHS tank, as depicted in Fig. 2. The thickness, height and outer diameter of shell are 1 mm, 320 mm and 450 mm, respectively. The outer diameter and thickness of tube is 22 mm and 1mm, respectively. Tubes are connected with longitudinal fins. The length, height and thickness of longitudinal fins are 40 mm, 230 mm and 1.5 mm, respectively. Copper is used as construction material for shell, tube and fins. Paraffin (RT44HC) is employed in shell as PCM, due to its excellent chemical stability, compatibility with copper, high latent heat storage capacity and low cost [12, 17]. The thermo-physical characteristics of RT44HC are listed in Table 1. Water is used as heat transfer fluid (HTF) in tube. The flow pattern of water within LHS tank is represented by blue arrows in Fig. 2.

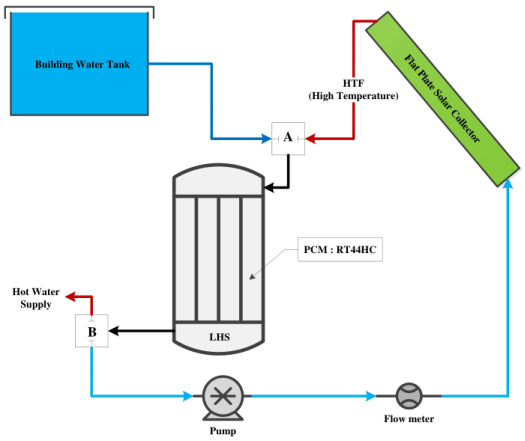

Fig. 1 Schematic of LHS system with flat plate solar collector

During melting process, water from mains supply is initially run through the whole system to make sure that the system is completely filled with water. Now, water supply from mains is turned off to make a close loop. Water is pumped through flat-plate solar collector, where solar radiations are converted to thermal energy. Thermal energy is transferred to water and therefore, it rises water temperature. Water at high temperature is now directed to pass through tubes in LHS tank, where it loses thermal energy to PCM. Thermal energy from water charges LHS system by melting PCM. The closed cycle is repeated until the entire mass of PCM is melted.

During solidification process, high temperature water supply from flat-plate collector is turned off at point A, as shown in Fig. 1. Also, the connection between LHS tank and pump is switched off at point B. Now, the connections for mains supply at point A and hot water supply at point B are switched on. Cold water from mains is made to run through tubes in LHS tank, where it extracts thermal energy from PCM. Solidification

of PCM starts as thermal energy is extracted. Open cycle is stopped once whole mass of PCM is solidified.

Table 1
Thermo-physical properties of RT44HC [6, 17]

Phase transition temperature T_{pc}	315.15-317.15 K
Latent heat of fusion	255 (kJ/kg)
Specific heat C_p	2.0 (kJ/kg. K)
Thermal conductivity k	0.2 (W/m. K) (solid); 0.2 (W/m. K) (liquid)
Density ρ	800 (kg/m^3) (solid); 700 (kg/m^3) (liquid)
Dynamic viscosity μ	0.008 (kg/m. s)
Coefficient of thermal expansion β	0.00259 (1/K)

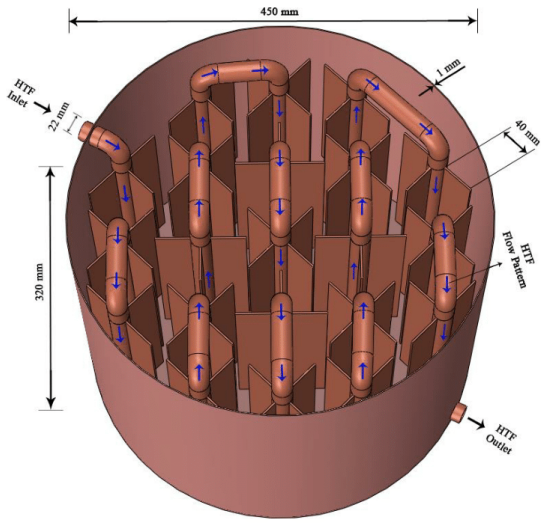

Fig. 2 Sketch of physical model of shell and tube based LHS tank

NUMERICAL MODEL AND BOUNDARY CONDITIONS

Numerical model for investigating phase transition rate and thermal storage capacity of LHS system is based on conservation of mass, momentum and energy equations. The conservation of mass equation is:

$$\frac{\partial \rho}{\partial t} + \rho \nabla \mathbf{u} = 0 \tag{1}$$

where $\mathbf{u}$ and ρ represent velocity vector and density, respectively. Similarly, momentum equation is expressed as follow:

$$\rho \frac{\partial \mathbf{u}}{\partial t} + \rho(\mathbf{u}.\nabla)\mathbf{u} = -\nabla p + \mu \Delta \mathbf{u} + \mathbf{F} + S\mathbf{u} \tag{2}$$

where p, μ, $\mathbf{F}$ and $S\mathbf{u}$ represent pressure, dynamic viscosity, buoyant force vector and momentum source term, respectively. Buoyant force term $\mathbf{F}$ in Eq. (2) can be calculated by employing Boussinesq approximation [18], as follow:

$$F = \rho \mathbf{g} \beta (T - T_{ref}) \tag{3}$$

where β and T_{ref} represent coefficient of thermal expansion and reference phase transition temperature. Similarly, momentum source term $S\mathbf{u}$ can be calculated by implementing Kozeny-Carman equation, which is calculated by using Darcy law for flow in porous medium, as follow[19]:

$$S\mathbf{u} = \frac{\kappa (1-f)^2}{(\alpha + f^3)} \mathbf{u} \tag{4}$$

where κ, α and f represent mushy zone constant, small constant value to avoid division by zero and fraction of phase transition, respectively. In current study, κ is set to 10^6 and α to 10^{-3}. Likewise, f can be described as follow:

$$f = \begin{cases} 0 & T < T_s \\ \dfrac{T - T_s}{T_l - T_s} & T_s \le T \le T_l \\ 1 & T > T_l \end{cases} \tag{5}$$

where T_s and T_l represent temperature of solid zone and liquid zone of PCM, respectively. Phase change of PCM initiates during interval of $T_s \le T \le T_l$. Likewise, the conservation of energy is illustrated as follow:

$$\rho \frac{\partial (C_p T)}{\partial t} + \rho \nabla .(C_p T \mathbf{u}) = k \Delta T + q \tag{6}$$

where C_p, T, k and q represent specific heat at constant pressure, temperature, thermal conductivity and heat source term, respectively. During phase transition, the effective specific heat capacity can be obtained by differentiating specific enthalpy of LHS system with temperature [6], as follow:

$$C_p = \frac{1}{\rho}\left(f_s\rho_s C_{p,s} + f_l\rho_l C_{p,l}\right) + \left(H_l - H_s\right)\frac{\partial}{\partial T}\left[\frac{\left(f_l\rho_l - f_s\rho_s\right)}{2\rho}\right] \quad (7)$$

where H represents specific enthalpy of LHS system. Solid and liquid phases of PCM are represented by indices s and l, respectively.

During melting process, the entire LHS system is assumed to be at initial room temperature, which is 291.15K. As discussed in Table 1, the phase transition temperature of PCM is 315.15K. Therefore, the initial temperature of LHS system guarantees that entire mass of PCM is in solid phase. Inlet temperature of HTF is set to three constant boundary temperatures, which have a temperature difference of 10K, 15K and 20K to phase transition temperature of PCM, respectively.

Likewise in solidification process, LHS system is set to 325.15K, which has a temperature difference of 10K with phase transition temperature. Therefore, it shows that initially entire mass of PCM is in liquid phase. In solidification process, the municipal cold water is employed as HTF. Thus, three inlet temperatures of HTF are investigated, which are 285.15K, 288.15K and 293.15K, respectively.

COMPUTATIONAL MODEL

Finite element analysis approach is implemented to discretise aforementioned governing equations. Coupled thermal energy transfer and non-isothermal techniques are adopted to simultaneously solve governing equations for both HTF and PCM. Second order backward differentiation formula is exercised to ensure relative tolerance for each time step. Relative tolerance is kept at constant value of 0.001. In order to simplify the computational model, the value for inlet temperature of HTF is assumed to be constant. Likewise, the influence of mesh size and time steps on phase transition rate is examined by conducting comparative investigations at constant inlet temperature. As depicted in Table 2, for initial three cases, the time step is kept constant at 1 min whereas mesh size is varied. The result indicates that for constant time step, the phase transition time for entire PCM in LHS tank is almost similar for case II and case III. However, a significant difference is noticed in phase transition time between case I and case II. Likewise, in case IV and case V, the time step is varied whereas mesh size is kept constant. It is noticed that the phase transition time for case IV and case V is having an insignificant percent error of 1.35 and 2.03 as compared to case II.

Therefore, the chosen time step and mesh numbers for this computational model are 1 min and 57861, respectively. Fig. 3 depicts mesh configuration adopted for this computational model. Parametric sweep is implemented to investigate the impact of various operating conditions on phase transition rate and thermal storage capacity.

Table 2
Validation of mesh independency and time stepping [6]

Case	Mesh Numbers	Time step (min)	Melt time (min)	Percent Error
I	28674	1	396	10.6
II	57861	1	443	-
III	61932	1	441	0.45
IV	57861	0.25	437	1.35
V	57861	0.5	452	2.03

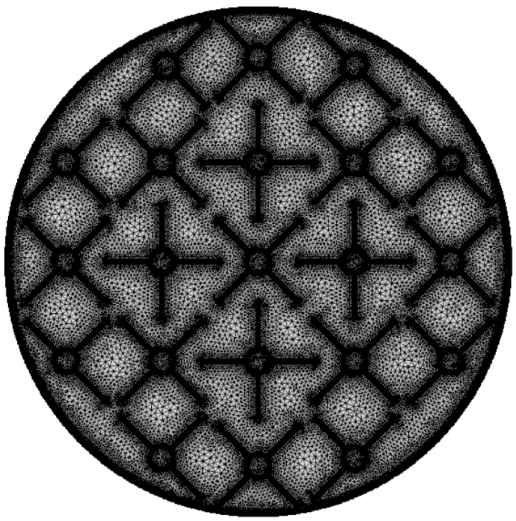

Fig. 3 Mesh configuration of shell and tube with longitudinal fins LHS tank

RESULTS AND DISCUSSION

In this section, the results attained from numerical investigations and experimental examinations are discussed.

PERFORMANCE OF TUBE IN SHELL WITH AND WITHOUT FINS

Prior to investigating thermal performance of shell and tube with fins, the computational model is implemented to shell and tube without fins. The inlet temperature of HTF is fixed at 335.15K. Four data points are selected to inspect the thermal performance of the system, as depicted in Fig. 4. It is noticed that due to less surface area for heat transfer, the rise in temperature is very slow. It is also observed that although the temperature difference between HTF and PCM in inlet zone is higher, it still requires 4.7 hours for complete melting of PCM. Likewise, the PCM in outlet zone needs almost 6.7 hours to completely melt. It shows that due to low thermal conductivity of PCM, the thermal performance of shell and tube heat exchanger without fins is poor. Thus, LHS system demands a

geometrical configuration that guarantees rapid charging and discharging.

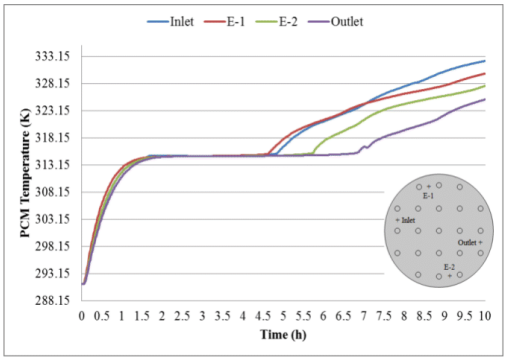

Fig. 4 Temperature plot of PCM in shell and tube without fins configuration. Inlet temperature is set to 335.15K. Four zones for inspecting temperature data within LHS tank are selected: 1) Inlet 2) Exterior E-1 3) Exterior E-2 4) Outlet.

Thermal performance of shell and tube heat exchanger with longitudinal fins is illustrated in Fig. 5. It is noticed that due to inclusion of longitudinal fins, the effective area for heat transfer increases which enhances thermal performance and heat distribution. As depicted in Fig. 5, the rise in temperature is faster as compared to shell and tube with no fins configuration. In this case, the inlet zone is completely melted in 1.7 hours and outlet zone in 2.25 hours. Melting time in inlet zone for shell and tube with fins configurations is reduced by 63.82% as compared to shell and tube configuration without fins. Therefore, it is recommended to use longitudinal fins to attain higher phase transition rate of LHS system.

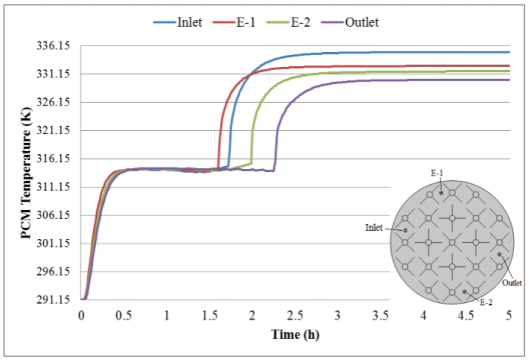

Fig. 5 Temperature plot of PCM in shell and tube with longitudinal fins orientation. Inlet temperature is kept constant at 335.15K.

GEOMETRICAL CONFIGURATIONS OF FINS

The geometrical configurations of longitudinal fins significantly influence the thermal behavior of LHS system. Therefore, parametric investigations are conducted to identify the impact of fins length and fins thickness on thermal storage behavior and melting rate. In all cases, the inlet temperature of LHS system is kept constant at 335.15K.

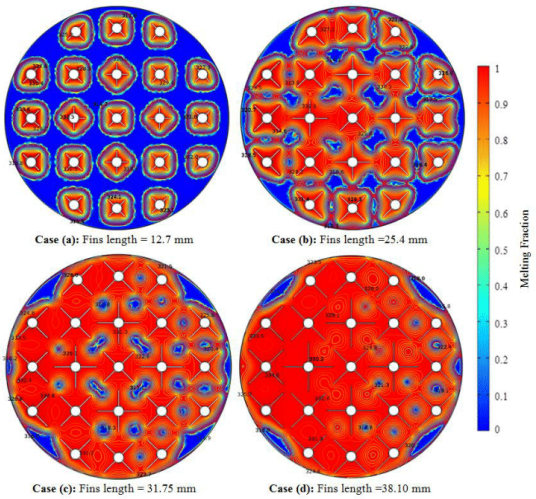

Fig. 6 Melting fraction and thermal contours of LHS system in response to varied fins lengths. Inlet temperature is set to 335.15 K.

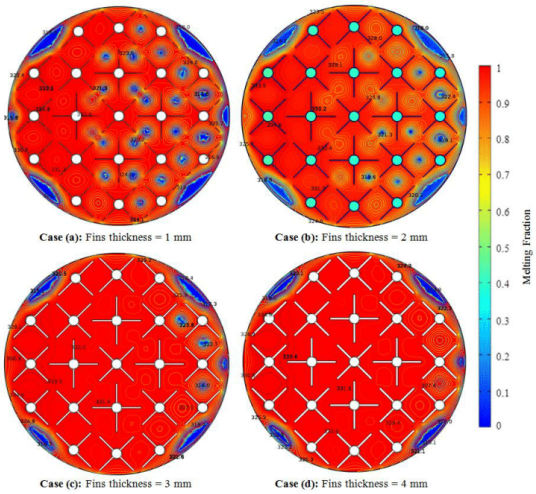

Fig. 7 Impact of fins thickness on melting fraction after charging LHS system with constant inlet temperature of 335.15 K for two hours.

It can be noticed from Fig. 6 that due to an increase in fins length, the melting rate of PCM in LHS system is significantly enhanced. Fins lengths are investigated in range of 12.70 mm to 38.10 mm. As depicted in Fig. 6, the distribution of temperature in entire system for 38.10 mm fins is better than others cases due to an increase in effective surface area for heat transfer. Likewise, after two hours of heat transfer from HTF to PCM at constant inlet temperature, the liquid fraction of PCM for case (a), (b), (c) and (d) are registered to be 64.34%, 82.80%, 92.06% and 96.86%, respectively. It shows that with an increase in fins length, the melting/charging time of LHS system can be significantly reduced. However, thermal storage capacity is slightly reduced due to inclusion of lengthy fins. Thermal storage capacity of 38.10 mm is 1.94% lesser than 12.70 mm. Nevertheless, the slight reduction in thermal storage capacity does not diminish the importance of rapid charging and discharging of LHS system produced by inclusion of lengthy fins.

Likewise, the influence of fins thickness ranging from 1 mm to 4 mm on thermal behavior of LHS system is studied. During this investigation, the fins length is set constant at 38.10 mm. As shown in Fig. 7, fins thickness displayed a moderate influence on melting rate as compared to fins length. Similarly, the effect on temperature distribution within LHS system is insignificant. The total melting time for case (b), (c) and (d) are reduced by 12.04%, 20.37% and 22.68% as compared to case (a). However, thermal storage capacity is compromised by using thicker fins. Thermal storage capacity for 4 mm is decreased by 4.3% as compared to 1 mm. Thus, it is recommended to use lengthy thin fins.

OPERATING CONDITIONS

In order to investigate the performance of shell and tube orientation with longitudinal fins under various operating conditions, the inlet temperatures of 325.15 K, 330.15 K and 335.15 K are inspected in melting process. Likewise, the inlet

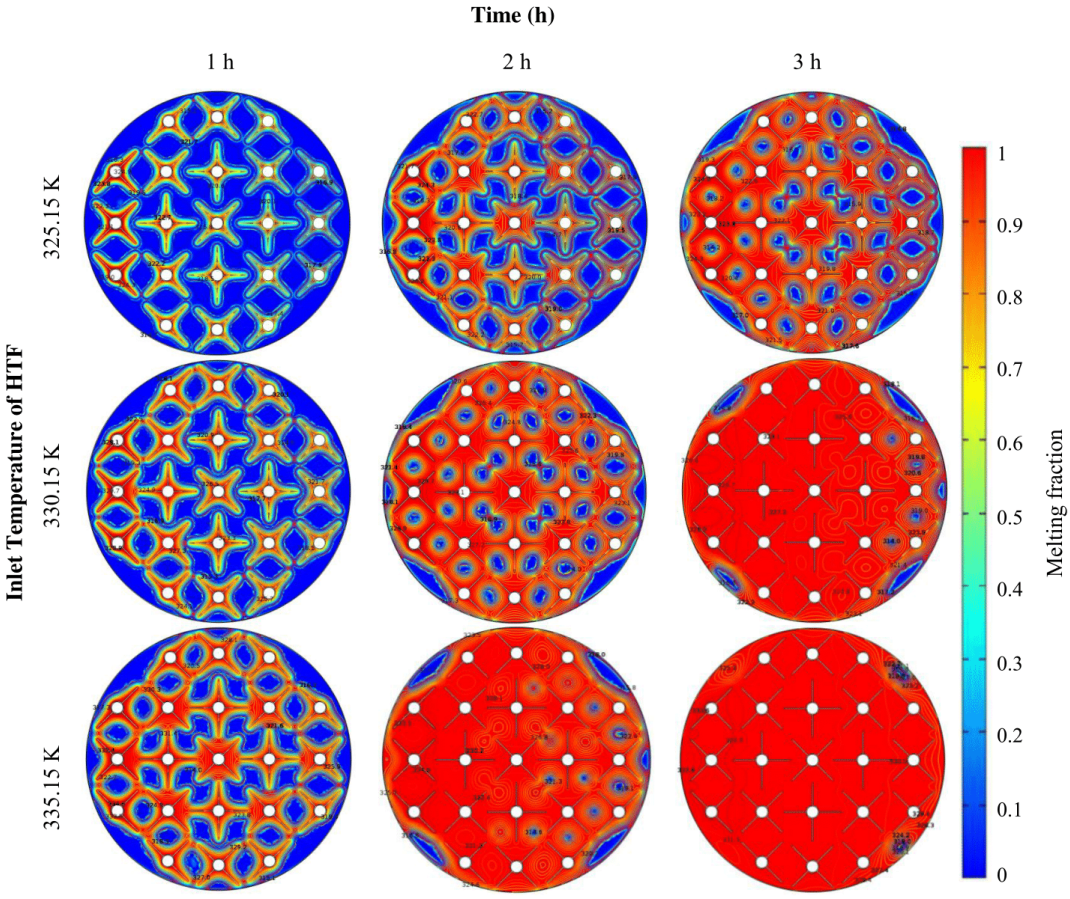

Fig. 8 Comparison of melting fraction of LHS system at various inlet temperatures of HTF

temperature of 285.15 K, 288.15 K and 293.15 K are tested in solidification process.

During melting process, it is observed that heat transfer between HTF and PCM is boosted due to higher temperature difference caused by an increase in inlet temperature of HTF. Due to higher heat transfer, the melting rate of PCM improves, as shown in Fig. 8. It can be observed that during 325.15 K as inlet temperature, due to higher temperature difference between inlet temperature of HTF and PCM in inlet zone (left side of Fig .8), the melting rate is higher and therefore HTF loses thermal energy to PCM. HTF drops temperature as it loses thermal energy. Thus, the melting rate in central zone and outlet zone (right side of Fig. 8) is comparatively lower due to smaller temperature difference.

Similarly, due to rise in inlet temperature, the temperature difference improves throughout the LHS tank, as depicted in Fig. 8. It can be noticed that in case of 335.15 K, almost entire mass of PCM is either in mushy zone or liquid form. After 3 hours of charging at constant inlet temperatures, it is observed that liquid fractions for 325.15 K, 330.15 K and 335.15 K are 86.71%, 97.84% and 99.9%, respectively. It indicates that with an increase in inlet temperature, the overall charging time of LHS system can be reduced. Moreover, with an increased inlet temperature, the sensible energy of system is boosted. Therefore, a higher overall thermal storage capacity is achieved. Overall system enthalpy can be increased from 317kJ/kg to 345kJ/kg by rising inlet temperature of HTF from 325.15 K to 335.15K.

During solidification process, the thermal energy is transferred from PCM to HTF. In this numerical investigation, three inlet temperatures of HTF are tested which are 285.15 K, 288.15 K and 293.15 K. These values are selected as the temperature of municipal water is in the range of 285.15 K to 293.15 K. The solidification times for entire LHS tank at all three inlet temperatures are 2.05, 2.32 and 2.78 hours, respectively. Due to higher temperature difference of PCM with HTF at 285.15 K, the solidification rate is higher.

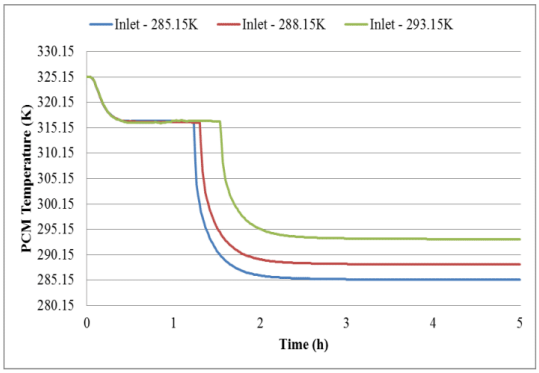

(A)

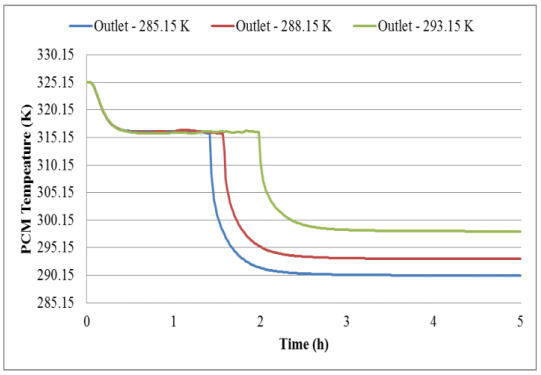

(B)

Fig. 9 Numerical examination of temperature response to PCM at inlet (A) and outlet (B) zones upon three different inlet temperatures

As shown in Fig. 9, thermal energy is promptly extracted from inlet zone with inlet temperature of 285.15 K as compared to inlet temperature of 293.15 K. Similarly in outlet zone, the solidification of entire PCM requires 1.4 hours and 1.98 hours for inlet temperature of 285.15 K and 293.15 K, respectively.

EXPERIMENTAL RESULTS

The experimental setup includes serpentine type flat-plate solar collector, LHS tank, water circulating pump, connections to mains water supply and K-type thermocouples with data acquisition unit. The serpentine type flat-plate solar collector is previously designed and commissioned by Helvaci and Khan [4, 5]. Based on numerical simulation results, the LHS tank is designed and manufactured as per specifications shown in Fig. 2. Prior to connecting LHS tank to flat-plate solar collector, leak tests are performed to ensure safety and system efficiency as otherwise water seepage will disturb thermo-physical properties of PCM. The joints and elbows are given special attention for any leakage. Initially, high pressure air equals to 4 bar is inserted to LHS tank by connecting it to a compressor. Foamy liquid leak detector is applied to all joints and elbows. After air leak test, the pressurised air is released. Similarly, water leak test is performed to cross check any seepage. In water leak test, the outlet valve is closed and water is pumped through inlet valve to generate pressure within tube loop of LHS tank. The inlet valve is also closed once sufficient pressure is developed. The pressurised water is left within tubes for 48 hours to identify any leakage. No seepage is detected in both air and water leak tests.

In order to conduct experimental investigations, the connections between flat-plate solar collector and LHS tank is made by following the schematic shown in Fig. 1. In data recording system, K type thermocouples are employed at inlet and outlet zone at various depths in LHS tank to investigate the

temperature response of PCM during melting and solidification process. Titan FT2 Hall Effect flow meter is utilised to measure and control the flow rate of water. Thermocouples and flow meter are connected to Agilent 34970A data acquisition unit to record data in computer interface. The time step for data recording is set to 10 s.

During melting/charging process, water is initially run from mains to confirm that the system is completely filled with water. Also, it helps in bringing down the temperature of PCM in LHS tank to approximately 291.15 K, which provides a better reference point for comparison. The water supply from mains is then turned off to make a close loop. Water circulating pump is operated to circulate water at various flow rates through flat-plate solar collector, where water absorbs thermal energy from collector and rises its temperature. Water at high temperature is directed through LHS tank, where it releases thermal energy to PCM. Three inlet temperatures of water are tested: 325.15 K, 330.15 K and 335.15 K. Likewise, the various volume flow rate of water range from 1.5 lpm to 3 lpm. The range of volume flow rate is selected in accordance to thermal performance of flat-plate solar collector.

In order to examine thermal behavior of PCM against various flow rates of water, the inlet temperature of water to LHS tank is kept constant at 335.15 K and three volume flow rates are experimented, as shown in Fig. 10. The selected volume flow rates are 2 lpm, 2.5 lpm and 3 lpm. The temperature data in Fig. 10 are collected from thermocouple installed at inlet zone with probe depth of 160 mm (central depth of LHS tank). It can be noticed from Fig. 10 that with an increase in volume flow rate of water, the melting time of PCM reduces and consequently, the charging time of LHS tank can be decreased. As depicted, the melting time for PCM at inlet zone is reduced by 9.65% and 22.81% as the volume flow rate is increased from 2 lpm to 2.5 lpm and 3 lpm, respectively. The sensible portion of heat storage, before and after phase transition, almost behaved in a similar manner for all flow rates. However, the latent portion of heat storage is considerably influenced by varying flow rates.

After charging the LHS tank, the entire mass of PCM is in liquid state. In order to conduct solidification/discharging test, the hot water connection between solar collector and LHS tank is turned off and cold water from mains supply is directed through LHS tank. Water extracts thermal energy from PCM as it runs through pipes of LHS tank. Solidification of PCM begins as it starts losing the latent portion of thermal energy to water. Experimental examinations are conducted to identify the impact of varying flow rates of cold water on thermal performance of PCM in LHS tank. Three volume flow rates of water are experimentally examined: 1.5, 2 and 2.5 lpm. Inlet temperature of cold water for all cases is constant at 285.15 K. As depicted in Fig. 11, the varying flow rate of water has a minimal impact on thermal performance of LHS system in solidification process. The temperature profiles for all three flow rates are almost identical. Due to higher temperature difference between inlet water temperature and liquid PCM, the extraction of thermal energy from PCM is rapid. Therefore, the phase transition of PCM from liquid to solid at inlet zone is faster than other zones within LHS tank.

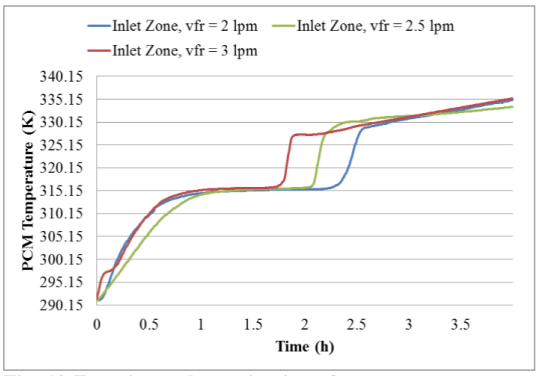

Fig. 10 Experimental examination of temperature response of PCM during melting process at various time intervals for various flow rates. The inlet temperature of HTF is kept constant at 335.15 K.

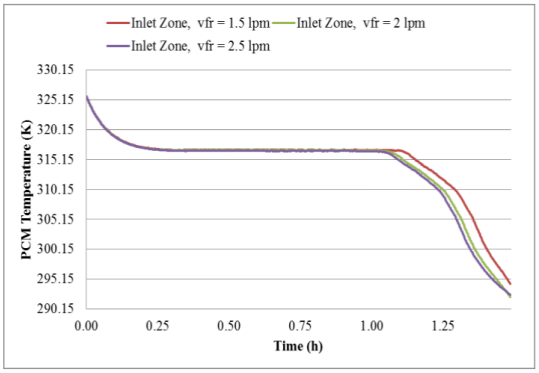

Fig. 11 Experimental investigation of temperature response of PCM during solidification process at various time intervals for various flow rates. The inlet temperature of water is kept constant at 285.15 K.

For validation purpose, experimental results at inlet zone for charging process is compared with numerical model simulation results, as shown in Fig. 12. The experimental data is collected from thermocouple at inlet zone with probe at central depth of LHS tank. It can be seen that both results are in good agreement, however the slight variation in experimental results is caused due to buoyancy driven natural convection. Liquid PCM molecules at higher temperature rise above the surface and subsequently, the rise in temperature in bottom and central surfaces are slower than the top.

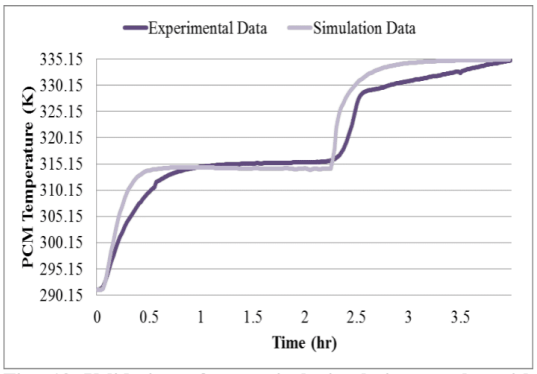

Fig. 12 Validation of numerical simulation results with experimental results. Inlet temperature and mass flow rate in both cases are set to 335.15 K and 2 lpm.

CONCLUSION

This paper is focused on identifying viable design solutions that would assure rapid charging and discharging rate of solar based LHS system. Numerical analyses are conducted on two dimensional transient computational models of longitudinal fins based LHS system. Parametric investigations have indicated that longitudinal fins length is an effective parameter as compared to fins thickness. Moreover, inlet temperature of HTF has shown significant influence on thermal performance as compared to volume flow rate. Numerical results are validated by experimental examination of LHS system. Both results have shown a good agreement. Shell and tube with longitudinal fins has exhibited an excellent thermal performance by quick charging and discharging rate of LHS system. Due to rapid charging rate, higher thermal storage capacity of LHS system can be achieved in shorter period of time. Similarly, prompt availability of required thermal energy can be guaranteed by adapting to the unique design of LHS system. Also, the LHS unit is flexible to scale-up or to operate in series in order to meet required energy demands. The improved thermal performance can yield good spatial, time and economic advantages in number of domestic and industrial applications.

ACKNOWLEDGMENTS

This research is joint funded by Bournemouth University, UK and National University of Sciences and Technology (NUST), Pakistan within their international collaboration initiative. The authors would also like to acknowledge Future Energy Source (FES) Ltd, UK for providing in-kind support and experimental resources during this research.

NOMENCLATURE

C_p	Specific heat (kJ/kg. K)
$\mathbf{F}$	Buoyant force (Pa/m)
f	Fraction of PCM in solid and liquid phase
$\mathbf{g}$	Gravitational acceleration (m/s^2)
H	Specific enthalpy (MJ)
k	Thermal conductivity (W/m. K)
L	Latent heat (kJ/kg)
T	Temperature (K)
T_{pc}	Phase transition temperature (K)
p	Pressure (Pa)
q	Heat source term (W/m^3)
$\mathbf{Su}$	Momentum source term
$\mathbf{u}$	Velocity vector (m/s)

Greek symbols

α	Small constant value
β	Coefficient of thermal expansion (1/K)
κ	Morphology constant of mushy zone
ρ	Density (kg/m^3)
μ	Dynamic viscosity (kg/m. s)

Subscripts

s	Solid phase of PCM
l	Liquid phase of PCM

Abbreviations

HTF	Heat transfer fluid
LHS	Latent heat storage
PCM	Phase change material
vfr	Volume flow rate
lpm	Liter per minute

REFERENCES

[1] International Energy Agency (IEA), 2015, "Energy and Climate Change " Proc. 21st UN Conference of the Parties (COP21).

[2] Suranovic, S., 2013, "Fossil fuel addiction and the implications for climate change policy," Global Environmental Change, 23(3), pp. 598-608.

[3] Modi, A., Bühler, F., Andreasen, J. G., and Haglind, F., 2017, "A review of solar energy based heat and power generation systems," Renewable and Sustainable Energy Reviews, 67, pp. 1047-1064.

[4] Helvaci, H., and Khan, Z. A., 2015, "Mathematical modelling and simulation of multiphase flow in a flat plate solar energy collector," Energy Conversion and Management, 106, pp. 139-150.

[5] Helvaci, H., and Khan, Z. A., 2016, "Experimental study of thermodynamic assessment of a small scale solar thermal system," Energy Conversion and Management, 117, pp. 567-576.

[6] Khan, Z., Khan, Z., and Tabeshf, K., 2016, "Parametric investigations to enhance thermal performance of paraffin through a novel geometrical configuration of shell and tube latent thermal storage system," Energy Conversion and Management, 127, pp. 355-365.
[7] Morrison, D., and Abdel-Khalik, S., 1978, "Effects of phase-change energy storage on the performance of air-based and liquid-based solar heating systems," Solar Energy, 20(1), pp. 57-67.
[8] Ghoneim, A., 1989, "Comparison of theoretical models of phase-change and sensible heat storage for air and water-based solar heating systems," Solar Energy, 42(3), pp. 209-220.
[9] Sharma, A., Tyagi, V., Chen, C., and Buddhi, D., 2009, "Review on thermal energy storage with phase change materials and applications," Renewable and Sustainable energy reviews, 13(2), pp. 318-345.
[10] da Cunha, J. P., and Eames, P., 2016, "Thermal energy storage for low and medium temperature applications using phase change materials–A review," Applied Energy, 177, pp. 227-238.
[11] Dhaidan, N. S., and Khodadadi, J., 2015, "Melting and convection of phase change materials in different shape containers: A review," Renewable and Sustainable Energy Reviews, 43, pp. 449-477.
[12] Khan, Z., Khan, Z., and Ghafoor, A., 2016, "A review of performance enhancement of PCM based latent heat storage system within the context of materials, thermal stability and compatibility," Energy Conversion and Management, 115, pp. 132-158.
[13] Khodadadi, J., Fan, L., and Babaei, H., 2013, "Thermal conductivity enhancement of nanostructure-based colloidal suspensions utilized as phase change materials for thermal energy storage: a review," Renewable and Sustainable Energy Reviews, 24, pp. 418-444.
[14] Fan, L., and Khodadadi, J., 2011, "Thermal conductivity enhancement of phase change materials for thermal energy storage: a review," Renewable and Sustainable Energy Reviews, 15(1), pp. 24-46.
[15] Salunkhe, P. B., and Shembekar, P. S., 2012, "A review on effect of phase change material encapsulation on the thermal performance of a system," Renewable and Sustainable Energy Reviews, 16(8), pp. 5603-5616.
[16] Giro-Paloma, J., Martínez, M., Cabeza, L. F., and Fernández, A. I., 2016, "Types, methods, techniques, and applications for Microencapsulated Phase Change Materials (MPCM): A review," Renewable and Sustainable Energy Reviews, 53, pp. 1059-1075.
[17] 2016, "Rubitherm® Technologies GmbH, http://www.rubitherm.eu/en/."
[18] Gray, D. D., and Giorgini, A., 1976, "The validity of the Boussinesq approximation for liquids and gases," International Journal of Heat and Mass Transfer, 19(5), pp. 545-551.
[19] Nield, D. A., and Bejan, A., 2006, Convection in porous media, Springer Science & Business Media.

Paper IV

Experimental investigations of charging/melting cycles of paraffin in a novel shell and tube with longitudinal fins based heat storage design solution for domestic and industrial applications

Zakir Khan [a]*, Zulfiqar Ahmad Khan [a]

[a] Bournemouth University, Faculty of Science and Technology, NanoCorr, Energy and Modelling (NCEM), Fern Barrow, Talbot Campus, Poole, Dorset BH12 5BB, UK.

E-mail: zkhan@bournemouth.ac.uk

Corresponding Author:

[a]* Bournemouth University, Faculty of Science and Technology, NanoCorr, Energy and Modelling (NCEM), Fern Barrow, Talbot Campus, Poole, Dorset BH12 5BB, UK.

E-mail: zkhan2@bournemouth.ac.uk

Tel.: +44 7459249069

Abstract

Due to vulnerability of solar energy based technologies to weather fluctuations and variations in solar thermal irradiance, thermal energy storage (TES) systems with their high thermal storage capacity offer a sustainable solution. In this article, experimental investigations are conducted to identify thermal performance of latent heat storage (LHS) unit in connection with flat plate solar collector during charging cycles. LHS unit is comprised of novel geometrical configuration based shell-and-tube heat exchanger with longitudinal fins, paraffin as thermal storage material and water as heat transfer fluid (HTF). In order to overcome the effect of low thermal conductivity of paraffin, the effective surface area and overall thermal conductivity for heat transfer is significantly improved by employing longitudinal fins. Moreover, the vertical orientation of longitudinal fins supports natural convection, which can assure rapid charging of paraffin in LHS unit. In experimental tests, the focus is on probing the heat transfer mechanism and temperature distribution in entire novel LHS unit, the influence of inlet temperature and volume flow rate of HTF on phase transition rate and mean power. Experimental results revealed that natural convection significantly influences the phase transition rate. Therefore, enthalpy gradient is noticed between paraffin at top, central and bottom positions in LHS unit. Likewise, the phase transition rate and mean power of LHS unit is significantly increased by a fraction of 50.08% and 69.71% as the inlet temperature of HTF is increased from 52 ^{o}C to 67 ^{o}C, respectively. Similarly, it is concluded that volume flow rate of HTF has a relatively moderate influence on thermal performance; however the influence declines with an increase in inlet temperature of HTF. Due to significant enhancement in thermal performance, the novel geometrically configured LHS unit can accumulate about 14.36 MJ of thermal energy in as less as 3 hours. Furthermore, a broad range of domestic and commercial energy demands can be fulfilled by simply assembling several LHS units in parallel sequence.

Keywords

Thermal energy storage, Latent heat storage, Phase change material, Shell-and-tube heat exchanger, Heat transfer, Natural convection.

1. Introduction

Energy is the backbone of a country economic development. Due to rapid increase in industrial and domestic energy demands, the dependency on fossil fuels to meet required energy demands have further increased. However, the excessive usage of fossil fuels have provoked global warming and climate change [1, 2]. Therefore, in order to limit environmental pollutions and to meet energy demands, developments in technologies are essential to utilise renewable energy sources. Solar energy is considered as a crucial renewable energy source due to its clean, free of cost and worldwide distribution of incident solar radiations [3, 4]. However, the fragmentary and inconsistent nature of solar radiations has affected the widespread applications of solar energy. To overcome the inconsistent and unpredictable nature of solar energy, TES system can provide a feasible solution. TES system can be utilised to capture thermal energy at solar peak hours and release it at solar off peak hours or night times. To shorten the energy supply and demand gap, LHS systems can be employed due to their higher thermal storage density, phase change materials (PCM) availability at wide range of temperatures, higher latent heat capacity at almost isothermal condition and lower vapour pressure [5, 6].

LHS systems are employed in number of applications including solar thermal systems, energy management and peak-shaving, waste heat recovery, building heating and air conditioning, agricultural drying units and automobile [7-13]. However, the widespread practical utilisation of LHS system is still under the influence of low thermal conductivity (≈ 0.2 – 0.4 W/m.K) of PCM, which handicaps the rapid charging and discharging of thermal energy [14]. Therefore, to improve thermal performance of LHS system, efficient and responsive heat exchanging techniques are essential to be adopted. A substantial number of research articles have been published that concern developments in thermal performance of LHS system including geometrical configuration [15], using extended surfaces [16], addition of thermal conductive additives [17], form stable and encapsulation of PCM [18, 19].

Thermal performance of LHS system is highly influenced by geometrical configuration of heat exchanger. Therefore, this article is focused on shell-and-tube heat exchanger based LHS systems due to the fact that it presents relatively better heat transferring performance and possesses excellent integration to number of engineering applications [20]. Wang et al. [21] conducted numerical investigations to examine thermal performance of n-octadecane in horizontal shell-and-tube heat exchanger. It was observed that with an increase in inlet temperature of HTF, the phase transition time was significantly reduced and the amount of thermal energy stored was non-linearly increased. However, with an increase in mass flow rate, the melting time was reduced whereas the amount of thermal storage was not significantly affected. Similarly, Tay et al. [22] performed experimental investigations on thermal performance of water as PCM in vertical tubes-in-tank heat exchanger. It was observed that an increase in mass flow rate from 0.01 kg/s to 0.07 kg/s reduced the phase transition duration from 215 min to 88 min. Hosseini et al. [23] conducted an experimental and numerical study to identify the influence of natural convection and inlet temperature of HTF on phase transition rate of paraffin in horizontal shell-and-tube heat exchanger. It was reported that natural convection highly influenced melting rate of paraffin in upper portion of shell. Likewise, it was noticed that the melting time was reduced by a fraction of 37% with an increase in inlet temperature from 70 ^{o}C to 80 ^{o}C. Likewise, Meng and Zhang [24] conducted an experimental and numerical investigation of melting behaviour of paraffin composite with copper form in vertical shell-and-tube heat exchanger. It was noticed that due to natural convection the temperature at top portion was higher as compared to other portions. Likewise, with an increase in inlet temperature of HTF from 75 ^{o}C to 85 ^{o}C, the melting time was reduced by a fraction of 41.67%. Moreover, an increase in flow velocities

of HTF from 0.1 m/s to 0.2 m/s had only reduced the melting time by 15.1%. Furthermore, Esapour et al. [25] numerically investigated the melting behaviour of paraffin in horizontal shell-and-tube heat exchanger. It was noticed that with an increase in number of HTF tubes from 1 to 4, the melting time was reduced by 29%. Likewise, Luo et al. [26] numerically examined the effect of HTF tubes number and their orientations in horizontal shell-and-tube heat exchanger on thermal performance. It was noticed that melting time for single HTF tube was 5 times as compared to nine HTF tubes case. Likewise, centrosymmetric configuration showed better thermal performance than staggered and inline configurations.

It can be construed from previous literature that shell-and-tube heat exchanger configurations have significant influence on thermal performance of LHS system. However, the optimal advantages are still hindered by low thermal conductivity of PCM. Therefore, the most appropriate and cost effective technique to enhance thermal performance is to incorporate extended surfaces. Rathod and Banerjee [27] conducted an experimental examination of melting behaviour of stearic acid in vertical shell-and-tube heat exchanger with three longitudinal fins configuration. It was observed that with longitudinal fins, the melting time was reduced by 24.52% as compare to no fins orientation. Yuan et al. [28] examined the impact of longitudinal fins on melting rate of lauric acid in horizontal shell-and-tube heat exchanger. It was noticed that complete melting time was reduced from 328 min for no fins orientation to 180 min for two fins orientation. Likewise, the peak melting enhancement ratio for inlet temperatures of 60 ^{o}C, 70 ^{o}C and 80 ^{o}C were 1.403 to 1.362, and 1.328, respectively. Li and Wu [29] conducted numerical investigations on thermal performance of $NaNO_3$ in horizontal shell-and-tube heat exchanger with and without longitudinal fins. It was noticed that average total heat flux of heat exchanger was increased by inclusion of six longitudinal fins and consequently, the melting time was reduced by 20%. Rabienataj Darzi et al. [30] numerically examined the influence of number of fins on melting time of n-eicosane in horizontal shell-and-tube heat exchanger. It was reported that as compared to no fins orientation, the melting time was reduced by 39%, 73%, 78% and 82% by incorporating 4, 10, 15 and 20 fins, respectively. However, with an increase in number of fins, the influence of natural convection on melting rate was affected. Likewise, Tao and He [31] recommended that non-uniform melting front and temperature distribution caused by natural convection could be improved by inclusion of longitudinal fins. However, the uniformity could be distorted again if excessively large fins number, height and thickness are employed. Wang et al. [32] conducted numerical analyses to identify the impact of various angles between three longitudinal fins on thermal performance of PCM in horizontal shell-and-tube heat exchanger. The selected angles between adjacent fins were 30^{o}, 60^{o}, 90^{o} and 120^{o}. It was reported that fins angle 60^{o} and 90^{o} displayed better heat transfer enhancement. Moreover, Liu and Groulx [33] experimentally investigated the thermal behaviour of dodecanoic acid in horizontal shell-and-tube heat exchanger with four longitudinal fins configuration. Longitudinal fins were installed in two orientations such as straight and angled. It was reported that natural convection was a dominant mode of heat transfer. Likewise, it was observed that inlet temperature of HTF has more prominent impact on thermal behaviour as compared to flow rate of HTF. Also, it was reported that angled fins showed a slightly lower melting time as compared to straight fins. However, the impact of angled fins declined with an increase in inlet temperature.

Beside longitudinal fins, the other proposed design solutions for thermal performance enhancement with extended surfaces are radial, helical, pinned and triplex fins. Tay et al. [34] conducted numerical investigations on three models of tubes-in-tank heat exchanger configurations without fins, with pins and with radial fins. It was concluded that radial fins based heat exchanger had better phase transition rate and average effectiveness as compared to without fins and with pins orientations. However, a

comparative study illustrated that longitudinal fins possess better thermal storage performance. Caron-Soupart et al. [35] experimentally studied the melting behaviour, heat exchanger power and thermal storage density of three vertical shell-and-tube heat exchanger configurations. The three selected orientations were tube without fins, with longitudinal fins and with radial fins. It was observed that heat exchanger orientations with longitudinal fins and circular fins showed significantly higher melting rate as compared to no fins orientation. Likewise, heat exchanger power was augmented by a factor of 10 as compared to no fins orientation. However, thermal storage density was noticeably reduced by radial fins orientation as compared to no fins orientation. Similarly, Agyenim et al. [36] experimentally examined the thermal performance of erythritol in horizontal shell-and-tube heat exchanger with three varied orientations of no fins, circular fins and longitudinal fins. It was reported that longitudinal fins orientation showed comparatively better thermal performance. Hence, it can be deduced from literature that longitudinal fins in vertical orientation of shell-and-tube heat exchanger has better thermal performance in terms of phase transition rate, thermal storage density and assisting natural convection. Moreover, it is noticed that major part of literature is based on numerical investigation of shell-and-tube heat exchanger with extended surfaces, lacking the experimental investigations of proposed shell-and-tube heat exchangers. Likewise, the literature also lacks the experimental investigation of multiple passes of tube with extended surfaces in shell-and-tube heat exchanger.

This article is focused on experimental investigation of a novel shell-and-tube heat exchanger with longitudinal fins based LHS unit, which is coupled with flat plate solar collector. The computational model of novel geometrical configuration of LHS unit is previously designed and simulated by authors in [37]. The optimum design of shell-and-tube heat exchanger configuration was developed by conducting numerical analysis to examine the impact of number of tube passes, their placement in the shell, geometry of longitudinal fins and construction material on phase transition rate and thermal storage capacity of LHS unit. In this paper, the unique geometrical configuration based LHS unit is connected to flat plate solar collector with solar simulators to perform charging cycles at various operating conditions. Moreover, this paper is focused on discussing the influence of natural convection, inlet temperature and volume flow rate of HTF on temperature distribution, phase transition rate and mean power. Furthermore, this article will give an understanding into how to utilise this novel LHS unit in wide ranging domestic and commercial applications to meet large scale thermal energy demands.

2. Experimental setup and procedure

2.1 Description of experimental setup

For present study, an experimental setup is designed as illustrated in **Fig. 1**. The system is comprised of flat plate solar collector with solar simulator, latent heat storage tank, circulation centrifugal pump, a flow meter, connection to building water tank and data acquisition unit with computer.

Flat plate solar collector consists of glazing cover, stainless steel absorber, serpentine copper tubing circulation system and insulations. Transparent glass sheet with 2 mm thickness is utilised as glazing cover to dampen convection and radiation losses from solar collector. The emissivity and transmittance of glazing cover are 0.92 and 0.9, respectively. Likewise, absorber is composed of 1mm thick stainless steel S280 sheet. In order to attain high absorptivity, the absorber is coated to dark black surface. The absorptivity, emissivity and thermal conductivity of absorber are 0.9, 0.9 and 50 W/m.K, respectively. Similarly, circulation system is comprised of serpentine copper tubing, where HTF gains thermal energy from absorber. The total length, outer diameter and thickness of copper tubing are 57.5 m, 10 mm and 1 mm, respectively. Moreover, Celotex is used as an insulating material

to reduce thermal losses from sides and rear of solar collector. The thickness and thermal conductivity of insulating material are 100 mm and 0.022 W/m K, respectively.

Solar simulator is utilised to provide steady thermal energy through radiations to collector. It consists of two lightening machines with twelve quartz-halogen lamps. Each lamp can emit 1 kW radiant heat output. Kipp & Zonen CMP3 pyranometer is operated to measure average irradiance and to identify optimum distance of solar simulator from collector. Consequently, solar simulator at a distance of 2 m from collector has shown almost constant radiations at each point on collector. Further details about selection of measured points and measuring average irradiance on collector surface can be found in [38, 39]. Solar simulator has inbuilt control system to adjust radiant heat output and operation time. During experiments, solar simulator is manually operated to generate required radiant heat output in order to sustain constant outlet temperature of HTF from collector.

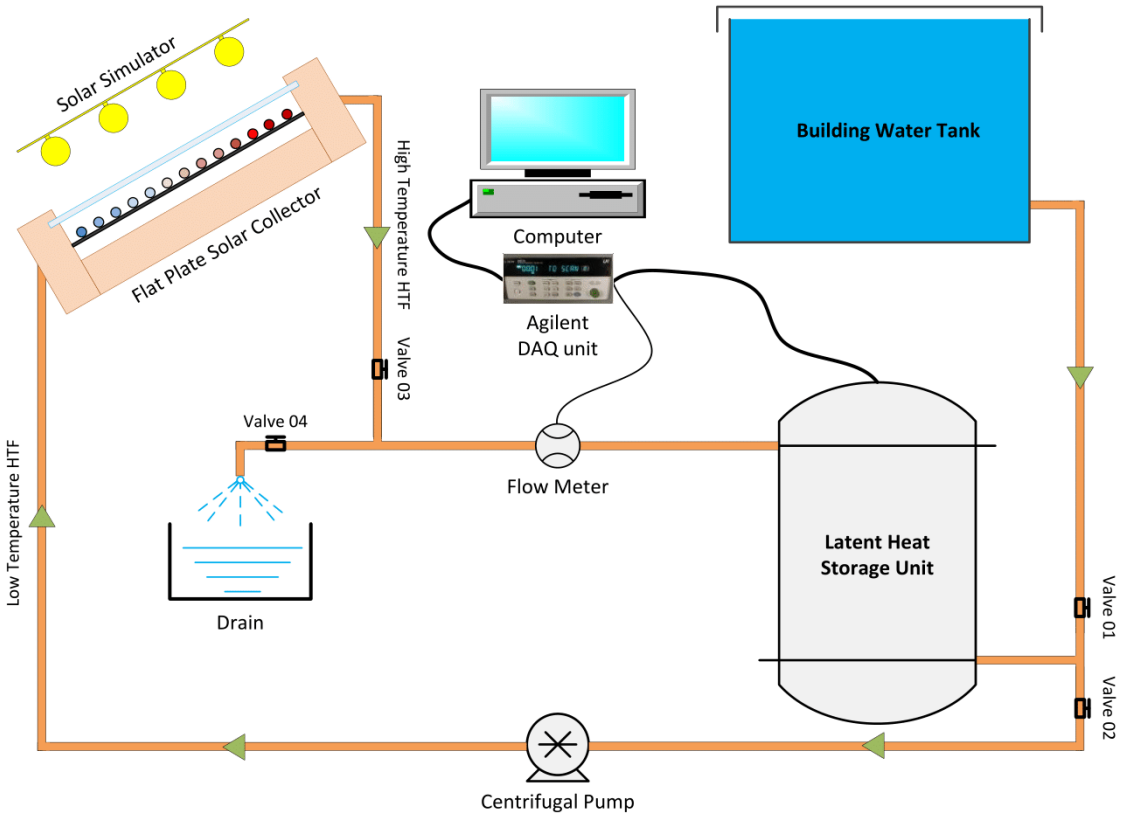

Fig. 1 Schematic representation of experimental setup

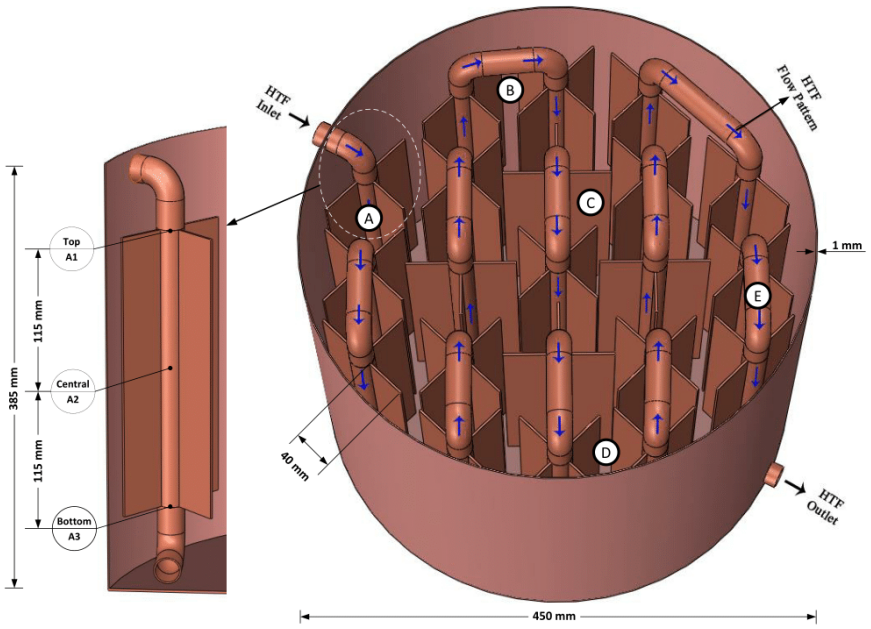

Fig. 2 Physical model of LHS unit and illustration of the vertical positioning of thermocouples at different zones A, B, C, D and E.

High temperature HTF from solar collector is directed to pass through LHS unit, where it transfers thermal energy to PCM. LHS unit consists of shell-and-tube heat exchanger with longitudinal fins and PCM, as illustrated in **Fig. 2**. Shell is made of copper and the outer diameter, height and thickness of shell are 450 mm, 385 mm and 1 mm, respectively. The exterior surface of shell is properly insulated with 50 mm thick chlorofluorocarbon-free envirofoam to reduce thermal losses to atmosphere. The tubes are made of copper and the outer diameter and thickness are 22 mm and 1 mm, respectively. The tubes have 21 passes in the shell and are connected to copper longitudinal fins of height, length and thickness as 230 mm, 40 mm and 1.5 mm, respectively. Further details about design specifications of LHS unit are provided in **Table 1**. Moreover, the detail description about geometrical orientation of tubes with longitudinal fins in shell can be found in [37]. Commercial grade paraffin (RT44HC) is filled in shell and water is employed as heat transfer fluid that is directed to run through tubes. Paraffin (RT44HC) is selected due to its high thermal storage capacity, good compatibility with copper and excellent thermo-physical stability [16, 40]. Thermo-physical properties of paraffin (RT44HC) are presented in **Table 2**.

Table 1
Specifications of shell-and-tube heat exchanger based LHS unit

Total volume of shell	V_S	60.7E+06	mm^3
Running length of tube		8.2	m
Volume occupied by tube	V_T	3.12E+06	mm^3
Surface area of longitudinal fins		1.43E+06	mm^2
Volume occupied by fins	V_F	1.05E+06	mm^3
Volume of LHS unit	$V_{LHS} = V_S - V_T - V_F$	56.5E+06	mm^3
Mass of paraffin		40	kg
Packing factor of PCM	$\frac{V_{PCM}}{V_S}$	0.824	solid
		0.942	liquid

Table 2
Thermo-physical characteristics of paraffin (RT44HC) [16, 40]

Phase change temperature	41-44	°C
Latent heat	255	(kJ/kg)
Specific heat capacity	2.0	(kJ/kg. K)
Thermal conductivity	0.2	(W/m. K) solid
	0.2	(W/m. K) liquid
Density	800	(kg/m^3) solid
	700	(kg/m^3) liquid
Coefficient of thermal expansion	0.00259	(1/K)

During charging cycle, high temperature water from solar collector is directed through tubes and heat is transferred to PCM in shell. The temperature distribution within PCM in shell is recorded by using fifteen K-type thermocouples. Five zones are selected within shell to investigate the temperature response of PCM, which are A, B, C, D and E, as shown in **Fig. 2**. The selected zones are regions closer to inlet (zone A), outlet (zone E), centre (zone C) and shell boundary (zone B and D) within LHS unit. Three thermocouples are installed at top, central and bottom position at each of five zones. The vertical distance between each thermocouple at each location is 115 mm, as shown in **Fig. 2**. Likewise, two thermocouples are mounted on copper tube at inlet and outlet of LHS unit to record the temperature response of HTF. Moreover, a turbine flow meter (Titan FT2 Hall Effect) is employed to record the volume flow rate of HTF. The accuracy of thermocouples and flow meter are ±0.18% and 1.5%, respectively. Also, a centrifugal pump (Grundfos type UPS 15-60) is utilised to circulate HTF between solar collector and LHS unit. Four flow control valves are installed before and after solar collector and LHS unit to control flow rate and direction of HTF. In order to record temperature and volume flow rate reading, a data acquisition unit (Agilent 34972A) is used to transfer data into computer. Agilent software is used to record data and display results on computer after each time step of 10 s.

2.2 Experimental procedure

During charging cycle, flow control valve 1 is switched on to direct water from mains to fill up the entire loop. The circulation of low temperature water from mains reduces the initial temperature of LHS unit to about 10 °C and therefore, a baseline for all experimental tests is established. Likewise, air release valve (not shown in **Fig. 1**) is switched on to ensure the release of trapped air in the loop. Flow control valve 4 is turned off and subsequently valve 1 is turned off to make a close loop for charging cycle. Likewise, flow control valve 2 and 3 are adjusted to operate charging cycle at specific volume flow rate. In this experimental study, four different volume flow rates of HTF are tested, which are 1.5, 2, 2.5 and 3.0 l/min. The range of volume flow rate of HTF is selected with accordance to thermal efficiency of flat plate solar collector. Further increase to volume flow rates would not generate the desired constant inlet temperature of HTF to LHS unit. Moreover, the thermal behaviour of LHS unit at various constant inlet temperature of HTF is experimentally investigated. The selected inlet temperatures values are 52, 57, 62 and 67 °C. This range is selected by considering temperature gradient of 10, 15, 20 and 25 °C between inlet temperature of HTF and melting point of PCM. The series of experimental tests conducted in this article is summarised in **Table 3**.

Solar simulator is operated to produce radiant heat output to increase thermal energy of HTF in collector. The high temperature HTF is guided to pass through the tubes in LHS unit, where heat transfer occurs between HTF and PCM. Due to release of thermal energy to PCM, the temperature of

HTF drops. Therefore, the low temperature HTF is pumped back from the outlet of LHS unit to collector to repeat the cycle. The charging cycle is completed when all thermocouples record temperature reading higher than phase change temperature.

However, it is observed that due to slow heating up process of solar collector, the temperature of HTF is gradually increased from ambient to selected range of temperature. Therefore at the start of charging cycle, entire set of 12 lamps of solar simulator are switched on to target more radiant heat at solar collector, in order to rapidly increase the temperature of HTF to selected range. Once the selected range of temperature of HTF is achieved, the solar simulator is manually operated to ensure constant inlet temperature of HTF to LHS unit.

Table 3
Range of experimental tests conducted

Set of experiments	Inlet temperature of HTF	Flow rate of HTF	Reynolds number
1-4	52, 57, 62, 67 °C	1.5 l/min	2950, 3200, 3450, 3700
5-8	52, 57, 62, 67 °C	2.0 l/min	4000, 4300, 4600, 4900
9-12	52, 57, 62, 67 °C	2.5 l/min	4950, 5350, 5750, 6150
13-16	52, 57, 62, 67 °C	3.0 l/min	5900, 6400, 6900, 7400

3. Results and discussion

3.1 Reliability and repeatability

Repeatability study is required to examine the consistency of experimental results. Therefore, a series of three charging cycle experiments are performed at constant inlet temperature of 62 °C and volume flow rate of 1.5 l/min. Transient temperature profiles are plotted for thermocouples installed at top, central and bottom positions at zone C, as shown in **Fig. 3**. It can be observed that phase transition time at all three positions for all experiments are clearly identical. Thus, it assures the reliability and repeatability of experimental results showing thermal performance. Moreover, statistical standard deviations for phase transition time at all three positions are calculated. The values of standard deviations for phase transition time at top, central and bottom positions are computed to be 0.008, 0.029 and 0.033, respectively. However, due to an expected slight variation in inlet temperature of HTF received from solar collector, the sensible heating of PCM at liquid phase shows a small variation in temperature.

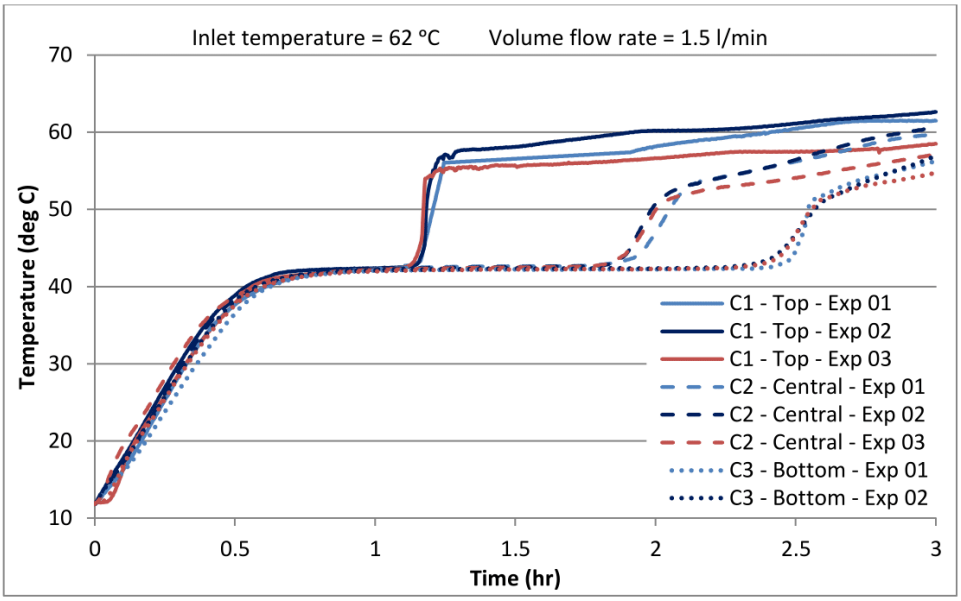

Fig. 3 Illustration of repeatability of transient temperature profiles at all three positions at zone C while charging system at constant inlet temperature of 62 °C and volume flow rate of 1.5 l/min.

3.2 Zonal temperature distribution

In order to examine the transient temperature distribution of PCM in LHS unit, temperature readings are recorded from all fifteen k-type thermocouples that are installed within LHS unit at three vertical positions at each of five zones (see **Fig. 2**). The transient temperature distribution can help in understanding the heat transfer rate and phase transition rate at different zones and positions within LHS unit. To conduct charging cycle, the high temperature HTF at 62 °C with volume flow rate of 1.5 l/min is directed from solar collector to pass through tubes in LHS unit. The initial temperature of PCM in LHS unit is nearly 10 °C.

Fig. 4 shows the pictorial depiction of phase transition performance of PCM in LHS unit. It can be noticed that due to higher temperature difference between inlet temperature of HTF and PCM, the phase transition rate at zone A is significantly higher as compared to other zones. After 0.5 hr of heat transfer, it can be noticed that top position of zone A is already either in mushy phase or liquid phase, whereas the rest of the zones are still in solid phase. Likewise, it can be observed that after 1 hr of charging cycle, the top positon of zone A is in complete liquid phase, zone B and C are in mushy phase and zone D and E are still in solid phase. Also, it can be noticed that at zone A, the PCM adjacent to tubes and longitudinal fins melts quickly and due to buoyant effect and volumetric expansion, the melted PCM rises upward to the top. Thus, it leads to rapid melting at top position whereas, central and bottom positions are still in mushy zone. After 1.5 hr, it can be seen that the top position of all zones are in liquid phase besides zone E, which is still in mushy phase. This is due to the fact that thermal energy is extracted from HTF at earlier zones and by the time HTF reaches zone E; the available thermal energy is lesser to generate higher temperature gradient. The effect of natural convection is evident in all zones. Liquid PCM at central and bottom positions rise above to top position due to density gradient and temperature difference. Thus it is expected that PCM temperature at top position will always be higher as compared to central and bottom positions. After 2.5 hr, it can be seen that the top and central positions of all zones are in liquid phase. Similarly, the bottom position at zone C is evidently showing liquid phase, however the PCM alongside shell boundary is

still in either mushy or solid phase. This is due to buoyant effect and weaker heat transfer at bottom position of LHS unit. Likewise, even after 3 hrs of charging cycle, there are still some portions of PCM in mushy phase alongside shell boundary, whereas the rest of the PCM is completely melted.

Transient temperature distribution at various positions and zones in LHS unit is represented in **Fig. 5**. It is evident from temperature profiles that due to small specific heat capacity of PCM in solid phase, the linear rise in temperature from initial value to about 40 ^{o}C is influenced by conduction heat transfer. This sensible portion of thermal energy storage is rapidly achieved. Subsequently, due to higher latent heat capacity, a comparatively slow and gradual rise in PCM temperature from 41 ^{o}C to 44 ^{o}C is observed. During this stage, as temperature increases, the phase transition of PCM from solid to mushy to liquid phase takes place. As latent portion of thermal energy is stored, an instant rise in PCM temperature is noticed, which indicates the sensible portion of thermal energy storage in liquid PCM.

It is evident from **Fig. 5** that in all zones, the increase in temperature at top position is faster as compared to central and bottom position. This is due to the fact that conduction is the dominant mode of heat transfer at earlier stages of charging cycle and consequently, phase transition from solid to liquid begins. However, with an increase in liquid fraction, natural convection becomes the dominant mode of heat transfer. Also, due to density gradient, volumetric expansion and upward rise of high temperature molecules, the temperature of PCM at top position is comparatively higher and thus phase transition rate at top is higher as compared to central and bottom positions. Likewise, as shown in **Fig. 5 (A)**, the phase transition rate at top position at zone A is 38.49% and 47.38% higher as compared zone D and zone E, respectively. This is due to the fact that temperature gradient between HTF and PCM at zone A is relatively higher and thus heat transfer is intense at zone A. Consequently, HTF transfers thermal energy to PCM at zone A and hence, the temperature gradient at zone D and zone E is comparatively smaller. Similarly, the phase transition rate at central position at zone A is reasonably higher as compared to other zones, as shown in **Fig. 5 (B)**. Besides zone A, the phase transition rates at central positions at zone B, D and E are fairly comparable. Likewise, due to natural convection and upward rise of higher temperature molecules, heat transfer is significantly smaller at bottom positions of LHS unit, especially in locations nearer to shell boundary, as shown in **Fig. 5 (C)**. It can be observed that the bottom positions at Zone B and Zone D exhibit considerably weaker phase transition rate and thus charging cycle completes after 3.12 hours.

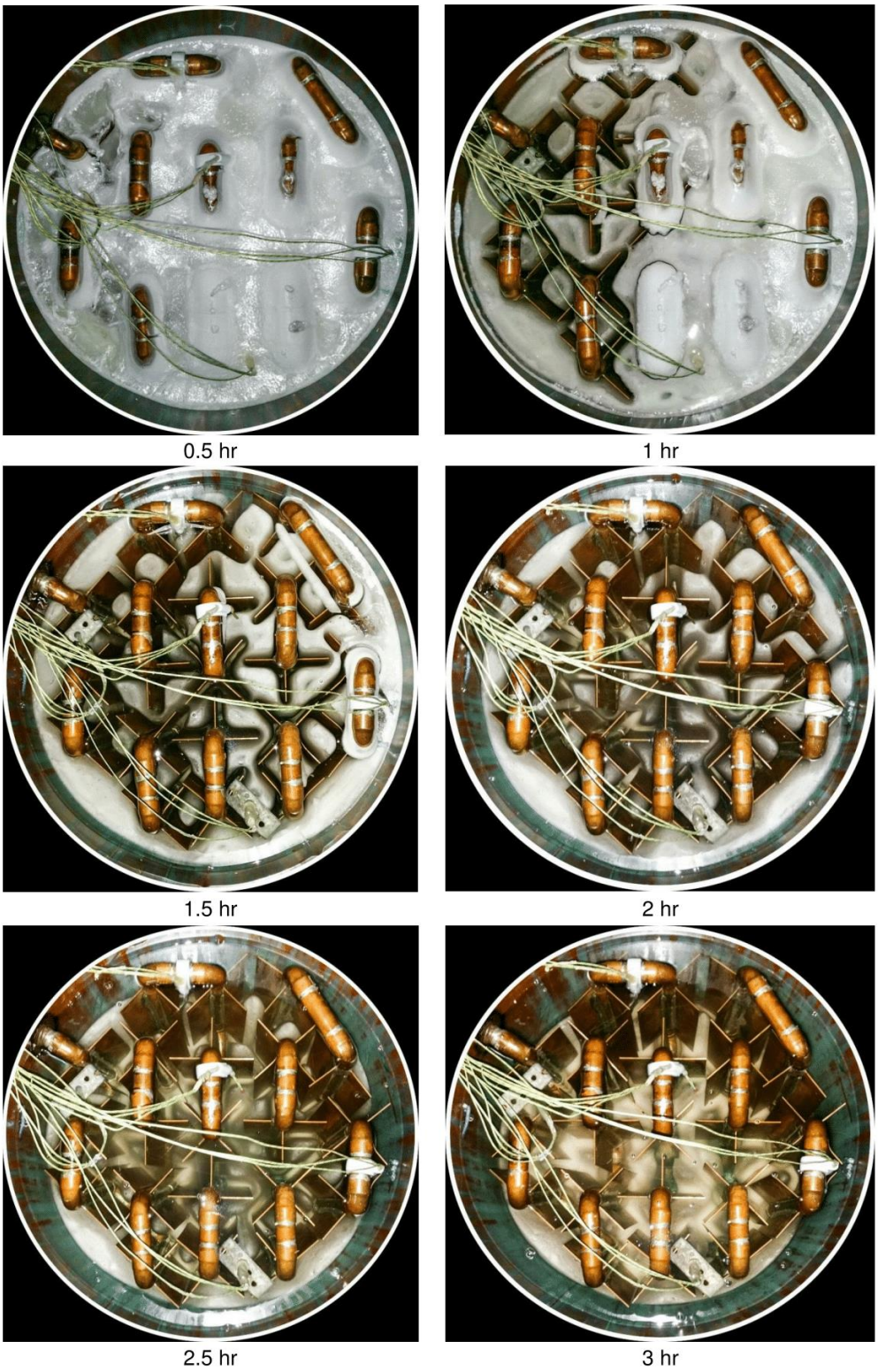

Fig. 4 Pictorial representation of PCM melting behaviour in LHS unit during charging cycle. Inlet temperature and volume flow rate of HTF are kept constant at 62 °C and 1.5 l/min, respectively.

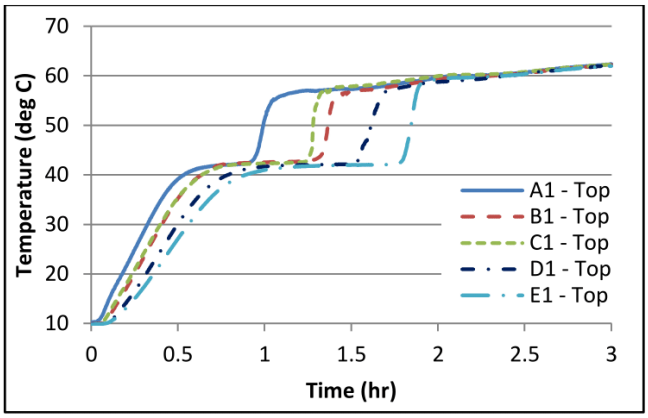

(A)

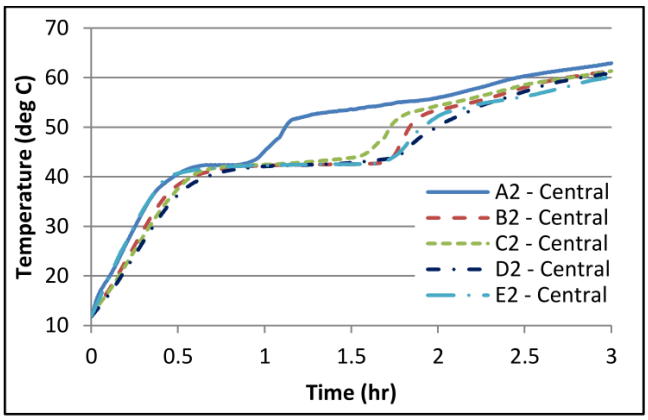

(B)

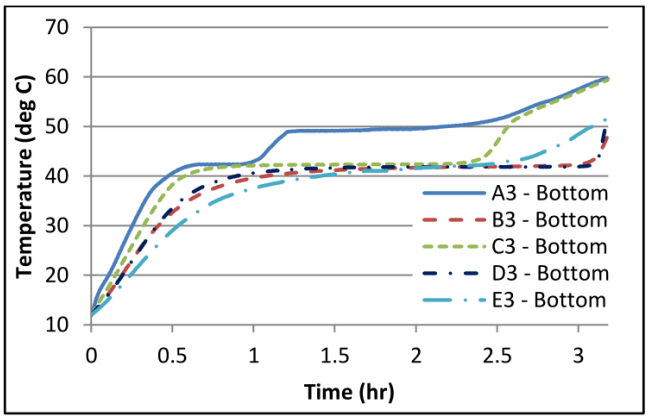

(C)

Fig. 5 Illustration of temperature profiles attained during charging cycle at all five zones (A, B, C, D and E) and all three vertical positions at each zone (1-Top, 2-Central and 3-Bottom). Inlet temperature and volume flow rate of HTF are set to 62 °C and 1.5 l/min, respectively. (A) Temperature profiles at top position at each zone, (B) central position at each zone and (C) bottom position at each zone.

3.3 Effect of inlet temperature on charging time

In order to examine the impact of weather fluctuations and solar off-peak hours on thermal performance of LHS unit, experimental tests are performed at four inlet temperatures of HTF and at constant volume flow rate of 1.5 l/min. The selected inlet temperatures of HTF are 52 °C, 57 °C, 62 °C and 67 °C. Likewise, the initial temperature of PCM is about 10 °C.

Transient temperature profiles of PCM at all three positions at zone D are illustrated in **Fig. 6**. It is evident that an increase in inlet temperature of HTF has a significant effect on phase transition rate and average temperature of PCM. Temperature gradient between PCM and HTF is the key driving force for heat transfer. With an increase in inlet temperature of HTF, higher temperature gradient can be achieved and consequently, higher heat transfer rate can be established. The accelerated heat transfer rate assures rapid phase transition from solid to liquid phase. Therefore, fraction of liquid PCM can be promptly increased, which can lead to quick natural convection and in consequence, less time will be required to complete charging cycle.

It is evident from **Fig. 6 (A)** that phase transition rate of PCM is considerably low for inlet temperature of 52 °C as compared to other inlet temperatures of HTF. Moreover, the total time required for PCM at top position at zone D to melt is 3 hr. However, with an increase in inlet temperature from 52 °C to 57 °C, 62 °C and 67 °C, the total melting time is reduced by 38.54%, 47.24% and 53.7%, respectively. Furthermore, with an increase in inlet temperature, the augmentation in sensible heating after phase transition can result in an increase in overall enthalpy of LHS unit.

As discussed in **section 3.2**, the heat transfer rate at central and bottom positions are affected due to upward rise of higher temperature molecules and buoyant effect. However, with an increase in inlet temperature, the phase transition rate can be significantly enhanced. The total time required for complete phase transition of PCM at central and bottom positions at zone D, for inlet temperature of 52 °C, are 3.14 hr and 4.48 hr, respectively (see **Fig. 6(B)** and **Fig. 6(C)**). However, with an increase in inlet temperatures to 57 °C, 62 °C and 67 °C, the total melting time at central position is reduced by 14.72%, 41.39% and 51.23%, respectively. Similarly, at bottom position, the total melting time is reduced by 15.22%, 28.49% and 45.32%, respectively. The overall reduction in melting time at zone D is calculated by taking an average of reduction in melting time at top, central and bottom positions, as shown in **Fig. 7**.

Therefore, it can be observed that the influence of an increase in inlet temperature on phase transition rate of PCM is higher at top position as compared to central and bottom positions. Additionally, it is noticed that a considerable amount of thermal energy is extracted from HTF at earlier zones, such as zone A, B and C, and thus only small fraction of thermal energy is available to generate good temperature gradient at later zones, such as zone D and E. Hence, an increase in inlet temperature can guarantee higher temperature gradient at earlier zones as well as a moderate temperature gradient at later zones.

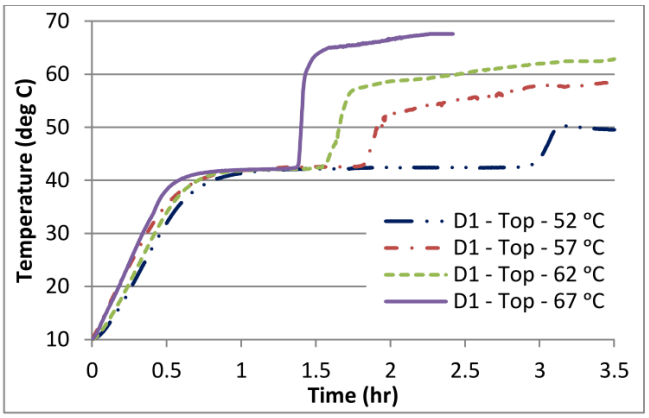

(A)

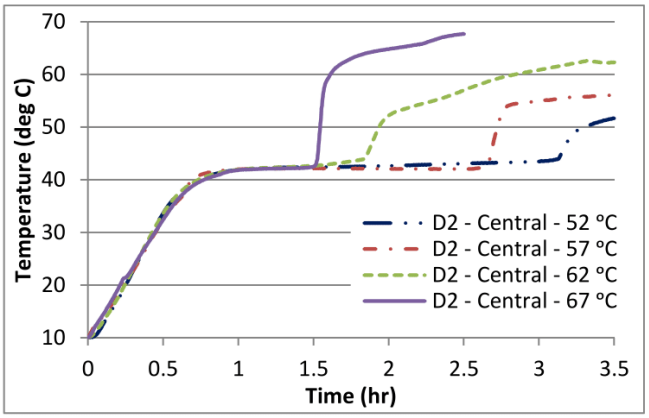

(B)

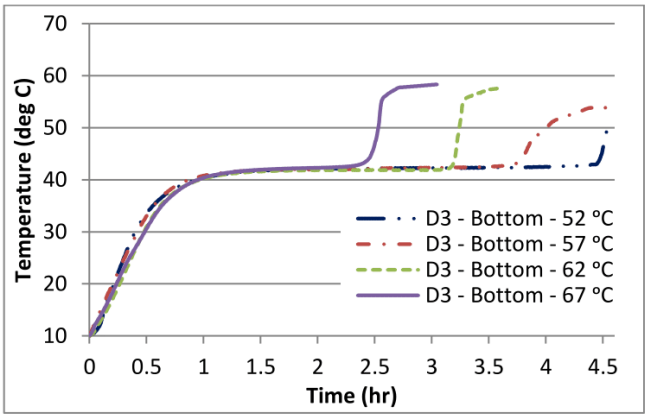

(C)

Fig. 6 Transient temperature profiles obtained from thermocouples at all three positions at zone D during charging cycle at various inlet temperatures of HTF and constant volume flow rate of 1.5 l/min.

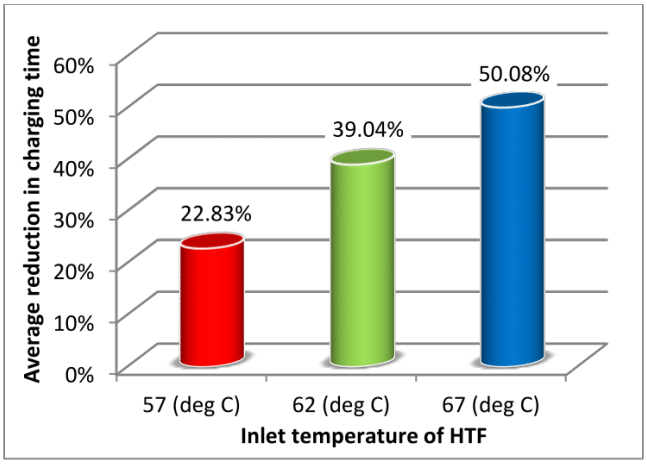

Fig. 7 Average reduction in charging time of LHS unit by increasing inlet temperature from 52 °C to 57, 62 and 67 °C.

3.4 Effect of volume flow rate on charging time

To investigate the influence of volume flow rate of HTF on phase transition rate and overall enthalpy of LHS unit, a series of sixteen experiments are conducted at four volume flow rates: 1.5, 2.0, 2.5 and 3.0 l/min and at four constant inlet temperatures: 52, 57, 62 and 67 °C, as shown in **Fig. 8**. The transient temperature profiles are obtained from thermocouples at bottom position at zone C and at central position at zone D.

As shown in **Fig. 8 (A)**, at constant inlet temperature of 52 °C, an increase in volume flow rate has no impression on enhancing the heat transfer rate at initial stages of charging cycle, which is dominated by conduction heat transfer. The reason behind is the low thermal conductivity of PCM at solid phase, due to which high thermal resistance is offered to conduction heat transfer and thus the overall heat transfer rate is affected. It is evident that the sensible heating from 15 °C to 41 °C is almost at same rate for all volume flow rates. However, the latent portion of thermal heating from 41 °C to 44 °C is highly influenced by an increase in volume flow rate. It is due to the fact that as phase transition occurs and the fraction of liquid PCM increases, natural convection starts dominating the heat transfer and therefore the overall thermal resistance offered by PCM is reduced. Thus, by increasing volume flow rate, the forced convection coefficient in tubes is improved, which enhances the heat transfer rate and reduces total time to complete charging cycle. Likewise, after the completion of latent heating, the sensible heating of liquid PCM shows an insignificant increase in temperature with an increase in volume flow rate.

Moreover, it can be observed from **Fig. 8 (A)** that by increasing volume flow rate from 1.5 l/min to 2.0, 2.5 and 3.0 l/min, the total phase transition time is reduced by 6.56%, 18.53% and 19.91%, respectively. Likewise, as shown in **Fig. 8 (B)**, the phase transition time at central position at zone D is lessened by 6.59%, 10.19% and 13.11%, respectively. Similarly, at constant inlet temperature of 57 °C, the total time required to complete phase transition at bottom position at zone C is reduced by 8.37%, 15.97% and 22.97%, respectively (see **Fig. 8 (C)**). Furthermore, the melting time at central position at zone D is decreased by 19.24%, 21.65% and 30.98%, respectively (see **Fig. 8 (D)**).

However, with higher constant inlet temperatures of 62 °C and 67 °C, the influence of volume flow rate is insignificant on phase transition rate. It is due to the fact that with higher constant inlet

temperatures, a strong temperature gradient across the unit is generated, which diminishes the further enhancement due to increase in volume flow rate. As illustrated in **Fig. 8 (G)**, at constant inlet temperature of 67 ^{o}C, the melting time at bottom position at zone C is slightly reduced by 1.67%, 2.04% and 7.72% by increasing volume flow rate from 1.5 l/min to 2.0, 2.5 and 3.0 l/min, respectively. Likewise, a trivial reduction in melting time is noted at central position at zone D. Therefore, it can be deduced that at higher constant inlet temperature, the occupancy period for HTF in tubes is reduced by increasing volume flow rate and hence, the heat transfer surface remains at almost isothermal condition.

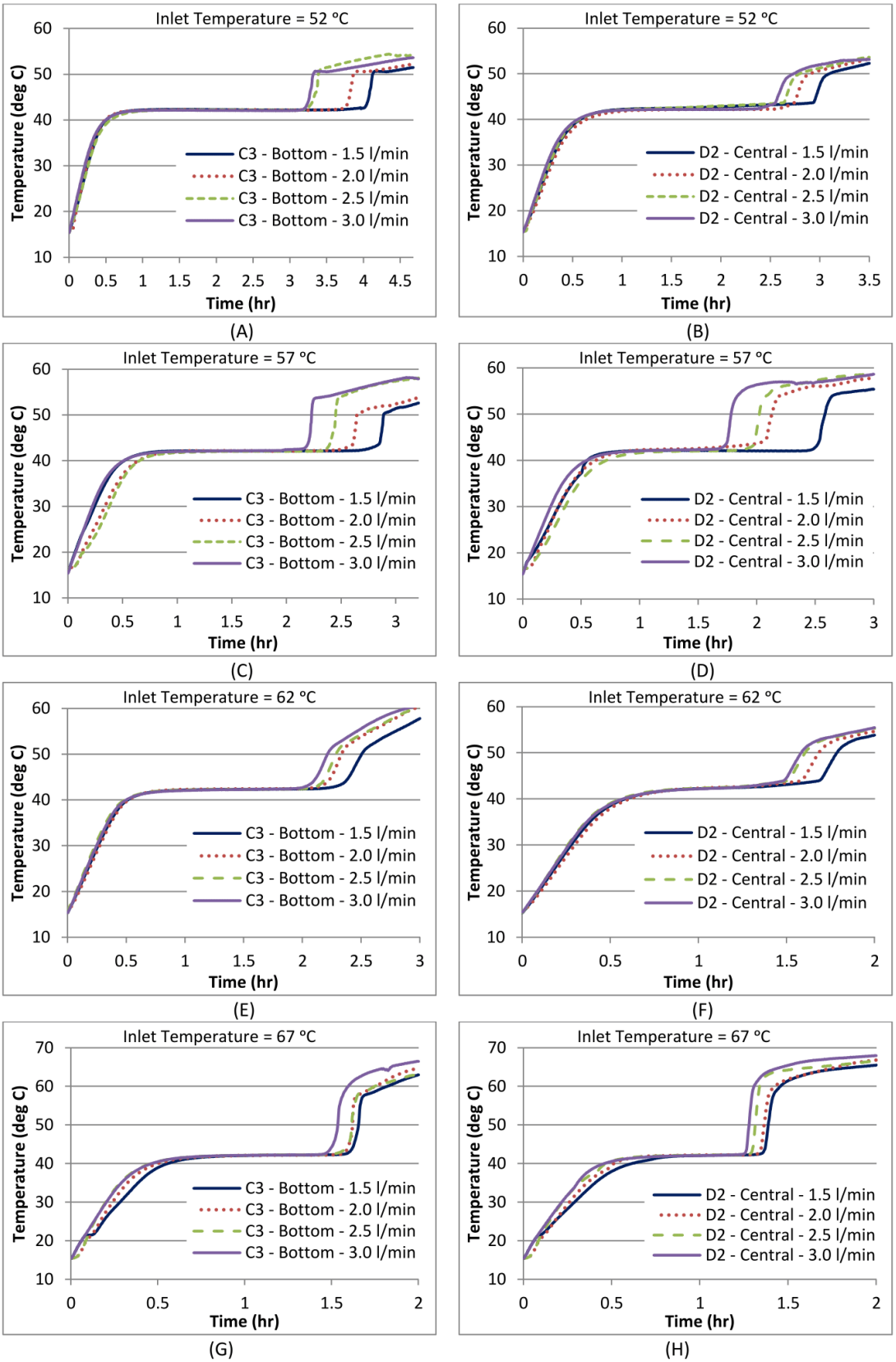

Fig. 8 Transient temperature profiles of PCM at bottom position at zone C and at central position at zone D during charging cycle at various volume flow rates and various constant inlet temperatures of HTF.

3.5 Mean power

To evaluate thermal performance of LHS unit, mean power is calculated from change in enthalpy of HTF. Thermocouples are installed at inlet and outlet of LHS unit, which can record the transient data of enthalpy change. Therefore, to calculate the total amount of thermal energy stored by LHS unit, the following subsection integral method is implemented which incorporates the variation in specific heat capacity and density of HTF with varying temperature:

$$Q_s = \sum \dot{V} \left(\frac{\rho_{in} + \rho_{out}}{2} \right) \left(\frac{C_{p,in} + C_{p,out}}{2} \right) \left(T_{HTF,in} - T_{HTF,out} \right) \Delta t \qquad (1)$$

where Q_s represents the amount of thermal energy storage (kJ), $\dot{V}$ is the volume flow rate of HTF (m^3/sec), ρ is the density of HTF (kg/m^3), C_p is the specific heat capacity of HTF (kJ/kg.K), T_{HTF} shows the temperature of HTF (°C) and Δt represents the time interval (sec) at which transient data is recorded. Further, the mean power for charging cycle is calculated as follow:

$$P_c = \frac{Q_s}{t_c} \qquad (2)$$

where P_c shows the mean power (kW) and t_c is the total time elapsed (sec) during charging cycle until all thermocouples display temperature higher than phase change temperature.

For all cases, the initial temperature and mass of PCM in LHS unit is fixed. Therefore, under different thermal conditions, the mean power is highly influenced by charging time. As illustrated in **Fig. 9**, inlet temperature of HTF has an evident impact on mean power. Refer to **section 3.3**, with an increase in inlet temperature of HTF, a stronger temperature gradient is generated between HTF and PCM, which increases the heat transfer and reduces the charging time. As a result, higher mean power is generated with an increase in inlet temperature of HTF. Likewise, the increase in volume flow rate enhances the heat transfer rate and thus the charging time is reduced. As a result, a moderate increase in mean power is noticed by increasing volume flow rate of HTF.

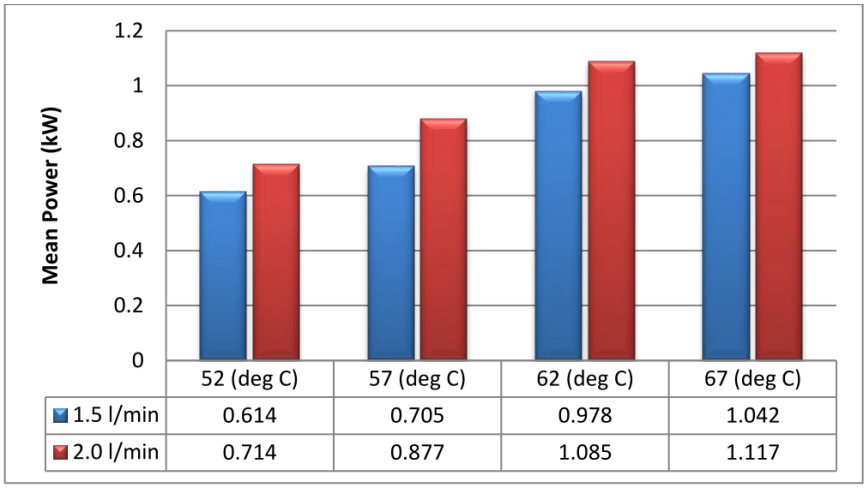

Fig. 9 Illustrating the influence of inlet temperature of HTF on mean power at two mass flow rates: 1.5 l/min and 2.0 l/min.

4. Conclusions

In this paper, experimental investigations of LHS unit connected to solar collector are performed to identify thermal performance during charging cycles. LHS unit is comprised of shell-and-tube with longitudinal fins heat exchanger and paraffin (RT44HC) as thermal storage material. Thermal performance of LHS unit is examined by conducting charging cycles at various inlet temperatures and volume flow rates of HTF. Based on experimental results, the following conclusions are derived:

- It is observed that the effective surfaces area for heat transfer and overall thermal conductivity is increased by introducing longitudinal fins in LHS unit. This novel configuration of LHS unit ensures higher thermal storage capacity and higher phase transition rate. For example, it can store 14.36 MJ of thermal energy in 3.12 hours when charged at inlet temperature of 62 °C and volume flow rate of 1.5 l/min.
- It is noticed that due to vertical orientation of shell-and-tube heat exchanger in LHS unit, the PCM at top position melts quickly as compared to central and bottom position. The reason behind is the natural convection and upward rise of high temperature liquid PCM molecules. Initially, the heat transfer is dominated by conduction. However, as the liquid fraction increases, natural convection is dominant mode of heat transfer. Moreover, longitudinal fins are employed for the reason that it does not restrict natural convection.
- Besides enthalpy gradient at top and bottom positions, it is noticed that significant quantity of thermal energy is extracted from HTF at earlier zones in LHS unit; therefore the later zones have smaller temperature gradient, which results in weaker phase transition rate. To overcome it, an increase in inlet temperature can assure better temperature gradient across entire LHS unit and therefore, phase transition rate can be significantly increased. For example, the average melting time is reduced by 22.83%, 39.04% and 50.08% as the inlet temperature is increased from 52 °C to 57, 62 and 67 °C, respectively. Likewise, the mean power is increased by 59.28% and 69.71% as the inlet temperature is increased from 52 °C to 62 °C and 67 °C, respectively.
- An increase in volume flow rate has a relatively moderate influence on thermal performance. The reason behind is that as natural convection starts dominating the heat transfer in LHS unit, an increase in volume flow rate of HTF in tubes enhances the forced convection coefficient in tubes and thus heat transfer improves. For example, at constant inlet temperature of 57 °C, the heat transfer is improved by increasing volume flow rate from 1.5 l/min to 2, 2.5 and 3 l/min and consequently, the melting time is reduced by 19.24%, 21.65% and 30.98%, respectively. However, with an increase in constant inlet temperature of HTF, the influence of volume flow rate on phase transition rate weakens. For example, at constant inlet temperature of 67 °C, as the volume flow rate is increased, the melting time is slightly reduced by 1.67%, 2.04% and 7.72%, respectively.
- Due to an upsurge in phase transition rate, the higher thermal storage capacity of LHS unit is completely charged in as less as 3 hours. Therefore, this novel LHS unit can provide time, spatial and financial benefits in range of household and industrial applications. Furthermore, depending on applications, thermal storage capacity and mean power can be enlarged by assembling several LHS units in parallel sequence. In this manner, LHS unit can serve as a versatile element for larger systems such as solar power plants, waste heat recovery and domestic heating systems.

Acknowledgement

The authors would like to acknowledge Bournemouth University, UK and National University of Sciences and Technology (NUST), Pakistan for their direct funding for conducting this research and the support they have provided.

References

[1] International Energy Agency (IEA). Energy and Climate Change 21st UN Conference of the Parties (COP21). Paris2015.
[2] Suranovic S. Fossil fuel addiction and the implications for climate change policy. Global Environmental Change. 2013;23:598-608.
[3] Jacobson MZ. Review of solutions to global warming, air pollution, and energy security. Energy & Environmental Science. 2009;2:148-73.
[4] Modi A, Bühler F, Andreasen JG, Haglind F. A review of solar energy based heat and power generation systems. Renewable and Sustainable Energy Reviews. 2017;67:1047-64.
[5] Sharma A, Tyagi VV, Chen C, Buddhi D. Review on thermal energy storage with phase change materials and applications. Renewable and Sustainable energy reviews. 2009;13:318-45.
[6] da Cunha JP, Eames P. Thermal energy storage for low and medium temperature applications using phase change materials–a review. Applied Energy. 2016;177:227-38.
[7] Tian Y, Zhao C-Y. A review of solar collectors and thermal energy storage in solar thermal applications. Applied Energy. 2013;104:538-53.
[8] Shukla A, Kant K, Sharma A. Solar Still with latent heat energy storage: A review. Innovative Food Science & Emerging Technologies. 2017.
[9] Pelay U, Luo L, Fan Y, Stitou D, Rood M. Thermal energy storage systems for concentrated solar power plants. Renewable and Sustainable Energy Reviews. 2017;79:82-100.
[10] Miró L, Gasia J, Cabeza LF. Thermal energy storage (TES) for industrial waste heat (IWH) recovery: a review. Applied Energy. 2016;179:284-301.
[11] Waqas A, Din ZU. Phase change material (PCM) storage for free cooling of buildings—a review. Renewable and sustainable energy reviews. 2013;18:607-25.
[12] Rabha D, Muthukumar P. Performance studies on a forced convection solar dryer integrated with a paraffin wax–based latent heat storage system. Solar Energy. 2017;149:214-26.
[13] Park S, Woo S, Shon J, Lee K. Experimental study on heat storage system using phase-change material in a diesel engine. Energy. 2017;119:1108-18.
[14] Cabeza LF, Castell A, Barreneche Cd, De Gracia A, Fernández A. Materials used as PCM in thermal energy storage in buildings: a review. Renewable and Sustainable Energy Reviews. 2011;15:1675-95.
[15] Dhaidan NS, Khodadadi J. Melting and convection of phase change materials in different shape containers: A review. Renewable and Sustainable Energy Reviews. 2015;43:449-77.
[16] Khan Z, Khan Z, Ghafoor A. A review of performance enhancement of PCM based latent heat storage system within the context of materials, thermal stability and compatibility. Energy Conversion and Management. 2016;115:132-58.
[17] Liu L, Su D, Tang Y, Fang G. Thermal conductivity enhancement of phase change materials for thermal energy storage: A review. Renewable and Sustainable Energy Reviews. 2016;62:305-17.
[18] Liu C, Rao Z, Zhao J, Huo Y, Li Y. Review on nanoencapsulated phase change materials: Preparation, characterization and heat transfer enhancement. Nano Energy. 2015;13:814-26.
[19] Giro-Paloma J, Martínez M, Cabeza LF, Fernández AI. Types, methods, techniques, and applications for microencapsulated phase change materials (MPCM): a review. Renewable and Sustainable Energy Reviews. 2016;53:1059-75.
[20] Agyenim F, Hewitt N, Eames P, Smyth M. A review of materials, heat transfer and phase change problem formulation for latent heat thermal energy storage systems (LHTESS). Renewable and sustainable energy reviews. 2010;14:615-28.
[21] Wang W-W, Zhang K, Wang L-B, He Y-L. Numerical study of the heat charging and discharging characteristics of a shell-and-tube phase change heat storage unit. Applied Thermal Engineering. 2013;58:542-53.
[22] Tay N, Bruno F, Belusko M. Experimental validation of a CFD model for tubes in a phase change thermal energy storage system. International Journal of Heat and Mass Transfer. 2012;55:574-85.

[23] Hosseini M, Ranjbar A, Sedighi K, Rahimi M. A combined experimental and computational study on the melting behavior of a medium temperature phase change storage material inside shell and tube heat exchanger. International Communications in Heat and Mass Transfer. 2012;39:1416-24.
[24] Meng Z, Zhang P. Experimental and numerical investigation of a tube-in-tank latent thermal energy storage unit using composite PCM. Applied Energy. 2017;190:524-39.
[25] Esapour M, Hosseini M, Ranjbar A, Pahamli Y, Bahrampoury R. Phase change in multi-tube heat exchangers. Renewable Energy. 2016;85:1017-25.
[26] Luo K, Yao F-J, Yi H-L, Tan H-P. Lattice Boltzmann simulation of convection melting in complex heat storage systems filled with phase change materials. Applied Thermal Engineering. 2015;86:238-50.
[27] Rathod MK, Banerjee J. Thermal performance enhancement of shell and tube Latent Heat Storage Unit using longitudinal fins. Applied thermal engineering. 2015;75:1084-92.
[28] Yuan Y, Cao X, Xiang B, Du Y. Effect of installation angle of fins on melting characteristics of annular unit for latent heat thermal energy storage. Solar Energy. 2016;136:365-78.
[29] Li Z, Wu Z-G. Analysis of HTFs, PCMs and fins effects on the thermal performance of shell–tube thermal energy storage units. Solar Energy. 2015;122:382-95.
[30] Darzi AAR, Jourabian M, Farhadi M. Melting and solidification of PCM enhanced by radial conductive fins and nanoparticles in cylindrical annulus. Energy Conversion and Management. 2016;118:253-63.
[31] Tao Y, He Y. Effects of natural convection on latent heat storage performance of salt in a horizontal concentric tube. Applied Energy. 2015;143:38-46.
[32] Wang P, Yao H, Lan Z, Peng Z, Huang Y, Ding Y. Numerical investigation of PCM melting process in sleeve tube with internal fins. Energy Conversion and Management. 2016;110:428-35.
[33] Liu C, Groulx D. Experimental study of the phase change heat transfer inside a horizontal cylindrical latent heat energy storage system. International Journal of Thermal Sciences. 2014;82:100-10.
[34] Tay NHS, Bruno F, Belusko M. Comparison of pinned and finned tubes in a phase change thermal energy storage system using CFD. Applied Energy. 2013;104:79-86.
[35] Caron-Soupart A, Fourmigué J-F, Marty P, Couturier R. Performance analysis of thermal energy storage systems using phase change material. Applied Thermal Engineering. 2016;98:1286-96.
[36] Agyenim F, Eames P, Smyth M. A comparison of heat transfer enhancement in a medium temperature thermal energy storage heat exchanger using fins. Solar Energy. 2009;83:1509-20.
[37] Khan Z, Khan Z, Tabeshf K. Parametric investigations to enhance thermal performance of paraffin through a novel geometrical configuration of shell and tube latent thermal storage system. Energy Conversion and Management. 2016;127:355-65.
[38] Helvaci H, Khan ZA. Mathematical modelling and simulation of multiphase flow in a flat plate solar energy collector. Energy Conversion and Management. 2015;106:139-50.
[39] Helvaci H, Khan ZA. Experimental study of thermodynamic assessment of a small scale solar thermal system. Energy Conversion and Management. 2016;117:567-76.
[40] Rubitherm® Technologies GmbH, http://www.rubitherm.eu/en/. 2017.

Paper V

An experimental investigation of discharge/solidification cycle of paraffin in novel shell and tube with longitudinal fins based latent heat storage system

Zakir Khan [a]*, Zulfiqar Ahmad Khan [a]

[a] Bournemouth University, Faculty of Science and Technology, NanoCorr, Energy and Modelling (NCEM), Fern Barrow, Talbot Campus, Poole, Dorset BH12 5BB, UK.

E-mail: zkhan@bournemouth.ac.uk

Corresponding Author:

[a]* Bournemouth University, Faculty of Science and Technology, NanoCorr, Energy and Modelling (NCEM), Fern Barrow, Talbot Campus, Poole, Dorset BH12 5BB, UK.

E-mail: zkhan2@bournemouth.ac.uk

Tel.: +44 7459249069

Abstract

In this article, the discharging cycles of paraffin in novel latent heat storage (LHS) unit are experimentally investigated. The novel LHS unit includes shell and tube with longitudinal fins based heat exchanger and paraffin as thermal energy storage material. The experimental investigations are focused on identifying the transient temperature performance, effective mode of heat transfer, accumulative thermal energy discharge and mean discharge power of paraffin in LHS unit. Moreover, the influences of operating conditions such as inlet temperature and volume flow rate of heat transfer fluid (HTF) on thermal behaviour of LHS unit are experimentally studied. The transient temperature profiles and photographic characterisation of liquid-solid transition of paraffin in LHS unit provide a good understanding of temperature distribution and dominant mode of heat transfer. It is noticed that during discharging cycles, natural convection has an insignificant impact on thermal performance of LHS unit. However, due to inclusion of extended longitudinal fins, conduction is the dominant mode of heat transfer. It is noticed that due to development of solidified paraffin around tubes and longitudinal fins, the overall thermal resistance is increased and thus, discharging rate is affected. However, by regulating inlet temperature or volume flow rate of HTF, the influence of overall thermal resistance is minimised. Mean discharge power is enhanced by 36.05% as the inlet temperature is reduced from 15 ^{o}C to 5 ^{o}C. Likewise, the mean discharge power is improved by 49.75% as the volume flow rate is increased from 1.5 l/min to 3 l/min. Similarly, with an increase in volume flow rate, the discharge time of equal amount of thermal energy 12.09 MJ is reduced by 24%. It is established that by adjusting operating conditions, the required demand of output temperature and mean discharge power can be attained. Furthermore, this novel LHS unit can meet large scale thermal energy demands by connecting several units in parallel and thus, it has potential to be employed in wide-ranging domestic and commercial applications.

Keywords

Thermal energy storage, Latent heat storage, Discharge cycle, Phase change materials, Heat transfer, Shell and tube heat exchanger

1. Introduction

Due to an increase in global economic growth, the urge for consistent supply of energy has increased in both industrial and domestic applications. Fossil fuels have been serving the purpose of generating desired energy for many decades. However, the harmful emissions from fossil fuels have caused climate change and global warming [1-3]. Therefore, the need for efficient and responsive technologies for renewable energy and heat recovery sources are imperative to abridge gap between energy supply and demand. Thermal energy storage (TES) is an environmental friendly technique to capture thermal energy at solar peak hours or from heat recovery sources and releases it to balance out energy demand. Latent heat storage (LHS) is considered as more attractive technique of TES due to its high thermal storage density, almost isothermal energy storage and retrieval, low vapour pressure, chemical stability and small variation in volume during phase transition [4-6].

LHS systems utilises phase change materials (PCM) to capture and release thermal energy during phase transition. LHS systems have been employed in number of practical applications ranging from solar thermal systems, waste heat recovery systems, energy balancing, management and peak shaving, agricultural drying and building air-conditioning systems [7-12]. However, the large scale practical utilisations of LHS systems are hindered by low thermal conductivity of phase change materials (≈ 0.2 W/m.K) [13, 14]. Due to low thermal conductivity, the rapid charging and discharging of LHS system is highly affected. Thus, a responsive heat transfer mechanism is essential to counter low thermal conductivity. Several methods have been proposed to improve heat transfer mechanism and consequently overall thermal performance of LHS system such as: container geometrical orientation, inclusion of extended surfaces, dispersion of high conductive additives and encapsulation [15-22]. The geometrical configuration of heat exchanger in LHS system plays a crucial role. Various types of heat exchangers for LHS systems are examined, however shell and tube configuration is intensely researched due to its easy installation into majority of industrial applications and design simplicity with minimal heat loss benefits [23].

Seddegh et al. [24] performed experimental investigations of paraffin (RT60) in vertical shell and tube configuration with varying tube radius. Four tube radiuses were tested with shell-tube radius ratio of: 8.1, 5.4, 4 and 2.7. It was noticed that by decreasing radius ratio from 8.1 to 2.7, the solidification time was reduced by 44%. Yazici et al. [25] performed an experimental examination of paraffin in horizontal shell and tube configuration of LHS system. The effect of eccentricity of heat transfer fluid (HTF) tube on discharging rate was investigated. Six locations were probed with eccentricity values of: -10, -20, -30, 0, 10 and 20. It was noticed that either upward or downward increase in eccentricity showed a reduction in discharging rate, whereas the concentric orientation had presented a relatively higher discharging rate. Similarly, Seddegh et al. [26] numerically examined the thermal behaviour of paraffin (RT50) in vertical and horizontal orientation of shell and tube based LHS system. It was noticed that geometrical orientation of shell and tube had minimal effect on solidification rate, due to conduction dominated heat transfer. Likewise, Longeon et al. [27] experimentally tested paraffin (RT35) in a vertical shell and tube configuration. It was noticed that conduction was the dominant mode of heat transfer during discharging cycle. Hosseini et al. [28] conducted discharging cycles on paraffin (RT50) in horizontal shell and tube based LHS system. It was observed that the initial temperature of liquid paraffin had a negligible impact on overall thermal efficiency. Avci and Yazici [29] conducted experimental investigations on discharging cycles of paraffin in a horizontal shell and tube orientation. It was deduced that conduction was the dominated mode of heat transfer. Moreover, it was observed that discharging rate can be enhanced by decreasing inlet temperature of HTF. Wang et al. [30] numerically examined the influence of inlet temperature and flow rate of HTF on solidification time of n-octadecane in horizontal shell and tube based LHS system. It was noticed that

temperature gradient between HTF and PCM was increased by reducing inlet temperature of HTF and thus, the solidification time was significantly reduced. Similarly, it was deduced that flow rate of HTF had an insignificant impact on overall thermal energy capacity of LHS system. Agarwal and Sarviya [31] performed an experimental study on paraffin wax in horizontal shell and tube based LHS system. It was noticed that solidification time was reduced by 19.09% as the mass flow rate was increased from 0.0015 to 0.003 kg/sec. Likewise, the cumulative thermal energy gain by HTF was increased by 8.7% with an increase in flow rate from 0.0022 to 0.003 kg/sec. Meng and Zhang [32] conducted numerical and experimental study to identify thermal behaviour of paraffin-copper foam composite in rectangular shaped shell and tube configuration of LHS system. It was observed that by increasing temperature gradient between PCM and HTF, the solidification time can be reduced by 34.76%. Likewise, by increasing inlet velocity of HTF from 0.1 m/sec to 0.2 m/sec, a moderate enhancement of 8.4% was observed in discharging rate. Wang et al. [33] performed experimental examination of erythritol as PCM in vertical shell and tube orientation of LHS system. It was noticed that inlet temperature and flow rate of HTF had a significant impact on discharging rate. However, an increase in pressure of HTF demonstrated a trivial impression on discharging rate.

It is evident from previous literature that temperature gradient and flow rate of HTF can influence the discharging rate. However, due to low thermal conductivity of PCM, the optimum benefits could not be achieved. Therefore, the most convenient and cost effective technique is to incorporate extended surfaces [34]. Rabienataj Darzi et al. [35] conducted numerical simulation of n-eicosane in horizontal shell and tube with longitudinal fins. It was noticed that as compared to without fins orientation, the solidification time was increased by 28% to 85% as the number of fins were increased from 4 to 20, respectively. Li and Wu [36] numerically investigated the thermal behaviour of $NaNO_3$ as PCM in horizontal shell and tube configuration with and without longitudinal fins. It was deduced that solidification time is reduced by 14% with inclusion of longitudinal fins. Rathod and Banerjee [37] conducted experimental examination of stearic acid in a vertical shell and tube with three longitudinal fins configuration. It was observed that due to inclusion of three longitudinal fins, the solidification time was reduced by 43.6%. Liu and Groulx [38] experimentally studied the influence of straight and angled longitudinal fins on discharging rate of dodecanoic acid in horizontal shell and tube configuration. Four longitudinal fins were attached to tube. It was noticed that due to conduction dominated heat transfer, both orientations presented almost identical discharging performance. Al-Abidi et al. [39] performed numerical simulation to investigate the solidification process of paraffin (RT82) in a horizontal triplex tube heat exchanger based LHS system. The discharge time was reduced by 35% with longitudinal fins as compared to no fins configuration. Also, the influence of longitudinal fins number, length and thickness were examined. It was reported that number of fins and length had a significant influence on solidification rate. However, the impact of fins thickness was moderate. Likewise, Almsater et al. [40] performed numerical and experimental investigation on solidification process of water as PCM and Dynalene HC-50 as HTF in a vertical triplex tube heat exchanger. It was observed that the solidification time was reduced from 3.67 hr to 3 hr and 2.31 hr by increasing mass flow rate from 0.02 kg/s to 0.044 kg/s and 0.074 kg/s, respectively. Kabbara et al. [41] conducted experimental investigation on solidification process of dodecanoic acid in a vertical shell and tube with rectangular fins configuration. It was noticed that the solidification rate and discharge power was slightly improved by increasing flow rate. However, more experimental tests could have conducted to help in drawing better conclusions. Agyenim et al. [42] experimentally investigated the influence of radial and longitudinal fins on thermal performance of Erythritol as PCM in shell and tube configuration. It was noticed that cumulative thermal energy discharge for no fins, radial fins and longitudinal fins were 4977.8 kJ, 7293.1 kJ and 8813.1 kJ, respectively. Similarly, Lohrasbi et al. [43] performed comparative examinations on thermal performance of PCM in vertical

shell and tube configurations with no fins, optimised circular fins and longitudinal fins. It was reported that the phase transition rate for optimised circular fins and longitudinal fins orientations were 3.55 and 4.28 times higher as compared to no fins orientation, respectively. Likewise, Caron-Soupart et al. [44] conducted experimental investigations of paraffin (RT35HC) in shell and tube with three configurations: no fins, radial fins and longitudinal fins. It was reported that longitudinal fins had generated better temperature gradient and thermal power as compared to no fins and radial fins. Therefore, it is concluded from previous literature that longitudinal fins have better thermal performance during solidification process as compared to no fins and radial fins configurations. Moreover, it is observed that shell and tube with single pass orientations are exclusively studied in previous literature, as detailed in **Table 1**. Therefore, the literature lacks experimental investigations of shell and tube with multiple passes and extended surfaces. Also, there is a lack of discussion on thermal energy discharge and mean discharge power of proposed LHS systems. Therefore, there is a need to experimentally investigate shell and tube with multiple passes and longitudinal fins based LHS system which can provide a viable solution for higher thermal storage capacity, discharge rate and discharge power. This article is focused on experimentally investigating a novel geometrical orientation of shell and tube with multiple passes and longitudinal fins which is not reported in previous literature. Furthermore, this article proposes a responsive and compact thermal storage design solution with higher discharge rate, cumulative heat capacity and discharge power.

Table 1
Summary of various studies conducted to examine thermal behaviour of PCM in shell and tube based LHS systems

Ref No.	Study type	Shell and tube		Extended surfaces		PCM
		Tube passes	Orientation	Type	No. of fins	
[24]	Exp.	Single	Vertical	-	-	Paraffin (RT 60)
[25]	Exp.	Single	Horizontal	-	-	Paraffin P56-58
[26]	Num.	Single	Ver. / Hor.	-	-	Paraffin (RT 50)
[27]	Exp./Num.	Single	Vertical	-	-	Paraffin (RT 35)
[28]	Exp./Num.	Single	Horizontal	-	-	Paraffin (RT 50)
[29]	Exp.	Single	Horizontal	-	-	Paraffin P56-58
[30]	Num.	Single	Horizontal	-	-	n-Octadecane
[31]	Exp.	Single	Horizontal	-	-	Paraffin (41-55)
[32]	Exp./Num.	Double	Vertical	-	-	Paraffin (54-64)
[33]	Exp.	Single	Vertical	-	-	Erythritol
[35]	Num.	Single	Horizontal	Longitudinal	4 - 20	n-Eicosane
[36]	Num.	Single	Horizontal	Longitudinal	6	$NaNO_3$
[37]	Exp.	Single	Vertical	Longitudinal	3	Stearic acid
[38]	Exp.	Single	Horizontal	Longitudinal	4	Dodecanoic acid
[39]	Num.	Single	Horizontal	Longitudinal	4 - 8	Paraffin (RT 82)
[40]	Exp./Num.	Single	Vertical	Longitudinal	8	Water
[41]	Exp.	Four	Vertical	Rectangular	58	Dodecanoic acid
[42]	Exp.	Single	Horizontal	Circular Longitudinal	8	Erythritol
Present study	Exp.	21	Vertical	Longitudinal	76	Paraffin (RT44HC)

In this article, the experimental examinations of discharging cycles of paraffin in a novel LHS system are conducted. The novel LHS system consists of shell and tube with longitudinal fins based heat exchanger and paraffin as thermal storage material. The geometrical orientations of novel LHS system is previously designed, simulated and discussed by authors in [45]. Numerical simulations were conducted to examine the influence of parameters such as number of tube passes and their orientations in shell, geometrical configurations of longitudinal fins and construction material; on thermal storage capacity and charging/discharging rate of LHS system. An optimum design of LHS system was developed and constructed to perform experimental investigations. Prior to performing discharging cycles, the paraffin are charged by connecting novel LHS system to flat plate solar collector [46]. In this article, the discharging cycles are performed by directing cold water from building water tank to extract thermal energy from paraffin in LHS system. The experimental investigations of discharging cycles are conducted at various operating conditions of inlet temperature and flow rate of HTF. Moreover, this paper is focused to examine the transient temperature performance, effective mode of heat transfer, total solidification/discharge time, cumulative thermal energy discharge and mean discharge power of paraffin in LHS unit. Furthermore, this article will give comprehensive knowledge of how to adjust operating conditions or connect several LHS units to meet required thermal energy demands.

2. Experimental Setup and Procedure

2.1 Experimental Setup

In this article, the focus is on investigation of thermal performance of LHS unit during discharging process. The schematic representation of experimental setup is demonstrated in **Fig. 1**. The experimental setup consists of flat plate solar collector (FPSC), solar simulator, latent heat storage (LHS) unit, paraffin as thermal storage material, water supply from municipal / building, centrifugal pump, flow meter and data acquisition with computer.

FPSC and solar simulators are utilised to conduct charging cycles at various operating conditions. Solar simulator is operated to deliver steady thermal radiations to FPSC which results in increasing thermal energy of HTF. The high temperature HTF is guided to pass through LHS unit where it loses thermal energy to paraffin. Charging cycle is repeated until the temperature of paraffin inside LHS unit is about 62 °C, which provides a good baseline for all discharging cycles.

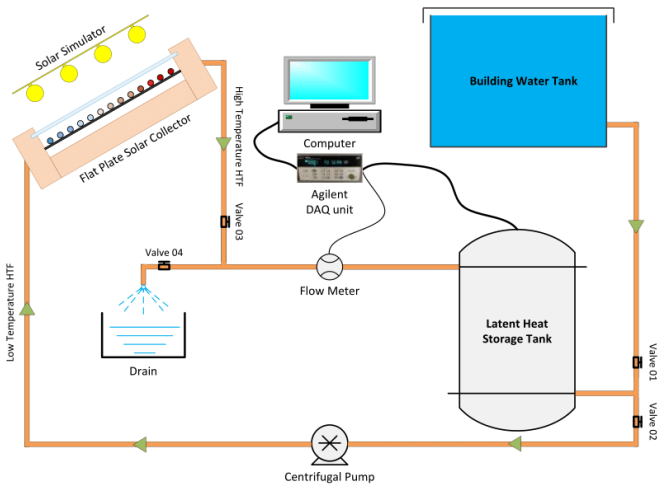

Fig. 1 Experimental setup layout for conducting discharging cycles of LHS unit.

During discharging cycle, the low temperature water is supplied from building water tank to extract thermal energy from paraffin in LHS unit. LHS unit is composed of vertical shell and tubes heat exchanger with longitudinal fins and paraffin as thermal storage material. The physical model of LHS unit is represented in **Fig. 2**. Shell and tubes with longitudinal fins are made up of copper. The outer diameter, length and thickness of shell are 450 mm, 385 mm and 1 mm, respectively. Likewise, the outer diameter and thickness of tubes are 22 mm and 1 mm. Longitudinal fins are connected to tubes having length, width and thickness of 230 mm, 40 mm and 1.5 mm, respectively. Chlorofluorocarbon-free envirofoam insulator of 50 mm thickness is muffled around the outer surface of shell to minimise thermal losses. Further design details on LHS unit can be found in [45]. Moreover, paraffin (RT44HC) is picked as thermal storage material due to its high thermal storage density, long term thermo-physical stability and good compatibility with copper [14, 47]. Thermal and physical characteristics of paraffin (RT44HC) are given in **Table 2**. Likewise, water is employed as heat transfer fluid (HTF).

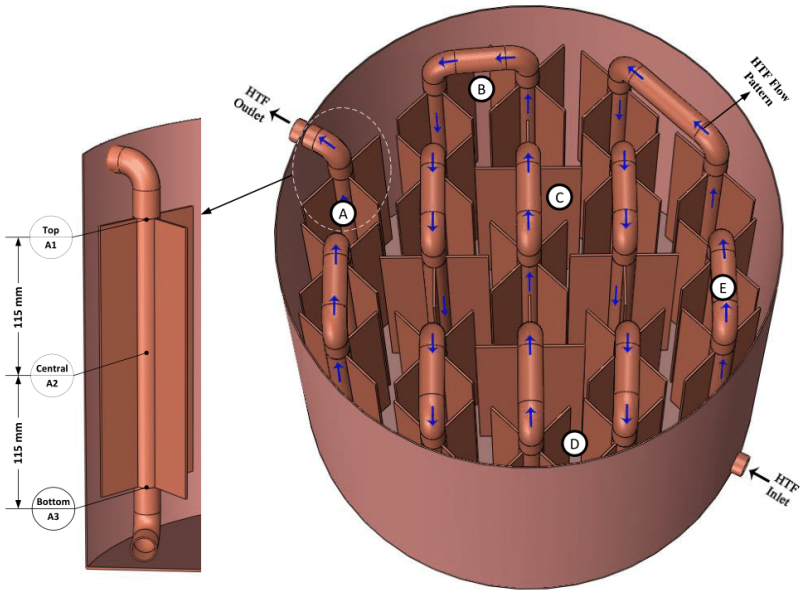

Fig. 2 Physical model representation of LHS unit with longitudinal fins, HTF flow pattern and vertical locations of thermocouples at various zones.

Table 2
Thermal and physical properties of paraffin (RT44HC) [14, 47]

Phase transition temperature	41-44 ^{o}C
Latent heat capacity	255 (kJ/kg)
Specific heat capacity	2.0 (kJ/kg. K)
Thermal conductivity	0.2 (W/m. K) solid, 0.2 (W/m. K) liquid
Density	800 (kg/m^3) solid, 700 (kg/m^3) liquid
Coefficient of thermal expansion	0.00259 (1/K)

Thermal response of paraffin in LHS unit is recorded by installing 15 K-type thermocouples at five zones i.e. A, B, C, D and E; at three vertical positions at each zone, as shown in **Fig. 2**. The vertical

positions of thermocouples are categorised as top, central and bottom position. Each thermocouple position is at a vertical distance of 115 mm. Moreover, two thermocouples are installed at inlet and outlet of HTF to LHS unit to register the amount of thermal energy discharge by paraffin to HTF. Likewise, a flow meter (Titan FT2 Hall Effect) is utilised to measure volume flow rate value of HTF. The thermocouples and flow meter have an accuracy of ±0.18% and 1.5%, respectively. In discharging cycle, flow control valve 2 and 3 are turned off to bypass FPSC and centrifugal pump, whereas valve 1 and 4 are operated to conduct discharging cycles at various controlled volume flow rates. The data acquisition (Agilent 34972A) is employed to register temperature and volume flow rate readings from thermocouples and flow meter into computer. Time step of 10 s is used to record data on computer.

2.2 Experimental Procedure

Prior to perform discharging experiments, the paraffin in LHS unit is charged at higher temperature to make sure that entire mass of paraffin is in liquid state. To provide a good baseline, the discharging cycles are started once all thermocouples at top positions at all zones display temperature equal to 62 ^{o}C.

Low temperature water from building water tank is supplied to conduct open loop discharging cycles. To regulate flow rate of water, valve 1 and 4 are adjusted to required value. Discharging cycles are examined at four different volume flow rates of water, such as 1.5, 2.0, 2.5, 3.0 l/min. Low temperature water from building water tank is guided to pass through tube passes in LHS unit. Due to temperature gradient between low temperature water and high temperature paraffin, heat transfer takes place. Paraffin loses thermal energy to water and thus the temperature of water is raised. The high temperature water at outlet of LHS unit can be utilised for desired application. Due to loss of thermal energy to water, paraffin starts solidifying. The discharging cycle is completed once all thermocouples display paraffin temperature less than its phase transition temperature and the temperature difference between inlet and outlet of water is less than 5 ^{o}C. Furthermore, to investigate the thermal response of paraffin at various inlet temperatures of water, three different inlet temperatures are tested which are 5, 10 and 15 ^{o}C.

In order to assess the reliability and repeatability of experimental results, a series of three discharging experiments are conducted at inlet temperature of 10 ^{o}C and flow rate of 1.5 l/min. The experimental results illustrate almost identical transient temperature profiles. The statistical standard deviations for discharging rate at top, central and bottom position at zone C are calculated to be 0.008, 0.029 and 0.033, respectively.

3. Results and Discussion

3.1 Temperature Distribution

To understand the thermal behaviour of paraffin during discharging process, the low temperature HTF at 10 ^{o}C is channelled through tubes in LHS unit. Due to temperature gradient, the low temperature HTF extracts thermal energy from high temperature paraffin. In consequence, the temperature of HTF is increased, whereas paraffin temperature is reduced. In order to understand the transient change in thermal energy of paraffin, the temperature data from all fifteen K-type thermocouples are registered. Transient temperature distribution can help in identifying the dominating mode of heat transfer and phase transition rate at various positions in various zones in LHS unit.

To perform discharging cycle, a first set of experimental test is conducted with an inlet temperature and flow rate of 10 ^{o}C and 1.5 l/min, respectively. The transient temperature profiles acquired from

thermocouples at top positions at all five zones are presented in **Fig. 3**. Due to higher temperature gradient between inlet temperature of HTF and paraffin in LHS unit, it is noticed that paraffin at top positions at all five zones rapidly discharges sensible portion of thermal energy to HTF. The sensible portion of thermal energy discharge to HTF is almost linear and as a result, paraffin temperature at top positions is reduced from initial temperature to 44 ^{o}C. Subsequently, latent portion of paraffin thermal energy discharge begins. Due to higher latent heat capacity of paraffin, the temperature of paraffin remains almost constant for a good period of time, as shown in **Fig. 3**. During this stage, the temperature of paraffin is gradually reduced from 44 ^{o}C to 41 ^{o}C. Due to discharge of latent portion of thermal energy, paraffin transforms from liquid phase to mushy phase and subsequently to solid phase. As latent portion of thermal energy is discharged, an instant decline in temperature is observed, which represents the sensible portion of thermal energy discharge.

Moreover, it can be observed that longitudinal fins are close-packed at zone C (centre of LHS unit), as shown in **Fig. 2**. Hence, the solidification/discharging rate of paraffin at top position at zone C is comparatively higher, as shown in **Fig. 3**. In succession, it can be noticed that due to relatively higher temperature gradient between inlet temperature of HTF and paraffin at zone E, the solidification rate is higher than zone A, B and D. The temperature of HTF increases as it extracts thermal energy from paraffin at zone E, D and C. Therefore, the temperature gradient for heat transfer is slightly reduced as HTF reaches zone B and zone A and thus, it affects the solidification rate of paraffin in those zones. Moreover, it can be observed from **Fig. 2** that HTF tube passes are connected at top at zone B, C and E, whereas it is connected at bottom at zone D. Therefore, due to geometrical orientation of connection between HTF tube passes and insignificant influence of natural convection, the discharge rate is comparatively lower at top position at zone D. Furthermore, an average of temperature profiles is obtained from all three thermocouples (top, central and bottom position) installed at each of five zones, as presented in **Fig. 4**. It is evident that due to higher temperature gradient between inlet temperature of HTF and paraffin, the discharging rate of paraffin at zone E is comparatively higher and is followed by zone C, zone B and zone A.

In order to give further insight into thermal performance of paraffin in longitudinal fins based LHS unit, the photographic illustration of discharge cycle is provided in **Fig. 5**. It can be observed that after discharging the system at inlet temperature of 10 ^{o}C and volume flow rate of 3 l/min for 0.25 hr, the paraffin around tubes and longitudinal fins are rapidly discharging latent portion of thermal energy to HTF and therefore the formation of solid layer is noticed. The transparent portion of paraffin represents the liquid phase, whereas the white portion displays the solid phase. It can be verified that the paraffin at inlet (zone E) is rapidly transforming to solid as compared to paraffin at outlet (zone A). This is due to the fact that conduction heat transfer and discharging rate is higher at inlet as compared to outlet. Likewise, after discharging for 0.5 hr, it can be noticed that thickness of solidified paraffin around tubes and longitudinal fins is increasing. The increase in thickness at zone E is more prominent. However, the paraffin in between longitudinal fins is still in liquid phase, which demonstrate the low thermal conductivity of paraffin. Similarly, after discharging for 0.75 hr, it is observed that a mushy phase of paraffin is created at top position, whereas the thickness of solidified paraffin has increased around tubes and longitudinal fins. It shows that natural convection has an insignificant impact on solidification of paraffin, whereas conduction is the dominant mode of heat transfer. Further, after discharging for 1 hr, it can be verified that paraffin at top position at zone C is completely solidified, whereas the top positions of the other zones display mushy phase. Finally, after discharging for 1.25 hr, it can be noticed that paraffin at top position at all zones have entirely discharged latent portion of thermal energy and have phase transformed to solid.

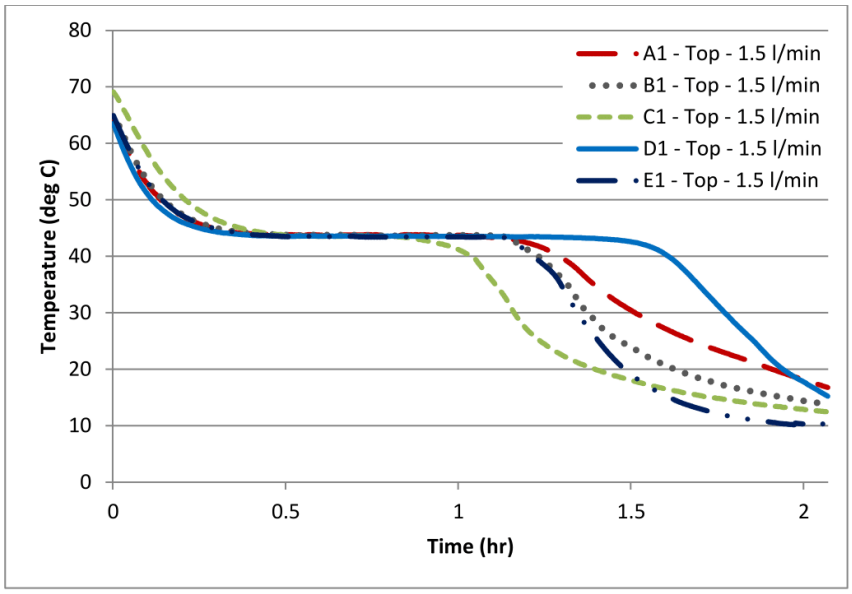

279

280 **Fig. 3** Illustration of transient temperature profiles recorded at top position at all five zones during discharging
281 process. Inlet temperature and volume flow rate of HTF are set to 10 °C and 1.5 l/min.

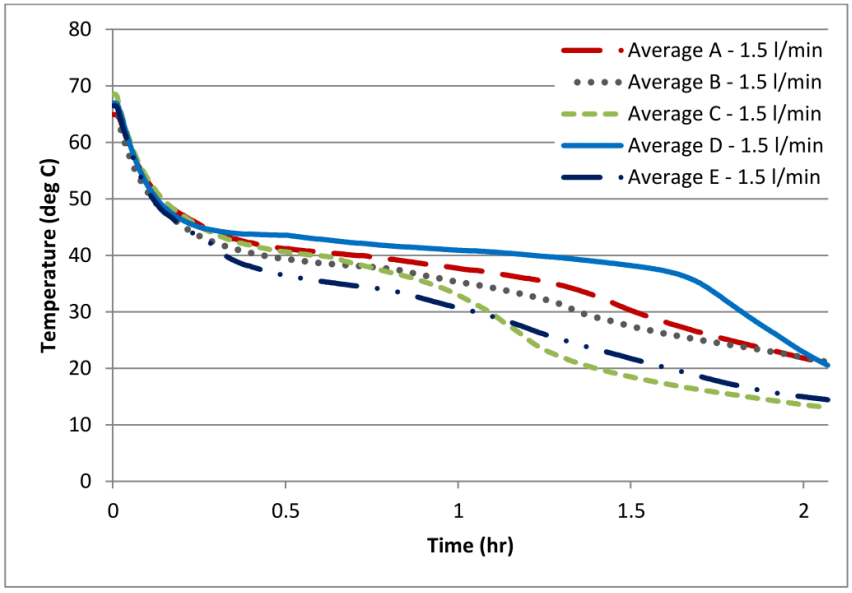

282

283 **Fig. 4** Time-wise variations in average temperature profiles obtained at all five zones during discharging cycle
284 at inlet temperature and volume flow rate of 10 °C and 1.5 l/min, respectively.

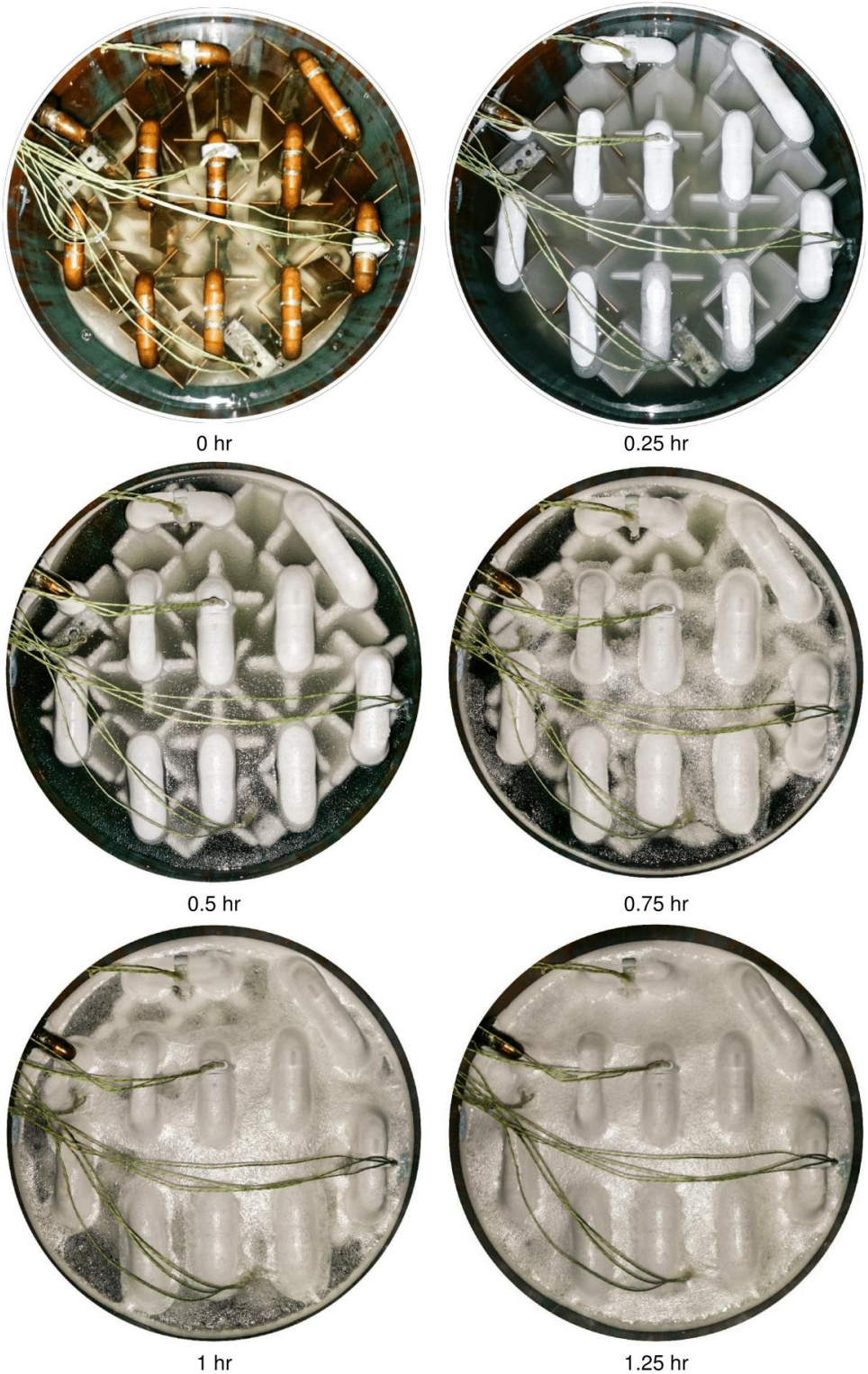

Fig. 5 Photographic illustrations of solidification front of paraffin in LHS unit during discharging cycle at inlet temperature and volume flow rate of 10 °C and 3 l/min, respectively.

3.2 Influence of Inlet Temperature

In order to investigate the effect of weather fluctuations on thermal behaviour of paraffin in LHS unit, a series of discharging cycle experiments are conducted at varied inlet temperatures of 5 °C, 10 °C and 15 °C. Whereas, the volume flow rate of HTF is set constant to 1.5 l/min. The transient temperature profiles of paraffin acquired from thermocouples installed at top, central and bottom positions within LHS unit are illustrated in **Fig. 6**. Similarly, the time-wise variations in outlet temperatures of HTF are registered, as presented in **Fig. 6**.

It is noticed from experimental investigations that inlet temperature of HTF has a significant impact on discharging rate of paraffin in LHS unit. As shown in **Fig. 6 (A)**, the transient temperature profiles of paraffin at top position at zone A display an identical thermal response to sensible portion of thermal energy discharge at varied inlet temperatures. Therefore, it is noted that inlet temperature of HTF has an insignificant effect on discharging of sensible portion of thermal energy. However, the discharging rate is noticeably influenced during latent portion of thermal energy discharge. The total solidification time for paraffin at inlet temperature of 15 °C is 1.38 hr. However, a higher temperature gradient can be generated by decreasing the inlet temperature of HTF. Therefore, the discharging rate is increased by 9.01 % and 17.43 % as the inlet temperature is decreased from 15 °C to 10 °C and 5 °C, respectively. Moreover, it can be observed that after solidification, the sensible portion of thermal energy discharge behave differently to varied inlet temperatures of HTF.

The influence of inlet temperature of HTF on transient temperature response of paraffin at central position at zone B and zone D are illustrated in **Fig. 6 (B)** and **Fig. 6 (E)**. It is evident that before solidification, the sensible portion of thermal energy discharge is almost identical for all inlet temperatures of HTF. However, the latent portion of thermal energy is discharged at higher rate by decreasing inlet temperature of HTF. The total solidification time required to discharge the latent portion of thermal energy at central position at zone B is 0.76, 0.88 and 1.06 hr for inlet temperature of 5 °C, 10 °C and 15 °C, respectively. Likewise, the discharging rate at central position at zone D is increased by 23.58% and 48.11% as the inlet temperature is decreased from 15 °C to 10 °C and 5 °C, respectively**.** After solidification, a linear identical decline in temperature profile is noticed. It shows that conduction is a dominant mode of heat transfer at central position of LHS unit.

Likewise, paraffin at top position at zone C indicates a significant enhancement in discharging rate, as shown in **Fig. 6 (D)**. It can be noticed that the discharging rate is increased by 20.36% and 32.95% as the inlet temperature is decreased from 15 °C to 10 °C and 5 °C, respectively. Likewise, paraffin at bottom position at zone D displays a significant reduction in solidification time, as presented in **Fig. 6 (F)**. The total solidification time is reduced by 9.18% and 16.41% as the inlet temperature is reduced to 10 °C and 5 °C, respectively. Similarly, paraffin at top position at zone E exhibits improvement in discharging rate, as shown in **Fig. 6 (G)**. It can be noticed that an enhancement of 12.37% and 28.04% is recorded by decreasing inlet temperature to 10 °C and 5 °C, respectively. The total solidification time of paraffin at various positions in LHS unit at varied inlet temperatures are presented in **Table 3**.

Inlet temperature of HTF has a notable impact on outlet temperature of HTF, as shown in **Fig. 6 (H)**. Due to decrease in inlet temperature of HTF, the temperature gradient between paraffin and HTF is magnified and therefore an enhanced discharge rate is obtained, which results in high temperature output of HTF for a short interval of time. However, with an increase in inlet temperature of HTF, the temperature gradient is reduced and thus a high temperature output is generated for a long period of time. Therefore, it can be predicted that by further increasing the inlet temperature of HTF during

discharging cycle, a high temperature output of HTF can be achieved for a longer span of time, which can be utilised for number of domestic or commercial applications.

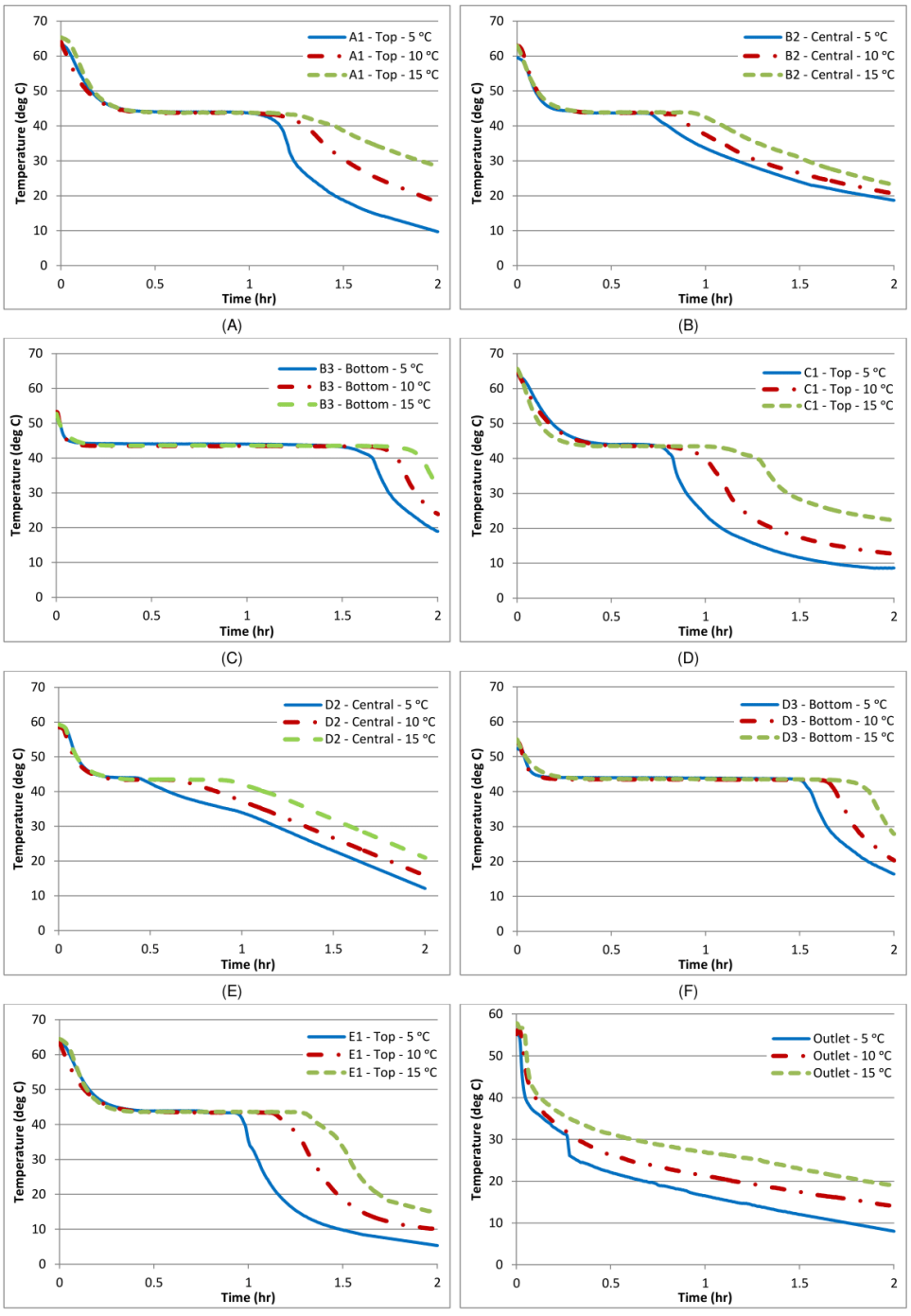

Fig. 6 Time-wise variation in temperature profile registered at top position (zone A, C and E), central position (zone B and D), bottom position (zone B and D) and outlet of LHS unit during discharging cycles at various inlet temperatures (5 °C, 10 °C and 15 °C) and constant volume flow rate of 1.5 l/min.

Table 3
Total solidification time recorded for varied inlet temperatures

Fig. No	Thermocouple		Inlet Temperature		
	Zone	Position	5 °C	10 °C	15 °C
Fig. 6 (A)	A	Top	1.14 hr	1.26 hr	1.38 hr
Fig. 6 (B)	B	Central	0.76 hr	0.88 hr	1.06 hr
Fig. 6 (C)	B	Bottom	1.63 hr	1.76 hr	1.89 hr
Fig. 6 (D)	C	Top	0.81 hr	0.97 hr	1.21 hr
Fig. 6 (E)	D	Central	0.55 hr	0.81 hr	1.06 hr
Fig. 6 (F)	D	Bottom	1.54 hr	1.68 hr	1.84 hr
Fig. 6 (G)	E	Top	0.97 hr	1.18 hr	1.35 hr

3.3 Influence of Flow Rate

To examine the influence of volume flow rate of HTF on heat transfer rate and solidification time of paraffin in LHS unit, experimental tests are conducted at constant temperature of 10 °C and four varied volume flow rates of 1.5, 2, 2.5 and 3 l/min. The time-wise variations in temperature profiles are obtained from thermocouples installed at top position at all five zones and outlet of HTF from LHS unit, as illustrated in **Fig. 7**.

As discussed in **section 3.1**, the discharging cycle of paraffin is composed of three phases. In initial phase, the sensible portion of thermal energy is discharged rapidly due to higher temperature gradient between HTF and paraffin. Natural convection is dominating the initial stage of discharging cycle and thus, the temperature drop of paraffin is fast. In second phase, the latent portion of thermal energy is discharged at almost isothermal temperature. During this phase, the phase transition from liquid to solid takes place and thus, the natural convection is weakened and conduction is the dominant mode of heat transfer. However, due to formation of solidified paraffin around tubes and longitudinal fins, the overall thermal resistance offered by paraffin is increased which effects the heat transfer rate. Therefore, it is noticed that latent portion of thermal energy is gradually discharged. In third phase, the sensible portion of thermal energy in solid phase is discharged which is dominated by conduction heat transfer. Similarly, it can be noticed from **Fig. 7** that initial sensible phase of thermal energy discharge is not affected by volume flow rate. However, the latent portion of thermal energy discharge is noticeably influenced.

Paraffin at top position at zone A has demonstrated an obvious enhancement in discharging rate and reduction in solidification time, as presented in **Fig. 7 (A)**. The total solidification time is reduced by a fraction of 9.03%, 14.98% and 28.19% as the volume flow rate is increased from 1.5 l/min to 2, 2.5 and 3 l/min, respectively. Likewise, paraffin at top position at zone B has illustrated an increase in discharge rate by a fraction of 7.16%, 11.55% and 21.01%, as shown in **Fig. 7 (B)**. Similarly, the solidification time for paraffin at top position at zone C is reduced by 11.04%, 21.22% and 27.32% as the volume flow rate is increased from 1.5 l/min to 2, 2.5 and 3 l/min, as presented in **Fig. 7 (C)**. Also, an enhancement in discharging rate is noticed for paraffin at top position at zone D, as illustrated in **Fig. 7 (D)**. The discharging rate is improved by a fraction of 10.72%, 16.52% and 27.76% as the volume flow rate is increased. Moreover, the improvement in heat transfer rate is observed for paraffin at top position at zone E, as shown in **Fig. 7 (E)**. Due to enhanced heat transfer rate, the solidification time is reduced by 6.76%, 13.05% and 19.81%, respectively.

It is evident that in case of constant inlet temperature of HTF, the heat transfer rate can be significantly influenced by varying volume flow rate of HTF and consequently, the discharging rate of

paraffin in LHS unit can be influenced. With an increase in volume flow rate of HTF, the discharging time is reduced. It is due to the fact that by increasing volume flow rate, the amount of thermal energy carried away by HTF is also increased. Therefore, the rapid decline in output temperature of HTF is noticed, as shown in **Fig. 7 (F)**. However, in order to maintain a higher outlet temperature of HTF for longer period of time, a small volume flow rate is recommended. In practical applications, the volume flow rate should be regulated to application based demands of outlet temperature and duration of discharge time.

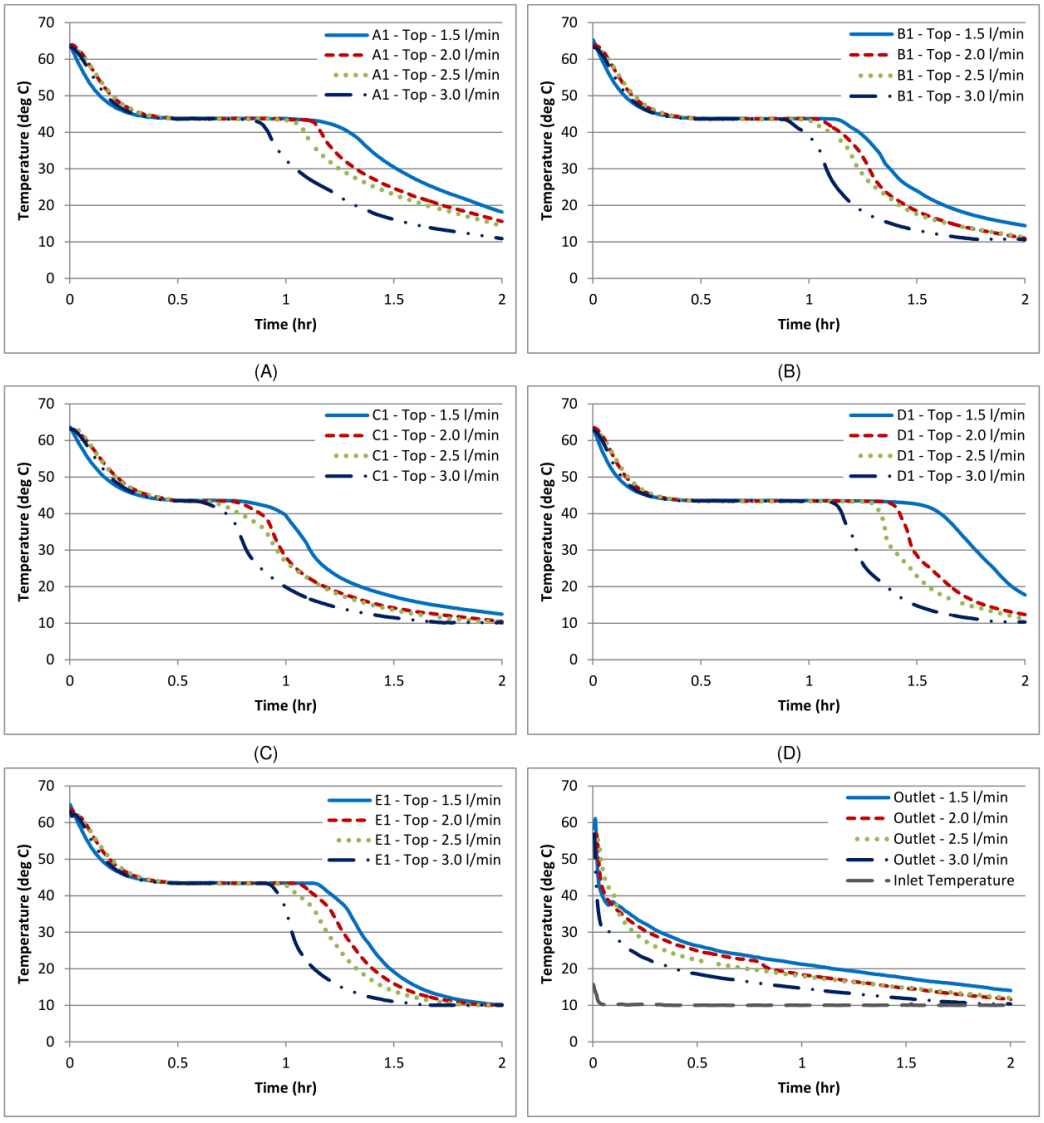

Fig. 7 Transient temperature variations recorded at top position at all five zones and outlet of LHS unit while conducting discharging cycles at four varied volume flow rates of 1.5, 2.0, 2.5 and 3.0 l/min and constant inlet temperature of 10 °C.

3.4 Energy Discharge and Mean Power

In order to investigate the thermal performance of paraffin in longitudinal fins based LHS unit during discharging cycles, the accumulative thermal energy discharge to HTF and mean discharge power of LHS system are calculated. To calculate thermal energy discharge by paraffin to HTF and mean discharge power, the following relations are implemented:

$$Q_{dis} = \sum \rho_{avg} \left(\frac{c_{p,in} + c_{p,out}}{2} \right) \left(T_{HTF,out} - T_{HTF,in} \right) \dot{V} \Delta t \quad (1)$$

$$P_{dis} = \frac{Q_{dis}}{t_{dis}} \quad (2)$$

where Q_{dis}, ρ_{avg}, c_p, T_{HTF}, $\dot{V}$ and Δt represent the measure of thermal energy discharge to HTF (kJ), average density of HTF (kg/m^3), specific heat capacity of HTF (kJ/kg. K), temperature of HTF (^{o}C), volume flow rate of HTF (m^3/sec) and time interval to record temperature data (sec), respectively. Likewise, P_{dis} represents the mean discharge power of LHS unit (kW) and t_{dis} is the total time elapsed by discharging cycle (sec).

Transient variations in thermal energy discharge to HTF is registered by conducting discharge cycles at constant inlet temperature of 10 ^{o}C and varied volume flow rates of 1.5, 2, 2.5 and 3 l/min, as illustrated in **Fig. 8**. It can be observed that volume flow rate has a significant impact on discharging rate of thermal energy to HTF. Due to higher temperature gradient at start of discharging cycle, the rate of accumulative thermal energy gain by HTF is higher. However, the temperature gradient is reduced owing to extraction of thermal energy from paraffin. Hence, the rate of accumulative thermal energy gain by HTF is affected. Despite that, with an increase in volume flow rate of HTF, the resistance to convective heat transfer in HTF can be decreased and thus, the discharging rate can be enhanced. It is noticed that after 1.5 hr of discharging cycles, the accumulative thermal energy discharge to HTF is recorded as 10604.41 kJ, 11150.88 kJ, 11521.10 kJ and 12055.03 kJ for volume flow rate of 1.5, 2, 2.5 and 3 l/min, respectively. Similarly, in order to discharge equal amount of thermal energy (12094.34 kJ), the required time is reduced by 24% as the volume flow rate is increased from 1.5 to 3 l/min.

The impact of inlet temperature and volume flow rate on mean discharge power of LHS unit is illustrated in **Fig. 9**. It can be observed that during inlet temperature of 15 ^{o}C, the increase in mean power is almost linear with an increase in volume flow rate. The discharge power is enhanced by 18.24%, 33.58% and 49.75% by increasing volume flow rate from 1.5 to 2, 2.5 and 3 l/min, respectively. Likewise, for inlet temperature of 10 ^{o}C, the discharge power is increased by 6.85%, 13.47% and 26.49%, respectively. Similarly, for inlet temperature of 5 ^{o}C, the discharge power is improved by 7.31%, 17.98% and 33.70%, respectively. Moreover, it can be noticed that inlet temperature also significantly influences the mean discharge power. For instance, at constant volume flow rate of 1.5, the discharge power is increased by 28.39% and 36.05% as the inlet temperature is decreased from 15 ^{o}C to 10 ^{o}C and 5 ^{o}C, respectively. Similarly, at flow rate of 3 l/min, the discharge power is increased from 1.959 kW to 2.125 and 2.38 kW, respectively. By regulating inlet temperature and volume flow rate of HTF, the desired output temperature and power demand can be achieved in practical applications.

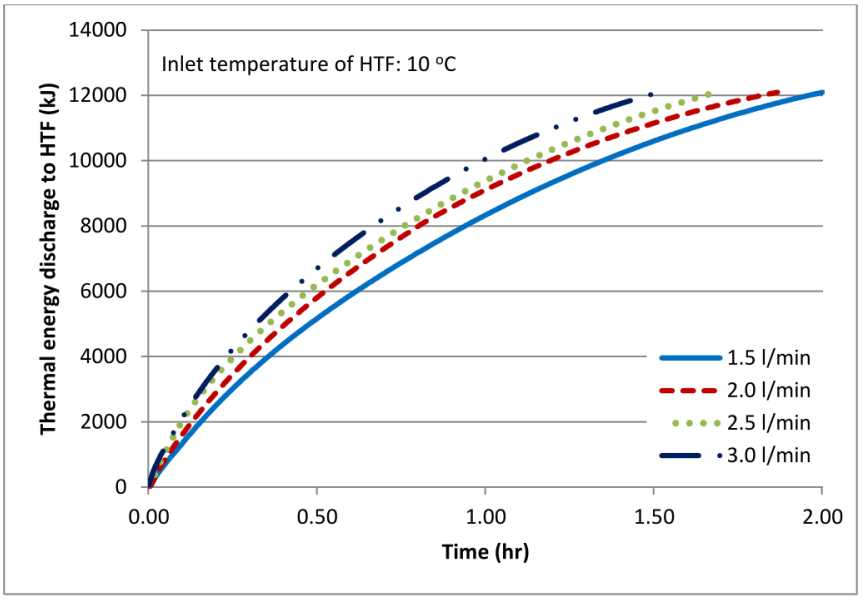

420

421 **Fig. 8** Transient variation in accumulative thermal energy gain by HTF during discharging cycles at constant
422 inlet temperature of 10 °C and four different volume flow rates of 1.5, 2.0, 2.5 and 3.0 l/min.

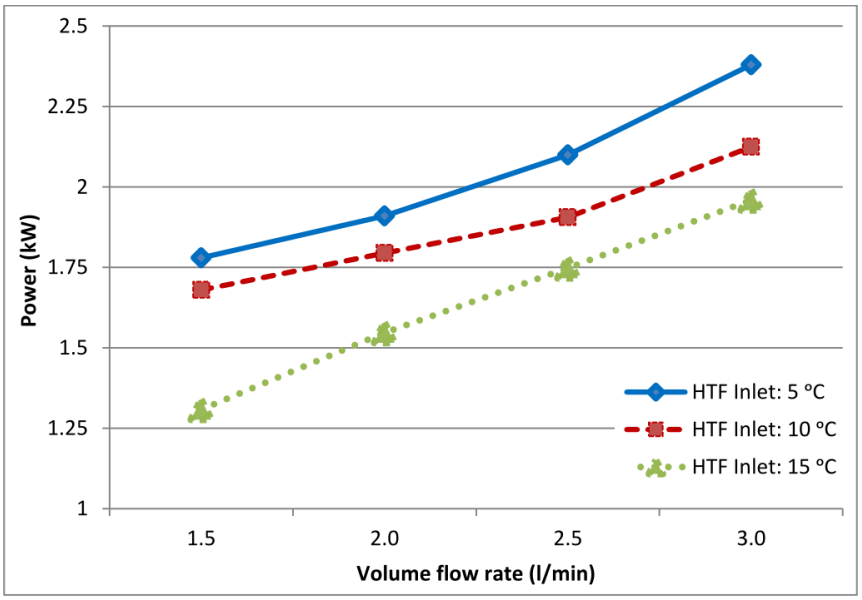

423

424 **Fig. 9** Influence of volume flow rate and inlet temperature of HTF on mean discharging power of LHS unit.

Furthermore, the results indicate that the discharge rate, accumulative thermal energy discharge and mean discharge power of our proposed LHS system is considerably higher as compared to LHS systems discussed in previous literature, as presented in **Table 4**. It can be noticed that none of the previously reported models could match the rapid solidification time (1.5 hr), accumulative thermal energy discharge (12 MJ) and mean discharge power (2.125 kW) of our proposed LHS system.

Table 4
Comparative thermal enhancement achieved by present study

	Discharge		
Ref No.	Time (hr)	Energy (kJ)	Power (kW)
[24]	12.5	575	-
[28]	8.67	772.4	0.025
[30]	0.56	80	-
[31]	18.35	1200	0.02
[32]	0.506	490	0.269
[33]	4.2	-	0.325
[40]	2.31	-	1
[41]	22	7500	0.1
[42]	1.67	7293.1	-
[42]	2.167	8813.1	-
Present study	1.5	12000	2.125

4. Conclusions

In this article, the experimental investigations of discharging cycles of paraffin in LHS unit are presented. LHS unit is comprised of shell and tube with longitudinal fins based heat exchanger and paraffin as thermal storage material. Water is employed as HTF and is channelled to pass through the tubes of LHS unit to extract thermal energy from paraffin. The discharging cycles are conducted at various operating conditions of inlet temperature and flow rate of HTF. The following conclusions are drawn from experimental investigations of discharging cycles:

- Due to inclusion of longitudinal fins, the effective surface area for heat transfer is enhanced and hence the impact of low thermal conductivity of paraffin on discharging cycle of LHS unit is significantly decreased. Consequently, the discharging rate is significantly improved. The novel geometrical orientation of shell and tube with longitudinal fins based LHS unit qualifies as an efficient and responsive thermal energy storage/discharge device. For instance, the novel LHS unit can discharge 12 MJ of thermal energy to HTF in 1.5 hours when it is discharged at inlet temperature and volume flow rate of 10 ^{o}C and 3 l/min, respectively.
- It is noticed that natural convection has minimal impact on discharging rate. However, due to presence of extended surfaces via longitudinal fins, conduction heat transfer is dominant mode for thermal energy discharge. Moreover, it is noticed that conduction is more prominent at central positon as compared to top and bottom positions of LHS unit. Heat transfer rate is relatively weaker at bottom position and therefore, the solidification time for paraffin at bottom position is higher as compared to central and top position.
- Discharging cycle involves three phases of paraffin. Initially, the sensible portion (liquid phase) of thermal energy is rapidly discharged due to higher temperature gradient. Secondly, during latent portion of thermal energy discharge, a rather steady and gradual reduction in temperature

454 is noticed due to high latent heat capacity of paraffin. Likewise, the formation of solidified
455 paraffin around tubes and longitudinal fins increase the overall thermal resistance, which
456 affects the discharging rate. Finally, due to low temperature gradient, the sensible portion (solid
457 phase) of thermal energy discharge is relatively slow as compared sensible portion of liquid
458 phase.

459 • It is observed that inlet temperature and volume flow rate of HTF have significant influence on
460 latent portion of thermal energy discharge. The influence of an increase in overall thermal
461 resistance can be controlled by adjusting inlet temperature or volume flow rate of HTF. It is
462 noticed that as the inlet temperature of HTF is decreased from 15 ^{o}C to 5 ^{o}C, the mean
463 discharge power is enhanced by 36.05%. This is due to the fact that with an increase in
464 temperature gradient, the conduction heat transfer overcomes the overall thermal resistance of
465 paraffin. Likewise, with an increase in volume flow rate from 1.5 l/min to 3 l/min, the
466 solidification time at constant inlet temperature of 10 ^{o}C is reduced by 24% to discharge same
467 amount of thermal energy 12.09 MJ. Moreover, in case of constant inlet temperature as 5 ^{o}C
468 and 15 ^{o}C, the mean discharge power can be enhanced by 33.70% and 49.75% by increasing
469 volume flow rate from 1.5 l/min to 3 l/min, respectively.

470 • It is deduced that by adjusting inlet temperature and volume flow rate, the required output
471 temperature and mean power can be achieved in practical applications. Likewise, the novel
472 LHS unit offers time, spatial and economic benefits. Moreover, in order to meet application
473 based energy demands, the mean power and thermal storage capacity can be augmented by
474 connecting several LHS units in parallel. Therefore, the LHS unit can be perfectly employed in
475 various domestic and commercial applications such as heating, ventilation and air conditioning
476 (HVAC) systems, water heating systems, waste heat recovery and solar power plants etc.

477

478 **5. Acknowledgement**

479 The authors would like to appreciate and acknowledge Bournemouth University, UK and National
480 University of Sciences and Technology (NUST), Pakistan to support and sponsor for conducting this
481 research.

482 **References**

483 [1] M.Z. Jacobson. Review of solutions to global warming, air pollution, and energy security. Energy
484 & Environmental Science. 2 (2009) 148-73.
485 [2] S. Suranovic. Fossil fuel addiction and the implications for climate change policy. Global
486 Environmental Change. 23 (2013) 598-608.
487 [3] International Energy Agency (IEA). Energy and Climate Change 21st UN Conference of the Parties
488 (COP21), Paris, 2015.
489 [4] J.P. da Cunha, P. Eames. Thermal energy storage for low and medium temperature applications
490 using phase change materials–a review. Applied Energy. 177 (2016) 227-38.
491 [5] M.M. Farid, A.M. Khudhair, S.A.K. Razack, S. Al-Hallaj. A review on phase change energy storage:
492 materials and applications. Energy conversion and management. 45 (2004) 1597-615.
493 [6] A. Sharma, V.V. Tyagi, C. Chen, D. Buddhi. Review on thermal energy storage with phase change
494 materials and applications. Renewable and Sustainable energy reviews. 13 (2009) 318-45.
495 [7] N. Soares, J. Costa, A. Gaspar, P. Santos. Review of passive PCM latent heat thermal energy
496 storage systems towards buildings' energy efficiency. Energy and buildings. 59 (2013) 82-103.
497 [8] Y. Tian, C.-Y. Zhao. A review of solar collectors and thermal energy storage in solar thermal
498 applications. Applied Energy. 104 (2013) 538-53.
499 [9] A. Waqas, Z.U. Din. Phase change material (PCM) storage for free cooling of buildings—a review.
500 Renewable and sustainable energy reviews. 18 (2013) 607-25.
501 [10] L. Miró, J. Gasia, L.F. Cabeza. Thermal energy storage (TES) for industrial waste heat (IWH)
502 recovery: a review. Applied Energy. 179 (2016) 284-301.
503 [11] A. Modi, F. Bühler, J.G. Andreasen, F. Haglind. A review of solar energy based heat and power
504 generation systems. Renewable and Sustainable Energy Reviews. 67 (2017) 1047-64.
505 [12] A. Shukla, K. Kant, A. Sharma. Solar Still with latent heat energy storage: A review. Innovative
506 Food Science & Emerging Technologies. (2017).
507 [13] L.F. Cabeza, A. Castell, C.d. Barreneche, A. De Gracia, A. Fernández. Materials used as PCM in
508 thermal energy storage in buildings: a review. Renewable and Sustainable Energy Reviews. 15 (2011)
509 1675-95.
510 [14] Z. Khan, Z. Khan, A. Ghafoor. A review of performance enhancement of PCM based latent heat
511 storage system within the context of materials, thermal stability and compatibility. Energy
512 Conversion and Management. 115 (2016) 132-58.
513 [15] S. Jegadheeswaran, S.D. Pohekar. Performance enhancement in latent heat thermal storage
514 system: a review. Renewable and Sustainable Energy Reviews. 13 (2009) 2225-44.
515 [16] L. Fan, J.M. Khodadadi. Thermal conductivity enhancement of phase change materials for
516 thermal energy storage: a review. Renewable and Sustainable Energy Reviews. 15 (2011) 24-46.
517 [17] P.B. Salunkhe, P.S. Shembekar. A review on effect of phase change material encapsulation on
518 the thermal performance of a system. Renewable and Sustainable Energy Reviews. 16 (2012) 5603-
519 16.
520 [18] J. Khodadadi, L. Fan, H. Babaei. Thermal conductivity enhancement of nanostructure-based
521 colloidal suspensions utilized as phase change materials for thermal energy storage: a review.
522 Renewable and Sustainable Energy Reviews. 24 (2013) 418-44.
523 [19] N.S. Dhaidan, J. Khodadadi. Melting and convection of phase change materials in different
524 shape containers: A review. Renewable and Sustainable Energy Reviews. 43 (2015) 449-77.
525 [20] C. Liu, Z. Rao, J. Zhao, Y. Huo, Y. Li. Review on nanoencapsulated phase change materials:
526 Preparation, characterization and heat transfer enhancement. Nano Energy. 13 (2015) 814-26.
527 [21] J. Giro-Paloma, M. Martínez, L.F. Cabeza, A.I. Fernández. Types, methods, techniques, and
528 applications for microencapsulated phase change materials (MPCM): a review. Renewable and
529 Sustainable Energy Reviews. 53 (2016) 1059-75.
530 [22] L. Liu, D. Su, Y. Tang, G. Fang. Thermal conductivity enhancement of phase change materials for
531 thermal energy storage: A review. Renewable and Sustainable Energy Reviews. 62 (2016) 305-17.

[23] F. Agyenim, N. Hewitt, P. Eames, M. Smyth. A review of materials, heat transfer and phase change problem formulation for latent heat thermal energy storage systems (LHTESS). Renewable and sustainable energy reviews. 14 (2010) 615-28.
[24] S. Seddegh, X. Wang, M.M. Joybari, F. Haghighat. Investigation of the effect of geometric and operating parameters on thermal behavior of vertical shell-and-tube latent heat energy storage systems. Energy. (2017).
[25] M.Y. Yazici, M. Avci, O. Aydin, M. Akgun. On the effect of eccentricity of a horizontal tube-in-shell storage unit on solidification of a PCM. Applied Thermal Engineering. 64 (2014) 1-9.
[26] S. Seddegh, X. Wang, A.D. Henderson. A comparative study of thermal behaviour of a horizontal and vertical shell-and-tube energy storage using phase change materials. Applied Thermal Engineering. 93 (2016) 348-58.
[27] M. Longeon, A. Soupart, J.-F. Fourmigué, A. Bruch, P. Marty. Experimental and numerical study of annular PCM storage in the presence of natural convection. Applied energy. 112 (2013) 175-84.
[28] M. Hosseini, M. Rahimi, R. Bahrampoury. Experimental and computational evolution of a shell and tube heat exchanger as a PCM thermal storage system. International Communications in Heat and Mass Transfer. 50 (2014) 128-36.
[29] M. Avci, M.Y. Yazici. Experimental study of thermal energy storage characteristics of a paraffin in a horizontal tube-in-shell storage unit. Energy conversion and management. 73 (2013) 271-7.
[30] W.-W. Wang, K. Zhang, L.-B. Wang, Y.-L. He. Numerical study of the heat charging and discharging characteristics of a shell-and-tube phase change heat storage unit. Applied Thermal Engineering. 58 (2013) 542-53.
[31] A. Agarwal, R. Sarviya. An experimental investigation of shell and tube latent heat storage for solar dryer using paraffin wax as heat storage material. Engineering Science and Technology, an International Journal. 19 (2016) 619-31.
[32] Z. Meng, P. Zhang. Experimental and numerical investigation of a tube-in-tank latent thermal energy storage unit using composite PCM. Applied Energy. 190 (2017) 524-39.
[33] Y. Wang, L. Wang, N. Xie, X. Lin, H. Chen. Experimental study on the melting and solidification behavior of erythritol in a vertical shell-and-tube latent heat thermal storage unit. International Journal of Heat and Mass Transfer. 99 (2016) 770-81.
[34] J. Liu, C. Xu, X. Ju, B. Yang, Y. Ren, X. Du. Numerical investigation on the heat transfer enhancement of a latent heat thermal energy storage system with bundled tube structures. Applied Thermal Engineering. 112 (2017) 820-31.
[35] A.A.R. Darzi, M. Jourabian, M. Farhadi. Melting and solidification of PCM enhanced by radial conductive fins and nanoparticles in cylindrical annulus. Energy Conversion and Management. 118 (2016) 253-63.
[36] Z. Li, Z.-G. Wu. Analysis of HTFs, PCMs and fins effects on the thermal performance of shell–tube thermal energy storage units. Solar Energy. 122 (2015) 382-95.
[37] M.K. Rathod, J. Banerjee. Thermal performance enhancement of shell and tube Latent Heat Storage Unit using longitudinal fins. Applied thermal engineering. 75 (2015) 1084-92.
[38] C. Liu, D. Groulx. Experimental study of the phase change heat transfer inside a horizontal cylindrical latent heat energy storage system. International Journal of Thermal Sciences. 82 (2014) 100-10.
[39] A.A. Al-Abidi, S. Mat, K. Sopian, M. Sulaiman, A.T. Mohammad. Numerical study of PCM solidification in a triplex tube heat exchanger with internal and external fins. International journal of heat and mass transfer. 61 (2013) 684-95.
[40] S. Almsater, A. Alemu, W. Saman, F. Bruno. Development and experimental validation of a CFD model for PCM in a vertical triplex tube heat exchanger. Applied Thermal Engineering. 116 (2017) 344-54.
[41] M. Kabbara, D. Groulx, A. Joseph. Experimental investigations of a latent heat energy storage unit using finned tubes. Applied Thermal Engineering. 101 (2016) 601-11.

582 [42] F. Agyenim, P. Eames, M. Smyth. A comparison of heat transfer enhancement in a medium
583 temperature thermal energy storage heat exchanger using fins. Solar Energy. 83 (2009) 1509-20.
584 [43] S. Lohrasbi, M. Gorji-Bandpy, D.D. Ganji. Thermal penetration depth enhancement in latent heat
585 thermal energy storage system in the presence of heat pipe based on both charging and discharging
586 processes. Energy Conversion and Management. 148 (2017) 646-67.
587 [44] A. Caron-Soupart, J.-F. Fourmigué, P. Marty, R. Couturier. Performance analysis of thermal
588 energy storage systems using phase change material. Applied Thermal Engineering. 98 (2016) 1286-
589 96.
590 [45] Z. Khan, Z. Khan, K. Tabeshf. Parametric investigations to enhance thermal performance of
591 paraffin through a novel geometrical configuration of shell and tube latent thermal storage system.
592 Energy Conversion and Management. 127 (2016) 355-65.
593 [46] Z. Khan, Z.A. Khan. Experimental investigations of charging/melting cycles of paraffin in a novel
594 shell and tube with longitudinal fins based heat storage design solution for domestic and industrial
595 applications. Applied Energy. (2017).
596 [47] Rubitherm® Technologies GmbH, http://www.rubitherm.eu/en/. 2017.

597

Paper VI

Experimental and numerical investigations of nano-additives enhanced paraffin in a shell and tube heat exchanger: a comparative study

Zakir Khan [a], Zulfiqar Ahmad Khan [a*]

[a] Bournemouth University, Department of Design & Engineering, NanoCorr, Energy and Modelling (NCEM) Research Group, Fern Barrow, Talbot Campus, Poole, Dorset BH12 5BB, UK.

E-mail: zkhan2@bournemouth.ac.uk

Corresponding Author:

[a*] Bournemouth University, Department of Design & Engineering, NanoCorr, Energy and Modelling (NCEM) Research Group, Fern Barrow, Talbot Campus, Poole, Dorset BH12 5BB, UK.

E-mail: zkhan@bournemouth.ac.uk

Tel.: +44 1202-961645

Abstract

The impact of metal oxides, metal nitrides and carbon allotropes based nano-additives on thermal conductivity and thermal storage performance of paraffin based latent heat storage (LHS) system is experimentally and numerically investigated. Aluminium oxide (Al_2O_3), aluminium nitride (AlN) and graphene nano-platelets (GnP) based nano-PCM samples are prepared with ultrasonic emulsification technique. Thermal performance enhancements of nano-PCM samples are investigated by conducting a series of charging and discharging experiments in shell and tube heat exchanger at various operating conditions. Moreover, a numerical model is developed to account for an impact of varying operating temperature, nano-additives particle size and volume fraction on the effective thermal conductivity and dynamic viscosity of nano-PCM. The numerical model is simulated to investigate the influence of effective thermal conductivity and dynamic viscosity on heat transfer and temperature distribution, phase transition rate and total enthalpy of the system. It is observed that the charging time for Al_2O_3, AlN and GnP based nano-PCM samples is significantly reduced by a fraction of 28.01%, 36.47% and 44.57% as compared to pure paraffin. Likewise, the discharging time is reduced by a fraction of 14.63%, 34.95% and 41.46%, respectively. However, the addition of nano-additives compromises the overall thermal storage capacity of LHS system. It is recorded that as compared to pure paraffin, the total enthalpy of the system is reduced by 20.58%, 19.64% and 2.88% for 5% volume fraction of Al_2O_3, AlN and GnP based nano-PCM samples, respectively. Also, an increase in volume fraction of nano-additives augments the dynamic viscosity which has an adverse impact on natural convection. Therefore, an optimum volume fraction of nano-additives is essential for an ideal enhancement in thermal performance of LHS system. In order to identify an optimum volume fraction of nano-additives, three Al_2O_3 based nano-PCM samples with volume fraction of 1%, 3% and 5% are experimentally examined in shell and tube heat exchanger at varied operating conditions. It is noted that the charging and discharging rate is significantly enhanced as the volume fraction is increased from 1% to 3%. However, an insignificant improvement is noticed for an increase in volume fraction from 3% to 5%. Therefore, the optimum volume fraction of 3% is established. Moreover, it is concluded that due to relatively smaller particle size, smaller density and higher thermal conductivity of GnP nano-additives, the effective thermal conductivity, charging/discharging rate and overall enthalpy of GnP based nano-PCM samples are considerably higher as compared to Al_2O_3 and AlN based nano-PCM samples.

Keywords

Thermal energy storage, Latent heat storage, Phase change materials, Thermal conductivity enhancement, Nano-PCM, Shell and tube heat exchanger

Nomenclature

C_p	specific heat capacity at constant pressure (kJ / kg. K)	ρ	density (kg / m^3)
d	diameter (m)	δ_{VF}	volume fraction of nano-additives
$\mathbf{F}$	buoyant force term (N / m^3)	μ	dynamic viscosity (kg / m. s)
g	gravitational acceleration (m / s^2)	ϕ	fraction of nano-PCM
k	thermal conductivity (W / m. K)	ψ	mushy zone constant
k_B	Boltzmann constant	Subscripts	
L	latent heat capacity (kJ / kg)	s	solidus phase
M_W	molecular weight	l	liquidus phase
N_A	Avogadro number	pc	phase change
Pr	Prandtl number of base material	np	nano-additives
p	pressure (N / m^2)	pcm	base material
q	heat source term (W / m^3)	$npcm$	nano-PCM
Re	Reynolds number of nano-additives	Acronyms	
S	momentum sink term	Al_2O_3	aluminium oxide
T	temperature of nano-PCM (^{o}C)	AlN	aluminium nitride
t	time (s)	GnP	graphene nano-platelets
$\mathbf{u}$	velocity (m / s)	HTF	heat transfer fluid
Greek		LHS	latent heat storage
α	small constant value	PCM	phase change material
β	thermal expansion coefficient (1 / ^{o}C)	TES	thermal energy storage

1. Introduction

The rapid increase in energy demands to meet world economic developments have escalated dependency on fossil fuels. The energy and fuel crisis along with environmental pollutions and climate change due to extensive usage of fossil fuels to meet industrial and domestic energy demands have raised serious challenges [1, 2]. To mitigate such serious concerns, the development in functional technologies for renewable energy sources or heat recovery systems is imperative to minimise the gap between energy demand and supply. Thermal energy storage (TES) is considered as a decisive technique to store excess thermal energy and utilise it at times to balance energy demand and supply. Latent heat storage (LHS) approach is more attractive category of TES system due to its higher thermal storage capacity and ability to an almost isothermal energy capture and release [3, 4]. LHS system employs phase change materials (PCM) to store and release thermal energy during phase change. LHS systems are integrated with numerous practical applications ranging from solar power plants, waste heat recovery systems, buildings temperature control systems, heating and air conditioning systems, energy balancing and peak shaving management systems, agricultural processing and drying [5-10]. However, due to low thermal conductivity of PCM, the charging and discharging rates of LHS systems are significantly affected, which hinders the widespread practical employability of LHS systems [11, 12]. Therefore, researchers have proposed several techniques to improve overall thermal performance of LHS systems which are: container geometrical orientation, addition of extended surfaces, incorporation of thermal conductive additives and encapsulation techniques [13-18].

Shell and tube heat exchanger based LHS systems are extensively studied in previous literature due to their better heat transfer performance, minimal thermal losses, design simplicity and easier integration to practical applications. Similarly, extended surfaces are widely adopted for thermal performance enhancement due to their better thermo-physical stability and cost effectiveness. Rathod and Banerjee [19] experimentally investigated the augmentation in charging and discharging rate of stearic acid in shell and tube heat exchanger without and with three longitudinal fins. It was informed that the inclusion of longitudinal fins reduced the charging and discharging time by 24.52% and 43.6% as compared to no fins configuration. Likewise, Rabienataj Darzi et al. [20] numerically examined the enhancement in charging and discharging rate of n-eicosane in shell and tube heat exchanger with and without longitudinal fins. It was reported that with an increase in number of longitudinal fins from 4 to 20, the melting and solidification rate was enhanced by 39-82% and 28–85% as compared to no fins configuration, respectively. Similarly, the phase transition rate and thermal storage capacity of paraffin is numerically examined in a novel geometrical orientation of shell and tube heat exchanger with longitudinal fins in [21]. It was discussed that the geometry and material of longitudinal fins had profound impact on charging rate of paraffin. It was reported that with an increase in fins length from 12.7 mm to 38.10 mm, the heat transfer was augmented and thus the melting rate was improved by 57.32%. Likewise, it was argued that charging rate and thermal storage capacity was improved by 68.8% and 18.06% as the inlet temperature was increased from 50 - 70 °C. Furthermore, this novel design was then developed and connected to flat plate solar collector to conduct experimental studies on charging and discharging cycles [22, 23]. It was noticed that as compared to shell and tube heat exchanger without extended fins orientations, the proposed design had displayed relatively higher charging/discharging rate, accumulative thermal energy charge/discharge and mean charge/discharge power. Besides

the extended surfaces technique, the inclusion of thermal conductive additives technique is largely acknowledged as an alternate solution to enhance thermal performance with relatively smaller increase in weight of the system.

Venkitaraj et al. [24] examined the influence of aluminium oxide (Al_2O_3) nano-particles on thermal performance of pentaerythritol. It was deduced that with an increase in mass fraction of Al_2O_3 from 0.1% to 1%, the effective thermal conductive was increased from 18.11% to 51.79% as compared to without nano-particle case. Moreover, the specific heat capacity and latent heat was reported to be decreased from 1.65% to 5.25% and from 1.45% to 4.60%, respectively. Similarly, Tang et al. [25] investigated the thermal performance enhancement of myristic acid with inclusion of Al_2O_3 and graphite nano-particles. It was reported that with an increase in mass fraction from 4% – 12%, the thermal conductivity was improved from 0.283 – 0.397 W/m.K for Al_2O_3 and 0.323 – 0.451 W/m.K for graphite based PCM composite. However, the latent heat capacity was recorded to be reduced from 122.87 – 109.45 kJ/kg for Al_2O_3 and 112.35 – 88.00 kJ/kg for graphite based composite. Harikrishnan et al. [26] experimented the improvement in thermal conductivity of lauric acid and stearic acid (LA/SA) mixture as base material with dispersion of 1 wt% of TiO_2, ZnO and CuO nano-particles. It was discussed that the thermal conductivity of LA/SA composite was improved by 34.85%, 46.97% and 62.12%, respectively.

Shi et al. [27] reported that thermal conductivity of paraffin was augmented by 10 times with inclusion of 10 wt% of exfoliated graphite nano-platelets. Likewise, Yu et al. [28] inspected the enhancement in thermal performance of paraffin wax with inclusion of short and long multi-walled carbon nanotubes (MWCNT), carbon nanofibers and graphene nano-platelets (GnP). It was discussed that GnP based paraffin composite had elaborated relatively higher thermal conductivity. Likewise, the dynamic viscosity was reported to be increased to 800 mPa.s for short/long MWCNT, 40 mPa.s for carbon nanofibers and 11.5 mPa.s for GnP based paraffin composites as compared to 5.892 mPa.s for paraffin wax. Likewise, Fan et al. [29] informed that the thermal conductivity of paraffin is improved by 164% with inclusion of 5 wt.% of GnP. Also, Yuan et al. [30] studied the impact of GnP and expanded graphite additives on thermal behaviour of palmitic-stearic acid mixture. It was observed that the thermal conductivity of composites was improved by 2.7 and 15.8 times as compared to base material. However, the latent heat capacity was reduced by 20.90% and 25.17%, respectively.

Wang et al. [31] conducted experimental analysis on thermal performance enhancement of polyethylene glycol with aluminium nitride (AlN). It was informed that with an increase in concentration from 5% – 30%, the thermal conductivity of composite was significantly improved from 0.3847 – 0.7661 W/m.K. It was also noticed that inclusion of AlN nano-particles had an insignificant impact on phase transition temperature. Zhang et al. [32] conducted thermal enhancement test on polymethyl methacrylate, polyethylene glycol and AlN nano-particles composite. The concentration of AlN nano-particles was ranged from 5 – 30 wt%. It was noticed that thermal conductivity was improved by 7.9% – 53.8%, respectively. However, the latent heat capacity was reduced from 168.5 kJ/kg for polyethylene glycol to 102.5 – 79.2 kJ/kg, respectively. Likewise, Fang et al. [33] reported that the thermal conductivity of paraffin wax was increased from 0.4 – 0.53 W/m.K by inclusion of 10 wt% of boron nitride. Similarly, Yang et al. [34] performed experimental investigation on paraffin and Si_3N_4 based composite. It was reported that thermal

conductivity was significantly enhanced by a fraction of 47% for 10 wt% composite. However, the latent heat capacity was observed to be reduced from 186.59 – 113.63 kJ/kg.

Arasu and Mujumdar [35] simulated Al_2O_3 nano-particles dispersed in paraffin wax in a square container. It was noticed that as the concentration of nano-additives increased, the dynamic viscosity was augmented which diminishes the impact of increased effective thermal conductivity on melting rate. Therefore, it was concluded that a smaller concentration of nano-additives should be adopted for thermal performance enhancement. Likewise, Mahdi and Nsofor [36] performed numerical examination of Al_2O_3 nano-particles based paraffin in a triplex-tube. It was reported that the solidification time was reduced from 8 – 20% as the volumetric concentration was increased from 3 – 8%, respectively. Moreover, Meng and Zhang [37] conducted experimental and numerical investigations on copper foam based paraffin in a rectangular tube in tank orientation. It was discussed that the charging and discharging power was significantly influenced by inlet temperature and flow rate of heat transfer fluid (HTF). Das et al. [38] conducted numerical simulation on n-eicosane and GnP composite in a vertical single tube in shell heat exchanger. It was concluded that for volumetric concentration of 2%, the melting time was shortened by 41% and 37% for inlet temperature of 60 ^oC and 70 ^oC, respectively.

It can be observed from previous literature that nano-additives based thermal performance enhancement can significantly improve the effective thermal conductivity of nano-PCM; however it will also augment the effective dynamic viscosity and reduce the overall thermal storage capacity. Also, it is noted that the inclusion of metal oxides, metal nitrides and carbon allotropes have presented excellent improvement in thermal conductivity, however the literature lacks a comparatively analysis of these three nano-additives families. It is also identified that the literature lacks an experimental and numerical examination of thermal performance enhancement of nano-PCM in an actual shell and tube heat exchanger. Moreover, it is perceived from the literature that the variation in dynamic viscosity with temperature and particle size of nano-additives had not been considered in previous numerical studies [35-38], which had certainly produced erroneous results.

This article is focused on the experimental and numerical investigations of metal oxides, metal nitrides and carbon allotropes based thermal performance enhancement of paraffin in a shell and tube heat exchanger. Thermal behaviour of nano-PCM samples are examined by conducting a series of charging and discharging cycles in shell and tube heat exchanger at various operating conditions. Moreover, this article proposes a numerical model that incorporates the operating temperature, particle size and volumetric concentration of nano-additives while calculating the effective thermal conductivity and dynamic viscosity of nano-PCM. The experimental and numerical studies are focused on identifying the impact of varying effective thermal conductivity and dynamic viscosity of nano-PCM on temperature distribution, liquid fraction, charging/discharging rate and overall enthalpy of the system. The experimental and numerical results discuss the significant enhancement achieved by the three types of nano-additives and identify an optimum volume concentration value to achieve an appropriate thermal performance.

2. Experimental

2.1 Materials and Nano-PCM samples preparation

In this article, paraffin (RT44HC) is selected as base material for all experimental tests. In order to enhance thermal conductivity of paraffin, three nano-additives are selected which are aluminium oxide (Al_2O_3), aluminium nitride (AlN) and graphene nano-platelets (GnP). The details about materials suppliers and their specifications are listed in **Table 1**. Likewise, the thermo-physical properties of pure paraffin and nano-additives are listed in **Table 2**. The materials are used as received from the dealers without any additional purification.

Table 1
List of dealers and specifications of materials used in this study

Materials	Dealers	Particle size	Purity
Paraffin (RT44HC)	Rubitherm Technologies GmbH		99.9%
Al_2O_3	EPRUI Nanoparticles and Microspheres Co. Ltd	30 - 60 nm	99.9%
AlN	Sigma-Aldrich Co. Ltd	<100 nm	99%
GnP	Ionic Liquids Technologies GmbH	6 - 8 nm	99.5%

The preparation of nano-PCM sample is accomplished by adopting ultrasonic emulsification technique, as shown in **Fig. 1**. In first step, the calculated amount of nano-additive is added to pre-melted base PCM and the suspension is formed by strong agitation using magnetic stirrer for 1 hr. In second step, to achieve complete dispersion of nano-additives in base PCM, the sample is subjected to intensive ultrasonication for 2 hr. In both steps, the temperature of sample is maintained at 60 °C to ensure that the base PCM remains in liquid state. In final step, the nano-PCM sample is poured into the shell of heat exchanger.

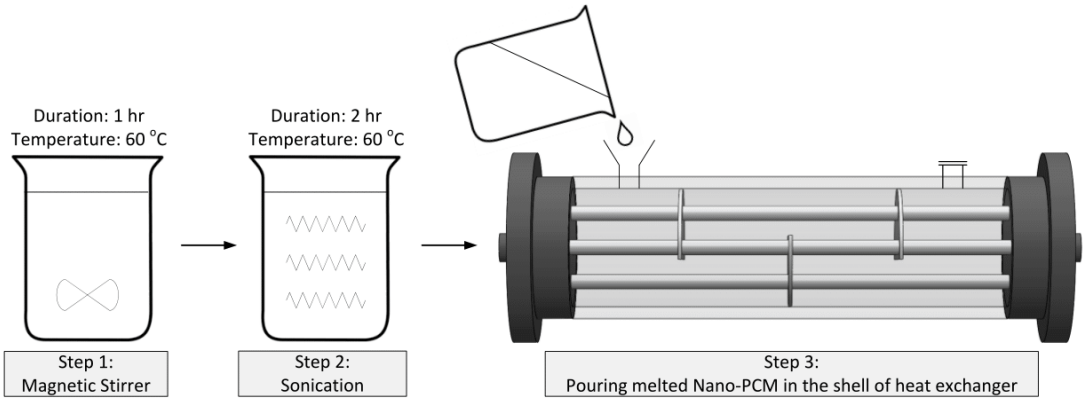

Fig. 1 Schematic illustration of nano-PCM sample preparation and loading in heat exchanger

In order to investigate the impact of various nano-additives, a sample for each nano-additive with volume fraction of 1% is prepared. Moreover, three samples of Al_2O_3 based nano-PCM are prepared with volume fraction of 1%, 3% and 5% to examine the influence of increasing volume fraction on thermal performance, as shown in **Table 3**. Prior to investigating nano-PCM in heat exchanger, a sample of pure paraffin is examined to provide a baseline for comparison.

Table 2
Thermo-physical properties of pure paraffin and nano-additives

Properties	Paraffin	Al_2O_3	AlN	GnP
Density (kg/m^3)	800 (solid) 700 (liquid)	3500	3300	400
Thermal conductivity (W/m.K)	0.2 (solid) 0.2 (liquid)	36	180	3000
Specific heat capacity (kJ/kg. K)	2.0	0.765	0.74	0.643
Latent heat of fusion (kJ/kg)	255	-	-	-
Phase change temperature (°C)	41-44	-	-	-

Table 3
Experimental tests of various nano-PCM samples

Sample	Nano-additives	Volume fraction	Mass of nano-additives added
A	Al_2O_3	1%	10.606 (gm)
B	Al_2O_3	3%	32.474 (gm)
C	Al_2O_3	5%	55.263 (gm)
D	AlN	1%	10 (gm)
E	GnP	1%	1.212 (gm)

2.2 Experimental setup

To investigate thermal behaviour of nano-PCM samples in a heat exchanger, an experimental setup is developed as shown in **Fig. 2**. The devised system includes water tank with electric heater, shell and tube heat exchanger, centrifugal pump, manual flow control valves, connections to municipal water and a versatile data acquisition system (VDAS) with computer.

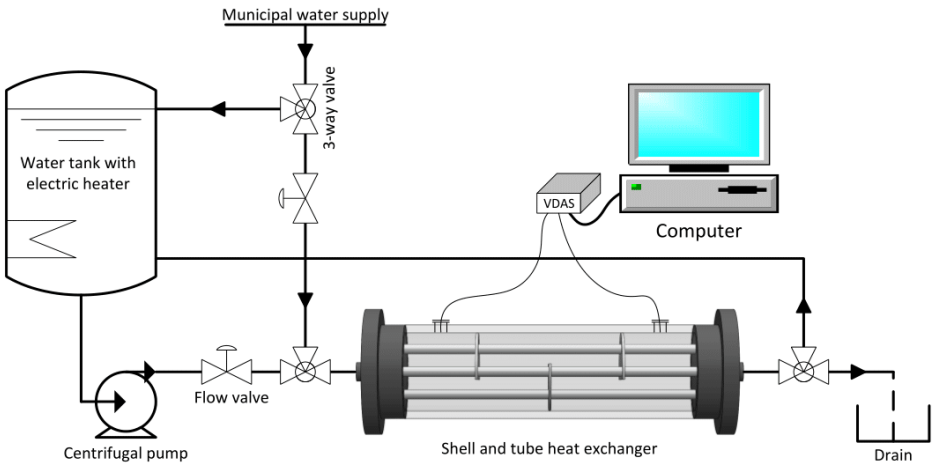

Fig. 2 Schematic illustration of experimental setup

The electric heater in water tank is governed by digital temperature controller to ensure constant temperature of HTF during charging cycles. Likewise, centrifugal pump is operated to direct high temperature HTF from water tank to shell and tube heat exchanger. The shell of heat exchanger is made of acrylic plastic and the outer diameter, length and thickness of shell are 60 mm, 185 mm and 5 mm, respectively. Similarly, the bundle of seven tubes is

made of stainless steel, with outer diameter and thickness of 6 mm and 1 mm, respectively. Moreover, the shell and tube heat exchanger is insulated with 50 mm thick glass wool to reduce thermal losses. The insulation layer can be untied to conduct visual inspection of phase transition process. The shell of heat exchanger is filled with nano-PCM sample and water as HTF is directed to circulate in the tubes.

In order to record transient temperature response of nano-PCM to charging/discharging cycles, four K-type thermocouples are installed within nano-PCM in the shell. As illustrated in **Fig. 3 (A)**, two zones are selected to investigate temperature distribution in nano-PCM. The selected zones are sections close to inlet and outlet regions. Two thermocouples are installed at each zone, at a vertical distance of ± 24 mm from central tube, as shown in **Fig. 3 (B)**. Likewise, two K-type thermocouples are attached to stainless steel tube at inlet and outlet to register temperature data of HTF. Manual operated flow control valve is installed at hot/cold circuit each to adjust and record the desired volume flow rate during charging/discharging cycles. To register temperature and flow rate data in computer, VDAS is operated to transfer data from sensors to computer. VDAS software is used to register temperature and flow rate reading at time step of 5 s.

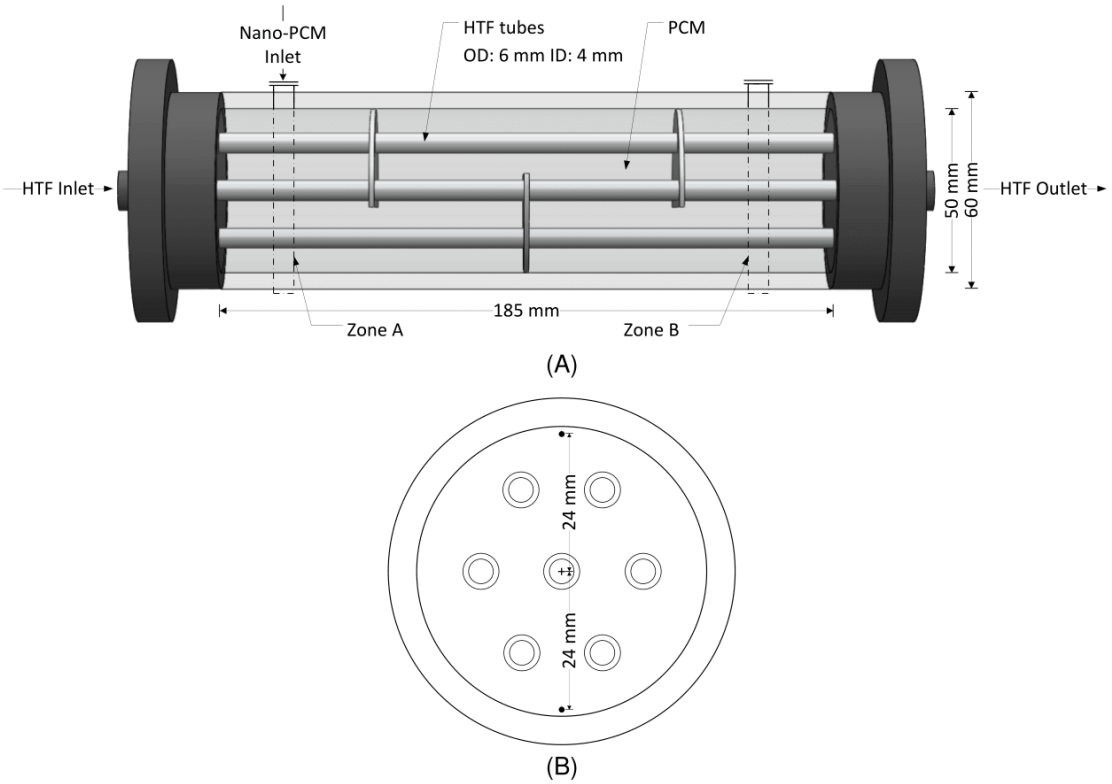

Fig. 3 Physical model of shell and tube heat exchanger with (A) description of dimensions and (B) vertical positioning of thermocouples at both zone A and B.

2.3 Experimental procedure

During charging cycles, the low temperature municipal water is initially circulated through the tubes of heat exchanger to provide a good baseline for all charging cycles with initial temperature of 15 °C. The desired temperature is set in digital temperature controller for electric heater to increase temperature of water in tank. Upon reaching the desired

temperature, the centrifugal pump is switched on to circulate high temperature HTF through the tubes of heat exchanger. The manual operated flow control valve is adjusted to specific volume flow rate value. In this study, the charging cycles are conducted at three inlet temperatures of 47, 52 and 57 °C and four volume flow rates of 1.5, 2.0, 2.5 and 3.0 l/min for each nano-PCM sample. HTF transfers thermal energy to nano-PCM in heat exchanger and the low temperature HTF at outlet of heat exchanger is directed back to water tank to repeat the cycle. Charging cycle is completed once all thermocouples register temperature value higher than melting temperature of PCM.

Prior to conducting discharging cycle, the inlet temperature of HTF is increased to maintain a uniform initial temperature of 50 °C for all discharging cycles. The discharging cycle is started by directing low temperature municipal water to extract thermal energy from nano-PCM. The discharging cycles are examined by regulating flow control valve to a specific flow rate value of 1.5, 2.0, 2.5 and 3.0 l/min. Due to thermal energy discharge to low temperature HTF, the solidification of nano-PCM begins. Discharging cycle is completed once the temperature gradient between inlet temperature and all thermocouples in shell is less than 2 °C.

3. Numerical Model

3.1 Mathematical formulation and governing equations

The physical model for numerical investigations is illustrated in Fig. 3. In order to simplify numerical model and shorten simulation time, the following assumptions are made:

a) The acrylic plastic shell is neglected and the outer boundary is considered as adiabatic by ignoring convective heat losses to surrounding.
b) The thickness of stainless steel tubes is neglected due to the fact that stainless steel possesses comparatively higher thermal conductivity to nano-PCM.
c) The liquid phase of nano-PCM is considered as incompressible Newtonian fluid and the change in density with temperature complies with the Boussinesq approximation.
d) The volumetric expansion of nano-PCM is neglected and natural convection is assumed to be laminar.
e) The computational domain of nano-PCM is considered to be at uniform initial temperature. Likewise, the inlet temperature and flow rate of HTF are assumed to be constant.

Based on above assumptions, a numerical model is formulated considering the governing equations of continuity, momentum and energy to investigate thermal performance of various nano-PCM samples in the computational domain of shell and tube heat exchanger. The governing equations are discussed as follow:

Continuity equation:

$$\frac{\partial \rho_{npcm}}{\partial t} + \nabla.(\rho_{npcm}\mathbf{u}) = 0 \quad (1)$$

Momentum equation:

$$\frac{\partial(\rho_{npcm}\mathbf{u})}{\partial t}+\nabla.(\rho_{npcm}\mathbf{uu})=-\nabla p_{npcm}+\nabla.(\mu_{npcm}\nabla\mathbf{u})+\mathbf{F}+S \quad (2)$$

Energy equation:

$$\frac{\partial(\rho_{npcm}C_{p,npcm}T_{npcm})}{\partial t}+\nabla.(\rho_{npcm}C_{p,npcm}T_{npcm}\mathbf{u})=\nabla.(k_{npcm}\nabla T_{npcm})+q \quad (3)$$

In Eq. (2), $\mathbf{F}$ represents buoyant force term which is responsible for upward rise of lower density and higher temperature molecules of nano-PCM. Buoyant forces control the natural convection in nano-PCM and it can be approximated by using Boussinesq approximation [39]:

$$\mathbf{F}=\rho_{npcm}\mathbf{g}\beta(T_{npcm}-T_{pc}) \quad (4)$$

Likewise, S in Eq. (2) defines momentum sink term which can be estimated by employing KozenyCarman equation, which is derived from Darcy law for porous medium [40]. This term is applied to equate for porosity in mushy zone, as follow:

$$S=\frac{\psi(1-\phi)^2}{(\phi^3+\alpha)}\mathbf{u} \quad (5)$$

where ψ is the mushy zone constant, which illustrates an approximate magnitude of damping in governing equation of momentum. In this study, the mushy zone constant value is set to 10^6, which presents good agreement between numerical and experimental results. Likewise, α denotes a small constant value equal to 10^{-4} and is used to prevent division by zero at liquid fraction $\phi = 0$. The range of liquid fraction with respect to temperature is defined as follow:

$$\phi=\begin{cases}0 & T_{npcm}<T_s\\ \dfrac{T_{npcm}-T_s}{T_l-T_s} & T_s\le T_{npcm}\le T_l\\ 1 & T_{npcm}>T_l\end{cases} \quad (6)$$

where s and l are the indices for solidus and liquidus phase of nano-PCM. The effective specific heat capacity in Eq. (3) is calculated by differentiating specific enthalpy with respect to temperature:

$$C_{p,npcm}=\frac{1}{\rho}\left(\phi_s\rho_{npcm,s}C_{p,npcm,s}+\phi_l\rho_{npcm,l}C_{p,npcm,l}\right)+L_{npcm}\frac{\partial}{\partial T}\left[\frac{\left(\phi_l\rho_{npcm,l}-\phi_s\rho_{npcm,s}\right)}{2\rho_{npcm}}\right] \quad (7)$$

The right hand side of Eq. (7) represents that specific heat capacity is the summation of sensible and latent portion of heat. Likewise, the thermo-physical properties of nano-PCM are estimated based on theoretical equations for mixture of two components, as follow:

$$\rho_{npcm}=\delta_{VF}\rho_{np}+\left(1-\delta_{VF}\right)\rho_{pcm} \quad (8)$$

$$C_{p,npcm} = \frac{\delta_{VF}\rho_{np}C_{p,np} + (1-\delta_{VF})\rho_{pcm}C_{p,pcm}}{\rho_{npcm}} \quad (9)$$

$$L_{npcm} = \frac{(1-\delta_{VF})\rho_{pcm}L_{pcm}}{\rho_{npcm}} \quad (10)$$

where δ_{VF} represents the volume fraction of nano-additives. Moreover, the effective dynamic viscosity and effective thermal conductivity of nano-PCM samples are evaluated by implementing the semi-empirical models proposed by Corcione [41] as given in Eq. (11) and Eq. (14), respectively. These propose models by Corcione, on contrary to earlier standard models and theories proposed by Einstein [42] and others [43-46] for estimating the effective dynamic viscosity and Maxwell [47] and others [48-50] for approximating the effective thermal conductivity, account for particle size of nano-additives, volume fraction and operating temperature. Therefore, these earlier standard models fail to predict an accurate increase in dynamic viscosity and thermal conductivity of nano-PCM due to the fact that these standard models are developed for larger particle size nano-additives and these models only depend on shape and volume fraction of nano-additives.

The effective dynamic viscosity is estimated as follow:

$$\mu_{npcm} = \frac{\mu_{pcm}}{1-34.87(d_{np}/d_{pcm})^{-0.3}\delta_{VF}^{1.03}} \quad (11)$$

where μ_{pcm}, d_{pcm} and d_{np} represents the dynamic viscosity of pure paraffin, equivalent diameter of pure paraffin and diameter of nano-additives, respectively. The dynamic viscosity and equivalent diameter of pure paraffin is determined as follow:

$$\mu_{pcm} = 0.001\exp\left(-4.25 + \frac{1790}{T_{pcm}}\right) \quad (12)$$

$$d_{np} = 0.1\left(\frac{6M_W}{\pi N_A \rho_{pcm,o}}\right)^{1/3} \quad (13)$$

where M_W, N_A and $\rho_{pcm,o}$ are the molecular weight of pure paraffin, Avogadro number and density of pure paraffin at $T_{pcm} = 20^oC$, respectively.

Similarly, the effective thermal conductivity is evaluated from the following equation:

$$k_{npcm} = k_{pcm}\left(1 + 4.4\,\mathrm{Re}^{0.4}\,\mathrm{Pr}^{0.66}\left(\frac{T_{npcm}}{T_{pc}}\right)^{10}\left(\frac{k_{np}}{k_{pcm}}\right)^{0.03}\delta_{VF}^{0.66}\right) \quad (14)$$

where Re and Pr represent the Reynolds number of nano-additives and Prandtl number of pure paraffin, respectively. Re and Pr can be calculated using the following relations:

$$\mathrm{Re} = \frac{2\rho_{pcm} k_B T_{npcm}}{\pi \mu_{pcm}^2 d_{np}} \quad (15)$$

$$\mathrm{Pr} = \frac{\mu_{pcm} C_{p,pcm}}{k_{pcm}} \quad (16)$$

Using Eq. (11) and Eq. (14), the effective dynamic viscosity and thermal conductivity of nano-PCM are computed for volume fraction of 1%, 2%, 3%, 4% and 5% of Al_2O_3, AlN and GnP nano-additives, as presented in **Fig. 4** and **Fig. 5**, respectively. It can be noticed that in all cases, the dynamic viscosity of nano-PCM as compared to pure paraffin is enhanced with an increase in volume fraction of nano-additives. However, the enhancement in effective dynamic viscosity of GnP based nano-PCM is more significant as compared to Al_2O_3 and AlN based nano-PCM. This is due to the fact that the effective dynamic viscosity is highly influenced by the particle size of nano-additives. Moreover, a higher dynamic viscosity can have an adverse impact on natural convection.

Likewise, the enhancements in thermal conductivity of nano-PCM due to varied volume fraction concentration of nano-additives are illustrated against temperature in **Fig. 5**. It can be observed that GnP based nano-PCM samples have shown significantly higher thermal conductivity due to their smaller particle size and higher thermal conductivity as compared to Al_2O_3 and AlN.

3.2 Initial and boundary conditions

During melting process, the initial temperature of nano-PCM is set to 15 °C which is less than phase change temperature, as shown in **Table 2**. Therefore, the initial temperature ensures that entire mass of nano-PCM is in complete solid state. Likewise, the HTF tubes are set to a constant inlet temperature of 52 °C for the complete charging cycle.

3.3 Computational procedure and model validation

The geometrical orientation and dimensions of shell and tube heat exchanger provided in **Fig. 3** are adopted for the computational model. The governing equations are discretised by implementing finite volume method. PISO algorithm is employed to solve the pressure-velocity coupling. PRESTO and second order upwind schemes are adopted for spatial discretisation of pressure, momentum and energy equations, respectively. The relative residuals values for the convergence criteria of continuity, velocity and energy equations are set to 10^{-6}, respectively. The time step and mesh independency study are conducted to ensure accuracy of numerical results. As a result, the time step of 0.1 s and mesh size of 27420 are selected for all nano-PCM samples in this study. The current computational model is validated with the experimental results obtained for pure paraffin and nano-PCM sample of 1% volume fraction of Al_2O_3, as presented in **Fig. 6**. The mean absolute percentage error between numerical and experimental results for pure paraffin and nano-PCM are 3.44% and 2.53%, respectively.

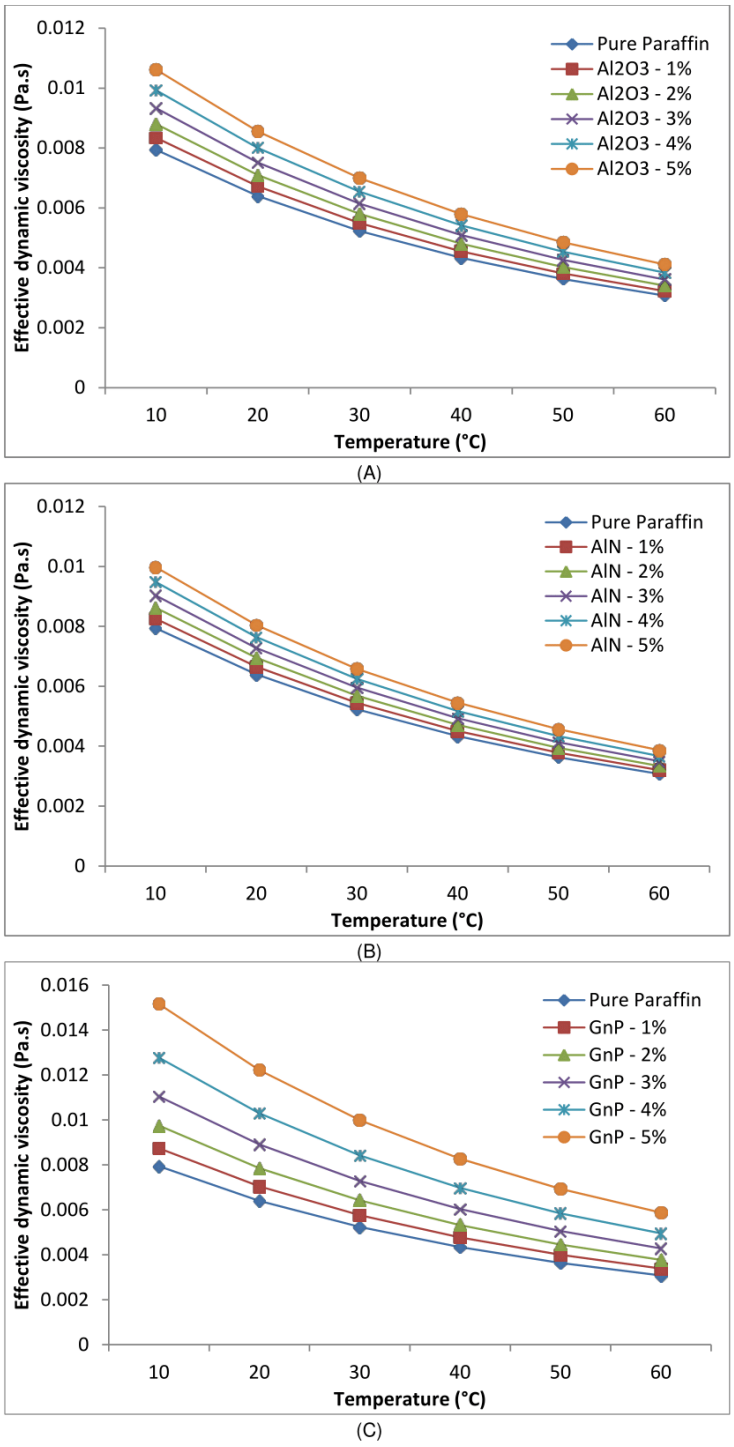

Fig. 4 Effective dynamic viscosity of nano-PCM samples with varied volume fractions and nano-additives (A) Al_2O_3, (B) AlN and (C) GnP.

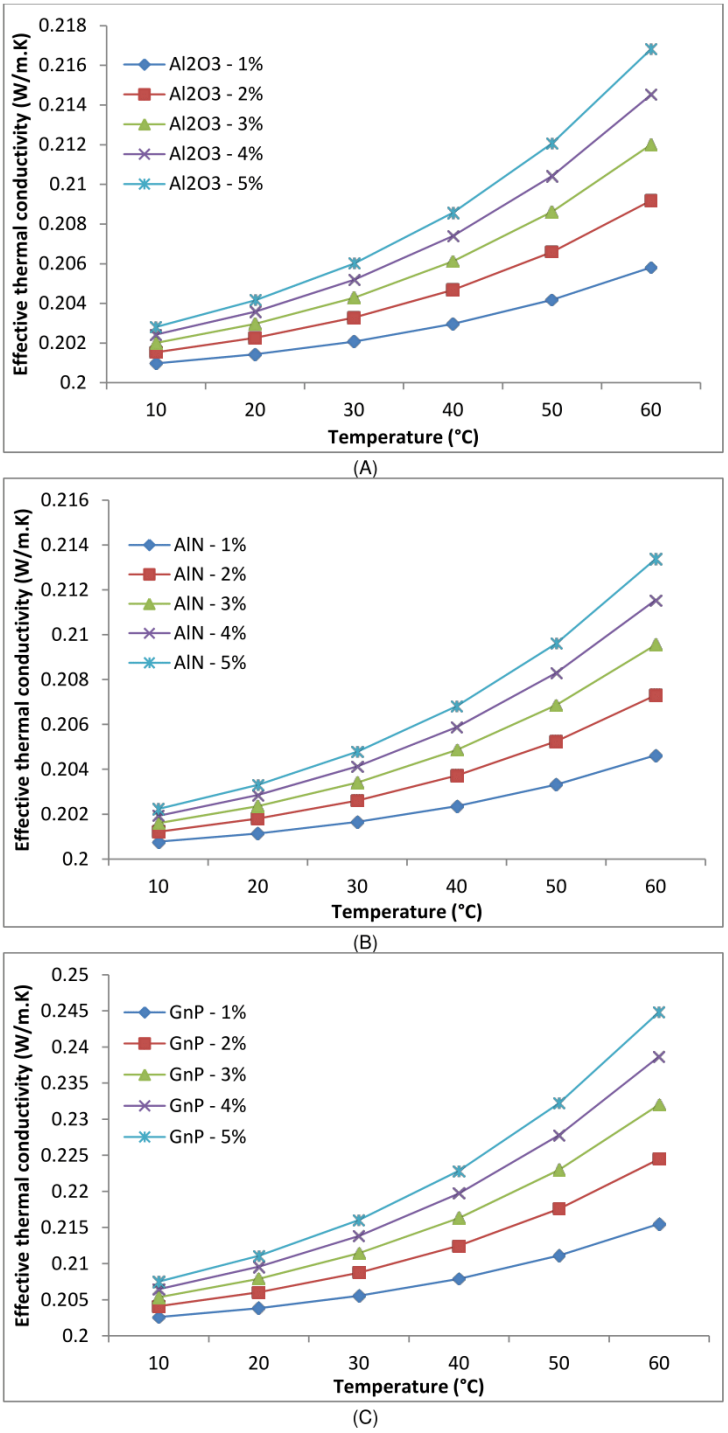

Fig. 5 Effective thermal conductivity of nano-PCM samples with varied volume fractions and nano-additives (A) Al_2O_3, (B) AlN and (C) GnP.

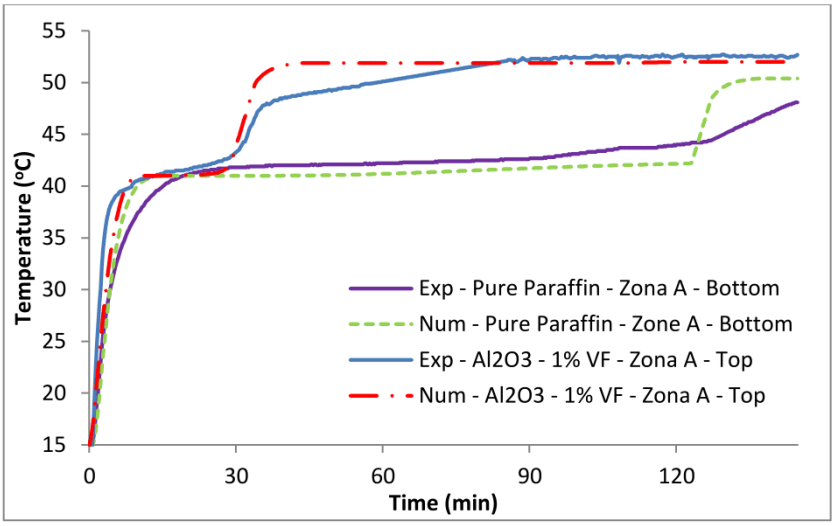

Fig. 6 Comparison of temperature profiles attained from experimental and numerical study of charging cycles at inlet temperature of 52 °C.

4. Results and discussions

4.1 Thermal performance of pure paraffin

In order to understand the thermal performance of nano-PCM samples in shell and tube heat exchanger, a sample of pure paraffin is initially examined to develop a good baseline for comparison.

4.1.1 Experimental

Pure paraffin sample is melted and poured in the shell of heat exchanger. In order to study the transient thermal response of pure paraffin to various inlet temperatures and volume flow rates of HTF, the data is registered from all four k-type thermocouples installed at zone A and B, as presented in **Fig. 3**. The temperature distribution in both vertical and horizontal positions in shell is examined at three inlet temperatures of 47, 52 and 57 °C. Likewise, the impact of varying flow rate of HTF is studied at four values of 1.5, 2.0, 2.5 and 3.0 l/min.

The melting behaviour of pure paraffin at various temperatures is presented in **Fig. 7**. It can be noticed that the linear rise from initial temperature to about 40 °C represents sensible heat and it is dominated by conduction heat transfer. The sensible heat capacity is rapidly stored due to small specific heat capacity of paraffin. Afterwards, a steady and gradual rise is observed, which represents the latent portion of heat storage. During this phase, the higher latent heat capacity is gradually stored as the temperature rises from 41 °C to 44 °C. Consequently, the phase transformation of solid paraffin to mushy and then to liquid state occurs. After completion of latent portion of heat storage, a relatively quicker increase in temperature is observed which again represent the sensible heat storage in liquid phase of paraffin.

Moreover, it can be observed from **Fig. 7** that phase transition at top position is quicker as compared to bottom position. The reason behind is that conduction dominates the heat transfer at initial stages and after phase transition; the amount of liquid paraffin increases

which results into upward rise against the gravity and thus it makes natural convection as dominant mode of heat transfer. Due to upward rise of high temperature molecules, the phase transition is relatively higher at top position as compared to bottom position. The natural convection is highly influenced by density and dynamic viscosity. Moreover, it can be noticed that with an increase in inlet temperature of HTF, the temperature gradient for heat transfer increases which results in relatively higher melting/charging rate of paraffin. Also, due to small volume capacity of shell and tube heat exchanger, the varying volume flow rate of HTF has insignificant influence on phase transition rate. It is noticed that with an increase in volume flow rate from 1.5 to 3.0 l/min, an almost identical transient temperature response is recorded with a relative standard deviation of 0.43%.

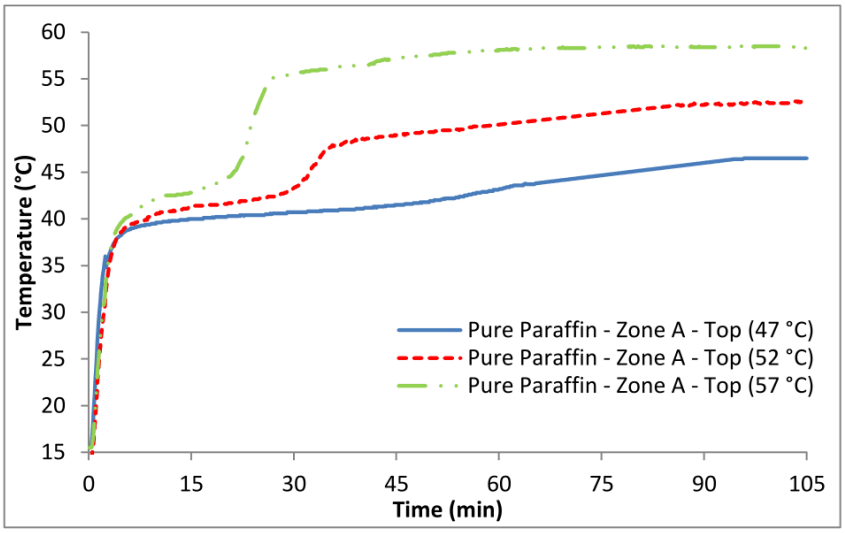

(A)

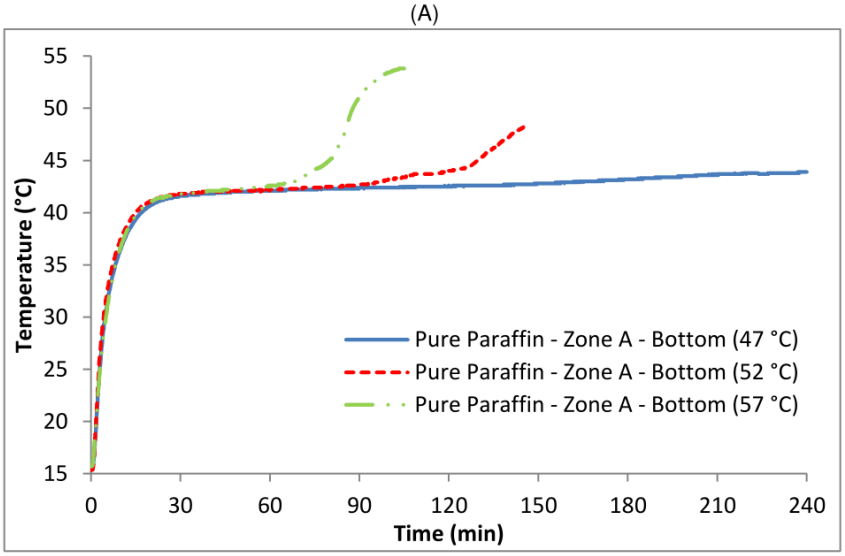

(B)

Fig. 7 Transient temperature response of pure paraffin to varied inlet temperatures of 47, 52 and 57 °C and constant volume flow rate of 1.5 l/min.

4.1.2 Numerical

In numerical simulation, the melting/charging cycles of pure paraffin sample are investigated at three constant inlet temperatures of 47, 52 and 57 °C. As presented in **Fig. 8**, the left side of plots indicates liquid fraction and the right side demonstrates temperature contours of pure paraffin in shell of heat exchanger. It can be observed that as liquid fraction around the HTF tubes increases, the buoyant forces enable liquid particles to rise above and thus, it results in comparatively higher melting rate at top position of shell. Likewise, the temperature contours demonstrate a relatively higher temperature of paraffin at top position as compared to bottom position. Moreover, it is noticed that with an increase in inlet temperature, the melting rate is significantly improved, as shown in **Fig. 8**. It is observed that with an increase in inlet temperature from 47 to 52 and 57 °C, the total melting time is reduced by a fraction of 56.96% and 72.60%, respectively. Furthermore, the sensible portion of heat storage in liquid phase is increased with an increase in inlet temperature, which enhances the overall thermal energy storage of LHS system. It is noticed that with an increase in inlet temperature from 47 to 52 and 57 °C, the overall enthalpy of LHS system is upgraded from 299 to 309 and 319 kJ/kg, respectively.

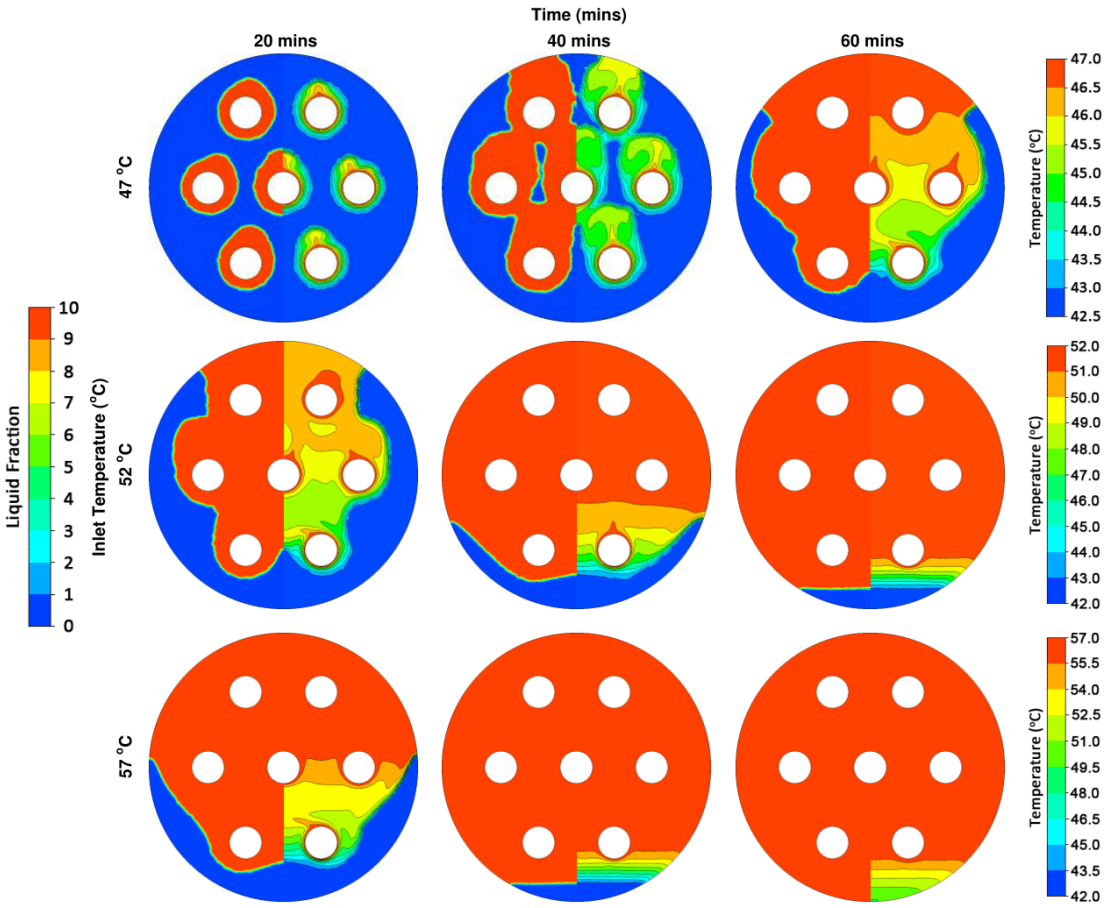

Fig. 8 Liquid fraction and temperature contours of pure paraffin at various inlet temperatures of 47, 52 and 57 °C.

4.2 Thermal performance of nano-PCM samples

After understanding the thermal behaviour of pure paraffin in shell and tube heat exchanger, the experimental and numerical examination of nano-PCM samples are conducted.

4.2.1 Experimental

As discussed in section 2.1, ultrasonic emulsification technique is adopted to prepare various nano-PCM samples and shell and tube heat exchanger is utilised to investigate thermal behaviour of the nano-PCM samples. Thermal conductivity of paraffin improves with an inclusion of nano-additives and thus, the total charging time can be significantly reduced. However, as illustrated in **Fig. 4**, an increase in volume fraction of nano-additives also augments the dynamic viscosity, which has an adverse impact on natural convection and therefore the thermal performance can be affected.

To begin with, three Al_2O_3 based nano-PCM samples are developed with volume fraction of 1, 3 and 5%. Nano-PCM sample in liquid phase is poured into the shell of heat exchanger and the experimental investigations are conducted at three varied inlet temperatures of 47, 52 and 57 °C. The transient temperature profiles for these three Al_2O_3 based nano-PCM samples are recorded by thermocouple installed at bottom position at zone B and are plotted against pure paraffin in **Fig. 9**.

It can be noticed that at constant inlet temperature of 47 °C, the melting/charging time at bottom position is significantly reduced by a fraction 33.75%, 55.41% and 56.25% for Al_2O_3 based nano-PCM samples with volume fraction of 1, 3 and 5% as compared to pure paraffin, respectively. Likewise, at constant inlet temperature of 52 °C, the charging time is considerably decreased by a fraction of 35.92%, 48.80% and 56.37%, respectively. Similarly, in case of constant inlet temperature of 57 °C, the charging time is lessened by a fraction of 11.36%, 21.71% and 24.74% for Al_2O_3 based nano-PCM samples as compared to pure paraffin, respectively. It can be noticed that for all three varied inlet temperatures, the melting/charging time is significantly reduced by incorporating Al_2O_3 based nano-additives to paraffin. However, with an increase in volume fraction from 3% to 5%, just a slight increment in thermal performance is observed which is due to adverse effects of higher dynamic viscosity on natural convection. Therefore, it can be deduced that an optimum volume fraction is essential to be identified for an appropriate enhancement in thermal performance.

Subsequently, the nano-PCM samples based on 1% volume fraction of Al_2O_3, AlN and GnP are prepared and experimentally investigated for thermal performance in shell and tube heat exchanger at three varied inlet temperatures of 47, 52 and 57 °C. In order to identify the thermal performance enhancement due to inclusion of same volume fraction of varied nano-additives in paraffin, the transient temperature profiles are recorded from thermocouples installed at top and bottom positions at zone A, as presented in **Fig. 10**.

It can be observed that at constant inlet temperature of 47 °C, the total melting time at top position for Al_2O_3, AlN and GnP based nano-PCM is reduced by a fraction of 9.04%, 18.74% and 37.85% as compared to pure paraffin, respectively. Similarly, the total melting time at bottom position is reduced by a fraction of 33.75%, 35.90% and 62.56%, respectively. Moreover, at inlet temperature of 52 °C, the reduction is melting time at top position is recorded to be 6.42%, 27.27% and 57.22%, respectively. Likewise, at bottom position, the melting time is lessened by 32.70%, 36.40% and 38.07%, respectively. Furthermore, at inlet

temperature of 57 °C, the total melting time is decreased by a fraction of 19.04%, 28.57% and 49.78% at top position and 28.01%, 36.47% and 44.57% at bottom position, respectively. It can be perceived from experimental results that nano-additives material plays a significant role in enhancing thermal performance of paraffin. For instance, it is noticed that thermal performance enhancement for GnP based nano-PCM sample is relatively higher than Al_2O_3 and AlN based nano-PCM samples due to relatively higher thermal conductivity and smaller particle size of GnP nano-additives.

Furthermore, similar to pure paraffin, the variations in volume flow rate of HTF from 1 to 3 l/min have presented an insignificant enhancement in charging rate of nano-PCM samples. This is due to small volumetric capacity of shell and tube heat exchanger and consequently, the tubes in shell are at same temperature throughout its length.

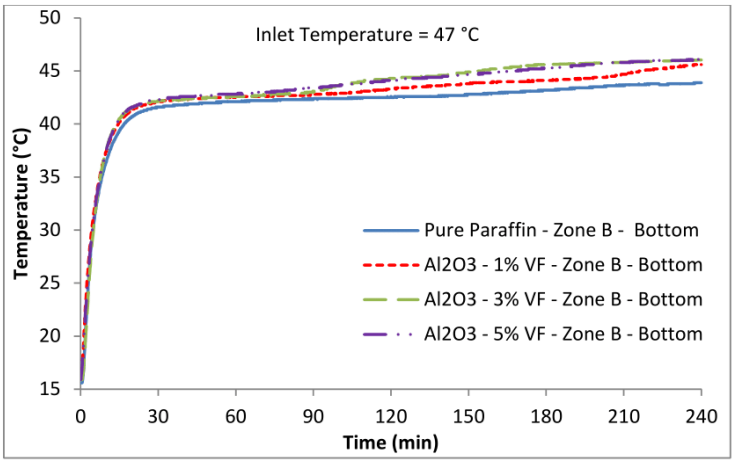

(A)

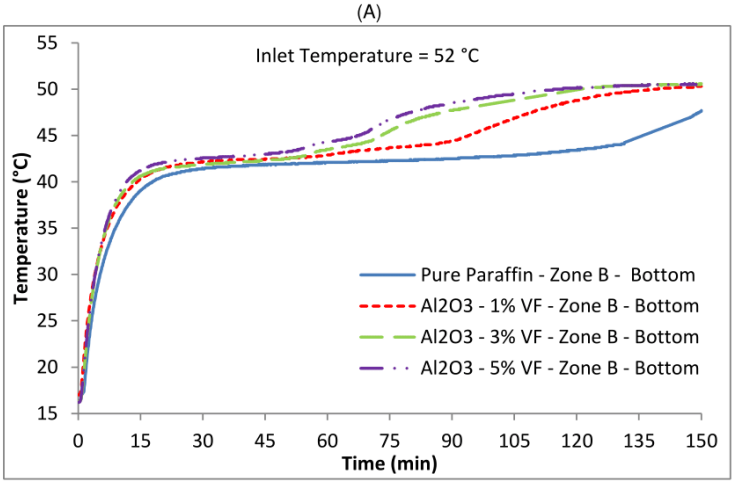

(B)

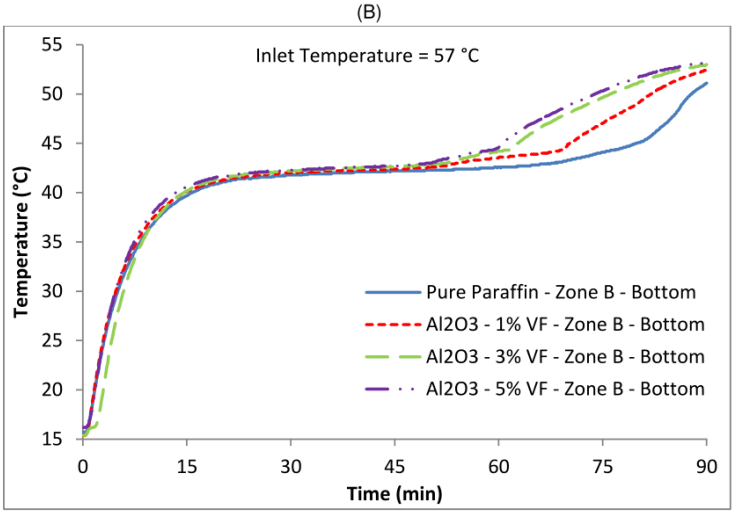

(C)

Fig. 9 Transient thermal performance of Al_2O_3 based nano-PCM samples with volume fraction of 1%, 3% and 5% at various inlet temperatures of 47, 52 and 57 °C and at constant volume flow rate of 1.5 l/min.

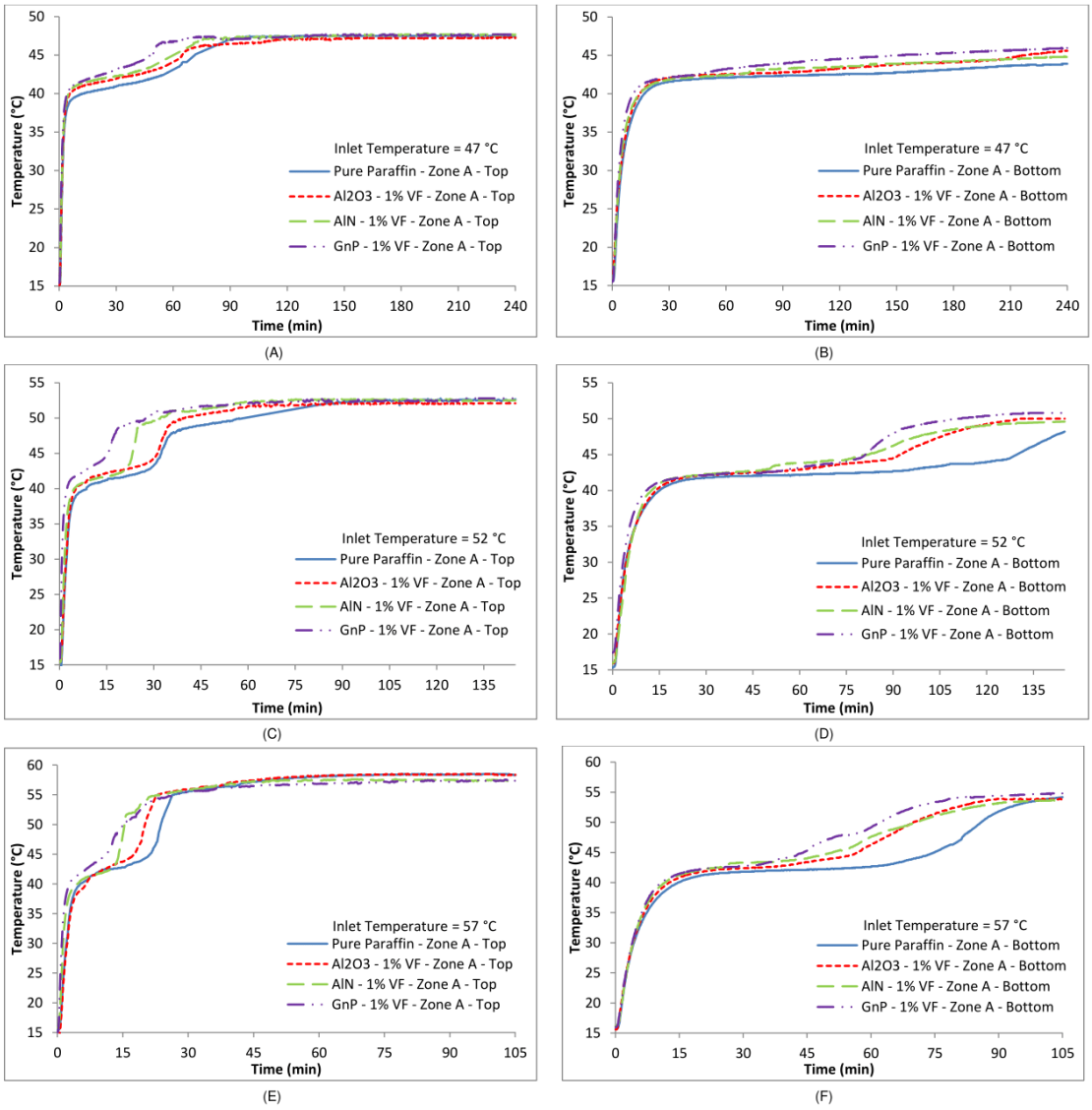

Fig. 10 Transient temperature plots attained from charging cycles of 1% volume fraction of Al_2O_3, AlN and GnP based nano-PCM samples at varied inlet temperatures of 47, 52 and 57 °C and at constant volume flow rate of 1.5 l/min.

4.2.2 Numerical

In this section, the numerical simulations of charging cycles of nano-PCM samples based on Al_2O_3, AlN and GnP nano-additives with volume fraction of 1%, 2%, 3%, 4% and 5% are conducted at constant inlet temperature of 52 °C, respectively. As illustrated in **Fig. 11**, the left sides of plots represent total enthalpy of nano-PCM based LHS system and the right sides demonstrate temperature contours. The plots are attained from simulation results at 30 mins of charging cycle.

It is observed that temperature contours for Al_2O_3, AlN and GnP based nano-PCM samples with varied volume fraction represent a small variation in temperature. This is contrary to the fact that GnP based nano-PCM possess higher effective thermal conductivity, as shown in **Fig. 4**. The reason behind is that GnP based nano-PCM also have relatively higher dynamic viscosity which limits the influence of buoyant forces and natural convection on temperature distribution and melting rate. Therefore, the temperature contours are indicating just a slight variation. However, it can be noticed from enthalpy plots that GnP based nano-PCM samples possess significantly higher enthalpy as compared to Al_2O_3 and AlN based nano-PCM samples for all respective volume fraction cases. This is due to the fact that Al_2O_3 and AlN nano-additives have relatively higher density and particle size which considerably reduces the overall thermal capacity and enthalpy of the system.

For control volume, the thermal storage capacity is reduced for nano-PCM as compared to pure paraffin because nano-additives occupy certain volume. Therefore, the total enthalpy is reduced for nano-PCM samples. As illustrated in **Fig. 12**, the total enthalpy of nano-PCM samples reduces with an increase in volume fraction of nano-additives as compared to pure paraffin (309 kJ/kg). It is recorded that with an inclusion of 1% volume fraction of Al_2O_3, AlN and GnP nano-additives, the total enthalpy of system is reduced by a fraction of 4.75%, 4.46% and 0.55%, respectively. Likewise, in case of 5% volume fraction of nano-additives, the total enthalpy is decreased by a fraction of 20.58%, 19.64% and 2.88%, respectively. It is noted that due to smaller density and particle size, the GnP based nano-PCM samples have illustrated higher thermal storage capacity as compared to Al_2O_3 and AlN based nano-PCM. Moreover, Al_2O_3 and AlN based nano-PCM have presented higher charging rate as compared to pure paraffin, however the increase in weight and reduction in thermal storage capacity can minimise their utilisation in widespread practical applications.

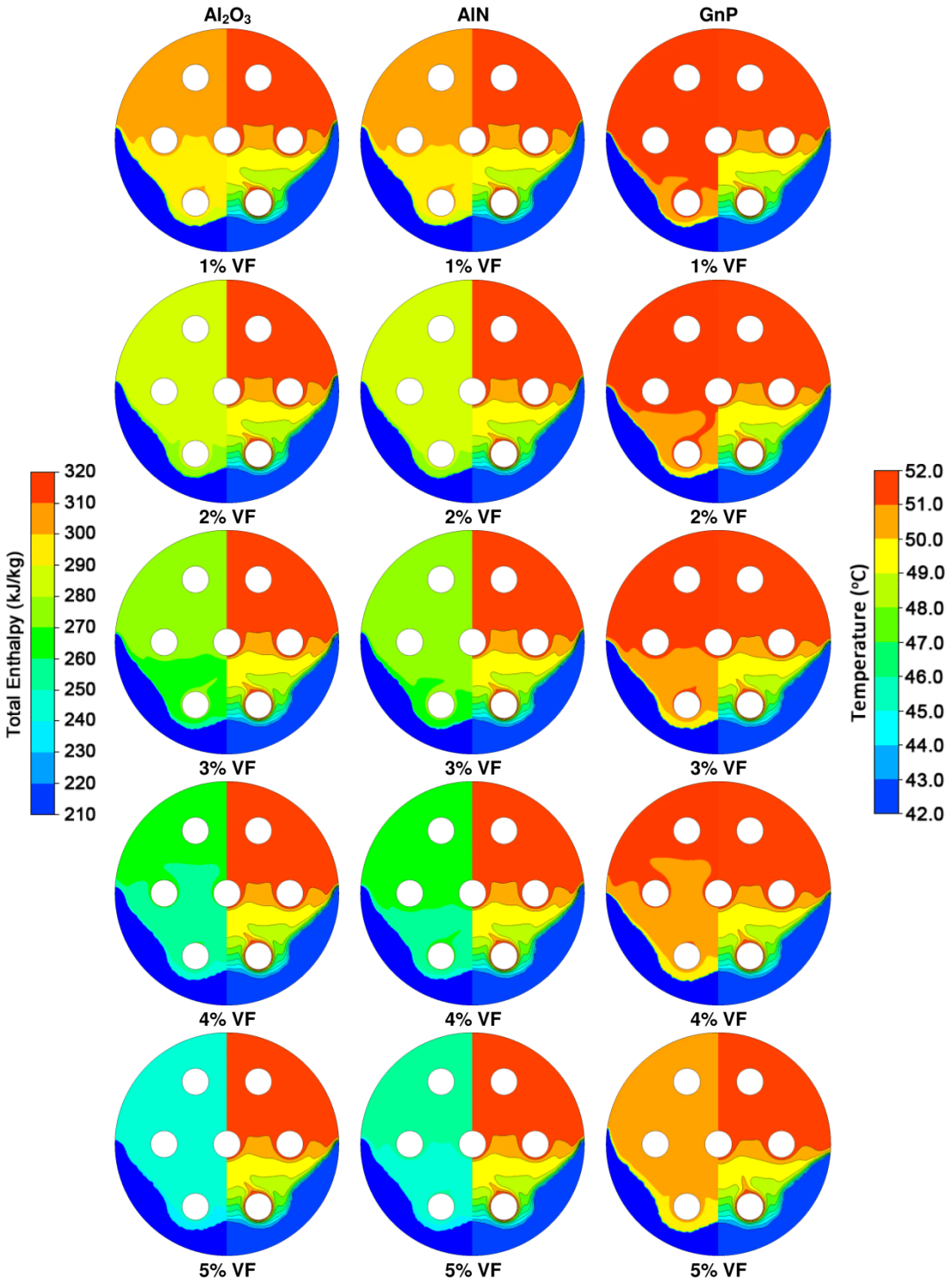

Fig. 11 Total enthalpy and temperature contours of Al_2O_3, AlN and GnP based nano-PCM samples with varied volume fractions attained after 30 mins of charging at constant inlet temperature of 52 °C.

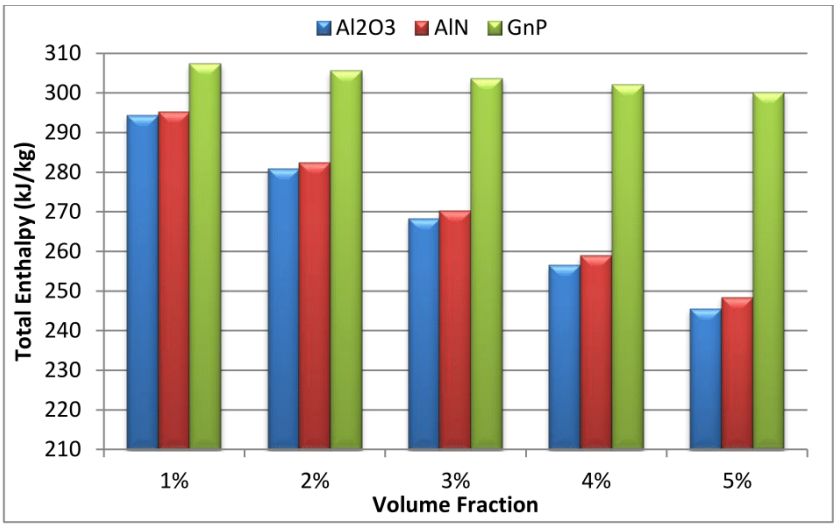

Fig. 12 Total enthalpy of nano-PCM samples with varying volume fraction of nano-additives.

4.3 Thermal performance of pure paraffin and nano-PCM during discharging cycles

After charging cycles, the thermal performance of various samples of nano-PCM in shell and tube heat exchanger are experimentally investigated during discharging cycles. Municipal water is directed through the tubes of heat exchanger to extract thermal energy from nano-PCM. In discharging cycles, the inlet temperatures for all cases are set constant to 15 °C.

Due to higher temperature gradient generated between HTF in tubes and nano-PCM in shell, the sensible portion of thermal energy is rapidly transferred to HTF. As a result, the temperature of nano-PCM is almost linearly declined to about 44 °C. After this stage, the discharge of latent portion of thermal energy starts. Due to higher latent heat capacity, the decrease in temperature from 44 to 41 °C is relatively slow and steady. During this period, the liquid phase nano-PCM transforms to mushy and then to solid phase. As the latent portion of thermal energy discharges, a rapid decline in temperature is observed which represents sensible portion of thermal energy discharge in solid phase.

Initially, the influence of varying volume fraction of nano-additives on thermal performance during discharging cycle is examined and plotted against pure paraffin in **Fig. 13**. It can be noticed that with inclusion of Al_2O_3 nano-additives, the thermal conductivity is enhanced and therefore, the discharging time is significantly reduced. It is observed that the time required to discharge latent portion of thermal energy at bottom position at zone A is reduced by a fraction of 28.45%, 39.05% and 39.52% for Al_2O_3 based nano-PCM samples with volume fraction of 1%, 3% and 5% as compared to pure paraffin, respectively. Moreover, it can be noticed that similar to charging cycles, an increase in volume fraction from 3% to 5% has an insignificant impact on phase transition rate of Al_2O_3 based nano-PCM.

Furthermore, in order to examine the impact of varying nano-additives material on thermal performance, the discharging cycles are experimentally investigated for 1% volume fraction of Al_2O_3, AlN and GnP based nano-PCM. The temperature data for nano-PCM samples registered by thermocouple installed at bottom at zone B are plotted against pure paraffin in **Fig. 14**. It can be noticed that the discharging time of latent portion of thermal energy is decreased by 14.63%, 34.95% and 41.46% for Al_2O_3, AlN and GnP based nano-PCM as

compared to pure paraffin, respectively. It can be perceived that due to higher thermal conductivity of GnP and AlN nano-additives, the discharge rate is significantly higher.

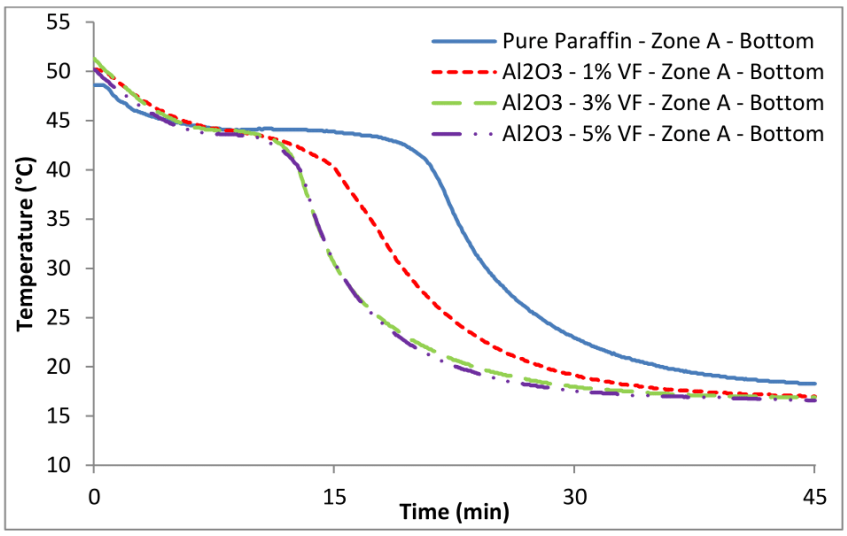

Fig. 13 Transient temperature profiles attained during discharging cycles of pure paraffin and Al_2O_3 nano-PCM samples of various volume fractions 1%, 3% and 5%. The inlet temperature of HTF is set to 15 °C for all cases.

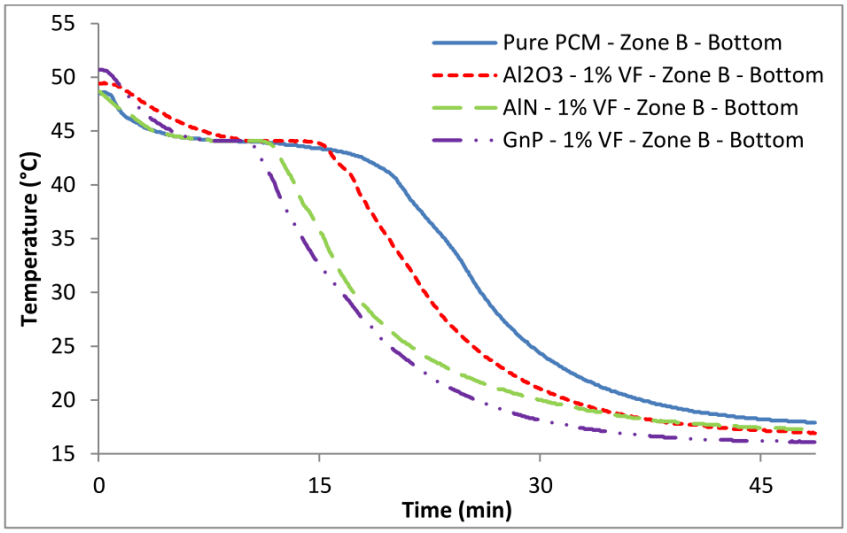

Fig. 14 Transient temperature plots acquired during discharging cycles of pure paraffin and nano-PCM samples of 1% volume fraction of Al_2O_3, AlN and GnP. The inlet temperature is kept constant to 15 °C for all cases.

5. Conclusions

In this article, experimental and numerical studies are conducted to identify the impact of metal oxides, metal nitrides and carbon allotropes based nano-additives on thermal performance enhancement of paraffin based LHS system. Ultrasonic emulsification technique is adopted to prepare Al_2O_3, AlN and GnP based nano-PCM samples with varied volume fractions. Thermal behaviour of nano-PCM samples are investigated in shell and tube heat exchanger by conducting series of charging and discharging cycles at various operating conditions. Meanwhile, a numerical model is developed and simulated to help understand and predict the effect of improved thermal conductivity and dynamic viscosity of nano-PCM samples on heat transfer mechanism, temperature distribution and overall enthalpy of the LHS system. The numerical model accounts for operating temperature, particle size and volume fraction of nano-additives while computing the effective thermal conductivity and dynamic viscosity of nano-PCM samples. Based on experimental and numerical investigations, the following conclusions are derived:

- It is observed that as the liquid fraction around the tubes increases during charging cycles, an upward rise of high temperature molecules due to buoyant forces enable natural convection to dominate the heat transfer in top position. Therefore, the melting rate is higher at top position as compared to bottom position of the shell and tube heat exchanger based LHS system. Likewise, it is noticed that with an increase in inlet temperature of HTF from 47 to 52 and 57 °C, the phase transition rate is significantly improved by a fraction of 56.96% and 72.60%, respectively. Moreover, the overall thermal enthalpy of the system is also improved with an increase in inlet temperature.

- It is deduced that the effective thermal conductivity and dynamic viscosity of paraffin is significantly enhanced with inclusion of nano-additives. Likewise, the particle size, volume fraction and operating temperature significantly influence the effective thermal conductivity and dynamic viscosity. The experimental and numerical results indicated that the thermal performance is improved for all nano-PCM samples. However, GnP based nano-PCM samples have illustrated relatively higher effective thermal conductivity and dynamic viscosity due to their smaller particle size and higher thermal conductivity as compared to Al_2O_3 and AlN. It is observed that while charging at inlet temperature of 47 °C, the charging time for Al_2O_3, AlN and GnP based nano-PCM samples is significantly reduced by 33.75%, 35.90% and 62.56% as compared to pure paraffin. Likewise, for inlet temperature of 52 °C, the charging time is decreased by 32.70%, 36.40% and 38.07%, respectively. Similarly, for inlet temperature of 57 °C, the charging time is reduced by 28.01%, 36.47% and 44.57%, respectively. Moreover, the discharging time is also decreased by a fraction of 14.63%, 34.95% and 41.46%, respectively. Therefore, it is concluded that all three nano-additives have presented significant improvement in charging/discharging rate. However, GnP based nano-PCM samples have illustrated relatively better thermal performance.

- An optimum volume fraction of nano-additives is critical for an ideal enhancement in thermal performance of LHS system. Al_2O_3 based nano-PCM samples with varying volume fractions of 1%, 3% and 5% are investigated at inlet temperature of 47, 52 and 57 °C. In case of inlet temperature of 47 °C, the charging time of Al_2O_3 based nano-PCM samples is significantly reduced by a fraction of 33.75%, 55.41% and 56.25% as

compared to pure paraffin. Likewise, in case of inlet temperature of 52 °C, the charging time is decreased by 35.92%, 48.80% and 56.37%, respectively. Also, in case of inlet temperature of 57 °C, the charging time is lessened by 11.36%, 21.71% and 24.74%, respectively. Furthermore, the discharging time is also reduced by a fraction 28.45%, 39.05% and 39.52%, respectively. It can be observed that Al_2O_3 based nano-PCM samples have illustrated higher charging and discharging rate. However for all charging/discharging cycles, a minimal enhancement in charging/discharging rate is noticed as the volume fraction of Al_2O_3 is increased from 3% to 5%. Therefore, the optimum volume fraction for Al_2O_3 based nano-PCM samples is identified as 3%.

- The inclusion of nano-additives captures certain volume and as a result, it reduces the overall thermal storage capacity of LHS system. It is noticed that with an addition of 5% volume fraction of Al_2O_3, AlN and GnP nano-additives, the total enthalpy of LHS system is reduced by 20.58%, 19.64% and 2.88% as compared to pure paraffin. It is noticed that GnP based nano-PCM samples have indicated a slight reduction in thermal storage capacity as compared to Al_2O_3 and AlN based nano-PCM samples. Due to significant reduction in thermal storage capacity and an increase in overall weight of the LHS system, the employability of Al_2O_3 and AlN based nano-PCM samples in large scale practical applications is limited.

Acknowledgement

The authors would like to acknowledge Bournemouth University, UK and National University of Sciences and Technology (NUST), Pakistan for their financial and in-kind support to conduct this research.

References

[1] International Energy Agency (IEA). Energy and Climate Change 21st UN Conference of the Parties (COP21), Paris, 2015.
[2] S. Suranovic. Fossil fuel addiction and the implications for climate change policy. Global Environmental Change. 23 (2013) 598-608.
[3] J.P. da Cunha, P. Eames. Thermal energy storage for low and medium temperature applications using phase change materials–a review. Applied Energy. 177 (2016) 227-38.
[4] A. Sharma, V.V. Tyagi, C. Chen, D. Buddhi. Review on thermal energy storage with phase change materials and applications. Renewable and Sustainable energy reviews. 13 (2009) 318-45.
[5] L. Miró, J. Gasia, L.F. Cabeza. Thermal energy storage (TES) for industrial waste heat (IWH) recovery: a review. Applied Energy. 179 (2016) 284-301.
[6] A. Modi, F. Bühler, J.G. Andreasen, F. Haglind. A review of solar energy based heat and power generation systems. Renewable and Sustainable Energy Reviews. 67 (2017) 1047-64.
[7] D. Rabha, P. Muthukumar. Performance studies on a forced convection solar dryer integrated with a paraffin wax–based latent heat storage system. Solar Energy. 149 (2017) 214-26.
[8] N. Soares, J. Costa, A. Gaspar, P. Santos. Review of passive PCM latent heat thermal energy storage systems towards buildings' energy efficiency. Energy and buildings. 59 (2013) 82-103.
[9] Y. Tian, C.-Y. Zhao. A review of solar collectors and thermal energy storage in solar thermal applications. Applied Energy. 104 (2013) 538-53.
[10] A. Waqas, Z.U. Din. Phase change material (PCM) storage for free cooling of buildings—a review. Renewable and sustainable energy reviews. 18 (2013) 607-25.
[11] L.F. Cabeza, A. Castell, C.d. Barreneche, A. De Gracia, A. Fernández. Materials used as PCM in thermal energy storage in buildings: a review. Renewable and Sustainable Energy Reviews. 15 (2011) 1675-95.
[12] Z. Khan, Z.A. Khan. Development in Paraffin Based Thermal Storage System Through Shell and Tubes Heat Exchanger With Vertical Fins. ASME 2017 11th International Conference on Energy Sustainability collocated with the ASME 2017 Power Conference Joint With ICOPE-17, the ASME 2017 15th International Conference on Fuel Cell Science, Engineering and Technology, and the ASME 2017 Nuclear Forum. American Society of Mechanical Engineers2017. pp. V001T11A3-VT11A3.
[13] N.S. Dhaidan, J. Khodadadi. Melting and convection of phase change materials in different shape containers: A review. Renewable and Sustainable Energy Reviews. 43 (2015) 449-77.
[14] Z. Khan, Z. Khan, A. Ghafoor. A review of performance enhancement of PCM based latent heat storage system within the context of materials, thermal stability and compatibility. Energy Conversion and Management. 115 (2016) 132-58.
[15] J. Giro-Paloma, M. Martínez, L.F. Cabeza, A.I. Fernández. Types, methods, techniques, and applications for microencapsulated phase change materials (MPCM): a review. Renewable and Sustainable Energy Reviews. 53 (2016) 1059-75.
[16] J. Khodadadi, L. Fan, H. Babaei. Thermal conductivity enhancement of nanostructure-based colloidal suspensions utilized as phase change materials for thermal energy storage: a review. Renewable and Sustainable Energy Reviews. 24 (2013) 418-44.

[17] L. Liu, D. Su, Y. Tang, G. Fang. Thermal conductivity enhancement of phase change materials for thermal energy storage: A review. Renewable and Sustainable Energy Reviews. 62 (2016) 305-17.
[18] M. Kibria, M. Anisur, M. Mahfuz, R. Saidur, I. Metselaar. A review on thermophysical properties of nanoparticle dispersed phase change materials. Energy Conversion and Management. 95 (2015) 69-89.
[19] M.K. Rathod, J. Banerjee. Thermal performance enhancement of shell and tube Latent Heat Storage Unit using longitudinal fins. Applied thermal engineering. 75 (2015) 1084-92.
[20] A.A.R. Darzi, M. Jourabian, M. Farhadi. Melting and solidification of PCM enhanced by radial conductive fins and nanoparticles in cylindrical annulus. Energy Conversion and Management. 118 (2016) 253-63.
[21] Z. Khan, Z. Khan, K. Tabeshf. Parametric investigations to enhance thermal performance of paraffin through a novel geometrical configuration of shell and tube latent thermal storage system. Energy Conversion and Management. 127 (2016) 355-65.
[22] Z. Khan, Z.A. Khan. An experimental investigation of discharge/solidification cycle of paraffin in novel shell and tube with longitudinal fins based latent heat storage system. Energy Conversion and Management. 154 (2017) 157-67.
[23] Z. Khan, Z.A. Khan. Experimental investigations of charging/melting cycles of paraffin in a novel shell and tube with longitudinal fins based heat storage design solution for domestic and industrial applications. Applied Energy. (2017).
[24] K. Venkitaraj, S. Suresh, B. Praveen, A. Venugopal, S.C. Nair. Pentaerythritol with alumina nano additives for thermal energy storage applications. Journal of Energy Storage. 13 (2017) 359-77.
[25] Y. Tang, D. Su, X. Huang, G. Alva, L. Liu, G. Fang. Synthesis and thermal properties of the MA/HDPE composites with nano-additives as form-stable PCM with improved thermal conductivity. Applied Energy. 180 (2016) 116-29.
[26] S. Harikrishnan, M. Deenadhayalan, S. Kalaiselvam. Experimental investigation of solidification and melting characteristics of composite PCMs for building heating application. Energy Conversion and Management. 86 (2014) 864-72.
[27] J.-N. Shi, M.-D. Ger, Y.-M. Liu, Y.-C. Fan, N.-T. Wen, C.-K. Lin, et al. Improving the thermal conductivity and shape-stabilization of phase change materials using nanographite additives. Carbon. 51 (2013) 365-72.
[28] Z.-T. Yu, X. Fang, L.-W. Fan, X. Wang, Y.-Q. Xiao, Y. Zeng, et al. Increased thermal conductivity of liquid paraffin-based suspensions in the presence of carbon nano-additives of various sizes and shapes. Carbon. 53 (2013) 277-85.
[29] L.-W. Fan, X. Fang, X. Wang, Y. Zeng, Y.-Q. Xiao, Z.-T. Yu, et al. Effects of various carbon nanofillers on the thermal conductivity and energy storage properties of paraffin-based nanocomposite phase change materials. Applied Energy. 110 (2013) 163-72.
[30] Y. Yuan, N. Zhang, T. Li, X. Cao, W. Long. Thermal performance enhancement of palmitic-stearic acid by adding graphene nanoplatelets and expanded graphite for thermal energy storage: A comparative study. Energy. 97 (2016) 488-97.
[31] W. Wang, X. Yang, Y. Fang, J. Ding, J. Yan. Enhanced thermal conductivity and thermal performance of form-stable composite phase change materials by using β-Aluminum nitride. Applied Energy. 86 (2009) 1196-200.
[32] L. Zhang, J. Zhu, W. Zhou, J. Wang, Y. Wang. Characterization of polymethyl methacrylate/polyethylene glycol/aluminum nitride composite as form-stable phase change material prepared by in situ polymerization method. Thermochimica acta. 524 (2011) 128-34.

[33] X. Fang, L.-W. Fan, Q. Ding, X.-L. Yao, Y.-Y. Wu, J.-F. Hou, et al. Thermal energy storage performance of paraffin-based composite phase change materials filled with hexagonal boron nitride nanosheets. Energy Conversion and Management. 80 (2014) 103-9.
[34] Y. Yang, J. Luo, G. Song, Y. Liu, G. Tang. The experimental exploration of nano-Si 3 N 4/paraffin on thermal behavior of phase change materials. Thermochimica Acta. 597 (2014) 101-6.
[35] A.V. Arasu, A.S. Mujumdar. Numerical study on melting of paraffin wax with Al 2 O 3 in a square enclosure. International Communications in Heat and Mass Transfer. 39 (2012) 8-16.
[36] J.M. Mahdi, E.C. Nsofor. Solidification of a PCM with nanoparticles in triplex-tube thermal energy storage system. Applied Thermal Engineering. 108 (2016) 596-604.
[37] Z. Meng, P. Zhang. Experimental and numerical investigation of a tube-in-tank latent thermal energy storage unit using composite PCM. Applied Energy. 190 (2017) 524-39.
[38] N. Das, Y. Takata, M. Kohno, S. Harish. Melting of graphene based phase change nanocomposites in vertical latent heat thermal energy storage unit. Applied Thermal Engineering. 107 (2016) 101-13.
[39] D.D. Gray, A. Giorgini. The validity of the Boussinesq approximation for liquids and gases. International Journal of Heat and Mass Transfer. 19 (1976) 545-51.
[40] D.A. Nield, A. Bejan, Nield-Bejan... Convection in porous media. Springer2006.
[41] M. Corcione. Empirical correlating equations for predicting the effective thermal conductivity and dynamic viscosity of nanofluids. Energy Conversion and Management. 52 (2011) 789-93.
[42] A. Einstein. Eine neue bestimmung der moleküldimensionen. Annalen der Physik. 324 (1906) 289-306.
[43] H. De Bruijn. The viscosity of suspensions of spherical particles.(The fundamental η-c and φ relations). Recueil des travaux chimiques des Pays-Bas. 61 (1942) 863-74.
[44] H. Brinkman. The viscosity of concentrated suspensions and solutions. The Journal of Chemical Physics. 20 (1952) 571-.
[45] I.M. Krieger, T.J. Dougherty. A mechanism for non-Newtonian flow in suspensions of rigid spheres. Transactions of the Society of Rheology. 3 (1959) 137-52.
[46] G. Batchelor. The effect of Brownian motion on the bulk stress in a suspension of spherical particles. Journal of fluid mechanics. 83 (1977) 97-117.
[47] J.C. Maxwell. A treatise on electricity and magnetism. Clarendon press1881.
[48] V.D. Bruggeman. Berechnung verschiedener physikalischer Konstanten von heterogenen Substanzen. I. Dielektrizitätskonstanten und Leitfähigkeiten der Mischkörper aus isotropen Substanzen. Annalen der physik. 416 (1935) 636-64.
[49] R. Hamilton, O. Crosser. Thermal conductivity of heterogeneous two-component systems. Industrial & Engineering chemistry fundamentals. 1 (1962) 187-91.
[50] Y. Xuan, Q. Li, W. Hu. Aggregation structure and thermal conductivity of nanofluids. AIChE Journal. 49 (2003) 1038-43.